Integrated Modeling of Process, Structures and Performance in Cast Parts

Kotas, Petr

Publication date:
2011

Integrated Modeling of Process, Structures and performance in Cast Parts

by

Petr Kotas

Ph.D. Thesis
Technical University of Denmark
Department of Mechanical Engineering
January, 2011

Integrated Modeling of Process, Structures and performance in Cast Parts

Process Modeling Group
Department of Mechanical Engineering
Technical University of Denmark
Kgs. Lyngby, Denmark
ISBN: 978-87-90416-54-6

To my cousin Pavel… see you in heaven

Preface

This thesis is submitted in partial fulfillment of the requirements for the Doctor of Philosophy degree in Mechanical Engineering (MEK) at Technical University of Denmark (DTU). The work presented in this thesis was supervised by Professor Jesper Henri Hattel during the period October 2007 through January 2011.

Acknowledgements

This work was made possible by the support, guidance, and encouragement of many people:

Above all, I would like to thank my supervisor Prof. Jesper Hattel for putting his trust in me and giving me this great opportunity to carry out my Ph.D. studies at his group, under his supervision. I am also very grateful for his continuous motivation, support and excellent guidance throughout the whole period of my Ph.D., and also for NOT being an old-fashioned fearful professor, but rather a mentor and a person who it is fun to be with.

Many sincere thanks go to Dr. Jesper Thorborg for always being ready for any kind of help and support, for inspiring and motivating me to stay focused but above all for being a true friend. Without you my Ph.D. would not be possible.

I would like to express my gratitude to all my fellow colleagues and friends from the process modeling group, especially to Dr. Cem Tutum for his close friendship, encouragement, leadership in evolutionary optimization and for teaching me to always push my limits further in order to get better. Next, my thanks go to Jon Spangenberg, Michael Wenani Nielsen and Jens Ole Frandsen for their encouragement, help and constant good, fun time.

Dr. Niels Tiedje, thanks for all our irreplaceable discussions on foundry technology and especially for your assistance with my experimental work.

I was privileged to meet Søren Andersen and Konstantin Nikolov from MAGMA Foundry Technologies who gave me a unique opportunity to spend two incredible months under their leadership. Thank you for teaching me so much about steel casting processes and optimization and for being my mentors who I can always turn to. Moreover, I would like to thank Dr. Erwin Flender from MAGMA GmbH, for providing me with their amazing software which made my Ph.D. possible.

I would like to express my sincere gratitude and appreciation to my family, especially my parents for loving, supporting and believing in me from the very beginning. I thank my beautiful wife Martina, for her deepest love, continuous encouragement and big sacrifice as we were apart many times due to my Ph.D. studies. My son Vojta, you are my greatest joy, source of a laughter and a genuine “thesis baby”.

I would like to devote this thesis to my best friend and cousin Pavel, who passed away so suddenly. You were my one and only role model and a brother to me. You are still deeply missed bro.

Last but not least I would like to thank Technical University of Denmark for its financial support and a pleasant working environment that is hard to find elsewhere.

Petr Kotas
Kgs. Lyngby, January 2011

Abstract

This thesis deals with numerical simulations of gravity sand casting processes for the production of large steel parts. The entire manufacturing process is numerically modeled and evaluated, taking into consideration mould filling, solidification, solid state cooling and the subsequent stress build up. The thermal analysis is then combined with evolutionary multi-objective optimization techniques in a search for the optimal thermal aspects and conditions for producing sound and competitive castings. The goals of the optimization procedure are related to the casting and rigging design and to defects occurrence. In other words, it is desired to eliminate all of the potential casting defects and at the same time to maximize the casting yield. The numerical optimization algorithm then takes these objectives and searches for a set of the investigated process, design or material parameters e.g. chill design, riser design, gating system design, etc., which would satisfy these objectives the most.

The first step in the numerical casting process simulation is to analyze mould filling where the emphasis is put on the gating system design. There are still a lot of foundry specialists who ignore the importance of a good gating system design. Hence, it is common to see, especially in gravity sand casting, “traditional gating systems” which are known for a straight tapered down runner a well base and 90^{o} bends in the runner system. There are theories supported by experimental results claiming that flow patterns induced by non-optimal gating systems can cause a variety of defects which are generally not considered to be filling related, such as hot tears and channel segregates. By improving the gating technology in traditional gating systems it is possible to achieve much higher casting integrity with less defects and also to reduce the amount of metal to be re-melted, hence reducing the energy consumption for melting in foundries. Guidelines on how to approach gating system design are given together with examples on how the separate elements constituting gating systems which affect filling patterns and subsequent defects occurrence.

Investigation and optimization of thermal behavior of steel castings is the main focus area of this thesis. The intention is to show and discuss a relation among three well-known casting defects, namely centerline porosity, hot tears and macrosegregation. It occurs that all of these defects depend on thermal gradients, cooling rate, pressure drop over the mushy zone and solidification pattern. It is not a standard procedure in daily foundry practice to run convection, macrosegregation and stress-strain calculations on all projects to identify macrosegregation and hot tearing, because of insufficient computational power in many foundries. As a result, many castings are being produced without any knowledge of these two defects. The consequences are known to everybody. The methodology or approach, adopted during the study, lies in utilizing the prediction of centerline porosity for the subsequent assessment of hot tears and macrosegregation. The Niyama criterion is used for this purpose. If there are any narrow areas or channels with high Niyama values, they indicate a presence of high thermal gradients over a narrow region and hence high thermal straining which may lead to hot tearing. If Niyama values are very low, flat thermal gradients are present in this area, which means that there is not a directional and progressive solidification pattern and there will be issues with centerline porosity. Moreover, flat thermal gradients imply large extent of the mushy zone which may promote macrosegregation and especially channel segregates. One can now see that indeed macrosegregation and hot tearing can be addressed by standard thermal calculations, just by using the Niyama criterion. This should not be understood as stress-strain analysis or convection calculations can be entirely omitted, not at all. But they can be reasonably substituted in the initial (informative) calculation or when there is not time to run proper stress-strain or convection calculations.

The methodology applied in the thermal analysis is then exploited in numerical optimization. It is shown and verified that it is possible to eliminate hot tears and macrosegregation issues by minimizing centerline porosity and by establishing the directional and progressive solidification pattern towards the heaviest area of the casting. Multi-Objective Genetic Algorithms are applied to handle this task. Three industrial case studies are presented in which minimization of riser volumes and minimization of the three aforementioned defects are pursued by modifying the riser and chill designs and their placement.

The thesis comprises the following five papers:

Paper I

Petr Kotas, Jesper Hattel, Jesper Thorborg, Ingvar L. Svensson, Salem Seifeddine. *Modeling of Filling, Microstructure Formation, Local Mechanical Properties and Stress – Strain Development in High-Pressure Die Cast Aluminium Castings*. Published at the International Ph.D. Foundry Conference, Brno, June 2007, Czech Republic.

Author's contribution: Performed modeling work except for the microstructure modeling and mechanical properties prediction, this was done by the co-authors. Contributed in writing the paper draft and in making all necessary corrections proposed by the co-authors. Also served as the corresponding author during the review process.

Paper II

Petr Kotas, Cem Celal Tutum, Olga Šnajdrova, Jesper Thorborg, Jesper Hattel. *A Casting Yield Optimization Case Study: Forging Ram*. Published in the International Journal of MetalCasting, Vol. 4, Issue 4, (2010).

Author's contribution: Carried out all numerical simulations including autonomous optimization and subsequently evaluated the results. Wrote the initial draft, except for the optimization theory which was written in collaboration with one of the co-authors. Moreover, incorporated all the corrections suggested by the co-authors and also performed the role of the corresponding author during the review process.

Paper III

Petr Kotas, Søren Andersen, Jesper Hattel, Cem Celal Tutum. *Autonomous Optimization of a Solidification Pattern and its Effect on Porosity and Segregation in Steel Castings.* Accepted for Oral Presentation at the 115th Metalcasting Congress, Schaumburg, April 2011, USA. Accepted for publication in AFS Transactions 2011.

Author's contribution: Carried out all the modeling and optimization work. Wrote the draft and made all the corrections and changes proposed by the co-authors. Was designated as the corresponding author during the review process.

Paper IV

Petr Kotas, Jesper Thorborg, Cem Celal Tutum, Jesper Henri Hattel. *Elimination of Hot Tears in Steel Castings by Means of Solidification Pattern Optimization.* Presented at the International Steel Casting Conference, October 2010, Dresden, Germany. Submitted to Metallurgical and Materials Transactions B – February 2011.

Author's contribution: Carried out the entire modeling and optimization work. The modeling work was supervised and discussed by the co-authors. Wrote the draft and made the corrections suggested by the co-authors. Presented the work at the conference and has been assigned the corresponding author for the review process.

Industrial Report

Petr Kotas, Jesper Henri Hattel. *Casting Process Optimization of a Large Steel Ring With Respect to Centerline Porosity and Channel Segregates.* Presented to the foundry management of Vitkovice Heavy Machinery in July 2010.

Author's contribution: Carried out the entire project work, i.e. modeling and subsequent optimization. The other co-author supervised and guided the work and was involved in making the overall structure of the final report delivered to the foundry personnel. The author presented the findings and proposals at the foundry and serves as a connection at Technical University of Denmark.

Table of contents

Chapter 1

1. Introduction

1.1. Objectives of the work

The foundry industry, probably more than any other branch of industry around the world, is constantly exposed to new challenges. Besides increased economical demands, especially regarding personnel and material resources, the foundry industry must comply with continuously increasing demands for high quality castings, documentation and delivery time.

The fundamental issue for design department in foundries is improving efficiency. Thus it is obvious that for foundries who want to succeed it no longer applies that the production is governed by experience-based innovation or trial-and-error methods only. In this area substantial changes have occurred over the last two decades by incorporating numerical casting process simulation, also referred to as virtual prototyping into daily foundry practice. This technology enables designers to set up robust and easy-to-optimize processes, working well before any tooling has been built, and hence resulting in savings of both cost and time and giving the industry a definite edge over the competitors.

Casting simulation aims at using physically realistic models that provide detailed information about material flow and heat flow, and with that, also information about the local microstructure evolution, non-uniform distribution of mechanical properties, residual stresses and distortion build-up, consequently leading to substantial improvement in predicting the in-service behavior of the final product.

The objective of this study is to apply numerical models for investigating, controlling and optimizing thermal conditions in various metal-casting processes. This means investigating how the melt flow and the subsequent heat flow influence local microstructure evolution, defects occurrence, the casting's soundness, mechanical properties and consequent residual stresses. All of this is done by means of numerical simulation and optimization techniques, respectively. Most of the investigations have been oriented on gravity sand casting of large steel castings.

Major focus has been put on solidification as the most influential stage in the whole casting process. The solidification pattern is initially governed by the flow field during mould filling which provides essential insights into the temperature fields, surface turbulence and resulting defects. The solidification pattern itself is influenced by the geometry of the casting, its alloy chemistry, the surrounding mould material and by the applied casting technique. Consequently, based on the thermal conditions it is possible to predict the microstructure at given areas of the casting, defects occurrence and final mechanical properties. On top of that, one should bear in mind that the solidification pattern is directly coupled to the subsequent mechanical behavior of the casting, providing valuable indications of hot tear susceptibility, thermally induced stresses and strains and final residual stresses that all together control the in-service properties of the given cast part.

In order to obtain a better overview of some of the fundamental mechanisms involved in all metal casting processes, the physical phenomena have been divided into two subsystems, i.e. thermal and mechanical behavior, followed by an approach referred to as integrated modeling where the coupled thermal and mechanical behavior is combined with the load situation.

Besides the casting process modeling investigations, autonomous optimization based on genetic algorithms has been applied to most of the presented case studies with the aim of finding optimal process parameters, casting geometry and thermo-physical properties with respect to predefined conflicting objectives. These objectives have been handled as multi-objective optimization problems.

It will be shown how fully automated optimization techniques, in our multi-objective genetic algorithms, can be exploited in solving both simple and complex casting-related issues. In addition, a methodology will be presented on how the Niyama criterion which predicts the presence of centerline porosity can be utilized in optimization of macrosegregation, channel segregates and hot tearing. It is not possible, at least computation time-wise to directly optimize hot tearing and macrosegregation

profiles in castings. One standard convection and segregation analysis which is necessary for this purpose takes roughly 24 hours on a standard up-to-date multi-core work station, using a reasonably fine computational grid and the same applies to stress-strain analysis which is necessary for hot tear prediction. Considering that a typical optimization cycle comprises from 1000 to 2000 independent designs, nobody in industry would afford doing this type of optimization. This explains why there is a gap in information in literature or in scientific papers on this type of optimization. Therefore, the idea of the optimization problems presented here has been to utilize the existing and well proven physical link between these defects and optimize the macrosegregation profiles and hot tears indirectly by means of the Niyama criterion. In other words, by finding proper riser and chill designs steeper thermal gradients and progressive-directional solidification pattern will be established and all of these defects should be eliminated.

The entire work throughout the Ph.D. studies has been devoted to numerical modeling of various aspects of the metal casting processes. Material and especially heat flow have been investigated with respect to evolution of microstructure, defects and transient as well as residual stresses during casting. All information and data have been provided by the simulation software MAGMAsoft® (MAGMA Giesserei Technologie GmbH), devoted solely to metal casting. All optimization cases have been dealt with using the built-in optimization module MAGMA*frontier* (MAGMA Giesserei Technologie GmbH).

1.2. Modeling of Foundry Processes

The following presentation is inspired by Hattel[1].

A need for modeling of foundry processes usually initiates from a technological problem, e.g. to test, analyze and/or optimize a certain casting layout or its manufacturing process. The first step in solving the given problem comprises describing this problem by the proper physical terms. For instance the mould filling can be taken as a fluid flow problem, solidification is recognized as a heat transfer problem and the distortions as a solid mechanical problem. The second step would be to describe these physical problems by a proper mathematical model applied in 3-D. In case of mould filling, a detailed flow analysis could be obtained by solving the 3-D Navier-Stokes equations. In the case of solidification a full 3-D heat conduction analysis involving various metallurgy-based models for solidification should be applied if a thorough analysis on a complex geometry should be carried out. Although, the numerical solution implies a complex mathematical model, the solution to the given technological problem always is an approximation of the original problem no matter the solution method.

Once the mathematical problem has been solved, the results should be interpreted. Even though this issue is not the major part of mathematical modeling, it is essential to all mathematical solution of real physical problems. In all manufacturing processes, casting as well, the misinterpretation of otherwise correct mathematical results could lead to totally wrong conclusions, and hence to no reasonable solution of the given problem. The basic flow of steps from the initial technological problem to the final solution is shown in **Figure 1.1**.

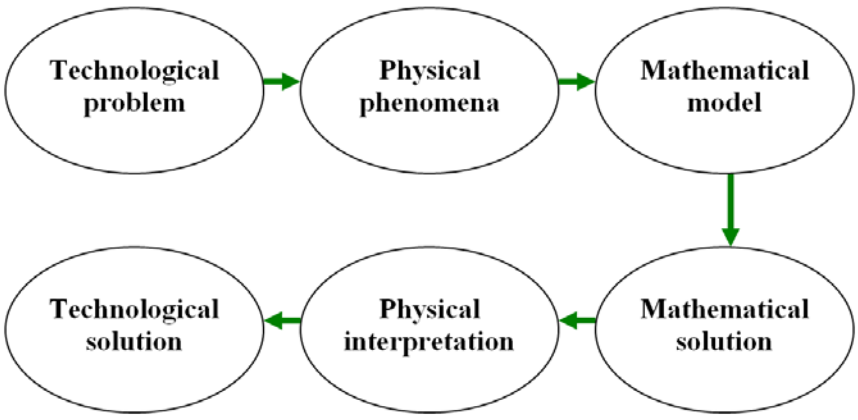

Figure 1.1: Flow of steps involved in the solution of a technological problem. Figure adapted from Hattel[1].

The starting point for a numerical modeling of casting processes is the geometry, provided by the design/construction department or by a customer. This geometry is then modified for better castability, e.g. sufficient draft, machining allowances, shrinkage allowances, etc., based on empirical knowledge and practical experience. The geometry then serves as the basis for the subsequent calculations that will result in a proper analysis or even in optimization of the casting process. The standard casting analysis includes evaluations of the layout, i.e. inlet, gating, feeding or cooling systems, various types of defects. The subsequent numerical optimization seeks for designs and layouts favorable in terms of lower susceptibility to hot tearing, residual stress and deformation, improved filling and feeding, increased casting yield etc., to increase the overall quality of the casting.

In a foundry or steel works, parameters such as alloys, process and geometry will often be predetermined to a high degree. Besides optimizing these parameters within narrow limits, the mathematical modeling and numerical simulations will be related especially to optimization of casting velocity, cooling rate and layouts, i.e. casting conditions, gating systems, chills, risers and local insulation.

The basic flow of any numerical model based calculation contains a pre-processing part, a calculation part and a post-processing part, **Figure 1.2**. These will be discussed I detail in the following.

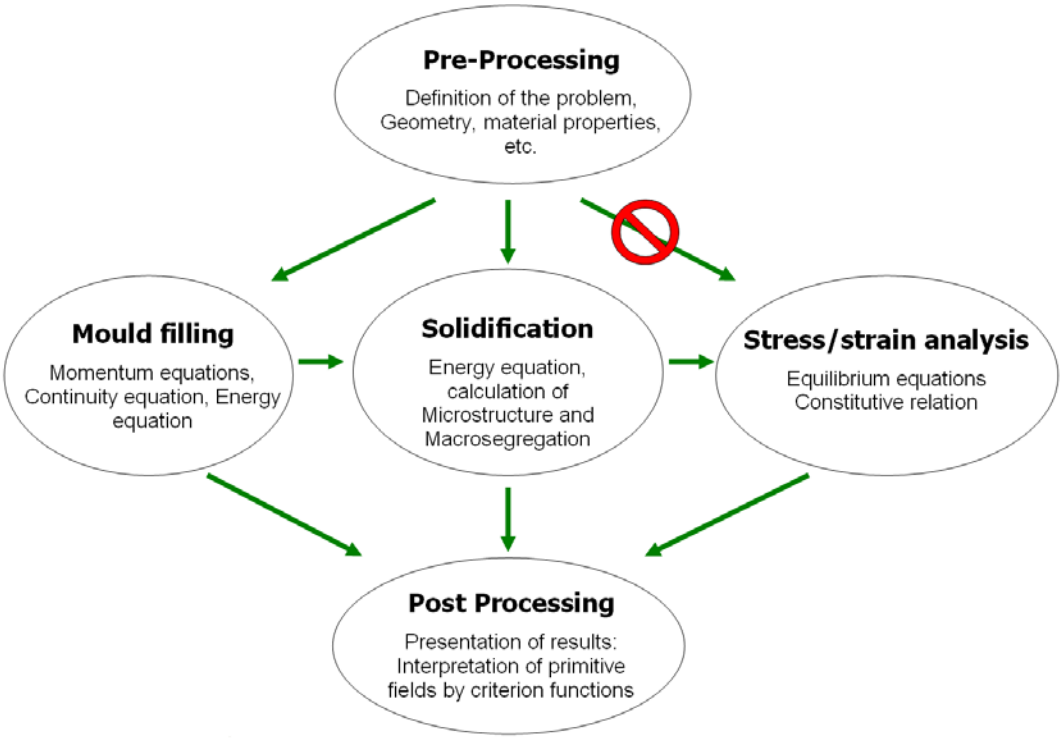

Figure 1.2: Flow diagram of the interrelationship of casting simulation modules, figure inspired by Hattel[1].

1.2.1. The Pre-Processing: Definition of the Problem

Casting simulation starts with a geometry defined by a CAD model of the casting, mold, gating, chills, risers, padding, etc. that are part of the casting system. It is of great importance to take into consideration all elements of the casting system that can have any impact on filling calculations and the subsequent solidification and cooling. In essence, the primary goal in numerical modeling should always be to "mimic" the real casting process as close as possible to achieve reality-resembling results.

As stated above, due to the geometrical complexity of industrial castings and the number of variables involved, it is virtually impossible to describe the entire casting process analytically. This issue can be relatively easily overcome by means of numerical methods based on suitable numerical models obtained by methods of discrete representation, i.e. control volumes, finite elements, finite differences or others. The analyzed domain is suitably split into a large number of volumes, the so-called mesh or the grid, which is based on simplified geometrical elements, e.g. cubic or tetragonal. Hence, the quality and precision of the subsequent results are directly related to both the employed algorithms and the accuracy of the computational mesh. On the other hand, as the mesh becomes finer, the computational time increases. Therefore, a balance needs to be found between the needed accuracy and the computational time that can be sacrificed for a particular simulation.

In essence, one could say that the major steps covering the whole casting process, i.e. mould filling, solidification and solid state cooling, can be described by means of a mathematical approach of varying complexity. But before the equations governing these physical phenomena can be solved, the necessary initial and boundary conditions, process parameters and the properties of the materials involved in the casting process must be available[2].

Boundary as well as initial conditions allow for parameters such as initial pouring temperatures, casting size and its geometrical configuration, i.e. feeder placement, cores, chills, insulation, mould / die configuration, i.e. placement of the gating system, cooling system, ventilation system, ejecting system, etc., to be taken into consideration. Besides that, to set up a reasonable simulation it is required to have detailed information concerning temperature dependent material and thermo-mechanical properties at disposal, such as:

- As to the cast alloy: extend of the solidification range, temperature dependent viscosity, density, thermal conductivity, diffusivity, temperature dependent Young's modulus and yield strength, thermal expansion coefficient, and many others.
- As to the mould / die: temperature dependent thermo-physical properties such as heat transfer coefficient at the metal/mould interface, sand density, thermal conductivity of the sand mould, specific heat capacity, thermal diffusivity, sand permeability, temperature dependent Young's modulus and yield strength, thermal expansion coefficient, and eventually chilling/cooling systems characteristics.

Apart from the material data themselves, information regarding process and work parameters must be known or at least estimated:

- High pressure die casting: definition of the velocity curve during filling, closing and opening time, lead time, coating application, operating time of the cooling system, ejection time, closing force of the machine, etc.
- Gravity sand casting: filling mode, i.e. manual ladle filling, lip-pour ladle, bottom-fill ladle, multiple stoppers in one ladle, height of the ladle above the pouring cup, simultaneous filling from multiple ladles, refilling of the open risers with fresh melt after certain time, time of removing the casting from the mould, referred to as shake out, time and temperature when risers and the gating system are burned off, type of heat treatment and its operating time and temperature, etc.

It is thus important to realize that the results of a foundry process simulation can only be as good as the material and process parameters applied in the simulation. For this reason, it is important to use the most accurate material, thermo-physical and thermo-mechanical data available and to specify the process in as much detail as possible in order to benefit the most from the casting simulation.

1.2.2. The Calculations Part

After the geometry and mesh definition, the most demanding part of the numerical simulation follows, with respect to the algorithmic development and the computational capacity requirements- the actual solution of the governing equations. It is clear that these calculations, in which primitive fields such as temperature, velocities, pressure, displacements, stresses, etc. are determined, require the solution of the governing differential equations. These equations often comprise several coupled partial differential equations with one or more dependent variables, e.g. temperature, and four independent variables, time and space (x, y, and z). All these equations express a certain balance or a conservation principle, established by specific physical quantities as dependent variables. These variables will be the temperature in the heat conduction equation, the concentration in the Fick`s 2nd law, the stresses in the equilibrium equations, displacements in the Navier equations, and the velocities in the momentum equations.

In general, the calculations connected with a numerical simulation of any kind of casting process contains of three major successive parts, i.e. fluid flow, solidification and solid state cooling and stress/strain analysis, as illustrated in **Figure 1.2**. These will be briefly discussed in the following.

1.2.2.1. Fluid Flow: Mould Filling

Fluid flow plays a very important role in the production of sound quality castings. Mould/die filling is the very first step of every casting process. For all castings processes, mould/die filling determines the quality of the final product. Excessive surface turbulence, air or gas entrapment, swirling, interrupted flow, oxidation, premature solidification, mould/die erosion, any of these factors can spoil the final product[3-8]. However, some casting techniques are more sensitive to an improper filling pattern than others, quality-wise. For instance in high-pressure die casting of thin-walled aluminum castings, the flow pattern is by far more decisive and influential for the casting's soundness as compared to rather slow gravity sand casting of large steel or cast iron castings. After the mould filling phase, during subsequent solidification of the casting, fluid flow steps in again. Buoyancy effects, segregation of the alloying (solute) elements, shrinkage flow, and flow due to gravity forces are the examples of fluid flow phenomena that can take place during the solidification[9-11]. Modeling of the fluid flow is required if the above phenomena need to be taken into account. In order to be able to model the mould filling properly, the following equations must be solved:

- The three momentum equations, i.e. momentum conservation, together with a suitable constitutive law relating stresses and velocities, typically incompressible, Newtonian fluid for metals.
- The continuity equation, i.e. mass conservation.
- The energy equation, i.e. energy conservation.

Important phenomena that should be taken into account are e.g. temperature dependent viscosity and tracking of free surfaces. These non-linear phenomena are often taken into consideration in an explicit manner in the numerical formulation. It should be noted that for especially thin-walled castings, surface tension could play an important role. This adds yet another non-linearity to the fluid flow analysis.

1.2.2.2. Solidification

After the mould filling the casting starts to solidify. In order to model this and the following solid-state cooling, a wide range of engineering and scientific disciplines including heat and mass transfer, thermodynamics, materials science, stability theory, metallurgy must in general be addressed. Tied together in rigorous solidification theory, this can be used in the design of castings or casting processes to control the mechanical, chemical and physical properties of the final product[12].

The basis of any solidification model is the energy equation, i.e. energy conservation and the momentum and continuity equations if fluid flow is not neglected, with release of latent heat. As mentioned before, fluid flow could also be necessary to include during the solidification analysis. However, in many cases, the convective terms are often neglected for the purpose of establishing a first impression of the temperature field during solidification.

1.2.2.3. Stress-Strain Analysis

After the mould filling and solidification analyses, the modeling of stress/strain phenomena should be carried out. In general, the solidification and stress/strain analyses are fully coupled problems, meaning that they should be made simultaneously. However, if suitable measures are taken, the thermo-mechanical analysis of a casting process may normally be performed in a semi-coupled way, that is, in a sequential manner, where the temperature analysis is performed first and the mechanical analysis follows within each time step, see **Figure 1.2**.

Some of the important phenomena to be addressed in the thermo-mechanical analysis are linear thermal contraction, solid-state phase transformations, shrinkage-dependent interfacial heat transfer due to relative motion between the casting and the mould, mould distortion, temperature and time-dependent plasticity, hydrostatic pressure from the liquid solidification and cold crack and/or hot tear formation. All of these phenomena are obviously not equally important and as for other branches of numerical process modeling, one of the keys to the successful stress/strain analysis of a casting process is to take into account only what matters for the solution of the problem at hand. The thermo-mechanical analysis involves the solution of the following equations in the general case:

- The energy equation, i.e. energy conservation.
- The three equilibrium equations together with a suitable constitutive law relating stresses and displacements or displacements rates. Typically, a rate independent thermo-elasto-plastic theory.

1.2.3. The post-processing: Presentation of the results

When all the relevant calculations are finished, the resulting basic fields, i.e. temperatures, velocities, pressure, displacements, stresses, etc., should be presented in an appropriate way.
In evaluating the results of a mould filling simulation, particular attention is commonly paid to the filling pattern of the casting in order to determine potential inadequacies or arising defects. For instance air/gas entrapment in various areas of the casting is a very common phenomenon that needs to be addressed by the filling pattern results. In gravity sand casting, velocities, e.g. at thin gates or inside the casting cavity, that are too high may lead to splashing, formation of melt fountains, melt disintegration referred to as fingering, recirculation of swirling indicating regions with mould erosion leading to sand inclusions, as well as where formation of oxide films can be expected and air may be entrained into the liquid metal resulting in air/gas bubbles. Observing the temperature field during filling can indicate whether cold runs can be expected. The temperature field right after filling establishes a starting point for the subsequent solidification calculations and helps to determine whether it supports the feeding of the volumetric shrinkage of the metal during solidification.

Based on this initial thermal field a proper heat flow calculation can be evaluated, giving the possibility of correlating the solidification pattern expressed by the so-called solidification parameters with the microstructural characteristics, i.e. dendrite arm spacing, and the macro- or micro-porosity content of the casting or the concentration profiles indicating issues with segregation. The solidification parameters are:

- *Local solidification time* is a parameter indicating the time at which particular areas of the casting dropped below the solidus temperature. It helps to detect potential hot spots. These are usually isolated areas that solidify slower and later than the surroundings, hence susceptible to porosity formation due to constrained feeding, and with deteriorated mechanical properties. The solidification time also highlights uneven solidification patterns. When a casting exhibits uneven solidification and subsequent cooling, thermally induced stresses and strains evolve, leading to casting deformations, residual stress or ultimate mechanical failure. Last, it is possible to relate local solidification time to characteristics of the dendritic structure, represented by secondary dendrite arm spacing and thus get an idea about the final quality of the microstructure and again, local mechanical properties.
- *Local thermal gradients* at the end of the solidification interval help to identify areas prone to centerline and microporosity due to flat thermal gradients. Moreover, flat temperature gradients imply potential issues with macrosegregation or channel segregates due to a large extend of the mushy zone with no apparent directional solidification. On the contrary, if very steep thermal

gradients are present as narrow channels or highly centralized, this could indicate a risk of hot tearing due to uneven volumetric shrinkage and high strain rates at those areas.

- *Cooling rate,* is an indicator of solidification rate, i.e. how rapidly do the dendrites grow in the opposite direction of the heat flow, and of the final size of grains. In areas with high cooling rates the solid network, i.e. dendrites, grow very rapidly and there is not enough time and "capacity" to adequately feed those areas with fresh melt to compensate for the volumetric reduction, resulting in high pressure drop in the liquid and a high risk of porosity formation.

In sand casting, the temperatures in sand cores are also of interest to provide information about the stability of the core during the solidification process. In permanent mould casting, i.e. die casting; the thermal balance in the die is of particular interest. The magnitude of temperature fluctuations in the die can be investigated to try to minimize thermal stresses and maximize die life. The time needed to reach a quasi-steady state thermal field in the die or the influence of a production interruption on the thermal balance can be determined by simulating several consecutive casting cycles.

For each phenomenon/problem to be treated, it is often necessary to have a criterion function that can transform the calculated basic fields into useful and readily available and understandable information, e.g.:

- Will the casting be sound?
- Will there be an even distribution of alloying elements? Or will there be issues with segregation or channel segregates?
- Will the part withstand tensile straining during solidification or will it tear?
- Does the part contain excessive residual stresses?
- Will the mechanical properties of the casting be satisfactory?
- Will the part maintain the prescribed geometrical tolerances?

Such criterion functions are at present still rather loosely defined, in other words they are primarily indicative. However, due to their key position there is a rapid development, and the area is thus under intense research. As the underlying primitive fields become more accessible vie improved calculation programs and increasing computational capacity, the criterion functions may be progressively better evaluated by comparing them with real casting experiments.

From this brief reasoning it follows, that the possibility of checking the behavior of the casting during its whole manufacturing process gives an engineer an opportunity to detect potentially critical regions of the casting which then provides valuable information for the subsequent validation, optimization and use of the casting itself ahead of its real-scale production.

1.3. Numerical Optimization

Due to the large number of factors affecting the quality of castings and rather complex interconnections of physics, metallurgy and casting geometry, empirical or experience-based knowledge was the only resource on which "optimized manufacturing engineering" depended on in the past. Numerical casting simulations can only test one "state" at a time, while conclusions from calculations or subsequent optimization still require an engineer's interpretation and decision after each of the simulation runs. Hence understanding the process enables a foundry engineer to make decisions that can affect both the part and the rigging to improve the final quality.

Thanks to rapid development of high performance computing the calculation time needed for one variant of the casting process to be analyzed has substantially shortened. Over night it is feasible to calculate numerous versions and layouts in almost unlimited configurations. The advantage of having such short calculation times can only be utilized providing that a computer can automatically analyze calculated variants with respect to some predefined objectives (e.g. maximum feeding, low porosity, low air entrapment etc.) and subsequently create new variants and analyze them in the same manner to achieve the optimal solution. By integrating software for casting process simulation with such an optimization algorithm (in this case the Multi-Objective Genetic Algorithm, MOGA which should

not be confused with the non-elitist MOGA developed by Fonseca and Fleming[13]), a computer based optimization tool is established which is able to determine optimal values of user-defined design variables thereby optimizing a given casting process with respect to defined objectives. Subsequently such system can readily provide optimal solutions for any kind of casting processes. A number of examples can be found both, in this thesis and in literature, first and foremost, in gravity sand casting. Here, especially optimization of riser technology, i.e. its shape, size and location [**Paper II**], should be mentioned[14], but also optimization of the gating system's geometry, optimization of filling[15-20], and a solidification pattern[21], [**Papers II, III** and **IV**], or optimization of thermo-physical data[22], are frequently applied.

Autonomous optimization represents a new approach when it comes to foundry industry, to overcome difficulties in the manufacturing process. When casting simulation software is incorporated into an optimization loop, the whole system can run without user interaction after optimization targets and degrees of freedom have been determined[23]. Multiple objectives, very often conflicting, can be pursued at the same time, e.g. riser size vs. level of porosity. To satisfy the optimization objectives, manufacturing variables, e.g. materials, casting conditions, mould/die temperatures, shot velocity curves, etc., and geometries, e.g. runner design, riser design and its location, chills design and position, gate dimensioning, etc., can be varied. At the same time, manufacturing constraints such as discrete values of riser shape, shake out time, cycle time can also be considered in the optimization run.

The first generation, also referred to as set of designs or technological variants, is defined as Design of Experiments (DOE), using the example of statistical experimental design- from the mostly very large number of possible variations. Several generations are then processed. According to the laws of genetics (since genetic algorithms are considered here), positive characteristics will "survive" to the next generation, such as reduced porosity or increased yield for instance. The best possible compromises between individual conflicting objectives are found in this way. The quantitative information on the impact of the varied process conditions obtained during optimization can also be used for sensitivity studies. Hence, the foundry expert obtains far more layout variants than only on the part in question. This way, the trial and error method is now replaced or transferred to the computer. This new trend in casting process simulation makes it possible to reach proposals for optimum parameter combinations or the optimal technological layout. To summarize the above, numerical models for foundry processes can be applied for the following purposes:

- *A priori prediction* and *evaluation* of the characteristics and potential of a newly set up foundry process, giving a decisive support to the design of mould / die and casting systems, as well as to the optimization of the process itself, accelerating the development and set up stage.
- *Diagnostics*, for figuring out and understanding the physical phenomena behind the cause of defects in castings, or drawbacks and inadequacies in their manufacturing processes, and for suggesting possible improvements.
- *Autonomous optimization* where the "most" optimal solution to one or multiple conflicting objectives is pursued. Based on the predefined objectives, design variables and constraints, the relevant optimization algorithm is seeking for a solution, i.e. technological design, which satisfies the given objectives the most. This often requires thousands of iterations and simulation runs that for an engineer would be impossible to set up and run independently and thus the optimal solution would never be found.

1.4. Outline of the Contents

The thesis comprises 6 chapters which are followed by 5 appended articles.

Chapter 1 summarizes basic objectives and motivation of the Ph.D. work, followed by a brief overview of numerical modeling and optimization of casting processes, the needs and potential benefits.

Chapter 2 is dedicated to numerical modeling of fluid flow phenomena in metal casting. The purpose of this thesis is to describe and subsequently optimize thermal aspects of considered casting

processes; hence the fluid flow chapter serves “only” as some sort of guidelines and proposals to the designers or foundry technologists. The chapter starts with an overview of fluid flow phenomena and basic conservation laws applied in metal casting. Later in the chapter, a general description of all major elements constituting a typical gating system is given together with their impact on the final quality of the filling process and of the casting itself. The primary focus of this chapter is on highlighting the importance of a gating system design in metal casting processes. It should be understood that casting engineers and designers have to, under all circumstances, pay very close attention to the layout of gating systems as it does not only influence filling patterns together with thermal fields and defects arising during solidification but it may also significantly contribute to residual stresses, deformations and hot tears in the casting body.

Chapter 3 is devoted to modeling of solidification and thermal phenomena in metal casting in general. Besides a brief description of heat transfer and guidelines for risering of steel castings, the main emphasis is on thermally-induced casting defects. Three well-known defects in steel castings are discussed, i.e. centerline porosity, hot tears and macrosegregation. It is shown that these defects are interconnected, meaning that there are few common factors which promote them. These factors are thermal gradients, pressure drop over the mushy zone and solidification patterns. This theory is backed and verified by few industrial case studies. Utilizing this interconnection of these defects, a methodology is developed on how hot tearing; macrosegregation and channel segregates can be addressed and “taken care of” by the minimization of centerline porosity, represented by the Niyama criterion. This methodology is then utilized in chapter 4 when optimizing these defects.

Chapter 4 presents a theory and practical use of evolutionary multi-objective optimization techniques in metal casting simulations. Principles of Multi-Objective Genetic Algorithms (MOGA) are thoroughly described and directly applied to industrial problems. Several case studies showing how fully automated optimization can be effectively applied into metal casting industry are presented. Since optimization is very broad discipline the focus is put only on optimization of thermal aspects and behavior of large steel castings.

Chapter 5 presents the overall conclusions of the thesis together with ideas and suggestions for a future research direction.

Chapter 6 is a summary of the four appended journal and conference papers and one industrial report which have been written during the Ph.D. period.

References

1. Hattel, J.H., *Fundamentals of Numerical Modelling of Casting Processes*, 1st ed., Kgs. Lyngby: Polyteknisk Forlag, (2005).
2. Bonollo, F., Odorizzi, S., *Numerical Simulation of Foundry Processes*. S.G.E., (2001).
3. Campbell, J., *Castings*. Second Edition. Elsevier Butterworth-Heinemann, (2003).
4. Campbell, J., *Castings Practice, the 10 Rules of Castings*, Elsevier Butterworth-Heinemann, (2004).
5. Kotas, P., "*Numerical Optimization of Die filling and of High-Pressure Die Cast Deformation*", Master Thesis, Technical University of Denmark, Lyngby, Denmark, (2007).
6. Hansen, S.S., "*Reduced Energy Consumption for Melting in Foundries*", Ph.D. Thesis, Technical University of Denmark, (2007).
7. Kotas, P., Hattel, J.H., Thorborg, J., Svensson, I.L., Seifeddine, S.," *Modelling of Filling, Microstructure Formation, Local Mechanical Properties and Stress – Strain Development in High-Pressure Die Cast Aluminium Castings*", *Proc. International Ph.D. Foundry Conference*, Brno, Czech Republic, (2009), i.e. [enclosed paper II].
8. Kotas P., Tutum, C.C., Šnajdrova, O., Thorborg, J., Hattel, J.H., "*A Casting Yield Optimization Case Study: Forging Ram*", International Journal of MetalCasting, Vol. 4, Issue 4, (2010).
9. Flemmings, M.C.: *Solidification Processing*. McGraw-Hill, Inc., (1974).
10. Fisher, K.: *Fundamentals of Solidification*. Trans Tech Publications LTD, (1986).
11. Schneider, M.C., Beckermann, C., "*Formation of Macrosegregation by Multicomponent Thermosolutal Convection During the Solidification of Steel*", Metallurgical and Materials Transactions A, Vol. 26A, (1995).
12. Dantzig, J., Rappaz, M., *Solidification*, CRC Press Taylor & Francis Group, (2009).
13. Fonseca, C., Fleming, P., "*Genetic algorithms for multi-objective optimization: Formulation, discussion and generalization*", 5th International Conference on Genetic Algorithms, USA, (1993).
14. Hahn, I., Sturm, J.C., "*Autonomous Optimization of Casting Processes and Designs*", Proc. World Foundry Congress, Hangzhou, China, (2010).
15. Masoumi, M., Hu, H., Hedjazi, J., and Boutorabi, M.A., "*Effect of Gating Design on Mold Filling*", AFS Transactions, 113, pp. 185-196, (2005).
16. Kor, J., Chen, X., Hu, H., "*Multi-Objective Optimal Gating and Riser Design for Metal-Casting*", IEEE International Symposium on Intelligent Control, Saint Petersburg, Russia, (2009).
17. Gramegna, N., Baumgartner, P., Kokot, V., "*Capabilities of New Multi-Objective Casting Process Optimization Tool*", IDEAL International Conference, Lecce, Italy, (October 2005).
18. Sun, Z., Hu, H., Chen, X., "*Numerical optimization of gating system parameters for a magnesium alloy casting with multiple performance characteristics*", Journal of Materials Processing Technology, 199, pp. 256–264, (2008).
19. Hahn, I., Hartmann, G., "*Automatic computerized optimization in the die casting processes*", Casting Plant & Technology, Vol. 24, no. 4, (2008).
20. Tsoukalas, V.D., "*Optimization of injection conditions for a thin-walled die-cast part using a genetic algorithm method*", Proc. IMechE Vol. 222 Part B: J. Engineering Manufacture, (2008).
21. Tsoukalas, V.D., "*Optimization of porosity formation in AlSi9Cu3 pressure die castings using genetic algorithm analysis*", Materials and Design Vol. 29, pp. 2027–2033, (2008).
22. Midea, A.C., Burns, M., Schneider, M., Wagner, I., „*Advanced Thermo-Physical Data for Casting Process Simulation – The Importance of Accurate Sleeve Properties*", International Foundry Research/Giessereiforschnung, Vol 59, No. 1, pp. 34 -43, (2007).
23. Kokot, V., Bernbeck, P., "*Integration and Application of Optimization Algorithms with Casting Process Simulation*", Proc. Int. Conf. On Modelling of Casting, Welding and Advanced Solidification Processes, MCWASP X, Destin, Florida, pp. 487- 494, (May 2003).

Chapter 2

2. Modeling of Fluid Flow in Casting Processes

Flow of the molten metal plays a remarkable role in the fabrication of sound and quality castings. Mould/die filling is the very first step of the whole casting process and it always affects the quality of the final product. There are many factors related to the flow influencing the whole process and hence the final casting quality; for instance a turbulent melt flow causing oxide films which impair the mechanical properties[1, 2], metal/mould impingement leading to mould erosion, splashing, disintegrated melt flow, air or gas entrapment within the mould cavity, interrupted flow causing cold shuts, inadequate cooling system, poor gating system[3], wrong fusible alloys with very little fluidity etc. Subsequent to filling, where solidification of the casting takes place, fluid flow phenomena such as buoyancy effects, feeding shrinkage- and gravity-driven flow, segregation of solute components are again of great importance. Modeling of the fluid flow is required if the above phenomena need to be taken into consideration.

Nowadays, in foundry practice, designers and engineers are aware how important it is to fully comprehend these phenomena in order to properly design the shape of castings as well as all elements and systems inside molds or dies. A rapidly increasing trend in various industrial sectors is integrating numerical simulation programs as part of the process and component design. In particular, different product components and tools are shape-optimized according to the results obtained from the prior numerical simulations and analyses of the flow and solidification. In this way it is feasible to reveal potential inadequacies and shortcomings in the design, thus to reduce a risk of consequential problems and defects in the product or in the steel die[4-7].

Modeling of fluid flow is a very extensive and complex subject matter therefore the objective of this chapter is restricted only to the introduction of the basics and fundamentals of fluid flow phenomena in casting processes, presentation of governing equations and laws of fluid mechanics and of aspects influencing processes in the most significant way. A more detailed analysis of impacts of inadequate flow patterns on the overall quality of cast parts analyzed throughout the PhD studies will be presented later in this chapter, as well as in the attached papers at the end of this thesis. There, one can find a presentation of numerical results together with explanations, discussions and subsequent proposals for improvements. No numerical optimization has been utilized in modeling fluid flow phenomena.

2.1. Equations Governing the Motion of Fluids

2.1.1. Introduction

Fluid mechanics and heat transfer textbooks give a firm theoretical basis of the mathematical description of the fluid and heat flow phenomena. On the macroscopic scales, fluids can be treated like a continuum, even though matter is not continuous but discrete, made of molecules. But its properties are averages over a large number of molecules. Our purpose is to simulate the mould filling and solidification of complex castings. The castings range in weight from fractions of a kilogram to several hundred tons. Our fluid is the melt of liquid metal. For our purposes, the mould filling and solidification of castings can be described by the continuum models. In this section, only a brief presentation of the basic conservation equations governing the fluid flow phenomena will be given.

General conservation laws of mass, momentum and energy are used to formulate mathematical models for mould filling and solidification of castings. In this context it means a balance of factors effecting changes. The derivation of the conserved property ϕ follows a general rule: *the rate of change of the conserved quantity inside the control volume is equal to the net influx plus appropriate*

contribution from the sources of ϕ inside of this control volume. A simple sketch illustrated in **Figure 2.1** explains the essence of the conservation principle.

Figure 2.1: Conservation principle, figure inspired by Hattel8.

To derive the conservation law for the property ϕ, one should select a control volume (CV) denoted by the grey area in Figure 2.1. Transport of ϕ by convection, diffusion, radiation or by other mechanisms may occur through the outer surface of the control volume. Inside the control volume ϕ may be generated or destroyed. The net inflow rate is defined as the rate of inflow of ϕ into the control volume minus the rate of outflow out of the control volume. Because of the net transport rate through the surface and the generation of ϕ inside the control volume, the ϕ contents of the control volume may change in time. Hence, it can be said that the property ϕ can be accumulated in the control volume. Conservation laws can be expressed in the following way8:

Rate of accumulation of the property ϕ inside the CV = Net rate of inflow of ϕ through the outer surface of the CV + Rate of generation of ϕ inside the CV.

where *CV* means the *control volume.*
When the mass conservation principle is applied to a fluid flow problem, the continuity equation is obtained. Conservation of momentum is expressed by Newton's Second Law of Motion. Applied to fluid flow problems, it yields the momentum equations. Application of the energy conservation principle, expressed by the First Law of Thermodynamics, leads to the energy equation. In order to obtain detailed point by point knowledge of the flow field, a differential form of the equations must be applied.

2.1.2. Conservation of Mass

The conservation of mass equation can be acquired by writing a mass balance over the stationary volume through which the fluid is flowing. The mass conservation principle denotes that the change of mass within the control volume is equal to the mass entering, minus the mass leaving the control volume. This can be interpreted as

Rate of accumulation of mass = net rate of inflow of mass by convection

The above statement can be rewritten in to the following equation

$$\frac{\Delta m}{\Delta t} = \sum_i \dot{m}_i \tag{2.1}$$

Eq. 2.1 is regarded as the starting point of deriving the mass conservation equation. However, this derivation will not be carried out due to lack of space and due to the scope of this work. For a complete derivation of the mass conservation equation, please refer to[8-10]. After performing derivations, substitutions and modifications we obtain the final continuity equation of the following partial differential equation

$$\frac{\partial \rho}{\partial t} + \frac{\partial (\rho u_1)}{\partial x_1} + \frac{\partial (\rho u_2)}{\partial x_2} + \frac{\partial (\rho u_3)}{\partial x_3} = 0 \tag{2.2}$$

Equation 2.2 represents the mass conservation valid for both compressible and incompressible fluids. Concerning the incompressible fluids (ρ = const.) this equation can be simplified and rewritten as

$$\frac{\partial u_1}{\partial x_1}+\frac{\partial u_2}{\partial x_2}+\frac{\partial u_3}{\partial x_3}=0 \tag{2.3}$$

Velocity components are ideally computed from the momentum equations, so the incompressible form of the continuity equation imposes an additional constraint on the velocity field[8].

2.1.3. Conservation of Linear Momentum

Newton`s second law of motion applied to a control volume gives the momentum equations. The momentum conservation principle must be formulated for all components of the velocity vector. Thus it is expressed by a vector equation from which it follows that we need two momentum equations in two dimensions and three momentum equations in three dimensions. In other words

Rate of accumulation of i-th direction momentum =

Net rate of inflow of i-th direction momentum +

Sum of forces acting on the system

This principle can be expressed by the following equation

$$\frac{\partial}{\partial t}\left(mu_i\right)=\left[\sum_{in}\left(\dot{m}u_i\right)-\sum_{out}\left(\dot{m}u_i\right)\right]+\left[\sum_j f_{i,j}+\sum_k b_{i,k}\right] \tag{2.4}$$

The first term in the brackets on the right side of the equation is the convection term. It brings the x-direction momentum into (or out of) the control volume. The second term on the right side of the equation comprises the sum of the x_i-direction components of the forces acting on the control volume. Two kinds of forces act on the CV. First, surface forces (e.g. pressure forces, viscous forces, surface tension forces) and, second, body forces (e.g. gravity force, centrifugal force, Coriolis force, electromagnetic force). In order to obtain the resulting momentum equation (for the x direction) quite a few modifications and substitutions have to be accomplished, and then we can write

$$\frac{\partial}{\partial t}\left(\rho u_1\right)=-\left[\frac{\partial}{\partial x_1}\left(\rho u_1 u_1\right)+\frac{\partial}{\partial x_2}\left(\rho u_2 u_1\right)+\frac{\partial}{\partial x_3}\left(\rho u_3 u_1\right)\right]-\left(\frac{\partial \tau_{11}}{\partial x_1}+\frac{\partial \tau_{21}}{\partial x_2}+\frac{\partial \tau_{31}}{\partial x_3}\right)-\frac{\partial p}{\partial x_1}+\rho g_1+X_1 \tag{2.5}$$

The brackets in the **Eq. 2.5** group various terms according to their origin. The first term on the right side in the square brackets represents the x_1 component of the convective transport. It originates from the bulk motion of the fluid. The second term is the diffusive transport term (again the x_1 component) arising from the viscous stresses. The third term originates from the gradient of the static pressure. The remaining two terms are the body force term and any additional terms denoted by X_1. This equation is valid for any fluid satisfying the continuum assumption. Before this equation can be used to solve problems, suitable expressions for stresses must be acquired in terms of the velocity and pressure fields.

$$\tau_{21}=\mu\left(\frac{\partial u_2}{\partial x_1}+\frac{\partial u_1}{\partial x_2}\right) \tag{2.6}$$

$$\tau_{31}=\mu\left(\frac{\partial u_1}{\partial x_3}+\frac{\partial u_3}{\partial x_1}\right) \tag{2.7}$$

$$\tau_{11}=-p-\frac{2}{3}\mu\nabla\cdot\vec{V}+2\mu\frac{\partial u_1}{\partial x_1} \tag{2.8}$$

If these expressions are introduced into the differential equation of motion (**Eq. 2.5**), we then obtain Navier-Stokes equation in the x_1-direction in 3-dimensions; equations for the other two directions could be obtained accordingly.

$$\frac{\partial}{\partial t}(\rho u_1) = \rho g_1 - \frac{\partial p}{\partial x_1} + \frac{\partial}{\partial x_1}\left[\mu\left(2\frac{\partial u_1}{\partial x_1} - \frac{2}{3}\nabla\cdot\vec{V}\right)\right] + \frac{\partial}{\partial x_2}\left[\mu\left(\frac{\partial u_1}{\partial x_2} + \frac{\partial u_2}{\partial x_1}\right)\right] + \frac{\partial}{\partial x_3}\left[\mu\left(\frac{\partial u_3}{\partial x_1} + \frac{\partial u_1}{\partial x_3}\right)\right] \qquad (2.9)$$

These equations can further be simplified when applied to incompressible flow with constant viscosity which applies quite well for casting processes. Under these conditions, the equation (for the x_1-direction) reduces to

$$\rho\left(\frac{\partial u_1}{\partial t} + u_1\frac{\partial u_1}{\partial x_1} + u_2\frac{\partial u_1}{\partial x_2} + u_3\frac{\partial u_1}{\partial x_3}\right) = \rho g_1 - \frac{\partial p}{\partial x_1} + \mu\left(\frac{\partial^2 u_1}{\partial x_1^2} + \frac{\partial^2 u_1}{\partial x_2^2} + \frac{\partial^2 u_1}{\partial x_3^2}\right) \qquad (2.10)$$

Navier-Stokes equations of fluid motion combined with the mass conservation equation (continuity equation) provide a sufficient description of the velocity field and an overall picture of the behavior of both compressible and incompressible moving fluids (e.g. die/mould filling) under various conditions. In order to fully describe the essence of fluid flow phenomena and primarily the temperature distribution within the calculation domain, one more governing equation must be introduced- conservation of energy.

2.1.4. Conservation of Energy

The energy equation for a stationary volume element can be in words formulated as:

Rate of accumulation of internal and kinetic energy =

Net rate of inflow of internal and kinetic energy by convection +

Net rate of heat addition by conduction +

Net rate of heat addition by radiation –

Net rate of work done by system on surroundings +

The strength of the internal heat sources/sinks

This statement is the first law of thermodynamics written for the open unsteady system. For weakly compressible and incompressible fluids (e.g. melt), the kinetic energy contribution to the total energy can be left out; hence the total energy equation will be replaced by the thermal energy equation. In addition, two terms small for casting processes can be excluded and neglected. The first one is the work against gravity forces and the second one is the rate of work done against the static pressure. It would be necessary to retain this term if we assumed that the melt is compressible. As we assume the melt as incompressible or at the most slightly compressible these terms can be easily omitted. The final non-conservative form of the energy equation is then written as[8]

$$\begin{aligned}\rho\frac{\partial}{\partial t}(cT) = -\Big[&(\rho u_1)\frac{\partial}{\partial x_1}(cT) + (\rho u_1)\frac{\partial}{\partial x_2}(cT) + (\rho u_1)\frac{\partial}{\partial x_3}(cT)\Big] \\ &+ \frac{\partial}{\partial x_1}\left(k\frac{\partial T}{\partial x_1}\right) + \frac{\partial}{\partial x_2}\left(k\frac{\partial T}{\partial x_2}\right) + \frac{\partial}{\partial x_3}\left(k\frac{\partial T}{\partial x_3}\right) \\ &+ \mu\Phi_v + \rho\Delta H_L\frac{\partial f_S}{\partial t} + S_T\end{aligned} \qquad (2.11)$$

The specific heat $c = c_p = c_v$ and the term Φ_v stands for the viscous dissipation function. For casting phenomena, this viscous dissipation function in the thermal energy equation should be retained if one wants to simulate the semi-solid process, otherwise it is negligibly small. Based on this equation it is possible to grasp and completely describe the behavior of the moving fluid in terms of the temperature. As for other variables in **Eq. 2.11** all of them are already known from the prior conservation laws (e.g. mass conservation and momentum conservation).

2.2. Background on Gating Technology

The purpose of, and the most important reason for having and designing the gating system is obviously to transport the molten metal from a ladle into the mould cavity, where the metal can then solidify to form the desired casting shape. The basic components of a simple gating system for a horizontally parted mold are shown in **Figure 2.2**. A pouring cup or a pouring basin provides an opening for the introduction of metal from a pouring device, i.e. a bottom-pour or a lip-pour ladle for gravity sand casting techniques. A sprue carries the liquid metal down to join one or more runners, which distribute the metal throughout the mold until it can enter the casting cavity through ingates, also referred to as thin gates. The first metal entering the gating system will generally be the most heavily damaged by contact with the mold medium and with air as it flows. To avoid having this metal enter the casting cavity, momentum effects can be used to carry it past the ingates into the runner extension. The ingates will then fill with the cleaner, less damaged metal that follows the initial molten metal stream.

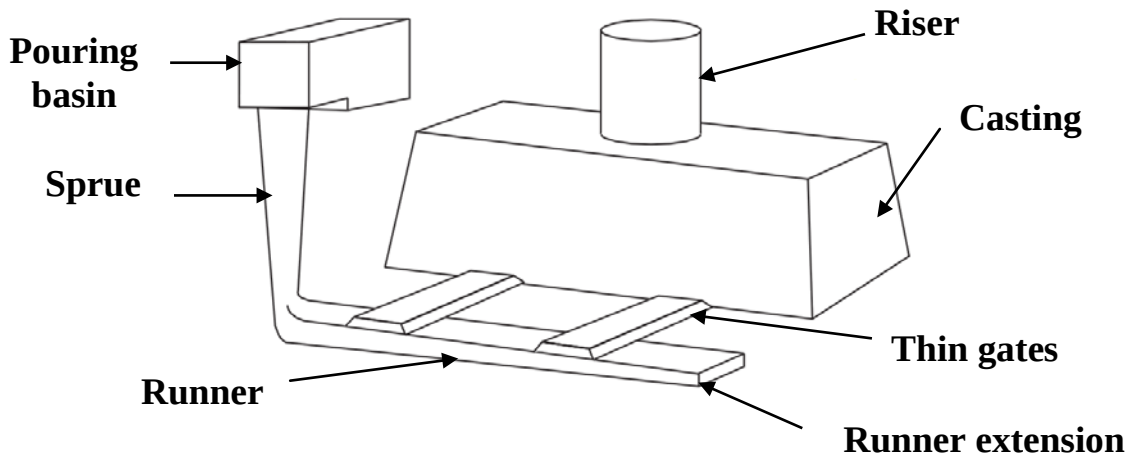

Figure 2.2: Schematic of a traditional gating system layout. Figure taken from[11].

At first glance this appears quite simple however, the gating system has to, at the same time fulfill a bunch of other demands as well. One of the first demands is that the rate and direction of metal flow must be such as to ensure complete filling of the mould before freezing. Furthermore, the gating system must ensure that the flow of the melt should be as calm and coherent as possible, i.e. with negligible surface turbulence, without being so slow that the melt solidifies before the mould is filled. Slowing down the melt before entering the mould cavity is another function of runner extensions. Providing that a runner extension is sufficiently large, or long, it will absorb a reasonable portion of the kinetic energy of the moving melt, making it slow down. One should be cautious when using runner extensions however, to prevent back waves when the melt reaches a blind end of the runner extension. It is important to slow down the melt gradually, not at once. The gating system should also be designed in a way that reduces jets, splashes, fountains, melt aspiration, formation of air pockets and vena-contracta as much as possible. Very often a poorly designed gating system can cause oxide formation and gas entrapment which compromise the final quality of the casting. Beside this a beneficial heat distribution in the castings is desired to ease the need for feeding and improve the efficiency of the risers. At the same time the gating system should weigh as little as possible to improve the ratio of the weight of castings produced to the weight of metal poured better referred to as “yield”. It must be mentioned that in this project only gravity driven mould filling in sand moulds is concerned.

Methods used to promote any of the mentioned demands and design considerations often conflict with another desired effect. For example, attempts to fill a mold rapidly can result in metal velocities that promote mold erosion or surface turbulence. As a result, any gating system will generally be a compromise among conflicting design considerations, with the relative importance of the consideration being determined by the specific casting and its molding and pouring conditions. The

design variables that should always be considered in designing gating systems regardless of the applied metal are briefly summarized[12]:

Rapid mold filling. Especially with thin-section castings, heat loss from the liquid metal during mold filling may result in premature freezing, producing surface defects (for example, cold laps) or incompletely filled sections (misruns). Superheating of the molten metal will increase fluidity and retard freezing, but excessive superheat can increase problems of gas pickup by the molten metal and exaggerate the thermal degradation of the mold medium. In addition, the mold filling time should be kept shorter than the mold producing time of the molding equipment to maximize productivity.

Minimizing turbulence. Turbulent filling and flow in the gating system and mold cavity can increase mechanical and thermal attack on the mold. More important, turbulence may produce casting defects by promoting the entrainment of gases into the flowing metal. These gases may by themselves become defects (for example bubbles), or they may produce dross or inclusions by reacting with the liquid metal. Turbulent flow increases the surface area of the liquid metal exposed to air within the gating system. The susceptibility of different casting alloys to oxidation varies considerably. For those alloys that are highly sensitive to oxidation, such as aluminum alloys; magnesium alloys; and silicon, aluminum, and manganese bronzes, turbulence can generate extensive oxide films that will be churned into the flowing metal, often causing unacceptable defects.

Avoiding mold and core erosion. High flow velocity or improperly directed flow against a mold or core surface may produce defective castings by eroding the mold surface (thus enlarging the mold cavity) and by entraining the dislodged particles of the mold to produce inclusions in the casting.

Removing slag, dross, and inclusions. This factor includes materials that may be introduced from outside the mold (for example, furnace slag and ladle refractory) and those that may be generated inside the system. Methods can be incorporated into the gating system to trap such particles (for example, filters) or to allow them time to float out of the metal stream before entering the mold cavity.

Promoting favorable thermal gradients. Because the last metal to enter the mold cavity will generally be the hottest, it is usually desirable to introduce metal in those parts of the casting that would already be expected to be the last to solidify. One obvious method of accomplishing this is to direct the metal flow from the gating system into a riser, from which it then enters the mold cavity. Because the riser is generally designed to be the last part of the riser/casting system to solidify, such a gating arrangement will help promote directional solidification from the casting to the riser. If the gating system cannot be designed to promote some desirable thermal gradient, it should at least be designed so that it will not produce unfavorable gradients. This will often involve introducing metal into the mold cavity through multiple ingates so that no location becomes a hot spot.

Maximizing yield. A variety of unrecoverable costs must go into the metal that will fill the gating system and risers. These components must then be removed from the casting and generally returned for remelting, where their value is downgraded to that of scrap. Production costs can be significantly reduced by minimizing the amount of metal contained in the gating system. The production capacity of a foundry can also be enhanced by increasing the percentage of salable castings that can be produced from a given volume of melted metal.

Ease of removal. Preferably the system should break off. As a next best option, it should be removable with a single stroke of a clipping press, or a straight cut. Curved cuts take more time and are more difficult to dress to finished size by grinding or finishing.

Avoiding casting distortion is especially important with rangy, thin-wall castings, in which uneven distribution of heat as the mold cavity is filled may produce undesirable solidification patterns that cause the casting to warp. In addition, the contraction of the gating system as it solidifies can pull on sections of the solidifying casting, resulting in hot tearing or distortion.

Controlled flow conditions. A steady flow rate of metal in the gating system should be established as soon as possible during mold filling, and the conditions of flow should be predictably consistent from one mold to the next.

2.3. Principles of the traditional gating system

This section will provide a more detailed description and overview of separate features of a gating system. As a part of it, useful tips, recommendations or guidelines will be given on how to design a better gating system especially for manufacturing of large steel castings. The guidelines will be reasoned based on results of various projects and research-oriented papers that the author has conducted throughout the Ph.D. study. These papers are attached at the end of the thesis. Separate elements of the gating system will be addressed based on the sketch in **Figure 2.2**.

2.3.1. Design of a Pouring Basin

One could define the pouring cup or pouring basin as the part of the gating system that receives the molten material from the pouring vessel, referred to as a ladle. This basin can be either built in the mould as a core of the given shape of the basin, or placed on top of the mould and tightly mounted by proper devices, i.e. glues or other tools. The size and shape of the pouring cup is meant to accommodate the way the melt is being poured. In many foundries the pouring is still done manually from a ladle in a crane. In these cases melt is poured from one side and the pouring cup is designed to calm down the melt to avoid splashing when being poured and to make it easier for the operator to pour as directly and precisely in every mould as possible.

2.3.1.1. Conical basin (pouring cup)

There are many recommendations and guidelines on how a pouring cup should be designed however most of these designs do not prevent vena-contracta in the upper part of the down runner. One type of the pouring basin used almost everywhere in the foundry industry is *the conical basin*, outlined in **Figure 2.3**. Campbell claims in his book[11] that this type of basin, i.e. conical, is very bad and responsible for the production of more casting scrap than any other single feature of the filling system due to the following factors[11]:

- The melt enters at high, unchecked velocity. Since the main problem with gating systems is to reduce the velocity, this adds to the difficulty of reducing surface turbulence.
- Any contaminants such as dross or slag that enter with the melt are necessarily taken directly down the sprue.
- The mould cavity fills differently depending on precisely where in the basin the pourer directs the pouring stream, whether at the far side of the cone, the centre, or the near side. Thus when pouring manually, the castings are not reproducible. This situation is overcome by automatic pouring devices.
- The small volume of the basin makes it difficult for the pourer to keep it full so that air is automatically entrained as the basin becomes partially empty from time to time during pouring. The pourer is usually unaware of this, since the aspiration of air usually takes place under the surface at the basin/sprue junction.
- This type of basin is the most susceptible to the formation of a vortex, because any slight off-axis direction will tend to start a rotation of the pool.

Nevertheless, in the author's personal opinion, this type of a pouring basin is not as bad as stated by Prof. Campbell. There are other elements of a gating system, e.g. non-tapered runners, thin gates, sharp corners, etc., that are by far more decisive or critical for the overall casting quality than a pouring cup. Although, this statement should not be interpreted as "do not care about the shape of pouring cups". On a contrary, in this section it will be clearly shown, that indeed an impact of a pouring cup must not be disregarded, especially when casting small or thin-walled castings where high quality is demanded.

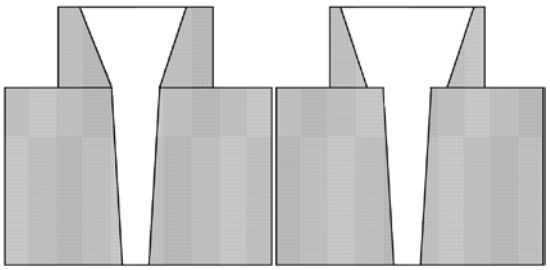

(a) *(b)*

Figure 2.3: Conical basin and sprue combinations showing (a) perhaps least damaging; (b) basin too large.

A basin that is too large for the sprue entrance, **Figure 2.3b** jets metal horizontally off the exposed ledge formed by the top of the mould, creating much turbulence and preventing the complete filling of the sprue. The problem is unseen by the caster, who, because he is keeping the basin full, imagines he is doing a good job however, the aspirated air can cause a staggering amount of bubble damage inside a casting that will be discovered later during machining or by ultrasonic testing (UT) or radiographic testing (RT). For very small castings weighing only a few grams and where the sprue is only a few millimeters in diameter, there is a strong element of control of the filling of the sprue by surface tension. For such small castings the conical pouring cup probably works tolerably well. It is simple and economical, and, probably fills well enough.

An example of how the conical pouring basin affects filling of a thin-walled aluminium casting are shown in **Figure 2.4**. In this experiment a thin-walled casting was cast into a sand mould using the "troublesome" conical pouring cup. The entire mould was tilted to ensure an uphill smooth filling of the casting. The filling sequence indicates that neither the cup nor the sprue gets completely filled and thus there is still an open space for massive oxidation and air entrapment in the liquid aluminium alloy. The pouring cup needs to be kept full of metal during the whole duration of the pour. If the pouring is carried out too slowly, allowing the stream to dribble down the sprue, or simply poured down the centre without touching the sides of the sprue, and without filling the basin at all (which was the case with the expanded sprue type applied in this experiment), then air and dross will enter the system.

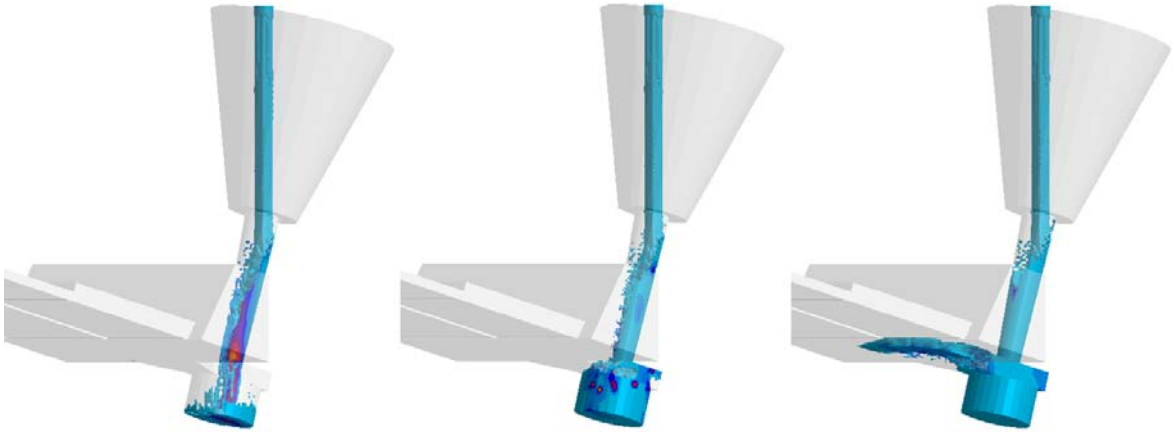

Figure 2.4: Air entrapment and splashing in the sprue and sprue base areas at 2, 3 and 6% filled, using the conical pouring basin for a light-weight, stair-shaped Al-Si based casting, (Kotas et. al., 2010).

This unfavorable filling pattern resulted in oxide bi-films and air bubbles present on the casting surface, as captured in **Figure 2.5(a, b)**. Moreover, it is believed that trapped oxide films together with other phenomena, e.g. low pouring temperature, interrupted pour, etc., contributed to the misrun in the thinnest section of the casting.

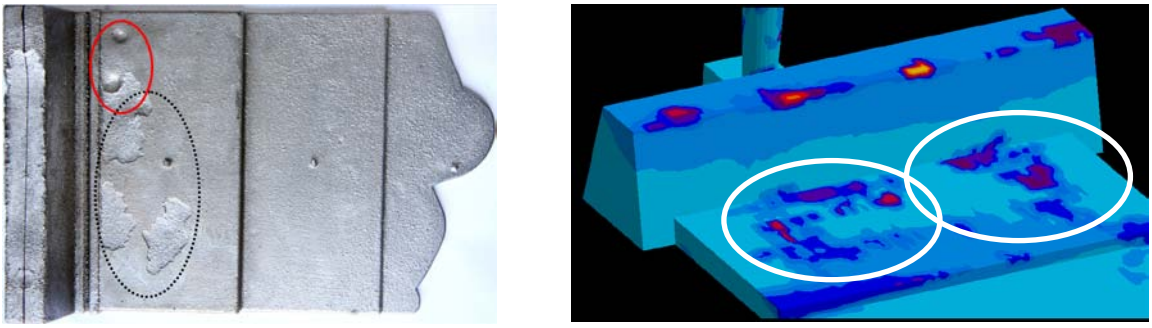

Figure 2.5: Filling related defects in the casting (a) the experimental result, (b) Air pressure criterion function in the simulation software MAGMAsoft, (Kotas, 2010).

Although, Campbell states that when the conical cup is filled with a hand ladle held just above the cone, the fall distance of about 50 mm above the entrance to the sprue results in a speed of entry into the sprue of approximately 1 m/s. At such speeds the basin is probably the least harmful.

On the other hand, where the conical cup is used to funnel metal into the running system when poured directly from a furnace, or from many automatic pouring systems, the distance of fall is usually much greater, often 200 to 500 mm. In such situations the rate of entry of the metal into the system is probably several meters per second. From the bottom-poured ladles in steel foundries the metal head is usually over 1m giving an entry velocity of 5 m/s. This situation highlights one of the drawbacks of the conical pouring basin; it contains no mechanism to control the speed of entry of liquid[11].

Alternatively, harm can be done by inattention, so that the pour is interrupted, allowing the bush to empty and air to enter the down-runner before pouring is restarted. Even so, because of the small volume of the basin, it is not easily kept full so that these dangers are a constant threat to the quality of the casting. Unfortunately, even keeping the pouring cup full during the pour is no guarantee of good castings if the cup exit and the sprue entrance are not well matched. This is the most important reason for moulding the cup and the filling system integral with the mould if possible. Finally, even if the pour is carried out as well as possible, any witness of the filling of a conical basin will need no convincing that the high velocity of filling, aimed straight into the top of the sprue, will cause oxides and air to be carried directly into the running system, and so into the casting. For castings where quality is at a premium, or where castings are simply required to be adequate but repeatable, the conical basin is definitely not recommended.

2.3.1.2. The offset step basin

Another design of a basin (sometimes called a bush) that has been recommended from time to time is the offset step basin. The provision of a vertical step, or weir, in the basin, **Figure 2.6,** brings the horizontal jet across the top of the sprue to a stop. It is an essential feature of a well-designed basin. The *offset* blind end of the basin is important in bringing the vertical downward velocity to a stop. The offset also avoids the direct inline type of basin, such as the conical basin, where the incoming liquid goes straight down the sprue, its velocity unchecked, and taking with it unwanted components such as air and dross, etc. The *step* (or weir) is essential to eliminate the fast horizontal component of flow over the top of the sprue, preventing it from filling properly. The provision of the step yields a further bonus since it reverses the downward velocity to make an upward flow, giving some opportunity for lighter phases such as slag and bubbles to separate prior to entering the sprue. Finally, the provision of a generous *radius* over the top of the step smoothes the entrance into the sprue, and further aids the smooth, laminar flow of metal.

The problem in the design of the pouring cup in **Figure 2.6** is that when the melt reaches above the height in the basin where the melt can flow to the down runner it will. The volume of this initial melt to reach the down runner will under no circumstance be sufficient to fill the cross section of the down runner. So unless it is possible to pour fast enough to completely fill the entire geometry instantaneously it will not be possible to keep the down runner full. To pour the molten metal in this way must be considered to be extremely difficult. This is especially because the pouring must be slowed down just as instantaneously as it was begun. If the pouring is not slowed down to the exact

same flow rate as the gating system is designed for the melt will just flow all over the top of the mould having an already full pouring cup. If the pouring is slowed down too much and the level of melt in the pouring cup drops below the top of the bend, the down runner will no longer be kept full. Hence it is highly unlikely that it is possible to keep the down runner full from the beginning to the end of pouring using the pouring cup shown. Designing a pouring cup that fulfils all the desired properties is not easy and therefore a wide range and very individually designed pouring cups is also seen used in the foundries[8].

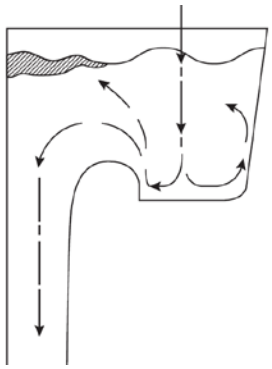

Figure 2.6: Offset step pouring basin[11].

In case of very large steel castings filled from the bottom-pour ladle it is practically impossible to use some sophisticated pouring basins as shown above due to very large pouring rates which would for sure cause overfilling and sand erosion of that pouring cup. In order not to overfill, the basin would have to be enormously deep which would decrease the yield substantially. Moreover it would be extremely difficult to control the pouring rate when filling multiple castings from one ladle, due to the decreasing pressure height when the ladle empties during filling. Therefore, still a common practice is to pour directly from the bottom-pour ladle and from its nozzle to the sprue which is made of refractory tiles. Just to make sure that the nozzle will not splash all around the very top refractory element of the sprue is tapered, resembling the much criticized conical basin. As to the author's knowledge many foundries casting large steel castings do not use any protective shroud, i.e. protective argon atmosphere to prevent oxidation, or contact pouring method either, conducting the pour completely unprotected, but successfully.

2.3.2. Sprue (the down-runner)

The sprue has the difficult job of getting the melt down to the lowest level of the mould while introducing a minimum of defects despite the high velocity of the stream. The fundamental problem with the design of sprues is that the length of fall down the sprue greatly exceeds the critical fall height[13]. The height at which the critical velocity is reached corresponds to the height of the sessile drop for that liquid metal. Thus for aluminum this is about 13 mm, whereas for iron and steel it is only about 8 mm. Since sprues are typically 100 to 1000 mm or even several meters long as in **Paper II** or in **Figure 2.7**, the critical velocity is greatly exceeded. How then is it possible to prevent damage to the liquid? It seems that the secret of designing a good sprue is to make it as narrow as possible, so that the metal has minimal opportunity to break and entrain its surface during the fall. The concept on protecting the liquid from damage is either (i) to prevent it from going over its critical velocity, or (ii) if the critical velocity has to be exceeded, to protect it by constraining its flow in channels as narrow as possible so that it is not able to jump and splash.

Most sprues are oversized. This is bad for metallic yield, and thus bad for economy. However, it is much worse for the metal quality, which is damaged in one important way: If the flow is directed down a straight-sided sprue, the falling stream will create a low-pressure area as it pulls away from the sprue walls and will aspirate air. Air is therefore taken down with the metal, causing severe surface turbulence especially when the stream reaches the base of the sprue, see **Figure 2.7**. This, of course, leads to a build-up of oxide in the sprue itself, and much consequential damage downstream from oxide and entrained air.

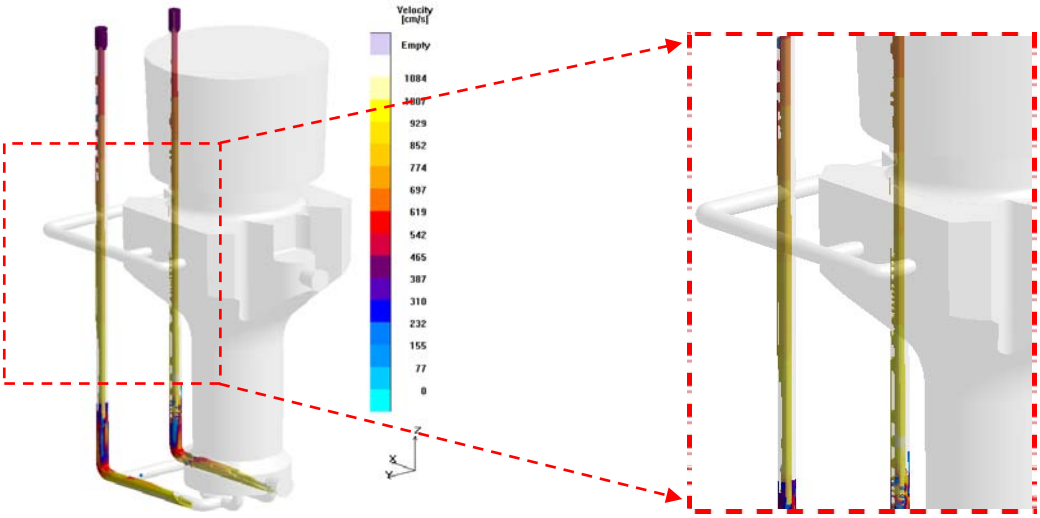

Figure 2.7: Air aspiration identified in the down-sprue as the metal accelerates during its free- fall. Note that the height of the sprue is approximately 4.5m, [ref. Paper II, (Kotas et al. 2010)].

The question then arises, how is it possible to make sure, that the sprue has the right size and shape? The answer can be found in the continuity equation. One practical implication of the law of continuity is seen in **Figure 2.8**, which illustrates the flow of metal from a pouring basin. Velocity increases as the stream falls, so the cross-sectional area of the stream must decrease proportionally to maintain the balance of the flow rate. The result is the tapered shape typical of a free-falling stream shown in **Figure 2.8**. Therefore, the sprue should be designed to mimic the taper that the falling stream adopts naturally as a result of its acceleration due to gravity. The shape is a hyperbola.

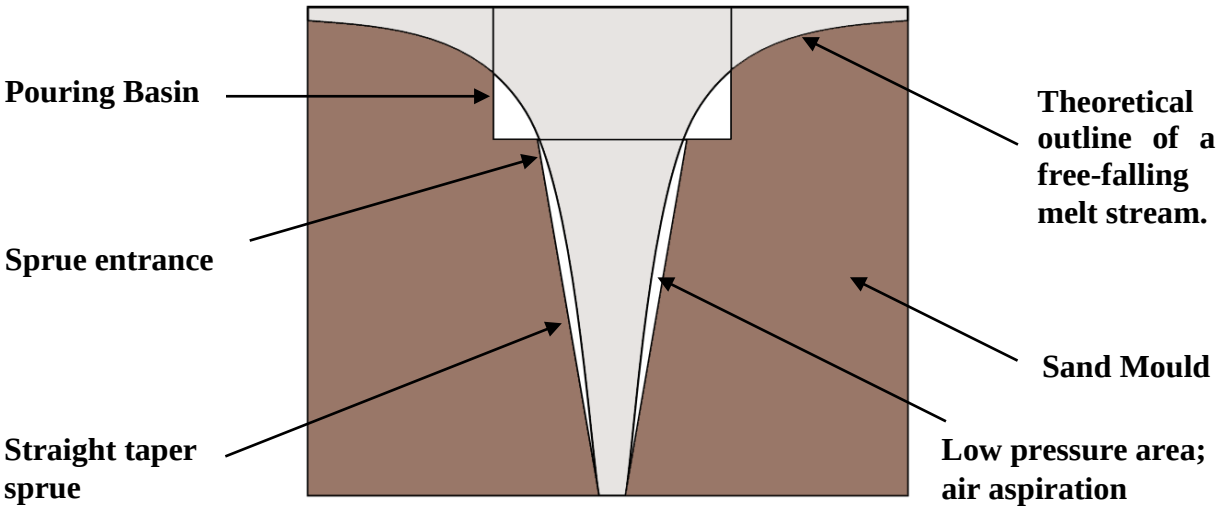

Figure 2.8: Schematic showing natural flow of the free-falling melt and flow behavior in the tapered sprue. Figure inspired by Hansen[14].

The straight-tapered sprue is designed to conform to the natural form of the flowing stream and therefore reduces turbulence and the possibility of air aspiration. Although, the curved sides of the stream still encourage metal to become detached from the walls at about half-way down, as shown in this figure. For modest-sized castings this issue can be corrected by making the sprue entrance about 20 per cent larger in area. Moreover, if the casting and hence the sprue is not too tall, the area of the free falling melt does not decrease too much and thus, straight tapered sprues are commonly used, and appear to be satisfactory[11].

For very tall castings the straight tapered approximation to the sprue shape is definitely not satisfactory. In this case it is necessary to calculate the true diameter of the sprue at close intervals along its length to create the so-called streamlined gating[14, 15]. The correct form of the falling stream can then be followed with sufficient accuracy, and air entrainment during the fall can be avoided.

The basic idea behind the streamlined gating system is to use the surface tension and boundary layer friction of the molten metal to keep the front of the flowing molten metal coherent during the mould filling. This is done primarily by keeping the runner width as small as possible. Based on experimental work, conducted by Tiedje and Larsen[16], it was clearly shown that sharp changes in the geometry and dead ends of the gating system cause pressure waves to form that eventually lead to defective castings. Therefore, all 90º bends are avoided and more soft curves are used instead. A comparison between the traditional and streamlined gating system for Disamatic automatic moulding machines is illustrated in **Figure 2.9**.

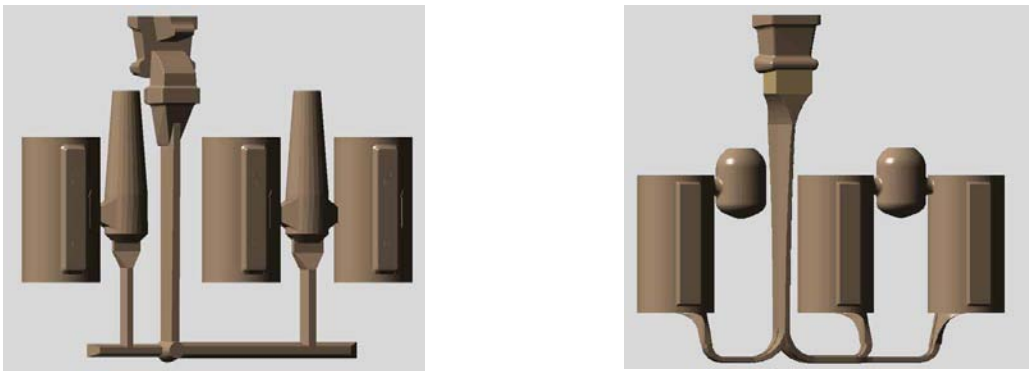

(a) ***(b)***

Figure 2.9: Schematic of a traditional gating system (a), and a concept of a streamlined gating system (b), for Disamatic moulding machines[14]. Courtesy of Niels Skat Tiedje.

Mould filling simulations for both types of gating system showed distinct flow behavior of the melt at various stages of the filling process. This is captured in **Figure 2.10**. In that figure filling by the traditional gating system is seen where melt disintegration and air aspiration takes place already in the upper section of the sprue, (a). Moreover, as a result of a back pressure, the first melt enters the riser areas very rapidly, causing jetting and massive surface turbulence, (b). On the contrary, the streamlined gating system minimizes the melt disintegration and uncontrolled down fall in the sprue, (c), and the shape of the runners with no sharp corners and dead ends reduce the back pressure and turbulent behavior leading to calmer entrance of the melt into the casting cavity, (d).

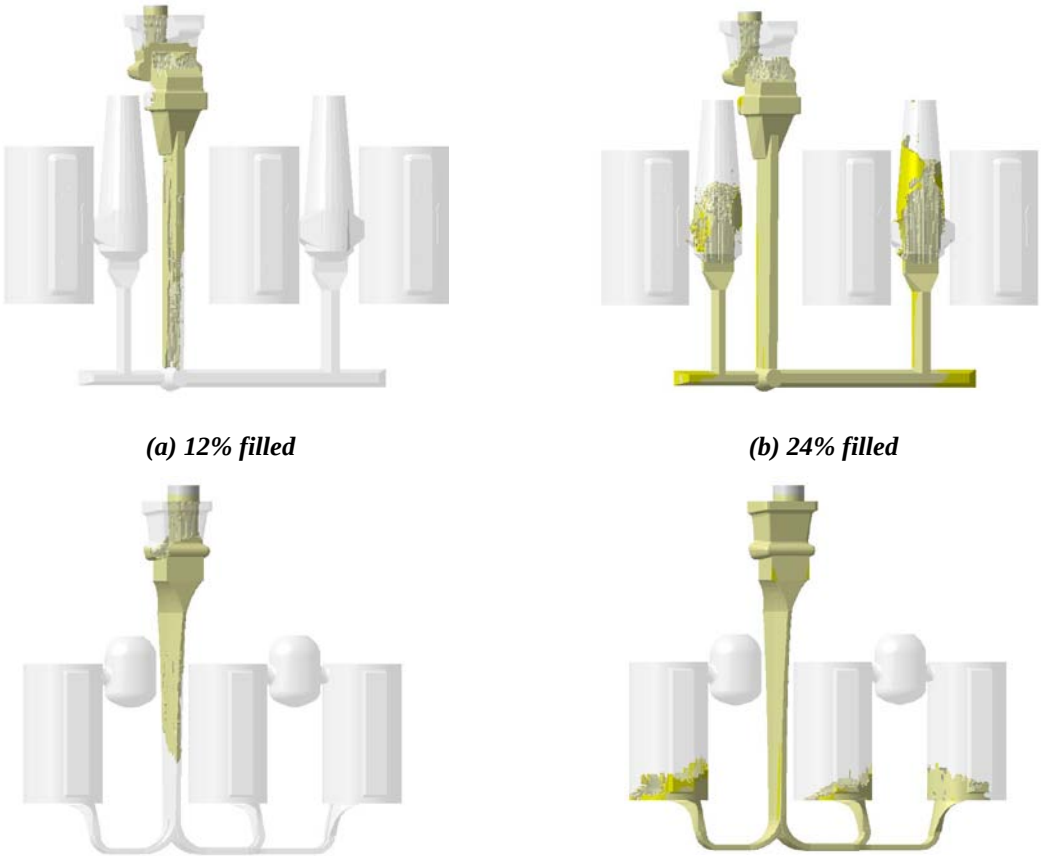

(a) 12% filled *(b) 24% filled*

(c) 12% filled *(d) 28% filled*

Figure 2.10: Filling sequence for both traditional and streamlined gating systems[14]. Courtesy of Niels Skat Tiedje.

It is well known to foundry engineers that many types of high-production molding units do not readily accommodate tapered sprues or the streamlined gating. But what is even worse or more disappointing is that in many foundries, technologists and designers are reluctant to accept or trust new trends or scientific findings, and apply them into the gating system design. It is still common, especially in gravity sand casting of large steel parts, to see non-tapered sprues and runners, sharp corners, and abrupt changes in cross sections or constant areas all over the gating system- hence a total neglect of the continuity equation. Their, i.e. foundry personnel, reasoning is:" This design has worked for us quite well for 30 years so why should we replace it?" or "gating systems are not that decisive for the overall quality". Note, that this statement is based solely on the author's personal experience. In cases where tapered sprues and runners are not feasible to accommodate, the gating system designer should at least try to approximate the effect of a tapered sprue by placing a restriction, the so-called choke elements, at or near the base of the sprue to force the falling stream to back up into the sprue.

2.3.2.1. Simple Equations for Designing the Sprue

The design and the dimensions of a gating system determine the character and the velocity of the liquid flow into the mould cavity. When an appropriate mould filling time has been determined, it can be then used for dimensioning the gating system. In foundry practice it is quite complicated to choose a correct filling time. Although thanks to the rapid development of numerical simulation tools, the whole design stage has become much easier than twenty years ago in that now a designer can test and improve his new designs virtually without destroying a real casting. Usually all foundries try to fill as fast as possible to increase their production rate. However, a short filling time will cause a turbulent flow pattern or erosion and damage of the molding material. Moreover, a short filling time will also need a more permeable mould or additional vents; otherwise the pressure in the mould might get too high. On the other hand too long filling times can result in cold shots, i.e. incomplete filling or scabs.

It is known by experience that for gravity sand casting of steel there is a relation between filling time and the casting's weight:

$$t = B \cdot \sqrt{G}$$
$$where\ B = 1.8\ \ for\ G < 500kg \qquad (2.12)$$
$$B = 0.6\ \ for\ G < 50000kg$$

It must be pointed out that the filling times calculated by this equation cannot be considered to be optimal. It only gives an estimation of practically used filling times for similar castings. When the filling time has been determined, the first section that needs to be calculated is the sprue. The reason is that the height of the sprue and the free fall of the molten metal determine the velocity of the melt. These very simple 1-D calculations are based on several fundamental principles of fluid flow. Among these principles are Bernoulli's theorem, the law of continuity, i.e. mass conservation principle shown in **Eq. 2.3**, and the effect of momentum. An argument could be raised that we are showing the same equations as in the beginning of this chapter, just simplified. It is true that for an accurate fluid flow calculation, the numerical solver has to deal with the governing equations in 3-D, described in section 2.1, but to get a first impression of how the gating system for any given casting should look like; these simplified versions of the governing equations are reasonable substitutes. Later on, when the gating system is designed, the full-extent 3-D flow calculations are carried out in the simulation software as verification or to identify potential design shortcomings.

A first way of expressing the velocity in the sprue is to use the Bernoulli's theorem seen in **Eq. 2.13**. Bernoulli's theorem relates the pressure, velocity, and elevation along a line of flow in a way that can be applied to gating systems. The theorem states that, at any point in a full system, the sum of the potential energy, kinetic energy, pressure energy, and frictional energy of a flowing liquid is equal to a constant. The energy terms can be expresses as follows:

$$mgh_1 + \frac{mv_1^2}{2} + \frac{mp_1}{\rho_1} = mgh_2 + \frac{mv_2^2}{2} + \frac{mp_2}{\rho_2} \qquad (2.13)$$

where p is a pressure in points 1 and 2, ρ is a density of the applied melt; v is a velocity of the liquid in points 1 and 2, h is a height in points 1 and 2 and g is acceleration due to gravity.
Equation **2.13** allows for prediction of the effect of the several variables at different points in the gating system, although several conditions inherent in foundry gating systems complicate and modify its strict application. For example:

- Equation 2.13. is for full systems, and at least at the start of pouring, a gating system is empty. This indicates that a gating system should be designed to establish as quickly as possible the flow conditions of a full system.
- It (**Eq. 2.13**) assumes an impermeable wall around the flowing metal. In sand foundry practice, the permeability of the mold medium can introduce problems, for example, air aspiration in the flowing liquid.
- Additional energy losses due to turbulence or to friction (for example, because of changes in the direction of flow) must be accounted for.
- Heat loss from the liquid metal is not considered, which will set a limit on the time over which flow can be maintained. Also, solidifying metal on the walls of the gating system components will alter their design while flow continues.

Bernoulli's theorem is illustrated schematically in **Figure 2.11**, and several practical interpretations can be derived. The potential energy is obviously at a maximum at the highest point in the system, that is, the top of the pouring basin, i.e. point 1. As metal flows from the basin down the sprue, potential energy changes to kinetic energy as the stream increases in velocity because of gravity. As the sprue fills, a pressure head is developed. Once flow in a filled system is established, the potential and frictional heads become virtually constant, so conditions within the gating system are determined by the interplay of the remaining factors[17]. The velocity is high where the pressure is low, and vice versa.

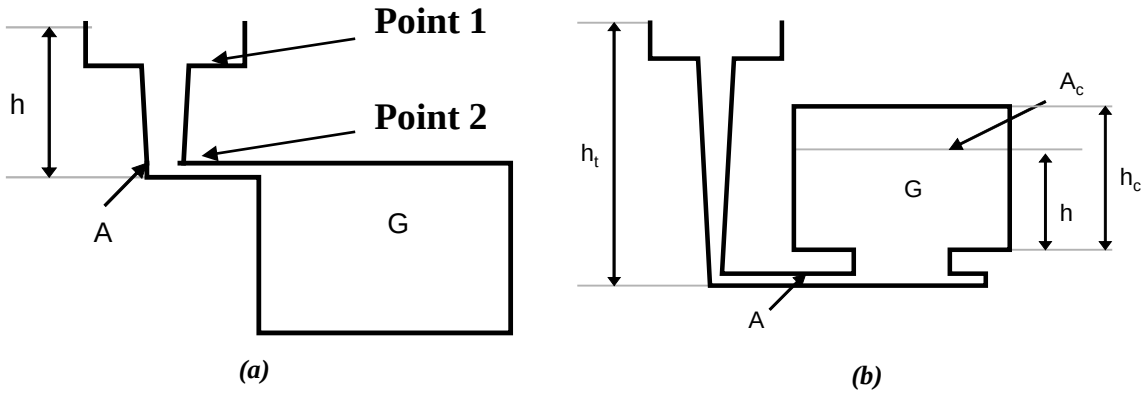

Figure 2.11: Schematic illustrating the application of Bernoulli's theorem to a gating system.

Considering only top filling, i.e. the entire casting lies below the lowest point of the down sprue, as in **Figure 2.11(a)**, the velocity at point 1 is considered to be zero, i.e. the kinetic energy is negligible. Using the height in point 2 as zero level, considering the two densities identical as well as the pressures in points 1 and 2, since the system is open, the Bernoulli's equation reduces to[18]

$$v_{top} = \sqrt{2 \cdot g \cdot h} \tag{2.14}$$

where *h* stands for a ferrostatic pressure height, i.e. height of the sprue. To achieve a more realistic result calculating the velocity a friction factor '*f*' is necessary. This factor can be seen as representing the percentage of loss in velocity due to friction between melt and mould wall and due to pressure drop. The new expression for the velocity is then seen in **Eq. 2.15**. The value for the loss factor is based upon experience, but a value 0.5 is commonly used.

$$v_{top} = (1 - f) \cdot \sqrt{2 \cdot g \cdot h} \tag{2.15}$$

In case of bottom filling where the entire casting lies above the lowest level of the down sprue, one has to assume the effect of back pressure on the flow velocity. The velocity at the bottom of the sprue is then calculated as:

$$v_{bottom} = \frac{\sqrt{2g}}{2} \cdot \left(\sqrt{h_t} + \sqrt{h_t - h_c}\right); \; With \; friction: v_{bottom} = (1 - f)\frac{\sqrt{2g}}{2} \cdot \left(\sqrt{h_t} + \sqrt{h_t - h_c}\right) \tag{2.16}$$

where h_t is the same as *h*, and h_c stands for the height of the casting above the bottom of the down sprue. The amount of the molten metal *V* [m^3] which passes a given cross section area *A* [m^2] is given as

$$\frac{V}{t} = A \cdot v \Rightarrow \quad \frac{M}{t} = \rho \cdot A \cdot v \tag{2.17}$$

Inserting **Eq. 2.15** into **2.17** we obtain the following solution for the governing cross sectional area at the bottom of the sprue for the case of top filling, seen in **Eq. 2.19**.

$$\frac{M}{t} = \rho \cdot A \cdot (1 - f) \cdot \sqrt{2 \cdot g \cdot h} \tag{2.18}$$

$$A = \frac{M}{(1 - f) \cdot \rho \cdot t \cdot \sqrt{2 \cdot g \cdot h}} \tag{2.19}$$

Where *M* is total weight of the casting in Kg, *f* is a friction loss coefficient (should be set to 0.5), *t* is the filling time estimated in **Eq. 2.12**. The same procedure would apply for bottom filling.

Equation 2.19 is typically used for estimating the area of the governing cross section in the gating system. The governing cross section can be understood as the reference area based on which the remaining cross sections are designed or defined to achieve a good design of the gating system[14]. It should be noted that the above derivations do not apply to high-pressure die casting (HPDC) of

aluminium based alloys. In HPDC high pressure is exerted by a moving plunger in a filling chamber, referred to as shot sleeve, which then induces rapid melt propagation throughout the die cavity, while in gravity sand casting only gravity is exploited as the only source of the melt flow. Hence, different rules and guidelines for designing gating systems apply and these will not be discussed in this work. This work will primarily focus on gravity sand casting of large steel parts.

The relation between the areas in two cross sections 1 and 2 in the sprue can be found based on the law of continuity, which has already been introduced in **Eq. 2.3**. In this case it can be expressed as:

$$A_1 \cdot v_1 = A_2 \cdot v_2 = Q \tag{2.20}$$

Where Q is a volume rate of flow, A is a cross section area of flow passage in points 1 and 2 and v is a linear velocity of flow in points 1 and 2

Again, the permeability of sand molds can complicate the strict application of this law, introducing potential problems into the casting process. When this principle is used in combination for instance with **Eq. 2.15** it yields:

$$A_1 = A_2 \cdot \sqrt{\frac{h_2}{h_1}} \tag{2.21}$$

2.3.2.2. Case study

To demonstrate the validity of the above statements and of the presented simple equations, a small "artificial" case study has been conducted using the commercial casting simulation tool MAGMAsoft. Filling of a casting cavity in a sand mould for two distinct gating system designs has been simulated. The first layout, **Figure 2.12 (a)** considers a constant cross section area of the sprue with an abrupt 90º bend to a horizontal runner 1, which then suddenly changes, i.e. decreases, its area to a runner 2 and then connects to a cylindrical casting with a larger cross-section area than the adjacent runner 2. The second layout, **Figure 2.12 (b)**, was designed based on equations presented in section 2.3. These calculations resulted in a tapered sprue with completely different cross section areas as compared to the first case, i.e. the case (a) was over dimensioned. Moreover, the runner in the second layout connects to the casting at the lowest point possible to reduce melt fall.

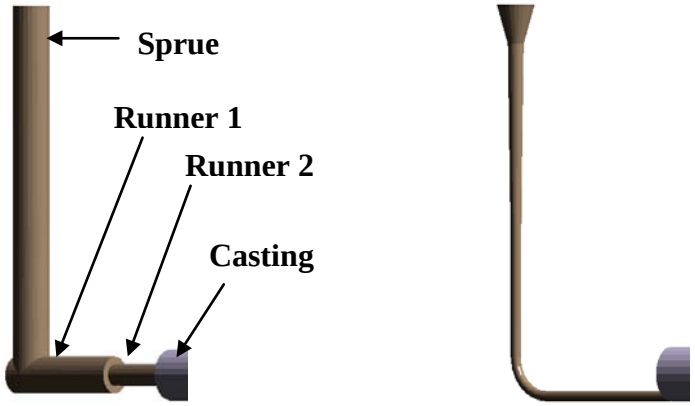

Figure 2.12: Outline of two geometrical layouts used in the test case, (Kotas, 2010).

Figure 2.12 indicates the following: first, it is seen that as the melt stream falls down through the sprue it really reduces its cross section and follows the hyperbolic shape as outlined in **Figure 2.8**. Therefore in the non-tapered sprue one can observe the separation of the melt from the mould walls and the following air aspiration due to low pressure into the melt stream.

Next, when the first melt reaches the bottom of the sprue it directly hits the mould walls due to a missing bend. The so far calm and coherent melt stream then breaks and splashes introducing severe

turbulence into the stream, **Figure 2.13 (a)**. It does not splash only horizontally but also upwards back to the sprue where it meets the new-coming melt. It again leads to disintegration of the melt stream. It should be noted that liquid metals and mainly aluminum based alloys readily oxidize in contact with air. Therefore, having turbulent and disintegrated melt flow increases the probability of having oxide films incorporated somewhere in the melt. There is no use of explaining here why and how oxides compromise the overall casting quality since many books and scientific papers are readily available; the reader should refer to the book of John Campbel[13].

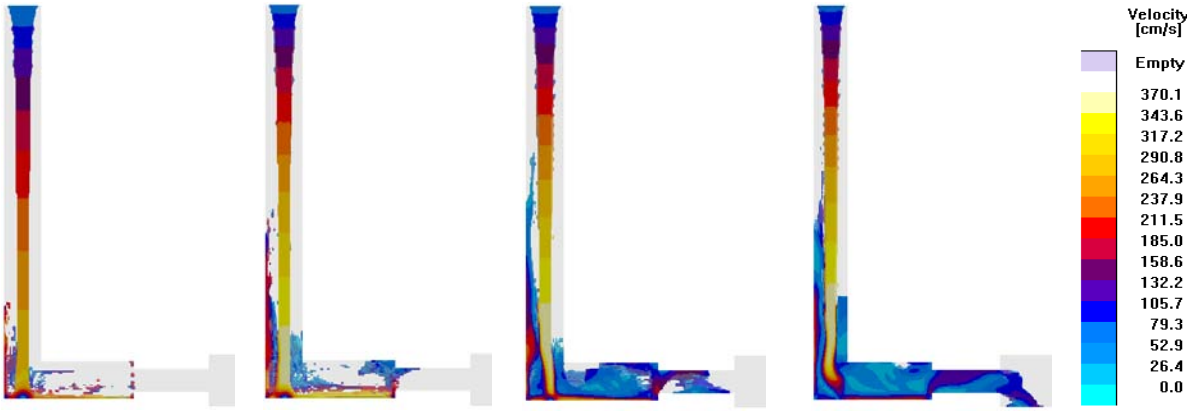

Figure 2.13: Filling sequence for the gating system with sharp and abrupt transitions in cross sections leading to splashes and back waves even before the melt gets to the mould cavity, (Kotas, 2010).

In **Figure 2.13 (b)** a formation of a back wave after the melt impinges the runner wall is seen. This undesirable feature will for sure will lead to air entrapment and also to folding of oxide films already present on the melt surface. When the melt enters the reduced flow channel, the melt does not fill the entire area and an area with low pressure forms along the walls, which is seen in **Figure 2.13 (c)**. Last, in **Figure 2.13 (d)** a situation when the melt reaches the casting is depicted. What happens is that the melt will fall down into the casting cavity and will create an empty area right below the cross section change. This area will consequently be filled with the metal but air will have no way to leave that area, resulting in air bubbles. Moreover, that "dead" area will solidify earlier than the rest of the casting since it is stagnant while the remaining sections are still being filled by the hot melt. As a consequence, the "dead" area will have different microstructure and possibly also distinct mechanical properties. More on this topic will be discussed in the section devoted to solidification.

Filling results for the second layout, redesigned according to the simplified equations in section 2.3 can be seen in **Figure 2.14**.

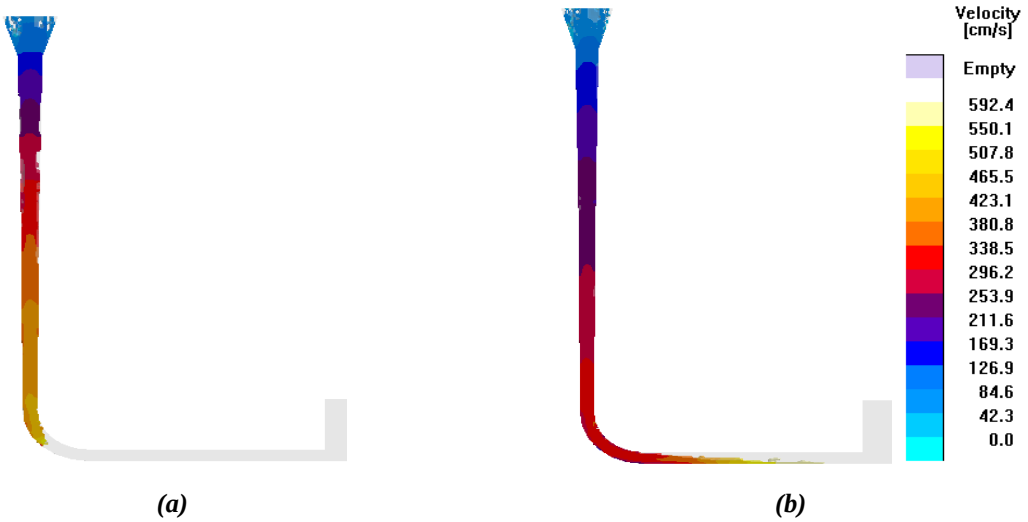

Figure 2.14: Filling sequence for the modified gating system where the sharp corners at the bottom of the sprue got replaced by a simple turn, (Kotas, 2010).

From the filling sequence in **Figure 2.14** it follows that the melt movement is much more uniform and coherent. It all started in the sprue area where air aspiration is not seen, the melt falls down with almost negligible separation from the mould wall. Due to the added bend, the melt does not hit the bottom wall, but propagates further to the horizontal runner and to the casting with no apparent disturbance. Also, thanks to the horizontal runner placed at the lowest point of the casting, the melt fall was eliminated.

It must be emphasized that this case study is only indicative. This test case was intended only to demonstrate the benefits of the properly calculated gating system in which the basic physical principles of the fluid flow, i.e. continuity and Bernoulli equations, were fully considered. For more detailed analysis of different designs of gating systems refer to the reference 16.

2.3.3. Sprue base

The point at which the falling liquid emerges from the exit of the sprue and executes a right- angle turn along the runner requires special attention. One of the widely used designs for a sprue base is a well which is shown in **Figure 2.15a**. Its general size and shape has been extensively researched by many research groups and individuals in an effort to provide optimum efficiency in the reduction of air entrainment in the runner. The idea of this bottom well has been to take in the first metal stream falling from the sprue and comfort it so that calm and non-turbulent melt flow throughout the horizontal runner is provided. However, based on many personal discussions with various metal casters, on literature search and also after performing many numerical simulations, it seems that the comforting and widely held image of the well as being a “cushion” to soften the fall of the melt is seen to be an illusion. In reality, the well has been an opportunity for the melt to churn, entraining quantities of oxide and bubble defects. This can also be seen in **Figure 2.15a**, where a bottom well has been used while filling a small casting. One can clearly see that as the melt impinges at the bottom of the well, it disintegrates and splashes causing severe surface turbulence and consequent air entrapment. These trapped air bubbles are then transported further into the casting cavity with the flowing melt compromising the final casting quality.

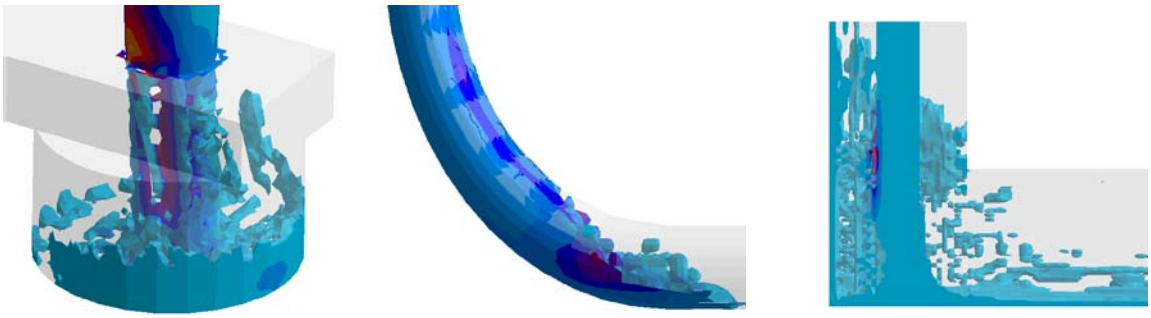

(a) ***(b)*** ***(c)***

Figure 2.15: Three common types of sprue/runner junctions. A sprue well (a), turn (b) and a sharp 90deg corner-element (c), (Kotas, 2010).

Campbell and his colleagues performed systematic X-ray radiographic studies which started in 1992 to investigate the effects of various sprue ends on filling patterns of various castings. They have shown that in a sufficiently narrow filling channel with a good radius at the sprue/runner junction, the high surface tension of the liquid metal assists in retaining the integrity of a compact liquid front, constraining the melt. These investigative studies on narrow channels in real moulds with real metals quickly confirmed that the sprue/runner junction was best designed as a simple turn (**Figure 2.15b**), provided that the channels were of minimum area. The studies showed that if a well of any kind was provided, the additional volume created in this way was an opportunity for additional surface turbulence, so damaging the melt. Furthermore, after the well was filled, the rotation of the liquid in the well was seen to act as a kind of ball bearing, reducing the friction on the stream at the turn. In this way the velocity in the runner was increased. These higher speeds observed out of right-angle turns provided by a well were unhelpful. For a narrow turn without a well the velocity of the metal in the runner had the benefit of additional friction from the wall, giving a small (approximately 20 %)

but useful reduction in metal speed. Thus the conclusion that the filling systems perform better without a well seems conclusive.

The worst case possible is to use a 90 degree angle junction between the sprue and the runner as seen in **Figure 2.15c**. Sudden changes in the direction of flow can produce low pressure zones. Moreover, these sudden changes in the flow direction or dead ends always lead to massive splashing and pressure back-waves, leading to surface turbulence of the propagating melt front and to subsequent air entrapment or folding of oxide films as also seen in work by Tiedje and Larsen[16]. The mentioned problems with the turbulent flow pattern can be minimized by making the change in flow direction more gradual or smooth. It may seem obvious that this solution, i.e. right angle junction, should never be applied but one would be unpleasantly surprised how often it is still used in foundry practice. Not especially in casting of large steel cast parts but in gravity sand casting of grey cast iron. This just shows how optimization of gating systems and filling patterns has been taken for granted by many metal casters and foundry technologists. A demonstration of how significantly simple changes in the design of the sprue base can influence the filling pattern is shown in case study one in section 2.3.2.2., and also in **Figures 2.13** and **2.14**.

2.3.4. Runner

The runner is that part of the filling system that acts to distribute the melt horizontally around the mould, reaching distant parts of the mould cavity quickly to reduce heat loss problems. The runner is usually horizontal because it simply follows the normal mould joint in conventional horizontally parted moulds. In other types of moulds, particularly vertically jointed moulds, or investment moulds where there is little geometrical constraint, the runner would often benefit from being inclined uphill. It is especially useful if the runner can be arranged under the casting, so that the runner is connected to the mould cavity by vertical gates. But above all, this so-called bottom gating will ensure more uniform and slower entry of the melt into the casting cavity. Placing the mould cavity below the runner causes an uncontrolled fall into the mould cavity, creating the risk of imperfect castings. For products whose reliability needs to be guaranteed, the arrangement of the runner at the lowest level of the mould cavity, causing the metal to spread through the running system and the mould cavity only in an uphill direction is a challenge that needs to be met. More on the methods of gating will be given in the following sections.

The objective of a runner is not solely to deliver a molten metal into the casting cavity but also to control the velocity of the flowing metal, i.e. to slow it down. In the horizontal runner the melt is no longer falling and therefore the velocity is no longer increasing as in the down runner and the bend below the down runner. This means that at least in theory, using the continuity equation **Eq. 2.22** it is possible to decrease the velocity by increasing the cross-sectional area throughout the horizontal runner. A traditional approach has been to enlarge the cross section area of a runner compared to the sprue exit to provide sufficient friction and hence to slow down the melt. A danger of this approach lies in that if the runner area is expanded too much it will cause the runner to be incompletely filled and so permit conditions for damage, i.e. surface turbulence and surface oxidation. Campbell states that if the runner's area is enlarged by more than 20% as to the sprue exit, the risk of incomplete filling rises[8]. One of the most effective devices to reduce the speed of flow in the runner is the use of a filter. The close spacing of the walls of its capillaries ensures a high degree of viscous drag. The flow rate can often be reduced by a factor of 4 or 5. This is a really valuable feature, and actually explains nearly all of the beneficial action of the filter (i.e. when using good quality metal in a well-designed filling system the filter does very little filtering. Its really important action in improving the quality of castings is its reduction of velocity).

2.3.4.1. Tapered runner

Very often, when casting larger castings it is necessary to use multiple thin gates or multiple runners. In order to facilitate a good filling pattern where melt will enter the casting cavity from all the thin gates at the same time, geometrical adjustments in the runner design have to be performed. The situation is shown in **Figure 2.16**. Clearly, the momentum of the flowing liquid causes the furthest gate, number 3, to be favored. The rapid flow past the opening of gate 1 will create a reduced-

pressure region in the adjacent gate at this point, drawing liquid out of the casting! In the case of a non-tapered runner it would have been best to have only gate 3.

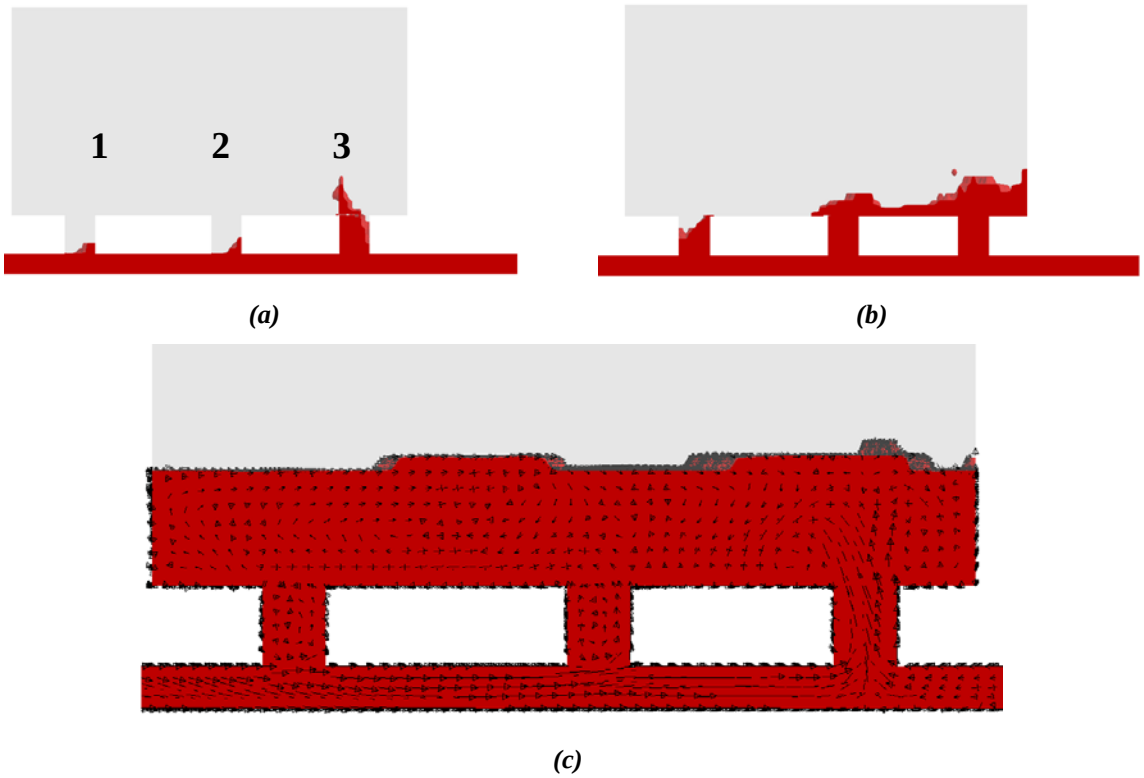

Figure 2.16: Filling sequence in the non-tapered runner, indicating issues with non-uniform metal entry into the mould cavity. Moreover, melt velocities differ for each thin gate. Simulation was performed based on an example given in Campbell[11].

Where more than one gate is attached to the runner, the runner needs to be reduced in its cross-section as each gate is passed, as illustrated in **Figure 2.17**. It has been common that such reductions have usually been carried out as a series of steps, producing the well-known stepped runner designs. For three ingates the runner would be reduced in section area by a step of one third the height of the runner as each gate was passed. However, real-time X-ray studies have noted how during the priming of such systems, because of the high velocity of the stream, the steps cause the flow to be deflected, leaping into the air, and ricocheting off the roof of the runner. Needless to say, the resulting flow was highly disturbed, and did not achieve its intended even distribution. It has been found that simply reducing the cross-section of the runner gradually, usually linearly, cures the deflection problem. A smooth, straight taper geometry does a reasonable job of distributing the flow evenly (**Figure 2.17**).

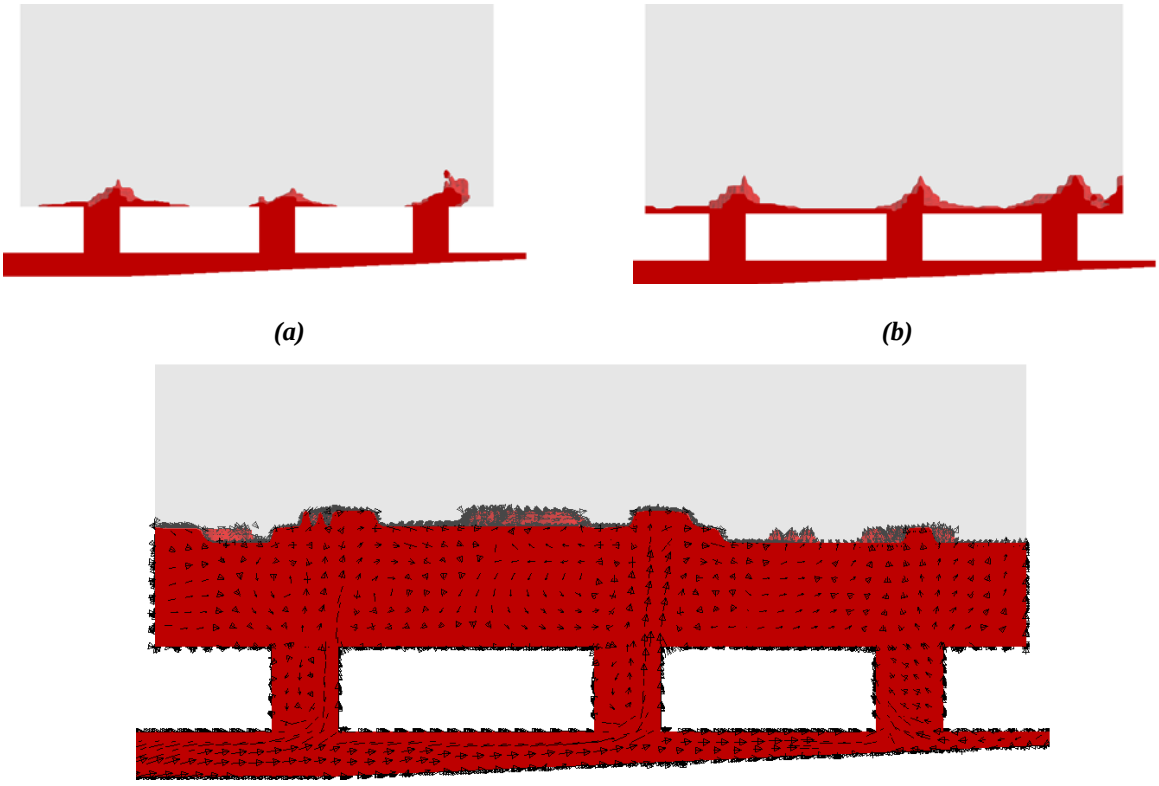

Figure 2.17: Filling sequence in the tapered runner. Much more uniform metal entry can be observed with more-or-less similar melt velocities in all thin gates. Simulation based on Campbell[8].

Figure 2.17c shows a much more favorable filling pattern using velocity vectors showing the velocity and direction of the flowing melt. The areas of our focus are the three gates which indicate a more directional flow pattern as compared to the non-tapered runner in **Figure 2.16**.

There is especially one casting technique in which gating systems are of utmost importance. In high pressure die casting, it really matters if the melt enters the die cavity from all the runners/thin gates at the same time. Filling velocities are so high, filling times so short and die cooling so intense that having melt coming at different velocities and at distinct times very often results in waves, splashes, air bubbles or even cold shuts due to inability of the melt streams exhibiting different temperatures, to fuse. One such example is given in the series in **Figure 2.18**. The two split horizontal runners are not tapered enough to ensure a uniform entry from all the thin gates at the same time, **Figure 2.18(a)**. Due to the geometry of the thin gates, in a combination with different melt velocities, several areas indicate potential problems with air entrapment in the early stages of filling, **Figure 2.18(b)**. The entire filling pattern is captured in **Figure 2.18(c)**. Notice the encircled area which suggests a wave forming in an area from which the air will not be able to escape, when entrapped. **Figure 2.18(d)** shows the air entrapment criterion which supports the just mentioned assumption that waves and vortices can cause entrapment of air inside the casting.

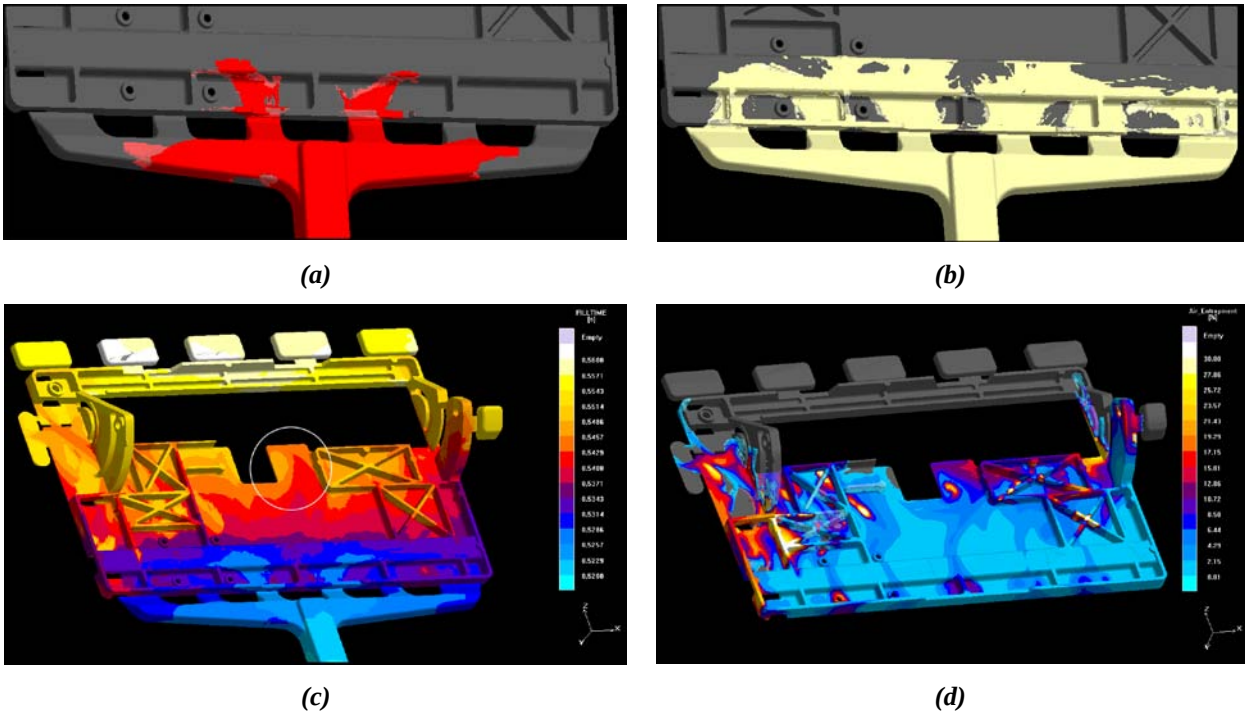

Figure 2.18: Filling of high-pressure die casting. (a) Initial stage of filling when the melt is entering the die cavity unevenly from the four thin gates due to inadequately tapered runners, (b) consequence of improper gating system- air entrapment at the lower part of the casting, (c) fill time criterion function indicating the overall filling pattern. Issues with surface turbulence and potential risk of air entrapment encircled, (d) air entrapment criterion implying air pockets which arise during filling. Figures taken from Kotas[7].

It should be noted that an improper design of the runners can promote not only filling-related issues as just demonstrated. The runners and primarily their robustness play a significant role in the solidification behavior of the entire casting. By this we mean that if the gating system is thick or bulky as compared to the adjacent casting, it will solidify later than the casting, and may form hot spots which can then result in shrinkage porosity just above the thin gates. Or, in a worse case, it may lead to deformation, e.g. bending or warping, and residual stresses inside the casting. Consider now the same HPDC cast part in **Figure 2.18**. It appears that when the robust and wide gating system, adjacent to a very thin-walled flat Al-based casting, tries to cool down and shrink, the entire casting can end up being distorted or containing residual stresses. This situation is well documented in **Figure 2.19**. Since the gating system is robust as compared to the actual casting, it solidifies and contracts a bit later. As it contracts, it forces the casting to bend down, i.e. bend it in the z-direction. The adjacent bottom area of the casting is already solid and relatively strong, thus exerting quite some resistance to any bending. This situation must naturally result in high stresses in the z-direction inside the casting, as shown in **Figure 2.19(a)**. When the gating system gets trimmed off, some of these "locked" stresses inside the casting get relieved **(Figure 2.19(b)),** in a form of permanent displacements, see **Figure 2.19(c, d)**. This phenomenon is referred to as elastic spring-back. Even though, the aforementioned findings may seem obvious, one would be very surprised how many foundry engineers have very little or no clue about thermally driven stresses and strains arising during metal casting. This explains why stress-strain analyses are commonly skipped when performing casting simulations. Moreover, some of them totally disregard the fact that even gating systems can substantially contribute to deformation or residual stresses inside castings. The author bases this statement on personal experience with both HPDC and steel foundries.

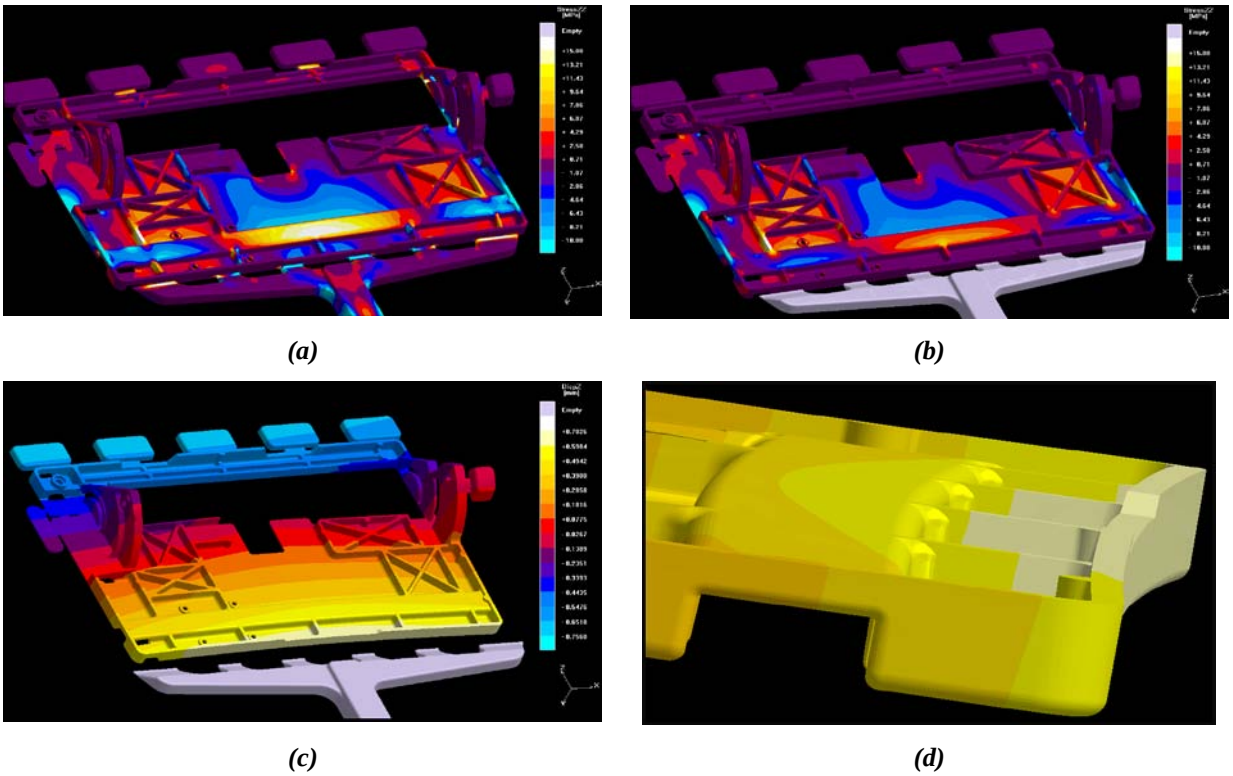

(a) *(b)*

(c) *(d)*

Figure 2.19: (a) stresses in the z direction due to the hindered thermal contraction of the casting caused by the robust gating system, (b) partial stress relaxation-elastic spring back, after trimming off the gating system, (c) permanent deformation of the casting after cutting off the gating system, (d) detailed view on the bottom distorted, i.e. bended, area of the casting. Figures are taken from ref. [7], Kotas, 2007.

Unlike in high-pressure die casting or gravity die casting, in gravity sand casting of large steel parts it is not possible or at least not common to use smooth tapering of the runners as shown above. The reason is that, refractory tiles (tubes) with constant inner diameters are used to construct gating systems. Such a gating system is depicted in **Figure 2.20**.

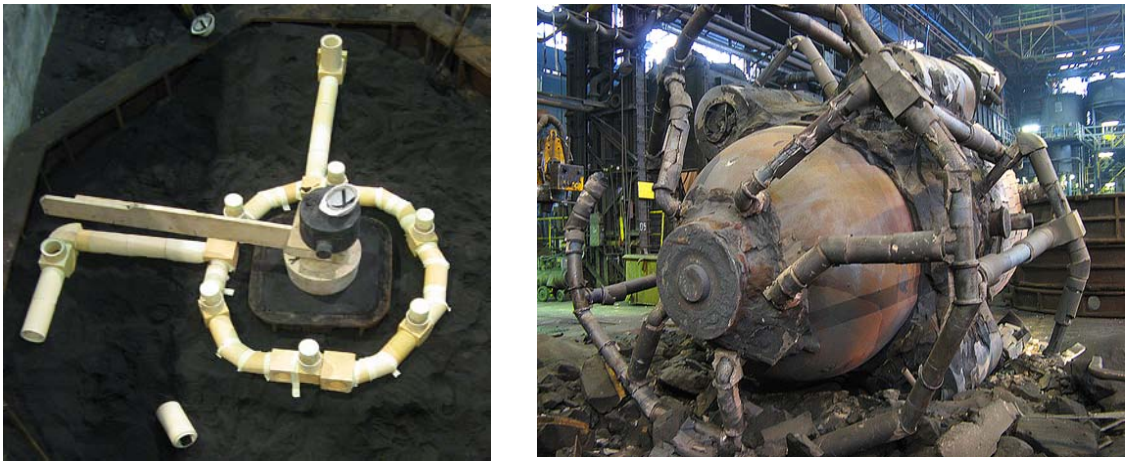

Figure 2.20: Gating systems for large steel casting are very often made of refractory tiles. Courtesy of Vitkovice Heavy Machinery.

When using the tile system it is impossible to use the smooth area reduction since most of the tile suppliers do not provide these. Therefore, the three possible scenarios are (i) to make the choke element as a sand core, (ii) use a tile with a smaller inner diameter, or (iii) leave it non- tapered. In the first case there is a high risk of sand erosion in that particular element since an extremely large amount of metal flows through and also, it is very difficult to integrate such element into the tile-gating system so that it holds firm. Using the second option, there is no smooth taper, but an abrupt

change of the runner's inner diameter which may introduce turbulence and vena contrata into the filling stage.

As shown in **Figure 2.21**, low-pressure zones-with a resulting tendency toward air entrainment can be created as the metal stream pulls away from the mold wall. With a sudden enlargement of the channel **Figure 2.21(a)**, momentum effects will carry the stream forward and create low-pressure zones at the enlargement. With a sudden reduction in the channel cross section, **Figure 2.21(b)** the law of continuity shows that the stream velocity must increase rapidly. This spurting flow will thus create a low-pressure zone directly after the constriction.

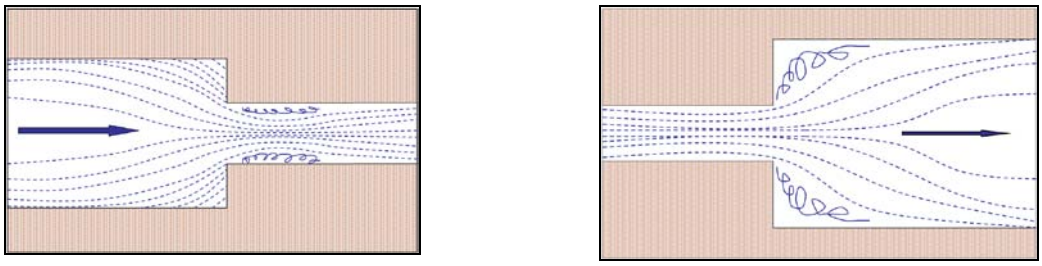

(a) ***(b)***

Figure 2.21: Schematic showing a theoretical formation of low-pressure areas due to abrupt changes in the cross section of a flow channel, e.g. a runner or a sprue.

If the third solution, i.e. non-tapered runner with no choke elements, is preferred, then a way of reducing the velocity of the flowing melt is to introduce runner extensions, also called overruns. The function of the runner extension was explained earlier, but in general it serves to absorb the kinetic energy and to lower the entrance velocity of the melt. A clear evidence of the usefulness of the runner extension is depicted in **Figure 2.22**. There, it is seen that without the runner extension the velocity in the runner was much higher leading to more severe impingement and splashing of the colliding melt streams, **Figure 2.22(a)**. While, when the small runner extensions were added, **Figure 2.22(b**), the velocity got lowered, eliminating the massive collision and splashing. If the size of those extensions was even larger, an even slower entry would be achieved.

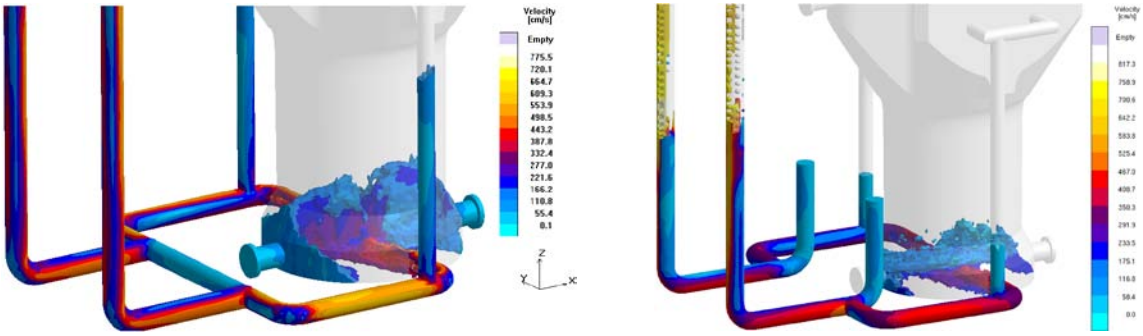

(a) ***(b)***

Figure 2.22: Effect of the runner extension on the flow velocity. Obviously, more profound effect on the velocity reduction could have been achieved if larger runner extensions were employed, [ref. Paper II, (Kotas et al. 2010)].

An example of non tapered runners in a commercial steel casting can be also seen in **Figure 2.23**. As a consequence of the improper runner design a non-uniform metal entry from separate thin gates is observed. Moreover, the runner system does not provide any velocity reduction thus the metal enters the casting cavity with a high velocity leading to jetting and subsequent splashing and surface turbulence. A remedy to this situation would either be to totally redesign the gating system, to enlarge the thin gates cross section area or to design it as a fan gate to increase friction losses. Additionally, if a runner extension was added, the kinetic energy of the flowing melt would be lowered somewhat and hence also the entrance velocity.

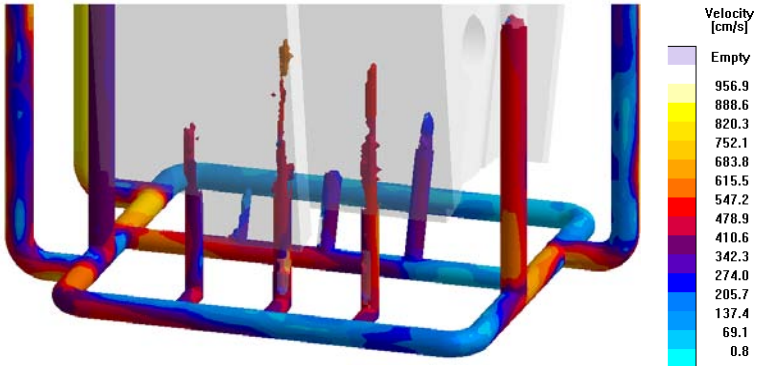

Figure 2.23: Non-tapered runner system contributing to the non-uniform entry of the metal into the casting cavity, [ref. Paper IV, (Kotas et al. 2010)].

A next example of how the non-tapered runner leads to a non-uniform entrance of the melt into the casting cavity is shown in **Figure 2.24**. In that case the thin gates were positioned horizontally, being filled by a circular runner with a constant cross section. The improper geometry of the runner has led to a situation where some gates got filled much earlier, depending on their position to the vertical sprues. Since this casting has been filled simultaneously from multiple ladles, the impingement of the multiple melt streams caused some gates to be filled with rather high velocity, due to the kinetic energy of the colliding melt streams. In such areas, the risk of mold wall erosion has increased tremendously. A reasonable solution to this problem would be to add few runner extensions to absorb some energy and to split the circular runner to several sections to prevent the impingement of the melt streams. Moreover, a tapered runner, by means of choke elements has also been proposed but the manufacturing foundry refused to apply it.

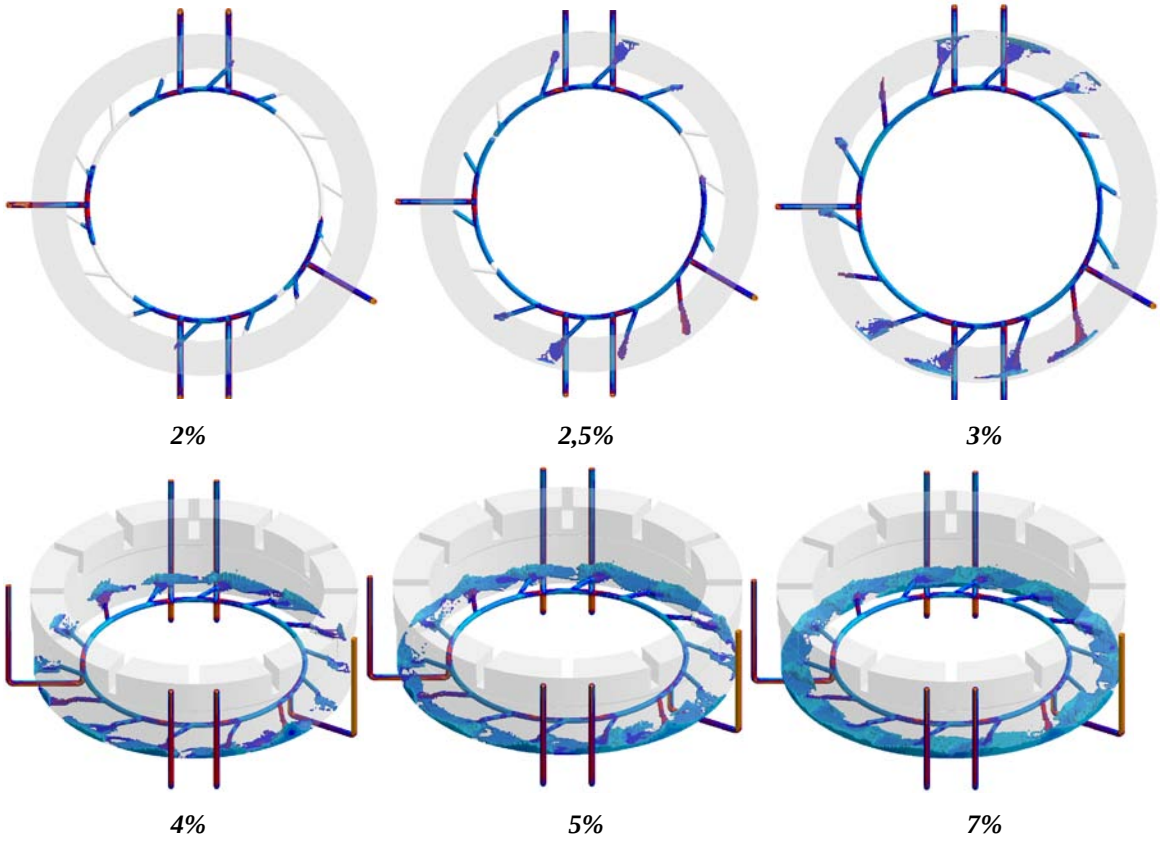

Figure 2.24: Non-uniform metal entry at the initial stages of the filling process of a large steel ring. This problem can be solved by making the runners tapered with gradually reduced cross section areas, [ref. Industrial report, (Kotas 2010)].

2.3.5. Thin gates

At this moment, a reader would expect one more section related to individual elements of a gating system. Till now, thin gates have not been addressed properly. Thin gates are elements of literally all gating systems. They can be found between runners and a casting and they directly deliver the melt into the casting cavity.

Thin gates in general play an important role in the overall quality of a filling procedure as they are the last elements which can control, i.e. slow down or accelerate the propagating melt. Naturally, there are few general guidelines which should be followed when designing thin gates. First of all the thin gate has to be connected to the casting in a way that gives a beneficial heat distribution in the casting after mould filling. In this way mechanical properties and feeding can be enhanced. Secondly it should be kept in mind that the cross-section area throughout the thin gate should be either the same or increased relative to the top cross-section of the 'bend under the casting'. At the same time the connection to the casting should be as thin as possible. These two parameters will help to decrease the velocity of the melt when entering the mould/die cavity. Thirdly the connection between the thin gate and the casting should be in a way that makes it as easy as possible to remove the gating system from the casting.

In casting of thin-walled or net shape castings, thin gates are one of the most, if not the most important features which affect filling. Therefore, a close attention must be paid to the thin gate design in HPDC-devoted foundries. However, this does not apply to the same extent to casting of large steel castings. Typically, thin gates look exactly the same as the runners; they are simply made of the same refractory tiles as the horizontal runners. Sometimes steel foundries use conical, i.e. upward expanding, thin gates which are usually made as sand cores and not as tiles, or fan gate-resembling thin gates can be applied as well, see **Figure 2.25**. As to the velocity reduction, it must be said, that in case of large steel castings, these gates do not slow down the melt almost at all since often the melt falls down from 2-5 meters and these small elements cannot remarkably slow it down. It is primarily the runner extension that significantly absorbs the kinetic energy and slows down the velocity.

The author's conviction is that for filling of small, thin-walled, net shaped castings the design of thin gates matters a lot, however, for filling of extremely large castings it does not-that much.

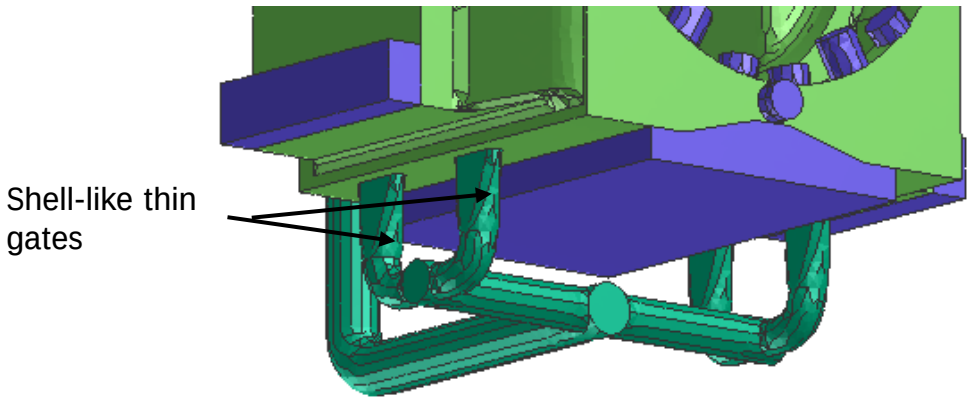

Figure 2.25: fan gate-like thin gates applied for large steel castings. This figure cannot be shown entirely due to copyright restrictions imposed by the manufacturing foundry.

2.4. Methods of Gating

Now, when the basic principles of traditional gating systems are known, three methods of gating will be introduced and discussed. It means how the melt gets to the casting cavity from the gating system, whether (a) it falls down from the top to the bottom of the cavity, (b) it flows from sides or, (c) it flows from the bottom of the cavity against gravity force, as sketched in **Figure 2.26**. Each method

has its pros and cons and thus it is up to the foundry technologist to select the most desirable tradeoff solution.

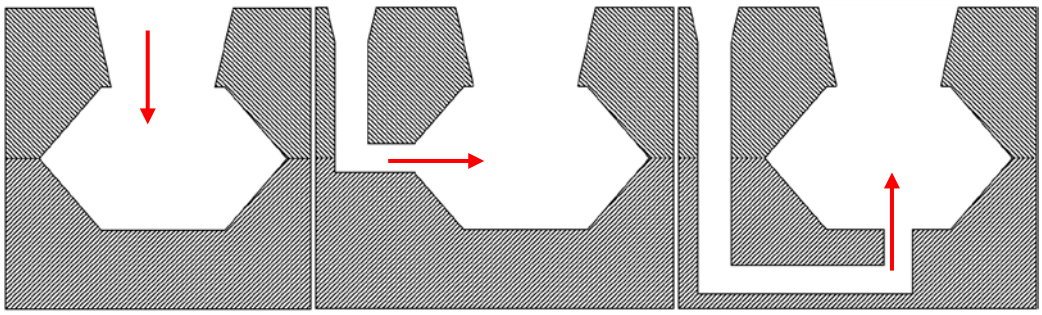

(a) *(b)* *(c)*

Figure 2.26: Methods of gating,(a) top filling, (b) side filling and (c) bottom filling. Figure inspired by Beeley[19].

2.4.1. Top gating

When metal is poured through a top gate or directly into an open feeder head, the melt stream impinges against the bottom of the mould cavity until a pool is formed; this is kept in a state of agitation until the mould is filled. The erosive effect of the unconfined stream can be severe, whilst the associated splashing gives an opportunity for oxidation. The mould surface can be protected at the point of impact by preformed refractory tiles; however, the massive splashing cannot be prevented. The principal advantages of top gating are its simplicity for moulding, its low consumption of additional metal and, above all, the generation of temperature gradients favorable to feeding from top heads; this arises from the proportionately rapid cooling of the first metal poured, followed by the progressive accumulation of metal from above until the mould is full.

In **Figure 2.27**, two examples coming from industry are shown. Both of them represent a combined filling, i.e. bottom and top filling. A function of the top runners is to supply a hot melt into the upper sections of the casting to establish a favorable thermal gradient so that the feeder feeds well. However, a huge downside of this solution is that the top runners get filled too early causing a waterfall of the new-coming melt. This will for sure lead to massive oxidation of the propagating melt, compromising the overall quality and integrity of the final product.

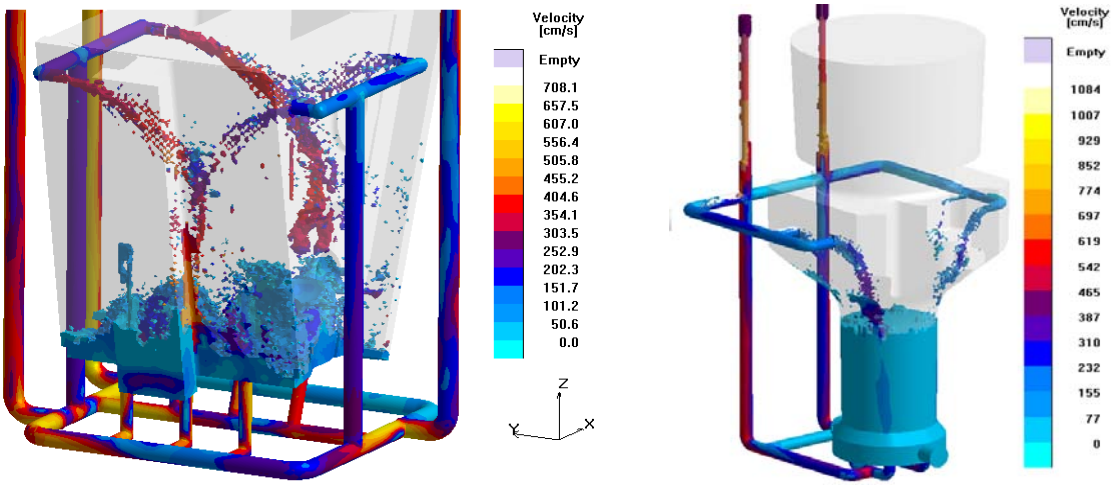

(a) *(b)*

Figure 2.27: Combined bottom and top filling in two industrial castings (a) a wedge casting, [ref. Paper IV, (Kotas et al. 2010)], (b) a steel forging ram, [ref. Paper II, (Kotas et al. 2010)].

A problem with oxide films is that nobody knows where they end up in the solidified structure. For instance, when the forging ram in **Figure 2.27(b)** was put into service, it collapsed after only a few forging cycles. After sectioning and a metallographic analysis it was found that it was the oxide films

together with porosity that caused this ultimate failure. Therefore, the author's personal conviction is that if possible, top filling should be completely avoided.

2.4.2. Bottom gating

Quiet entry of metal into the mould cavity is best achieved by its introduction at the lowest level. Using this method the metal rises steadily through the mould, splashing and metal/mould impingement are nearly eliminated and dislodged moulding material tends to be carried away to the surface. If bottom gates are used with top feeder heads the resulting temperature gradients are opposed to feeding, but various measures are available to reduce this effect. Despite the greater complexity of moulding, the method is much used for heavy castings. Nevertheless, one should always provide that the entrance velocity will be sufficiently low to prevent jetting and splashing as seen in **Figure 2.28** (left) illustrating the forging ram again. Due to missing elements for velocity control such as choke elements of runner extensions, the melt was so fast inducing very undesirable jetting. The identical feature was also seen in **Figure 2.23** because of the same reasons.

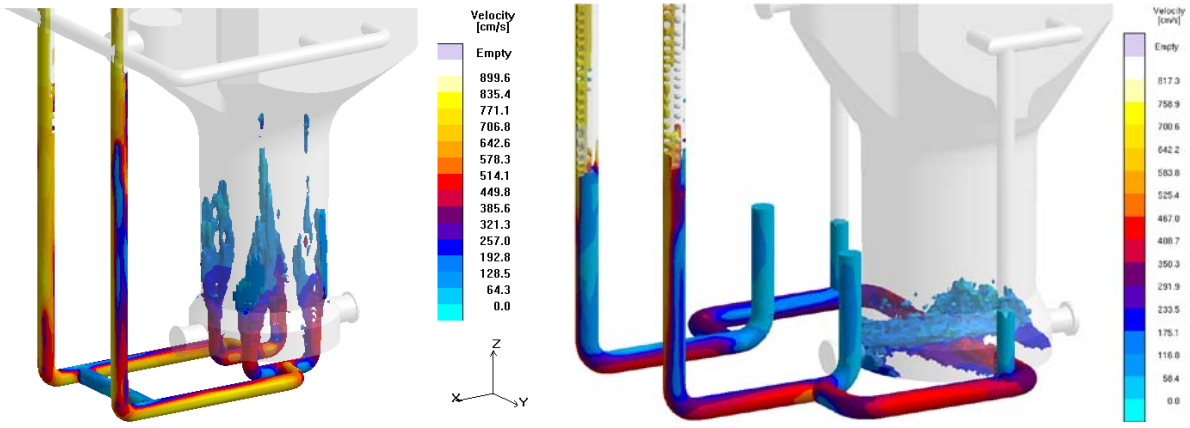

(a) *(b)*

Figure 2.28: Bottom and side gating and its impact on the filling pattern of the large steel forging ram [ref. Paper II, (Kotas et al. 2010)].

2.4.3. Side gating

Moulding can be simplified by the discharge of metal into the side of the mould cavity through ingates molded along a parting line; this practice frequently offers the best compromise between moulding convenience and the ideal gating arrangement, **Figure 2.28** (right). Using side gating, progressive mould filling can be achieved by tilting the mould towards the ingates to provide uphill casting conditions, as seen in **Figure 2.4**. If multiple runners and gates are used for filling of a single casting, it should always be insured that the melt streams will not directly collide as depicted in **Figure 2.28** (right). If they do collide it introduces surface turbulence into the filling stage leading to oxidation. Moreover, a direct impingement on the mould or core wall could relatively easily evoke sand erosion. Therefore a very common procedure is to apply so-called tangential thin gates, **Figure 2.29**.

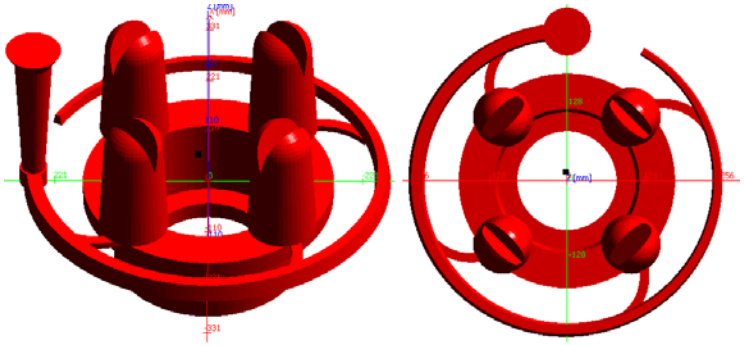

Figure 2.29: Combined bottom and top filling of a flange-shaped cast iron casting. Tangential thin gates have been employed in this case to prevent the melt impinging directly on the central sand core, which may cause sand erosion, (Kotas, 2008). This casting has been used in a course on modeling of casting processes as an example of an improperly positioned gating system.

It means that the gates will not be connected or directed to the casting cavity with a 90 degree angle but with lower as for instance in the case of the steel ring in **Figure 2.24**. The tangential gates will then induce the melt to sort of rotate and propagate relatively smoothly, minimizing a risk of surface turbulence.

2.5. Filling Related Defects

As far as casting defects are concerned, many books and atlases have been written giving very thorough descriptions of all so far known casting defects[20, 21]. Hence in this chapter, only defects primarily induced by improper gating and pouring techniques will be briefly addressed. It obviously does not mean that no other features such as casting and pattern design, moulding sand, risering, melting practice etc. evoke these defects. Only, due to the lack of space, these other features will not be discussed. The three major defects typically initiated by wrong design of the gating system, i.e. wrong basin, non-tapered sprue and runners, sharp bends etc., or by a metal caster while pouring, too rapid or slow filling, interrupted pour, are: (a) misruns or cold laps, (b) gas inclusions, i.e. gas bubbles and (c) inclusions, i.e. sand grains, slag or other dirt. These three will be discussed in the following three sections.

2.5.1. Misruns and cold shuts

A misrun casting is one which lacks completeness due to failure of the metal to fill the entire mold cavity. A portion of the casting is missing, usually on the cope surface or at a location remote from the gate area. The edges surrounding the missing portion are rounded[20]. Adjacent surface are generally shiny. The gates and runners are well-filled.

A cold shut casting is one in which a definite discontinuity exists due to imperfect fusion where two streams of metal have converged. This defect may have the appearance of a crack or seam with smooth, rounded edges[21]. See **Figure 2.30**.

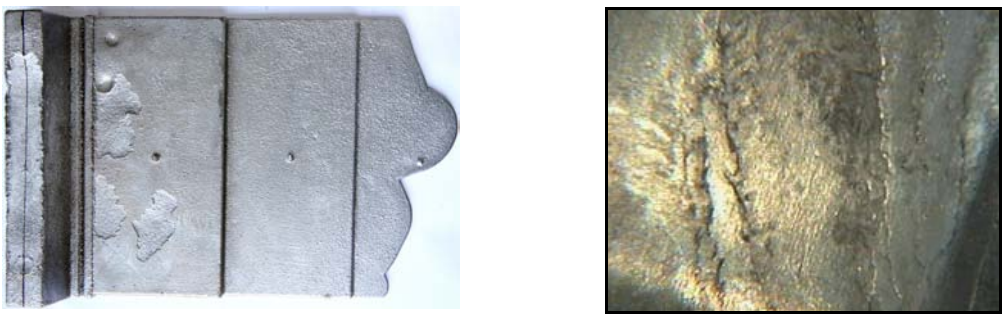

Figure 2.30: (left) typical misrun casting, (Kotas, 2009), (right) a cold shut casting.

There is more than one cause for occurrence of these two defects, among the most decisive are[21]:

- *Improper sizing of gates, runner and sprue*. The gating system must be designed so that the sprue and runners are of adequate size to supply metal to all gates evenly, and to keep the gates full in order to avoid interrupted metal flow.
- *Gates not properly located.* The proper location depends entirely upon casting design. How the mold cavity will fill and the probable flow pattern must be visualized and the gates located accordingly.
- *Pouring temperature is too low.*
- *Interrupted pouring* produces uneven filling and permits oxide films or gas to prevent proper fusion, the so-called knitting of the metal after pouring is resumed. Letting the sprue drop (not keeping the sprue filled) also acts as an interrupted pour.
- *Reducing the rate of pour too soon* may reduce the pressure needed to finish filling the mold cavity
- *Slag, dirt or ladle refractory which stops off the gate* acts as an interrupted pour or a reduced pouring rate.
- *Not keeping the sprue, runner and gates full* acts as an interrupted pour or inadequate pressure. In addition, this practice permits air entrapment which reduces fluidity of metal (especially nonferrous), or allows rapid oxide film formation in metals such as steel.

2.5.2. Gas Defects (air bubbles)

Blows or gas holes in castings are cavities, spherical, flattened or elongated, see the encircled red area in **Figure 2.5(a)**. Fundamentally, they are caused by localized gas pressure that exceeds the metal pressure in any locality during solidification of the metal. Gas follows the path of least resistance and hence moves usually toward the cope portions of the casting. Blows or gas holes may appear as depressed areas in the surface of the casting or as a subsurface cavity.

Pinholes, blisters and body scars as well as certain types of porosity are variations of gas holes or of a blow. A great deal of confusion can occur because of the frequent similarity in appearance to the shrinkage defect. There are two areas of possible confusion which must be analyzed carefully. In the first place, gas defects may occur in combination with a shrinkage area. In the second place, shrinks and blows tend to occur in the same general location. Both are likely to be located in the section of the casting that solidifies last. It is also wrong to define a blowhole as a cope defect and it is false to conclude that a similar defect in the drag must be a shrink. It is true that gas tends to rise and, therefore, flow to the cope. On the other hand, if the gas is created in the drag, it may not have time to travel upwards. In this case the blow is the drag defect. The general causes for this defect to form are[21]:

- *Casting and pattern design.*
- *Gating causing turbulence*. The use of non-tapered sprues, sharp bends in the runner and gate systems should be avoided.
- *Gating system that causes interrupted flow of metal*.
- *Improper sprue or gate design allowing air or mold gas to enter the metal stream.* Round design, i.e. conical, pouring basins should be avoided as this will create a vortex. Straight sprues, i.e. non-tapered, should not be used for tall castings at all. Sharp bends in the runner system should be avoided. All of these factors cause aspiration of air.
- *Gating system not full*. Tapered runners or at least choke elements should be used when having multiple gates to provide full channels with no melt oxidation or back waves.

2.5.3. Inclusions

Inclusions are particles of foreign material embedded in the metal. If these inclusions are found at the surface, they may be removed during cleaning, leaving only the holes. In this case, they may be referred to as dirt holes. Since this defect involves an unintended object or foreign body, determining the exact cause may involve clever detection. For example, the defect may be due to "any foreign materials getting into the mold, sprues, or open risers through carelessness[21]." Just looking for careless molding may not be adequate. The carelessness may be a matter of equipment, design, placement or maintenance. For example, the sand distribution belt may be spilling sand into open molds below.

It is obvious that the presence of a scab, erosion, or cut in the casting will produce sand or slag inclusions somewhere in the casting. It may not be equally obvious that such defects on any part of the gating system can create an identical problem. Since the gating system is usually detached before the casting is inspected and rejected, the source of trouble becomes mysterious. Inclusions involving a given pattern should be studied by inspection after cleaning, but with the gating system attached. The presence of any expansion, erosion, or cut defect on the gate, runner or the sprue may easily be the cause even though at some distance from the inclusions in the casting itself. The most probable causes are[21]:

- *Those design factors which contribute to scabs, cuts washes and erosion* will intensify the tendency towards inclusions which result from such defects in casting. Such designs involve abrupt changes of section, irregular contours, deep pockets and sections which detract from uniform mold hardness or excessive metal flow over confined surfaces.
- *Improper gating*. Gates should be located so the first metal will cushion the remainder of the metal and keep the sand covered until the mold cavity has been filled. This applies equally to the area at the base of the sprue where cuts are common. Gating systems that create slow pouring can cause scabs, particularly on cope surfaces. Slow pouring exposes the cope surface to radiant heat without a protective metal covering. This applies equally to the cope surface or runners. Gating formulas which create an unfilled runner should be avoided since the cope of such runners will eventually scab and drop sand into the gating system. An inadequate number of gates creates cuts and washes in the casting. An inadequate runner of excessive choke can likewise cause a cut or wash of the gating system. Weak skim cores may break down and wash into the casting especially if the amount of metal through the core is excessive. A gating system may be designed in such a way as to create, permit, or increase the formation of inclusions. For example, the choke may be inadequate to stop the flow of slag or dross coming into the sprue. The slag traps may be located incorrectly so as to permit further slag formations after the trap or they may be too small to retain the slag entering the system. The pouring basin designs should avoid a vortex and must permit retention of slag in the cup.
- *Pouring temperature*. Low pouring temperature is a common source of trouble. A gating system with adequate choke for relatively hot, clean metal may fail to separate slag from a colder, dirtier ladle of iron.
- *Interrupted or slow pouring*. Failure to keep the sprue full destroys the effectiveness of the slag trap in the gating system and permits slag to drop down the sprue instead of remaining in the pouring cups where it belongs.

Obviously there are many other causes for inclusions such as metal composition, melting and pouring practice, molding sand, core and molding practice, pattern equipment, flask equipment and rigging, or risering techniques. These will not be discussed in detail here. The interested reader should refer to references 20 and 21.

References

1. Dai, X., Yang, X., Campbell, J., Wood, J., "*Influence of oxide film defects generated in filling on mechanical strength of aluminium alloy castings*", Materials science and Technology, Vol. 20, Nr. 4, pp. 505- 513, (2004).
2. Mi, J., Harding, R.A., Campbell, J., "*Effects of the Entrained Surface Film on the Reliability of Castings*", Metallurgical and Materials Transactions A, Vol. 35A, (2004).
3. Dai, X., Yang, X., Campbell, J., Wood, J., "*Effects of runner system design on the mechanical strength of Al_/7Si_/Mg alloy castings*", Materials Science and Engineering A354, pp. 315- 325, (2003).
4. Gunasageram, D.R., Finnin, B.R., Polivka, F.B., "*Melt flow velocity in high pressure die casting: its effect on microstructure and mechanical properties in an Al-Si alloy*", Materials Science and Technology, Vol. 23, Nr. 7, pp. 847-856, (2007).
5. Kotas, P., Hattel, J.H., Thorborg, J., Svensson, I.L., Seifeddine, S.," *Modelling of Filling, Microstructure Formation, Local Mechanical Properties and Stress – Strain Development in High-Pressure Die Cast Aluminium Castings*", *Proc. International Ph.D. Foundry Conference*, Brno, Czech Republic, (2009), i.e. [enclosed paper II].
6. Domkin, K., Hattel, J.H., Thorborg, J., "*Modeling of high temperature- and diffusion-controlled die soldering in aluminum high pressure die casting*", Journal of Materials Processing Technology, (2009).
7. Kotas, P., "*Numerical Optimization of Die filling and of High-Pressure Die Cast De0formation*", Master Thesis, Technical University of Denmark, Lyngby, Denmark, (2007).
8. Hattel, J.H., "*Fundamentals of numerical modeling of casting processes*", Polyteknisk Forlag, (2005).
9. Fox, R.W., McDonals, A.T., "*Introduction to fluid mechanics*", fourth edition, John Wiley & sons, Inc. (1994).
10. White, F.M., "*Fluid mechanics*", sixth edition, McGraw-Hill, (2007).
11. Campbell, J., "Castings Practice, the 10 Rules of Castings", Elsevier Butterworth-Heinemann, (2004).
12. *ASM Handbook*, Volume 15, "*Casting"*, ASM International, (1998).
13. Campbell, J., "Castings", Elsevier Butterworth-Heinemann, (2003).
14. Skov-Hansen, S., "*Reduced Energy Consumption for Melting in Foundries*", Ph.D. Thesis, Technical University of Denmark, (2007).
15. Tiedje, N., Skov-Hansen, S. – Streamlined Gating Systems with Improved Yield – Dimensioning and Experimental Validation, World Foundry Congress, Harrogate, UK, (2006)
16. Tiedje, N.S., Larsen, P., "Investigation of the stability of melt flow in gating systems", Metallurgical and Materials Transactions B, (in press) (2010).
17. Wallace, J.F., Evans, E.B., "Principles of Gating", *Foundry*, Vol. 87, Oct (1959).
18. Fredriksson, H., Åkerlind, U. – *Materials Processing During Casting*, John Wiley & Sons, Ltd., (2006).
19. Beeley, P., *Foundry Technology*, Second Edition, Butterworth – Heinemann, (2001).
20. International atlas of casting defects, edited by Marvin T. Rowley, American Foundry Society, Inc., (1993).
21. Analysis of Casting Defects, American Foundry Society, (2007).

Chapter 3

3. Heat transfer during casting

All casting processes are very closely related to heat release and heat transport during solidification and solid state cooling. The rate of heat removal is very important as it determines the solidification time of the casting and the temperature distribution in the material. These phenomena affect both directly and indirectly the structure of the material, precipitation of pores and slag inclusions, distribution and shape of shrinkage pores and thus ultimate qualities and properties of castings. Heat transport and solidification processes in casting are very complex and often difficult to fully comprehend; nevertheless the knowledge of the basic laws of heat transport and their applications in the field of casting is of utmost importance. This knowledge is then the basis for the possibilities of modeling casting methods and designing casting processes for given purposes.

3.1. Thermal conduction

It is well known, that whenever a temperature gradient is present in any kind of matter or a subject, there is an energy transfer from the high temperature region to the low temperature region. This phenomenon is referred to as conduction and the heat flow per unit area is proportional to the normal temperature gradient, where the proportionality constant is the thermal conductivity[1]. The basic Fourier`s law of thermal conduction can be written as:

$$q = -kA\frac{\partial T}{\partial x} \tag{3.1}$$

Where q, [W], is the diffusive heat flow (heat flux) perpendicular through the surface of the area A[m^2], k is the thermal conductivity, [W/mK], T is the temperature, [K] or [°C], and x is the descriptive space parameter perpendicular to the surface, [m]. The minus sign in **Eq. 3.1** indicates that the heat is calculated positive in the direction it actually flows. Note that this equation is the defining equation for thermal conductivity, k.

3.2. Thermal convection

Both thermal conduction and radiation leads to transport of energy but not of material. Convection means transport of material together with its heat content. One type of convection present in the continuous casting of a metal melt is caused by cooling the surface of the solidified metal or the mould with water. The heated medium disappears from the neighborhood of the metal surface and the mould to be continuously replaced by cold air or cold cooling water. As for high-pressure die casting, the main source of convection is the motion of the melt in the shot sleeve and the die cavity.

There are two principal means of thermal convection: *forced and free convection*. Forced convection involves external source of motion of air or any other type of cooling/heating medium. The cooling of a die or a mold by flowing liquid (water, oil) is a very good example of forced convection. On the contrary, free or natural convection in a fluid is caused by density differences that are present in the fluid without any influence from outside. The main convection takes place due to the transport of the melt, and the contribution from the corresponding velocities can be seen in the energy equation (**Eq. 2.11**). The velocities themselves can be found from the momentum equations (**Eq. 2.5**) and the continuity equation (**Eq. 2.1**). Newton's law of cooling which is applied in order to express the overall effect of convection can be used commonly as a boundary condition or to describe the convection during the solidification or solid state cooling[1]

$$q = -hA\left(T_\infty - T_S\right) \tag{3.2}$$

where T_∞ and T_s are the temperatures of the surface of the body and the cooling fluid, respectively. *h* is referred to as the convection heat transfer coefficient, [W/m^{2}K] and **Eq. 3.2** is the defining equation. The heat transfer coefficient *h* is dependent on the speed of the flowing cooling medium and the shape and size of the surface of the casting.

3.3. Thermal radiation

The last mode of heat transfer is called thermal radiation and arises due to electromagnetic wave propagation, which can occur both in a total vacuum and in a medium. We will focus on electromagnetic radiation as a result of a temperature difference. For the ideal emitter, a blackbody, the Stefan-Bolzmann law is applied[1]

$$q = \sigma A T^4 \tag{3.3}$$

where σ is the proportionality constant and is called the *Stefan-Bolzmann constant* with the value of $5.669 \cdot 10^{-8}$W/ (m^{2}K^4). *T* is the temperature which must be inserted in Kelvin [K]. Regarding all other surfaces distinct from the ideal black body, their radiation is considerably lower, however, the total radiation emitted by these bodies still follow the fourth order proportionality stated in the Stefan Bolzmann law.

For our purposes, the analysis of the casting processes, however, we only consider two simple cases with radiant heat exchange between two surfaces A_1 and A_2. In both cases the net heat exchange can be found from the following expression[1]

$$q = -A_1 \varepsilon_{mean} \sigma \left(T_2^4 - T_1^4 \right) \tag{3.4}$$

where ε_{mean} states for the mean emissivity. Again it should be noted, that the sign convention from Fourier's law is adopted. The mean emissivity can be found for the aforementioned two cases which are particularly relevant in casting processes.

Case 1: $A_1 << A_2$, corresponding to, e.g. the surface one being completely enclosed by the much larger surface 2. In this case the mean emissivity will be equal to that of the small surface, i.e. $\varepsilon_{mean} = \varepsilon_1$.

Case 2: The two surfaces are immediately adjacent. In this case the mean emissivity will be given by

$$\varepsilon_{mean} = \frac{1}{\frac{1}{\varepsilon_1} + \frac{1}{\varepsilon_2} + 1} \tag{3.5}$$

Eq. 3.4 is often rewritten in a form more suitable for calculations:

$$q = -A_1 \varepsilon_{mean} \sigma \left(T_1^3 + T_1^2 T_2 + T_1 T_2^2 + T_2^3 \right) \left(T_2 - T_1 \right) \tag{3.6}$$

When introducing the equivalent heat transfer coefficient for radiation h_{rad}, given by:

$$h_{rad} = \varepsilon \sigma \left(T_1^3 + T_1^2 T_2 + T_1 T_2^2 + T_2^3 \right) \tag{3.7}$$

Eq. 3.6 can be written in the same form as Newton's law of cooling

$$q = -h_{rad} A \left(T_2 - T_1 \right) \tag{3.8}$$

These phenomena can be very complex and all the calculations are very rarely as simple as presented here. But for our purposes of introducing basic heat transfer modes in casting processes, these expressions are sufficient enough.

3.4. Heat Conduction equation

All thermal models, regardless of their complexity rely on the solution of the heat conduction equation, **Eq. 3.9**. This partial differential equation provides the basic tool for heat conduction analysis. From its solution, it is possible to obtain the temperature distribution in a medium, e.g. a casting or a mould, resulting from conditions imposed on its boundaries as a function of time.

$$\frac{\partial}{\partial x}\left(k\frac{\partial T}{\partial x}\right)+\frac{\partial}{\partial y}\left(k\frac{\partial T}{\partial y}\right)+\frac{\partial}{\partial z}\left(k\frac{\partial T}{\partial z}\right)+q_{vol}=\rho c_p\frac{\partial T}{\partial t} \tag{3.9}$$

where ρ denotes the material density [kg/m^3], c_p the specific heat capacity [J/kgK], T is the temperature field [K], and q_{vol} the volumetric heat source term [W/m^3]. It is often possible to work with simplified versions of Eq. 3.9. For example, if the thermal conductivity is a constant, the heat conduction equation becomes

$$\frac{\partial^2 T}{\partial x^2}+\frac{\partial^2 T}{\partial y^2}+\frac{\partial^2 T}{\partial z^2}+\frac{q_{vol}}{k}=\frac{1}{\alpha}\frac{\partial T}{\partial t} \tag{3.10}$$

Where α is the thermal diffusivity of material which is a measure of how fast temperature is conducted in a solid. In words, the heat conduction equation states that *at any point in the medium the rate of energy transfer by conduction into a unit volume plus the volumetric rate of thermal energy generation must equal the rate of change of thermal energy stored within the volume*[2]. Once the distribution of the temperature is known, the conductive heat flux at any point in the medium or on its surface may be computed from Fourier's law. Other important quantities of interest may also be determined. For a solid, knowledge of the temperature distribution could be used to determine structural integrity through determination of thermal stresses, expansions and deflections. The temperature distribution could also be used to optimize the thickness of an insulating material, e.g. insulating padding around risers, or to determine the compatibility of special coatings used during casting.

In addition to the heat conduction equation it is necessary to specify appropriate initial and boundary conditions in order to describe fully the physical problem under consideration[1]. The initial boundary conditions specify the initial temperature distribution throughout the body. In many problems, also in casting processes, the initial temperature might often be assumed constant.

With regard to the boundary conditions, there are five principal boundary conditions which are used in mathematical theory of heat conduction as idealizations of the actual physical processes. Basically, these boundary conditions are based on the three aforementioned modes of heat transfer. For more detailed analysis, refer to[1-3].

3.5. Heat transfer between materials and thermal resistance

The casting consists of a number of materials in addition to the metal, e.g. sand mould, die, chills, cooling circuit etc. The contact between them is not ideal and can lead to a significant temperature drop across the interface due to the thermal resistance to heat transfer. This temperature change is attributed to what is known as the thermal contact resistance. The existence of a finite contact resistance is due principally to surface roughness effects. Contact spots are interspersed with gaps that are, in most cases air filled. The mechanism of heat transfer at the interface between materials can be due to conduction and/or convection in the material (usually air) located in the small gaps between the materials in contact, and radiative transfer across these gaps can also be significant if the temperature difference between the two materials is large. Since it is difficult to model all of these effects on the microscopic level, the overall resistance to heat transfer across the gap is usually accounted for by using an equivalent interface heat transfer coefficient (HTC) between the materials. This is illustrated in **Figure 3.1**.

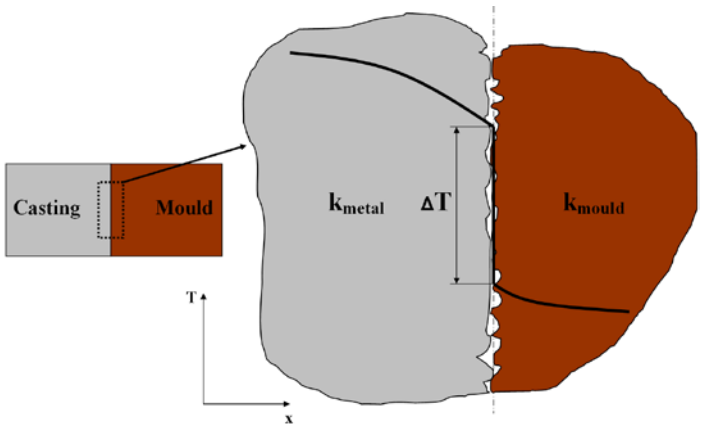

Figure 3.1: Temperature drop due to thermal contact resistance at the interface between the casting and mould. Figure inspired by Hattel[1].

As an example to how this contact resistance affects the heat transfer between two materials, consider the contact resistance between the casting and the mould. The total resistance to heat transfer between a location in the metal and a location in the mould is given by[1]

$$R_{total} = \left[R_{conduction}^{metal} + R_{interface} + R_{conduction}^{mould}\right] = \left[\frac{d_{metal}}{k_{metal}} + \frac{1}{h_{interface}} + \frac{d_{mould}}{k_{mould}}\right] \qquad (3.11)$$

Where $h_{interface}$ is the interface heat transfer coefficient, d_{metal} and d_{mould} are distances in the metal and the mould away from the interface, and k_{metal} and k_{mould} are the thermal conductivities of the metal and the mould, as illustrated in **Figure 3.1**.

3.6. Solidification and feeding of castings

During cooling and solidification in the mold most metals and alloys undergo volumetric changes, i.e. they shrink. The combined effect of metal shrinkage and mold behavior during casting solidification dictates casting soundness. Improper management of heat flow may result in casting defects such as cold shuts or shrinkage defects. These defects are responsible for considerable financial loss in the metal casting industry.

3.6.1. Metal shrinkage

It is convenient to distinguish four different types of volume changes: liquid contraction, solidification, solid contraction and solid state transformations, **Figure 3.2**.

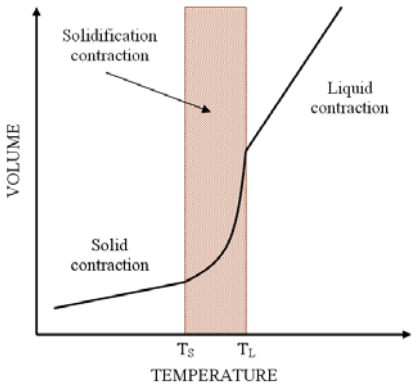

Figure 3.2: The solidification and cooling processes of an alloy.

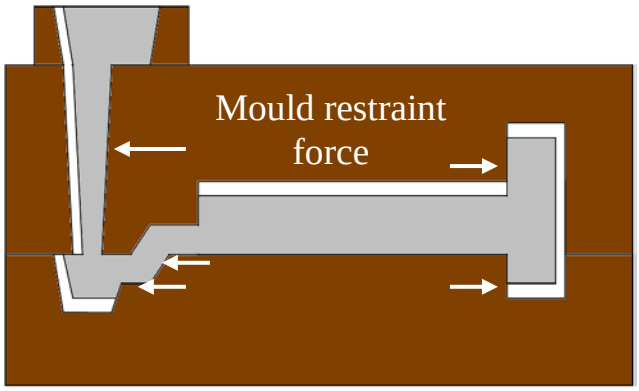

Figure 3.3: Casting constraint. Arrows indicate points where free volumetric contraction of the casting is not permitted[4].

1. *Liquid contraction*

The contraction occurring from the pouring temperature to the liquidus temperature is rarely a problem in casting. As long as the liquid level of the ingate system is above the level of the casting, the liquid contraction within the latter will be easily compensated.

2. Solidification shrinkage

As the liquid metal cools down and reaches the liquidus temperature, it starts to solidify. This means that the randomly distributed atoms of the liquid start to arrange themselves according to well-defined patterns, so-called crystals. The formation of a solid crystal is always accompanied by a change in molar volume, for pure metals usually a decrease[5]. We therefore talk about solidification shrinkage. Some typical values for solidification shrinkage are given in **Table I**.

Table I. Overview of volumetric solidification contraction for various metal casting alloys.

Material	Volumetric solidification contraction, %	Material	Volumetric solidification contraction, %
carbon steel	2.5 to 3	Cu-30%Zn	4.5
1% carbon steel	4	Cu-10%Al	4
white iron	4 to5.5	aluminum	6.6
gray iron	-2.5 (expansion) to 1.6	Al-4.5%Cu	6.3
ductile iron	-4.5 (expansion) to 2.7	Al-12%Si	3.8
copper	4.9	magnesium	4.2
zinc	6.5		

It is seen that for graphitic cast iron expansion may occur during solidification. This is because the graphite formed during solidification has a lower density than the liquid from which it is formed. Gray and ductile iron expand during solidification because of graphite precipitation, and when poured in non - rigid green sand molds an additional 15% feed metal requirement above that needed to satisfy the calculated liquid and solidification shrinkage may be required. Solidification shrinkage can also be compensated through liquid feeding from the risers. However, since feeding channels may be interrupted during solidification before all parts of the casting are fully solid, local shrinkage cavities may occur.

3. Solid contraction

By solid contraction, also called patternmaker shrinkage, we mean the change in molar volume of a material when its temperature changes. In general it means that the molar volume decreases (and the density increases) as the temperature goes down. The amount of volume change is given by the coefficient of volumetric thermal expansion / contraction, β

$$\beta = \frac{\Delta V}{V_0} \cdot \frac{1}{\Delta T} \tag{3.12}$$

which in one dimension is related to the elongation according to:

$$\alpha = \frac{\Delta L}{L_0} \cdot \frac{1}{\Delta T} = \varepsilon^{th} \cdot \frac{1}{\Delta T} \tag{3.13}$$

The constant of proportionality α is called the coefficient of linear thermal expansion. In words α expresses how much relative deformation the body experiences when exposed to a temperature change of one degree if allowed to contract or expand freely[1]. If a body, e.g. a casting, is unrestrained and it will contract an equal amount (proportional to the temperature drop) uniformly in all three direction, then it applies that $\beta = 3\alpha$. The solid contraction is accommodated by allowing suitable corrections to the dimensions of the pattern used for making the mold. It is apparent that because of liquid and solidification shrinkage a mass deficit may result in certain regions of the casting. This mass deficit translates into shrinkage cavities that may cause rejection of the castings. Therefore, it is important to understand and control the feeding of all regions of mass deficit.

Linear (solid) contraction according to **Eq. 3.12** will, however, only act upon the parts of the casting which are unconstrained, i.e. allowed to shrink freely. In many cases the mould or the casting itself will prevent this, see **Figure 3.3**. The result will be a gradual build-up of internal stresses, resulting in plastic deformation, cold cracking or residual stress. More on this topic will be given in section 3.7.3.

4. Solid state transformations

At certain temperatures, the atoms of some solid structures tend to rearrange themselves in order to decrease their energy. These solid state transformations have a great impact in many ways; e.g. volume changes, residual stresses and change of mechanical properties and are therefore very important to understand and also to control. The controlling parameters are mainly composition and cooling rate. More on this topic can be found in devoted literature.

3.6.2. Feeding – the five mechanisms

By feeding, one usually means that liquid metal should be supplied and transported to areas in the casting suffering from a lack of material due to the solidification shrinkage. Campbell distinguishes between five different feeding mechanisms, some of them involving solid material and acting during different stages of the solidification process. The feeding mechanisms are summarized in **Figure 3.4** as suggested by Campbell[4], for alloys with a freezing range.

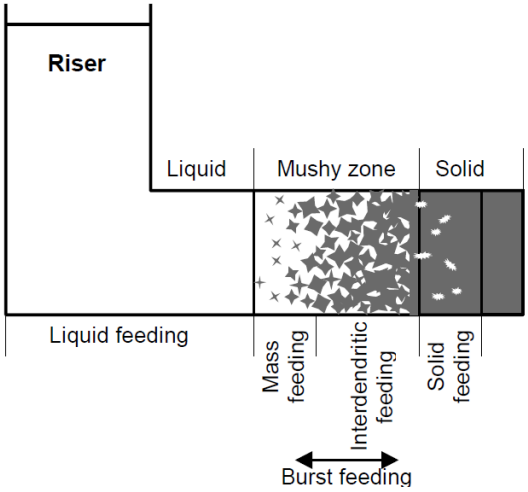

Figure 3.4: Schematic representation of the five feeding mechanisms[6].

In order to analyze the feeding, the so-called feeding velocity, V_f, is introduced and it is defined as the average velocity of the mass moving to fill the mass deficit. It can be expressed as $V_f = f_L V_L + f_S V_S$, where V_S and V_L are the velocity of the solid and liquid, respectively.

During *liquid feeding*, which is the most "open" feeding mechanism and generally occurs before the beginning of solidification, $f_S = 0$ and thus $V_f = V_L$. Inadequate liquid feeding is often seen to occur when the feeder has inadequate volume. Thus liquid flow from the feeder terminates early and subsequently only air is drawn into the casting.

When solidification starts, solid particles (grains) form in the liquid. As long as these particles are not in contact with one another, that is when $f_S < f_S^{cr}$, it may be assumed that the solid moves with the liquid ($V_S = V_L$), and the metal behaves like a slurry (semi-solid). Its relative viscosity is increased (fluidity is decreased). Because of this increased viscosity, during *mass* (semisolid) *feeding*, the flow velocity (of the slurry) decreases to $V_f < V_L$. This movement of the slurry is arrested when the volume fraction of solid reaches anywhere between 50 and 100%, depending on the pressure differential driving the flow, and depending on what percentage of dendrites are free from points of attachment to the wall of the casting.

As solidification proceeds, dendrite coherency (i.e. a rigid network of contiguous dendrites) will occur when $f_S < f_S^{cr}$, and a fixed solid network will form. Then, since $V_S = 0$, the feeding velocity

becomes $V_f = f_L \cdot V_L$, meaning a further decrease in feeding. Only *interdendritic feeding* is possible at this point.

If a part of the casting is cut off from feeding possibilities by a solid barrier, the hydrostatic tension in the remaining liquid of this region will increase dramatically. At a certain amount of tension, the solid barrier may burst, letting metal into the formerly cut off region. This is called *burst feeding*. Burst feeding is very hard to predict since it depends upon the relation between the amount of hydrostatic tension and the strength of the solid barrier, quantities which are difficult to estimate. Nevertheless, it is important to know that it may occur.

Solid feeding is related to burst feeding in a way that the gradual build-up of hydrostatic tension in an isolated liquid region deforms the surrounding solid shell inwards. The solid shell does not, however, burst but compensates the solidification shrinkage by decreasing the size of the entire casting, i.e. the surrounding solidified shell is being sucked inwards by plastic or creep flow[4]. This inward flow of the solid relieves the internal tension, like any other feeding mechanism. For effective feeding to occur during solidification four main requirements must be satisfied. They also must be fulfilled independently; if one is neglected, no matter how carefully the feeding system is designed in other respects, the result will be an unsound casting:

- a feeding source (riser) that solidifies after the region to be fed must be available- heat transfer requirement;
- sufficient liquid must be available to feed the shrinkage- volume requirement;
- unrestricted feeding channels (path of flow from the feeder to the shrinkage);
- sufficient pressure on the liquid to make it flow toward the shrinkage region.

These four feeding requirements will be briefly discussed in the next section.

3.6.3. Feeding requirements

It has already been mentioned that most of the commercial ferrous and non-ferrous cast alloys experience volumetric shrinkage during solidification. Additional volume reduction occurs during cooling of the liquid metal after pouring. These contractions will create internal unsoundness, i.e. porosity unless a riser of liquid metal reservoir provides liquid feed metal until the end of the solidification process. The riser also serves as a heat reservoir, creating a temperature gradient that induces directional solidification. Without directional solidification, liquid metal in the casting may be cut off from the riser, resulting in the development of internal porosity **[ref. Papers II, III, (Kotas et al. 2010)]**.

- **Heat transfer requirement**

To be effective, a riser should continue to feed liquid metal to the casting until the casting has completely solidified. Thus, the riser must have a longer solidification time than the casting. Since the critical factor affecting solidification time is heat loss, minimizing heat loss from the riser is an important consideration. It has been shown that the solidification time of any solidifying body is controlled by its ratio (volume)/ (cooling surface area), known as its modulus, *m*, i.e. Chvorinov's rule. Thus the problem of ensuring that the feeder has a longer solidification time than that of the casting is simply to ensure that the feeder modulus m_f is larger than the casting modulus m_c. To allow a factor of safety, particularly in view of the potential for errors of nearly 20 per cent when converting from modulus to freezing time, it is normal to increase the freezing time of the feeder by 20 per cent, i.e. by a factor of 1.2. Thus the heat-transfer condition becomes simply[7, 8]

$$M_f > 1.2 * M_c \tag{3.14}$$

A sphere represents the maximum volume-to-surface-area ratio and therefore freezes at the slowest rate according to Chorinov's rule. However, spherical risers present molding problems. A cylinder with a height, *H*, equal to its diameter, *D*, is the typically recommended riser geometry, since it is a simple, easily moldable shape having a high volume to surface-area ratio. The modulus of a feeder can be artificially increased by the use of an insulating or exothermic sleeve. It can be further increased by an insulating or exothermic powder applied to its open top surface after casting.

- **Mass-transfer (volume) requirement**

At first sight it may seem surprising that when the first requirement is satisfied then the volume requirement is not automatically satisfied also. However, this is definitely not the case. Although a feeder may have been provided of such a size that it theoretically would contain liquid until after the casting is solid, in fact it may still be too small to deliver the volume of feed liquid that the casting demands. Thus it will be prematurely sucked dry, and the resulting shrinkage cavity will extend into the casting. **Figure 3.5** illustrates that normal feeders are relatively inefficient in the amount of feed metal that they are able to provide[9].

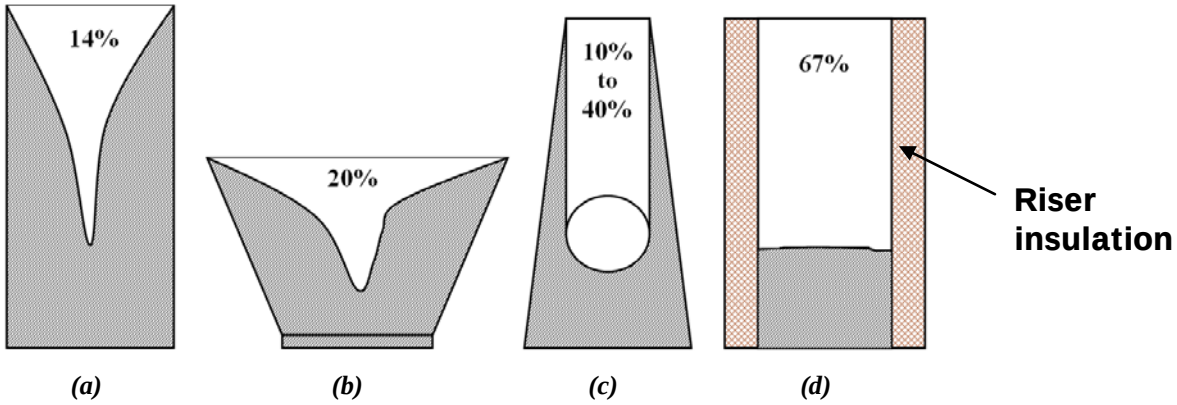

Figure 3.5: Metal utilization of feeders of various forms molded in sand. The numbers represent fed volume in percent of total volume, Figure adapted from Beeley[9].

This is because they are themselves freezing at the same time as the casting, depleting the liquid reserves of the reservoir. Effectively, the feeder has to feed both itself and the casting. We can allow for this in the following way. If we denote the efficiency ε of the feeder as the ratio (volume of available feed metal) / (volume of feeder, V_f,) then the volume of feed metal is, of course, $\varepsilon * V_f$. If the solidification shrinkage of the liquid is β during freezing, then the feed demand from both the feeder and casting together is $\beta (V_f.V_c)$, and hence:

$$\varepsilon \cdot \mathrm{V_f} = \beta \cdot \left(V_f + V_c\right) \tag{3.15}$$

Solving for the riser volume yields

$$\mathrm{V_f} = \frac{\beta \cdot V_c}{\left(\varepsilon - \beta\right)} \tag{3.16}$$

It follows that the smaller solidification shrinkage of ferrous alloys reduces the feeder volume considerably. For graphitic cast irons the value reduces even further of course, becoming approximately zero in the region of 3.6 to 4.0 per cent carbon equivalent. Curiously, a feeder may still be required because of the difference in timing between feed demand and graphite expansion.

- **Feed path requirement**

The third requirement amounts to efficient feeding channels. The efficiency of the feeding channels is affected by the type of alloy as well as by the geometry of the casting. The type of alloy influences the width of the mushy zone (the solidification interval). Wide mushy zone alloys (T_L -T_S > 110°C) that solidify typically with equiaxed grains, rely heavily on semisolid and interdendritic feeding. Thus their feeding velocity is small and significant difficulties are experienced in feeding the numerous tortuous channels. The resistance to flow is relatively high. Alloys with narrow mushy zone (T_L -T_S < 50°C), that exhibit columnar structure, rely mostly on liquid feeding, and therefore their feeding velocity is high. They are called *skin forming alloys*.
It is easy to appreciate that in normal conditions it is to be expected that there will be a limit to how far feed liquid can be provided along a flow path. Up to this distance from the feeder the casting will

be sound. Beyond this distance the casting will be expected to exhibit porosity. Hence, the feeding distance determines the number of risers needed. The feeding distance is always measured from the edge of the riser to the furthest point in the casting section to be fed by that riser. The feeding distance depends in part on the temperature gradient, which is the change in the temperature per unit length during solidification. **Figure 3.6** illustrates how a steep temperature gradient facilitates the feeding of a casting[6]. The shape of the solid skin surrounding the liquid metal varies with the steepness of the temperature gradient during freezing. When there is no, or very shallow temperature gradient parallel solidification fronts will move from the mold wall to the center of the casting, **Figure 3.6(a)**. The flow of liquid metal is gradually restricted, because liquid feeding is gradually replaced by interdendritic feeding. Eventually the feeding channel will be closed and porosity, known as dispersed centerline shrinkage, will occur between the dendrites. In the case of a solidifying wedge (**Figure 3.6(b)**); a steep temperature gradient from the center to the edge of the casting exists. Steep gradients provide open, more accessible feeding passages and liquid feeding is possible until the end of solidification, see **Papers II** and **III** in the supplements of this work. There exists a critical tapering angle for the liquid pool feeding the solidification shrinkage. For liquid pool angles smaller than this critical angle, centerline shrinkage will form in the isolated pools of liquid that are cut off from the feeding path[10]. The feeding distance also depends on the cooling rate of the steel during solidification, and hence the section thickness[11, 12]. For large cooling/solidification rates (small section thicknesses), the feeding distance is smaller because the velocity at which the feed metal must flow to compensate for shrinkage is larger. Accompanying this larger feed metal velocity is an increased pressure drop along the feed path, which in turn promotes the formation of porosity[13]. Since both the temperature gradient and the cooling rate are influenced by factors such as the section geometry, pouring conditions, steel type and molding material, the feeding distance will vary with all of these parameters.

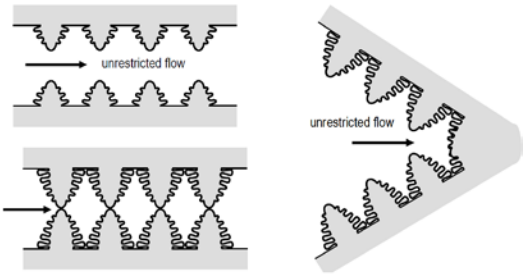

(a) parallel solidification fronts ***(b) converging solidification fronts***

Figure 3.6: Plate- and wedge-type solidification[6]

There are two terms that are important to understand when considering feeding distances: *riser zone* and *end zone*. Consider now the case of the L-shaped casting presented in **Figure 3.7**.

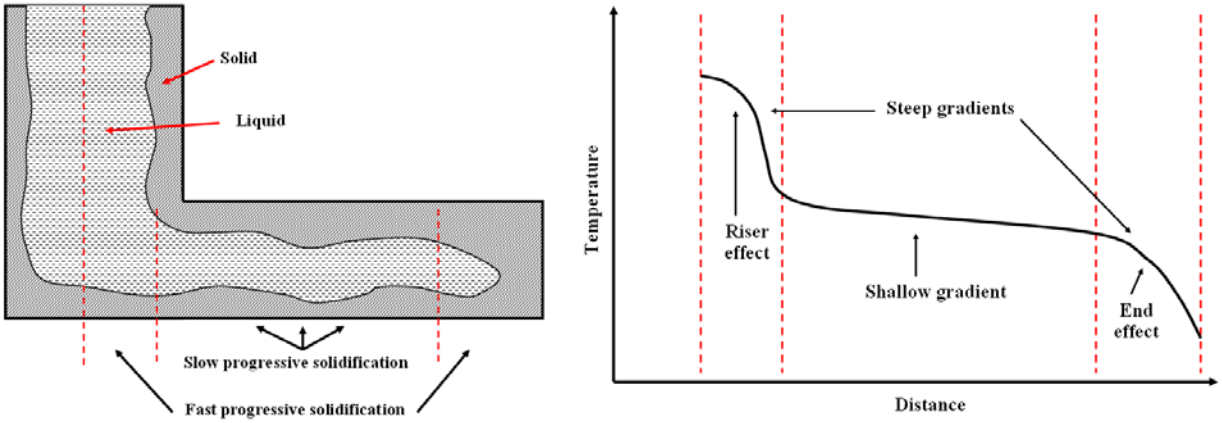

Figure 3.7: Directional (progressive) solidification in an L - shaped casting resulting from increasing temperature gradient from the extremity of the casting to the riser. Figure inspired by Stefanescu[6].

Since the riser remains hotter than the casting section to be fed, it provides a temperature gradient that facilitates feeding. The length over which this *riser effect* acts to prevent shrinkage porosity is called the *riser zone length, (RZL)*. The cooling effect of the mold at the end of a casting section also provides a temperature gradient along the length of the casting section to be fed. This is called the *end effect*, and it produces a sound casting over the so-called *end zone length*[14], *(EZL)*. The feeding distances are functions of RZL and EZL. In the long, horizontal part of the casting, parallel solidification fronts due to shallow gradients converge toward the center of the plate, and center-line dispersed shrinkage is to be expected, the grey area in **Figure 3.8**. This is why criteria attempting to predict the position of centerline shrinkage include the thermal gradient in their formulation.

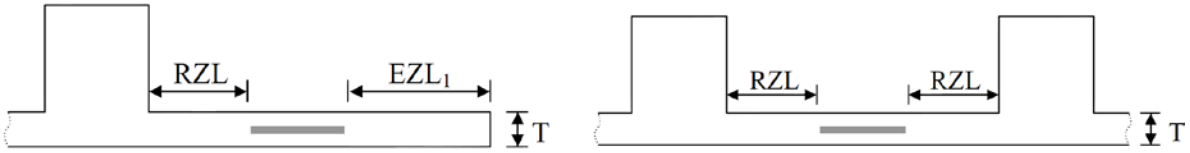

(a) ***(b)***

Figure 3.8: Top-risered plate (a) with end effect and (b) with lateral feeding. The plate is sound if (a) the riser zone and the end zone extending from the right edge of the casting section are tangent or overlap and (b) if the riser zones are tangent or overlap. The plate has centerline shrinkage between these zones if they do not meet[14].

Nowadays, numerical simulation tools are heavily utilized in predicting the effect of a casting design on the solidification behavior of the casting with subsequent analysis of the casting defects which are directly coupled to the solidification pattern. **Figure 3.9** is an example of how the geometry used in **Figures 3.7** and **3.8** affect thermal gradients and subsequent formation of centerline porosity inside the casting. **Figure 3.9(a)** implies that the whole horizontal section, especially its central region does not undergo directional solidification. The end zone is very short, leaving the major part of the casting with very shallow thermal gradients. Eventually the residual liquid will be cut off from the primary feeding path from the riser and centerline porosity will form which is seen in the same figure (b and c).

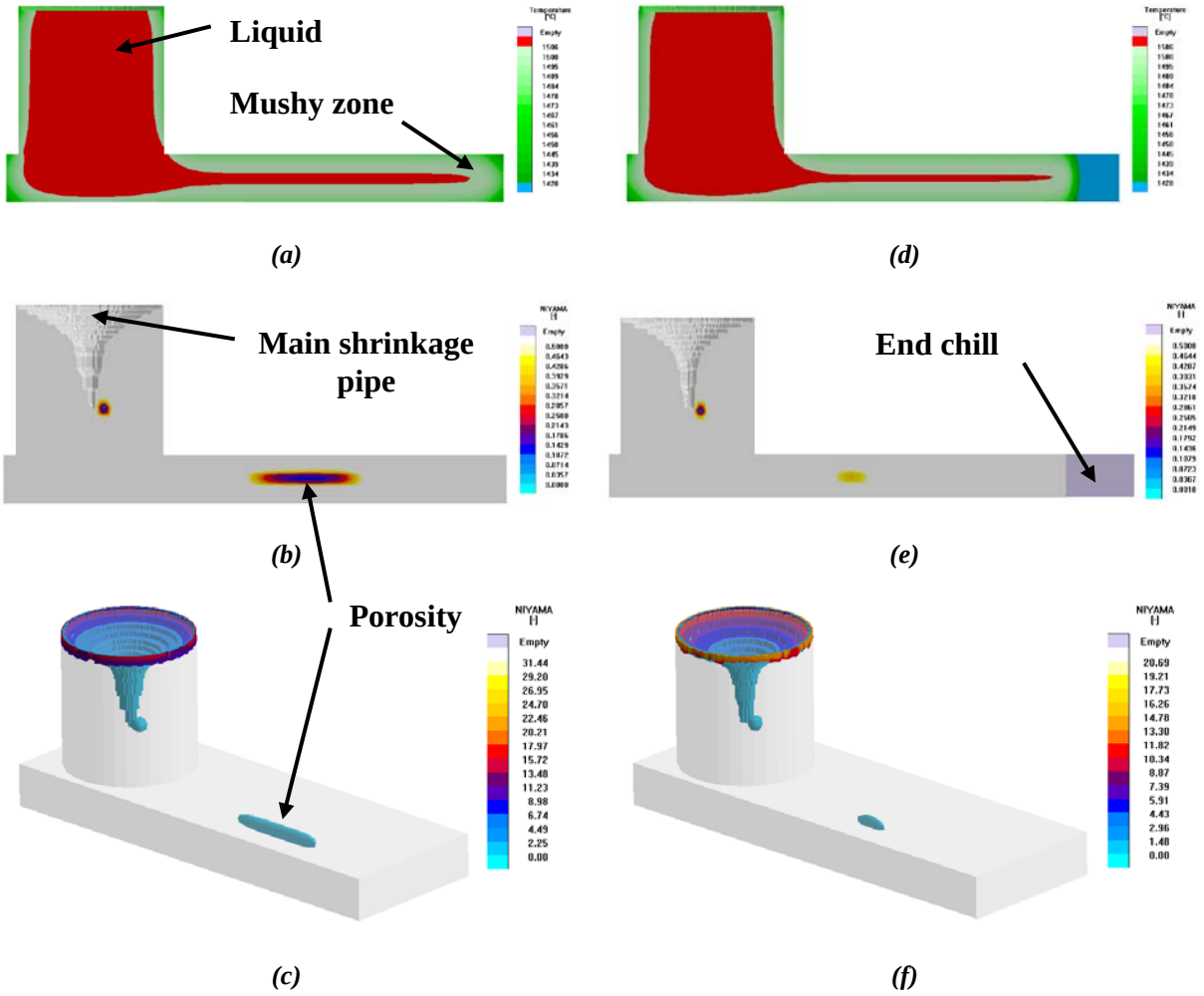

Figure 3.9: Numerical simulation of a solidification pattern and its effect on the defect distribution, (a-c) no chill, (d-f) with the end chill, (Kotas 2010).

Sometimes methods are used to increase feeding distances. *End chills* create an additional temperature gradient and enhance the end zone length (and thus the feeding distance), but have no effect on the riser zone length. The benefits of the end chill are shown in **Figure 3.9 (d-f)**. Obviously the end chill enhances the cooling effect and increases the end zone length. Due to that steeper thermal gradients will be induced in the central plate region, establishing directional and progressive solidification and hence minimizing the extent of the porous region, **Figure 3.9 (e and f)**. In order to fully avoid the porous region, more adjustments would have to take place. For instance, the plate should be tapered towards the riser, the riser should be shifted to the right or chilling would have to be intensified. The lateral feeding distance can be enhanced by the use of *drag chills*. A drag chill does not increase the riser zone length, but rather it causes a temperature gradient that essentially creates an end effect between the risers. An open feed path is also promoted by a *taper*, where the section thickness continually increases toward the riser. In fact, a sufficiently large taper can result in an infinitely long feeding distance.

The above concept is well described and documented in the work by Kotas et al**.** [**ref. paper II** and **III**]. **Figure 3.10** highlights the effect of the solidification pattern on feeding efficiency of the top riser. Due to inadequate external cooling from the chills in **Figure 3.10a**, very shallow thermal gradients were induced along the cylindrical section. The parallel solidification fronts gradually restricted the flow of liquid to the lower sections, causing the complete isolation of the residual liquid, **Figure 3.10(b)** which eventually transformed into shrinkage porosity, **Figure 3.10(c)**.

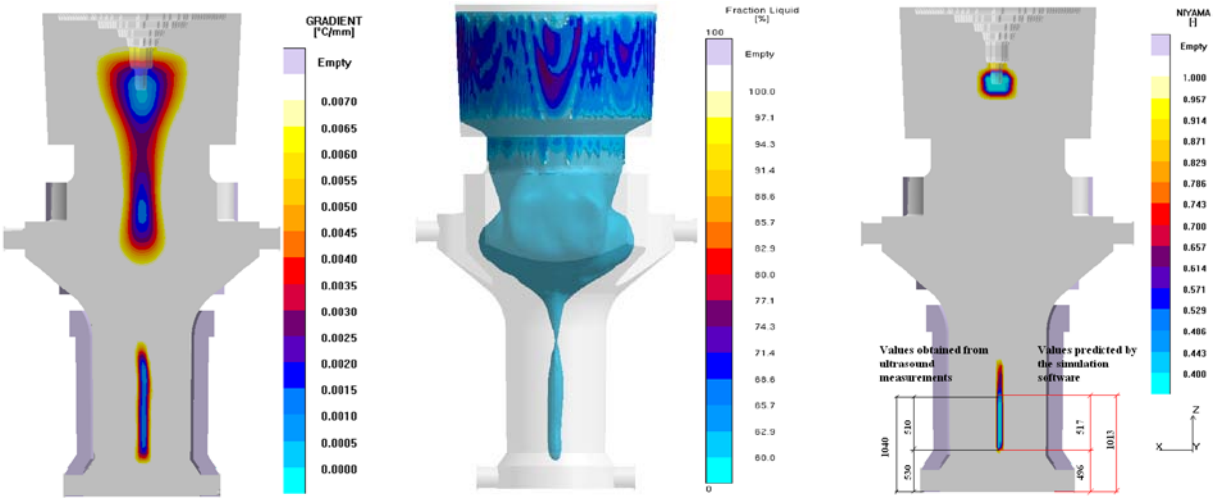

(a) *(b)* *(c)*

Figure 3.10: Negative effect of the solidification pattern on thermal gradients leading to porosity formation in the casting, [ref. Paper II, (Kotas et al. 2010)].

On the contrary, when adequate cooling is established due to the new chills around the cylindrical section, directional and progressive solidification towards the thermal axis and the riser is evoked, **Figure 3.11**. It means that the solidifying front progresses towards upper areas in a V-shape pattern which is desirable mainly with respect to the elimination of multiple casting defects- this will be dealt with in detail in the section devoted to casting defects.

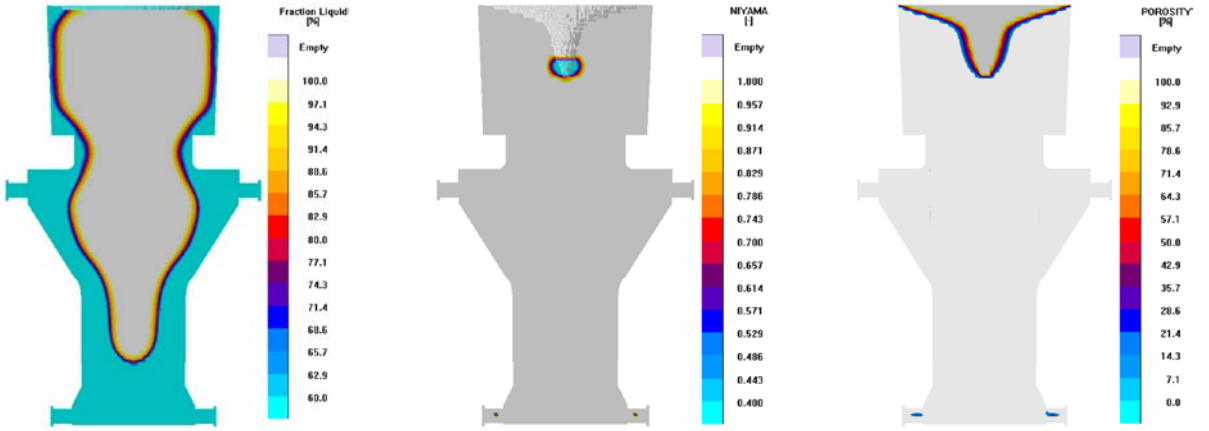

(a) *(b)* *(c)*

Figure 3.11: The effect of the intense cooling on the solidification pattern, on thermal gradients and on porosity elimination in the casting, [ref. Paper II, (Kotas et al. 2010)].

- **Pressure gradient requirement**

Although all of the previous feeding rules may be met, including the provision of feed liquid and a suitable flow path, if the pressure gradient needed to cause the liquid to flow along the path is not available, then the feed liquid will not flow to where it is needed. Internal porosity may therefore occur. A fluid flowing down a channel will experience various resistances against its motion. For a feeding liquid the important resistances will be offered by friction against the mould walls, the viscosity of the liquid itself and gravitational forces. The force which has to overcome all these resistances is the metallostatic pressure. The friction against the mould wall is usually low as long as no solid is formed. When the solid phase starts to grow, the feeding path narrows down and the pressure gradient increases. The feeding is now very much dependent on whether the alloy solidifies in a eutectic or a dendritic mode. Eutectic growth is accompanied by smooth walls of the flow channel while dendritic growth exhibits a rugged surface with great resistance to fluid flow.

The viscosity of the liquid is mostly dependent on the presence of equiaxed grains. At pouring, the viscosity corresponds to that of water but as the content of the solid phase increases it becomes more like porridge or paste. For both dendritic and eutectic alloys the amount of equiaxed grains depends on the temperature gradient in such a way that a flat gradient promotes equiaxed growth. This explains why permanent mould castings are easier to feed.

The gravitational force constrains the feeding system design in a way that a feeder can never feed a higher located part of the casting, unless the feeding system is pressurized in some way. The feeder should therefore be positioned well above the casting regions it should feed. It is also very important to preserve the atmospheric pressure inside the feeder when the liquid level starts to sink. Both of these conditions are fulfilled by an *open riser*, see **Figures 3.9-3.11**. This type of a riser is usually placed at the top or the side of a casting with its upper surface open to atmosphere. A valuable feature of such risers is their function in venting the mould cavity during pouring. The principal disadvantage of an open riser is the heat loss to atmosphere by radiation: in the absence of insulation the exposed surface is susceptible to premature freezing, with corresponding loss in feeding efficiency[9]. A type of the riser which is not in contact with the upper mould surface is referred to as a *blind riser*. These blind risers will be ineffective unless placed in such a position that metallostatic pressure is available for feeding. Blind risers required for the feeding of sections at lower levels are usually modified to exploit the atmospheric effect for feeding, the so-called *atmospheric blind riser*. This can be done by using an atmospheric vent, a type of a porous core[7]. The general arrangement of such a head is shown in **Figure 3.12**.

After casting, a solidified shell of metal forms round the periphery of the entire mould cavity, the gating system having become sealed off due to its relatively small cross-section area. As the remaining liquid continues to contract and a partial vacuum is created, the solid envelope will puncture at its weakest point which, due to the slow rate of freezing at re-entrant angles in the casting surface, is at the end of the puncture core. Atmospheric pressure is thus brought to act on the liquid, creating the conditions for feeding to an appreciable height. Even though Beeley in his book[9] points out that "atmospheric blind risers can feed to a height considerable greater than that of the head itself where gravity is opposed to feeding", after talking to quite a few foundry men, the general conviction is that atmospheric blind risers can feed well to approximately 2/3 of their height- if they are well "ventilated". Some foundry engineers even follow a theory; always try to rearrange your casting so that blind risers can be avoided. If an atmospheric vent is not used, this could have dramatic consequences in some casting geometries. When a solid shell has formed, the pressure inside the feeder will significantly decrease. If at the same time, there is contact between liquid and the sand mould in some part of the casting which is to be fed; it could lead to a situation where the feeder is fed from the casting.

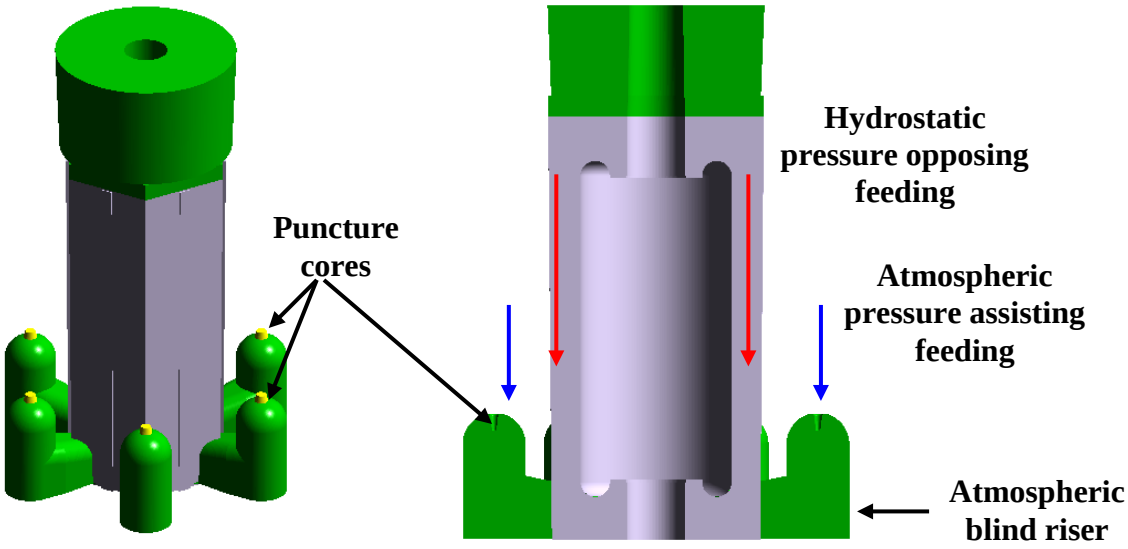

Figure 3.12: The principle of atmospheric blind risers used in steel castings, (Kotas, 2010).

The casting in **Figure 3.12** is an additional example from industry how improper rigging and casting arrangement can lead to an improper, i.e. non-directional, solidification pattern, induce low pressure and thermal gradients and hence promote solidification related defects, i.e. centerline porosity. Due to the inability of the top riser to feed the entire height of the casting and due to missing chills that would split the feeding zone, progressive solidification could not have been established and thus solidification propagated only from the casting walls inwards eventually choking off small liquid pools almost over the entire height of the casting. These isolated pools did not have a chance to compensate for the volumetric shrinkage during the temperature drop which resulted in centerline shrinkage in the problematic area, see **Figure 3.13**. A remedy, which is seen in a work by Kotas, is an addition of new chills to divide the feed zones into smaller regions to increase the efficiency of the risers, and addition of a second row of atmospheric blind risers.

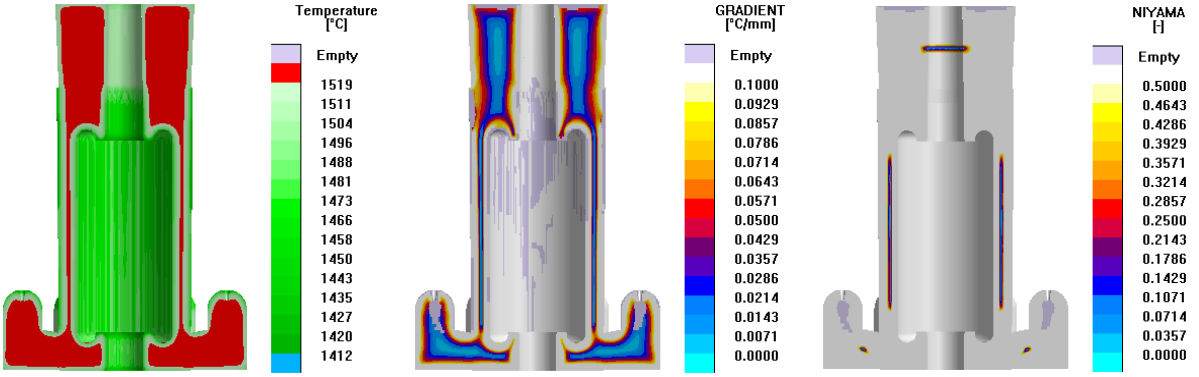

Figure 3.13: (left) Temperature distribution in the steel crusher roll shell, causing shallow thermal gradients in the vertical section (middle), and centerline porosity as a consequence (right), (Kotas, 2010).

An alternative to the casting arrangement in **Figure 3.12** could be the one in **Figure 3.14**. In this way, one could replace the blind risers only with open risers. However, the casting yield would decrease substantially and machining costs would increase.

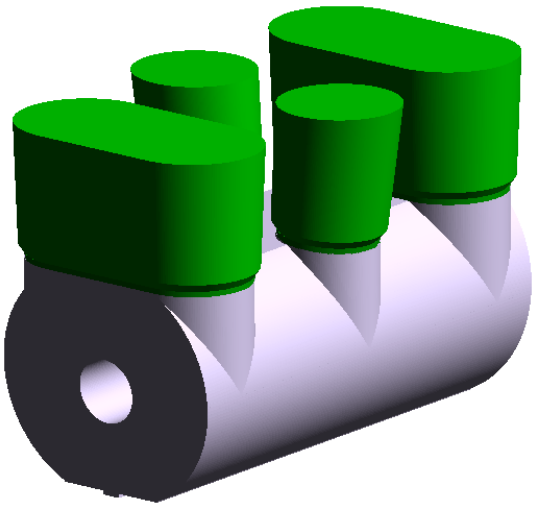

Figure 3.14: An alternative solution if blind risers should be avoided. However, the casting yield will get substantially increased, (Kotas, 2010).

3.6.4. Risering procedure

It must be emphasized that this section was highly inspired by a brochure "*Feeding & Risering Guidelines for Steel Castings*" of the Steel Founders' Society America[14].

The risering of steel castings should proceed in a systematic manner. The first step is to represent the casting as a collection of simple, plate-like sections. Representing the casting with simply shaped sections allows for the calculation of the solidification modulus, i.e. Chvorinov's rule (volume-to surface-area ratio) for each casting section. Although, Chvorinov's rule can be applied not only to plate-like sections, but also to cylinders and spheres. As already mentioned**,** the larger the solidification modulus, the longer the solidification time. If a casting section has a larger modulus than all of the surrounding casting sections, it will still be solidifying after the surrounding sections are completely solidified. The last region to solidify in such a casting section is termed a *hot spot*. Once the hot spots in a casting are identified, a riser must be placed adjacent to each hot spot. This ensures that feed metal will be available to feed each hot spot until solidification is complete.

The reason that the collection of simple sections used to represent the casting should be plate-like is that the risering rules presented in this manual were developed for simple, plate-like shapes. Thus, it is necessary to use such shapes in order to apply these rules. Once this has been accomplished, the edges of each casting section with and without the benefit of end effect must be identified. The feeding distance between a riser and an edge without end effect should be calculated as a lateral feeding distance (LFD), instead of as a regular feeding distance (FD).

Once the casting has been represented with a collection of plate-like shapes, the feeding zones of the casting must be identified. A *feeding zone* is a solidifying region of the casting that solidifies in such a manner that it must be risered separately from the rest of the casting (a region containing a hot spot is an example of a feeding zone). A feeding zone may require more than one riser to feed it, depending on the feeding distances involved. Feeding zones can be identified by their solidification moduli (V/A ratio). Sections with the smallest solidification moduli will solidify first, and might therefore divide the casting into distinct feeding zones. Sections having larger moduli will require feed metal until the end of solidification. Risers must be added to such sections to prevent shrinkage during the final stages of solidification. Feeding zones for simple castings might be the simple, plate-like parts that make up a casting. This is not always trivial for complex castings.

Once the feeding zones have been identified, a *feeding path* must be determined for each feeding zone. Regions of the casting where sufficient taper and directional solidification exist must be identified. Such regions need not be considered in determining the feeding distance.

Also, for such cases, there is no end effect in determining the feeding distance. The principle of directional solidification should be considered in placing the riser. The feeding path should be identified so that it proceeds from the first region in the feeding zone to solidify to the last region to solidify. The riser should be placed at the last position along the feeding path to solidify. Ingates should be placed so that the metal enters below top risers, and always through side risers.

The final step prior to calculating feeding distances and riser sizes for each feeding zone is to define the feeding dimensions. The feeding dimensions of the section to be fed are the length L, width W, and section thickness T. Two examples of a section with L, W, and T indicated are shown in **Figure 3.15**. As shown in this figure, a feeding zone and a feeding path must be identified in order to assign risering dimensions.

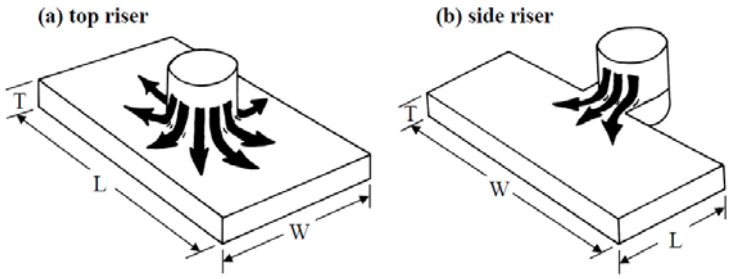

Figure 3.15: Dimensions for casting sections fed by (a) a top riser, and (b) a side riser (adapted from [15]).

To summarize, the recommended procedure for risering steel castings is[14]:

(a) Representation of the casting as a collection of simple, plate-like shapes

- **locate hot spots, and place a riser on each one**
- **for each plate-like shape, determine edges with and without end effect**

(b) Determination of feeding zones, feeding paths and feeding dimensions

(c) Determination of feeding distances

(d) Determination of riser sizes

Obviously, this procedure is to be followed when designing an initial casting and risering layout. All of these aforementioned steps should be considered and respected regardless of the circumstances, as they have been thoroughly analyzed and verified by many foundry-oriented researchers over the years, and successfully applied by thousands of foundry engineers world-wide. They are not just some rules of thumb.

Today's generation of foundry engineers has been very fortunate in that numerical casting simulation tools, which are based on various complex physical models, are readily available to assist and help during a design stage. For those who are familiar with numerical casting simulations, there is no need to manually split the casting into simple shapes and calculate solidification times for each of them whatsoever, since the numerical tool does it for them in a few minutes. Afterwards, it is very simple to thoroughly investigate a thermal behavior of a given casting in a search for potentially critical areas above which a riser(s) or a chill(s) should be placed. It is also feasible to evaluate the feeding efficiency of separate risers meaning, how far and for how long they are able to supply the necessary hot melt to compensate for volumetric shrinkage. Moreover, information on subsequent defects occurrence, based on the thermal analysis, is also provided to users of any given numerical casting-devoted tool.

Last, when casting simulation and numerical optimization tools are coupled, the entire procedure for risering steel or any metal alloy-based castings can be fully automated. A potential outcome of such an automated procedure would be proposals for the most optimal riser shapes and their location, positioning of chills or insulation, which would yield a totally sound cast part. The truth is, that a skilled and experienced foundry engineer, who knows the physics and understands all the complex and coupled physical phenomena behind the foundry processes, is still highly demanded to properly define and set up each project, but above all to be capable of interpreting and assessing the results and proposals provided by the numerical solver as to their applicability to real production.

3.7. Casting Defects

3.7.1. Introduction

Compared to forming processes, solidification of a melt can produce very complex shapes in a single operation, thus limiting the number of subsequent joining steps. However, this major advantage is offset in some cases by the formation of defects, which may prevent the use of castings for high integrity automotive parts, such as suspension arms, or aircraft components. Among those defects, porosity and hot tears are the most serious. They are both induced by a lack of feeding of the mushy zone[16], i.e. the zone where solid and liquid phases co-exist. Ultimately, these voids can initiate premature fractures or at least compromise mechanical properties significantly[17- 19].

In the case of porosity, the volume change is associated with solidification shrinkage. In most materials, the liquid is less dense than the solid. The difference in density in turn requires a flow from the liquid, through the mushy zone to the regions where final solidification takes place. The pressure decreases with distance into the mush, due to viscous losses, and if the pressure loss is large enough, a pore might nucleate and grow[20, 21]. This type of porosity is often referred to as shrinkage porosity because it occurs deep in the mushy zone and is primarily induced by the density difference.

Such pores become filled by gaseous elements that come out of the melt. Among those elements, hydrogen is the most important one in metallic alloys. Hydrogen becomes dissolved in the melt from the reaction between the melt and water either adsorbed at the surface of the mould or simply contained in the air, thus leading to the formation of oxides and hydrogen. Other gases are also important in some alloys. If the composition of such gaseous elements in the melt is high, voids can form fairly early in the mushy zone, and this is referred to as gas porosity. Although the pore morphology and the main mechanisms leading to their formation are quite different, both types of porosity are described using the same governing phenomena and equations[22].

In the case of hot tearing, the volume change is associated with strains in the partially coherent solid, which add to solidification shrinkage. These strains are induced by the contraction of the solid in a thermal gradient and are localized at the weakest parts of the mushy zone, the grain boundaries[22]. Although the equations governing both defects are similar, the topic of hot tearing is presented separately.

Another problem encountered in solidification processes is the inhomogenity of compositions at large scale, known as macrosegregation[23]. Indeed, such defects cannot be eliminated after solidification since they involve solute diffusion at long range and thus very long homogenization times (typically a few centuries for diffusion distance on the order of 10cm). Although the melt itself usually has a uniform composition, microsegregation at the scale of the microstructure induces local variations of the concentration. If the enriched or depleted liquid moves with respect to the solid, it leads to a final average composition that differs from the nominal one. Among the various sources of macrosegregation, four main mechanisms are generally distinguished: solidification shrinkage, natural or forced convection, grain sedimentation and deformation of the solid[22].

3.7.2. Porosity

The soundness of the casting depends on uninterrupted flow of liquid metal to the region that solidifies to feed the mass deficit resulting from solidification contraction. Failure to feed the mass deficit will produce shrinkage defects[24], referred to as porosity. There are many types of porosity and thus they cannot be all addressed in detail in this work, only the most severe, miscroporosity will be the subject of this chapter. For more detailed analysis of porosity see for example the books by Campbell[4] or Frederiksson[8]. Only a brief classification and definition will be given, see **Figure 3.16**. Shrinkage defects that are open to the atmosphere, also called shrinkage cavities are a consequence of metal contraction while cooling in liquid state and during solidification. This defect is a macro-scale defect that can be also termed *macroshrinkage*. The mass deficit produced by this shrinkage is compensated by atmospheric gasses, a process that is independent of the gas content of the metal and which does not require gas pores nucleation and growth. On the contrary, closed shrinkage defects

correlate well with pores nucleation and growth in the mushy zone or the amount of bifilms, and thus seem to depend on the impurity level and the amount of gas dissolved in the metal. They can be either *macroporosity* or *microshrinkage* (microporosity) defects[6]. In summary, shrinkage cavities are driven only by metal contraction (shrinkage flow) while shrinkage porosity is driven by both metal contraction and pore nucleation and growth or bifilms growth[22].

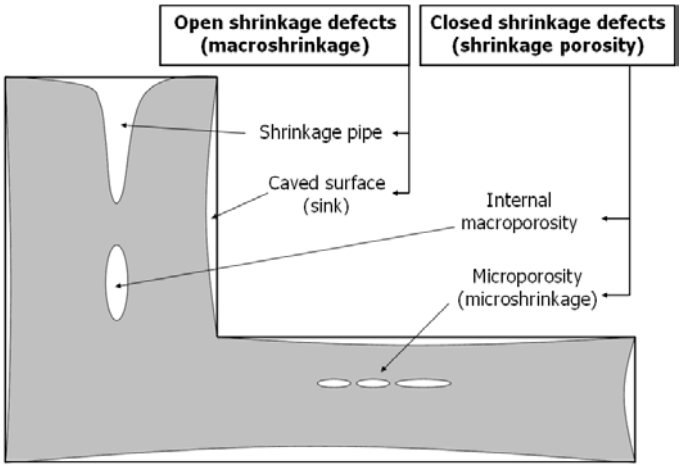

Figure 3.16: Definition and classification of shrinkage defects, adapted from Stefanescu[6].

From this analysis it is apparent that the accurate prediction of shrinkage cavity formation must be based on three-phase (liquid, solid, and gas) mass conservation, coupled with energy conservation. To include casting distortion, stress must be also modeled.

Microporosity, which will be discussed in this chapter, has a strong negative effect on mechanical properties, especially on ductility and fatigue life, because internal pores act as local stress concentrators and crack initiation sites. In many instances the appearance of the pore is not spherical but follows the dendrites shape. Both, the size and the shape of the microshrinkage are important. As the solidification time increases the secondary dendrite arm spacing increases[25, 26], and so does porosity. This trend is well captured in **Figure 3.17** for the case of an aluminum-based, i.e. AlSi9Cu3 alloy, high-pressure die cast part. In areas where the solidification time is the longest, the microstructure is the coarsest and the severity of microporosity is the largest. Obviously, the same trend could be seen in all castings regardless of a cast alloy and size.

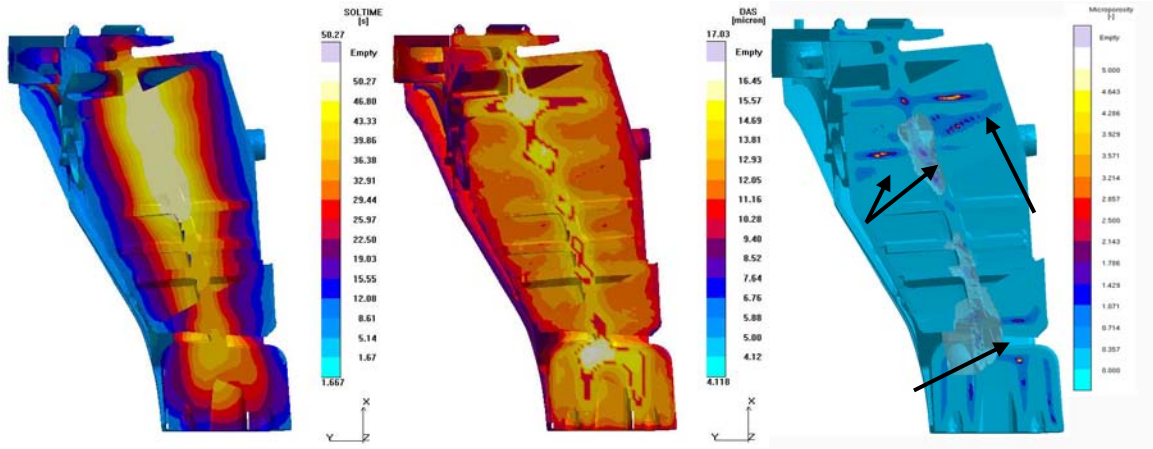

Figure 3.17: Left: Cut through the casting – solidification pattern indicating areas which solidify the last,. Middle: cut through the casting – SDAS distribution after the casting process, the coarsest microstructure is found in areas solidifying the last, Right: Microporosity is the most pronounced in areas solidifying the last- transparent and yellow areas signify the porous regions inside the casting, [ref. Paper I, (Kotas et al., 2009)].

In addition, the fatigue strength and ductility also decrease[27]. In well-degassed melts, microshrinkage takes the shape of the interdendritic liquid that remains just before eutectic solidification, see **Figure**

3.18, and the stress concentration factors resulting from these shapes are much higher than for spherical pores[6].

The present understanding of microporosity formation is that metal flows toward the region where shrinkage is occurring until the flow is blocked, either by solid metal or by a solid or gaseous inclusion. Recent numerical models assume that when a gas pore appears in the mushy zone during late solidification, after dendrite coherency, it is entrapped in the dendritic network. When the metal flow toward the solidification front is blocked, the pore becomes the starting point of microshrinkage. Thus, microshrinkage formation depends on the nucleation and growth of micro-pores[6]. This concept can be understood from the analysis of the local pressure which will be given later in this section.

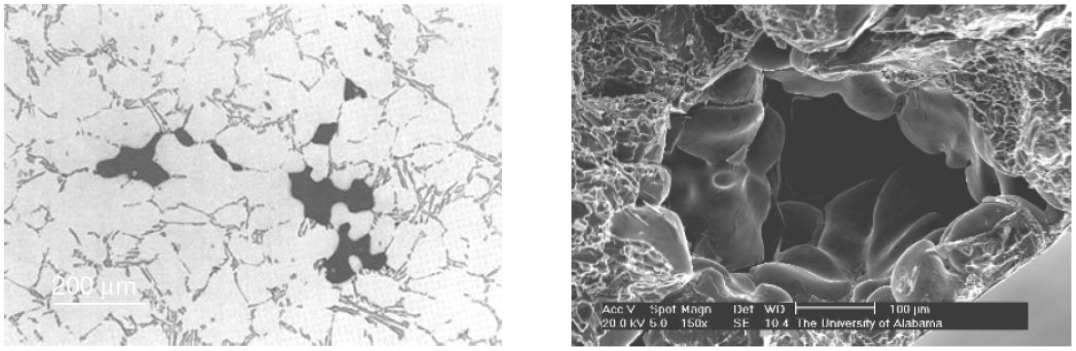

Figure 3.18: (a) Optical micrograph of interdendritic micro- shrinkage in Sb refined Al-Si alloy[6]. (b) SEM image; unmodified Al-Si alloy[6].

One could thus state that there are two main causes of microporosity in castings: *shrinkage porosity*, due to the volume change upon solidification combined with restricted feeding of liquid to the final solidification region; and *gas porosity*, due to the condensation of dissolved gases in the melt upon freezing, as a result of the difference in solubility of such gases in the liquid and solid phases. The two types of porosity manifest themselves in different ways: where they form in the mushy zone, their morphologies and the extent to which they interconnect are quite distinct. Dantzig and Rappaz[22] give a very nice description of both of the defects. They conclude that gas porosity forming early in the mushy zone, is associated with a certain gas precipitation and is nearly spherical because it grows in a fairly open dendritic network. In contrast to gas porosity, shrinkage porosity forms deep in the mushy zone in fairly large solidification interval alloys. It is induced primarily by the difficulty to provide shrinkage flow required by the final solidification of a solid phase that is denser than the interdendritic liquid.

Both types of porosity involve the nucleation and growth of pores, in one case due mainly to the evolution of dissolved gases, and in the other as a result of failure to feed solidification shrinkage. Although the two types each have different morphology, both can be described using the same set of governing equations to determine the pressure drop in the mushy zone associated with liquid feeding and the segregation of dissolved gases. These governing equations are based on the extended mass conservation equation, derived in chapter 2, i.e. **Eq. 2.3**, where a compressible phase is now present.

$$\frac{\partial \rho}{\partial t} + \nabla \cdot \rho u = 0 \tag{3.17}$$

The density rho is averaged over the various phases:

$$\rho = \rho_l g_l + \rho_s g_s + \rho_p g_p \tag{3.18}$$

Where g stands for volume fraction of the given phase and the subscript p refers to the pore. When the density of gaseous phases is neglected and the average mass flow is expressed (also neglecting the mass transport associated with the gaseous phase) as:

$$\rho u = \rho_l g_l u_l + \rho_s g_s u_s \tag{3.19}$$

the following expression is acquired:

$$\frac{\partial \rho_0}{\partial t} - \rho_l \frac{\partial g_p}{\partial t} + \nabla \cdot (\rho_l g_l u_l) + \nabla \cdot (\rho_s g_s u_s) = 0 \tag{3.20}$$

The first term on the left in **Eq. 3.20** represents the change in density due to the combined effects of solidification shrinkage and thermal contraction of the solid and liquid phases. This change in density must be compensated by three phenomena: void growth in the liquid (second term), inward flow of interdendritic liquid (third term) or compression of the solid phase (fourth term). If the solid phase is under a tensile load, arising for instance from external constraints, void growth and interdendritic flow must produce additional compensating volumes, which can lead to hot tears, as discussed in the dedicated section. Three cases are illustrated in **Figure 3.19**: the compensation of shrinkage by interdendritic flow in (a), void formation in (b) and the additional effect of tensile strains in (c).

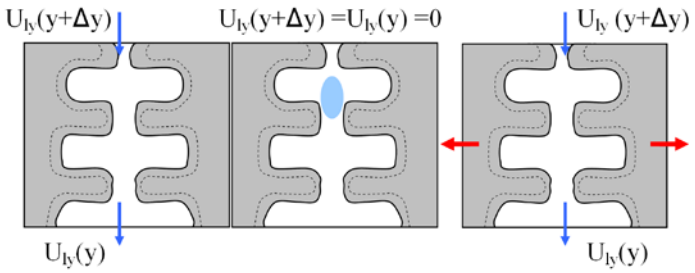

Figure 3.19: (a) solidification occurs between times t (dashed interface) and t + Δt (solid line) and is compensated by liquid flow along the y-axis. In (b), solidification shrinkage is compensated by pore growth alone. In (c), tensile strains on the dendrites perpendicular to the growth direction add to the solidification shrinkage to induce more flow. Figure adapted from[22].

In this chapter the focus is on porosity ignoring strains in the solid for now, to be taken up again in the section devoted to hot tearing. The mass conservation equation then reduces to

$$\frac{\partial \rho_0}{\partial t} - \rho_l \frac{\partial g_p}{\partial t} + \nabla \cdot (\rho_l g_l u_l) = 0 \tag{3.21}$$

There are two unknown fields in this equation, the pore fraction $g_p(x, t)$ and the velocity field $u_l(x, t)$. We treat only the case of fluid flow in the mushy zone without pore formation. The pore formation is not considered here, for more information on this topic, refer to Dantzig and Rappaz[22].

3.7.2.1. Flow through the mushy zone and pressure drop

The mushy zone is a region where solid and liquid phases coexist as a mixture. As long as the equiaxed dendrites are free to flow with the liquid, it may be assumed that the flow velocity is affected only by the change in viscosity. However, when dendrite coherency is reached and a fixed solid network is formed or if the dendrites are columnar, the flow will be considerably influenced by the morphology of the mushy zone. In most solidification models, the flow through the mushy zone is treated as flow through porous media and *Darcy's* law is used for its mathematical description. Darcy's law, **Eq. 3.22**, relates the velocity to pressure drop[13]:

$$u_l = -\frac{K}{\mu_l g_l} \frac{dP}{dx} \tag{3.22}$$

where u_l is the liquid velocity in the mushy zone (i.e., shrinkage velocity), g_l is the liquid volume fraction, μ_l is the dynamic viscosity of the interdendritic liquid, P is the melt pressure, and x is the spatial coordinate, as indicated in **Figure 3.20**, and K is the specific permeability of the mushy zone. Darcy's law is valid under the following assumptions[28]:

- Slow flow ($u_l \rightarrow 0$); this allows ignoring inertial effects
- Steady flow
- Uniform and constant volume fraction of liquid

- Negligible liquid-liquid interaction forces

3.7.2.2. Centerline porosity - The Niyama criterion

In modeling of casting processes, special criteria have been developed to indicate areas of the casting where particular problems, e.g. shrinkage, hot tears or mould erosion, can be expected. A very important part of the solidification analysis is the evaluation of the feeding efficiency. Several criterion functions have been suggested for that purpose. A criterion function based on only the temperature gradient for predicting centerline porosity was suggested by Pellini[29] as early as in 1953. Later on, in 1982, this criterion was improved by Niyama[30]. By comparing the results of solidification simulations and observations of centerline shrinkage problems in steel castings, Niyama and co-workers were able to relate the development of centerline shrinkage to the temperature gradient and the cooling rate, both of which are assessed at a specified temperature near the end of solidification, see **Eq. 3.23**.

$$Niyama = \frac{G}{\sqrt{\dot{T}}} \tag{3.23}$$

Shrinkage porosity predicted by the Niyama criterion usually forms in the mushy region at high solid fractions. At lower solid fractions, the pressure drop which governs this type of porosity is negligibly small. Therefore, in a casting simulation, the Niyama criterion is always evaluated at a temperature near the end of the solidification interval.

With the help of the Niyama criterion, it is feasible to predict the presence of centerline shrinkage porosity, i.e. micro- and macro-shrinkage in alloys with short freezing range such as steels, caused by shallow temperature gradients[11, 13, 31], see also **Figures 3.10** and **3.13**. It indicates that in regions that solidify quickly, there must be hot metal nearby to establish a high gradient to feed the shrinkage during solidification.

Although at first appearance, the Niyama criterion may appear to be a purely empirical relationship, it also has a physical interpretation. The model begins with Darcy's law, which relates the interdendritic feeding-flow velocity to the pressure drop across the mushy zone. Assuming that the liquid and solid densities (ρ_s and ρ_l) are constant during solidification, one can define the total solidification shrinkage, i.e. the coefficient of volumetric expansion/contraction as in **Eq. 3.12**, in terms of these densities as $\beta = (\rho_s - \rho_l)/\rho_l$. Using β to simplify the 1-D mass conservation equation and then integrating the result, it can be shown that the shrinkage velocity throughout the mushy zone is constant and can be expressed as $u_l = -\beta R$, where R is the constant isotherm velocity **(Figure 3.20)**. Niyama noted that the isotherm speed R is difficult to measure, whereas the cooling rate and the thermal gradient are relatively easy. He therefore replaced R and expressed it in terms of the temperature gradient, $G = dT/dx$, and the cooling rate, $\dot{T} = dT/dt$. The cooling rate mainly depends on the mould material and the air gap formed at the metal-mould interface, which affect the rate at which heat is extracted from the metal. The cooling rate during the time of solidification affects the grain size. The shrinkage velocity in the mushy zone can then be written as:

$$u_l = -\beta R = -\beta \frac{\dot{T}}{G} \tag{3.24}$$

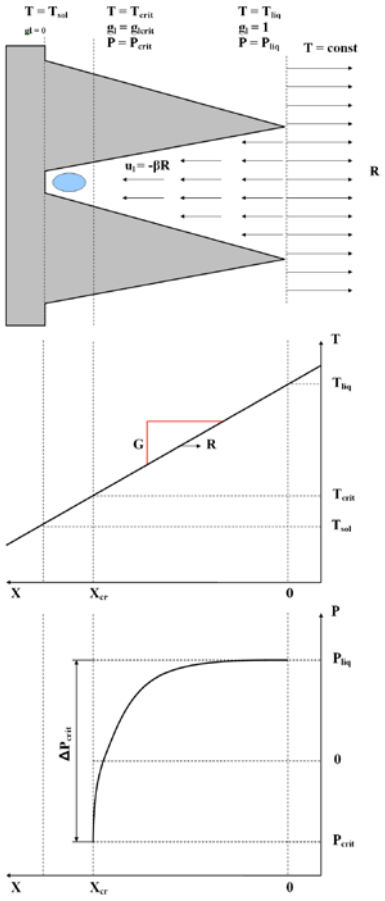

Figure 3.20: Schematic of a 1-D mushy zone solidifying with constant temperature gradient, G, and isotherm velocity, R. Figure adapted from Beckerman et. al.[13]

In words, the microscopic velocity of the fluid in the mushy zone is uniform under steady state conditions and only the superficial velocity $U_l = u_l \cdot g_l$, which is proportional to the mass flow rate, varies[22]. The flow rate attains its maximum near the liquidus temperature, since it has to compensate for the shrinkage of the entire mushy zone. As one moves deeper into the mushy zone, part of the flow has already been used to compensate shrinkage of solid ahead of this location, leaving only the flow to compensate for the remaining part of the mushy zone. After deriving this expression, i.e. **Eq. 3.24**, Niyama used Darcy's equation to write an expression in terms of pressure. Inserting **Eq. 3.24** into **Eq. 3.22**, yields

$$\frac{dP}{dx} = \frac{\mu_l \beta \dot{T} g_l}{KG} \tag{3.25}$$

Figure 3.20 illustrates that, as the solid fraction increases, the melt pressure decreases from the value at the liquidus, P_{liq}, down to some critical pressure, P_{cr}, at which point shrinkage porosity begins to form. For convenience, the critical pressure drop can be defined as $\Delta P_{cr} = P_{liq} - P_{cr}$. The pressure at liquidus is simply the sum of the ambient pressure of the system and the local head pressure. The critical pressure is determined by considering the mechanical equilibrium necessary for a stable pore to exist. This equilibrium is given by the Young–Laplace equation as $P_{cr} = P_p - P_\sigma$, where P_p is the pressure inside the pore and P_σ is the capillary pressure. The capillary pressure is given by $P_\sigma = 2\sigma / r_0$, where σ is the surface tension between the pore and the surrounding liquid and r_0 is the initial radius of curvature at pore formation. For pure shrinkage, in the absence of dissolved gases in the melt, the pressure inside the pores is negligibly small (due only to the vapor pressure of the elements in the melt). With this, the Young–Laplace equation simplifies to

$$P_{cr} = -P_\sigma = -\frac{2\sigma}{r_0} \tag{3.26}$$

Note that **Eq. 3.26** implies that the critical pressure is a negative number; this is reasonable, because the surface tension must be overcome before porosity can form. Generally, the capillary pressure at pore formation, P_σ, is an unknown quantity, primarily because the initial radius of curvature of the pores is unknown. Shrinkage pores typically nucleate heterogeneously from pre-existing bubbles associated with oxides, other inclusions, and small cavities in mold walls. The radius of curvature when porosity forms is a function of the nature, size, and geometry of the nucleation sites, which in turn are influenced by melt quality.

The point in space at which shrinkage porosity begins to form can be determined by integrating **Eq. 3.25** over the mushy zone from the critical point to the liquidus, assuming that the viscosity, temperature gradient, and cooling rate are constant over the interval being considered. After performing necessary integrations and modifications, the final expression is obtained:

$$\Delta P_{cr} = \frac{\mu_l \beta g_l \Delta T_{cr}}{K} \cdot \frac{\dot{T}}{G^2} = \frac{M}{Niyama^2} \tag{3.27}$$

where ΔP_{cr}, g_{lcr} and ΔT_{cr} are the critical pressure drop over the mushy zone, critical liquid fraction and critical temperature interval at which the melt pressure drops to P_{cr} and porosity begins to form, see **Figure 3.20**. This inverse relationship shows that the pressure drop increases as the *Niyama* value decreases. If an assumption is made that porosity forms at a critical pressure drop, then this critical value is more likely to be exceeded when the *Niyama* value is small[1].

By comparing experimentally observed shrinkage porosity patterns in cast-steel cylinders to corresponding casting simulations, Niyama et al. discovered that, indeed there was a threshold value of *Niyama* below which shrinkage was typically present. When the *Niyama* value decreases below a critical value, small amounts of micro-shrinkage begin to form. As the *Niyama* value decreases further, the amount of micro-shrinkage increases until it becomes detectable on a standard radiograph. This transition occurs at a second critical value. Both of these threshold values are heavily dependent on the composition of the alloy and in some cases on the casting process conditions. For instance, it has been experimentally found; see the enclosed **Paper II**, that for low-carbon steel cast alloys, the second critical value below which the centerline porosity becomes apparent on the radiographs is approximately 0.45-0.5. A comparison of experimental and numerical results is seen in **Figure 3.10 (c)** and in **Figure 3.21**.

While the presence of the temperature gradient in **Eq. 3.23** is not surprising, and implies that shrinkage porosity will form in regions of low *G*, the presence of the cooling rate in the denominator may at first seem counterintuitive. The Niyama criterion predicts that shrinkage porosity increases with increasing cooling rate, because the feeding-flow velocities and the resulting pressure drop across the mushy zone are higher for higher solidification rates. In other words, low gradient implies that even if liquid metal is available at a neighboring region, there is insufficient thermal 'pressure' for the flow to actually take place, while high cooling rate implies that even if liquid metal and sufficient gradients are available, the time available is too short and the liquid metal freezes before reaching the hot spot. It follows that the beneficial effect of a chill, for example, is due to the increase in the temperature gradient the chill provides; the concomitant increase in the cooling rate near a chill is actually counterproductive with regard to avoiding shrinkage porosity[13].

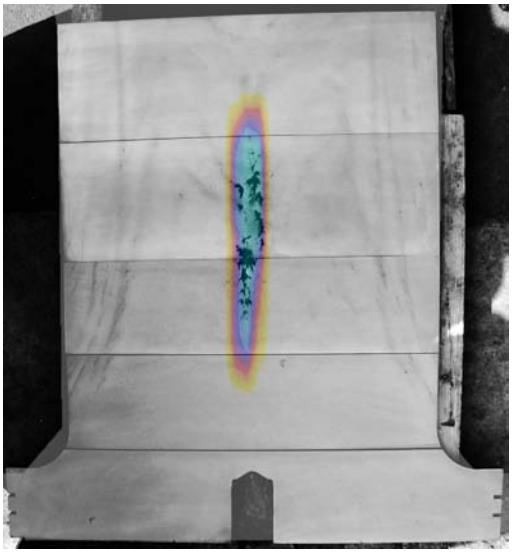

Figure 3.21: Prediction of the centerline macro/micro shrinkage and its experimental validation obtained from the foundry. The cyan color indicates regions with the Niyama value below 0.45, [ref. Paper III, (Kotas et al. 2010)].

As already mentioned, Niyama applied a few simplifications in his pressure drop and centerline porosity calculations. One of them was an assumption that the permeability of the mushy zone is proportional to the fraction liquid, i.e. $K = \alpha f_L$. However, measurements of the permeability of alloys show that the data fit the Kozeny–Carman model[13] given in **Eq. 3.28**:

$$K = K_0 \frac{g_l^3}{(1-g_l)^2} \tag{3.28}$$

Where, as a first approximation, $K_0 = \frac{\lambda_2^2}{180}$ in which λ_2 is the secondary dendrite arm spacing (SDAS). **Eq. 3.28** indicates that when the arm spacing is large, it leads to a large permeability of the mushy zone and low porosity. As the SDAS decreases, i.e. the grains are getting finer, which is usually associated with increasing cooling rate, the resistance to feeding flow is increased and thus the likelihood of porosity formation is higher. However, the porosity will not be centralized but distributed all over the casting forming very small voids. So, what is commonly observed is that, the total pore volume is increased but the even distribution of very small pores will actually lead to increase in mechanical properties of the given casting. This phenomenon is very typical when modification of cast alloys is applied[32, 33].

In essence, one could thus argue that the original Niyama criterion accounts for thermal conditions, i.e. cooling rate and thermal gradient, but it does not account for the effect of the thermal conditions on the SDAS, which can significantly affect the resulting pore volume. If proper modifications are done, the "modified" Niyama criterion can easily account not only for the local thermal conditions considered by the original Niyama criterion, but also for the properties and solidification characteristics of the alloy (μ_l, β, ΔT_{cr}, and λ_2) and the critical pressure drop across the mushy zone ΔP_{cr}. The difference from the original Niyama criterion in the dependence on thermal conditions is due solely to the SDAS and the effect that this arm spacing has on the permeability in the mushy zone[13].

The Niyama criterion was developed specifically for feeding-distance related shrinkage in short freezing range cast alloys such as steels, although, attempts have been performed by a research group at the University of Iowa to develop a dimensionless Niyama criterion, which would be suitable also for long freezing range alloys based on aluminum or magnesium. Note that the Niyama criterion does not explicitly predict hot spots in a casting, and it does not predict gas porosity, which forms by a completely different mechanism[30].

Foundries use the Niyama criterion primarily in a qualitative fashion, to identify regions in a casting that are likely to contain shrinkage porosity. The reason for such limited use is twofold: (1) the threshold Niyama value below which shrinkage porosity forms is generally unknown, other than for steel, and can be quite sensitive to the type of alloy being cast and sometimes even to the casting conditions (e.g., sand mold vs. steel mold, application of pressure, etc.); and (2) the Niyama criterion does not provide the actual amount of shrinkage porosity that forms, other than in a qualitative fashion (i.e., the lower the Niyama value, the more shrinkage porosity forms). Various industrial applications of the Niyama criterion can be seen in the work of the author, i.e. **Papers II, III, IV** and **Industrial report** which are enclosed at the end of this thesis.

In the following sections, it will be shown how the Niyama criterion can be effectively utilized in predicting other casting defects such as macrosegregation and hot tearing. To make it clear, it is not the criterion itself, but the physics behind it, i.e. thermal gradients, cooling rate and pressure drop, through which the Niyama criterion can be related to the defects prediction and their elimination.

3.7.3. Deformation during solidification and hot tearing

It was shown in the previous chapter and it can also be found in literature, that porosity can be caused by the inability to feed solidification shrinkage due to pressure losses through the mushy zone (shrinkage porosity), or by the segregation of too much dissolved gas in the liquid (gas porosity). Although the same equations[22] are used to describe the two cases, they differ in both the mechanism and possible preventive measures for pore formation. Gas porosity can be eliminated by an appropriate melt treatment, such as degassing, which removes excess dissolved gas prior to casting, or by preventing reactions between the melt and oxygen or water which lead to excess gas in the melt. However, the alloy's tendency to form shrinkage porosity is a more intrinsic characteristic, caused by the formation of a dense phase during late-stage solidification. Consequently it is harder to avoid.

One way to eliminate shrinkage porosity is to compress the mushy zone during solidification. It is shown in literature[22], that the partially coherent solid of a mushy zone can be compacted or expanded like a sponge. Putting this concept into context of **Eq. 3.20**, in regions of a casting that are under

compression, i.e. where $\nabla \cdot u_s < 0$, the deformation of the solid can counterbalance the density increase and thus maintain $g_p = 0$, even where there is no feeding, i.e. for $u_l = 0$. This is the idea behind the squeeze casting process, in which an extra compressive stress is applied at certain locations at prescribed times[34].

However, in many solidification processes such as shape casting, i.e. gravity sand or die casting, continuous casting or welding, some locations are subjected to tension rather than compression during solidification. In this case, the deformation of the solid skeleton adds to the solidification shrinkage, thereby inducing even more liquid suction in the mushy zone. A lack of feeding of the semisolid regions under tension will result in what is called hot tearing or hot cracking, a defect that is similar to shrinkage porosity, but that also requires tensile stresses. Whereas microporosity is fairly uniformly distributed within the mushy zone, hot tears are localized at grain boundaries.

3.7.3.1. Thermomechanics of castings- governing equations

In this section, the origin of deformation and stress during solidification and solid state cooling will be discussed. Dimensional changes are required to accommodate the volume change upon solidification, and more importantly, the thermal contraction of the solid upon cooling to room temperature. These dimensional changes produce stresses if one or more of the following conditions are met: non-uniform temperature, non-uniform mechanical properties, constraints induced by the mould or the casting geometry[22].

The foundation of all classical mechanics is the Newton laws of motion. And the equilibrium principle is a consequence of Newton's 2nd law of motion which states that the summation of the external forces on a body equals the mass times the acceleration. However, in casting processes, after the filling of the mould, the accelerations are close to zero. This will simplify Newton's 2nd law to the static equilibrium as follows:

$$\sum_{i=1}^{3} F_i = 0 \quad \Rightarrow \quad \sigma_{ij,i} + p_j = 0 \tag{3.29}$$

Where p_j is the body force at any point within the plate and σ_{ij} is the stress tensor. A very important consequence of **Eq. 3.29** is that every arbitrarily chosen part of the casting and the mould has to be in static equilibrium. This also means that the forces, if any, acting on the boundary of the geometry together with volume forces, e.g. gravity, must even themselves out, finally adding up to zero. If this is not true the part will start to accelerate, thus violating the static nature of the problem[1].

Thermal strain

It is a well-known phenomenon that a body when heated will expand and when cooled will contract, if allowed to deform freely. This is a consequence of the thermal deformation or thermal strain. If the temperature of a body is raised uniformly and if its bounding surfaces are unrestrained then it will expand uniformly in all directions. The constant of proportionality is called the coefficient of linear thermal expansion which was already introduced in **Eq. 3.13** and the strain that the body will experience will be equal to the thermal strain given by

$$\varepsilon^{th} = \int_{T_1}^{T_2} \alpha dT \tag{3.30}$$

In words, α expresses how much relative deformation the body experiences when exposed to a temperature change of one degree if it is allowed to contract or expand freely. For this type of application, i.e. casting processes, it is desired to relate elastic strains to stresses. This is in general called a constitutive law within the field of solid mechanics. The word elastic indicates that the deformation that the body undergoes will be entirely recovered while unloading. This leads to the 1-D Hooke's law:

$$\sigma = E\varepsilon^{el} \tag{3.31}$$

which states that there is a linear relationship between the stress and elastic strain. At this point the material behavior is not taken into account. If it was, it would lead to the Hooke's generalized law which is discussed in the next section.

Thermal stress and constraints

It is commonly known that internal stresses may occur in a heated or a cooled body either due to a highly local heating/cooling or external constraint, or a combination of both causes. These internal stresses are referred to as thermal stresses.

In casting processes, one distinguishes between internal and external constraints on castings. The casting constraint which is a result of uneven cooling is an example of the internal constraint; furthermore, constraining from the mould/die on the casting could be regarded as the external constraint. This type of constraining is readily understood and quite easy to visualize. The rate of constraining is determined via the shape complexity of the casting, which plays an important role for the mould/die constraint. One very important rule follows.

Thermal contraction/ expansion can result in:

- **Deformation only** (the body is allowed to contract/expand freely).
- **Stress only** (the body is totally restrained).
- **A combination** of deformation and stress (almost always the case in practice).

This is also closely coupled with the relationship between total, elastic, plastic and thermal strain, which is known as the decomposition of the strain component, and in 1D can be written as

$$\varepsilon^{tot} = \varepsilon^{el} + \varepsilon^{pl} + \varepsilon^{th} \tag{3.32}$$

This so-called total strain is the one that the body experiences, i.e. the strain seen from outside the casting. The elastic strain is often regarded as the strain driving the stresses, since they are related very simply by the Hooke`s law. Therefore, in this respect, the thermal strain cannot produce stresses by itself. It can be understood as a thermal load that promotes elastic strains, and these elastic strains cause stresses[1]. For the 1-D thermo-elastic case, the relationship between the stresses and strains is obtained combining **Eq. 3.31** and **Eq. 3.32**:

$$\sigma = E\varepsilon^{el} = E\left(\varepsilon^{tot} - \varepsilon^{pl} - \varepsilon^{th}\right) \tag{3.33}$$

The elastic behavior of the body subjected to the external heat is an idealization which does not correspond to the reality, at least not for metal casting processes. In terms of casting processes the behavior of the materials differs quite considerably from the elastic description which now becomes inadequate. The material in general is then said to behave elasto-plastically, i.e. the material deformation also becomes irreversible. A very important consequence of this is that in general it is not possible to express the stresses as functions of the strains on total form as was the case for Hooke`s law. In plasticity, it is in general possible to express only changes in stresses as changes in strains. This is called an incremental constitutive law. We then introduce the mechanical strain which is defined as the sum of the elastic and plastic strains[1]

$$\varepsilon^{mech} = \varepsilon^{el} + \varepsilon^{pl} \tag{3.34}$$

This definition is very important in the case of thermo-mechanical modeling of casting processes because the thermal strain is very dominant, so that the total strain in thermo-elasto-plastic case can be formulated as:

$$\varepsilon^{tot} = \varepsilon^{mech} + \varepsilon^{th} = \varepsilon^{el} + \varepsilon^{pl} + \varepsilon^{th} \tag{3.35}$$

where the plastic strain accounts for all inelastic behavior, e.g. time-independent plasticity where time-dependent plasticity like creep or visco-plasticity is typically dominating inelastic behavior at high temperatures, of the deformed body.

3-D thermo-elasticity, Hooke's generalized law

Now if we consider a general multi dimensional stress state during loading, it will bring us to Hooke's generalized law for linear-elastic, isotropic material where stresses are expressed in terms of strains in 3D:

$$\begin{aligned}
\sigma_{11} &= \frac{E}{1+\nu}\left\{\varepsilon_{11} + \frac{\nu}{1-2\nu}\left(\varepsilon_{11}+\varepsilon_{22}+\varepsilon_{33}\right)\right\} - \frac{E\alpha\Delta T}{1-2\nu} \\
\sigma_{22} &= \frac{E}{1+\nu}\left\{\varepsilon_{22} + \frac{\nu}{1-2\nu}\left(\varepsilon_{11}+\varepsilon_{22}+\varepsilon_{33}\right)\right\} - \frac{E\alpha\Delta T}{1-2\nu} \\
\sigma_{33} &= \frac{E}{1+\nu}\left\{\varepsilon_{33} + \frac{\nu}{1-2\nu}\left(\varepsilon_{11}+\varepsilon_{22}+\varepsilon_{33}\right)\right\} - \frac{E\alpha\Delta T}{1-2\nu}
\end{aligned} \tag{3.36}$$

where ν is Poisson's ratio and E is the Young's modulus in case of isotropic material. In tensor notation it can be written as

$$\sigma_{ij} = \frac{E}{1+\nu}\left\{\varepsilon_{ij} + \frac{\nu}{1-2\nu}\delta_{ij}\varepsilon_{kk}\right\} - \delta_{ij}\frac{E\alpha\Delta T}{1-2\nu} \tag{3.37}$$

The version of Hooke's generalized law expressing stresses in terms of strains is normally the version that is used in a numerical formulation of a thermo-mechanical problem. This is because the governing equations are the equilibrium equations and these are expressed in terms of stresses[1]. Just for clarity, **Eq. 3.32** can be extended to 3D and expressed in tensor notation as

$$\varepsilon_{ij}^{tot} = \varepsilon_{ij}^{el} + \delta_{ij}\varepsilon^{th} \tag{3.38}$$

3-D thermo-elasto-plasticity

To include and describe plastic behavior in the material model, the standard J_2-flow theory can be applied. The elastic domain is limited by the yield stress, via the yield function which describes when the material starts to behave plastically. The yield function used to evaluate the elastic/plastic behavior in the J_2 flow theory is based on the von Mises hypothesis which states that "plastic flow in a general stress state is initiated when the second invariant J_2 reaches the critical value of the second invariant J_2 that initiates plastic flow in the uni-axial stress state[1]". This hypothesis leads to the definition of the effective von Mises stress which is used to predict yielding of materials under any loading condition from results of simple uni-axial tensile tests. In other words it is possible to evaluate the general stress state via the effective stress and compare it with the actual yield stress of the material.

The calculation of the effective stress based on the second invariant of the deviatoric stress tensor in **Eq. 3.39**, known as the J_2 invariant is given by the following relation.

$$\sigma_e = \sqrt{3\cdot J_2} = \sqrt{3\cdot\frac{1}{2}s_{ij}s_{ji}} = \sqrt{\frac{3}{2}s_{ij}s_{ji}} \quad \textit{where} \;\; s_{ij} = \sigma_{ij} - \frac{1}{3}\delta_{ij}\sigma_{kk} \tag{3.39}$$

The component s_{ij} stands for the deviatoric part of the stress tensor. The last component on the right hand side represents the hydrostatic pressure which does not contribute to plastic deformation. This leads to the definition of the yield function of the form, **Eq. 3.40**

$$f(\sigma_e, \varepsilon_e^{pl}, T) = \sigma_e(s_{ij}) - \sigma_y(\varepsilon_e^{pl}, T) \tag{3.40}$$

Where ε_e^{pl} is the equivalent plastic strain, σ_e is the effective von Mises stress and σ_y is the temperature and plastic strain dependent yield stress. This leads to the following definition of the elastic and the plastic states expressed in terms of the yield function. If $f < 0$ the material behaves elastically, while if $f = 0$, the material starts to behaves plastically, i.e. it starts to yield. The plastic

deformation outside the yield surface ($f > 0$) is not physically possible. The evolution of the yield surface is described by the consistency criterion which enforces the solution to stay on the yield surface during the plastic load increment.

The associated flow rule (**Eq. 3.41**) indicates how the plastic strain develops by using the yield criterion function (yield surface) and this relation is formulated as

$$d\varepsilon_{ij}^{pl} = d\lambda \frac{\partial f}{\partial \sigma_{ij}} \quad where \quad \frac{\partial f}{\partial \sigma_{ij}} = s_{ij} \tag{3.41}$$

where λ is a load parameter which stands for the size of the plastic strain increment, while the direction of this increment is given by the second term which is the outwards pointing normal to the yield surface. The load parameter is obtained from the consistency criterion in **Eq. 3.42**.

$$\dot{f} = \dot{f}(s_{ij}, \varepsilon_{ij}^{pl}, T) = \frac{\partial f}{\partial s_{ij}} \dot{s}_{ij} + \frac{\partial f}{\partial \varepsilon_{ij}^{pl}} \dot{\varepsilon}_{ij}^{pl} + \frac{\partial f}{\partial T} \dot{T} \tag{3.42}$$

This condition relates the development of stress in the domain to the change in yield stress of the material governed by the isotropic hardening and the softening of the material as function of the temperature increment during the applied load increment[1].

Generally, the behavior of temperature softening and the generation of plastic strain can be illustrated by the 2D plane stress representation of the yield surface given in **Figure 3.22**. These two illustrations show how the general stress level drops when the temperature increases and how the stress level increases during any production of plastic strain.

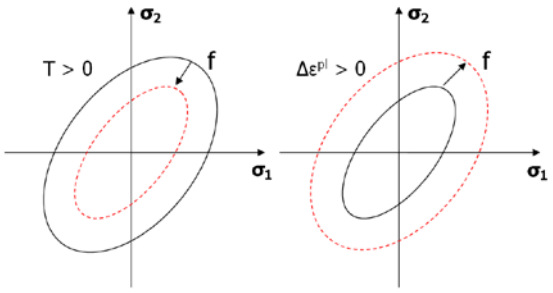

Figure 3.22: Development in the yield surface as function of temperature softening (left) and generation of plastic strain (right). 2D plane stress case given in terms of principal stresses. Figure adapted from Hattel[1].

The aforementioned theory of stresses and strains occurring in a solidifying casting has been presented for one reason. All this and much more needs to be calculated by the numerical stress solver implemented in MAGMAsoft, in order to model and predict phenomena such as deformation, residual stresses, i.e. von Mises stress, hot tears or cold cracks within a given casting. Considering just hot tearing, if it was not for these stress-strain calculations, it would not be possible to evaluate strains, strain rates, transient stresses, etc., which all contribute substantially to this very common defect in steel castings. Obviously, one should never forget that thermal calculations need to be carried out as well to get an idea on how the casting cools down, i.e. if uniformly or not, since non-uniform solidification and thermal contraction drive the formation of thermal stresses and strains.

3.7.3.2. Coherency

Before we turn to the description of hot tearing the term "coherency" which is commonly used in discussion of hot tearing should be introduced. The coherency point can be defined as the volume fraction of solid, or the temperature at which a given alloy starts to develop mechanical resistance. In order to understand the complexity of defining a unique coherency point, it is necessary to study the evolution of the mushy zone over the entire solidification range. When we look at **Figure 3.23**, we can see a sequence of six micrographs taken during growth of columnar dendrites.

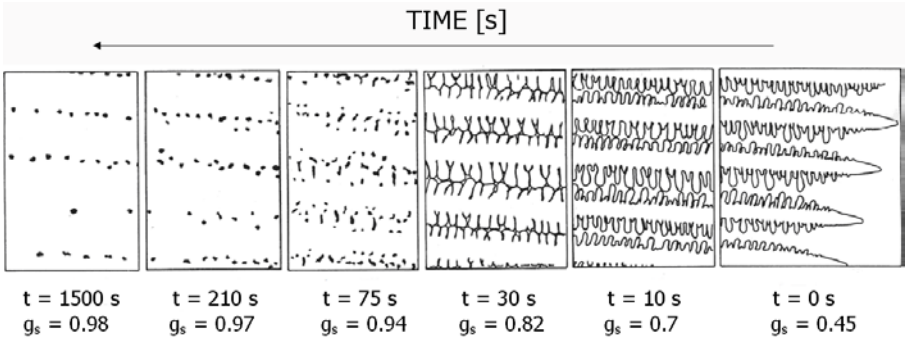

Figure 3.23: Growth and coalescence of dendrite arms within a single grain of succinonitrile-acetone. The microstructure has been redrawn from the original micrographs to highlight the solid-liquid interface. The volume fractions of solid are indicated below each image. Figure adapted from [22].

Observing the microstructure deeper within the mushy zone, one first notices that the dendrite arms become coarser and thicker. At t = 30s, the dendritic network fills nearly the entire frame, but g_s is still only 0.82. Note that, at this point, the columnar dendrites remain separated from their neighbors by continuous liquid films. Between t = 30s and t = 75s, a dramatic change in topology occurs. The dendrite arms coalesce or bridge, transforming the continuous liquid films into isolated liquid pools or droplets. Coalescence should not be confused with coarsening; it is defined as the replacement of two solid-liquid interfaces by one solid bridge. This intragranular bridging does not have to overcome any grain boundary energy barrier, and thus occurs at a fairly low volume fraction of solid (~0.9), as soon as two dendrite arms touch[22]. The temperature at which this takes place is designated $T_b^{\text{int } ra}$. Below g_s = 0.82, dendrite trunks do not pose much resistance to tensile stresses applied perpendicular to their growth direction, whereas above g_s = 0.94, the mushy zone behaves as a coherent solid, slightly weakened by the presence of the liquid droplets.

If the simplest possible polycrystalline specimen consisting of two columnar dendritic grains growing with a symmetric tilt boundary between them is considered, see **Figure 3.24**, one can see again the same coalescence occurring at around $T_b^{\text{int } ra}$ within each grain.

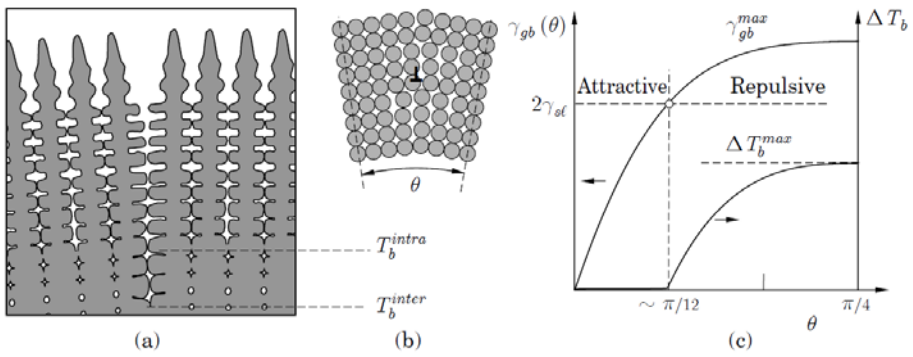

Figure 3.24: (a) A schematic diagram of two columnar dendritic grains in a symmetric tilt boundary configuration. (b) The configuration of the atoms located at the grain boundary after solidification. (c) The surface energy of a tilt boundary, $\gamma_{gb}(\theta)$, as a function of the misorientation angle θ. The bridging undercooling ΔT_b is shown on the right hand scale. The transition between an attractive and repulsive boundary occurs at around $\pi/12$. Figure taken from [22].

Below this temperature, the grains are already close to being fully solid, with a few isolated liquid pools. On the other hand, dendrite arms located on both sides of the future grain boundary must overcome the grain boundary energy, which depends on the relative misorientation between the two grains. For values of the misorientation angle small enough there would be a decrease in energy upon coalescence and hence this boundary would be attractive and the coalescence would occur around $T_b^{\text{int } ra}$. However, for larger misorientations, the grain boundary is said to be repulsive and the bridging occurs at a lower temperature given by an undercooling $\Delta T_b(\theta)$.

In summary, for a polycrystalline columnar specimen in which all of the grain boundaries are nearly parallel to the thermal gradient, all of the dendrites are surrounded by liquid films for $T > T_b^{\text{int } ra}$. Accordingly, there is little mechanical resistance in the direction along which thermal strains develop. However, any lateral separation of the dendrites can be compensated by interdendritic liquid flow, since permeability is high. Therefore, the range is characterized by high ductility and low strength. On the other hand, for $T < T_b^{\text{int } ra}$, all of the boundaries are solid, and the specimen exhibits both high ductility and high strength. For $T_b^{\min} < T < T_b^{\text{int } ra}$, films of liquid remain at some of the grain boundaries, thereby weakening the material. Any opening of such grain boundaries by thermal strains cannot be compensated easily by liquid flow, since the permeability of the mushy zone is low in this range ($\sim 0.94 < g_s < 1$). Therefore this range typically corresponds to low ductility and an intermediate strength of the mushy zone. The material is very sensitive to hot tearing, due to the remaining liquid films acting as a brittle phase and concentrating the thermal strains.

3.7.3.3. Hot tearing

As discussed in the first part of this chapter, thermally induced stresses and strains during casting develop mainly in the fully solid part. These are then transmitted to the mushy zone and tend to localize at the weakest regions, i.e. at the continuous liquid films remaining between the grains. Some of these films are still present even at low temperatures and the low permeability of the mushy zone in such regions prevents feeding of any grain boundary opening. This leads to hot tearing[22]. The next section reviews the main characteristics of such defects after which factors influencing this defect will be introduced and discussed. The theory on hot tears will be explained by considering an industrial project.

Characteristics of hot tears

Hot tearing is one of the most common and serious defects encountered in large steel castings. Hot tear defects require extensive rework, which significantly increases costs. In some instances, several iterations of part inspection repair and heat treatment can be required, which is both labor and energy intensive. Hot tear defects that are not properly repaired or are not discovered, can result in failure initiation sites during service. These troublesome defects can occur internally in a casting or on the surface of the casting, see **Figures 3.25 and 3.26**. These cracks may be large and visible to the naked eye or small and found only by magnetic particle inspection.

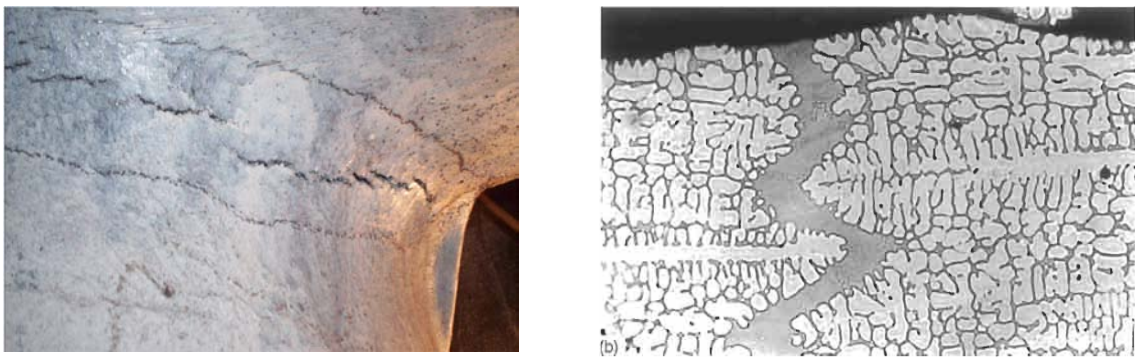

(a) ***(b)***

Figure 3.25: (a) The jagged and discontinuous surface appearance of a hot tear on the surface of a casting, (b) An optical micrograph of a "healed" or filled hot tear in an Al-10%Cu specimen[35].

Figure 3.26: View on the location of a hot tear in the middle rib of a steel casting, [ref. Paper IV, (Kotas et al. 2010)].

The defect is easily recognized from one or more of a number of characteristics[4]:

- Its form is that of a ragged, branching crack.
- The main tear and its numerous minor offshoots generally follow inter-granular paths. This is particularly clear on a polished section viewed under the microscope.
- The failure surface reveals a dendritic morphology. The failure surface is often heavily oxidized (prior, of course, to any subsequent heat treatment). This is particularly true for higher temperature alloys such as steels.
- Its location is often at a hot spot, and where contraction strain from adjoining extensive thinner sections may be concentrated.
- It does not always appear under apparently identical conditions; in fact it seems subject to a considerable degree of randomness in relation to its appearance or non-appearance, and to its extent.
- The defect is highly specific to certain alloys. Other alloys are virtually free from this problem.

Hot tears are caused by a combination of thermal effects, such as hot spot size, and casting restraint, such as cores in cylindrical castings. In addition, composition can affect hot tearing tendency. Physically, two factors contribute to hot tearing in the mushy zone. Hot tears are formed when the mushy zone is cut off from liquid feeding and is under tensile loading[36].

First, liquid feeding is the flow of liquid metal into the mushy zone to account for volumetric shrinkage as the liquid becomes solid. The mushy zone accumulates volumetric changes both through shrinkage, which is the density change as liquid metal solidifies to solid metal, and by the externally imposed volumetric strain. The mushy zone is analogous to a sponge shown in **Figure 3.27**. Initially, liquid may flow through, like the sponge, but as solidification continues the permeability of the sponge decreases which restricts liquid metal flow. Eventually the flow is cut off and the remaining liquid pockets become isolated. As long as the liquid pressure is sufficient to drive liquid into the pockets, no porosity will form. But when the pockets become isolated then the liquid will not feed the contraction during solidification and porosity forms.

Second, tensile solid deformation is also necessary for hot tears. In the sponge analogy, tensile deformation stretches the sponge. Alternatively, compressive deformation squeezes the sponge and may eliminate porosity and hot tears. Tensile deformation can result when the thermal contraction of the solid areas of the casting are restrained.

Restrained thermal contraction may occur, when metal surrounds a core or if an already solid casting feature pins the contraction at a hot spot. When the mushy zone in a hot spot is being deformed in tension, solid dendrites or grains are pulled apart. This circumstance is illustrated schematically in **Figure 3.27**.

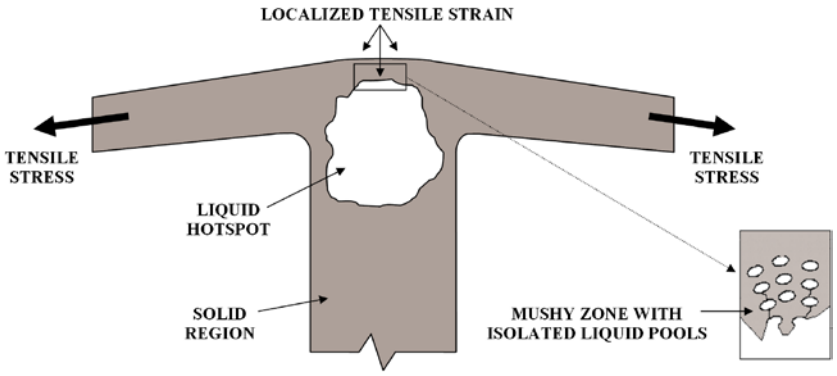

Figure 3.27: Schematic of a deformed mushy zone. Tensile stress in one area can evoke tensile strains localized in a distinct area. If that area is still mushy and improperly fed, the tensile strains can easily facilitate hot tearing in that weak spot. Figure inspired by Monroe[16].

As the solid colder pieces at the edge of the mushy zone are pulled apart by contraction, additional liquid metal must flow into the mushy zone to fill this space. If liquid is not available under tensile loading, due to the feeding flow being cut off, additional porosity may form. This porosity forms late in solidification, along grain boundaries and it is the initiation site for a hot tear.

The initiating conditions for hot tearing can occur from (1) casting design; normal contraction of thinner sections causing deformation or restraint of thicker sections which cool more slowly, or (2) bulk resistance of the mold and core, which prevents contraction of a casting, or (3) the rigging design, especially if feeding is marginal, by providing additional restraints or due to the high thermal gradients that are often needed to achieve directional solidification. In a complex-shaped casting, tearing may occur as a result of the combined effect of the aforementioned causes.

Alloy composition

Susceptibility to hot tearing is closely associated with the mode of freezing and thus with alloy composition. The tendency is loosely related to the length of the temperature range over which the alloy possesses certain cohesion yet ductility is minimal. This range is related to the freezing range of the alloy, since cohesion, i.e. coherency is attained at some critical proportion of solid to residual liquid. The extent of the brittle range determines the total contraction occurring in a cast member of a given length whilst the alloy is in the vulnerable condition. Alloys with very short freezing range, therefore, including those of near eutectic composition, show little tearing tendency. Alloys containing small amounts of eutectic, with their relatively long temperature range of primary dendrite cohesion, are especially prone to tearing. Larger amounts of eutectic enable liquid flow to heal incipient tears until the eutectic temperature is attained, accounting for the low susceptibility to hot tearing in grey cast irons and in the eutectic aluminum–silicon alloy.

Apart from the basic alloy composition, susceptibility to hot tearing is influenced by segregation of alloying elements and impurities. Microsegregation or coring extends the true freezing range and increases the tendency for prolonged retention of interdendritic liquid films, with consequent increase in the accumulated strain during the critical period of weakness. This accounts for the serious lowering of resistance to hot tearing by high sulfur and phosphorus contents in steel. Carbon, C, is known to diffuse relatively well in ferrite and austenite whereas phosphorus, P, like sulfur, S, diffuses slowly. These two elements have a low partition coefficient and are known to produce interdendritic segregate of low melting point[37] and depress the solidus temperature. This last liquid to solidify is on grain boundaries, which under tensile deformation will easily separate. The depressed solidus temperature increases the time that tensile strain may accumulate when flow is cut off[38]. Hence one can see that unfavorable macrosegregation profiles in the casting also facilitate hot tearing to a large extent.

The hot tearing tendency of an alloy is, on the other hand, diminished by precipitation of gaseous impurities during freezing, since the resulting volume expansion partly offsets the contraction during the critical film stage.

Design and production factors in hot tearing

Design and production conditions influence hot tearing mainly through effects upon temperature distribution and resistance to contraction. Temperature distribution is of crucial importance in respect of all types of contraction defect, since it governs the distribution of mechanical properties and at the same time creates the pattern of stress–strain relationships due to differential contraction. As a general rule the probability of tearing is increased by longitudinal temperature differentials, which produce hot spots during cooling. The more confined and intense the hot spot the greater the tearing tendency, since the strain resulting from the hindered contraction of the whole member is then concentrated within a narrow zone of weakness, where it must be accommodated by relatively few films of residual liquid. Temperature distribution and hot spot intensity are influenced by design, by gating technique, and by selection of pouring speed and temperature, all of which can be used to reduce the strain concentration.

- **Design**

Much can be achieved at the design stage of the casting. A hot spot generally occurs at any intersection or local section increase. The basic aim, therefore, should be to equalize cooling rate by designing for uniform section thickness. Where this is impossible, cooling can be equalized with the aid of chills. The chilling of the hot spot is a useful technique. This reduces the temperature locally, thus strengthening the metal by taking it outside of its susceptible temperature range before any significant strain and stress is applied. By reducing the temperature locally nearer to that of the casting as a whole, the temperature differential that drives the process is reduced, and any strain concentration is redistributed over a larger region of the casting. Local chilling is therefore usually extremely effective. Although one should be aware of one fact, it is very common for chills which are in direct contact with the casting wall that they may induce local surface tears. This is because the chills will induce high thermal gradients localized over a small or narrow area and thus the strain rates will be very high at that place. However, if feeding is sufficient at that section nothing may happen. A rule of thumb that the author learned while collaborating with the steel casting industry is that if more brick-shaped or cylindrical chills in direct contact with the casting are applied in one area, the minimum distance between them should be at least the same as the width of each of these chills, not smaller. If this condition cannot be provided, the given chills should be substituted by one single big chill to prevent hot tearing.

An industrially-oriented project has been performed by the author to investigate and subsequently optimize the hot tear formation in a large steel wedge-shaped casting, **see Paper IV**. It is a perfect example of how the improper solidification pattern and insufficient chilling can cause massive hot tearing in the 85 ton large casting. The casting is seen in **Figure 3.28** and it should be instantly clear that the chilling will be insufficient. Since hot tearing is a thermally induced defect, it was important to thoroughly analyze the whole solidification interval.

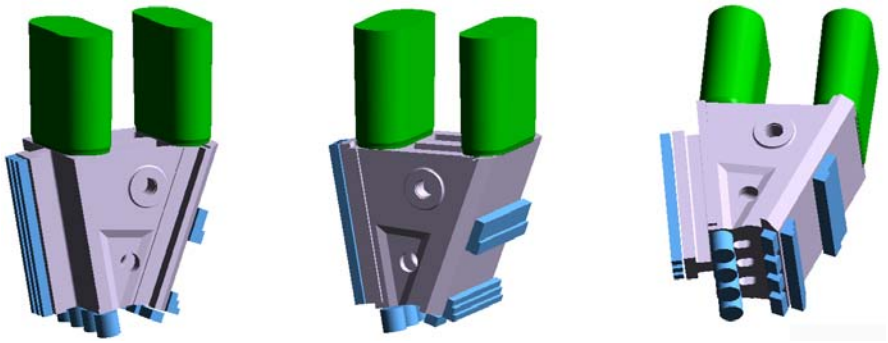

Figure 3.28: 3-D visualization of the original casting layout with its characteristic feeder design and chill patterns applied in the initial numerical calculations, [ref. Paper IV, (Kotas et al. 2010)].

Figure 3.29 outlines the Niyama criterion for the casting shown in **Figure 3.28**, and this criterion is generally used to indicate regions prone to centerline porosity due to low thermal gradients. Although, at the same time it can be used to highlight regions with very steep gradients and hence

areas prone to hot tearing. Having large temperature differences over a small or narrow region implies that large thermal strains will be evoked due to this sudden temperature change. One can see that the area above the top cylindrical core experiences large temperature changes in two very narrow channels, exactly at the area where the hot tear was found in the real casting. Since the Niyama criterion is evaluated at the end of the solidification interval it was necessary to check how the casting behaves thermally speaking during the entire solidification interval to identify the most critical time for hot tear formation.

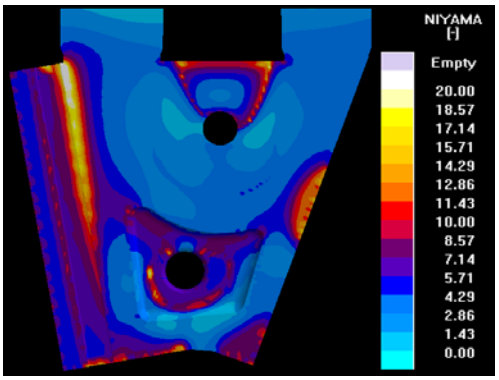

Figure 3.29: The Niyama criterion used to highlight areas with high thermal gradients for the casting shown in Figure 3.28. Areas with high Niyama values exhibit steep thermal gradients and low cooling rates, [ref. Paper IV, (Kotas et al. 2010)].

Figure 3.30 implies that already at 40% solidified a small region above the top core solidifies at a much higher rate than the surrounding areas. This trend persists throughout the entire solidification interval. Having an area which solidifies much quicker than the surroundings generally leads to large thermally induced tensile strains. Also, the cold area has gained strength and volumetrically contracts while the surroundings are still semi-solid and weak. The consequence of this thermal imbalance can easily be a hot tear located at the boundaries of the cold and hot regions.

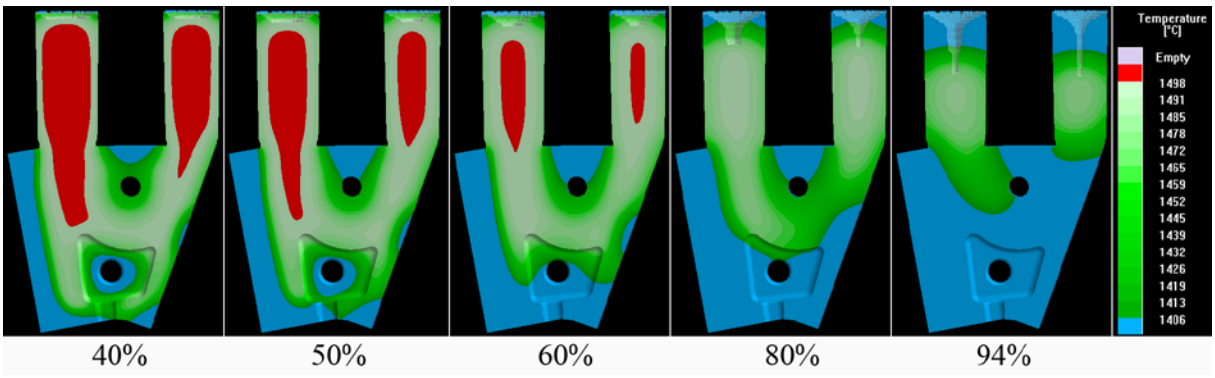

Figure 3.30: Temperature distribution in the solidification interval of the original casting layout. It is expected that the sudden temperature change in the area between the risers might induce thermal straining at the boundaries of the cold and hot regions and consequently a hot tear. Blue color denotes a completely solid region, all of the shades of green stand for the mushy zone and the red color stands for the liquid, [ref. Paper IV, (Kotas et al. 2010)].

Figure 3.31 captures the maximal principal strain rate inside the casting at two different stages of solidification. One might argue why we should be concerned about what goes on at that early stage of solidification when hot tears usually form much later. The reason is that at 40% solidified; the cold "triangular" area starts to form above the top core, as indicated in **Figure 3.30**. Therefore, that particular area is already in the late stage of its solidification, due to the uneven solidification pattern of the entire casting and thus hot tears can form there already now. Indeed, one can see in **Figure 3.31** that the significant temperature difference coupled with volumetric contraction lead to rather severe thermally induced tensile straining in that area. Also, it is now obvious that the top core represents a mechanical restraint to the free contraction as the peak values of the strain rate are

adjacent to the core. Hence one may assume that the hot tear initiated there and propagated diagonally to the top.

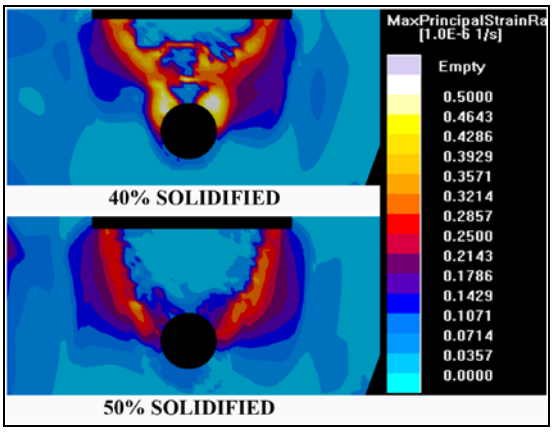

Figure 3.31: Maximal principal strain rate contributing to hot tearing. The effect of the top cylindrical core as a mechanical restraint to free contraction is seen. The "fastest" deformation occurs right at the region where the hot tear was found in the real casting, [ref. Paper IV, (Kotas et al. 2010)].

Figure 3.32 depicts the final prediction of the hot tear occurrence in the casting as a consequence of the coupled physical phenomena mentioned above. Notice a very good correlation with the results obtained from the casting trial. There is one more area in the hot tear results that might be of concern. It is located in the lower central section of the casting above the bottom cylindrical core. One of the probable reasons why the hot tear did not occur in the bottom area in reality is the stress redistribution in the casting after the top hot tear opened up. So, when the hot tear formed in the central rib, the residual stress stored in the casting got released in a form of deformation and the stress pattern of the entire casting changed and the bottom tear did not initiate.

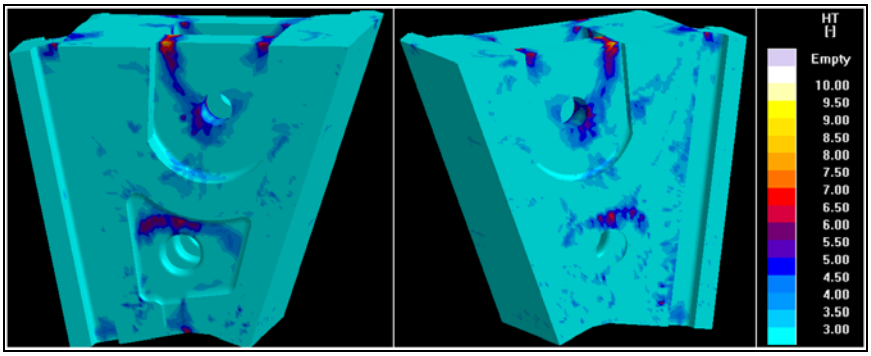

Figure 3.32: Hot tear prediction obtained from the numerical stress-strain analysis. Colored areas indicate regions most susceptible to hot tearing. A good agreement with the experimental results (Figure 3.26), is seen in terms of the predicted hot tear in the central rib, [ref. Paper IV, (Kotas et al. 2010)].

A conclusion can be that the hot tear was in essence evoked by a combination of multiple factors, (i) an uneven temperature distribution inducing high thermal gradients concentrated over the very narrow area, (ii) by unfavorable concentration profiles of solute elements which are also heavily dependent on the temperature profiles, (this will be shown and discussed in the section dedicated to macrosegregation), and, (iii) by a mechanical restraint due to the presence of the top core which hindered free volumetric contraction of the solidifying cast part.

- **Gating technique**

Hot spots may also exist as by-products of the pour, the ingate regions forming frequent sites for tears. Gating practice can be designed to reduce this risk by the use of multiple ingates positioned to achieve a wide distribution of the molten metal, so avoiding intensive heating at a single ingate. Care is required, however, to avoid creation of a stress framework embodying the gating system itself.

Based on Campbell's arguing that hot tears are strongly linked to the presence of bifilms and various inclusions[4], a conclusion can be made that simply upgrading the filling system is one of the most important techniques for dealing with hot tearing problems. By using filters in the gating system or by avoiding air aspiration or sand mould erosion, the melt will travel more uniformly and will contain fewer impurities and potential nucleation sites for hot tears. Basically, the less turbulent filling, the lower the risk of hot tearing. An example of a gating system applied in practice is given in **Figure 3.33**. This highly turbulent flow pattern will for sure cause excessive oxidation and providing that Campbell's theory is correct, it will be the inclusions and bifilms which most likely will promote hot tearing.

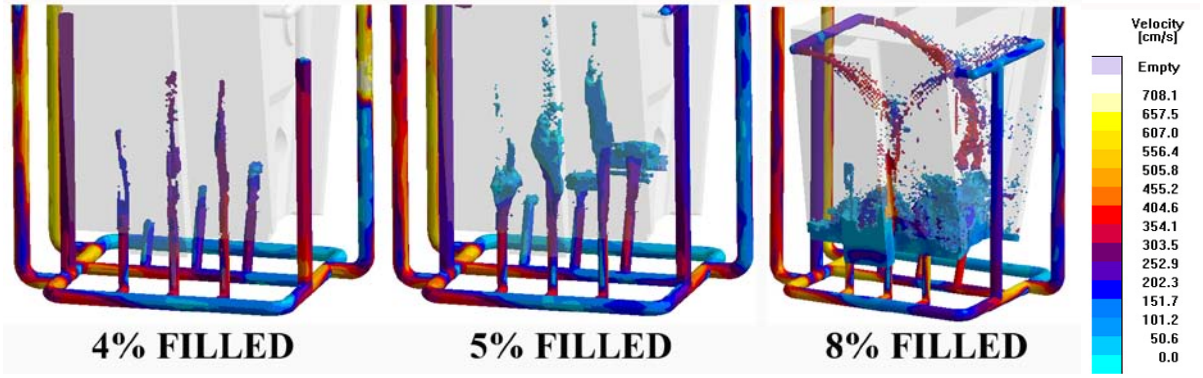

Figure 3.33: Initial stages of the filling process in case of the original casting arrangement suggesting highly turbulent entry of the metal to the mould causing jetting and also a waterfall effect due to improperly designed gating system, [ref. Paper IV, (Kotas et al. 2010)].

A Few simple changes in the design of the gating system, namely increasing the cross section area of the ingates and adding three more gates would slow down the melt while entering the mould cavity. Additionally, the vertical runners were eliminated to prevent the waterfall effect, see **Figure 3.34**.

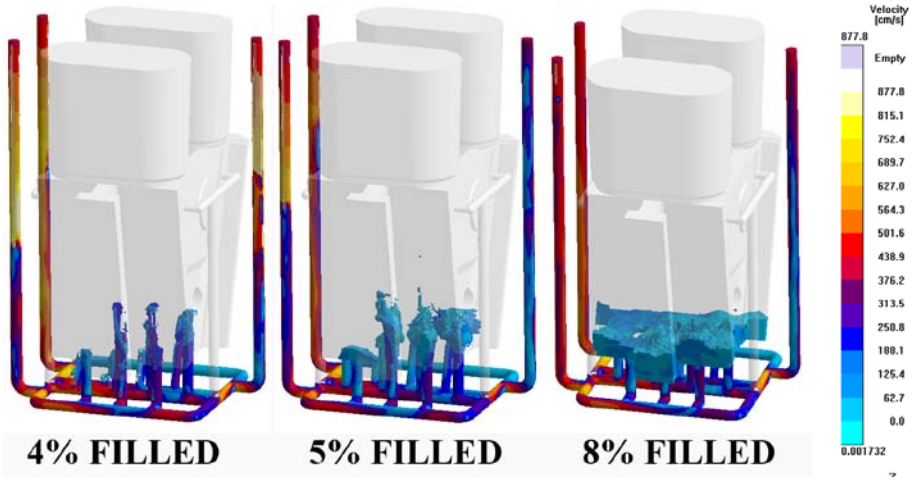

Figure 3.34: Initial stages of the filling process after shape optimization of the gating system. The entry is much smoother and quiet which may eliminate oxidation and most likely also hot tear susceptibility.

- **Melt treatment and pouring conditions**

The grain refinement of the alloy is expected to be helpful in reducing tear initiation in that for finer grains more strain can be accommodated by easy slip along the lubricated grain boundaries without the danger of tearing. Since a hot tear generally grows or propagates along the grain boundaries, having much more fine grains exposes higher resistance to the free movement of the growing hot tear. From this, it is obvious that having a mushy zone comprised of very fine grains, i.e. small SDAS, will lower the permeability of the mushy zone[39] and lower the risk of hot tearing.

A high casting temperature is associated with increased incidence of tearing. This can be explained partly by its effect upon transverse temperature gradients in the casting member. Pouring with

excessive superheat, by preheating the mould, produces shallow transverse gradients during solidification, so that an increased proportion of the cross section passes simultaneously through the brittle range. Steep transverse gradients, on the other hand, favor progressive inward growth of a solid layer, of which the weaker inmost region has constant access to the residual liquid whilst the skin develops full solid cohesion. These conditions are favored by moderate pouring temperatures and by greensand moulds. The influence of a high pouring temperature can also be partly attributed to a grain size effect, since a coarse structure produces concentration of longitudinal strain at fewer inter-crystalline liquid film sites[9]. The influence of pouring speed on hot tearing arises primarily from its effect upon long range longitudinal temperature gradients: rapid pouring promotes uniformity and reduces hot spot intensity, enabling the strain to be accommodated at a maximum number of sites.

Note that hot tearing follows the same trend as centerline porosity, represented by the Niyama criterion in, that if proper thermal gradients with proper cooling rate are present in the casting and if directional and progressive solidification is ensured, the extent and the permeability of the mushy zone are decreased and hence the resistance to centerline porosity and hot tearing is increased. This leads to the assumption that in essence hot tears which are considered as "thermo-mechanical" defects can be treated by the Niyama criterion. In other words, if we minimize the presence of the centerline porosity by establishing a proper solidification pattern, the risk of hot tears will decrease as well. This assumption has been verified in **Paper IV, (Kotas et al. 2010).**

- **The mould**

The resistance to contraction of a mass of moulding material depends partly upon its bulk properties at normal temperatures and partly upon properties in the heated layers adjacent to the casting. In a greensand mould bulk properties predominate and there is little tendency to form hot tearing in the casting when compared with dry sands and core sands: contraction is accommodated by deformation of the whole mass. The traditional assumption that organically bonded cores suppress hot tearing is only valid if sufficient time elapses for breakdown of the binder to an adequate depth before the casting cools through the susceptible temperature ranges. Before this stage heating of the sand actually makes the problem worse through expansion. Owing to the low thermal diffusivity of moulding materials, the conditions for collapse are only achieved with castings of extremely heavy sections. For light section castings, which cool rapidly to the tearing temperature, it is the high dry strength of the unchanged coresand that is significant, producing a strong tearing tendency[9]: the contrasting situations arising from the time dependence of the sand properties are schematically illustrated in **Figure 3.35**.

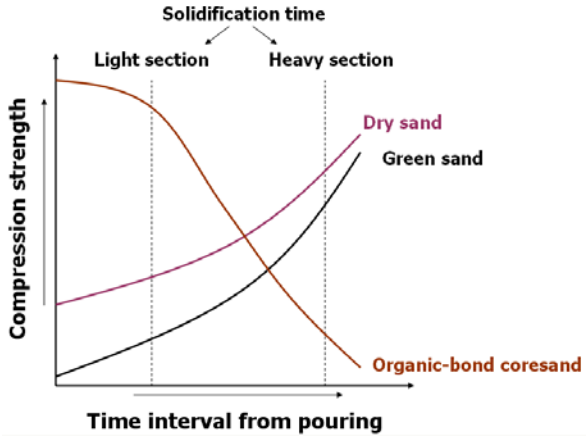

Figure 3.35: Strength changes in moulding materials after casting. Schematic comparison of clay bonded and organically bonded sands, adapted from [9].

Campbell[4] lists the sand binders in increasing hot-tearing tendency for casting sections of less than 30 mm. These are: Greensand *(least hot tearing tendency)*, Dry sand (clay bonded), Sodium silicate bonded (CO, and ester hardened types), Resin-bonded shell sand, Alkyd resin/oil (perborate or isocyanate types), Oil sand, Phenol formaldehyde resdisocyanate, Furan resin (*highest hot tearing tendency*). Although the strengths give a rough indication of hot tearing tendency, the capacity for deformation is the crucial factor. For a sand of high initial dry strength, the capacity for high

temperature deformation in the surface layers alone must be sufficient to accommodate the whole of the contraction. The extent of this deformation is a function of metal temperature, binder composition, ramming density and other variables. Deformation of a mould can be enhanced by special additions such as sawdust, wood flour, or chopped straw; this is also one of the functions of cereal binders. The contraction resistance of larger moulds and cores may also be reduced by centre fillings of loose materials such as coke and unbonded sand. Certain mould and core sections may be completely hollowed out by the use of dummy pattern blocks in moulding. The mechanical construction of the mould must be designed to avoid hindrance from box bars, reinforcing grids and irons. Sprues and feeder heads emerging at the cope surface must be kept well clear of these obstructions, a considerable amount of free movement being required for long dimensions. This movement can be helped by removal of moulding material from between heads and runners immediately after casting, a practice aided by relief cores which can be extracted after a suitable interval. However, it has to be emphasized that removal of constraints after casting is not always a reliable technique. This is because the timing is difficult to control precisely; too early an action may result in a breakout of liquid metal, and too late will cause cracking[9]. Therefore, other improving measures should be applied, for instance optimized chilling to induce a favorable solidification pattern, i.e. progressive and directional.

Specific precautions against hot tears can be embodied in the casting design. Apart from the overall aim of section uniformity, section changes should be gradual and all corners provided with adequate radii to reduce stress concentration. Reinforcement can be introduced in the form of thin webs and brackets across critical regions; these may be temporary to be removed in fettling or may be retained as a permanent feature of the design. Their function is to accelerate cooling and so to strengthen vulnerable zones during their cooling through the critical temperature. These brackets can be seen in **Figure 3.36**. Corrugated, i.e. wavy, surfaces have been suggested as one means of sharing the strain concentration between numbers of sites in members prone to tearing.

Figure 3.36: Application of strengthening brackets, i.e. ribs, in steel castings to prevent hot tearing [ref. Paper IV, (Kotas et. at. 2010)].

Much effort has been devoted to the understanding of the hot tearing phenomenon over the past decades. Several mechanisms of hot tearing and conditions that may lead to it are already suggested in literature[40]. In conclusion to this section, some of those are outlined and summarized in **Figure 3.37.** It also shows that the conditions for and causes of hot tearing can be considered on different length scales, from macroscopic to microscopic, and some of these conditions are important on both mesoscopic and microscopic scales[41]. This figure also gives a support to the assumption that the Niyama criterion can be effectively utilized in assessing and predicting the presence of hot tears. The first link can be seen in the pressure drop over the mushy zone which favors a pore or void to nucleate. This newly nucleated pore then represents an initiation site of the subsequent hot tear. The second link between centerline porosity and hot tears is the thermal gradient, which has already been discussed earlier in this work.

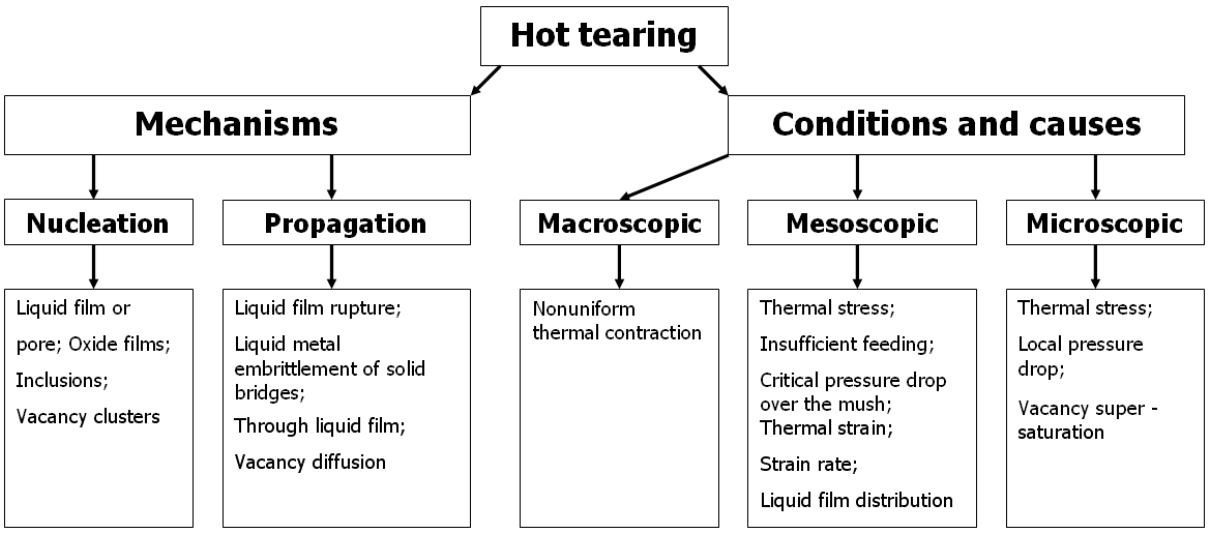

Figure 3.37: Summary of mechanisms, conditions, and causes of hot tearing, as suggested to date. Figure adapted from [41].

3.7.4. Macrosegregation

Macrosegregation refers to spatial variations in composition that occur in metal alloy castings and range in scale from several millimeters to centimeters or even meters. These compositional variations have a detrimental impact on the subsequent processing behavior and properties of cast materials and can lead to rejection of cast components or processed products. Macrosegregation is present in virtually all casting processes, including continuous, ingot[42- 44] and shape casting of steel and aluminum alloys, iron casting, casting of single crystal super-alloys, semisolid casting, and even growth of semiconductor crystals[23]. Macrosegregation is especially important in large castings and ingots. Because of the low diffusivity of the solutes in the solid state and the large distances involved, such inhomogenity cannot be removed through processing of the casting after solidification is complete, i.e. by heat treatment, as the time required for solid state diffusion to occur at this scale is prohibitive[22]. Therefore, not surprisingly, modeling of macrosegregation is still a very active research field, for instance the research group of Prof. Beckermann[45] at University of Iowa, has contributed substantially in this field, when the first pioneering contributions were made by Flemings[20, 46, 47] and co-workers in the beginning of 1960s. They discovered the importance of convection within the mushy zones of solidifying alloys, and derived the basic equation describing macrosegregation due to interdendritic flow[20].

The cause of macrosegregation is relative movement or flow of segregated liquid and solid within the mushy zone during solidification. Most alloy elements have a lower solubility in the solid than in the liquid phase as is shown by phase diagrams, see **Figure 3.38**.

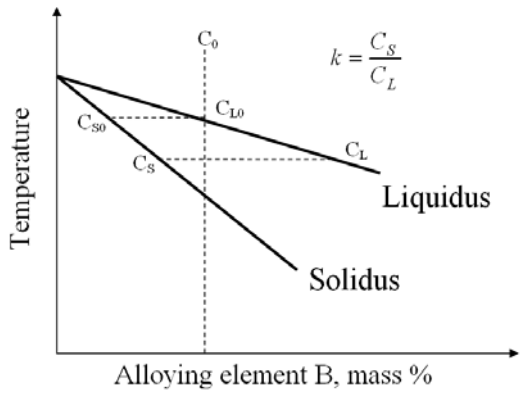

Figure 3.38: Schematic of a partial equilibrium phase diagram of a binary alloy.

During solidification, the solutes are therefore rejected into the liquid phase, leading to a continuous enrichment of the liquid and lower solute concentrations in the primary solid. The segregation occurs on the scale of the microstructure that is forming, which often consists of dendrites having arm spacing of the order of 10 to 100 μm. It is therefore termed microsegregation and results in a nonuniform, cored solute distribution in the dendrite arms. Despite this localization of segregation at the micron scale, macrosegregation can nevertheless occur by several mechanisms, as illustrated in **Figure 3.39**.

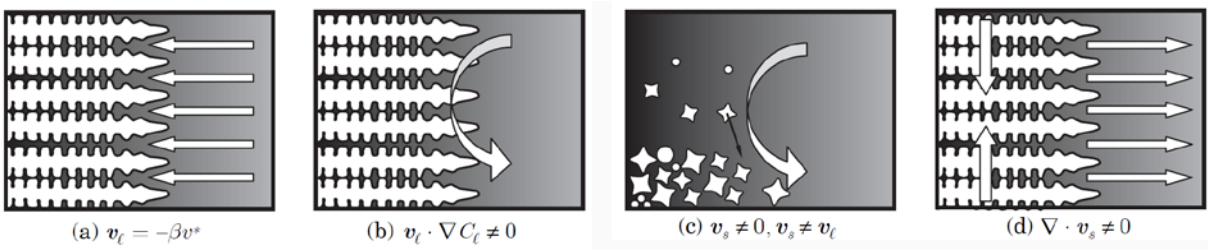

Figure 3.39: Various types of macrosegregation induced by (a) solidification shrinkage, (b) fluid flow, (c) grain movement and (d) deformation of the solid[22].

In all of them, macrosegregation takes its origin in the relative movement of one phase with respect to another. Indeed, as the solid and liquid phases do not accept the same amount of solute, microsegregation will give rise to macrosegregation in which one phase moves relative to the other. When such movement or flow generally occurs over large distances, the casting becomes macroscopically segregated. Macrosegregation at a given location in a casting is said to be negative when the average composition measured over a representative volume element is lower than the nominal value. It is positive in the opposite case. The four main causes of macrosegregation are illustrated in **Figure 3.39** and are briefly treated in the following:

(a) *Macrosegregation associated with solidification shrinkage*, i.e. flow that feeds the solidification shrinkage and the contractions of the liquid and solid during cooling, **Figure 3.39(a)**,

(b) *Macrosegregation associated with natural or forced convection*. If the velocity of the liquid is perpendicular to the solute gradient, no macrosegregation occurs. However, macrosegregation is induced when the flow enters or exits the mushy zone, **Figure 3.39(b)**.

(c) *Macrosegregation associated with grain movement*. As long as the grains move with the same velocity as the liquid, there is no macrosegregation. However, equiaxed grains have a tendency to sediment or, in certain cases, to float, giving rise to macrosegregation, **Figure 3.39(c)**.

(d) *Macrosegreation associated with deformation of the solid network* in the mushy zone due to thermal and shrinkage stress, head pressure, or external forces on the solid shell. In other words, the mushy solid behaves like a sponge causing the liquid to be expelled (when in compression) or sucked in (when in tension), **Figure 3.39(d)**.

All efforts to prevent macrosegregation are aimed at controlling liquid flow and movement of solid. Examples include adjustments to the alloy composition or thermal gradients to induce a stable density stratification in the liquid; application of nozzles, baffles, porous materials, or electromagnetic fields to redistribute the flow; controlled deformation such as soft reduction during continuous casting of steel to squeeze highly enriched liquid away from the centerline of slabs; changing the cooling rate or the alloy composition to decrease the dendrite arm spacing and hence increase the resistance to flow through the solid network; and increasing the prevalence of equiaxed grains in a casting, for example, by inoculation or stirring, in order to obtain a more uniform and dense solid distribution[48].

3.7.4.1. Macrosegregation induced by fluid flow

In this section, quite a few equations related to macrosegregation phenomena will be presented and briefly discussed. It has not been the aim to explain the theory and various aspects of macrosegregation just based on these equations. It is for sure not a scope of this thesis. The reason for showing all of these equations is that they serve as a basis for the modeling and analysis of macrosegregation in MAGMAsoft, which has been used throughout the PhD study. It was considered

interesting to show a brief overview of what goes on inside this numerical solver. To link the theory to the practical aspects of metal casting, several practical casting-related examples are shown indicating and supporting the results and theoretical findings of most of these equations.

Liquid flow through the mushy zone, where the developing solid network can be assumed to be rigid and fixed, is the most common cause of macrosegregation. Such macrosegregation can be best understood by considering the local solute redistribution equation (LSRE) derived by Flemings and co-workers[20, 47], see **Eq. 3.43**. They considered the flow of interdendritic liquid through a fixed dendritic solid network as illustrated in **Figure 3.40** while accounting for the different densities of the solid and liquid. This equation is based on a solute balance on a small-volume element inside the mushy zone. Flemings and co-workers assumed that: (i) local solute diffusion in the solid phase is neglected, and (ii) the liquid flowing through the volume element is assumed to be well mixed and in local equilibrium with the solid, i.e. the liquid is not undercooled. These are the same assumptions as made in the derivation of the Scheil equation[1]. Then, the solute concentration in the liquid, C_L, is given as a function of temperature by the liquidus line of an equilibrium phase diagram (**Figure 3.38**) according to $C_L = (T - T_m)/m$ (where T is the temperature, T_m is the melting point of the pure solvent, and m is the slope of the liquidus line).

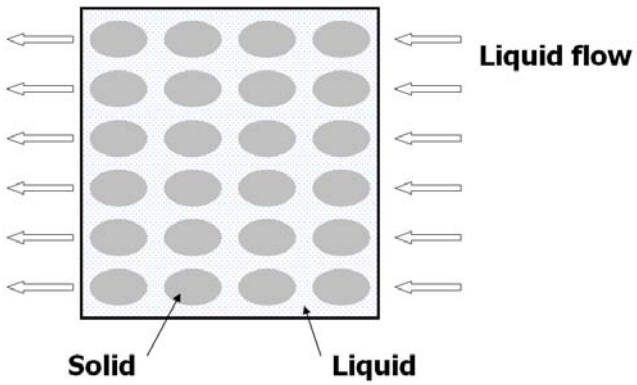

Figure 3.40: Schematic of liquid flowing through a small volume inside the mushy zone. The gray ovals represent cuts through dendrite arms. Figure inspired by Beckermann[48].

Accounting for advection of solute by the liquid flow in or out of the volume element, and for the different densities of the solid and liquid phases, the following LSRE results:

$$\frac{df_s}{dC_L} = \frac{(1-f_S)}{C_L}\frac{(1-\beta)}{(1-k)}\left(1-\frac{u_n}{R}\right) \tag{3.43}$$

where f_S is the solid volume fraction, k is the partition coefficient, u_n is the liquid flow velocity in the direction normal to the isotherms and R is the isotherm velocity and β is the solidification shrinkage described in section **3.7.2.2**.

In one dimension, mass conservation yields that the liquid velocity needed to feed the solidification shrinkage is given by:

$$u_{n-shrink} = R\cdot\left(1-\frac{\rho_S}{\rho_L}\right) = -R\cdot\frac{\beta}{(1-\beta)} \tag{3.44}$$

Note that shrinkage-driven flow is in the direction opposite to the isotherm velocity, that is, in the direction of decreasing temperature toward regions of higher solid fraction. Only if the alloy expands upon solidification, $\beta < 0$, and $u_{n\text{-}shrink}$ has the same sign as R. Defining the flow factor, ξ, as:

$$\xi = (1-\beta)\left(1-\frac{u_n}{R}\right) \tag{3.45}$$

Equation **3.43** can be integrated to yield a modified Scheil equation:

$$\frac{C_L}{C_0} = (1 - f_S)^{(k-1)/\xi} \tag{3.46}$$

where k and ξ are assumed constant. The physical significance of Equations **3.43** or **3.46** can be understood as follows (for k < 1):

- **Eq. 3.46** reduces to the Scheil equation, implying no macrosegregation if the flow factor is equal to unity. There are two obvious cases for which $\xi = 1$:
  a. No shrinkage and no liquid flow normal to the isotherms, i.e. $u_n = 0$.
  b. When the liquid velocity is just that required to feed solidification shrinkage, i.e. $u_n = -R \cdot \beta / (1 - \beta)$ or $u_n = u_{n\text{-shrink}}$.

- For $\xi \neq 1$, macrosegregation occurs, since the liquid concentration, C_L, varies differently from that predicted by the standard Scheil equation. Based on **Eq. 3.46**, three different macrosegregation mechanisms and outcomes can be identified.

  a. **Negative segregation**: $\xi > 1$ or $u_n / R < -\beta/(1-\beta)$, or equivalently, $u_n < u_{n\text{-shrink}}$. At the same solid fraction, C_L is lower than for $\xi = 1$, indicating that negative macrosegregation will result. For the case of $\beta \geq 0$, this condition is met if the liquid flows in the direction of decreasing temperature toward regions of higher solid fraction ($u_n < 0$) and with a speed (absolute value of velocity) that is greater than the shrinkage velocity $u_{n\text{-shrink}}$.

  b. **Positive segregation**: $0 < \xi < 1$ or $1 > u_n / R > -\beta/(1-\beta)$, or equivalently $R > u_n > u_{n\text{-shrink}}$. At the same solid fraction, C_L is higher than for $\xi = 1$, indicating that positive macrosegregation will result. This can be rephrased as, both flow in the same direction as the shrinkage flow, but with a speed less than the shrinkage velocity, as well as flow in the opposite direction (in the direction of increasing temperature towards regions of lower solid fractions) result in positive macrosegregation. Examples include centerline and under-riser segregation in steel castings.

  c. **Local remelting**: $\xi < 0$ or $u_n > R$. This condition is met if the liquid flows in the direction of increasing temperature toward regions of lower solid fraction and with a velocity that is higher than the isotherm velocity. Based on **Eq. 3.46**, such flow results in the solid fraction decreasing, rather than increasing, with decreasing temperature. This means that remelting occurs and that open (solid-free) channels can form inside the mushy zone. Once the casting is solidified, the macrosegregation inside of these channels is positive. Such situation is depicted schematically in **Figure 3.41**. Assume that a columnar mushy zone grows at steady state with a velocity R. If a small element of liquid deep in the mushy zone, where C_L is large, moves toward the dendrite tips because $u_n > R$, the average composition in the liquid at this point increases. On the other hand its temperature remains almost unchanged. From the standpoint of the average composition C_{AVG}, increasing the liquid composition increases C_{AVG} at the highest location. If the temperature remains fixed, this obviously decreases the solid fraction, i.e. local remelting occurs, in order to maintain local equilibrium at the solid-liquid interface[22]. This phenomenon is responsible for freckle formation often referred to as channel segregation. More on this topic will be given later in this chapter.

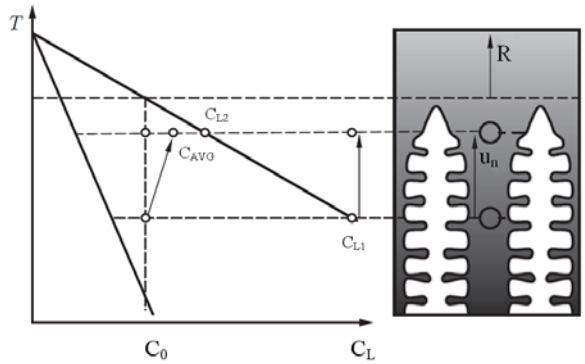

Figure 3.41: Local remelting inside a mushy zone when $u_n > R$. Adapted from [22].

The direction and magnitude of the liquid flow velocities in the mushy zone depend on numerous factors. For a given driving force, the permeability of the mush is the single most important parameter that limits the flow[49]. In general, the permeability decreases with increasing solid fraction. A smaller dendrite arm spacing also reduces the permeability. The following examples illustrate in more detail the aforementioned macrosegregation mechanisms.

Inverse Segregation. Near a chill face, positive macrosegregation is often observed[50]. This so-called inverse segregation[51] is a consequence of the second macrosegregation mechanism discussed previously. At an impenetrable chill face, the liquid velocity vanishes ($u_n = 0$). Moreover, the condition $u_n > u_{n\text{-shrink}}$ is always satisfied at the chill face, and positive macrosegregation results. If a gap is present between the mold and the casting, the solute-rich interdendritic liquid can be pushed into the gap by the metallostatic pressure. This is termed exudation and results in even higher positive macrosegregation at the surface. In direct chill casting of aluminum ingots, this macrosegregation can be so severe that the exuded surface layer must later be removed by scalping the ingot.

A very similar case is seen in **Figure 3.42** where due to the presence of an inner chill a tendency towards positive segregation is seen. Since a non-contact chill was applied in this case, we cannot talk strictly about the inverse segregation but rather just a tendency. This tendency is denoted by the two black arrows.

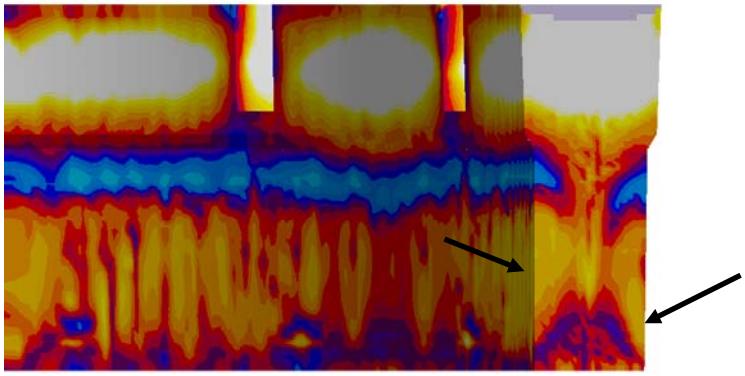

Figure 3.42: Carbon compositional profile in an optimized steel casting. Everything what is white contains more solute elements than is the nominal composition in the liquid state. The two black arrows emphasize the tendency towards inverse segregation in areas very close to chills, [ref. Industrial report, (Kotas et al. 2010)].

Macrosegregation due to Buoyancy-Driven Flow. The first and second macrosegregation mechanisms can be observed simultaneously if the liquid flow pattern in the mushy zone is of a recirculating nature. This has been demonstrated for the large steel ring casting shown in **Figure 3.43**.

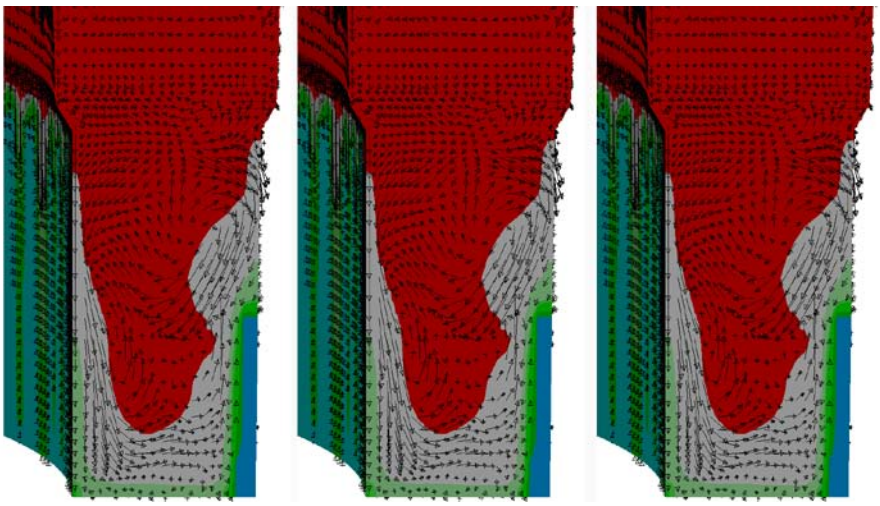

Figure 3.43: Temperature field with suggested thermal convection profiles at 8, 10 and 12% solidified, [ref. Industrial report, (Kotas et al. 2010)].

Here, a clockwise recirculating flow pattern is induced in the liquid by thermal and solutal buoyancy forces. **Figure 3.43** shows that the flow in the bulk liquid region penetrates into the mushy zone. In the upper right part of the mushy zone, the flow is in the direction of decreasing temperature ($u_n < 0$), i.e. flowing from the liquid area to the mushy zone. According to the first macrosegregation mechanism, such flow causes negative macrosegregation. The same trend, but less pronounced, is seen on the casting's inner side. Negative macrosegregation was indeed measured in the upper part of the casting on its both i.e. inner and outer surfaces, as shown in **Figure 3.44**.

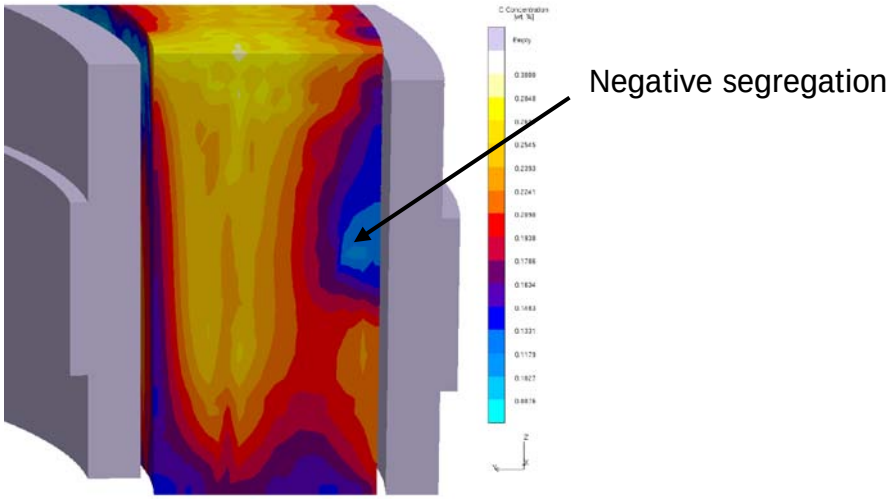

Figure 3.44: A detailed view on a concentration profile of carbon in the original casting layout [ref. Industrial report, (Kotas et al. 2010)].

Conversely, in the lower part of the mushy zone, the interdendritic liquid flows in the direction of increasing temperature ($u_n > 0$), back into the bulk liquid region. This causes positive macrosegregation according to the second mechanism. This was again verified by the macrosegregation profile (**Figure 3.44**). Buoyancy-driven flow is also responsible for the positive macrosegregation seen in the riser of large steel castings and ingots, as shown in **Figure 3.45**. In steel castings, the interdendritic liquid is often lighter than the bulk liquid and flows up. This up-flow is in the direction of increasing temperature ($u_n > 0$), since the riser is the last part of the casting to solidify. Consequently, positive macrosegregation results according to the second mechanism. More on this topic can be found in **Papers III, IV** and **Industrial Report**, written by the author.

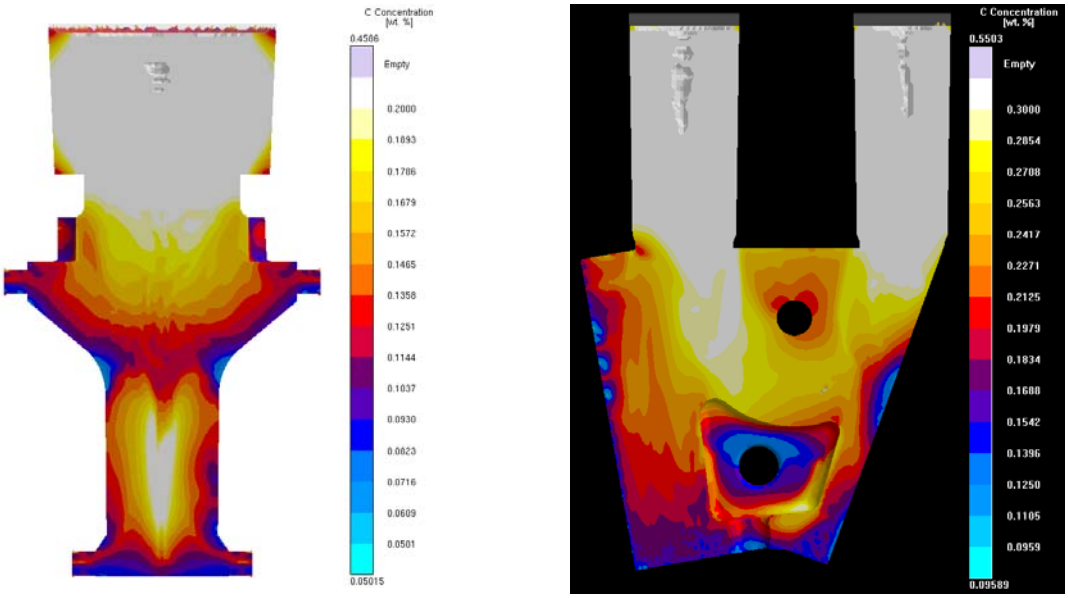

Figure 3.45: Macrosegregation profiles for two distinct industrial castings, [ref. Paper III, (Kotas et al. 2010) and Paper IV, (Kotas et al. 2010)]. White color indicates positively segregated regions.

Channel segregation. Flow due to thermal and solutal gradients in the liquid leads to formation of so-called channel segregates, commonly referred to as A- segregates or freckles, an example of which is shown in **Figure 3.46**.

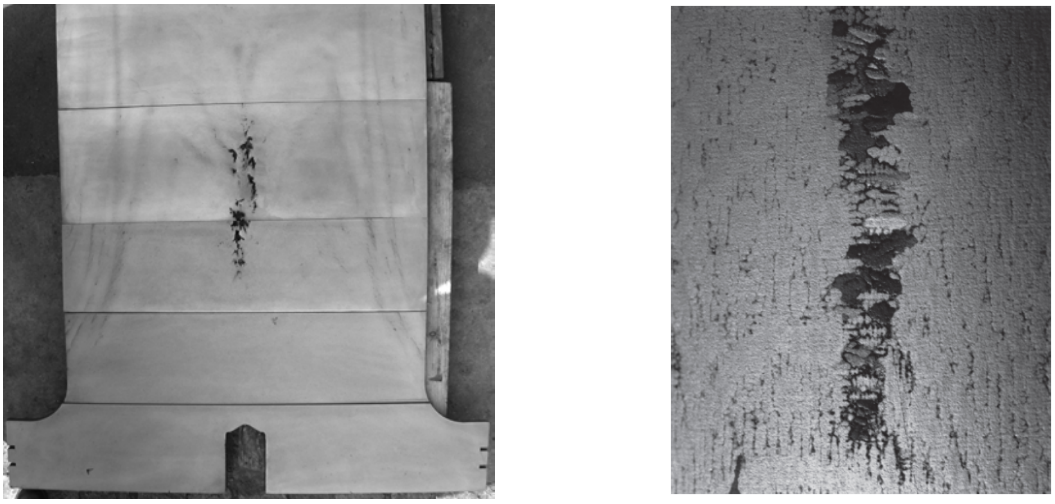

Figure 3.46: (a) Presence of porous areas and channel segregates in a steel casting [paper II, (Kotas et al., 2010)], (b) Close-up of a single freckle[52].

Freckles have been the subject of intense research efforts for about 40 years due to their importance as a defect in alloy casting and the interesting fluid-mechanical phenomena associated with their formation. Freckles are chains of small equiaxed grains in an alloy otherwise solidified with a columnar structure. They are typically initiated by convective instabilities in the high-liquid-fraction region of the mushy zone near the primary dendrite tips[53], i.e. when the velocity of the liquid in the mush exceeds that of the isotherm ($u_n > R$). During upward directional solidification into a positive temperature gradient, the melt inside the mushy zone can become gravitationally unstable due to chemical segregation of alloy elements at the scale of the dendrite arms. Such microsegregation can cause local melt density to decrease during solidification if the light alloy elements are preferentially rejected into the melt (for $k < 1$), or if heavy alloy elements are preferentially incorporated into the solid (for $k > 1$). If the melt overcomes the retarding frictional force in the porous medium-like mushy zone, convection cells form. Since the mass diffusivity of the liquid is much lower than the heat diffusivity, the segregated melt retains its composition as it flows upward through the mush into regions of higher temperature. There, the melt causes delayed growth which eventually leads to open channels, i.e. local remelting due to solid fraction decrease, in the mush through which the solute-rich and low-density liquid flows upward into the bulk liquid region (according to the third macrosegregation mechanism). These open channels are associated with local increase in permeability which allows for the liquid to flow more easily, thus enhancing remelting and macrosegregation. When the channels eventually freeze, they appear as pencil-like chains of equiaxed crystals that are highly enriched in solute[54]. At the lateral boundary of the channels, higher-order dendrite arms can become detached from the main trunk, most likely by a local remelting process. These dendrite fragments either, (1) remain in the channels and grow into the equiaxed grains later observed as freckles chains or (2) are advected out of the channels by the flow and, if not remelted completely, may form spurious grains inside the columnar structure or even cause a columnar-to-equiaxed transition[44].

There have been many empirical studies over the years that have attempted to identify the process variables that influence or drive the formation of channel segregates, i.e A- and V-type, primarily in steel castings and ingots. For instance the work by Suzuki and Miyamoto[55] revealed the effects of thermal conditions on the formation of A-segregates and found that segregation in an 0.7 wt. % carbon steel occurs when the product of the solidification rate and cooling rate are below a certain value. They also discovered that channel segregates are initiated in areas with a solid fraction between 0.3 and 0.35. Suzuki and Miyamoto also reported that the tendency to form V-segregates in steel ingots increased for larger height-to-diameter ratios of the mold. Since this ratio controls the extent of cooling on the sides versus the bottom of the ingot, it was deduced that when the rate of

solidification is large in a direction perpendicular to the buoyancy driven flow (large H/D), V-segregation is promoted. Later on, this theory was supported by showing that V and A-segregates can be eliminated by unidirectional, vertical solidification, i.e. where solidification proceeds in the same direction as the solute enriched liquid. This is exactly why both types of channel segregates occurred in the large steel forging ram depicted in **Figure 3.46(a)** (refer to **Papers II and III**). In the original casting arrangement, i.e. prior to the numerical optimization, the bottom of the casting was not cooled whatsoever, while the entire height of the cylindrical section was surrounded by the chill bricks, leading to pronounced cooling perpendicular to the buoyancy driven flow, thus promoting segregation. An additional supporting case experienced by the author was that when large steel rings were cast, channel segregates occurred in those with large heights. For those problematic rings, a cooling/chilling system had to be entirely reworked to induce and support a favorable solidification pattern to minimize the segregation issues, see **Industrial report**. Frawley (1981) discovered that the formation of channel segregates can be further eliminated by increasing the amount of the mold taper in steel ingots, i.e. having larger top diameter as compared to the bottom diameter of the ingot[56]. Nowadays, this has been a common method in ingot casting to find the most suitable taper of the ingot to reduce segregation issues, i.e. channel segregates or/and under-riser segregation[57]. The importance of proper thermal conditions on formation of segregation but also centerline porosity is also known in the steel foundry industry in shape casting, where there is an interest in selecting the proper insulation and toppings for casting risers or shapes of the risers to minimize the aforementioned problems.

Since the formation of channel segregates is due to buoyancy driven flow, the types and amount of the various solutes present in the melt has a significant effect on the formation of macrosegregation. These solutes can be either alloying elements or residual elements present through the remelting of scrap. One example is provided in the earlier mentioned work of Suzuki and Miyamoto (1981) who observed that the addition of 1 wt. % molybdenum to 0.7 wt. % carbon steel significantly reduced the occurrence of A-segregates[56]. The alloying elements nickel, chromium and vanadium, however did not have much influence on the formation of A-segregates. In the same steel, increasing the silicon content from 0.1 to 0.5 wt. % substantially increased the extent of A-segregates.

Clearly, the onset of freckling depends on the complicated interplay of the stabilizing thermal gradient (G); the speed of the isotherms (R) relative to the flow velocities; the structure and permeability of the mush, which, in turn, depend on the casting conditions G and R as well as on the variation of the solid fraction in the mush; the variation of the liquid density in the mush and, thus, the segregation behavior of the solutes as a function of the alloy composition and solidification path; and the casting geometry and growth direction relative to gravity. Copley et al.[58] suggested a criterion for freckle formation that is based on a critical cooling rate, $\dot{T}$ (i.e. the product of imposed casting speed, *R*, and temperature gradient, *G*), below which freckles are likely to form (if *G* is below a certain critical value). One could thus argue that in this regard centerline porosity and channel segregations follow a similar trend although; they are not necessarily governed by the same physical phenomena. It means that in principle enhanced thermal gradients which in essence decrease the extent of the mushy zone, and progressive directional solidification with sufficiently tapered pool of liquid metal[10] should decrease the risk of both of these defects. This statement is well supported in the work by the author; refer to **Paper III** and **Industrial report,** enclosed at the end of this thesis. Pollock and Murphy[59] performed directional solidification experiments using Ni-base superalloys. They found a strong correlation between the primary dendrite arm spacing and freckle initiation, and, for one superalloy, the critical spacing above which freckles form was found to be 320 μm. However for superalloys, the primary spacing has been experimentally found to be well correlated by $\dot{T}^{-1/3}$,[60] lending support to Copley et al. as well.

Several investigators have attempted to interpret their experimental results in terms of a non-dimensional mushy zone Rayleigh number[61, 62]. The Rayleigh number measures the ratio of the driving buyoancy force to the retarding frictional force associated with the permeability of the mush. Beckermann and Gu[63] developed a Rayleigh number based criterion for predicting the formation of freckles in Ni-base superalloy castings. This criterion relies on finding the maximum local Rayleigh number in the mush, where the ratio of the driving buoyancy force to the retarding frictional force is the largest. They discovered that a maximum value of the Rayleigh number for freckle formation is

reached at a fairly low volume fraction of solid, approximately around 0.25. If the Rayleigh number in a superalloy casting is below this critical value, freckles are not expected to form because the driving force for convection is not large enough, whereas above this value, the average permeability is too low. The main advantage of a Rayleigh number based criterion for freckle initiation over the aforementioned purely thermal criteria is that the influence of alloy composition is taken into consideration. For a review, refer to Beckermann et al.[63].

We will conclude this section with two final remarks about freckle formation. Freckles initiate in regions of the mushy zone where the permeability is the largest. Freckles are most likely to start at the location of the largest primary spacing where the resistance to interdendritic flow is low. This also explains why freckles are very often observed at the surface of a casting, where dendrites can be seen to diverge from it. The microstructure there is thus naturally more permeable due to the branching mechanisms that are necessary to fill the space.

In large ingots, where the interdendritic liquid is less dense than the initial liquid, cooling from the side and the bottom will induce U-shaped isotherms. The flow moving upward will have a tendency to take the easiest path, i.e., move in the direction of the liquidus from the point of initiation. This leads to so-called A-type segregate channels, which are simply inclined freckles[22].

Case study I – Forging ram

This case study presents findings from numerical simulations of solidification and thermal convection in a large steel forging ram shown in **Figure 3.47**. The main objective of this study was to try to accurately predict the effect of the solidification pattern on freckle formation. It is still not possible to accurately capture and predict freckle formation just by the overall macrosegregation profiles using commercial casting oriented software packages. This is due to the necessity of an extremely fine mesh, i.e. it is an extremely computationally-heavy calculation especially for large castings. For this reason simulation of thermal convection was applied to identify the flow instabilities within the mush which then lead to freckling. Due to improper cooling/ chilling of the cylindrical section, the thermal gradients were very shallow, see **Figure 3.10(a)**, and an unfavorable temperature distribution caused choking of the liquid pool, **Figure 3.10(b)** which eventually resulted in porosity, **Figure 3.10(c)** and **3.21**.

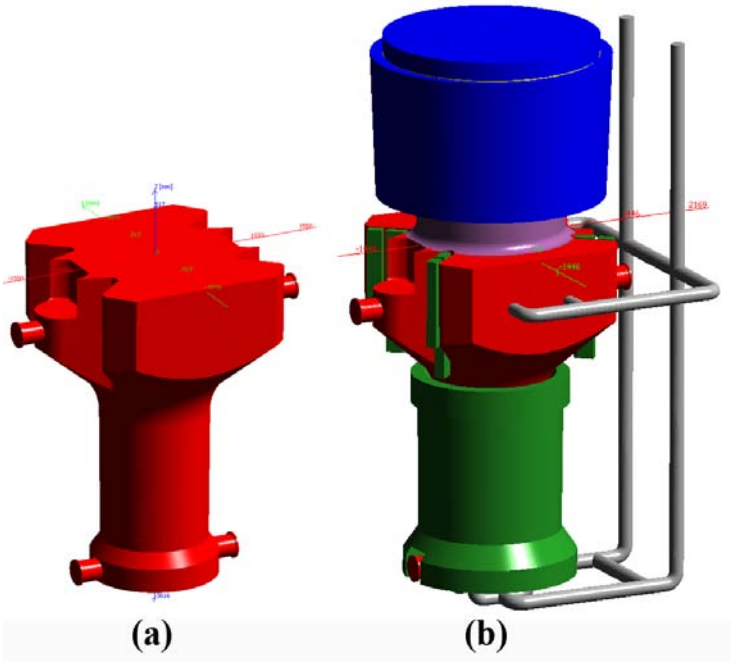

Figure 3.47: The cast part used in Case Study I, and the initial casting layout. The casting is indicated red, chills indicated green; insulation is denoted dark blue, [ref. Paper III, (Kotas et al. 2010)].

Due to the presence of very shallow thermal gradients, the mushy zone of the solidifying metal was very extensive, see **Figure 3.48**. As it was argued before if the stabilizing thermal gradient is very low it affects also the cooling rate which if it is low, it promotes freckling. This could be rephrased as

follows: if directional, progressive and pronounced solidification is not provided, the interdendritic liquid in the mush behaves “chaotic” and the buoyancy forces will “win” over the retarding frictional forces and freckling will be enabled. So the solidification pattern should be established so that it exhibits a direction, progressiveness and so that the thermal gradients are increased. In this way, the extent of the mushy zone will be decreased; more fine grains will be nucleated and present in the mush, lowering the permeability of the mush and hence imposing larger resistance to this “chaotic” interdendritic flow.

Figure 3.48 is a plot of the predicted convection patterns in the bulk liquid and mushy zones during solidification, namely at 7, 11 and 20% respectively. The vectors indicate the direction and velocity of both, the liquid and the mush during solidification. Based on this information one can estimate whether channel segregates will form or not, and where. In essence, just due to density changes the solidifying elements in the mush have higher density than the liquid in the central areas and thus they will sediment down and push the lighter liquid upwards. However, if a strong upward flow within the solidifying mush occurs this could indicate that a narrow channel has been opened, local remelting has occurred and highly segregated liquid can flow through, giving rise to a freckle. Indirectly it implies that the cooling ability of the surrounding chills is poor to retain steep thermal gradients and thus to prevent upward, localized flow. Obviously in practice it is nearly impossible to completely avoid channel segregation since the geometry of the casting together with the shape of the chills and of the riser would have to be designed extremely well and still it would not be 100% sure that no problems would occur. Nevertheless, by establishing a proper directional and progressive solidification pattern, potential freckles can be either pushed deep into the casting so that they do not show on the surface during machining operations or, get partially eliminated. The highest priority should always be to eliminate freckles due to the fact that their microstructure is totally different from the surroundings. Freckles are characterized by equiaxed grains, while the surrounding areas are mostly composed of columnar grains. Therefore, freckles represent narrow band-like areas inside the casting with deteriorated mechanical properties as compared to the surroundings. When considering that most castings and this steel ram in particular are subsequently loaded during the life service, all of a sudden these yet hidden freckles may promote cracking of even an ultimate failure of the cast parts. Problematic areas with a high risk of freckles are implied by black arrows in the figure. As compared to the casting trial depicted in **Figure 3.46(a)**, quite good agreement with the numerical prediction of freckles has been found.

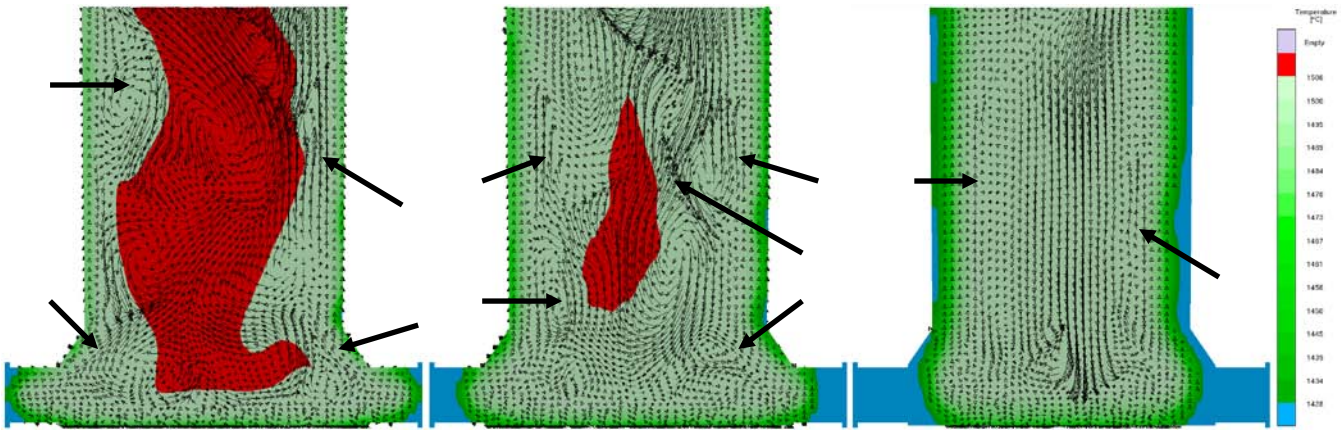

Fig. 3.48: Convection patterns and velocity vectors at 7, 11 and 20% solidified, [ref. Paper III, (Kotas et al. 2010)].

To demonstrate that the numerical simulation of thermal convection can provide accurate results, **Figure 3.49** has been used. In that figure the convection pattern from 20% solidified is overlapped by the photo obtained from the casting experiment. It suggests that indeed, the A-segregates match well with those numerically predicted. **Figure 3.50** shows the predicted carbon macrosegregation pattern in the completely solidified casting placed on top of the photo of the sectioned casting, while **Figure 3.45(left)** shows the numerical predictions for the entire cast part. It can be seen that the strong flow has created a carbon rich region in the centre of the casting. It affirms that areas solidifying last, i.e. the hot spots, will be rich in solute elements. These elements have been rejected and pushed away to the remaining liquid by the progressing solidifying front due to their lower solubility at decreasing

temperatures, causing positive segregation in the last area to solidify. Due to the isolated liquid pool which has also been a hot spot, all solute elements ended in that region with nowhere to escape, causing positive segregation.

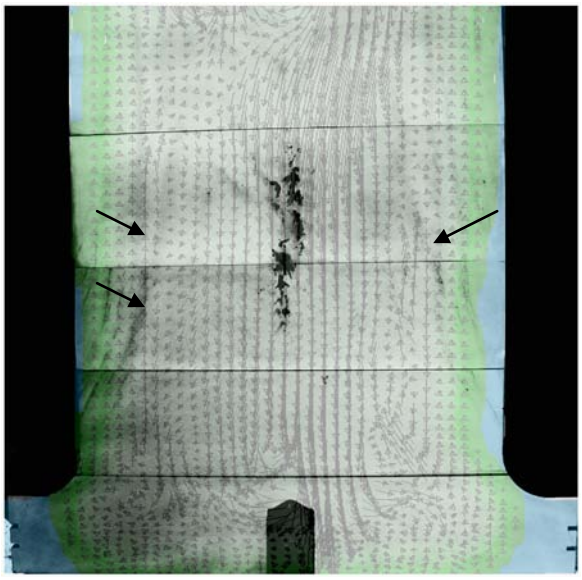

Fig.3.49: Comparison of the numerically and experimentally obtained information regarding A-segregates in the steel casting, [ref. Paper III, (Kotas et al. 2010)].

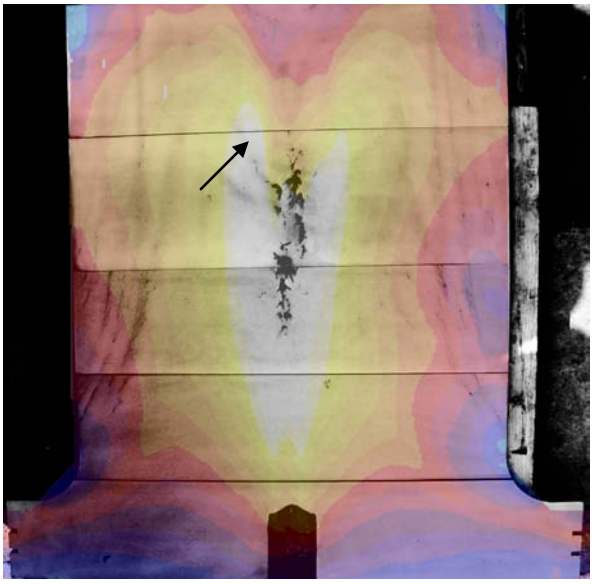

Fig. 3.50: Calculated and experimentally obtained final C macrosegregation pattern, [ref. Paper III, (Kotas et al. 2010)].

These macrosegregation predictions have been compared with the experiment, i.e. samples from the central region have been analyzed with respect to solute composition, and a reasonable agreement has been found. It can also be seen that the V-shaped segregates that formed in the real casting, seen in the photo in **Figure 3.46(a),** match very well with the predicted pattern which also resembles a V shape. This might however be a coincidence as the resolution of small scale macrosegregation features such as A- or V-segregates in large castings is still beyond the current capabilities of the macrosegregation model in the applied software.

Case study II – Steel ring

The second case study is based on the findings listed in Industrial report I. The objective of this project was very similar to the first case study, eliminate the presence of freckles inside the steel ring seen in **Figure 3.51**, and at the same time, propose a way how to increase the casting yield. However, even after the yield optimization, the overall quality of the casting had to remain superior, i.e. concentration profiles, freckles, shrinkage porosity and hot tears had to be avoided. The procedure was the same as in the first case study, i.e. at first try to accurately identify where and why the freckles would form and secondly, if they appear, find a way how to eliminate them. The results from the second objective are discussed in the chapter dedicated to optimization. Standard convection calculation was applied for identifying the freckle formation inside the casting.

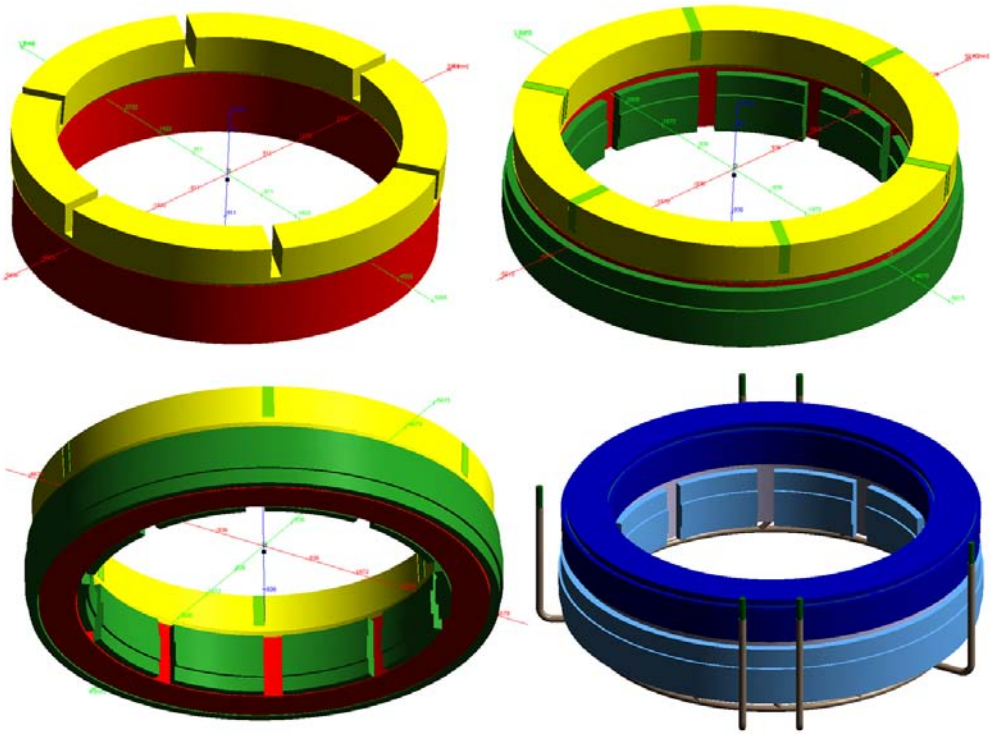

Figure 3.51: Original casting arrangement with its rigging, [ref. Industrial report, (Kotas 2010)].

In **Figure 3.52** potential initiation sites for A-segregates, i.e. freckles are indicated by the black arrows. A sudden upward-oriented flow in the mush suggests that the permeability of the mushy zone got decreased and that the interdendritic liquid rich on solute elements is enabled to float up. This means that the buoyancy force causing this flow overruled the retarding frictional force and made the interdendritic liquid flow up as explained earlier in the text. Moreover it is observed both with the numerical results and with experimental findings in **Figure 3.53** that the inner surface of the ring will be more prone to freckling due to suppressed heat removal compared to the outer surface meaning that the inner core will heat up fast due to the "converging" heat transfer. As one could see, a relatively good agreement with reality was achieved using the convection profiles during solidification.

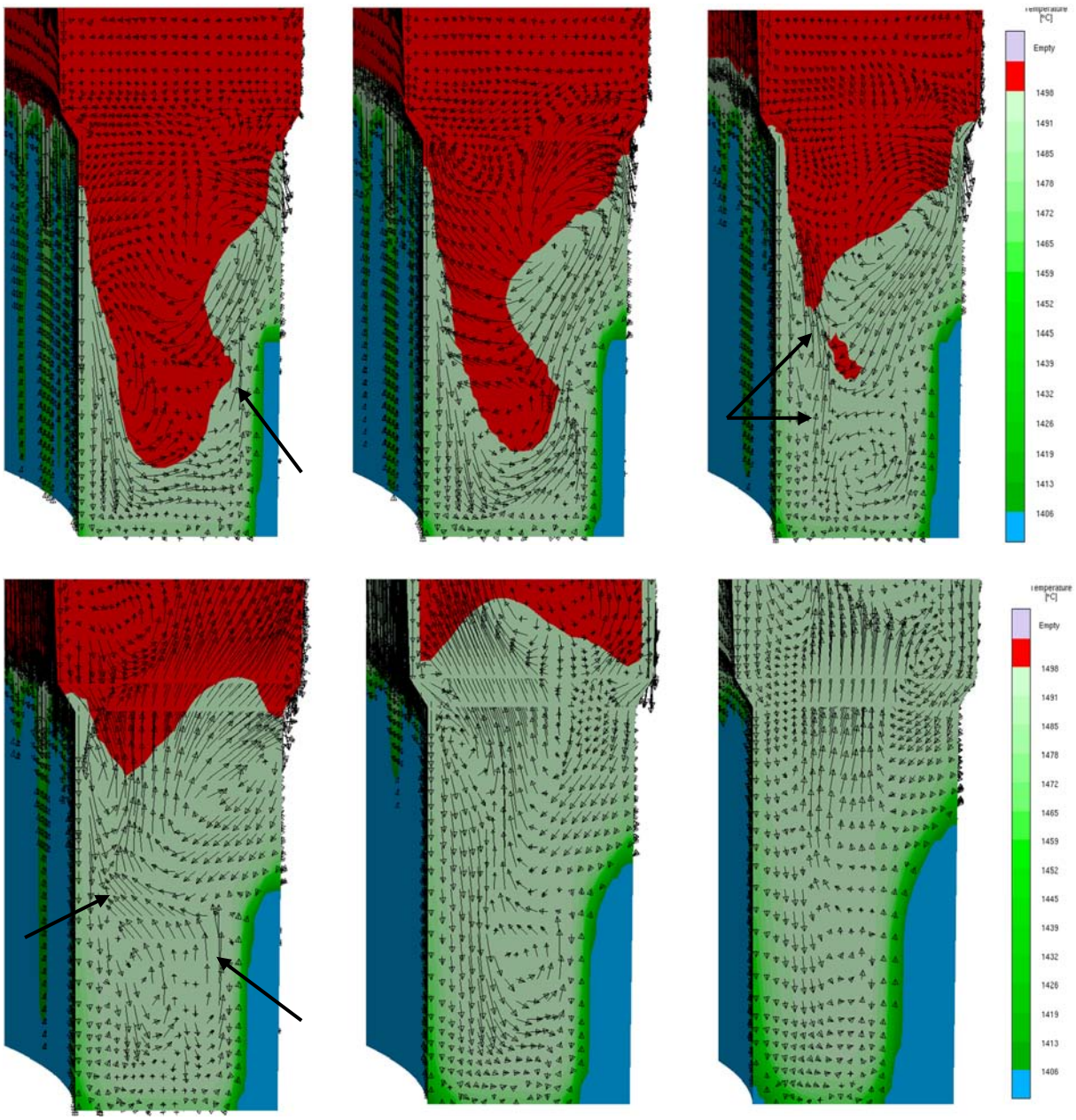

Figure 3.52: temperature profiles and convection patterns in a solidifying steel ring casting at 8, 10, 12, 14, 20 and 30% solidified. Black arrows indicate potential initiation sites for freckles [ref. Industrial report, (Kotas 2010)].

It must be noted that it is practically impossible to fully eliminate issues with channel segregates or with macrosegregation in general. The geometry of the casting would have to be designed extremely carefully and well, moreover process and working parameters would have to be extremely precise and well selected and last but not least, nothing would have to go wrong during the melting and pouring process of the casting itself. For this reason, foundry technologists generally try to design the casting geometry and the casting process in such a way that the channel segregates are pushed inwards and partially eliminated by a proper solidification pattern so that they do not appear on the casting surface after machining. If they are present on the surface, they still can be removed by welding operations, although this gets very costly if large amount of freckles are present. Such a case is depicted in **Figure 3.54** where freckles were spotted on the surface after the top riser has been remover. These black dots were among others a cause for rejection of this particular casting. The optimized solution will be shown and discussed in the chapter dedicated to numerical optimization.

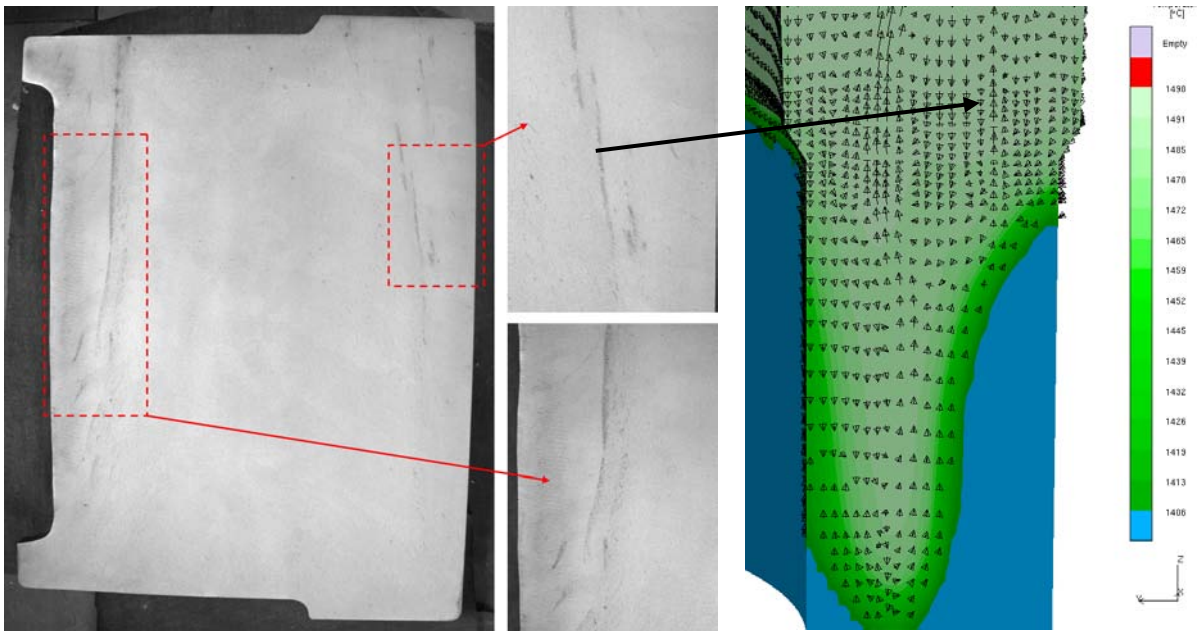

(a) *(b)*

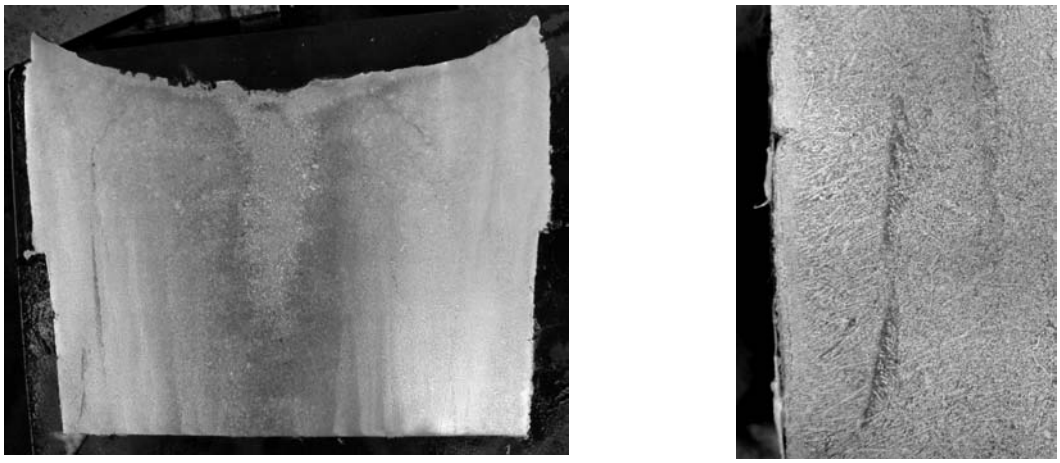

(c) *(d)*

Figure 3.53: (a) longitudinal cut through the steel ring with highlighted A-segregates, (b, temperature profile and the convection pattern in a solidifying steel ring casting at 40% solidified, the black arrow denotes a good agreement with the experimental results regarding the A-segregates (c) cut through the riser showing the pronounced macrosegregation and also porosity and (d) a detailed view on the A-segregated in the riser area, [ref. Industrial report, (Kotas 2010)].

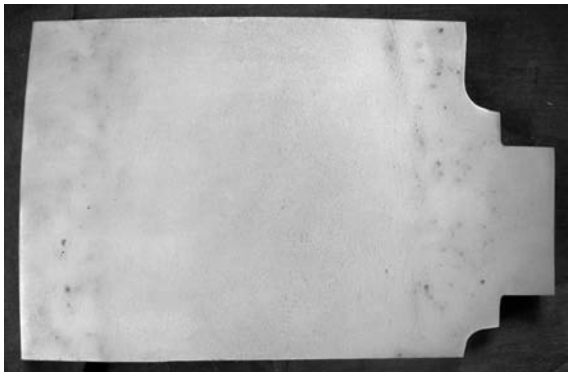

Figure 3.54: Transverse cut through the under-riser area of the steel ring denoting the appearance of channel segregates as black dots, [ref. Industrial report, (Kotas 2010)].

References

1. Hattel, J.H., "*Fundamentals of numerical modeling of casting processes*", Polyteknisk Forlag, (2005).
2. Incropera, F.P., DeWitt, D.P., "*Fundamentals of heat and mass transfer*", 4th ed., John Wiley & sons, Inc., (1996).
3. Cengel, Y.A., "*Heat and mass transfer: a practical approach*", 3rd ed., McGraw-Hill Education, (2007).
4. Campbell, J., "*Castings*", Elsevier Butterworth-Heinemann, (2003).
5. Porter, D.A., Easterling, K.E., "*Phase transformations in metals and alloys,*" 2nd ed., Taylor & Francis Group, (2004).
6. Stefanescu, D.M., "*Science and engineering of casting solidification*", 2nd ed., Springer Science+ Business Media, LLC, (2009).
7. Campbell, J., "*Castings Practice, the 10 Rules of Castings*", Elsevier Butterworth-Heinemann, (2004).
8. Frederiksson, H., Åkerlind, U., "*Materials processing during casting*", John Wiley & sons, Inc., (2006).
9. Beeley, P., "*Foundry technology*", 2nd ed., Butterworth – Heinemann, (2001).
10. Sigworth, G.K., Wang C., *AFS Trans*., vol. 100, pp. 989–1004, (1992).
11. Carlson, K.D., Ou, S., Hardin, R.A., and Beckermann, C., "*Development of New Feeding Distance Rules Using Casting Simulation; Part I: Methodology*," Metall. Mater. Trans. B, Vol. 33B, pp. 731-740, (2002).
12. Ou, S., Carlson, K.D., Hardin, R.A., and Beckermann, C., "*Development of New Feeding Distance Rules Using Casting Simulation; Part II: The New Rules*," Metall. Mater. Trans. B, Vol. 33B, pp. 741-755, (2002).
13. Carlson, K.D., Beckermann, C. "*Prediction of Shrinkage Pore Volume Fraction Using a Dimensionless Niyama Criterion*", Metallurgical and Materials Transactions A, Vol. 40A, pp. 163-175, (2009).
14. Steel Founders' Society of America, "*Feeding & Risering Guidelines for Steel Castings*", Steel Founders' Society of America, (2001).
15. Steel Founders' Society of America, "*Risering Steel Castings"*, Steel Founders' Society of America, (1973).
16. Monroe, C., *Ph.D. Thesis*, University of Iowa, (2008).
17. Hardin, R.A., and Beckermann, C., "*Effect of Porosity on the Stiffness of Cast Steel*", Metallurgical and Materials Transactions A, Vol. 38A, pp. 2992-3006, (2007).
18. Deegan, P.T., Stephens, R.I., Hardin, R.A., and Beckermann, C., "*The Effect of Porosity on the Fatigue Life of 8630 Cast Steel*," AFS Transactions, Vol. 115, Paper No. 07-120, pp. 787-803, (2007).
19. Hardin, R.A., and Beckermann, C., "*Prediction of the Fatigue Life of Cast Steel Containing Shrinkage Porosity*," Metall. Mater. Trans. A, Vol. 40A, pp. 581-597, (2009).
20. Flemmings, "Solidification Processing",
21. Kurz, W., Fischer, D.J., "Fundamentals of Solidification," Trans Tech Publications, (1998).
22. Dantzig, J.A., Rappaz, M., "S*olidification"*, EPFL Press, (2009).
23. Beckermann, C., "*Modeling of macrosegregation: applications and future needs*", International Materials Reviews, Vol. 47, No. 5, pp. 243-261, (2002).
24. Monroe, R., "*Porosity in castings*", AFS Transactions, pp. 519-547, (2005).
25. Juan, H., Jian-min, Z., Along, Y., "*Effects of Solidification Parameters on SDAS of A357 Alloy*", Advanced Materials Research, Vol. 51, pp 85-92, (2008).
26. Zhanga, L.Y., Jianga, Y.H., Maa, Z., Shanc, S.F., Jia, Y.Z., Fanc, C.Z., Wangc, W.K., *"Effect of cooling rate on solidified microstructure and mechanical properties of aluminium-A356 alloy*", Journal of materials processing technology, 207, pp 107–111, (2008).
27. Boileau J.M., Allison, J.E., "*The effect of solidification time and heat treatment on the fatigue properties of a cast 319 aluminum alloy*", Metallurgical and Materials Transactions A, Vol. 34, Issue 9, pp 1807-1820, (2003).

28. Ganesan, S.; Poirier, D. R., "*Conservation of mass and momentum for the flow of interdendritic liquid during solidification*," Metallurgical and Materials Transactions B, Vol.21, Issue.1, pp173-181, (1990).
29. Pellini, W.S., "*Factors which determine riser adequacy and feeding range*," AFS Transactions, Vol. 61, pp 61-80, (1953).
30. Niyama, E., Uchida, T., Morikawa, M., Saito, S., "*A method of shrinkage prediction and its application to steel casting practice*," *AFS Int. Cast. Met. J.*, Vol. 7, No. 3, pp 52-63, (1982).
31. Carlson, K.D., Ou, S., and Beckermann, C., "*Feeding of High-Nickel Alloy Castings*," Metallurgical and Materials Transactions B, Vol. 36B, pp. 843-856, (2005).
32. Dinnis, C.M., Otte, M.O., Dahle, A.K., Taylor, J.A., "*The Influence of Strontium on Porosity Formation in Al-Si Alloys*," Metallurgical and Materials Transactions A, Vol. 35, Issue 11, pp 3531-3541, (2004).
33. Tavitas-Medrano, F.J., Gruzleski, J.E., Samuel, F.H., Valtierra, S., Doty, H.W., "*Effect of Mg and Sr-modification on the mechanical properties of 319-type aluminum cast alloys subjected to artificial aging*," Materials science and engineering A, Issue 480, pp 356- 364, (2008).
34. Vinarcik, E.J., "*High integrity die casting processes*," John Wiley & sons, (2003).
35. Spittle, J.A., Cushway, A.A., "*Influences of superheat and grain structure on hot tearing susceptibilities of Al-Cu castings*," Metals Technology, Vol. 10, part 1, pp 6-13, (1983).
36. Monroe, C., and Beckermann, C., "*Development of a Hot Tear Indicator for Steel Castings*," Materials science and engineering A, Vol. 413-414, 2005, pp. 30-36.
37. Y. M. Wong, H. N. Han, T Yeo and K. H. OH, "*Analysis of solidification cracking using the specific crack susceptibility*," ISIJ International, vol. 40 (2000), no. 2, pp. 129-136.
38. Monroe, C., and Beckermann, C., "*Simulation of Hot Tearing and Distortion During Casting of Steel: Comparison with Experiments*," in Proceedings of the 60th SFSA Technical and Operating Conference, Paper No. 5.7, Steel Founders' Society of America, Chicago, IL, 2006.
39. Oryshchyn, Danylo B.; Doğan, Ömer N., "*An examination of effects of solidification parameters on permeability of a mushy zone in castings*," Journal of Materials Science, Vol.43, Issue.4 , pp 1471-1479, (2008).
40. Sigworth, G.K., "*Hot Tearing of Metals*," AFS Transactions, Vol.104, pp 1053- 1063, (1996).
41. Eskin, D.G., Katgerman, L., "*A quest for a new hot tear criterion*," Metallurgical and materials transactions A, Vol. 38, Issue 7, pp 1511- 1519, (2007).
42. Combeau, H., Založnik, M., Hans, H., Richy, P.E., "*Prediction of Macrosegregation in Steel Ingots: Influence of the Motion and the Morphology of Equiaxed Grains*," Metallurgical and materials transactions B, Vol. 40, Issue 6, pp 289- 304, (2009).
43. Combeau, H., Kumar, A., Založnik, M., "*Modeling of equiaxed grain evolution and macrosegregation development in Steel Ingots*," Transactions of The Indian Institute of Metals, Vol. 62, Issues 4-5, pp. 285-290, (2009).
44. Gu, J.P., and Beckermann, C., "*Simulation of Convection and Macrosegregation in a Large Steel Ingot*," Metall. Mater. Trans. A, Vol. 30A, pp. 1357-1366, (1999).
45. Solidification Laboratory at the University of Iowa: http://css.engineering.uiowa.edu/~becker/
46. Flemmings, M.C., "*Solidification processing*,"Metallurgical transactions A, Vol.5, Issue.10, pp 2121-2134, (1974).
47. Fujii, T., Poirier, D. R., Flemings, M. C., "*Macrosegregation in a multicomponent low alloy steel*," Metallurgical Transactions B, Vol.10, Issue.3, pp 331-339, (1979).
48. Beckermann, C., "*Macrosegregation*," in ASM Handbook, Volume 15: Casting, ed. S. Viswanathan, ASM International, Materials Park, OH, pp. 348-352, (2009).
49. Poirier, D.R., "*Permeability for Flow of Interdendritic Liquid in Columnar-Dendritic Alloys*," Metallurgical Transactions B, Vol. 18, pp 245–255, (1987).
50. Ohnaka, I., Matsumoto, M., "*Computer Simulation of Macrosegregation in Ingots*," Tetsu-to-Hagane (J. Iron Steel Inst. Jpn.), Vol. 73, pp 1698–1705, (1987).
51. Kirkaldy, J.S., Youdelis, W.V., "*Contribution to the Theory of Inverse Segregation*," Trans. Met. Soc. AIME, Vol. 212, pp 833–840, (1958).

52. Giamei, A.F., Kear, B.H., "*On the nature of freckles in nickel base superalloys*," Metallurgical transactions, Vol.1, Issue.8, pp 2185-2192, (1970).
53. Fredriksson, H., "*Solidification mechanisms. A study of the crystallization process in metal alloys*," Scandinavian Journal of Metallurgy, Vol.20, Issue.1, pp 43-49, (1991).
54. Schneider, M.C., Gu, J.P., Beckermann, C., Boettinger, W.J., Kattner, U.R., "Modeling of Micro- and Macrosegregation and Freckle Formation in Single-Crystal Nickel-Base Superalloy Directional Solidification," Metall. Mater. Trans. A, Vol. 28A, pp. 1517-1531, (1997).
55. Suzuki, K., Miyamoto, T., "*Study on the formation of A segregation in steel ingot*," Transactions ISIJ, Vol. 18, pp 80- 89, (1978).
56. Schneider, M.C., "*Ph.D. Thesis*," The University of Iowa, Iowa City, IA, (1995).
57. Kermanpur, A., Eskandari, M., Purmohamad, H., Soltani, M.A., Shateri, R., "*Influence of mould design on the solidification of heavy forging ingots of low alloy steels by numerical simulation*," Materials and Design, Vol. 31, pp 1096–1104, (2010).
58. Copley, S. M.; Giamei, A. F.; Johnson, S. M.; Hornbecker, M. F., "*The origin of freckles in unidirectionally solidified castings*," Metallurgical Transactions, Vol.1 Issue.12, pp 3455-3455, (1970).
59. Pollock, T.M., Murphy, W.H., "*The breakdown of single-crystal solidification in high refractory nickel-base alloys*," Metallurgical and Materials Transactions A, Vol. 27, Issue. 4, pp 1081-1094, (1996).
60. Quested, P.N.; McLean, M., "*Solidification morphologies in directionally solidified superalloys*," Materials Science and Engineering, Vol.65, Issue.1, pp 171-180, (1974).
61. Sarazin, J. R.; Hellawell, A., "*Channel formation in Pb-Sn, Pb-Sb, and Pb-Sn-Sb alloy ingots and comparison with the system NH_4CI-H_2O*," Metallurgical Transactions A, Vol.19, Issue.7, pp 1861-1871, (1988).
62. Bergman, M.I., Fearn, D.R., Bloxham, J., Shannon, M.C., "*Convection and channel formation in solidifying Pb−Sn alloys*," Metallurgical and materials transactions A, Vol.28A, Issue 13, pp 859- 866, (1997).
63. Beckermann, C., Gu, J.P., and Boettinger, W.J., "*Development of a Freckle Predictor via Rayleigh Number Method for Single-Crystal Nickel-Base Superalloy Castings*," Metall. Mater. Trans. A, Vol. 31A, pp. 2545-2557, (2000).

Chapter 4

4. Optimization

4.1. Introduction

Let us start this chapter with a simple question, what is optimization? Optimization in general may be assumed as an attempt of finding an optimal or the best solution(s) to meet under some limitations a given objective(s) either in a trial-and-error or a systematic way[1]. Optimization has played a big role since the dawn of creation and has been found in literally all fields, disciplines and activities of mankind such as daily life applications, the field of mathematics, engineering and operations research or being presented by so many brilliant examples in nature. People have always strived, or they have been forced to optimize ways of doing things, working procedures, life styles and habits to make their lives easier, earn more money, become successful or just to survive. The same principles apply to nature around us where only the fittest survive.

Nature is a great inspiration and a teacher in optimization for scientists, engineers, or whoever interested in improving any kind of design, process or schedule, etc. More specifically, e.g. in structural optimization, a number of efficient optimization and search algorithms mimicking evolutionary principles, i.e. selection and survival of the fittest, has been developed. For instance one could mention genetic algorithms (GAs) which are motivated by the principles of natural evolution. These principles are then borrowed and used artificially to construct search algorithms that are robust and require minimal problem information and which are then able to solve various search and optimization problems of science, engineering and commerce.

Let us leave nature and restrict ourselves only to engineering activities and to casting processes in particular. One may realize that this manufacturing process has gone hand in hand with optimization for ages. Metal casters have always been improving their layouts with an intention of satisfying the customer's needs, saving material, increasing mechanical properties and production rate, or eliminating scrap percentage to win over the competitors. However, for many years, even centuries, optimization of casting processes has been solely based on intuition, experience and on trial-and-error method. If optimization failed, a foundry instantly ended up with a financial loss. Therefore, much money and resources have been invested into research and development in order to understand "mysterious" physical phenomena behind the casting process, which directly influence quality of castings. A lot of important phenomena taking place during casting were described and understood over the last century which, in turn has led to a substantial increase in the quality of foundry processes and of the final casting products. However, optimization was still only manual and intuitive and a lot of castings got spoiled, rejected and wasted as a result. For this reason people from foundry industry started calling for a development of any reliable numerical simulation tool which would simulate casting processes virtually on a personal computer, evaluate and reveal potential shortcomings before any money would be lost in a real scale production. Implementation of such numerical simulation software has been a significant threshold in the history of foundry industry. The same applies to optimization; even though it was still based on the trial-and-error method at least, all of these "improving" trials and efforts started to be performed virtually without remarkable financial or material loss.

Twenty years after the introduction of simulation software for foundries into the industry, casting process simulation has become an accepted tool for process and design lay-out[2].

Metal casting process simulation is used to provide detailed information about the mold filling, solidification and solid state cooling, heat treatment and with that, also information about the local microstructure, non-uniform distribution of mechanical properties and subsequently residual stress and distortion build-up[3-8]. Moreover, physical modeling and simulation of core shooting, binder hardening and binder degradation during casting is now possible to carry out[9]. Casting simulation

tries to use physically realistic models without overtaxing the computer. At the same time the simulations need to give applicable results in the shortest time possible.

Due to the multitude of factors affecting the quality of castings and the complex interactions of physics, metallurgy and casting geometry, empirical knowledge is still the main source on which "optimized manufacturing engineering" is based. Foundry simulation can quantify experience but unfortunately, it can only test one "state" or layout. It provides insights into the root causes of problems, while conclusions from calculations or subsequent optimization still require an engineer's interpretation and decision after each of the simulation runs. This means that a continuous improvement involves "trial and error"- both in reality and in simulation.

In recent years the use of simulations software has increased and is now integrated with parallel processing computers. It is feasible to calculate numerous versions and layouts in almost unlimited configurations. The advantage of having such short calculation times can only be utilized providing that a computer can automatically evaluate different combinations of design variants with respect to predefined objectives (e.g. maximum feeding, low porosity, low air entrapment etc.) and subsequently produce new variants and analyze them in the same manner to achieve the optimal solution. By integrating such software for casting process simulation with an optimization algorithm, GA for instance, a computer based optimization tool is established which is able to determine optimal values for user-defined design variables thereby optimizing a given casting process with respect to the objectives[10].

Autonomous optimization uses the simulation tool as a virtual test field. By modifying pouring conditions, gating designs or process parameters, the software tries to find the optimal route to fulfill the desired objective(s). Several parameters can be changed at the same time and be evaluated independently from each other. Autonomous optimization tools combine the classical approach of foundry engineers, to find the "best compromise" with validated physics. This not only further reduces the need for trial runs to find the optimal process window, but also allows an in-depth evaluation of many parameters and their individual impact on providing a robust process. Subsequently such system can readily provide optimal solutions for any kind of casting processes[11-16].

In this chapter, it is intended to give a basic overview of one particular optimization technique called multi-objective genetic algorithms which have been applied for casting process optimization during this PhD study. Genetic algorithms[17] and mainly the Multi-Objective Genetic Algorithms[18] (MOGA) for handling multiple conflicting objectives have been applied, because they are incorporated in the software called MAGMA*frontier* which is the add-on optimization module of a commercial casting solidification software package MAGMAsoft®. One should bear in mind that there are other multi-objective optimization techniques and algorithms, e.g. MOGA-II[19], NSGA[20] or NSGA-II[21] (successor of NSGA), that would suit our purposes the same as MOGA; maybe even better, nevertheless these are not discussed here. Later in the chapter, several industrial case studies are presented to demonstrate how multi-objective optimization can be effectively utilized in solving various casting process-related issues.

4.2. Genetic algorithms

In this section, working principles of genetic algorithms is first described. The theory is demonstrated on a simple foundry-related case study concerning optimization of a riser volume. Thereafter, a discussion on how to apply and utilize multi-objective optimization in which several conflicting objectives are present, in daily engineering problems will be given.

4.2.1. Genetic algorithms – working principles

Genetic algorithms (GA) are computerized search and optimization algorithms developed by mimicking the evolutionary principles and chromosomal processing in natural genetics. A GA begins its search with a number of solutions, collectively known as a population of solutions, usually created at random within a specified lower and upper bound on each design variable, e.g. a height of a riser should not exceed 1000 mm and not drop below 400 mm. Since GAs work with a set of solutions (population) instead of a single point as in gradient based (classical) methods this gives an opportunity to attack a complex problem (discontinuous, noisy, multi-modal, etc.) in different directions allowing the algorithm to explore as well as exploit the search space. This capability gives an advantage for having a more robust search strategy compared to traditional algorithms. Since genetic algorithms do not need any gradient information, they are very suitable for black-box (e.g. commercial software) optimization applications. Moreover, compared with classical optimization strategies based on gradient methods, genetic algorithms can effectively utilize distributed computing facilities because all individuals (designs) can be computed independently. Due to their population based search strategy, they have been very popular for the Multi-Objective Optimization (MOO) problems, often having conflicting objectives resulting not only in a single optimum solution, but in a set of trade-off solutions (Pareto-optimal set). The availability of trade-off solutions, representing varying preference levels between chosen objectives, makes it easier for a user to choose a particular solution for subsequent implementation[22-29]. A flowchart of the working principle of a simple genetic algorithm is shown in **Figure 4.1**.

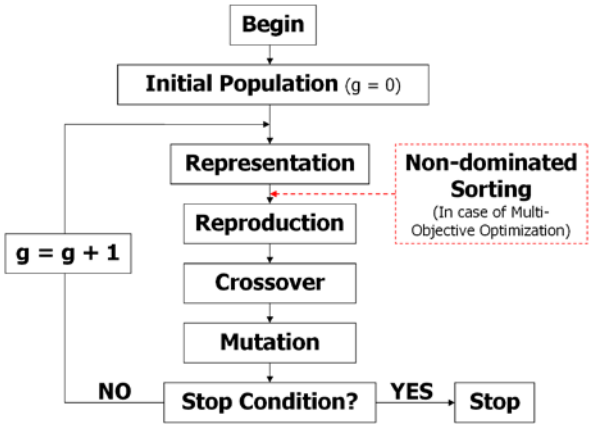

Figure 4.1: A flowchart of the working principle of genetic algorithms. The non-dominated sorting is implemented just in case of multi-objective optimization problem. Figure inspired by Deb[30].

4.2.1.1. Representation

In classical genetic algorithms[17] (Goldberg, 1989), the internal representation is based on binary encoding that each design variable is represented as a binary string, i.e. 0100, 1101101, etc., where the length of the string depends on the desired accuracy for each design variable. Therefore in order to find the optimal values from the set of design variables, e.g. diameter and height of a riser which are used to evaluate the objective function, it is necessary to represent the parameter values in binary strings. For instance, a casting riser of diameter 50 cm and height 110 cm can be represented by the following string 110010, 1101110, respectively. Since the representation of a solution or a variable in a genetic algorithm is similar to a natural chromosome and GA operators (which will be discussed later) are similar to genetic operators, the above procedure is named “genetic algorithm”. It is

important to mention that the binary-coding of the design variables in not absolutely necessary. There exist some studies where GAs are directly used on the variables themselves, the so-called real-coded genetic algorithms[31, 32], however these are not discussed here. After this, each member of the initial population, in our case each technological solution is sent into the casting simulation software MAGMAsoft®, which performs standard casting simulations for all the designs. When this is done, the user would have, let us just say 100 distinct casting layouts, completely analyzed. But there would be no information as to which design is better or worse.

The user himself would have to check each design manually and find the best one from those 100 layouts. This is obviously not an effective way of doing things. In a GA instead, each design created either in the initial population or in the subsequent generations must be evaluated in terms of the predefined objective functions and constraints. In other words, it must be assessed how well it meets the predefined objective(s) and whether it does not violate the constraint(s). For example when the minimization of the riser is our objective see **Figure 4.2(left)**, each design must be evaluated with respect to the optimization objective, i.e. the minimization of the riser volume, and designs with low riser volumes are regarded better. Then the designs or solutions are sorted by the GA (say from best to worst) in the population. Often, such an ordering can be established by creating a real-valued fitness function derived from objective and constraint values[30]. A solution is usually called better than the other, if its fitness function value is better. Again, the fitness value indicated how "fit" a given design is with respect to the objectives and constraints, how well it fulfills them. This analogy can be understood from **Figure 4.2(right)** where our riser volume optimization problem is schematically shown. One can see the initial population of all considered riser shape variants. Moreover now, each riser design is equipped with a number representing its fitness, i.e. the objective function (riser volume). Since the objective function, in our case, is to be minimized, risers with lower volumes are ranked or assumed better than the big ones. We can say that the designs have been sorted. Up till now, only a single-objective optimization has been assumed. For multi-objective optimization problems, one of the ways to achieve the ordering is to sort the population based on the domination principle proposed by Goldberg[17] (1989).

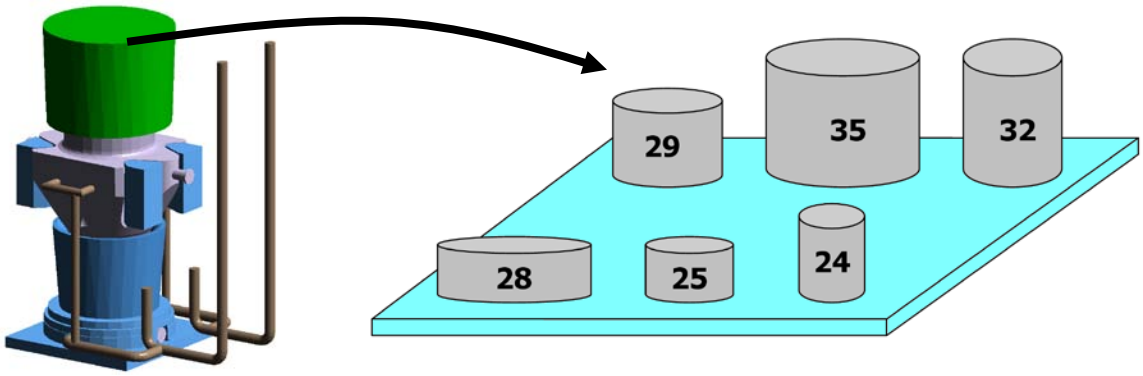

Figure 4.2: (left) The steel forging ram for which an optimal riser design with the lowest volume is sought by optimization techniques, see Papers II and III, (right) a random population of six top risers is created by GAs. Each riser design is assigned with a fitness value representing how well it fulfills the objective function.

Most engineering design activities require a solution of multi-objective and multi-disciplinary optimization problems. When multi-objective optimization is utilized, the user defines not only the degrees of freedom for the process parameters, i.e. ranges of variation, but also a number of objective functions, each of which may have a *different* individual optimal solution. It is very common, that engineers have to deal with multiple objectives which are conflicting to each other, and are to be either minimized, maximized, or a combination of these. It means that a satisfaction of one objective leads to a sacrifice in the other one. This often results in having multiple *trade-off* solutions associated with different amounts of *gains* and *sacrifices* among multiple criteria, providing that the objectives are conflicting. One common example of two conflicting objectives in foundry industry is to fill the mould as fast as possible to increase the production rate and simultaneously to keep the flow uniform and smooth without surface turbulence to promote good quality of the given cast part.

In case of single-objective optimization problems, it is easier to identify the optimal solution as compared to the case of Multi-Objective Optimization (MOO) where there is more than one criterion to investigate and satisfy, hence more than one best (elite) solution to consider. Because in case of conflicting objectives, in general, the best solution for one objective is the worst solution for the other objective.

As it was put forward by Goldberg[17] "if we refuse to compare apples to oranges, then we must come up with a different definition of optimality, one that respects the integrity of each of our seperate criteria" which points out the concept of Pareto Optimality, correlated to the fundamental concept of domination. Since the concept of domination allows a way to compare solutions with multiple objectives, most MOP algorithms use this domination concept to search for non-dominated solutions, i.e. the ones that constitute the Pareto-front as shown in **Figure 4.3(c)**. This concept can be explained with a simple example in a 2D objective space, in which the minimization of both objective functions (i.e. f_1 and f_2) is considered, as shown in **Figures 4.3(a-c)**. In **Figure 4.3(a)**, point-1 representing a solution or a design which splits the 2D objective space into two zones: the first zone (the shaded region); the set of the points dominated by point-1, and the second zone; the set of points not dominated by point-1 (the remaining three quadrants), i.e. the non-dominated or noninferior set of points. Thus, the two conditions stated below need to be satisfied if point-1 dominates point-i, where point-i is any other design point in the objective space[33]

- point-1 is no worse than point-i in all objectives.
- point-1 is strictly better than point-i in at least one objective.

These two statements give a general description for the comparison of the two solutions in terms of "betterness", hence emphasizing the applicability of this comparison for other types or combinations of conflicting objectives besides the minimization – minimization type as shown in **Figures 4.3(a-c**), i.e. maximization - maximization, maximization – minimization as well as minimization - maximization. . In case of the aforementioned minimization-minimization problem, it is formulated as follows[17, 34]

$$(\forall j : f_j(x_1) \leq f_j(x_i)) \bigcap (\exists k : f_k(x_1) < f_k(x_i)) \qquad (4.1)$$

where x_1 represents point-1 in **Figure 4.3(a)** and x_i represents any design point-i in the same 2D objective space. **Eq. 4.1** can be put in words as; at least ($\exists$) in one objective, design-1 is "strictly less" than design-i, while in others ($\forall$) they might be equal.

In case of having a population composed of e.g. five points as shown in **Figure 4.3(b)**, a need for an overall relation of dominance arises, i.e. the one-to-one comparison made for point-1 should be generalized for each point. **Figure 4.3(b)** shows the distribution of these five points together with their domination regions which are distinguished with different tones of colors and it is clearly seen that point-4 dominates points-1, 2 and 5 with respect to all objectives, while point-3 dominates all other points (i.e. strictly better) only with respect to the first objective for the given distribution. However, since points-3 and 4 are not dominated by any other points, they constitute the non-dominated front which is also called the Pareto-optimal front, see **Figure 4.3(c)**, in an MOO context. A similar comparison will reveal that point-1 and point-5 constitute the next domination front which in itself is dominated by the Pareto front and shown as the closest dashed line to the Pareto front in **Figure 4.3(c)**[19].

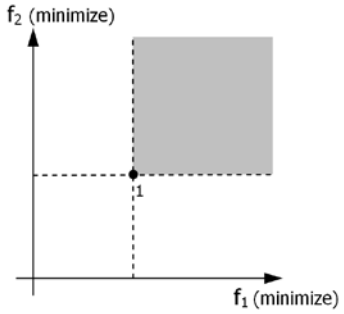

Figure 4.3(a): The two separate sets of solutions defined with respect to point-1: i) the set of dominated solutions (the shaded region), ii) the set of non-dominated solutions (adapted from [19]) [1].

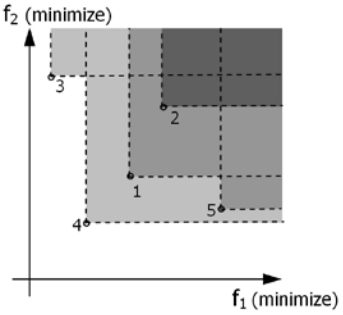

Figure 4.3(b): Each solution in a population has its own sets of dominated and non-dominated solutions (inspired by [34]) [1].

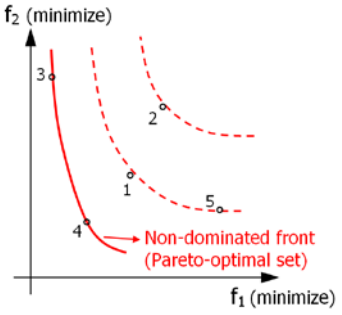

Figure 4.3(c): The dominated and non-dominated (Pareto-optimal) fronts [1].

After the population members, i.e. various technological solutions are evaluated and sorted with respect to their fitness, the next step is to select the good solutions, i.e. to emphasize the non-dominated members, for the next generation.

4.2.1.2. Reproduction

Reproduction is usually the first operator applied on a population. The primary objective of the reproduction operator is to select good solutions and to form a mating pool and to eliminate bad solutions in a population, while keeping the population size constant- in classical GAs. This is achieved by performing the following tasks:

- Identifying good (usually above-average) solutions in a population-with respect to the fitness function.
- Making multiple copies of good solutions.
- Eliminating bad solutions from the population so that multiple copies of good solutions can be placed in the population.

There exist a number of ways to achieve the above tasks. Some common methods are tournament selection[35], proportionate selection, ranking selection, and others (Goldberg & Deb, 1991)[36]. In the following, we illustrate the binary tournament selection. As the name suggests, tournaments are played between two solutions (technological designs) and the better solution is chosen and placed in a population slot also referred to as a mating pool. Two other solutions are picked again and another population slot is filled up with the better solution. If done systematically, each solution can be made to participate in exactly two tournaments. The best solution in a population will win both times, thereby making two copies of it in the new population. Similarly, the worst solution will lose in both tournaments and will be eliminated from the population. This way, any solution in a population will have zero, one, or two copies in the new population[30].

Again, assume the case where we would like to design a casting with a riser which has the lowest possible volume (**Figure 4.2**). **Figure 4.4** shows the six different tournaments played between the old population members (each gets exactly two turns) shown in **Figure 4.2(right)**. When risers with a cost of 25 units and 29 units are chosen at random for tournament, the riser costing 25 units is chosen and placed in the new population, because we want to minimize the cost. Both risers are replaced in the old population and two risers are chosen for other tournaments in the next round. This is how the mating pool, i.e. the blue area in **Figure 4.4**, is formed and the new population of designs (risers) is stored there.

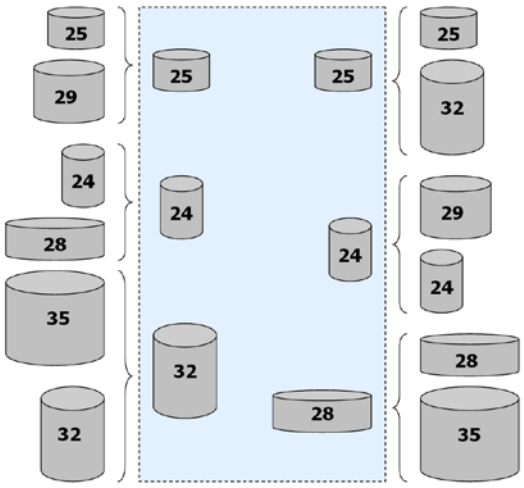

Figure 4.4: Tournaments played between six population members are shown. Solutions which have won their tournaments found themselves within the dashed box which represents the so-called mating pool. Figure adapted from Deb[30].

It is interesting to note how better solutions (having lesser costs) have made themselves have more than one copy in the new population, i.e. risers 25 and 24, and worse solutions have been eliminated from the population, i.e. risers 29 and 35. It can be concluded that the reproduction operator cannot modify any designs in the population. It only makes more copies of good solutions at the expense of not-so-good solutions. This is precisely the purpose of a reproduction operator.

4.2.1.3. Crossover

The ***crossover operator*** is next applied to the solutions, i.e. riser designs, which won their tournaments and found themselves in the mating pool. Unlike the reproduction operator, creation of new solutions is performed in crossover and mutation operators. Just like the reproduction operator, there exist a number of crossover operators in the GA literature (Spears & De Jong 1991)[37]. The classical (single-point) cross-over is a well-known genetic algorithm operator in which two parents (individuals or designs from the mating pool) are randomly chosen and some portions of these binary strings are exchanged between each other. In a single point cross-over operator, the crossing site is randomly chosen and all bits on the right side of the crossing site are swapped[1] as shown schematically in **Figure 4.5.**

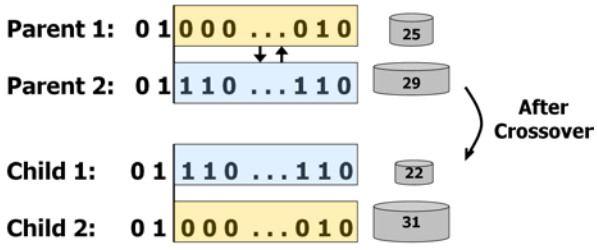

Figure 4.5: Schematic procedure of single-point crossover. Two parents are chosen from the mating pool to create two new children. Explanation, binary strings and real values next to them, obtained after decoding are all schematically given. Figure inspired by Tutum[1]

The crossover operator can be well illustrated by picking two solutions (called parents) from the new population created after a reproduction operator, i.e. those designs placed in the mating pool in **Figure 4.4**. The process creates two new solutions, i.e. riser designs (called children).

Notice that when the crossover operation was performed in **Figure 4.5** we have been quite lucky and have created a solution – Child 1 (22 units) which is better in cost than both parent solutions, i.e. it fulfills the optimization objective better than its parent solutions. One may wonder whether if another cross site was chosen or two other solutions from the mating pool were chosen for crossover, we would have a better child solution every time. It is true that every crossover between any two

solutions from the new population is not likely to find children solutions better than parent solutions; however, the likelihood of creating better solutions is far higher than random. This is because parent solutions being crossed are not just any two arbitrary random solutions, they have already survived tournaments played with other solutions during the reproduction phase. Thus, they are expected to have some good bit combinations in their string representations. Since a single-point crossover on a pair of parent solutions can only create l different solution pairs with bit combinations from either solution, the created children solutions are also likely to be good solutions. If bad solutions are created, for instance our Child 2 in **Figure 4.5**, they will get eliminated in the next reproduction operator and hence have a short life. When a good solution is created, since it is better, it is likely to get more copies in the next reproduction operator and it is likely to get more chances to perform crossovers with other good solutions. Thus, more solutions are likely to have similar chromosomes, i.e. properties, like it. This is exactly how biologists and evolutionists explain the formation of complex life forms from simple ones[38- 40]. In order to preserve some good solutions selected during the reproduction operator, not all solutions in the population are subjected to crossover. If a crossover probability of p_c is used then $100p_c$% solutions in the population are used in the crossover operation and $100(1 - p_c)$ % of the population is simply copied to the new population.

4.2.1.4. Mutation

The ***mutation operator*** is applied to a single solution to create a new perturbed solution. This means that it changes a 1 to a 0 and vice versa with a small mutation probability, *Pm.* Mutation probability is the probability of performing a mutation operation. This refers to, on average, the proportion of decision variables participating in a mutation operation to a solution. A fundamental difference with a crossover operator is that mutation is applied to a single solution, whereas when crossover is applied more parents are involved. The mutation operator can be said to be responsible of the local search as well as maintaining the diversity in the population[31]. In other words, mutation can make local improvement of one particular solution. **Figure 4.6** shows how a solution obtained after reproduction and crossover operators has been mutated to another solution. In our case when talking about casting, the child represents a slightly different riser shape and volume as compared to its parent.

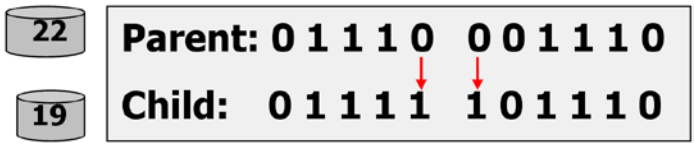

Figure 4.6: An illustration of the mutation operation. The third, fifth and sixth bit are mutated to create a new string. Figure inspired by Deb[30].

To summarize the benefits of these three operators, one could say that the reproduction operator selects good solutions and the crossover operator recombines good substrings from two good solutions together to hopefully form a better substring. The mutation operator alters a solution locally to hopefully create a better solution. Even tough none of these claims are guaranteed and-or tested while creating a new population of solutions, it is expected that if bad solutions or designs are created they will be eliminated by the reproduction operator in the next generation and if good solutions are created, they will be emphasized and further improved.

After the application of reproduction, crossover and mutation in the whole population, one generation of a GA is completed. The new population is further evaluated and tested for termination. If the termination criterion is not met, the population is iteratively operated by the above three operators and evaluated. This procedure is continued until the termination criterion is met[31].

4.2.2. Principles of multi-objective optimization (MOO)

In the context of multi-objective optimization, the extremist principle of finding the optimum solution cannot be applied to one objective alone, when the rest of the objectives are also important. Different solutions may produce trade-offs (conflicting outcomes among objectives) among different objectives.
A solution that is extreme (in a better sense) with respect to one objective requires a big sacrifice in other objectives. In relation to our riser volume optimization problem one could picture an extreme solution as follows: Our two conflicting objectives are to minimize the riser volume as much as possible and to minimize the presence of porosity in the casting. An extreme solution to this problem could be for instance total preference of the sound casting with minimum porosity but with a big riser that ensures zero porosity or, vice versa, see **Papers II, III** in the appendix for a complete case study on this topic. This prohibits one to choose a solution which is optimal with respect to only one objective. This clearly suggests two ideal goals of multi-objective optimization[35]:

1. Find a set of solutions which lie on the Pareto-optimal front, and
2. Find a set of solutions which are diverse enough to represent the entire range of the Pareto-optimal front.

However, one fundamental difference lies between single- and multi-objective optimization. In a single-objective optimization problem only one solution is evaluated the best while in the multi-objective optimization problems a whole group of non-dominated Pareto solutions is provided to a user. From a practical standpoint a user needs only one solution, no matter whether the associated optimization problem is single- or multi-objective. The user is now in a dilemma. Since a number of solutions are optimal, the obvious question arises: Which of these optimal solutions must one choose? This is not an easy question to answer. It involves higher-level information which is often non-technical, qualitative and experience-driven. However, if a set of many trade-off solutions are already worked out or available, one can evaluate the pros and cons of each of these solutions based on all such non-technical and qualitative, yet still important, considerations and compare them to make a choice. Thus, in a multi-objective optimization, ideally the effort must be made in finding the set of trade-off optimal solutions by considering all objectives to be important. After a set of such trade-off solutions are found, a user can then use higher-level qualitative considerations to make a choice. This methodology for handling multiple conflicting objectives can be summarized in the following two steps[35]:

Step 1 Find multiple non-dominated points as close to the Pareto-optimal front as possible, with a wide trade-off among objectives.

Step 2 Choose one of the obtained points using higher-level information.

Figure 4.7 shows schematically the principles, followed in an MOO procedure. Obviously step 2 can be disregarded in case of a single-objective optimization problem, because only one preferred or the "most optimal" solution is found already in Step 1.

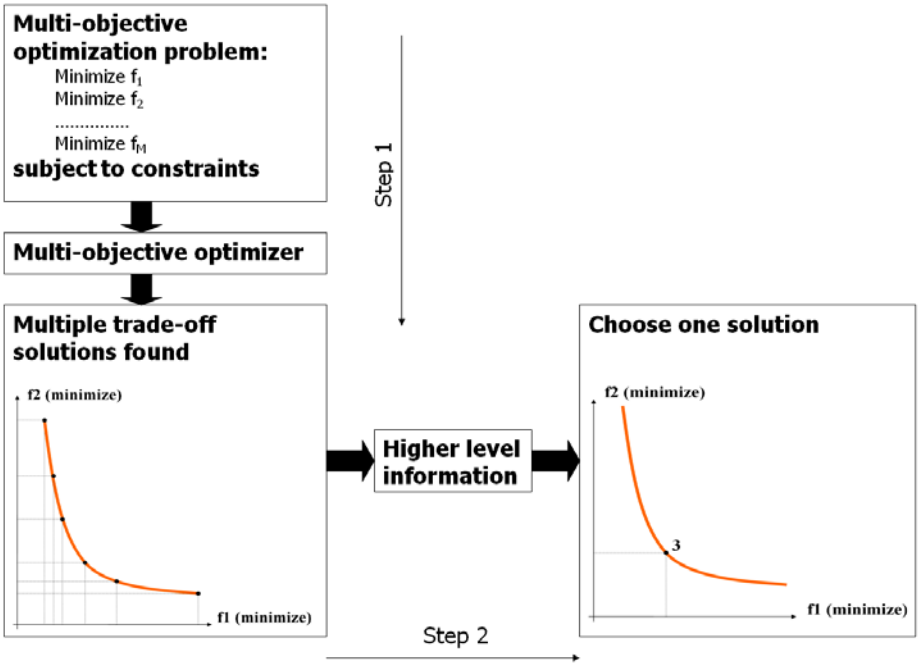

Figure 4.7: Schematic of a two-step multi-objective optimization procedure. Figure inspired by Deb[33].

4.3. Optimization of thermal behavior of large steel castings

In this section, several multi-objective optimization case studies are presented. Since thermal aspects and phenomena play a major role in obtaining high quality castings and a large number of all so-far known defects are also related or driven by thermal processes, the major emphasis has been put on optimization of the thermal behavior of these large castings with an objective of increasing the overall quality of the castings. It will also be shown how complex phenomena such as macrosegregation, channel segregates and hot tearing can be effectively related and eliminated by simple optimizing solidification patterns. The entire work, both modeling and optimization has been performed using the commercial casting simulation software package MAGMAsoft[41] and its add-on optimizer MAGMAfrontier. No advanced models or features that a regular user would not have an access to have been exploited.

4.3.1. Coupling of Simulation and Optimization Tools

Before the optimization process can be started, a standard project must be defined in the simulation software environment. This includes geometry definition in the pre-processor, furthermore a suitable mesh must be generated and all relevant process parameters defined adequately. The optimization itself is based on performing a large sequence of "standard" calculations, each with different design variants, therefore all of these design variables must be defined in a parametric way.

In essence any constrained optimization method is based on the following scheme: a user formulates the problem in a mathematical way by means of several parameters[42]:

- **Input (design) variables** together with allowed ranges of variation. Design variables (initial temperatures, riser dimensions, alloy composition, process parameters, etc.) are modified by the optimization algorithm in order to meet the given objectives.
- **Output variables** usually represent values calculated in a standard casting simulation. The optimization objectives are usually formulated by using the output variables, (e.g. when the porosities and the volumes of the feeders in one design need to be assessed for a feeder optimization).
- **Constraints** are conditions for designs. They limit the design space or the range of solutions. If a design does not satisfy these constraints, it is considered as unacceptable.

- **Objective functions –** These are the aims and targets that are the goal to achieve by means of optimization. They maximize or minimize certain combinations of output variables, e.g. **min** (volume of a riser) or **min** (max. porosity).

4.3.2. Optimization procedure

The actual optimization cycle is initiated by establishing a first generation, i.e. set of solutions, containing a user-defined amount of individuals, referred to as initial population or Design of computational Experiments (DOE). Each individual represents one configuration for the considered set of design variables. For each of these designs an analysis of solidification and solid-state cooling is performed and the values for the requested output variables are calculated. The output data is used to evaluate and compare the different designs. After the first generation has been calculated, the optimization algorithm evaluates the designs with respect to the objective functions and constraint(s) and subsequently generates a new set of solutions using mathematical mechanisms that follow the concept of natural genetics, i.e. selection, reproduction, cross-over and mutation. From the algorithmic point of view the procedure can be described as follows:

1. Create the initial set of designs (initial population).
2. Calculate all designs and grade their performance in terms of the objectives.
3. Generate a new set of designs (new generation) by performing statistical evaluations (selection, cross-over, mutation).
4. Repeat this procedure for the user-defined number of generations.

The optimization cycle terminates when the stopping criterion, i.e. usually the total number of generations, is reached. The flow chart of the above described optimization procedure is depicted in **Figure 4.8**.

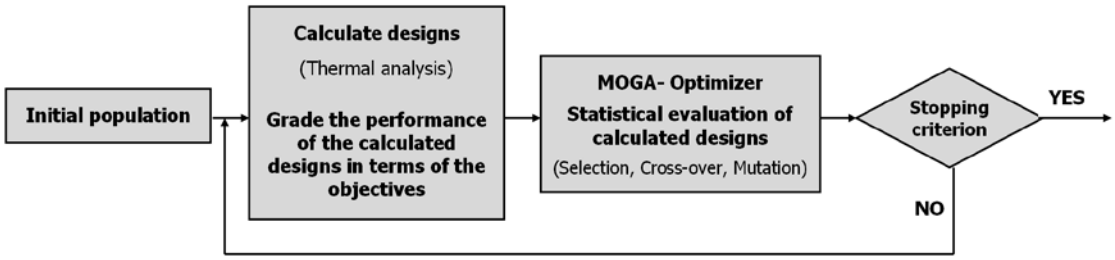

Figure 4.8: Flow chart of the optimization process, [ref. Paper II, Kotas et al. 2010].

In the following, several industrial case studies which are intended to show that the previously described concept of a Multi-Objective Optimization Problem (MOOP) is applicable and reliable for a variety of casting related issues are presented. All of these examples deal with optimization of solidification pattern and its effect on different casting defects occurrence and distribution.

4.3.3. Case study 1 - A casting yield optimization

The optimization case presented here was the first one considered in the PhD project, see **Paper II**. The multi-objective optimization problem is stated as the goal of finding the optimum set of design variables, i.e. dimensions of the riser and the chills which provide a set of trade off solutions for the two conflicting objectives. These are the minimization of the remaining volume of the top open riser and the minimization of shrinkage porosity inside the casting. The optimization problem is subjected to a constraint on centerline porosity.

The iterative product design cycle includes five different layouts of a steel forging ram (as seen in **Figure 3.47**) manufactured by a gravity sand casting process. The initial layout is obtained from a foundry, Vitkovice Heavy Machinery a.s., which manufactures the forging ram. The second layout with manually rearranged gating system and chills is also provided by the foundry, and last three layouts are generated by using numerical optimization. The first two designs are analyzed both in terms of filling and solidification using MAGMAsoft® and then the results are compared with experimental casting trials; no numerical optimization is involved at this stage. The last three designs are optimized numerically using MOGA (Multi- Objective Genetic Algorithm[42]) implemented in MAGMAfrontier ,and are assessed only in terms of solidification since the filling pattern remains unchanged; however temperature fields at the beginning of the solidification are inherited from the filling stage.

4.3.3.1. Case Study Description 1– Original Casting Arrangement

The project involves a large, 60 ton steel forging ram, shown in **Figure 3.47.** During design stage a riser is designed and placed on top of the heaviest section, based on the thermal analysis of the part itself. In order to enhance the feeding ability of the riser, insulation is applied. The main cylindrical padding is insulating, the melt surface is covered by an exothermic powder and on top of that additional insulating powder is applied. Next, it is determined that the part will be bottom-filled using a gating system comprised of refractory tiles. The cross-section area of the tiles is constant over the entire gating system. Last, the chills are added around the cylindrical section of the casting to establish directional solidification and to push the macrosegregation-related flaws from the surface further inside the casting.

After casting and machining operations, it was found during quality tests, i.e. NDT techniques, that there is a rather extensive porous area present in the lower section of the cylindrical area of the ram, see **Figure 3.21**. Shrinkage porosity, together with channel segregates penetrating to the machined surface was the two major causes of rejection of the casting. Thus, the objective of this case study was to find a solution to this problem by means of numerical optimization techniques.

The original casting layout is simulated using casting conditions and parameters listed in **Table II**. Both, filling and solidification analyses are conducted. A stress analysis is not considered in any of the presented cases. Results from the filling and the solidification analysis of the original casting layout are given in **Figures 2.7, 2.27(b), 2.28(a)** and **Figure 3.10**, respectively.

Table II. Material settings in MAGMAsoft®

Material of the casting	GS20Mn5 (DIN 1.1120)
Material of the mould	Furan Sand
Initial (pouring) temperature of the casting	1540 °C (2804 F)
Initial temperature of the mould	20 °C (68 F)
Filling time	120 s
Weight of the casting- incl. risers and gating system	59596 kg (131111.2 lbs)

4.3.3.2. Case Study Description 2– Manually modified Casting Arrangement

After the original casting got rejected, a new layout with a manually redesigned gating system and rearranged chills is developed. The new layout in **Figure 4.9** is manufactured for a different customer who requested minor geometrical adjustments as compared to the very original layout, i.e. a slightly larger diameter of the cylindrical section and geometrical adjustments in the ram's head. However, none of these adjustments will deteriorate the purpose of this study.

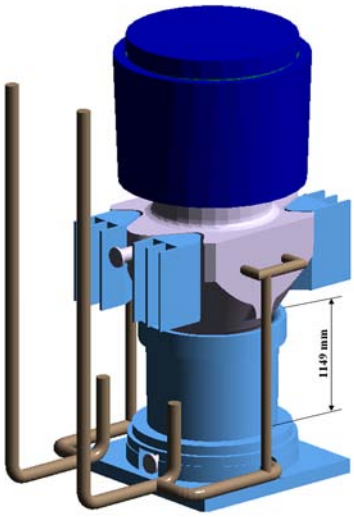

Figure 4.9: Manually optimized casting design (the result of the case study 2). The gating system is now side-fill to accommodate the bottom chill plate. Cylindrical chills are more robust and four wedge-shaped chills are implemented at the casting's head area, [ref. Paper II, Kotas et al. 2010].

The aim is now to investigate the effects of the redesigned system of chills, particularly of a cooling plate located underneath the casting, on the solidification behavior of the casting. In order to place the cooling plate, the gating system has to be changed from bottom filling to side filling. Also, new vertical runners are added to support filling in higher sections of the casting. Furthermore, the chills are rearranged a bit. In order to ensure sufficient cooling of the very bottom, thicker chills are added around the conical bottom section of the casting. Furthermore new chills are incorporated into the top head section of the casting. The changes are seen in **Figures 4.9**. Besides the mentioned geometrical changes, the total weight, all casting and simulation parameters remain the same as in the first casting arrangement. It should be noted that up till now, no numerical optimization has been applied. All of these modifications have been done by intuition. Findings from the thermal analysis for the redesigned casting are captured and discussed in **Figure 3.11**.

4.3.3.3. Case Study Description 3– Optimization of the riser and chills

After inserting all datasets and parameters into the standard simulation environment, the manually refined casting layout is used to create a reference solution to compare the optimization results with. It has been decided to try to reduce the size of the top riser as much as possible to increase the casting yield, providing that there will be no defects occurring in the casting due to the riser's reduced size. When the riser and the chills are transformed into parametric objects, the optimization process is initiated. The design variables (those which are subjected to optimization) are: dimensions of the chills- height and thickness of the bottom cylindrical chills, and of the top riser –its height, bottom and top diameters, and the top diameter of the riser neck, see **Table III**.

Table III. Design variables for optimization.

Design Variable	Lower limit	Upper limit	Step
Cylindrical chill- Height	549 mm	1149 mm	50 mm
Cylindrical chill- Thickness	100 mm	200 mm	10 mm
Riserneck- Top diameter	1200 mm	1300 mm	10 mm
Riser- Bottom diameter	1260 mm	1660 mm	20 mm
Riser- Top diameter	(1260* 1.06) mm	(1660* 1.06) mm	20 mm
Riser- Height	500 mm	1350 mm	50 mm

Again, this optimization problem is stated as the goal of finding such a design of the top riser so, that the casting is sound (i.e. with minimum shrinkage and centerline porosity) and at the same time having the top riser's volume as small as possible to increase the casting yield. In this context, 'casting yield' is defined as the weight of the fettled casting divided by the gross weight including the riser and the gating system. In terms of the MOOP we deal with minimization of two conflicting objectives (**min.** porosity in the casting body vs. **min.** riser volume). The optimization problem is further subjected to a constraint on centerline porosity.

In many engineering cases there are more than two optimization targets to address. However, it is more complex or unfeasible to graphically visualize and reasonably evaluate more than two objectives. Then the only way for the optimization algorithms to take the other optimization targets into consideration without prescribing them as objectives, is to express them by means of optimization constraints. Of course one can then expect the presence of unfeasible designs that do not comply with the prescribed constraints. Subsequently, these solutions are automatically rejected by the optimizer. Our optimization problem is constrained only by the predefined ranges of variation of the design variables, see **Table III.**

Based on the number of design variables and their ranges of variation, the optimizer generates the total number of feasible combinations (the initial DOE sequence), by a DOE sequence technique referred to as Full Factorial Design. Obviously, it would be very time-demanding to calculate all possible designs, thus the initial population is provided by the Sobol DOE sequence generating technique[43] which is a quasi-random sequence. The points in this type of sequence are maximally avoiding each other, so the initial population fills the design space in a uniform manner. The optimization run has been executed using the following parameters:

Initial Population: Sobol Sequence

Population Size: 100

Number of Generations: 10

Probability of Directional Cross-Over: 60%

Probability of Selection: 30%

Probability of Mutation: 10%

Elitism: Enabled

Treat Constraints: Penalizing Objectives

Algorithm Type: MOGA Steady

4.3.3.4. Simulation results – Optimized riser and the chilling system

From **Figure 3.11(c)** it is seen that the manually optimized chills completely eliminated the presence of shrinkage porosity in the casting and that the major shrinkage pipe in the riser is still too far from the actual casting body to be considered critical. One could stop here and argue that the optimal solution has already been found. This would be true for a very conservative and old-fashioned foundry which is not concerned with saving its material resources whatsoever. At this stage, the best solution in terms of competitiveness is to apply the state of the art optimization techniques and utilize them in the riser volume reduction to obtain the increased casting yield.

The objective space for the optimization problem in **Figure 4.10** is constructed by the two following objectives: The minimization of shrinkage porosity and the minimization of the remaining volume of the top riser. The first objective is represented by a Weighted Volume Porosity criterion function which stands for the total volume of areas having issues with shrinkage porosity or with feeding in general. The remaining volume of the riser is then calculated as the geometrical volume of the riser minus the volume of the shrinkage pipe in the riser.

The blue line is the Pareto set which is comprised of all the non-dominated solutions, although, it is up to the user to determine which solution out of the Pareto set will be the most desirable. In other words, the user has to figure whether he/she wants to minimize the riser as much as possible, at a cost of increased porosity or to have a porosity-free casting with a slightly larger riser. In our case, three distinct designs were selected. The first one, marked 1 in **Figure 4.10** does not lie on the Pareto set and represents the most modest solution- i.e. the largest riser volume. It should be emphasized that although it may not be clear from the figure, solution 1 is dominated by solution 2. The second one, marked 2 resembles a single optimum case- the lowest amount of porosity and the third one, marked 3 stands for a trade-off solution.

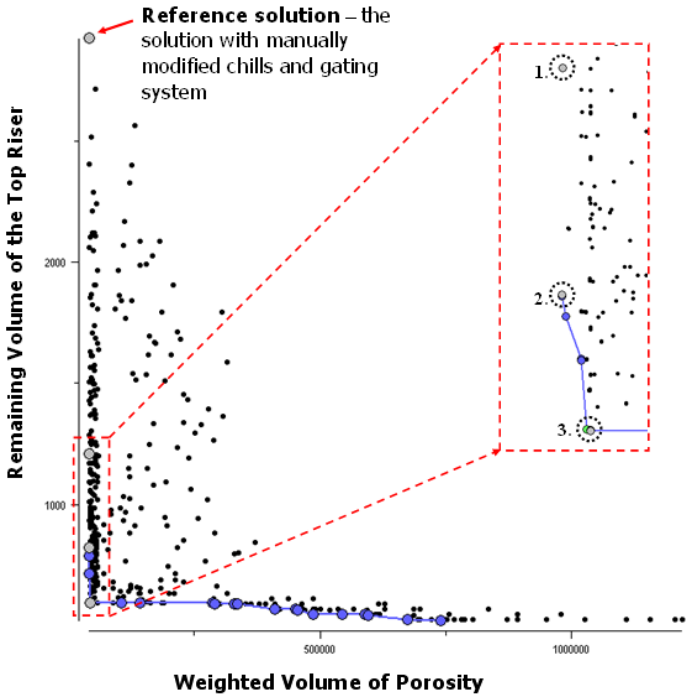

Figure 4.10: Design space with all the calculated designs, i.e. each design is represented by a black dot. The non-dominated trade-off solutions constitute the Pareto set, i.e. the blue line. Three designs are selected for further analysis, two lie on the Pareto line and one does not, [ref. Paper II, Kotas et al. 2010].

Then, the three designs have then been analyzed in the standard simulation environment. In order to obtain realistic temperature fields during solidification, filling has also been considered in the simulation, but its results are not shown here. The reason for choosing such designs was the following: the primary aim has been to keep the level of porosity very low- possibly not above the value of the original design, but still increasing the casting yield. That is why the focus was put on

the solutions very close to the Y-axis. Moreover, the manufacturing foundry wanted to see different layouts-from "modest" to those "on the edge" to make a better comparison and decision as to which solution to select for the subsequent production. From the optimization perspective it is given that the best solutions constitute the Pareto line, so why should we pick a design not on the Pareto line that is solution 1? Many foundries will rather prefer a very safe solution to compensate for potential flaws during production, e.g. human factors, deviations from alloy compositions, etc. Solution 1 was selected for the subsequent analysis because it has a large enough riser to keep porosity far from casting and still has its total volume remarkably smaller than the original layout. **Figure 4.11** depicts the three selected designs. Information regarding dimensions of the optimized designs is listed in **Table IV**.

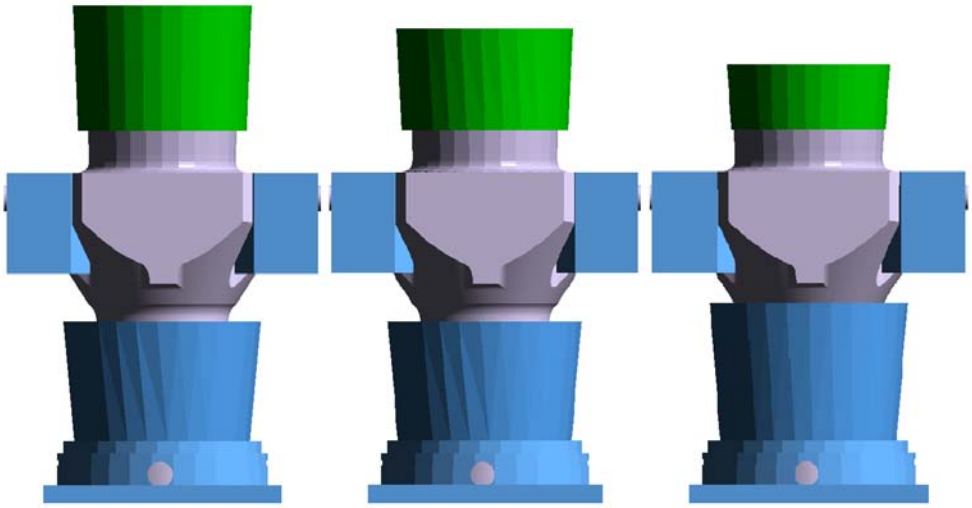

(a) ***(b)*** ***(c)***

Figure 4.11: Three distinct designs proposed by the optimization tool, [ref. Paper II, Kotas et al. 2010]

Table IV. Comparison of the three optimized designs.

	Solution 1	**Solution 2**	**Solution 3**
Total height	4037 mm	3837 mm	3537 mm
Total weight	48406.8 kg	45850 kg	40968 kg
Height of the bottom cylindrical chills	999 mm	999 mm	1149 mm
Thickness of the bottom cylindrical chills	160 mm	160 mm	160 mm

Regarding the solidification pattern of the three optimized designs, no isolated liquid areas are forming in the bottom area as compared to the original layout which is depicted in **Figure 3.10(b)**. The bottom chill plate and the stair-type chill around the conical section induced directional solidification towards the thermal axis and the riser. Solidification patterns were checked over the entire solidification interval. It was found that none of these designs exhibit apparent isolated liquid areas although solution 3 is really on the edge later in solidification in an area right below the riser-neck, see **Figure 4.12**. The reason is that the riser is too small and the heaviest section of the casting slowly begins to be the last to solidify. If one should fully rely on the numerical results, solution 3 would be good enough for production. However, simulation does not take into account all crucial factors that occur in practice. For instance the quality of the melt can be compromised by a dirty ladle with residuals from the previous batch. Next could be the human factor, which often compromises the quality of a casting process. Having all this in mind it was decided together with the foundry not to go for solution 3 to avoid failure in production. But this solution is still shown and discussed here.

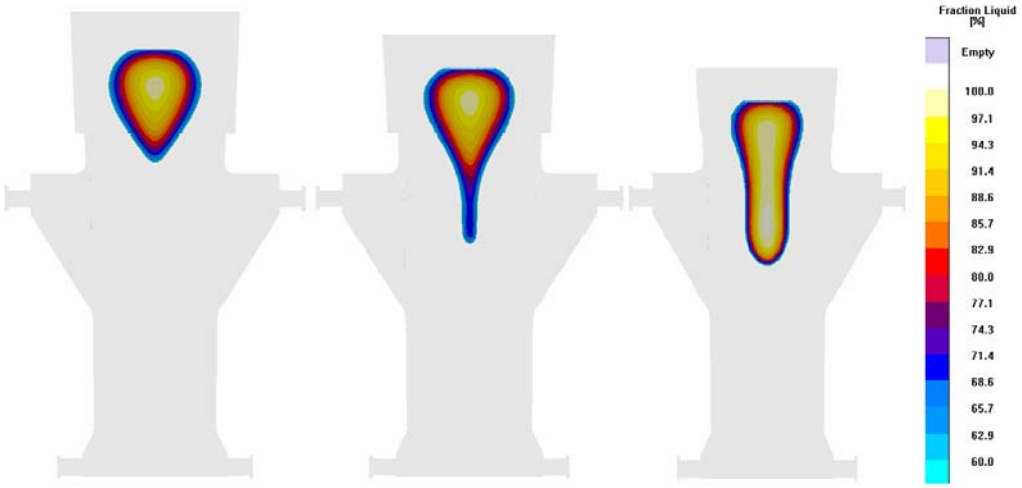

(a) *(b)* *(c)*

Figure 4.12: Solidification pattern, i.e. fraction of liquid, of the three optimized designs at 90% solidified, [ref. Paper II, Kotas et al. 2010]

In **Figure 4.13**, the centerline porosity is expressed by the Niyama criterion. The light blue areas stand for values of 0.4 and lower which will contain macroscopic shrinkage. Everything above the 0.45 up to 1 will most likely be microporosity not detectable by the radiography techniques. It is seen that despite solution 3 being on the edge, it still shows no occurrence of porosity in the casting body. Only the bottom pins contain small porous areas. The reasonable remedy for this would be to enlarge the taper towards the casting. One can see a remarkable improvement in presence of this defect, compared to the original solution in **Figure 3.10(c)**.

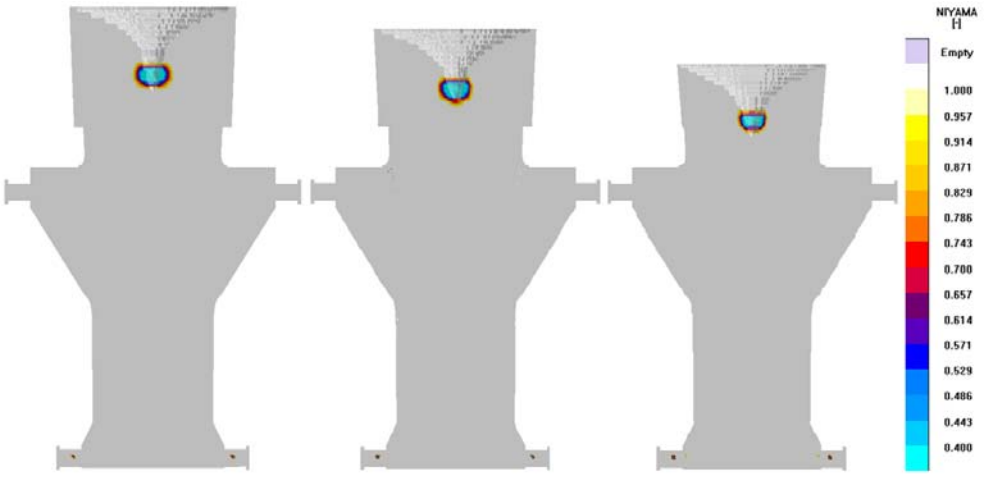

(a) *(b)* *(c)*

Figure 4.13: Occurrence of centerline porosity in the optimized designs, [ref. Paper II, Kotas et al. 2010].

A similar situation applies for shrinkage porosity shown in **Figure 4.14**. The casting body appears to be porosity free in all three cases, except for the pins again.

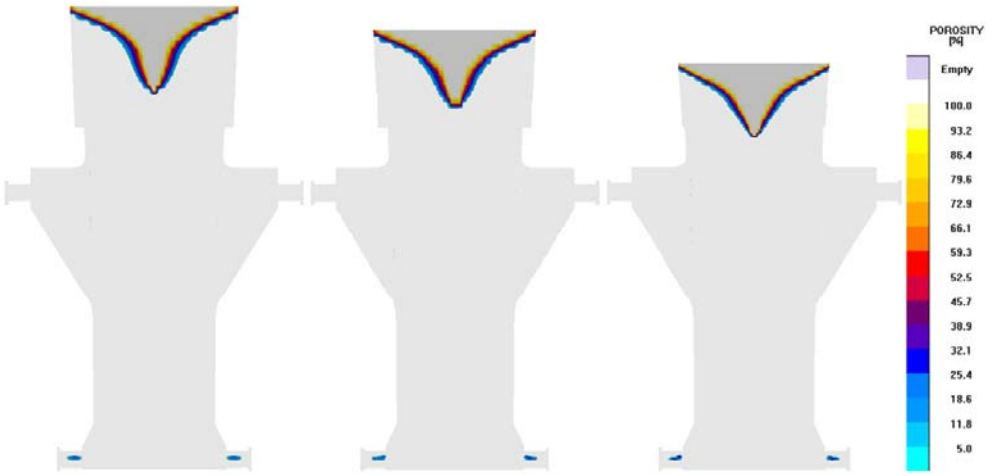

(a) ***(b)*** ***(c)***

Figure 4.14: Occurrence of macroscopic shrinkage in the optimized designs, [ref. Paper II, Kotas et al. 2010].

The last assessment concerns the casting yield. The aim of the entire project has been primarily to eliminate the presence of various casting defects. Once this was achieved, the next step was to optimize the riser volume for the casting yield improvement. The results of this assessment are given in **Table V**. Compared to the original design the casting yield could be increased by approximately 25% if the optimized solution 3 was applied. Due to a high risk a shrinkage occurrence below the riser neck, solution 3 was not approved for production.

Table V. Casting yield assessment

	Original solution	**Optimized Solution 1**	**Optimized Solution 2**	**Optimized Solution 3**
Total height	4337 mm	4037 mm	3837 mm	3537 mm
Total weight	59640 kg	48406.8 kg	45850 kg	40968 kg
Casting Yield	55.36 %	61.76 %	72.01 %	80.59 %

4.3.3.5. Conclusion – case study 1

This work showed a study of a multi-objective optimization problem that has been carried out for a steel forging ram produced by the gravity sand casting technique. The main idea of this case study was to demonstrate how the fully computerized optimization can be effectively utilized in daily foundry practice. The optimization objectives were minimization of the remaining volume of the top riser and the avoidance (minimization) of shrinkage and centerline porosity in the casting body.

Three distinct solutions were selected from the design space. The first one represented a modest approach (relatively large riser), the middle one was still a safe solution but the riser was much smaller and the third solution represented the very risky solution with the highest casting yield. It turned out that all three designs yielded different solidification patterns compared to the initial design. This was attributed to the change in the riser dimensions and the rearranged chills. No residual liquid pools were spotted, however there were some indications of potential problems in the third solution. Concerning the macro and micro-shrinkage in the optimized designs, the only problematic areas were in the riser head and in the bottom pins. The casting body seemed free of porosity. Eventually it was decided together with the foundry not to consider the last solution for production due to a high risk of failure in production. In other words, when taking the human factor into consideration, the risk of porosity extending from the riser to the casting body is too high. Last, findings regarding the casting yield showed that when correctly utilizing multi-objective optimization, it is feasible to substantially increase the casting yield and thus reduce production costs.

4.3.4. Case study 2 - Optimization of the Solidification Pattern and its Effect on Porosity and Segregation in Steel Castings

The second case study is based on the same forging ram which was subjected to optimization in the previous section (**Section 4.3.3**). This time the aim is to optimize the solidification pattern of the same forging ram while simultaneously considering its impact on centerline porosity and macrosegregation distribution. As it was demonstrated in chapter 3, there is a physical relation or at least the same driving force for occurrence of both, centerline porosity and macrosegregation. It is a thermal gradient in a solidifying casting which drives both of these defects. It is not possible, at least computation time-wise to directly optimize macrosegregation profiles in castings. One standard convection and segregation analysis which is necessary for this purpose takes roughly 24 hours on a standard up-to-date multi-core work station, using a reasonably fine computational grid. Considering that a typical optimization cycle comprises from 1000 to 2000 independent designs, nobody in industry would afford doing this type of optimization. This explains why there is a lack of information in literature or in scientific papers on this type of optimization. Therefore, the idea of this optimization problem has been to utilize the existing and well proven physical link between these two defects and optimize the macrosegregation profiles indirectly by means of the Niyama criterion. In other words, by finding proper riser and chill designs steeper thermal gradients and progressive-directional solidification pattern will be established and both of these defects should be eliminated. The multi-objective genetic algorithm has been applied to handle this problem.

4.3.4.1. Problem Statement – Optimization of the riser and chills

The initial casting layout is identical with the casting layout presented and described in section 4.3.3.1. The manually refined casting layout described in section 4.3.3.2 is taken as a reference solution to compare the optimization results with. The design variables are: dimensions of the chills-height and thickness of the bottom cylindrical chills, and of the top riser –its height, bottom and top diameters, and the top diameter of the riser neck. As already discussed, it would not be feasible to calculate thermal convection and segregation for each design during the optimization cycle. Thus, only selected designs constituting the final Pareto line are analyzed with respect to macrosegregation.

The two conflicting objectives can be formulated in the following way: Design the top riser and the chills so that (i) the casting yield is increased, i.e. minimize the riser volume, and (ii) so that the casting is sound, i.e. with minimum centerline porosity, and evenly distributed concentration profiles of solute elements.

The initial population for the MOGA algorithm containing 100 unique designs is provided by the Sobol DOE sequence generating technique. The assumed optimization problem is constrained only by the predefined ranges of variation of the design variables. The directional cross-over, the selection and the mutation probabilities of 0.6, 0.3 and 0.1, respectively, are chosen for running 20 generations giving in a total number of 2000 possible solutions. In addition, elitism is applied to support convergence in the optimization problem. Elitism is a GA operator (in general, an evolutionary algorithm operator) to keep the best designs found so far in the evolution of the generations.

4.3.4.2. Optimized riser and chilling system

The objective space for the optimization problem in **Figure 4.15** is constructed by two following objectives: Minimization of centerline porosity and minimization of the remaining volume of the top riser. The non-dominated trade-off solutions constitute the Pareto optimal front, i.e. the blue line shown in **Figure 4.15**.

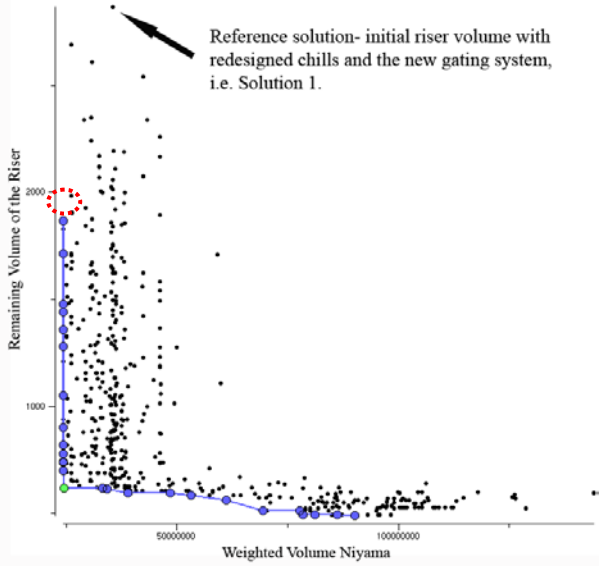

Figure 4.15: Design space with the highlighted Pareto set, [ref. Paper III, Kotas et al. 2010].

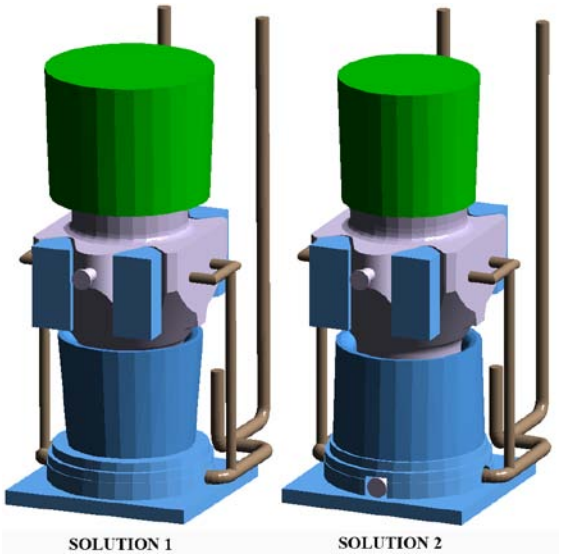

Figure 4.16: Two selected designs proposed by the optimizer, [ref. Paper III, Kotas et al. 2010].

Two distinct designs have been selected. The first one does not lie on the Pareto front and represents the reference solution with the largest riser volume, i.e. the manually optimized solution from case study 1. This solution, even though it appears in the optimization results has not undergone a proper multi-objective optimization. It is entirely based on the manual rearrangement of the chills and the top riser remained unchanged, i.e. it has the same dimensions and casting yield as the original solution. The second design highlighted by the red dashed circle represents the case with the lowest amount of centerline porosity and somewhat reduced remaining volume of the riser.

The two selected designs have then been evaluated with respect to filling and solidification in the standard simulation environment. The results from filling of solution 2 are not presented. The filling pattern of solution 1, which is the reference solution here and is the same as the solution in section 4.3.3.2 is seen in **Figure 2.22**. The geometries of the two designs are captured in **Figure 4.16.** There are a few reasons for choosing what at first glance could appear as modest or conservative designs. First, the primary goal has been to eliminate the presence of centerline porosity and to minimize macrosegregation issues, especially A-segregates as compared to the original solution. To satisfy this objective the focus has been on solutions located very close to the Y-axis, representing minimum centerline shrinkage in **Figure 4.15**. Moreover, as discussed in chapter 3, centerline shrinkage is directly affected by a pressure drop inside the casting, derived from Darcy`s law of flow in porous media, which represents a resistance to feeding in a given area. To keep the pressure gradient sufficiently high to ensure efficient feeding flow, the height and the total volume of the riser should not be too small. Next, centerline shrinkage usually forms at areas with shallow thermal gradients. To establish steep thermal gradients, the riser should again be sufficiently large and the dimensions of the chills should be chosen so that progressive and directional solidification towards the riser is provided. Considering segregation, it is also known that having steep thermal gradients due to intense chilling results in a finer dendritic microstructure imposing higher resistance for channel segregates to form. Moreover, if a progressive and directional solidification pattern exists, it helps to move the highly segregated remaining liquid towards the riser.

If macrosegregation was not considered in the optimization case, designs with much smaller riser volumes could be chosen with no major risk of issues with porosity. This has been shown in the previous work, see section 4.3.3.4, where macrosegregation has been disregarded; therefore the selected designs reached much higher casting yields. Information regarding dimensions of the optimized designs is listed in **Table VI**.

Table VI. Comparison of the two optimized designs

	Solution 1	Solution 2
Riser height	1350 mm	1300 mm
Riser bottom D	1660 mm	1380 mm
Riser top D	1760 mm	1463 mm
Height of the cylindrical chills	1150 mm	1050 mm
Bottom thickness of the cylindrical chills	100 mm	220 mm
Top thickness of the cylindrical chills	190 mm	190 mm
Total weight	59650 kg	51143 kg

Regarding the solidification patterns of the two selected designs, no isolated liquid areas have been forming in the bottom area as in the original layout, depicted in **Figure 4.17**. The bottom chill plate and the new chills around the cylindrical section evoked directional solidification towards the thermal axis and the riser. Solidification patterns were checked over the entire interval. It is also seen, that solution 2 has a more pronounced progressive solidification pattern compared to solution 1, meaning that the solidifying front progresses towards upper areas in a V shape pattern which is desirable mainly with respect to segregation. The favorable solidification pattern in solution 2 has to do with the dimensions of the top riser and the chills which are different as compared to solution 1. Solution 1 has conical chills extending upwards while solution 2 has conical chills extending downwards, see **Table VI**. Due to more intense heat removal at the top of the cylindrical chills in solution 1, a tendency for choking the remaining liquid pipe is observed, similar to the initial case.

Figure 4.18 shows the new distribution of centerline porosity. It shows that due to the optimized design of the chills, steeper thermal gradients inside the casting have been achieved. These gradients have changed the morphology of the mushy zone, i.e. decreased its extent, decreased its permeability due to finer grains giving rise to very small and widely distributed pores not detectable via radiographs, etc. Besides that, a more favorable solidification pattern has been evoked, which has led to more enhanced feeding of the remote bottom area. The light blue areas stand for values of 0.45 and lower which will contain macroscopic shrinkage. Everything above 0.45 up to 1 will most likely be microporosity not detectable by radiography techniques. It shows that the casting body and even the riser neck will be free of any porosity issues. Only the bottom pins contain small porous areas. The reasonable remedy would be to enlarge the draft towards the main casting body.

The same pattern applies for shrinkage porosity. The main porous region has been found in the top riser, forming a shrinkage pipe which in both cases has not penetrated even to the riser neck. This can be seen in **Figure 4.18** as the missing area on the top of the riser.

Figure 4.17: Fraction liquid at 45% solidified for the two optimized solutions, [ref. Paper III, Kotas et al. 2010].

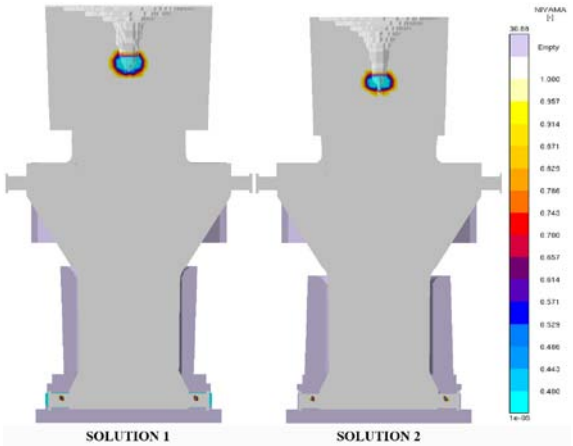

Figure 4.18: Comparison of centerline porosity in the optimized designs, [ref. Paper III, Kotas et al. 2010].

Figure 4.19 illustrates how the solidification progresses inside the casting and its influence on the convection pattern for both of the optimized designs. Now it is obvious that the optimized chills have induced steeper thermal gradients that have decreased the size of the mushy zone denoted by green color. As compared to the initial situation depicted in **Figure 3.48**, the liquid area is present for a longer period of time and in a much larger scale. Steeper gradients have caused an evolution and growth of much finer grains, thereby decreasing the permeability of the mush. Consequently, resistance towards liquid/solid movement and to opening liquid channels which give rise to channel segregates is therefore much higher. Convection is denoted by the vector arrows.

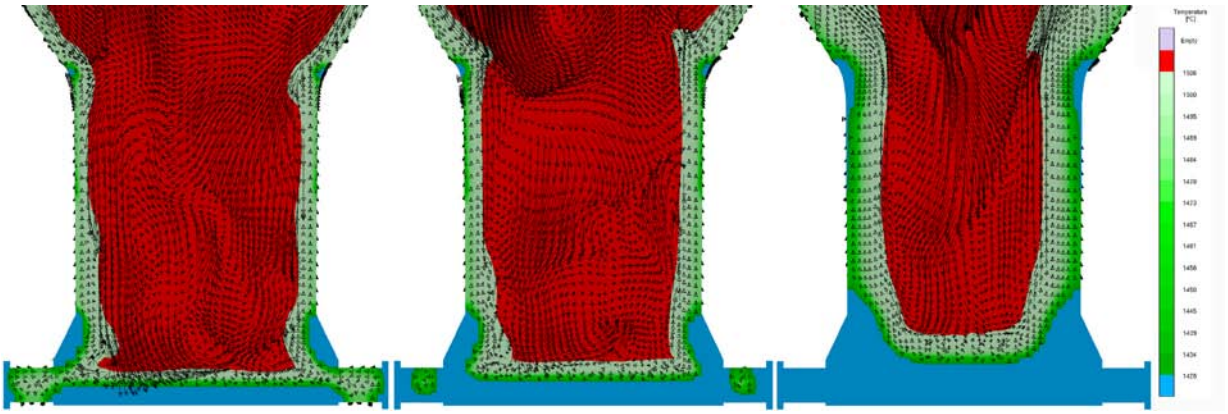

Figure 4.19(a): Solidification processing and convection patterns at 7, 11 and 20% solidified respectively for SOLUTION 1, [ref. Paper III, Kotas et al. 2010].

Potential issues with channel segregates are again highlighted by the black thick arrows. At 7% solidified, areas adjacent to the bottom pins are very prone to channel segregation because of a sudden increase of velocity oriented upwards and a subsequent local remelting. Moreover due to choking the pins from the open feed path, porosity will form and a positively segregated region will occur which is subsequently proven in **Figure 4.21**. At 20% solidified the first indications of minor channel segregates at the cylindrical area are noticed, **Figure 4.19(b)**. However, there is very little chance that these will form at all since they are in direct contact with the liquid melt which is highly permeable.

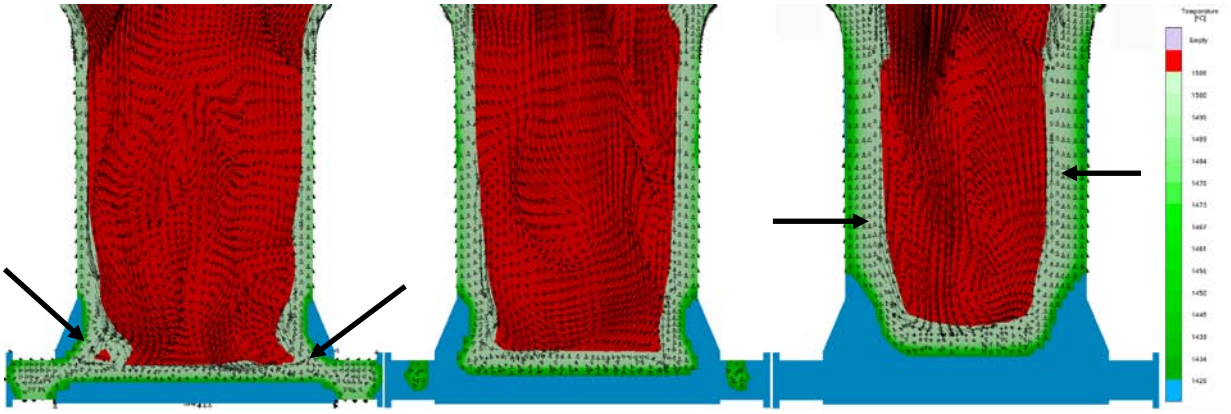

Figure 4.19(b): Solidification processing and convection patterns at 7, 11 and 20% solidified respectively for SOLUTION 2, [ref. Paper III, Kotas et al. 2010].

Figure 4.20 implies the situation at 31% solidified. The probability of forming some channel segregates is rather high for both solutions as quite large streams of upward moving liquid/solid have been observed. Although if any such channel segregates form, they will be found deep enough in the casting not to show on the casting surface after machining operations.

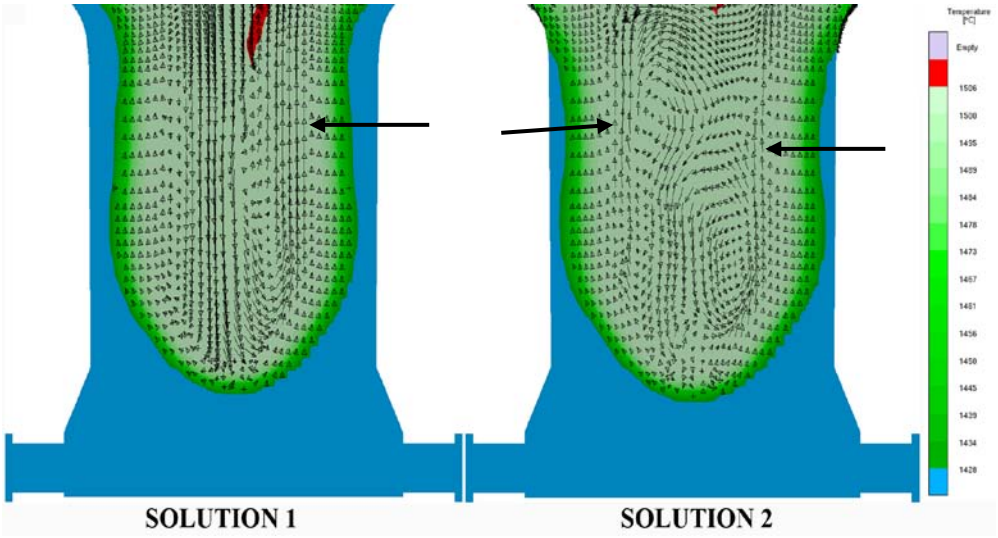

Figure 4.20: Convection patterns at 31% solidified for the two optimized solutions, [ref. Paper III, Kotas et al. 2010].

As a consequence of the modified solidification and convection pattern new macrosegregation profiles have been expected for both optimized solutions. These are captured in **Figure 4.21**. One can recognize an apparent improvement in the sense that the carbon is distributed more uniformly over the entire lower section which exhibited high positive segregation in the initial layout, see **Figure 3.45(left)**. When it comes to the under-riser section, solution 1 appears to have a slightly more favorable carbon distribution, while solution 2 seems to have that region highly segregated and thus worse as compared to the original solution. This is for sure attributed to the riser size and shape.

The forging application, for which this part is used, sets high requirements on the under-riser area which should exhibit very good mechanical properties. For this reason, solution 1 would be more beneficial. It should be noted that solution 1 has already been cast according to the optimization results. It has been evaluated, tested and no problems have occurred whatsoever.

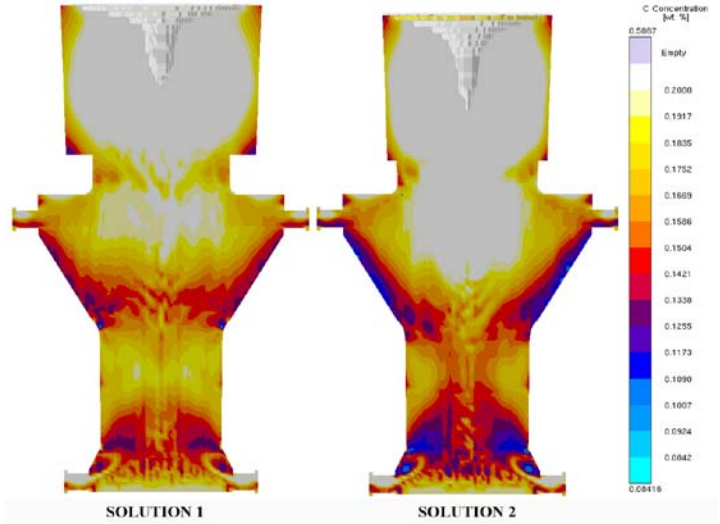

Figure 4.21: Carbon macrosegregation patterns for the two optimized solutions, [ref. Paper III, Kotas et al. 2010].

The effect of optimization on the casting yield has been also assessed in this study. The aim of the entire project has been primarily to eliminate the presence of various casting defects via determination of the proper design of the riser and chills. It has also been very desirable to increase the casting yield somewhat but not at the cost of impaired soundness of the casting. Results of this assessment are given in **Table VII**.

Table VII. Casting yield assessment

	Original solution	Solution 1	Solution 2
Total weight	59640 kg	59640 kg	51143 kg
Casting Yield	55.36 %	55.36 %	64.9 %

Now it is actually very interesting to make a small mutual evaluation of the two case studies which are based on the same casting, in terms of the casting yield. In the first case study, the only concern was to get rid of the shrinkage porosity and to reduce the volume of the riser. While in the second case study, the objectives have been changed a bit and macrosegregation came into the game. The second case study shows that when considering macrosegregation we do not have that much freedom in lowering the riser volume due to its effect on the solidification pattern and on the under-riser macrosegregation profiles at the same time. In the first case study, just by looking at the optimization results, one would vote for the solution 2 which seems very safe and reasonable. However, when macrosegregation is considered, solution 1 from case study 2 would be the most reasonable solution since it suggests the lowest under-riser segregation. This comparison just shows that in order to obtain a valuable and trustworthy numerical assessment of any given casting process, it is very important to include as many factors, which may have any negative effect on the quality of the casting, as possible.

4.3.4.3. Conclusion – case study 2

The main intention of this study was to prove that macrosegregation can be addressed by optimization even without prescribing it as one of the objectives which would not be feasible time-wise. It was found that by optimizing the solidification pattern so that directional and progressive solidification with steep thermal gradients is established, one could relatively easy handle multiple issues like porosity and segregation.

The optimization objectives were minimization of the remaining volume of the top riser and the avoidance (minimization) of centerline porosity through which the elimination of macrosegregation issues, particularly channel segregates in the casting body was expected.

The manually-optimized solution, i.e. solution 1, served as a reference or starting solution for the autonomous multi-objective optimization of the solidification pattern. In the optimization problem, the dimensions of the riser and the chills were applied as design variables together with the allowed ranges of variation. After optimization, one solution was selected from the design space.

The new chill arrangement caused significant improvements in the solidification patterns in both of the solutions. More pronounced cooling established steeper temperature gradients and induced progressive and directional solidification in the problematic bottom area, totally eliminating the shrinkage-related defects. The only porous areas were found in the riser head and in the bottom pins. The casting body seemed free of porosity.

New convection and macrosegregation patterns were obtained giving favorable and promising results. Due to steeper thermal gradients the mushy zone got reduced, its permeability was lowered imposing higher resistance for liquid-solid movement and for potential channel segregation. The resulting carbon distribution seemed more uniform over the casting body, mainly in case of solution 1. As to the under-riser area (in solution 1) which will be heavily cyclically loaded during service, it is likely to have similar mechanical properties as compared to the initial solution.

4.3.5. Case study 3 - Elimination of Hot Tears in Steel Castings by Means of Solidification Pattern Optimization

In the following sections a methodology of how to exploit the Niyama criterion for elimination of various defects such as centerline porosity, macrosegregation and hot tearing in steel castings is presented. The tendency for forming centerline porosity is governed by the temperature distribution close to the end of the solidification interval, specifically by thermal gradients and cooling rates. The physics behind macrosegregation and hot tears indicate that these two defects are also heavily dependent on thermal gradients and pressure drop in the mushy zone, more on this topic can be found in chapter 3. The objective of this work is to show that by optimizing the solidification pattern, i.e. establishing directional and progressive solidification with the help of the Niyama criterion, hot tears issues can be at least minimized or entirely eliminated.

4.3.5.1. Description of the project

The project involves a large (84,6 ton, max height = 4280mm, max width = 2881mm) steel wedge-shaped casting made of a low carbon steel alloy DIN 1.1165, (GS30Mn5), poured into a furan bonded silica sand mould. Two insulated top risers are placed on top of the casting, directly above the critical regions with the highest mass accumulation to ensure sufficient feeding. The entire geometry is shown in **Figure 4.22**.

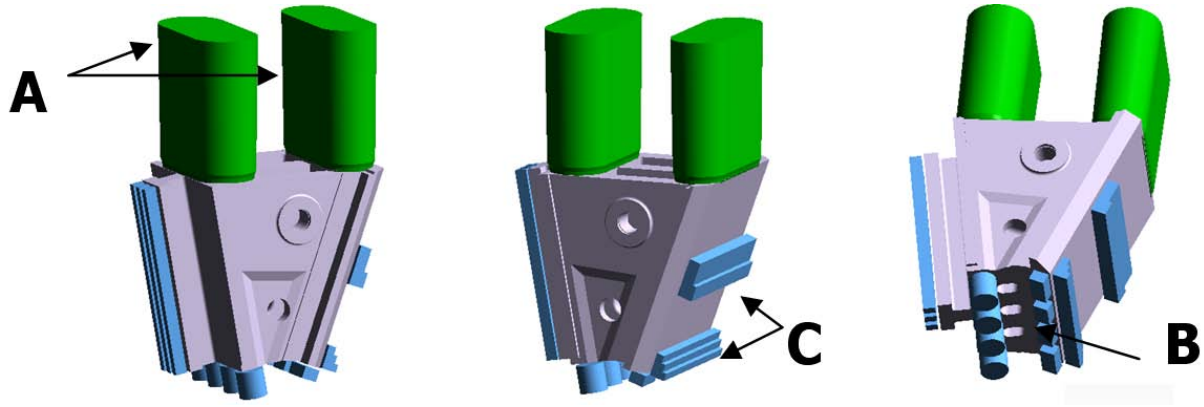

Figure 4.22: 3-D visualization of the original casting layout with its characteristic feeder design and chill patterns applied in the initial numerical calculations. This layout was then subjected to optimization. Letters A, B, C indicate groups of design variables for the subsequent optimization, [ref. Paper IV, Kotas et al. 2010].

The original casting arrangement was cast and left in the sand mould for a few weeks to solidify and cool to a certain temperature. After shake out, a thorough visual inspection took place and a massive hot tear was identified in the middle rib, going diagonally from the left top riser down to the right, across the top cylindrical core, see **Figure 4.23**. The rib was found to be torn completely from both sides. Obviously, this defect was impossible to repair weld, making the casting a scrap. The hot tear was found before burning off the two top risers which disproved all the hypotheses and arguments that it formed due to stress relief while removing the risers and not due to an improper technological solution. Therefore, the major aim of this case study is to find the reason why the hot tear formed and subsequently to eliminate it by means of the solidification pattern optimization.

Figure 4.23: View on the location of the hot tear in the middle rib of the steel casting. This hot tear occurred on both sides of the middle rib, [ref. Paper IV, Kotas et al. 2010].

4.3.5.2. Optimization problem statement

Unknown optimal shapes and sizes of the two top risers as well as the chills are sought by means of autonomous optimization to obtain a better solidification pattern of the casting which would eliminate the likelihood of hot tearing. This issue has been addressed by defining the problem as a multi-objective optimization problem (MOP) via combining multiple conflicting criteria, i.e. the minimization of the riser volume together with the minimization of the presence of centerline porosity. The decisive factors for the occurrence of centerline porosity, macrosegregation and hot tears are the same, i.e. the low thermal gradients combined with an unprogressive solidification pattern. Therefore, the focus has been put on eliminating hot tears by the minimization of centerline porosity by establishing enhanced thermal gradients and progressive solidification pattern inside the casting. This unconstrained multi-objective problem can then be expressed in mathematical terms as

$$\begin{aligned} &\text{Minimize:} \quad f_1(\mathbf{x}) = \mathbf{V_{riser}} \\ &\text{Minimize:} \quad f_2(\mathbf{x}) = \mathbf{Weighted\ Volume\ Niyama} \\ &\mathrm{x} = \{a_{1-5}, b_{1-4}, c_{1-12}\} \end{aligned} \tag{4.3}$$

$$\text{where } \mathbf{Weighted\ Volume\ Niyama} = \sum_{\substack{i=1 \\ Niyama_i < Niyama_{cr}}}^{N_{cell}} V_i \cdot 2^{\,\mathrm{int}\left(10 \cdot \frac{Niyama_{crit} - Niama_i}{Niyama_{crit}}\right)} \tag{4.4}$$

where V_i is a volume of a cell, $Niyama_{crit}$ is a critical value of 0.7. Information received from the weighted volume Niyama values is regarding the volume of the mesh affected by a poor Niyama value, i.e. below the critical value of 0.7.

In total there have been 21 independent design variables (those which are changed / updated during optimization) used in the optimization procedure, which are: placement and dimensions of the chills-height, width and thickness, and of the top risers –their height, bottom and top diameters. The design variables were split into three groups and are highlighted in **Figure 4.22,** where group A (a_{1-5}) contains all variables for the two top risers, group B (b_{1-4}) contains variables for the four bottom brick-like chills and group C (c_{1-12}) comprises variables for the two sets of chills on the right hand side of the casting. It would be very time consuming to calculate thermal convection, segregation and hot tears prediction for each design during the optimization cycle. Thus, only the selected designs constituting the final Pareto line are analyzed with respect to macrosegregation and hot tearing.

The initial population for the MOGA contains 100 unique sets of designs. The directional cross-over, the selection and the mutation probabilities of 0.6, 0.3 and 0.1, respectively, are chosen for running 20 generations giving in a total number of 2000 solutions. In addition, elitism is applied to accelerate convergence in the optimization problem.

4.3.5.3. Casting and simulation results – optimized layout

As mentioned above, the primary goal of autonomous optimization based on process simulations has been to find a more suitable design of the two top risers and of the surrounding chills to establish a directional and progressive solidification pattern. A more favorable solidification pattern should then eliminate the formation of solidification related issues such as centerline porosity, shrinkage porosity, macrosegregation and hot tears which were present in the original casting layout. A thorough analysis on why the hot tear formed in this particular casting can be found both, in **section 3.7.3.3.3** and in **Paper IV** in the attachments.

The gating system has been changed somewhat to achieve a more uniform and smooth flow pattern to avoid excessive oxidation, see **Figures 3.33** and **3.34** for comparison. On top of that, chills and risers have been transformed into parametric objects and subjected to optimization as design variables. The most important condition in assessing the size of the riser has been to avoid the shrinkage pipe penetrating into the riser neck area or even to the casting body. Such designs are then instantly rejected since they are unsuitable.

The objective space for the optimization problem is constructed by two following conflicting objectives (i) minimization of the remaining riser volume and (ii) minimization of the weighed volume Niyama of the casting body, **Figure 4.24**.

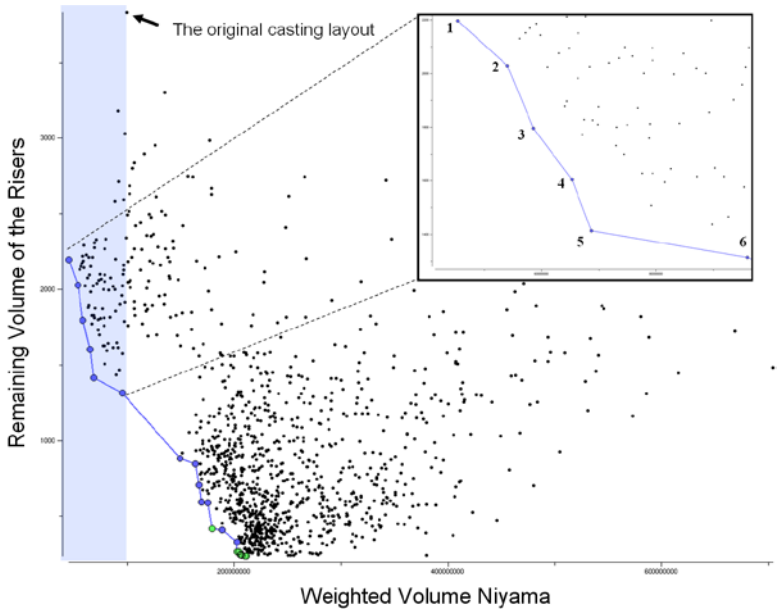

Figure 4.24: The objective space where all the computed designs are stored. The blue line represents the Pareto optimal front which comprises the best trade-off solutions in terms of the predefined optimization objectives. The light blue color indicates the area from which the best solution is selected. The enlarged view on the six Pareto designs is located on the right upper corner, [ref. Paper IV, Kotas et al. 2010].

After the optimization run the user has to decide which design among multiple optimal solutions will be the most desirable for him/her. Whether he/she wants to minimize the riser as much as possible, at the cost of increased porosity or to have a porosity-free and sound casting with a slightly larger riser, but still smaller than the initial design. Obviously, the optimized design must contain less centerline porosity than the original casting layout. This is why only Pareto optimal solutions located in the blue region are considered. All other solutions are disregarded since they exhibit more centerline porosity than the initial layout, which is not desirable. These six solutions were subsequently analyzed in terms of shrinkage porosity, which is an additional criterion for evaluating the overall soundness of the casting. It was found out that the solution 4 had the best response in terms of the shrinkage porosity and solution 1 was only slightly worse than solution 4. The other four designs showed much worse response and therefore they were disregarded. Since the primary aim of the optimization procedure was to search for the solution with the lowest amount of centerline porosity, solution 1 was selected, although it had the largest volume of the two top risers from all of the trade-off solutions. However, the objective of minimizing the riser volume was still met by solution 1, which actually

exhibited a significant decrease in the riser volume as compared to the original solution. By picking solution 1, one could argue that single objective optimization could have been applied. True, however, the benefit of multi-objective optimization is that the user has a selection of many trade-off solutions lying on the Pareto line which may fulfill his/her preferences that he/she would never be able to explore, or be aware of other potential alternatives, while using the single objective approach.

The selected design has then been evaluated with respect to filling, solidification as well as stresses and strains in the standard simulation environment. The geometry of the preferred design, i.e. solution 1 from **Figure 4.24**, is captured in **Figure 4.25**.

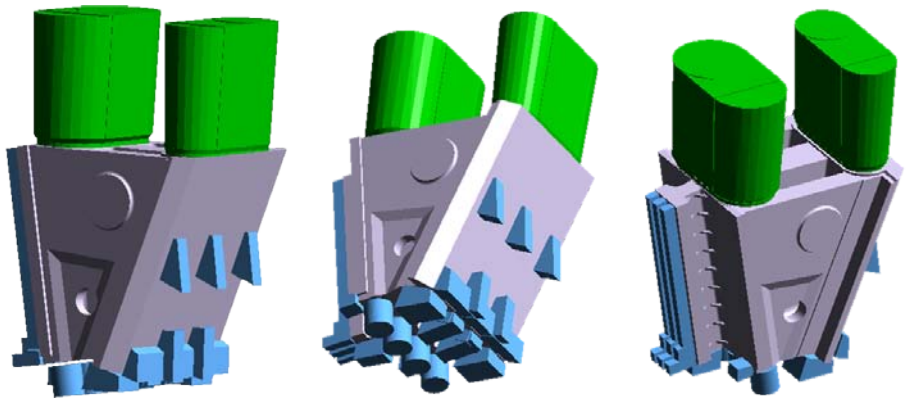

Figure 4.25: New casting layout after optimization. Dimensions of the two top risers together with dimensions and location of the surrounding chills were varied during optimization, [ref. Paper IV, Kotas et al. 2010].

Figure 4.26 shows how the thermal gradients inside the casting changed due to the performed optimization adjustments. It is seen that due to the new shape of the risers, combined with newly placed chills with optimized design and due to the removed top core, the high thermal gradients got eliminated from the area where the hot tear occurred. The large area on the left hand side of the casting indicates steep thermal gradients accumulated over a relatively narrow region, hence implying potential hot tearing. In reality, there are narrow ribs placed along that area to prevent hot tearing as seen in **Figures 4.25** and **4.31**. Since they are very narrow and it would require an extremely fine mesh to consider them during calculations, these were not modeled. Hence, this critical area predicted by the numerical solver can be disregarded.

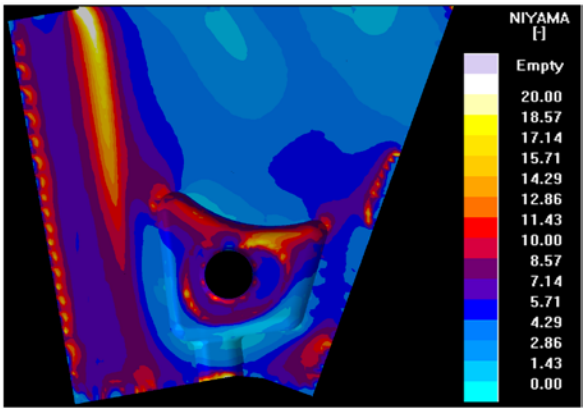

Figure 4.26: Thermal gradients in the cast part after optimization. No obvious high thermal gradients located in a narrow band-like area as in the original casting arrangement are seen. The risk of hot tears has been minimized in the previously critical region, [ref. Paper IV, Kotas et al. 2010].

The optimization adjustments have also led to a new distribution of temperature in the casting domain, **Figure 4.27**. There is no longer that "triangular" area solidifying much faster as compared to the surroundings, evoking thermal imbalance and subsequent thermal tensile strains. Now it appears that the casting solidifies directionally and progressively from the bottom and from the sides towards

the two top risers. This should for sure lower the risk of hot tearing in that problematic area as well as in the entire casting domain.

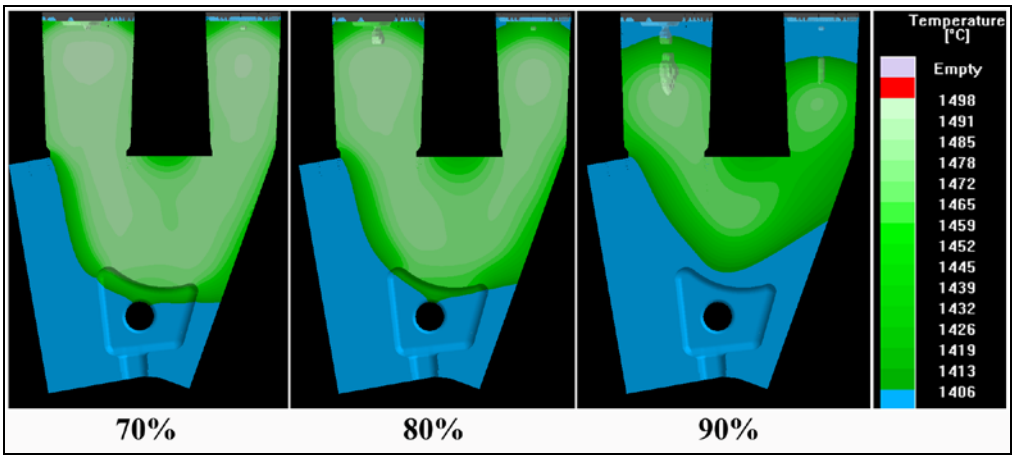

Figure 4.27: Temperature profiles at different stages of solidification in the optimized layout. No indications of sudden temperature changes as were identified in the original layout. The likelihood of a hot tear is very low in the previously critical area. Blue color denotes a completely solid region, all of the shades of green stand for the mushy zone and the red color stands for the liquid phase, [ref. Paper IV, Kotas et al. 2010].

The changes in the solidification pattern have naturally led to a redistribution of the characteristic solute elements in the casting, represented by their concentration profiles. It is shown in **Figure 4.28** that the concentration profiles of the selected three elements are now more balanced and favorable implying that the positively segregated region will be found mostly in the riser region.

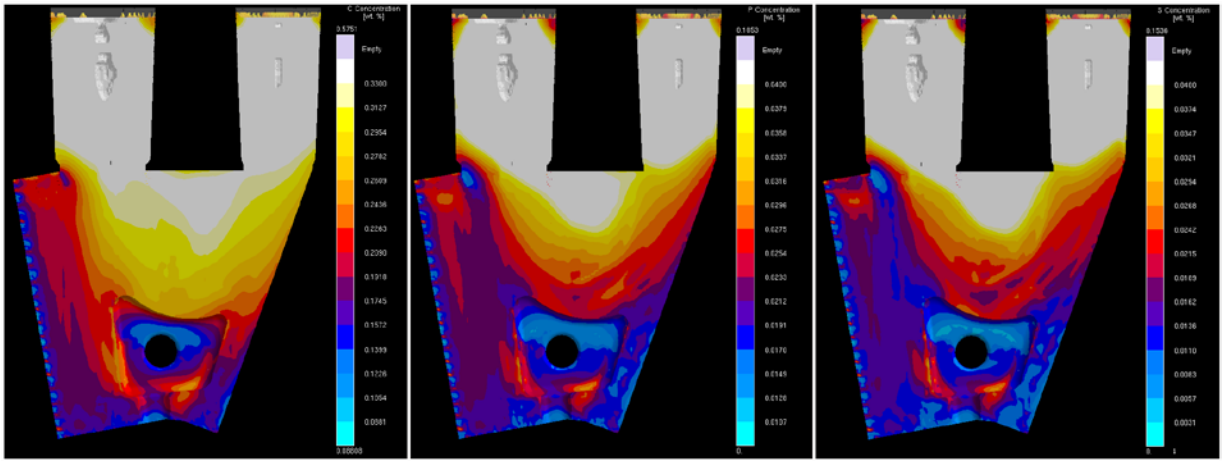

Figure 4.28: More uniform concentration profiles in the optimized steel casting due to the more favorable solidification pattern, (left) carbon, (middle) phosphorus, (right) sulfur. The positively segregated area is now located mainly in the two top risers and partially in the under-riser region, [ref. Paper IV, Kotas et al. 2010].

This state is much more beneficial with respect to hot tear susceptibility as compared to the original state. However, a question arises whether the mechanical properties would be sufficiently good in the area between the two risers due to positive segregation. The manufacturer noted that no special requirements for that specific area as to the mechanical properties were determined by the final customer. Therefore this solution would be suitable for subsequent production. Minor improvements in the segregation might be expected during the heat treatment that the part will undergo afterwards, especially during homogenization.

When we look at the maximal principal strain rates during the solidification interval of the optimized layout in **Figure 4.29** it shows that, in the previously critical area there are no more signs of high tensile straining hence eliminating the risk of hot tearing. The potentially critical area in the lower central region of the casting is not to be worried about. Each numerical solver always highlights some

risky areas, but it is very important to assess also the magnitude of it. The peak values on the scale are so low as compared to the state in the original layout (see **Figure 3.31)**, that it becomes apparent that the thermally induced strains will not cause any major problems in relation to hot tearing.

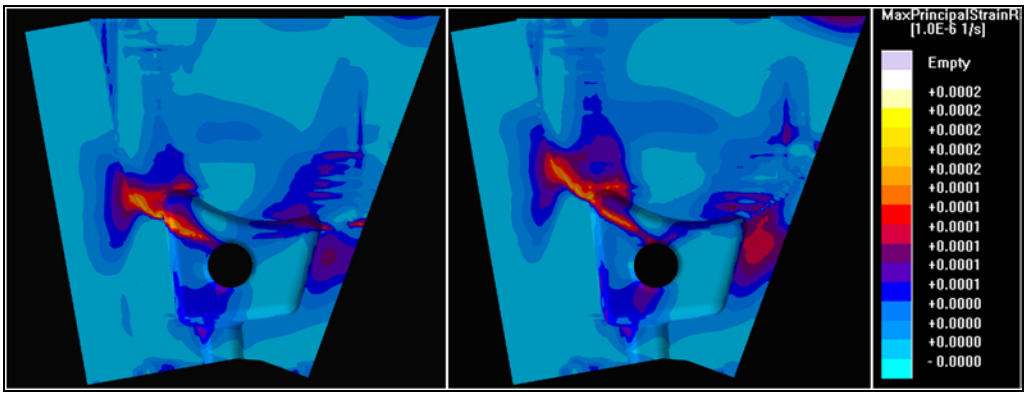

Figure 4.29: Maximal principal strain rate in the optimized layout. Note the difference in the scale as compared to Figure 3.31, [ref. Paper IV, Kotas et al. 2010].

Consequently, due to the optimized solidification pattern in which directional and progressive solidification toward the heaviest section has been established, the risk of hot tearing got entirely eliminated in the problematic area in the middle rib, **Figure 4.30**, compared to the situation in **Figure 3.32**. There is only one small place in the casting which might be prone to hot tearing. It is found in the lower central area, right above the bottom core. However, when considering all the above investigated criteria such as temperature profiles during solidification, the Niyama criterion, segregation profiles and strain rates, it can be assumed that this area will not be of concern in production and hot tear will most likely not form. Also, the peak value on the scale is much lower as compared to the original solution where the tear was found.

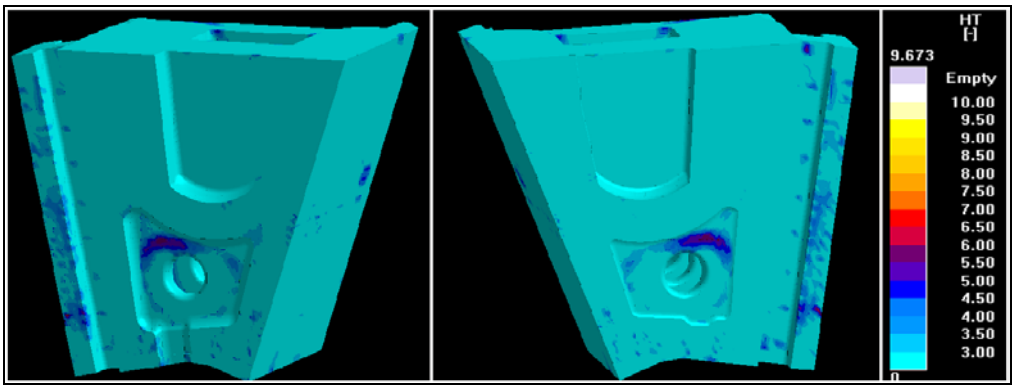

Figure 4.30: Hot tear prediction in the optimized casting layout. The middle rib appears hot tear free. The other indication in the lower central area will most likely induce no hot tearing. This can be deduced from its value on the color scale, [ref. Paper IV, Kotas et al. 2010].

Based on the findings obtained from the multi-objective optimization run, a new casting layout has been proposed and applied in production, see **Figure 4.31**. After it was cast, the part was inspected, both visually and by the prescribed NDT techniques, and no major defects or problems that would ultimately destroy the casting were found.

Figure 4.31: The steel casting which was manufactured based on the optimization results, after its shakeout. It exhibited no hot tears whatsoever. Protective ribs have been applied for the real casting. They were not assumed during simulations since they would require extremely fine meshing, [ref. Paper IV, Kotas et al. 2010].

4.3.5.4. Conclusion - case study 3

The main purpose of the work was to demonstrate and to prove that hot tearing can be relatively easily addressed by optimization even without prescribing it as one of the objectives which would not be feasible computational time-wise. It was found that by optimizing the solidification pattern so that directional and progressive solidification with favorable thermal gradients is established, one could relatively easily handle multiple phenomena like centerline porosity, macrosegregation, and hot tears.

The optimization objectives were prescribed as (i) minimization of the remaining volume of the top riser and (ii) minimization of centerline porosity through which the elimination of hot tear occurrence in the middle rib was expected.

The first step was to analyze the original casting arrangement provided by the foundry to figure out the major reasons for the hot tear to form. Filling, solidification and stress/strain analyses were performed to capture all physical phenomena and potential flaws and defects which may contribute to hot tearing. Findings from this first step are listed in section 3.7.3.3. These findings were verified by casting trials performed at the foundry. A very good agreement with the casting results was found.

In the optimization problem, the dimensions and positions of the two top risers and the chills were prescribed as design variables together with the allowed ranges of variation. After optimization, one solution was selected from the design space.

The new shapes of the top risers and the new chill arrangement led to significant improvements in the solidification pattern of the selected optimized solution. More pronounced cooling established favorable temperature gradients and induced progressive and directional solidification not only in the problematic area but also in the entire casting. New convection and macrosegregation patterns were obtained giving favorable and promising results. Due to steeper thermal gradients the mushy zone got reduced, its permeability was lowered imposing higher resistance for liquid-solid movement and for potential channel segregation. The resulting carbon, phosphorus and sulfur distributions seemed more uniform over the casting body. After removing the top sand core there was no longer a mechanical restraint to free volumetric contraction of the casting in the area just below the top core. All of these features and improvements completely eliminated the susceptibility to hot tearing in the entire casting which was also proved during the subsequent production.

References

1. Tutum, C.C., *PhD thesis*, Technical University of Denmark, Lyngby, (2009).
2. Flender, E., Sturm, J., "*Thirty years of casting process simulation*," International Journal of Metalcasting, Vol. 4, Issue 2, (2010).
3. Sturm, J.C., Busch, G., "*Cast iron- a predictable material*," World Foundry Congress, Hangzhou, China, (2010).
4. Domkin, K., Hattel, J.H., Thorborg, J., "Modeling of high temperature- and diffusion-controlled die soldering in aluminum high pressure die casting," Journal of Materials Processing Technology, (2009).
5. Dedmon, S.L., Dutler, S., Pilch, J., Galbraith, J., "*Simulation of Solidification of a 19 inch Diameter, Double Length Steel Ingot*," Proc. Fall Conference of the ASME Rail Transportation Division RTDF2008, Chicago, Illinois, USA, (2008).
6. Svensson, I.L., Seifeddine, S., Hattel, J.H., Thorborg, J., Kotas P., "*On Modelling of Microstructure Formation, Local Mechanical Properties and Stress-Strain Development in Aluminium Castings*," Proc. Int. Conf. On Modelling of Casting, Welding and Advanced Solidification Processes, MCWASP XII, Vancouver BC, Canada, pp. 129-136, (2009).
7. Egner-Walter, A., "*Prediction of distortion in thin-walled die castings*," CP+T Casting Plant + Technology International , Vol. 23, no. 1, pp. 24-29, (2007).
8. Kotas, P., "Numerical Optimization of Die filling and of High-Pressure Die Cast Deformation", Master Thesis, Technical University of Denmark, Lyngby, Denmark, (2007).
9. Schneider, M., Heisser, C., Serghini, A., Kessler, A., "*Experimental investigation, physical modeling and simulation of core production processes*," AFS Transactions, (2008).
10. Kokot, V., Bernbeck, P., "*Integration and Application of Optimization Algorithms with Casting Process Simulation*," Proc. Int. Conf. On Modelling of Casting, Welding and Advanced Solidification Processes, MCWASP X, Destin, Florida, pp. 487- 494, (May 2003).
11. MAGMAfrontier 4.4 Reference Manual, (2005).
12. Hahn, I., Hartmann, G., "*Automatic computerized optimization in die casting processes*," Casting Plant & Technology, Vol. 24, no. 4, (2008).
13. Hahn, I., Sturm, J.C., "*Autonomous optimization of casting processes and designs*," Proc. World Foundry Congress, Hangzhou, China, (2010).
14. Tsoukalas, V.D., "*Optimization of injection conditions for a thin-walled die-cast part using a genetic algorithm method*," Proc. IMechE, Vol. 222, Issue 9, Part B: J. Engineering Manufacture, (2008).
15. Tsoukalas, V.D., "*Optimization of porosity formation in $AlSi_9Cu_3$ pressure die castings using genetic algorithm analysis*," Materials and Design, Vol. 29, pp. 2027–2033, (2008).
16. Gramegna, N., Baumgartner, P., Kokot, V., "*Capabilities of New Multi-Objective Casting Process Optimization Tool*," IDEAL International Conference, Lecce, Italy, (October 2005).
17. Goldberg, D.E., *Genetic Algorithms in Search, Optimization & Machine Learning*, Addison Wesley Longmann, Inc., (1989).
18. Poloni, C., Pediroda, V., *GA coupled with computationally expensive simulations: tools to improve efficiency, chapter Genetic Algorithms and Evolution Strategies in Engineering and Computer Science*, pp 267-288, John Wiley and Sons, (1997).
19. Poles, S., "*MOGA-II, an improved multi-objective genetic algorithm*," Technical Report 006, ESTECO s.r.l., (2003).
20. Srinivas, N., and Deb, K., "*Multi-objective optimization using non-dominated sorting in genetic algorithms*," Evolutionary Computation, 2, pp 221-248, (1994).
21. Deb, K., Agrawal, S., Pratap, A., and Meyerivan, T., "*A fast and elitist multi-objective genetic algorithm: NSGA-II*," IEEE Transactions on Evolutionary Computation, 6, pp 182-197, (2002).
22. Kotas, P., Tutum, C.C., Snajdrova, O., Thorborg, J., Hattel, J.H., "*A Casting Yield Optimization Case Study: Forging Ram*," *International Journal of MetalCasting*, Vol. 4, Issue 4, (2010).

23. Tutum, C.C., Hattel, J.H., "*Optimization of Process Parameters in Friction Stir Welding Based on Residual Stress Analysis – A Feasibility Study*," Science and Technology of Welding and Joining, Vol. 15, No. 5, pp. 369- 377, (2010).
24. Deb, K., "*Unveiling innovative design principles by means of multiple conflicting objectives*," Engineering Optimization, Vol. 35, No. 5, pp 445-470, (2003).
25. Kor, J., Chen, X., Hu, H., "*Multi-Objective Optimal Gating and Riser Design for Metal-Casting*," IEEE International Symposium on Intelligent Control, Saint Petersburg, Russia, (2009).
26. Hartmann, G.C., Kokot, V., Seefeldt, R., "*Numerical Optimization of Casting Processes – Leveraging Coupled Process Simulation and Multi-Object Optimization to the Manufacturing Level*," 21st CAD-FEM Users' Meeting, International Congress on FEM Technology, Berlin, Germany, (2003).
27. Kotas, P., Tutum, C.C., Andersen, S., Hattel, J.H., "*Autonomous Optimization of a Solidification Pattern and its Effect on Porosity and Segregation in Steel Castings*," 115th Metalcasting Congress, Schaumburg, USA, (2011), (accepted for oral presentation).
28. Deb, K., "*Unveiling innovative design principles by means of multiple conflicting objectives*", Engineering Optimization, Vol. 35, No. 5, pp 445-470, (2003).
29. Tutum, C.C., Deb, K., Hattel, J.H., "*Hybrid Search for Faster Production and Safer Process Conditions in Friction Stir Welding*," SEAL 2010, pp. 603–612, Springer-Verlag Berlin Heidelberg, (2010).
30. Deb, K., "*An introduction to genetic algorithms*," Sadhana, Vol. 24, Parts 4 & 5, pp. 293-315, (1999).
31. Deb, K., *Optimization for engineering design, algorithms and examples*, Prentice-Hall of India Pvt.Ltd, (2006).
32. Deb, K. and Kumar, A., "*Real-coded genetic algorithms with simulated binary crossover: Studies on multi-modal and multi-objective problems*," Complex Systems, 9, pp 431-454, (1995).
33. Deb, K., *Multi-Objective Optimization using Evolutionary Algorithms*, JohnWiley and Sons, Ltd., Chichester (2001)
34. Zitzler, E., *Ph.D. Thesis*, Swiss Federal Institute of Technology (ETH), Zurich, (1999).
35. Branke, J., Deb, K., Miettinen, K., Słowinski, R., *Multiobjective Optimization Interactive and Evolutionary Approaches*, Springer-Verlag Berlin Heidelberg, (2008).
36. Goldberg D.E., Deb, K., "*A comparison of selection schemes used in genetic algorithms*," In Foundations of genetic algorithms FOGA, San Mateo, CA, USA, pp 69-93, (1991).
37. Spears, W.M., De Jong, K.A., "*An analysis of multi-point crossover*," In *Foundations of genetic algorithms* FOGA, San Mateo, CA, USA, pp 310-315, (1991).
38. Dawkins, R., *The selfish gene*, New York: Oxford University Press, (1976).
39. Dawkins, R., *The blind watchmaker*, New York: Penguin, (1986)
40. Eldredge, N., *Macro-evolutionary dynamics: Species, niches, and adaptive peaks*, New York: McGraw-Hill, (1989).
41. MAGMAsoft simulation software, MAGMA GmbH, Aachen, Germany
42. Poloni, C., Poles, S., Odorizzi, S., Gramegna, N. and Bonollo, F., "*MAGMAfrontier: state of the art of an optimisation tool for the MAGMASOFT environment*," MAGMASOFT International User meeting, (2002).
43. Sobol, I., "*On the systematic search in a hypercube*", SIAM Journal on Numerical Analysis 16, (1979).

Chapter 5

5. Concluding remarks and future work

5.1. Concluding remarks

The work presented in this thesis is devoted to two major subjects; first, modeling of metal casting processes, with a primary focus on gravity sand casting of large steel castings, where all stages of this manufacturing process are taken into consideration, and second, to optimization of thermal aspects of the casting process by means of multi-objective genetic algorithms which belong to evolutionary computation techniques. The main conclusions and findings are briefly addressed below.

Modeling and simulations of casting processes are generally divided into two steps, i.e. fluid flow calculations where mould filling is modeled and thermo-mechanical modeling in which thermal behavior during solidification and solid-state cooling is investigated together with its effect on stress-strain formation inside the casting.

The fluid flow phenomena are addressed first as metal pouring is the first stage in casting processes. It represents the driving force for various defects, such as air bubbles, oxide films; cold shuts, misrun, hot tears, etc., and has a direct influence on the temperature distribution inside the casting which then affects its thermal behavior. The purpose of this thesis has been to describe and subsequently optimize thermal aspects of the considered casting process; hence the fluid flow chapter serves "only" as some sort of guidelines and proposals to the designers or foundry technologists. The idea has been first, to briefly introduce the fundamental physical laws based on which the flow calculations can be carried out. Then each single element of a typical gating system is described and commented on to give an overview on how these elements influence final filling patterns. Furthermore, useful tips on how to proceed when designing the gating systems are given together with one example of how improperly designed gating systems may evoke residual stress and deformation in castings. This example is shown on a HPDC casting. In essence, the chapter devoted to filling aims at showing how important it is to focus not only on thermal aspects of a casting, but also on the design of gating systems. One should come to realize and always have in mind that gating systems and subsequent filling patterns greatly influence the overall quality of castings and stand behind many types of defects, found in castings, regardless of their size or material.

The chapter dedicated to solidification and thermal behavior of castings is the core of the thesis. In the beginning, governing equations for the heat transfer and temperature distribution in castings are given. Feeding rules and mechanisms are discussed and used for designing a proper riser to avoid subsequent solidification related defects. The greatest portion of this chapter concerns casting defects. Three major defects, i.e. centerline porosity, hot tears and macrosegregation, are presented and thoroughly analyzed. When discussing casting defects, it is the most important to determine their causes of occurrence. When doing so, it was found that there exists a link between all three defects. Thermal gradients, the pressure drop over the mushy zone and the solidification pattern are the three common links between these defects. Centerline porosity starts to form when the pressure drop over the mush exceeds a critical value. The pressure drop decreases as the thermal gradient increases. It was also shown that when establishing a progressive and directional solidification pattern, centerline porosity does not occur. One of the theories found in literature claims that the pressure drop is also accountable for initiation and growth of hot tears, therefore the thermal gradient gets on the scene again. Hot tears are also promoted by the extent or size of the mushy zone. The longer the area stays in a semi-solid state, the higher probability of hot tears. The thermal gradient is again the factor which decreases or increases the size of the mush. If tensile stresses are found in the casting, they can cause localized tensile straining in the weak, semi-solid area which will not impose any major resistance to the straining and a hot tear will be initiated.

As to macrosegregation and A-segregates in particular, these are investigated in large steel castings. Macrosegregation is caused by convective flow inside the solidifying melt. Again, it was found that if

the extent of the mushy zone gets decreased by the increased thermal gradient, there will not be that much time and chances to form the A-segregates. If a directional and progressive solidification pattern towards the heaviest section, i.e. the riser, the residual liquid being rich on the solute elements, will be pushed into the riser. It is very desirable for the structural integrity of castings to have the positively segregated liquid in the riser(s) and the uniform solute distribution in the casting body. One can see that it is possible to address hot tears and macrosegregation by optimizing, i.e. minimizing, centerline porosity. In other words, if centerline porosity is eliminated by proper thermal gradients and directional solidification, the other two defects should be eliminated as well. This is clearly shown in the optimization section. The aforementioned theory is always backed and supported by industrial examples and case studies carried out during the PhD period.

The thermal model implemented in MAGMAsoft, predicting the behavior of castings during solidification and solid state cooling is subsequently coupled with evolutionary multi-objective algorithms (MOGA- in MAGMA*frontier*) in a search for the optimal casting design parameters, namely the riser(s) and chills design, which would minimize the issues with centerline porosity by establishing a directional and progressive solidification pattern. By minimizing centerline porosity and based on its relationship to hot tears and macrosegregation, it is possible to optimize these two defects without a need of prescribing them as optimization objectives. There is no need to run the very time-consuming macrosegregation, convection and stress-strain analysis for all the designs in the optimization run. Only simple thermal analyses are required to assess the thermal behavior of each of the casting designs. When the optimal design with respect to minimized centerline porosity is found and selected, just this one casting layout is subjected to macrosegregation, convection and/or stress-strain analyses. Three case studies are shown in the optimization chapter to support this theory.

Findings from the solidification and optimization chapters are, in the author's opinion, valuable for many foundry engineers who deal with these defects on a daily basis. It was shown that one can obtain reasonable information on macrosegregation and hot tears already from the standard thermal analysis in MAGMAsoft, by checking the Niyama criterion, the thermal gradient criterion function and the temperature distribution inside the casting. This should not be understood as if stress-strain analysis can be now totally neglected. Those who have access to the optimization tool MAGMA*frontier* can directly benefit from this work by learning that macrosegregation and hot tears can be effectively optimized without even prescribing them as the objectives and without running the time-demanding analyses.

5.2. Future work

The major area of focus during the PhD study has been numerical modeling and optimization of large steel castings using MAGMAsoft. Since the author has always intended to relate and apply the theory behind casting processes to industrial applications, a research-oriented collaboration with Vitkovice Heavy Machinery (VHM), Czech Republic, has been established during the studies. Thus, all of the case studies and examples, presented in this thesis, come from this foundry. Therefore, a natural follow-up is that the future work will be closely related to this foundry and to MAGMA GmbH, applying its numerical simulation tool.

Besides classical end products, i.e. shape castings, many steel foundries also cast steel ingots which are then taken as inputs for the subsequent forging operations. It is clear that the forged parts are not always perfect, including internal/external defects or residual stresses which are then a cause of rejection. Such a rejection of let us say, a 70 ton crank shaft is extremely costly for the foundry since approximately 140 tons of metal plus labor work got used just to manufacture this shaft. For such foundries it is extremely important to determine where the defects come from, whether from the ingot casting or from the forging operation. There is basically no information or work done in this field that would be described in literature. Therefore, a personal aim of the author is to fill this gap. Of course this is not practically feasible without help and leadership of the participating partners, i.e. the process modeling group of DTU, MAGMA GmbH and Vitkovice Heavy Machinery.

The idea is to model ingot castings, as precise as possible, to closely mimic the reality. Based on the first assessment, the most critical aspects of the casting process will be identified. The most common defects in ingot castings are centerline and shrinkage porosity, macrosegregation and sometimes hot

tears. The optimization methodology presented in this thesis will be applied in the following optimization procedure which will aim at modifying the casting layout and process parameters to minimize the aforementioned defects. This optimized ingot layout will be subsequently exported from MAGMAsoft together with its complete thermal history and defects prediction, and inserted as an initial layout for FEA software to model the forging operation.

By taking the thermal history of the ingot into account, the forging operation should deliver much more reality-resembling results. At this moment, when modeling forging it is standard procedure to assume a homogeneous distribution of mechanical properties, no residual stresses and no defects inherited from the casting operation. When coupling these two independent manufacturing processes, it will be possible to see where the defects, for instance porosity, will end up after forging, or whether stress peaks will be located at areas which will be subsequently severely loaded during service. Moreover, even though it is a long and very challenging run, it is then possible to simulate the load situation on the forged part to see how the part behaves in its real working conditions.

One big advantage of having industrial partners involved in this project is that they, i.e. Vitkovice H.M., will provide us with experimental, real-scale results and microstructure analyses to compare our results with. Having MAGMA GmbH involved gives us assurance of having access to the state-of-the-art numerical solvers which will make the modeling part as accurate as possible.

Besides this project, the author's focus will be put on applying various optimization techniques to casting processes. Although the performance of the MOGA algorithm, implemented in MAGMAfrontier, is promising, giving good results, it could be nice to test the performance of a different and newer optimization algorithm, e.g. NSGA-II. A custom NSGA-II algorithm has been developed and tested on the chosen benchmark cases (in-house) by Dr. Tutum. The plan is to couple this custom algorithm with MAGMAsoft, through the MAGMA API interface to test its performance on real industrial cases where the Pareto front is not known.

Chapter 6

6. Summary of Appended Papers and Reports

Paper I

Petr Kotas, Jesper Hattel, Jesper Thorborg, Ingvar L. Svensson, Salem Seifeddine.

Modelling of Filling, Microstructure Formation, Local Mechanical Properties and Stress – Strain Development in High-Pressure Die Cast Aluminium Castings.

Published at the International Ph.D. Foundry Conference, Brno, June 2007, Czech Republic.

In this work, a concept of integrated modeling in casting processes, namely in high pressure die casting is presented. The objective is to demonstrate how the manufacturing process influences the defect distribution, local microstructure, final mechanical properties and subsequent in-service behavior of the casting. A test case of a complex high-pressure die cast part in an aluminium silicon-based alloy is considered including the simulation of the entire casting process, i.e. filling, solidification and solid state cooling. The focus is on (i) filling and its effect on defects occurrence and on final temperature distribution which directly influences the solidification pattern. (ii) How the temperature fields coming from filling affect local microstructure formation and its coupling with mechanical properties such as elastic modulus, yield stress, ultimate strength and elongation as well as residual stresses. Subsequently, the casting is subjected to external service loads and the results of this analysis are discussed in relation to the predicted local properties as well as the residual stresses originating from the casting simulation.

Paper II

Petr Kotas, Cem Celal Tutum, Olga Šnajdrova, Jesper Thorborg, Jesper Hattel.

A Casting Yield Optimization Case Study: Forging Ram.

Published in the International Journal of MetalCasting, Vol. 4, Issue 4, (2010).

This paper summarizes the findings of multi-objective optimization of a gravity sand-cast steel part for which an increase of the casting yield via riser optimization was considered. This was accomplished by coupling a casting simulation software package MAGMAsoft® with its optimization add-on module MAGMA*frontier*. First, analyses of filling and solidification of the original casting design were conducted in the standard simulation environment to determine potential flaws and inadequacies. Based on the initial assessment, the gating system was redesigned and the chills rearranged to improve the solidification pattern. After these two cases were evaluated, the adequate optimization targets and constraints were defined. One multi-objective optimization case with conflicting objectives was considered in which minimization of the riser volume together with minimization of shrinkage porosity and limitation of centerline porosity were performed.

Paper III

Petr Kotas, Cem Celal Tutum, Søren Andersen, Jesper Hattel.

Autonomous Optimization of a Solidification Pattern and its Effect on Porosity and Segregation in Steel Castings.

Accepted for an Oral Presentation at the 115th Metalcasting Congress, Schaumburg, April 2011, USA.

Accepted for publication in AFS Transactions 2011.

The present paper considers optimization of the solidification pattern of a gravity sand-cast steel part. That is, the choice of proper riser and chill designs has been investigated using genetic algorithms while simultaneously considering their impact on centerline porosity and macrosegregation distribution. This was accomplished by coupling a casting simulation software package with an optimization module. The casting process of the original casting design was simulated using a transient 3D thermal model incorporated in MAGMAsoft® to determine potential flaws and inadequacies. After this initial assessment, a new geometrical model was suggested with the redesigned gating system and rearranged chills to obtain better filling and solidification patterns. Based on the improved model, relevant optimization targets and constraints were defined. One multi-objective optimization case with two conflicting objectives was considered in which minimization of the riser volume together with minimization of centerline porosity and elimination of macrosegregation issues were performed.

Paper IV

Petr Kotas, Jesper Thorborg, Cem Celal Tutum, Jesper Henri Hattel.

Elimination of Hot Tears in Steel Castings by Means of Solidification Pattern Optimization.

Presented at the International Steel Casting Conference, October 2010, Dresden, Germany.

Submitted to Metallurgical and Materials Transactions B – February 2011.

In this paper, a methodology of how to exploit the Niyama criterion for elimination of various solidification-related defects such as centerline porosity, macrosegregation but primarily hot tearing in steel castings is presented. The tendency of forming centerline porosity is governed by the temperature distribution very close to the end of the solidification interval, specifically by thermal gradients and cooling rate. The physics behind macrosegregation and hot tears indicate that these two defects are also heavily dependent on thermal gradients and pressure drop in the mushy zone. The objective of this work is to show that by optimizing the solidification pattern, i.e. establishing directional and progressive solidification with the help of the Niyama criterion, macrosegregation and hot tears issues can be both minimized or entirely eliminated.
The casting process of an original casting layout was simulated using a transient 3D thermal fluid model incorporated in a commercial simulation software package MAGMAsoft®, to determine potential shortcommings. Based on the initial casting process assessment and when the major causes for hot tearing were determined, multi-objective optimization (using MAGMA*frontier*), of the solidification pattern of the considered steel part followed. That is, the choice of proper riser and chill designs has been investigated using genetic algorithms while simultaneously considering their impact on centerline porosity, the macrosegregation pattern and primarily on hot tear formation.
One multi-objective optimization case with two conflicting objectives was considered in which the minimization of the riser volume together with the minimization of centerline porosity and elimination of hot tear susceptibility were performed.

Industrial Report

Petr Kotas, Jesper Henri Hattel

Casting Process Optimization of a Large Steel Ring With Respect to Centerline Porosity and Channel Segregates

Presented to the foundry management of Vitkovice Heavy Machinery, July 2010, Ostrava, The Czech Republic.

This report deals with optimization of an entire casting process of a large (246 ton) steel ring with the objective of eliminating problems with macrosegregation, particularly with channel segregates. Moreover, it was requested to optimize the shape of the top riser to increase the casting yield.
Two thorough numerical analyses of mould filling and solidification took place; both accomplished using the commercial simulation software package MAGMAsoft®. These analysis gave detailed information about the filling pattern, subsequent defects prediction and the temperature distribution in the casting evoked by the mould filling process, the temperature distribution during solidification and the subsequent solid state cooling. Moreover, it was possible to identify critical areas such as hot spots, areas with inadequate and/or restricted feeding, or areas with thermal imbalance that may evoke thermal stresses and strains. Last, convection and macrosegregation profiles were assessed in order to predict possible issues with macrosegregation and with channel segregates.
The optimization was defined as a goal of finding the "most optimal" solution to the predefined objectives, which were: (i) the minimization of the riser volume and (ii) the minimization of the presence of centerline porosity. When centerline porosity is minimized by increasing thermal gradients and by establishing a progressive solidification pattern, concentration profiles suggesting macrosegregation are positively affected as well, thereby suppressing the tendency to channel segregation in the cast part. For this purpose, a built-in optimizer MAGMA*frontier* was applied.
After selecting the most favorable design, this design was analyzed with respect to filling, solidification and stress-strain to assess the impact of the optimized features on the overall behavior. The findings and proposals from this study were presented to the management of the foundry and were evaluated as suitable for subsequent implementation.

A PAPER – I

Kotas, P., Hattel, J.H., Thorborg, J., Svensson, I.L., Seifeddine, S., "*Modelling of Filling, Microstructure Formation, Local Mechanical Properties and Stress – Strain Development in High-Pressure Die Cast Aluminium Castings*", International Ph.D. Foundry Conference, Brno, June 2007, Czech Republic.

Brno University of Technology
Czech Foundrymen Society – CFS

International PhD Foundry Conference

3rd June 2009

Modelling of Filling, Microstructure Formation, Local Mechanical Properties and Stress – Strain Development in High-Pressure Die Cast Aluminium Castings

Petr Kotas, Jesper Hattel, Jesper Thorborg, Ingvar L Svensson and Salem Seifeddine
Technical University of Denmark, Department of Mechanical Engineering
Jönköping University, School of Engineering, Department of Mechanical Engineering

MODELLING OF FILLING, MICROSTRUCTURE FORMATION, LOCAL MECHANICAL PROPERTIES AND STRESS – STRAIN DEVELOPMENT IN HIGH-PRESSURE DIE CAST ALUMINIUM CASTINGS

Petr Kotas[1] Jesper Hattel[1] Jesper Thorborg[1, 3] Ingvar L Svensson[2] and Salem Seifeddine[2]

[1]Technical University of Denmark, Department of Mechanical Engineering

Building 425, DK-2800, Lyngby, Denmark.

[2]Jönköping University, School of Engineering, Department of Mechanical Engineering

Box 1026, 551 10 Jönköping, Sweden

[3]MAGMA GmbH, Kackertstrasse 11, D-52072, Germany

Keywords: Aluminium alloy, high-pressure die casting, filling, local mechanical properties, stress strain, material data

ABSTRACT

Today, the industrial demands are to reduce product development time as well as costs of producing prototypes. In this context, virtual prototyping by numerical simulation offers an efficient way of lowering costs and shorten lead time.

Castings are produced by a manufacturing method which inherently affects the component's properties depending on design, metallurgy and casting technique. The wall thickness influences the coarseness of the microstructure and the material will have properties depending on the local metallurgical and thermal histories. This is independent on the material, i.e. whether the casting is based on cast iron- or aluminium-alloys. The distribution of local properties in a casting might vary substantially which makes it complex to optimize the casting with good accuracy. Often, mechanical simulations of the load situation are based on the assumption that the cast product has constant material properties throughout the entire casting. Thus, if the microstructure is determined or predicted at a given point, it gives the possibility to calculate the local material behavior more realistically.

In the present work, a test case of a complex high-pressure die cast part in an aluminium alloy is considered including simulation of the entire casting process with emphasis on microstructure formation related to mechanical properties such as elastic modulus, yield stress, ultimate strength and elongation as well as residual stresses. Subsequently, the casting is subjected to service loads and the results of this analysis are discussed in relation to the predicted local properties as well as the residual stresses originating from the casting simulation.

INTRODUCTION

Today, there is a big need for production of complex and compound components to lower the manufacturing costs and shorten the lead times. A substantial portion of costs in the manufacturing of cast components is production of physical prototypes and the following execution of physical testing. It is not only the production cost that is large, but also the production time is long. Only to produce/prepare/ one cast prototype can take from 2-10 weeks. Since the properties depend to a large extent on the casting process [1-4], the prototypes must imitate the" true" component in an attractive way; which in turn makes the cost high and production time long.

If one instead could establish a methodology for development of cast components where parameters from the casting and production process are taken into account to predict for example properties and residual stresses, reliability will be increased and the precision of simulations and the number of physical prototypes will be drastically decreased.

The automotive, telecom and manufacturing industries are moreover strongly depending on sophisticated and complex geometries of cast components in continuation of improvement of their products. In order to become more efficient in product and production development, the time for the experimental testing must decrease or nearly entirely be eliminated. Therefore new and improved simulation methods and more reliable mathematical models are needed.

Furthermore, improved simulation tools become the strongest competition means for producing complex cast components with high knowledge- and technology contents. Through combining a traditional production method with a sophisticated technology an old method can get a world-leading position within the component production technology area by Virtual product production (VPF).

To optimize a cast component, all main parameters and variables in the process must be taken into consideration in the subsequent analyses, calculations and simulations. Examples of parameters are metallurgy treatment, chemical analysis, cooling conditions and resulting properties and residual stresses. Geometry and process relations will and lead to components containing a wide variety of properties over the entire geometry. In addition, residual stresses arise during solidification and solid-state cooling and they will be geometry dependent [3,5,6]. These effects and new boundary conditions are necessary to be addressed in the following work.

So far, it has been a common procedure for the designers to assume that the cast material has similar properties in all areas. In most of the cases the properties are taken from a standardized test bar, which then leads to incorrect results and conclusions. Therefore, it is of importance to consider properties depending on the local metallurgical and thermal histories directly inherited from the manufacturing process. By means of integrated modeling [7,8] of multi-process steps (casting, solidification, stress-strain analysis) and materials modeling, it is feasible to obtain the final mechanical properties and thereby predict the behavior of the component during in-service loading.

In the present work a test case of a console for a front bumper on a truck is analyzed, see Figure 1. First the casting process is simulated in MAGMAsoft® [9], taking the entire cycle of mould filling, solidification using microstructure formation and solid state cooling into account. Focus is on solidification pattern, microstructure formation related to mechanical properties such as elastic modulus, yield stress, ultimate strength and elongation as well as residual stresses. Subsequently, the casting is subject to service loads and the results of this analysis are discussed in relation to the predicted local properties as well as the residual stresses originating from the casting simulation.

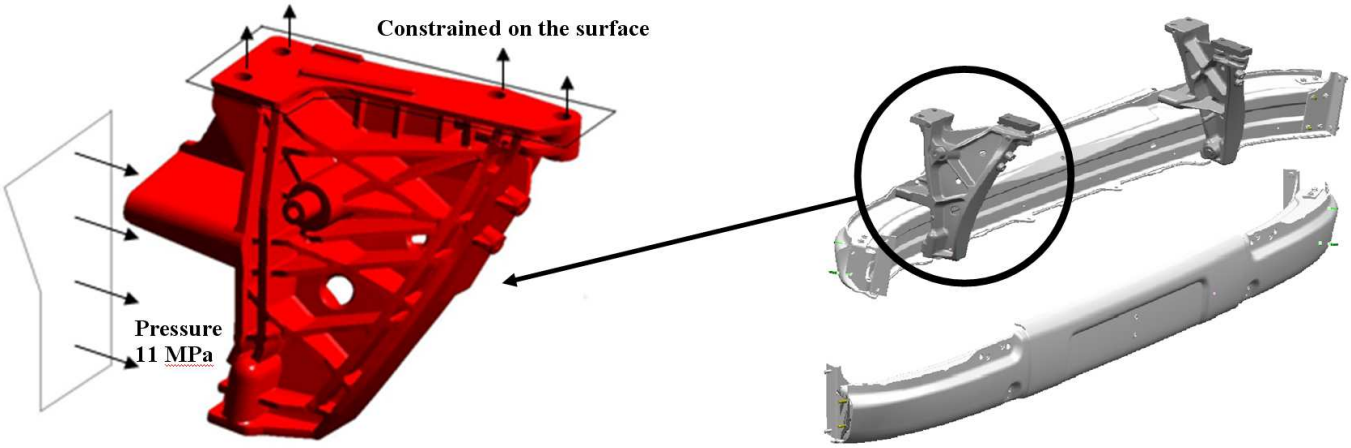

Figure 1 Left: Detailed view of the console with prescribed constant compressive stress corresponding to an equivalent crash force of 160 kN (worst case according to Swedish standards). Right: Positioning of a similar console on the front bumper.

However, since as earlier mentioned, the microstructural and mechanical analyses are in focus in the present work, they will be briefly explained in the following.

MICROMODELLING OF SOLIDIFICATION AND MECHANICAL PROPERTIES

Today's generation of computer simulation programs for cast components has mainly focused on fluid flow/mould filling, solidification and prediction of shrinkage and residual stresses.

However, the development goes toward that simulation can predict microstructures, porosities and shrinkage and mechanical properties of the material that along with the design gives the component its mechanical properties. Here, one can see several development trends with the common aim that the resulting mechanical properties can to be imported into simulation programs to predict stresses and deformations arising from the in-service loads.

The mathematical models used [10,11], describe the microstructure formation during solidification, including nucleation and growth kinetics for the phases and algorithms that describe the relation between the microstructure and mechanical properties. Note that the present investigation aims to develop a relationship based on the isolated effect of microstructure on the mechanical properties, therefore, the influence of defects are not considered here.

The microstructure of aluminium cast alloys is widely defined as the distance of the spacing between the dendrite arms in terms of secondary dendrite arm spacing, SDAS. In this paper the SDAS is described as a function of local solidification time t_s, equation (1), depicting the fineness of the microstructure constituents; C and n are constants which are related to the material's chemical composition.

$$SDAS = C \cdot t_s^{\,n} \tag{1}$$

The commercial cast aluminium alloy A354, that is commonly used when casting automotive components, is used in this study. As seen in Figure 2, the finer the microstructure, (a), the stronger the material and vice versa, (b) and (c).

A comparison of three identical tensile test samples at each SDAS has been performed and the material characteristics as Young's modulus, strength coefficients and deformation hardening have been evaluated from the experimental curves. The scatter in data is mainly due to a lower degree of inhomogenities between the samples and different levels of defects. The filled circles on the curves indicate the fracture points. The material has been gradient solidified to get low spread in material properties.

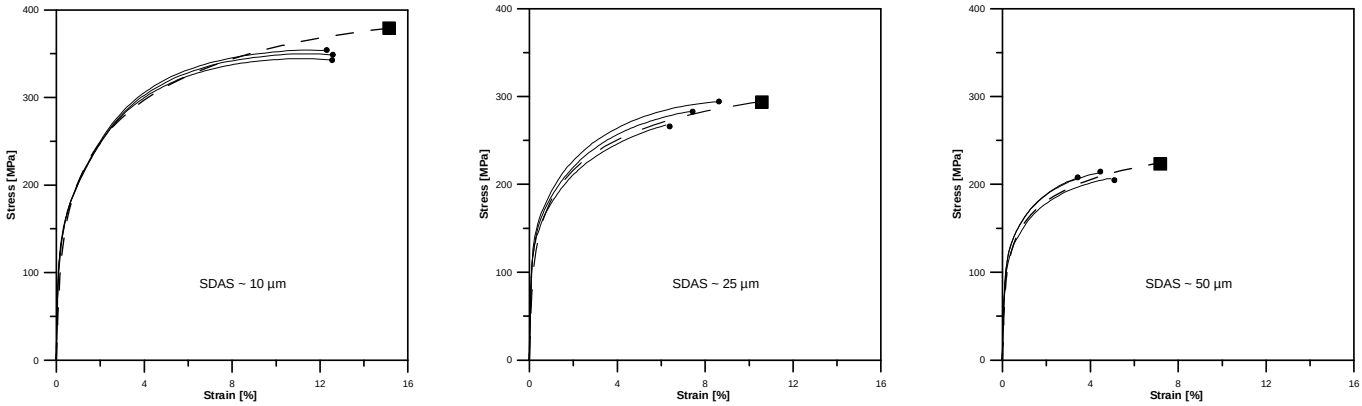

Figure 2. Tensile test curves illustrating the tensile behavior of an Al-9%Si-1%Cu-0.4%Mg cast alloy where SDAS in a) is ~ 10 µm, b) is ~ 25 µm, and c) is ~ 50 µm. The dashed curves are the corresponding simulated tensile curves and the filled squares imply that the quality of the material i.e. defect content, will determine where the fracture occurs. The filled circles denote the fracture of the particular tensile test sample.

The influence of defects such as porosities and/or harmful intermetallic phases are incorporated in the modelling of the tensile test curve and assumed to affect the mechanical performance, as seen from the simulated curves. The filled squares are to be considered as indicators, emphasizing that the inherent strength potential of the alloys might have not been reached due to the factors mentioned above.

MECHANICAL ANALYSIS

A mechanical analysis is carried out during the casting process as well as the subsequent loading situation of the cast part. In both cases, a standard mechanical model based on the solution of the three static force equilibrium equations is used, i.e.

$$\sigma_{ij,i} + p_j = 0 \tag{2}$$

where p_j is the body force at any point within the volume and σij is the stress tensor.

The well-known Hooke's law, linear decomposition of the strain tensor into an elastic, a plastic and a thermal part as well as small strain theory are applied

$$\sigma_{ij} = \frac{E}{1+\nu}\left\{\frac{1}{2}\left(\delta_{ik}\delta_{jl} + \delta_{il}\delta_{jk}\right) + \frac{\nu}{1-2\nu}\delta_{ij}\delta_{kl}\right\}\varepsilon_{kl}^{el} = E_{ijkl}^{el}\varepsilon_{kl}^{el} \tag{3}$$

$$\varepsilon_{ij} = \varepsilon_{ij}^{el} + \varepsilon_{ij}^{pl} + \varepsilon_{ij}^{th}$$

$$\varepsilon_{ij} = \frac{1}{2}\left(u_{i,j} + u_{j,i}\right)$$

where the thermal strain is given by $\varepsilon_{ij}^{th} \cdot \left(T_1 - T_2\right) = \delta_{ij} \cdot \int_{T_1}^{T_2} \alpha \cdot (T) dT$

In both cases the plastic strain is based on standard J2-flow theory with a temperature dependent yield surface. During the load analysis, isothermal conditions at room temperature are assumed and hence the thermal strain is set to zero in this case. The conditions during yielding are described by the associated flow rule; the von Mises yield surface and the consistency condition, i.e.

$$\dot{\varepsilon}_{ij}^{pl} = \lambda \dot{s}_{ij} \tag{4}$$

$$f\left(\sigma, \varepsilon_e^p, T\right) = |\sigma| - \sigma_Y\left(\varepsilon_e^p, T\right) \leq 0$$

$$\dot{f} = \dot{f}\left(s_{ij}, \varepsilon_e^{pl}, T\right) = \frac{\partial f}{\partial s_{ij}}\dot{s}_{ij} + \left.\frac{\partial f}{\partial \varepsilon_e^{pl}}\right|_T \dot{\varepsilon}_e^{pl} + \left.\frac{\partial f}{\partial T}\right|_{e^{pl}} \dot{T} = 0$$

This material description is considered to be adequate for the casting simulation where the first order effect is the yield strength of the material as a function of temperature.

In general, the temperature fields obtained during the casting simulation will be the driver for the thermally induced strains and stresses via the thermal strain. During the subsequent load situation, it is the mechanical load emulating a crash situation, which in general is the driver for the strains and stresses. The temperature dependent Young's modulus and virgin yield stress used during the casting simulation are depicted in Figure 3 (left), whereas the hardening curve at room temperature is depicted in Figure 3 (right).

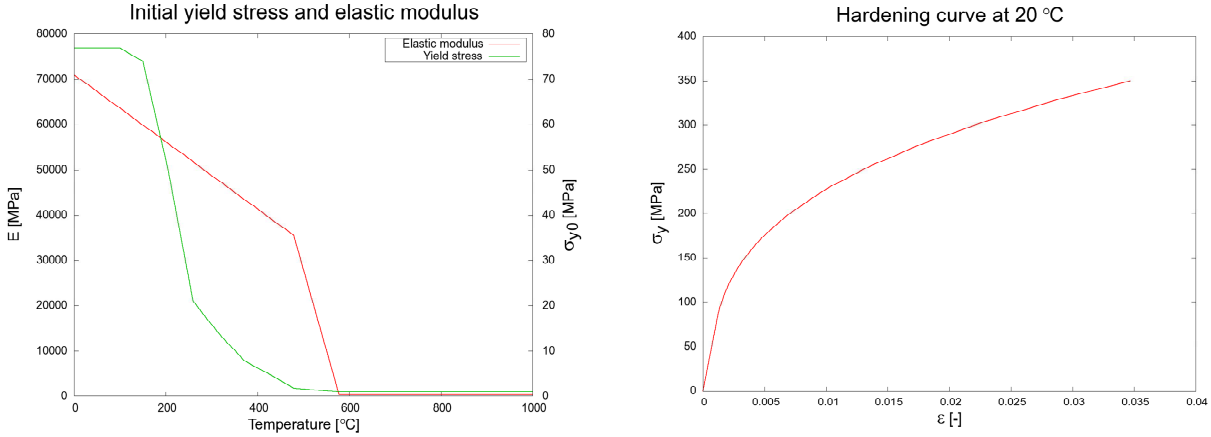

Figure 3 Left: Temperature dependent Young's modulus and virgin yield stress used for the casting simulation. Right: Hardening curve at 20 ºC used in the load simulation.

In MAGMASOFT the mechanical field problem outlined above is solved in an FE-framework using 8-node brick elements. A more thorough description of the mechanical models implemented in MAGMASOFT can be found in [12, 13].

RESULTS AND DISCUSSION

Casting simulation

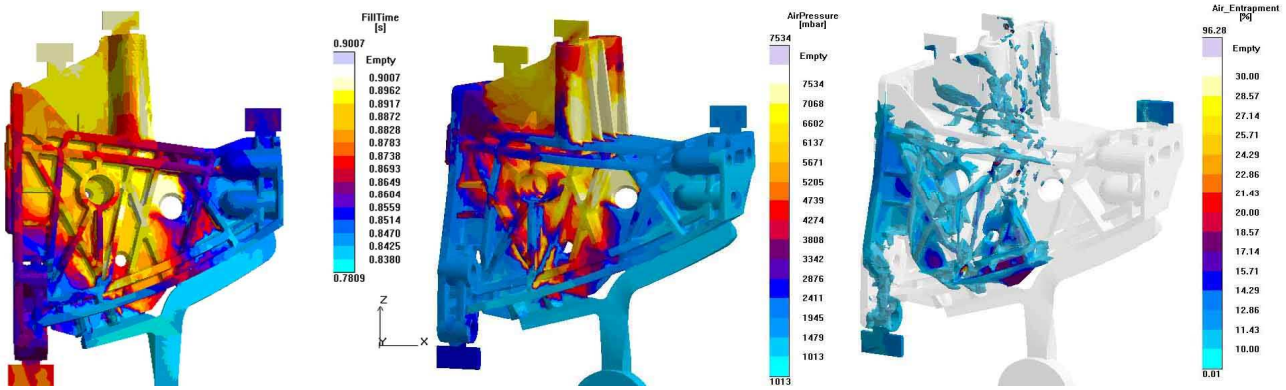

Figure 4 Left: Filling pattern when filling is completed. Middle: Amount of air pressure in the melt after filling. Right: Percentage of entrained air in the melt when filling is completed.

The *filling time* criterion depicted in Figure 4 (left) implies that the filling pattern is not favorable at all. The central area of the casting gets filled as almost the last, rising the likelihood of entrained air or bubbles there. The reason for the uneven filling is that the gating system is split into two main runners with the division just adjacent to the central area of the casting. As a natural consequence, most of the entrapped air is located in the very bottom of that problematic central area. This is well captured by the *air entrapment* Figure 4 (right) and *air pressure* Figure 4 (middle) criteria. It is obvious to all foundry engineers that there is no entirely sound casting produced by any known technique. There is always a certain amount of locked air in the microstructure due to filling and its related inadequacies or faults amongst other wrong design of the gating system, surface turbulence, excessive velocity in thin gates and insufficient venting [1-5, 14-16]. Nevertheless, entrained air gets dangerous and unacceptable only when exceeding a certain value. Therefore, a question comes up, namely which percentage should serve as a threshold value from which the locked air could compromise the internal and structural integrity of the part. There is no "the best answer" therefore, after a discussion with a specialist on HPDC processes [17], the value of 25% entrapped air (on MAGMAsoft® scale) was recommended to use as the value from which the air locked in the casting structure could cause impairment in the casting's soundness. This value closely corresponds to 5% of locked air experimentally measured in real HPDC castings. For this reason, when using an X-Ray function in MAGMAsoft®, everything below 25% was considered too low to affect the casting quality. As seen from figure 4 (right), air entrapped in the material structure did not exceed this agreed value and it is therefore unlikely to encounter problems like air/gas porosity.

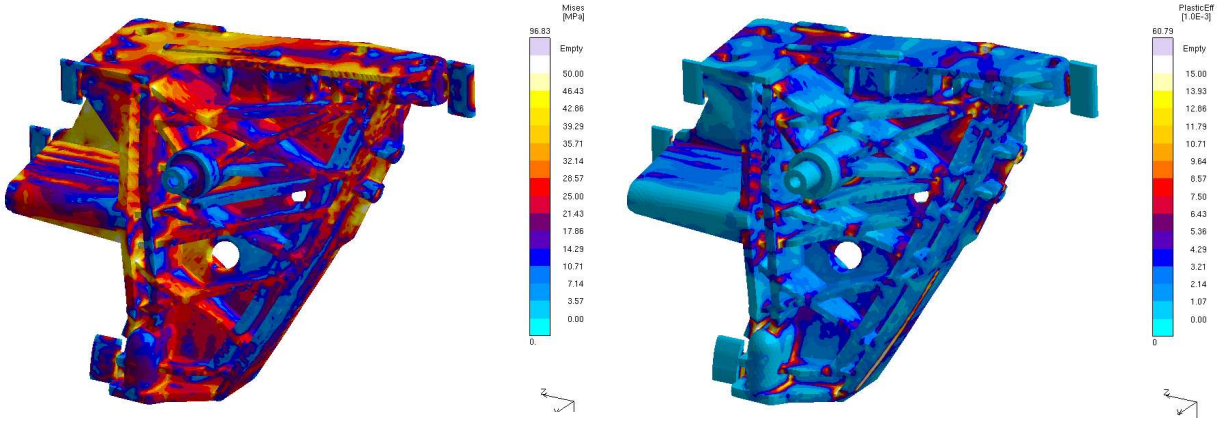

Figure 5 Left: Residual Mises stresses after the casting process. Right: Residual effective plastic strain after the casting process.

In Figure 5 the residual Mises stress and effective plastic strain after the casting process are shown. It is seen that the Mises stresses are in the range up to 96 MPa (Figure 5 left) assuming the highest values in the areas where noticeable effective plastic straining of up to around 6.0 % has taken place (Figure 5 right).

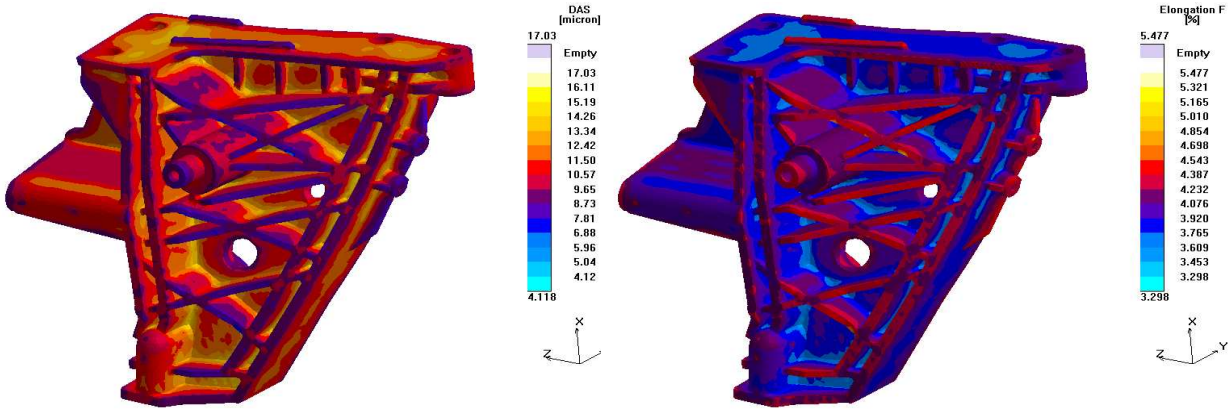

Figure 6 Left: SDAS distribution after the casting process. Right: Elongation distribution after the casting process.

Figure 6 (left) depicts the predicted dendrite arm spacing (SDAS), whereas Figure 6 (right) shows the corresponding elongation of the final casting. It is quite obvious to see that the finer the structure, the higher the elongation. This is in full correspondence with the expected outcome of the presented microstructural model.

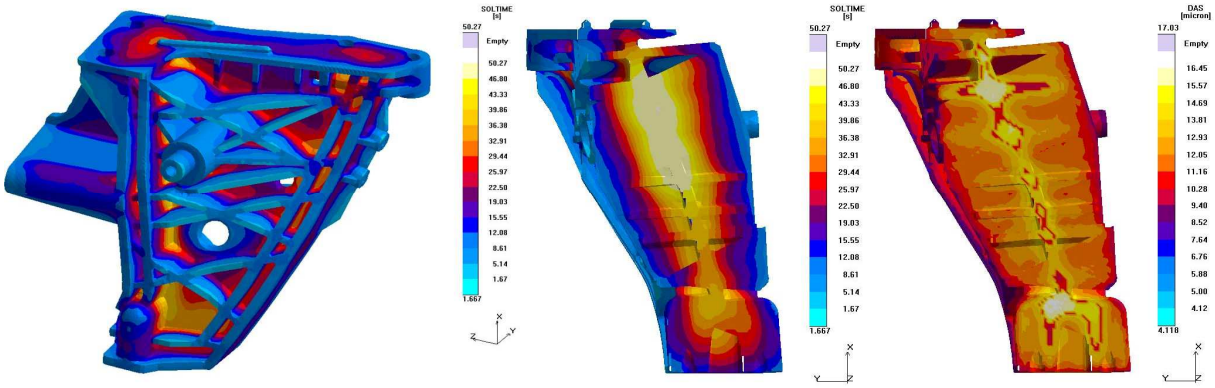

Figure 7 Left: Solidification pattern in the casting. Middle: Cut through the casting – solidification pattern. Right: cut through the casting – SDAS distribution after the casting process

Figure 7 (left) captures an overall solidification pattern of the cast component. The employed criterion SOLTIME employed denotes the time necessary for each element to drop from the initial pouring temperature below its solidus. Factors which are decisive for the solidification pattern are amongst other the composition of an alloy, mode of freezing, filling pattern, casting geometry and design of the die (die material- its cooling capacity, cooling system, and type of coating). As mentioned earlier in the text, the local solidification time directly affects the scale of the secondary dendrite arm spacing (SDAS), thereby the fineness of the microstructure and the final mechanical properties of the component respectively [3,18-21]. In high pressure die casting, it is a very common feature that castings solidify and cool down nearly uniformly over the entire domain. This is due to a complex cooling system present within the die blocks and the wall thickness which in many cases does not change significantly over the casting. However, one can never neglect the effect of the gating system. If a gating system is designed improperly- too robust, thick or cooled poorly, the entire solidification pattern gets impaired, a thermal imbalance is established, giving rise to damaging thermally induced stresses [5,6,22]. Figure 7 (middle) shows the same solidification pattern inside the casting revealing areas to solidify last, so-called hot spots. Figure 7 (right) shows the predicted dendrite arm spacing inside the casting, implying the widely recognized relation between solidification time and coarseness of the microstructure, equation (1). In other words, the longer solidification time, the larger dendrite arm spacing, the coarser microstructure and the poorer mechanical properties of the final product. This phenomenon is well captured in figure 8. Values have been obtained from the numerical model for predicting the microstructure and local mechanical properties in Al-based cast alloys developed by Svensson[2] . It applies, that the elongation (pink line) decreases quite substantially with increasing dendrite arm spacing DAS, causing the material to become brittle, while the Yield strength (blue line) seems to be more or less insensitive towards variations in DAS. Very similar results were experimentally obtained by Campbell [3] for different Al-based alloys.

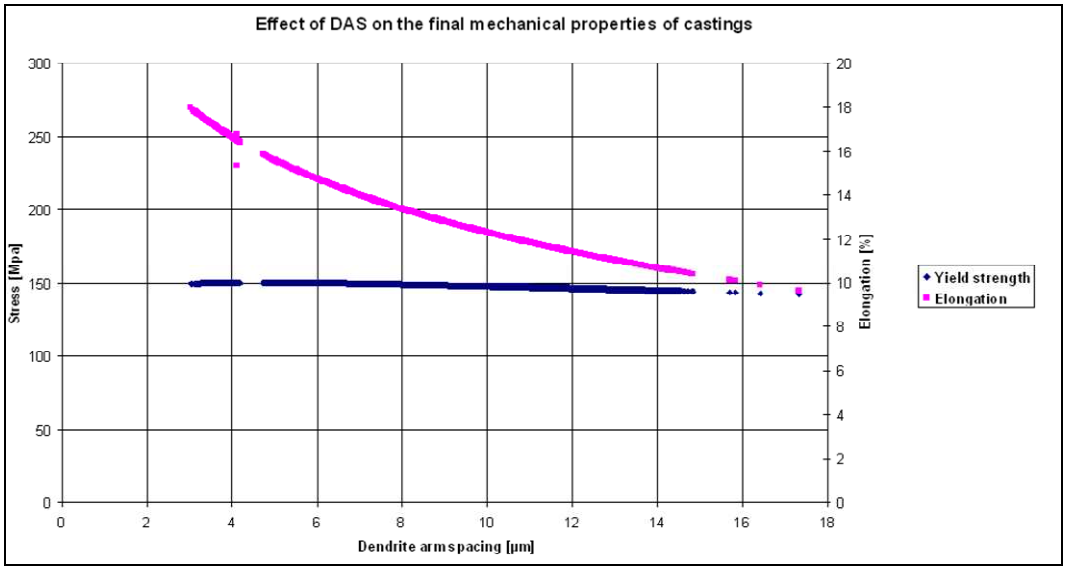

Figure 8: Effects of DAS on the final mechanical properties of the AlSi9Cu3 alloy casting as predicted by the applied model by Svensson.

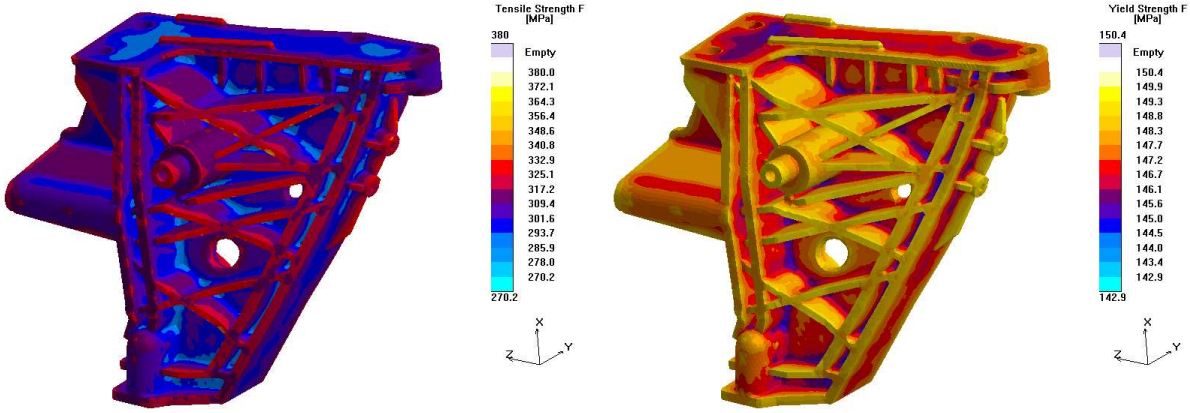

Figure 9 Left: Ultimate tensile strength (UTS) distribution after the casting process. Right: Yield stress at 0.2 % effective plastic strain after the casting process.

Finally, in Figure 9 the ultimate tensile strength (UTS) and the yield stress at 0.2 % effective plastic straining after the casting process are depicted. It is interesting to notice the substantial difference in levels, i.e. the UTS varies between 270 and 350 MPa, whereas the 0.2 yield strength is more or less constant at a level of 150 MPa. For the part under consideration this is an important result in the sense that for effective plastic strains lower than 0.2% the different sections of the casting will yield almost equally whereas for substantially higher strains there will be a noticeable difference in the corresponding stress levels for the same effective plastic strain depending on the location in the cast part. Moreover, since the part is supposed to obtain crash loads during service, it is of vital importance that the elongation is sufficiently high and the UTS is substantially higher than the virgin yield stress.

Load simulation

The above predicted mechanical properties were used in the subsequent load simulation. As a preliminary approach, no spatial distribution of these properties was applied, i.e. the same behavior in all elements was assumed. As discussed above, the yield stress at 0.2 % could be taken as constantly equal to 150 MPa. Combining this with average UTS of 300 MPa and an elongation of 4 %, the stress strain curve shown in Figure 2 right was generated.

Note that the values of the Young's modulus and virgin yield stress correspond to the values at room temperature shown in Figure 2 left.

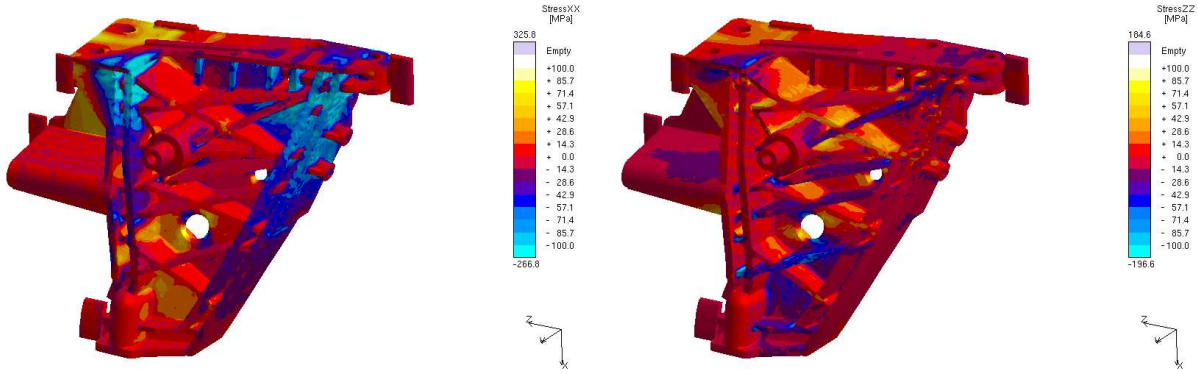

Figure 10 Left: Normal stress in vertical direction as a result of the crash load. Right: Normal stress in horizontal direction as a result of the crash load.

The results of subjecting the as-cast part to the crash load are presented in Figures 10 and 11. The normal stress in vertical direction in Figure 10 (left) shows the expected tensile stress in the most upper left corner and the corresponding compressive stresses in the uppermost right corner. This corresponds to the reactive force moment making equilibrium with the crash load. Note the localized compressive zone in the uppermost part of the outer stiffening flanges in the left part of the casting. These stresses are a result of the load attacking the structure a little eccentric to the right as seen from the load (seen from the left of the casting in the figure). This results in an out-of-plane bending force moment.

Figure 10 (right) shows the horizontal normal stress component. First of all, the boundary condition of a prescribed normal stress of -11 MPa is recognized at the left part of the casting.

Moreover, the mission of the crisscross-wise inclined stiffeners in the middle of the casting acting by and large as bars in alternating tension and compression is noticed.

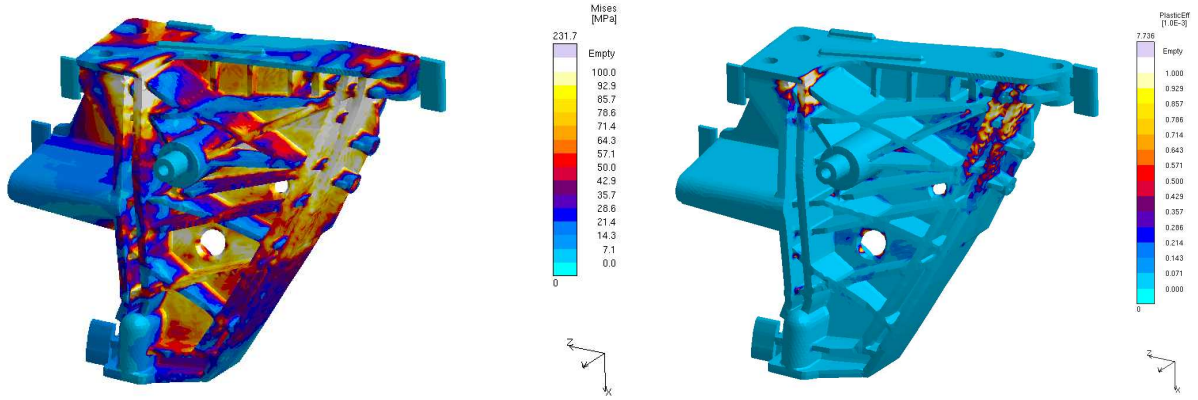

Figure 11 Left: Mises stress as a result of the crash load. Right: Effective plastic strain as a result of the crash load.

In Figure 11 (left) the Mises stress field from the load situation is depicted. Both the distribution and the level of the Mises stress are coherent with the two normal stress components shown in Figure 10. It is interesting to compare the load induced Mises stress with the casting induced Mises stress field shown in Figure 5 (left). First of all, it is obvious that the casting Mises stresses are lower, however, not negligible. Secondly the distribution is somewhat different which is no surprise since the two fields are originating from substantially different "loads", i.e. i) a thermal contraction at high temperature in a mould presenting constraints and ii) a prescribed compressive stress at room temperature with the part constrained at the upper plane surface where it is mounted. Moreover, in Figure 11 (right) it is noticed that the effective plastic strain due to the loading is very low in most of the part and reaches its maximum in localized areas which coincide with the values of the high Mises stress. This is of course to be expected.

CONCLUSION

As mentioned earlier, development of cast components without considering all of the parameters and properties that the component directly inherits from the production process very often leads to incorrect and misleading results and predictions of the in-service behavior of the cast components. Thus, the present work could be considered a preliminary attempt to do an integrated analysis of the casting process and the subsequent loading situation for a complex aluminium casting. This comprises simulation of the entire casting process with focus on microstructure formation related to local mechanical

properties such as elastic modulus, yield stress, ultimate strength and elongation as well as residual stresses. Subsequently, the casting is subject to service loads and the results show the relation between the predicted local properties as well as the residual stresses originating from the casting simulation.

ACKNOWLEDGEMENT

The authors would equally like to thank Swedish Governmental Agency for Innovation Systems (VINNOVA) for financially supporting the project VIKTOR, Product development for cast components and to Scania CV AB for supplying the component as well as Technical University of Denmark for all necessary financial support.

REFERENCES

[1] D.R. Gunasegaram, B.R. Finnin and F.B. Polivka, " *Melt flow velocity in high pressure die casting: its effect on microstructure and mechanical properties in an Al-Si alloy*", Materials Science and Technology, Vol. 23, No. 7, pp. 847-856, 2007

[2] R. Zamora et. al, "*Experimental Investigation of Porosity Formation During the Slow Injection Phase in High-Pressure Die-Casting Processes*", Journal of Manufacturing Science and Engineering, Vol. 130, October 2008

[3] J. Campbell,.: *Castings*. Second Edition. Elsevier Butterworth-Heinemann, 2003, ISBN 0 7506 4790 6

[4] Y. Yan et. al., *„Effects of Casting Process Parameters on Porosity and Mechanical Properties of High Pressure Die Cast ADC12Z Alloy*", Shape Casting: The 2nd International Symposium, Orlando, Florida, USA, 2007

[5] P. Kotas, " *Numerical Optimization of Die filling and of High-Pressure Die Cast Deformation*", Master Thesis, Technical University of Denmark, Lyngby, Denmark, 2007

[6] J.H. Hattel, : *Fundamentals of Numerical Modelling of Casting Processes.* First edition. Kgs. Lyngby: Polyteknisk Forlag, 2005, , ISBN 87-502-0969-8.

[7] J.H. Hattel, J. Thorborg, K.V. Dahl and J. Hald, *„ Integrated Modelling of Manufacturing Processes and Service Conditions*", Proc. 8th Int. Seminar on ‚Numerical analysis of weldability', Seggau, Graz, Austria, September 2006, (Keynote)

[8] J.H. Hattel, *„ Integrated Modelling in Materials and Process Technology-Review*", Materials Science Technology, Vol. 24, No. 2, pp.137-148, 2008

[9] MAGMAsoft simulation software, MAGMA GmbH, Aachen, Germany

[10] S. Seifeddine, T. Sjögren, I.L. Svensson, "*Variations in Microstructure and Mechanical Properties of Cast Aluminium EN AC 43100 Alloy",* the Journal of Metallurgical Science & Technology, Vol. 25, No. 1, pp. 12-22, 2007

[11] S. Seifeddine and I.L. Svensson, "*The effect of cooling conditions and variation of alloying elements on the microstructural and mechanical properties of Al-7%Si cast alloys",* Journal of International Foundry Research, Vol. 58, No.1, 2006.

[12] J. Thorborg, J.H. Hattel and A. Bellini, "*Thermomechanical conditions in heat treated aluminium cast parts*", Proc. Int. Conf. On *Modelling of Casting, Welding and Advanced Solidification Processes, MCWASP* XI, May 2006, Sophia Antipolis, France, 193-200, (2006)

[13] A. Bellini, J.H. Hattel and J. Thorborg, "*Thermo-mechanical modelling of aluminium cast parts during solution treatment*", Modelling and Simulation in Materials Science and Engineering Vol. 14**,** No. 4, pp. 677-688, 2006

[14] E.A. Herman, : *Die casting dies: Designing*, Society of Die Casting Engineers Inc., 1979

[15] E.A. Herman,: *Gating Die Casting Dies*, North American Die Casting Association, Rosemont, Illinois, USA, 1995

[16] J. Campbell, : *Castings Practive, The ten rules of castings*, Elsevier Butterworth-Heinemann, 2004, ISBN 07506 4791 4

[17] Ing. Petr Vrábel, AXIOM Tech, s.r.o., personal communication

[18] S. Seifeddine.: *„On the Microstructure Formation and Mechanical Properties of Aluminium-Silicon Cast Alloys"* Ph.D Thesis, Jönköping University, Jönköping, 2006, ISBN 91 85643 42 4

[19] P. Beeley, : *Foundry Technology*. Second Edition. Butterworth – Heinemann, 2001, ISBN 0 7506 4567 9

[20] K. Fisher, : *Fundamentals of Solidification*. Trans Tech Publications LTD, 1986, ISBN 0 87849 522 3

[21] M.C. Flemmings, : *Solidification Processing.* McGraw-Hill, Inc., 1974, ISBN 0 07 021283-x

[22] B.A. Boley, J.H.Weiner, : *Theory of Thermal Stresses*. Dover Publication, Inc., 1997, ISBN 0 486 69579 4

B PAPER – II

Kotas, P., Tutum, C.C., Snajdrova, O., Thorborg, J., Hattel, J.H., "*A Casting Yield Optimization Case Study: Forging Ram*", International Journal of MetalCasting, Vol. 4, Issue 4, (2010).

A CASTING YIELD OPTIMIZATION CASE STUDY: FORGING RAM

P. Kotas, C. Tutum and J. Hattel
Technical University of Denmark, Lyngby, Denmark

O. Šnajdrová
Vitkovice Heavy Machinery A.S., Ostrava, Czech Republic

J. Thorborg
Technical University of Denmark, Lyngby, Denmark
MAGMA GmbH, Aachen, Germany

Abstract

This work summarizes the findings of multi-objective optimization of a gravity sand-cast steel part for which an increase of casting yield via riser optimization was considered. This was accomplished by coupling a casting simulation software package with an optimization module. The benefits of this approach, recently adopted in the foundry industry worldwide and based on fully automated computer optimization, were demonstrated. First, analyses of filling and solidification of the original casting design were conducted in the standard simulation environment to determine potential flaws and inadequacies. Based on the initial assessment, the gating system was redesigned and the chills rearranged to improve the solidification pattern. After these two cases were evaluated, the adequate optimization targets and constraints were defined. One multi-objective optimization case with conflicting objectives was considered in which minimization of the riser volume together with minimization of shrinkage porosity and limitation of centerline porosity were performed.

Keywords: *casting process simulation, genetic algorithms, riser volume optimization, casting yield, steel casting, centerline porosity, macro-porosity*

Introduction

Today, there is a general trend to reduce production costs as much as possible in order to stay competitive and attractive for potential and current customers. Production is no longer governed only by experience-based innovation or trial-and-error method. In this context, virtual prototyping and testing by numerical simulation offers an efficient way of reducing product development time, reducing costs of producing prototypes, shortening lead time and, above all, eliminating scrap.

Metalcasting process simulation is used to provide detailed information about mold filling, solidification and solid state cooling, as well as, information about the local microstructure, non-uniform distribution of mechanical properties and subsequently residual stress and distortion build-up.[1-9] Casting simulation tries to use physically realistic models without overtaxing the computer. At the same time the simulations need to give applicable results in the shortest time possible. Unfortunately, numerical simulations can only test one "state", while conclusions from calculations or subsequent optimization still require an engineer's interpretation and decision after each of the simulation runs. Understanding the process enables a foundry engineer to make decisions that can affect both the part and the rigging to improve the final quality.

The objectives which drive designers are generally well defined: improve the component quality, achieve homogeneous mechanical characteristics, maximize the casting yield, increase the production rates, etc. It may sound easy, but the truth is that in reality it is very complex and time consuming to achieve all these objectives at the same time, due to the high number of variables involved. In many foundries, the only applied optimization is still based on experience and thus on the trial-and-error method. When using numerical simulation, only a virtual casting is spoiled, in the case of an error. No raw material is wasted, no mould is produced and, above all, no production loss is experienced.

Recently, rapid development of high performance computing has substantially shortened the calculation time needed for one variant of the casting process to be analyzed. It is feasible to calculate numerous versions and layouts in almost unlimited configurations over night. The advantage

of having such short calculation times can only be utilized with a computer that can automatically analyze calculated variants with respect to the predefined objectives (e.g. maximum feeding, low porosity, low air entrapment etc.) and subsequently create new variants and analyze them in the same manner to achieve the optimal solution. By integrating such software for casting process simulation with an optimization algorithm (in this case the Multi-Objective Genetic Algorithm, [MOGA][10] which should not be confused with the non-elitist MOGA developed by Fonseca and Fleming),[11] a computer-based optimization tool is established which is able to determine optimal values of user-defined design variables, thereby optimizing a given casting process with respect to defined objectives. Subsequently, such a system can readily provide optimal solutions for any kind of casting process.[12-14]

This paper details multi-objective optimization of filling and solidification patterns, together with the riser volume of a steel forging ram cast into a furan sand mould, and presents the results obtained from the study. Numerical multi-objective optimization is carried out by coupling the general-purpose casting simulation software package MAGMASOFT® with the add-on optimization module MAGMA*frontier*.

This study includes five different layouts. The initial layout is obtained from a foundry that manufactures the forging ram. The second layout with manually rearranged gating system and chills is also provided by the foundry. Three layouts are generated by numerical optimization. The first two designs are analyzed both in terms of filling and solidification, and the results are compared with the experimental casting trials. No computerized optimization is involved. The three optimized designs are assessed only in terms of solidification since the filling pattern remains unchanged; however the temperature fields at the beginning of the solidification are inherited from the filling stage. Conclusions and proposals are made from the various investigations and findings in the study and presented in the last section of the paper.

Coupling of Simulation and Optimization Tools

Before the optimization process can be started, a standard project must be defined in the simulation software environment. This includes a definition of geometry in the pre-processor. Furthermore, a suitable mesh must be generated and all relevant process parameters adequately defined. The optimization itself is based on performing a large sequence of "standard" calculations, each with different design variants. Therefore all design variables must be defined in a parametric way.

In essence, any constrained optimization method is based on the following scheme: a user formulates the problem in a mathematical way by means of several parameters:[15]

- **Input (design) variables** together with allowed ranges of variation. Design variables (initial temperatures, riser dimensions, alloy composition, process parameters, etc.) are modified by the optimization algorithm in order to meet the given objectives.
- **Output variables** usually represent values calculated in a standard casting simulation. The optimization objectives are usually formulated by using the output variables (e.g. when the porosities and the volumes of the feeders in one design need to be assessed for a feeder optimization).
- **Constraints** are conditions for designs. They limit the design space or the range of solutions. If a design does not satisfy these constraints, it is considered unacceptable.
- **Objective functions –** These are the aims and targets that are the goal to achieve by means of optimization. They maximize or minimize certain combinations of output variables, e.g. min (volume of a riser) or min (max. porosity).

When all this information is available an optimization loop can be started.

Optimization Methodology

In the next few sections, a multi-objective optimization problem in the gravity sand casting process of a forging ram is presented. The objectives for this case study are the following: minimize the top riser volume, minimize shrinkage porosity, and limit centerline porosity, by means of an optimized arrangement of the chills.

The actual optimization cycle is initiated by establishing a first generation, i.e. a set of solutions, containing a user-defined amount of individual variables referred to as the initial population or Design of Experiments (DOE) in the applied software package. Each individual represents one design for the considered design variables, e.g. dimensions of the riser and the chills. For each of these designs a thermal (solidification) analysis is started, and the values for the requested output variables are calculated. The filling analysis is not performed during optimization since the gating system is kept the same as in the previous side-filled case. The output data is used to compare and evaluate the different designs. After the first generation has been calculated, the optimization algorithm evaluates the designs relative to the objective function(s) and constraint(s). Afterwards, it generates a new set of solutions using mathematical mechanisms that follow the concept of genetics, i.e. selection, cross-over and mutation. This strategy is consequently referred to as a genetic algorithm.[16] From the algorithmic point of view, the procedure can be described as follows:

1. Create the initial set of designs (initial population)
2. Calculate all designs and grade their performance in terms of the objectives

3. Generate a new set of designs (new generation) by performing statistical evaluations (selection, cross-over, mutation)
4. Repeat this procedure for the user-defined number of generations

The optimization cycle terminates when the stopping criterion, i.e. the total number of generations, is reached. The flow chart of the above described optimization procedure is depicted in Figure 1.

Multi Objective Optimization Problem (MOOP)

Most engineering design activities require a solution of multi-objective and multi-disciplinary optimization problems that in many cases deal with conflicting objectives. When considering these objectives, a number of alternative trade-off solutions, referred to as Pareto-optimal solutions, have to be evaluated. None of these Pareto designs can be said to be better than the other without any additional information about the problem under consideration. In order to define the Pareto set, one has to apply the concept of domination, which allows comparing solutions with multiple objectives. Most multi-objective optimization algorithms use the domination concept to search for non-dominated solutions, i.e. the ones that constitute the Pareto-optimal set,[18] which is schematically shown in Figure 2. Since the Pareto set includes numerous designs, from an engineering viewpoint it is more practical to select only a few or even one solution among them. The selection of the "most optimal" design depends on the user's preference of importance of the different design criteria (e.g. porosity-free casting is more important than having the highest casting yield).

Genetic algorithms work with a set of solutions (population) instead of a single point, as in gradient based (classical) methods. This gives an opportunity to attack a complex problem (discontinuous, noisy, multi-modal, etc.) in different directions, allowing the algorithm to explore as well as exploit the search space. This capability gives a more robust search strategy compared to traditional algorithms. Since genetic algorithms do not need any gradient information, they are suitable for black-box (e.g. commercial software) optimization applications. Moreover, compared with classical optimization strategies based on gradient methods, genetic algorithms can effectively utilize distributed computing facilities because all individuals (designs) can be computed independently. Besides that, they are typically able to provide a larger spectrum of Pareto-optimal designs without requiring additional problem definition. The availability of trade-off solutions, representing varying preference levels between chosen objectives, makes it easier for a user to choose a particular solution for subsequent implementation.[17-20]

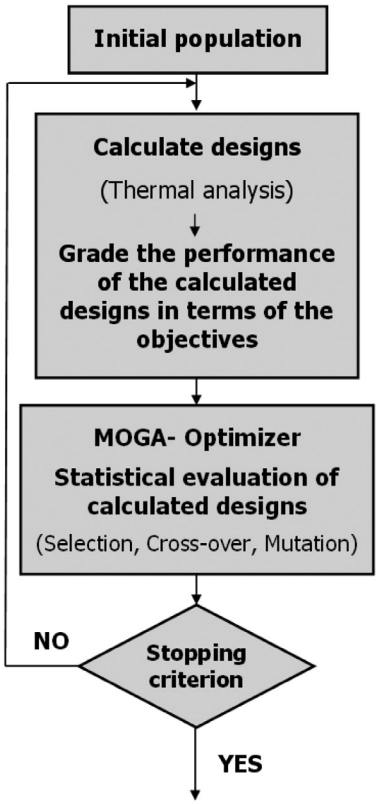

Figure 1. Flow chart of the optimization process.

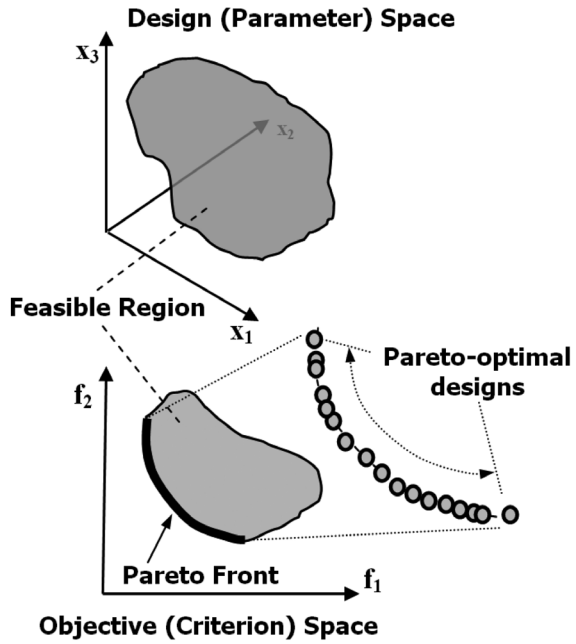

Figure 2. Design and objective space related to a multi-objective optimization problem, taken from reference.[17]

The following case study shows that the previously described concept of a Multi-Objective Optimization Problem (MOOP) is applicable and reliable for a variety of casting related issues.

Case Study Description 1—Original Casting Arrangement

The project involved a steel forging ram manufactured by a gravity sand casting process shown in Figure 3. Based on the thermal analysis of the part itself, a riser was designed and placed on top of the heaviest section. In order to enhance the feeding ability of the riser, insulation was applied (Figure 4). The main cylindrical padding is insulating, the melt surface is covered by an exothermic powder, and on top of that additional insulating powder is applied. Next, it was determined that the part be bottom-filled using a gating system comprised of the refractory tiles. The cross-section area of the tiles is constant over the entire gating system. Last, the chills were added around the cylindrical section of the casting to establish directional solidification and to push the macrosegregation-related flaws from the surface to further inside the casting.

The original casting layout was simulated using the casting conditions and parameters listed in Table 1. Both filling and solidification analyses were conducted. A stress analysis was not considered in any of the presented cases.

Heat Transfer Coefficients (HTC) at the casting/mould interface, are assumed to be temperature independent. This assumption holds only in the case of gravity sand casting. The reasoning is that in sand casting the contact between the melt and the mould is poor from the beginning due to the rough surface of the mould. As a result, there is a high resistance to heat removal, resulting in low interface HTCs. When the casting shrinks during solidification and solid state cooling, an air gap is formed in the casting/mould interface, inducing even more resistance to the heat removal. Nevertheless, since the heat transfer has been poor from the beginning, the decrease in HTC due to volumetric changes is not that significant to the results, and the HTC can be assumed more or less constant (low) over the entire casting process. Moreover, it is not primarily the interface that induces the largest resistance to heat transfer, but rather the large sand mould and its poor thermal properties that really govern the heat removal. Thus, the HTC between the casting and the sand mould was set to be 800 W/m^{2}K.

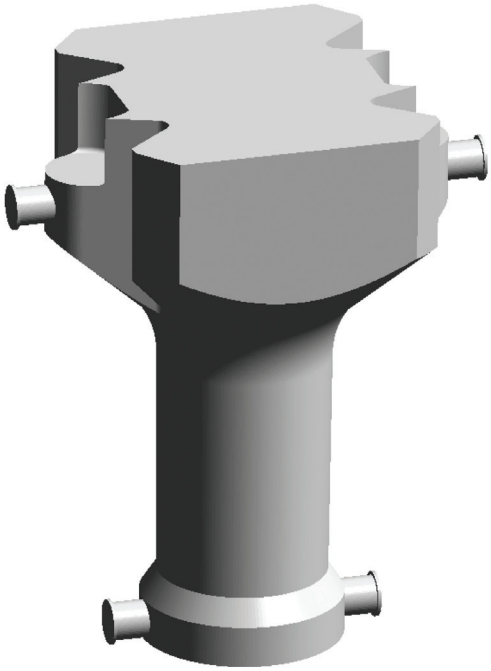

Figure 3. 3-D view of the cast part used in the project (Courtesy of Vitkovice Heavy Machinery, a.s.).

Case Study Description 2—Manually Modified Casting Arrangement

Next, the new casting arrangement with manually redesigned gating systems and rearranged chills were developed. The shape of the forging ram (Figure 5) was somewhat different compared to the initial one in Figure 3, due to the fact that the second layout was manufactured for a

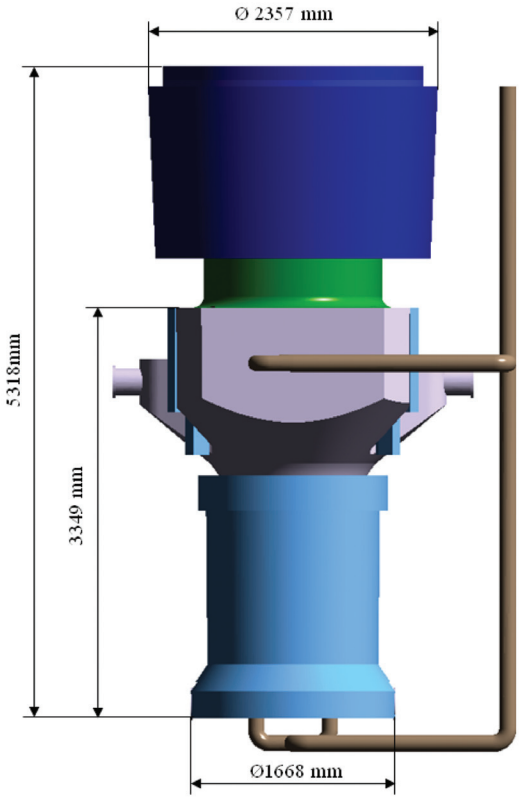

Figure 4. Initial casting layout. The riser is indicated by green, chills indicated by light blue, and insulation is denoted by dark blue (Courtesy of Vitkovice Heavy Machinery, a.s.).

different customer who requested these geometrical adjustments, i.e. a larger diameter of the cylindrical section and geometrical adjustments in the ram's head. The aim was to investigate the effects of a cooling plate located underneath the casting. In order to place the plate, the gating system had to be changed from bottom filling to side filling. New vertical runners were added to support filling in higher sections of the casting and the chills were rearranged. In order to ensure sufficient cooling of the very bottom, thicker chills were added around the conical bottom section of the casting. New chills were incorporated into the top head section of the casting. The changes are seen in Figures 5 and 11. Besides the mentioned geometrical changes, all casting and simulation parameters are the same as in the first casting arrangement.

Case Study Description 3— Optimization of the Riser and Chills

After inserting all datasets and parameters into the standard simulation environment, the manually refined casting layout in Figure 5 was assessed to create a reference solution to compare with the optimization results. It had been decided to try to reduce the size of the top riser as much as possible to increase the casting yield, providing that there were no defects occurring in the casting due to the riser's reduced size. When the riser and the chills were transformed into parametric objects, the optimization process was initiated. The design variables (those which are subjected to optimization) are dimensions of the chills, height and thickness of the bottom cylindrical chills, and of the top riser, height, bottom and top diameters, and top diameter of the riser neck, see Table 2.

The main optimization objectives are to design the top riser so the casting is sound (i.e. with minimum shrinkage and centerline porosity) and at the same time the top riser's volume is as small as possible to increase the casting yield. In this context, 'casting yield' is defined as the gross weight including the riser and the gating system divided by the weight of the fettled casting. In terms of the MOOP, we deal with minimization of two conflicting objectives (min. porosity in the casting body vs. min. riser volume).

Table 1. Material Settings in MAGMAsoft®

Material of the casting	GS20Mn5 (DIN 1.1120)
Material of the mould	Furan Sand
Material of chills	Common steel
Material of the insulating padding	IN5
Material of the exothermic powder	Ferrux
Material of the insulating powder	Vermikulit
Initial (pouring) temperature of the casting	1540 °C (2804 F)
Initial temperature of the mould	20 °C (68 F)
Filling time	120 s
Feeding effectivity of the applied steel alloy	40%
Sand permeability	Activated-value taken from a standard database
Weight of the casting- incl. risers and gating system	59596 kg (131111.2 lbs)
Weight of the casting itself (fettled)	29898 kg (65775.6 lbs)

Table 2. Design Variables for Optimization

Design Variable	**Lower Limit**	**Upper Limit**	**Step**
Cylindrical Chill -Height	549 mm	1149 mm	50 mm
Cylindrical Chill -Thickness	100 mm	200 mm	10 mm
Riserneck -Top Diameter	1200 mm	1300 mm	10 mm
Riser - Bottom Diameter	1260 mm	1660 mm	20 mm
Riser - Top Diameter	(1260* 1.06) mm	(1660* 1.06) mm	20 mm
Riser - Height	500 mm	1350 mm	50 mm

In many engineering cases, more than two optimization targets are addressed. However, it is more complex or unfeasible to graphically visualize and reasonably evaluate more than two objectives. The only way for the optimization algorithms to take the other optimization targets into consideration without prescribing them as objectives is to express them by means of optimization constraints. Of course, one should then expect the presence of unfeasible designs that do not comply with the prescribed constraints. Our optimization problem is constrained only by the predefined ranges of variation of the design variables (Table 2).

Based on the number of design variables and their ranges of variation, the optimizer generates the total number of feasible combinations (the initial DOE sequence) by a DOE sequence technique referred to as Full Factorial Design. Obviously, it would be very time-demanding to calculate all possible designs, thus the initial population is provided by the Sobol DOE sequence generating technique,[21] which is a quasi-random sequence. The points in this type of sequence are maximally avoiding each other, so the initial population fills the design space in a uniform manner. The optimization run has been executed using the following parameters:

Initial Population: Sobol Sequence
Population Size: 100
Number of Generations: 10
Probability of Directional Cross-Over: 60%
Probability of Selection: 30%
Probability of Mutation: 10%
Elitism: Enabled
Treat Constraints: Penalizing Objectives
Algorithm Type: MOGA Steady

The last task is to assess how the optimized riser influences the formation of the centerline porosity, represented by the Niyama criterion[22- 24] in the simulation software environment. The minimization of the centerline porosity is neither prescribed as an objective nor a constraint in the optimizer. The optimization results are simply analyzed with respect to the Niyama criterion in order to select the "most" optimal solution on the Pareto line.

The Niyama criterion is a local thermal parameter defined as the relationship between the gradient (G) in K/mm and the cooling rate (R) in K/s, both of which are assessed at a specified temperature near the end of solidification, when the solidification shrinkage forms (Equation 1). In the present study, the Niyama criterion is evaluated at a temperature 10% of the solidification range above the solidus temperature. This is important to state, since the choice of Niyama evaluation temperature can remarkably affect the resulting Niyama values.[25]

$$Niyama = \frac{G}{\sqrt{R}} \qquad \text{Equation 1}$$

With the help of the Niyama criterion, it is feasible to predict the presence of centerline shrinkage porosity, i.e. micro- and macro-shrinkage in steels caused by shallow temperature gradients.[26, 27] It indicates that in regions that solidify quickly, there must be hot metal nearby to establish a high gradient to feed the shrinkage during solidification.

It has been proven by numerous trials that for sufficiently large Niyama values, no shrinkage porosity forms. When the Niyama value decreases below a critical value, small amounts of micro-shrinkage begin to form. As the Niyama value decreases further, the amount of micro-shrinkage increases until it becomes detectable on a standard radiograph. This transition occurs at a second critical value. Both of these threshold values depend on the composition of the alloy and, in some cases, on the casting process conditions.

Based on a literature search and results obtained from the manufacturing foundry, it is determined that the critical Niyama value for macro-porosity for this particular steel alloy is Ny_{macro}= 0.45 $(K \cdot s)^{1/2}$/mm. Everything above this value is assumed to be micro-shrinkage that will not be detected via common radiography. The second threshold value for micro-porosity, above which the material is completely sound, is set to be Ny_{micro}= 1 $(K \cdot s)^{1/2}$/mm. It should be emphasized that the Niyama criterion only predicts feeding-distance related shrinkage; it does not explicitly predict hot spots in a casting, and it does not predict gas porosity.[22]

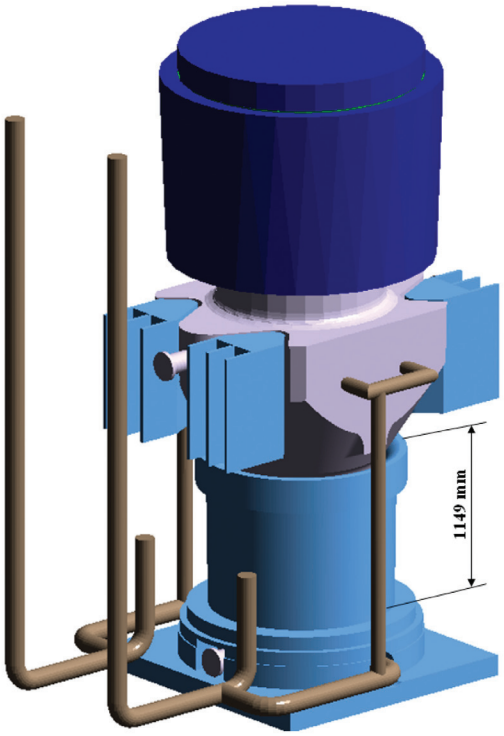

Figure 5. Manually optimized casting design (the result of the case study 2).

Results and Discussion

In the three following sections, results obtained from the simulations and casting trials are presented and discussed. First, the numerical and experimental results from the original casting assembly are analyzed to establish a base case. Then, the numerical results of the mould filling and solidification processes based on the reworked chills and gating system are listed. In the last section, the results from the multi-objective optimization problem (riser volume and chill size optimization) are presented. At the end a comparison of the casting yield of the original and optimized designs is carried out.

Simulation and Casting Trial Results—Original Layout

The original casting arrangement, Figure 4, was simulated both with respect to filling and solidification using the casting conditions listed in Table 1. The filling analysis is supposed to indicate whether the current gating system will provide uniform filling without any melt aspiration in the downsprue or surface turbulence that would likely lead to excessive oxidation of the propagating melt, causing various filling-related defects, e.g. reoxidation inclusions, entrapped air pockets, etc.[28] The primary source of oxygen in reoxidation inclusion formation is air, which contacts the metal stream during pouring as well as the metal free surface in the mold cavity during filling. The oxide mixture that forms during pouring of carbon and low-alloy steel is partially liquid,[29] as opposed to the solid oxide films or particles that form during casting of high-alloy steel or light metals. Figure 6 captures three different stages of the filling process.

It can be seen in Figure 6(a) that due to a constant cross-section area over the entire downsprue, the melt starts to spire from the mould walls and becomes oxidized. This phenomenon can be explained by the continuity equation. The melt experiences a free fall from the nozzle of the pouring ladle down to the bottom of the gating system. During the free fall, it accelerates due to the effect of gravity and changes its area (the area decreases with the increasing velocity). In order to compensate for the area reduction resulting in the aspiration from the mould walls, one has to decrease the area of the downsprue accordingly. The nearly ideal solution would be an application of a stream-lined gating system.[30] However, for such a large cast part, this solution is unfeasible. The stream-lined gating system is used mainly in gravity die casting. Another option would be the use of "choke" conical elements at several locations in the downsprue.

Figure 6(b) shows that due to no velocity control during the early stage of the filling process, the melt reaches the mould cavity with a high velocity (approx. 5m/s). A very rapid entrance naturally leads to a formation of fountains (1.47 m high) inside the mould cavity. When the melt starts to fall down again, it splashes, becoming highly turbulent and disintegrated. In most of the bottom-filled casting assemblies it is a difficult task to fully avoid this formation. Nevertheless, it should always be the primary objective of a designer to design such a gating system with all necessary attributes to keep this phenomenon at a minimum.

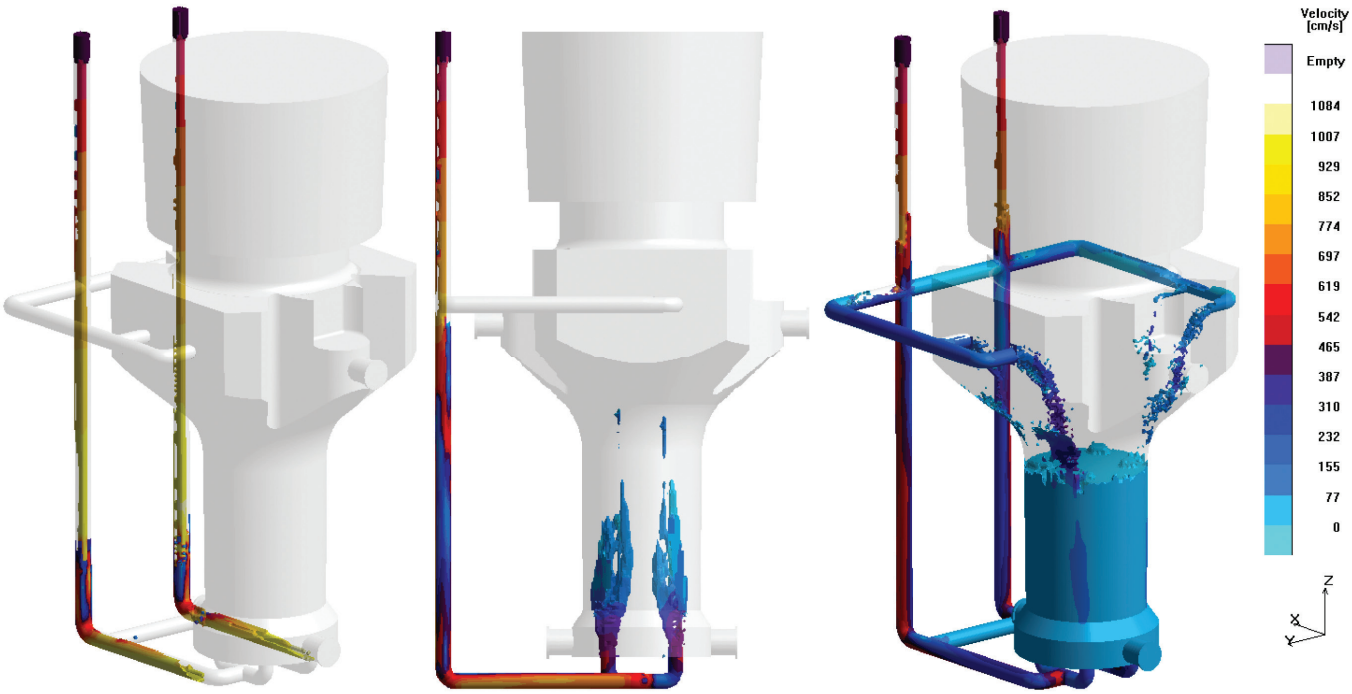

(a) 1% filled *(b) 2.5% filled* *(c) 16% filled*

Figure 6. Three different stages of the filling process of the bottom-filled forging ram.

Figure 6(c) indicates the melt falling down from the two top runners on top of the melt front progressing from the bottom of the mould cavity. This is again a feature that should be kept at a minimum during filling for the same reason as the fountains, i.e. oxidation. Moreover, an oxide layer is already present on top of the melt front coming from the bottom, which likely gets torn apart by the melt streams, and establishes surface turbulence and disintegration of the melt front. The thermal analysis during solidification evaluates the effect of the top riser and the cooling effect of the chills placed around the cylindrical section of the cast part.

In Figure 7 one can see that during the solidification process, particularly at 42% solidified, there are indications of isolated liquid pools in the lower section of the casting. This fact raises a probability of porosity formation due to a lack of liquid feeding. The chills cool the cylindrical section too rapidly, compared to the very bottom area in which the cooling rate is lower due to the enlarged cross-section, thus creating a hot spot. A potential remedy might be either to increase the thickness of the chills towards the bottom area or to redesign the gating system so that there is a chance to add a chill plate underneath the casting bottom. This would significantly promote cooling of the bottom of the casting and directional solidification towards the riser. This will be addressed in the following section.

A direct consequence of having both isolated liquid pools (Figure 7) and very flat temperature gradients (Figure 8) in the casting domain is the presence of a shrink (porous area). Areas solidifying early always "suck out" the liquid melt from areas solidifying last to compensate for the volumetric changes evoked by the solidification process. As long as there is an open and active feeding path to these areas, no problem occurs. However, when the liquid melt supply is cut off and drained, areas solidifying last will be short of melt, so when the time comes for them to solidify, no compensation for the volumetric shrinkage will be available, giving rise to porosity. This issue is addressed by means of the Niyama criterion function in Figure 9.

Figure 9 shows the numerically predicted presence of centerline porosity in the lower areas together with results obtained from the casting trials (by the radiographic technique). It is seen that the porous areas occured in the casting where the isolated pools of liquid were once present. Looking at the dimensions of the defect area, one can see a very good agreement between the two types of results (numerical- red [right] *vs.* experimental- black [left]). The close correlation also justifies the use of the Niyama threshold value of 0.45 for this particular steel alloy. However, it should be emphasised that the geometrical extension of the shrinkage obtained numerically, to some extent is approximate due to its dependency on the mesh quality.

Figure 10 shows the results obtained from the casting trials. The cast part was cut into several sections, and the po-

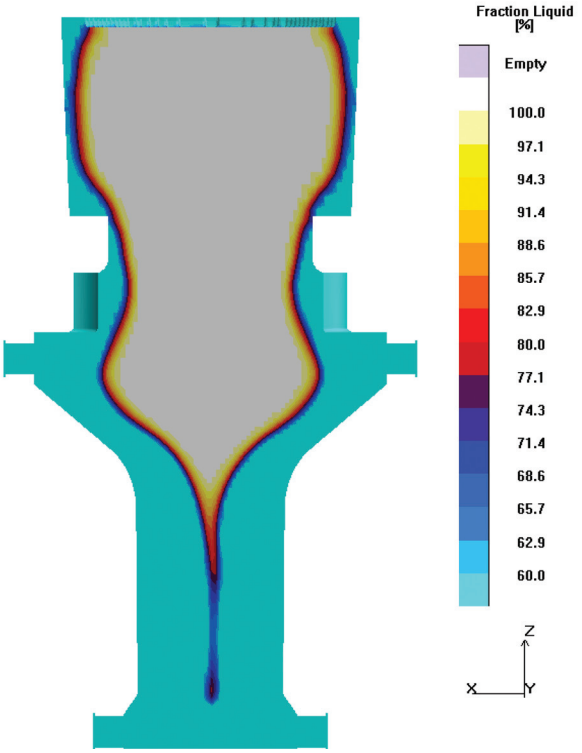

Figure 7. Fraction liquid criterion function indicating an isolated liquid pool in the bottom section of the cast part at 42% solidified.

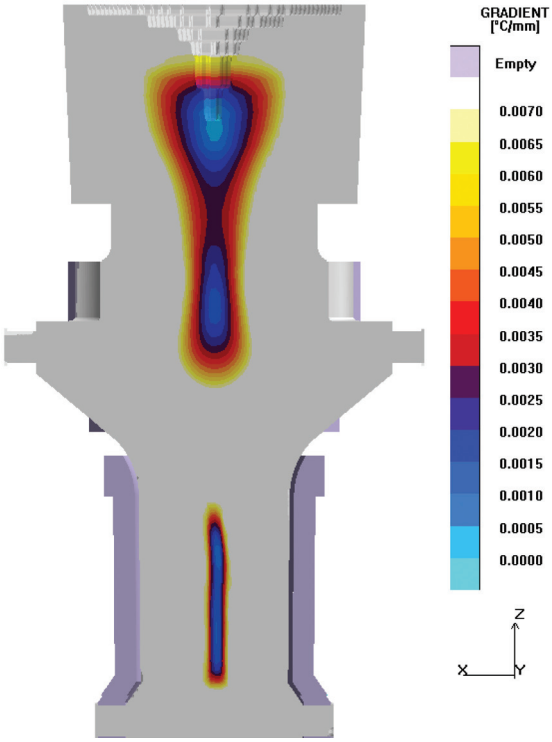

Figure 8. Gradient criterion function depicting a very shallow gradient in various areas of the casting.

rous area (also predicted by the simulation) was detected and measured. Besides the macro-shrinkage, both V- and A-type macrosegregation bands are spotted in the casting. A general cause of the macrosegregation is relative movement or flow of segregated liquid and solid during solidification. The most common form of solid movement is the settling or floating up of small solid pieces formed early in the solidification process.

These solid pieces may be dendrite fragments that separated from an existing solid structure or equiaxed grains that nucleated in the bulk liquid. They settle or float, depending on their density relative to the liquid. The solid pieces generally have a composition different from the nominal alloy composition, and their movement to different parts of the casting thus induces macrosegregation.[31-33]

Simulation Results—Manually Refined Layout

After the initial assessment of various stages of the manufacturing process, potential drawbacks and defects were recognized. This was then verified through casting trials by creating a solid ground for subsequent improvements and optimization.

Since centerline porosity depends primarily on thermal gradients and the cooling rate, the next step was to induce steeper thermal gradients in the section surrounded by the chills and to establish a directional solidification towards the heaviest top section where the riser is placed to keep the feeding path open as long as it is necessary. This was pursued by the rearrangement of the chills and by adding a chill plate underneath the casting bottom. Due to the chill plate, the bottom filling was no longer feasible. Therefore, the gating system was somewhat redesigned, which after the first filling analysis was strongly recommended anyhow. The reason for adding the vertical extensions of the two horizontal runners is to reduce the kinetic energy of the melt. This is a very easy way to slow down the melt front. However, in many foundries worldwide it has been overlooked and not applied.

Figure 11 shows early stages of the filling process. One can argue that the new gating system really improved the filling pattern. The two vertical extension channels significantly slowed down the melt (approx. 4m/s in the runners compared to almost 10m/s in the original layout) and thus it propagates uniformly towards the thin gates. When the melt reaches the cavity it does not form fountains but creates a relatively small splash during impingement of the streams. A solution to this problem might be an application of tangentially oriented thin gates, which then help to avoid any impingement of propagating melt fronts.

However, since the shape of the downsprue remained untouched, melt aspiration is still seen at that area. This issue should really be addressed by the manufacturing foundry to eliminate oxidation of the melt in the downsprue area.

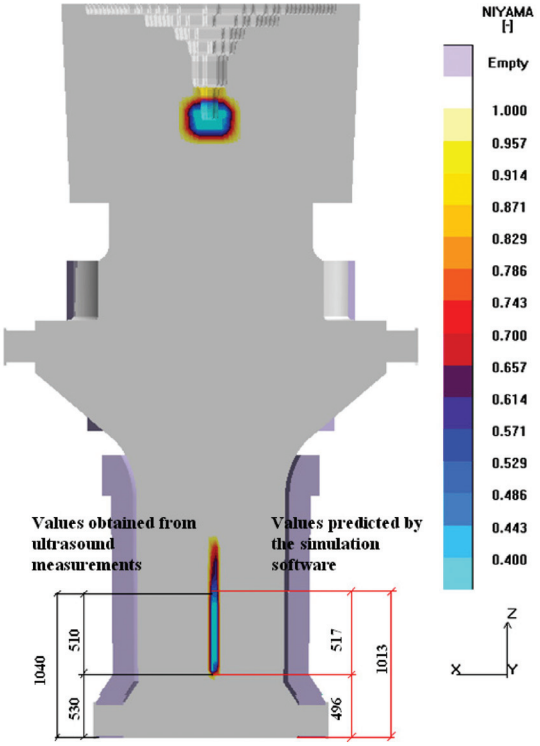

Figure 9. Prediction of the centerline macro/micro shrinkage and its experimental validation obtained from the foundry.

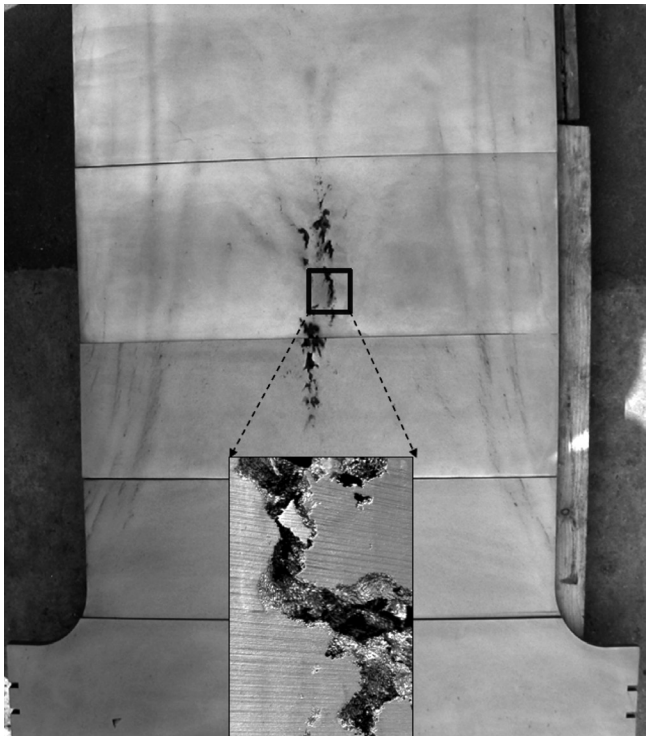

Figure 10. Results from the casting trial - presence of porous areas and bands of macrosegregation, (Courtesy of Vitkovice Heavy Machinery, a.s.).

It was expected that the new system of chills will change the solidification pattern of the casting and will have positive effects on the formation and distribution of the defects. The results are captured in Figures 12-14. In Figures 12a, b a new solidification pattern was predicted by means of the fraction liquid function at 42% and 75% solidified.

The size of the riser together with the new arrangement of the chills obviously positively affected solidification, completely avoiding the isolation of the liquid pools seen in Figure 7. Moreover, the steel plate placed below the casting evoked rapid cooling and facilitated directional solidification toward the riser. The comparison of centerline porosity indicates that the increased temperature gradients via enhanced chilling readily eliminated likelihood of its formation see Figure 13. The only two areas that might be of concern are the two bottom pins. In the original layout, no porosity was present in these areas however this is not true for the current layout. This is depicted in Figures 13 and 14. Considering that part is used for transportation purposes and the entire casting weighs around 58 tons, this porosity cannot be neglected as it corrupts the mechanical properties and weakens those areas. This issue can be eliminated by adding a sufficient draft to the pins and changing their solidification pattern. The critical value for porosity in Figure 14 has been set to 1%. Areas containing less than 1% porosity are considered "healthy" and thus they are filtered out by the X-Ray function.

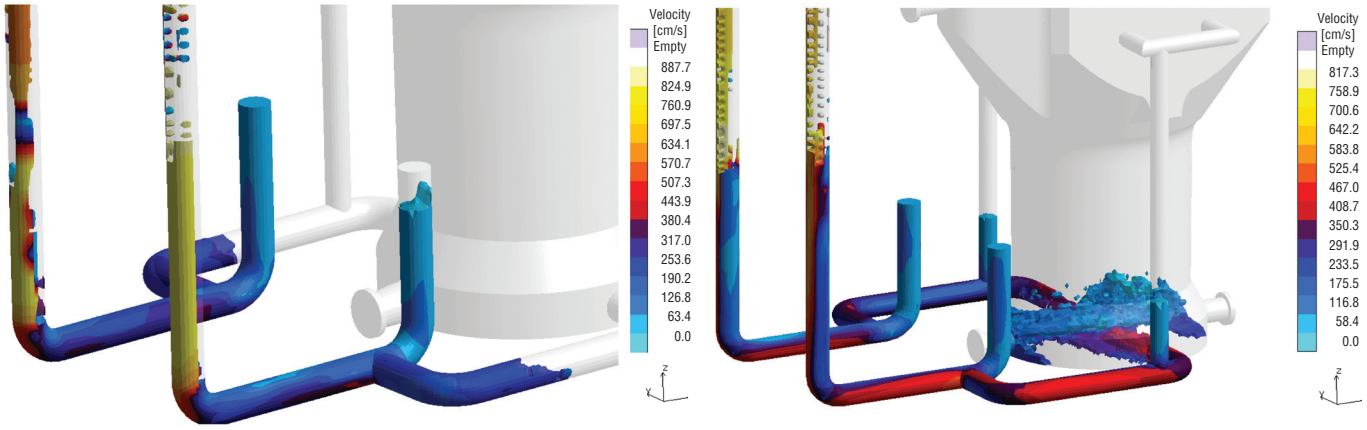

(a) (b)

Figure 11. New filling pattern due to the redesigned gating system.

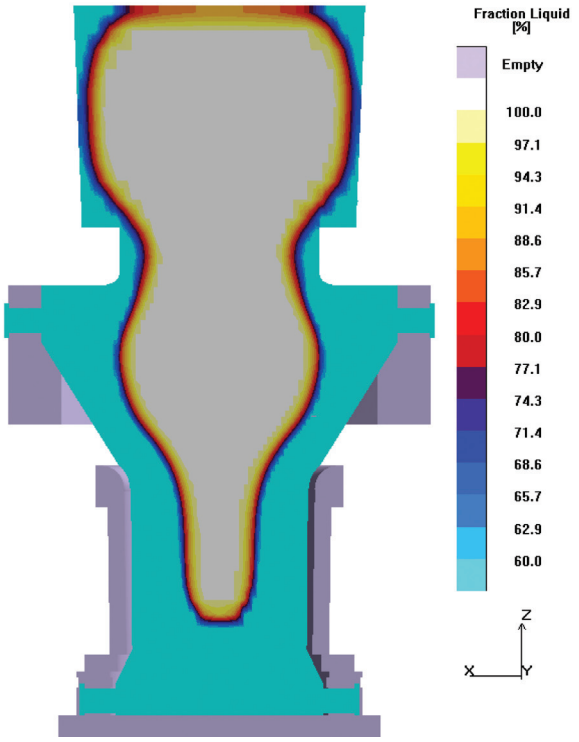

Figure 12a. Improved solidification pattern due to the reworked system of the chills- 42% solid.

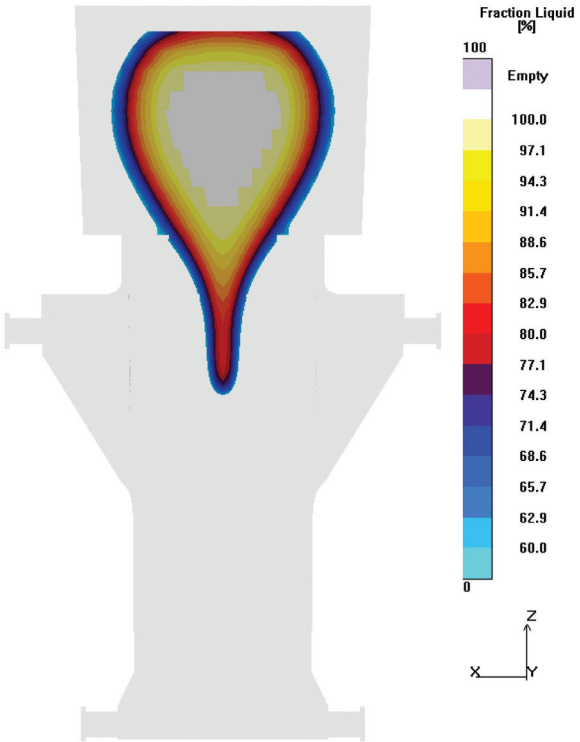

Figure 12b. Fraction liquid at 75% solidified

Simulation Results— Optimized Riser and the Chilling System

After the two preceding analyses, one might think that a reasonably good solution has been found. The gating system has been improved; the solidification pattern changed and fewer defects are present. This was also confirmed by the manufacturing foundry which is using this improved design at the present state. Thus it is a favorable state for a subsequent geometry optimization. Both of the previous designs weighed approximately 60 tons together with the riser and gating system. From Figures 13 and 14, it is seen that the major shrinkage pipe in the riser is still too far from the actual casting body to be critical. Therefore, there is room for a volume reduction to obtain an increased casting yield. From now on, only the solidification results will be discussed since the gating system remained unchanged, and thus the filling pattern did not change.

The objective space for the optimization problem in Figure 15 is constructed by the two following objectives: minimize shrinkage porosity and minimize the remaining volume of the top riser. The first objective is represented by the Weighted Volume Porosity which stands for the total volume of areas having issues with porosity. The remaining volume of the riser is then calculated as the geometrical volume of the riser minus the volume of the shrinkage pipe in the riser. Several features in that figure should be addressed. The blue line is the Pareto set which is comprised of the non-dominated solutions, but, it is up to the user to determine which solution out of the Pareto set will be the most desirable. In other words, the user has to figure whether he/she wants to minimize the riser as much as possible, at the cost of increased porosity, or to have a porosity-free casting with a slightly larger riser. In our case, three distinct designs were selected. The first one, marked 1 in Figure 15, does not lie on the Pareto set and represents the most modest solution- i.e. the largest riser volume. It should be emphasized that although it may not be clear from the figure, solution 1 is dominated by solution 2. The second one, marked 2, resembles a single optimum case, the lowest amount of porosity, and the third one, marked 3, stands for a trade-off solution, see Figure 15.

The three designs have then been analyzed in the standard simulation environment. In order to obtain realistic temperature fields during solidification, filling has also been considered in the simulation, but its results are not shown here. The reason for choosing such designs was: The primary aim has been to keep the level of porosity very low-possibly not above the value of the original design, but still increasing the casting yield. That is why the focus was put on the solutions very close to the Y-axis. Moreover, the manufacturing foundry wanted to see different layouts-from "modest" to those "on the edge" to make a better comparison and decision as to which solution to select for the subsequent production. From the optimization perspective it is given that the best solutions constitute the Pareto line, so why should we pick a design not on the Pareto line that is solution 1? Many foundries prefer a

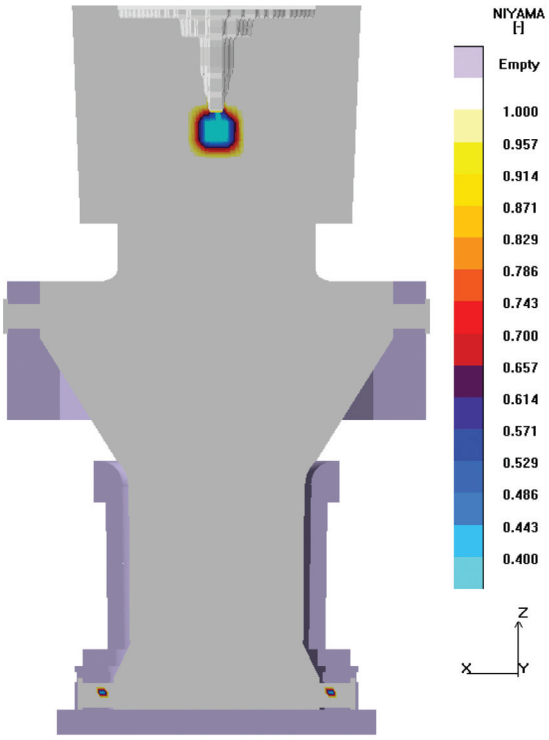

Figure 13. Prediction of centerline porosity.

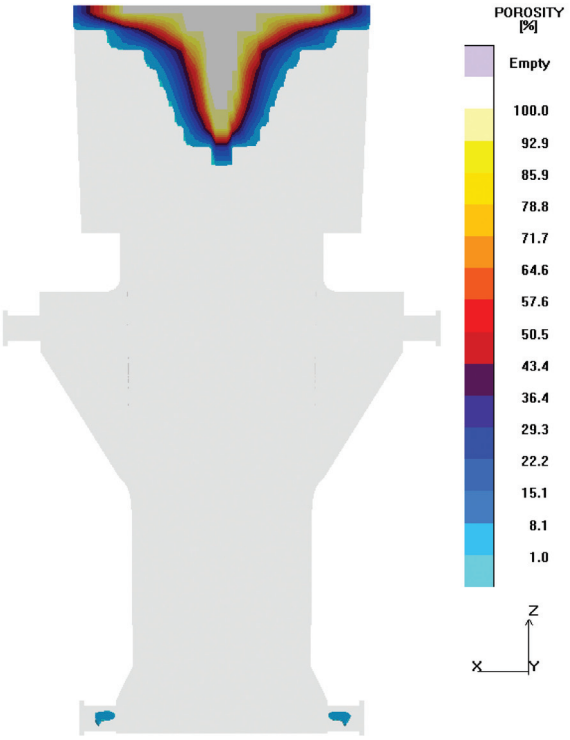

Figure 14. Distribution of macroscopic shrinkage.

very safe solution to compensate for potential flaws during production, e.g. human factors, deviations from alloy compositions, etc. Solution 1 was selected for the subsequent analysis because it has a large enough riser to keep porosity far from the casting and still has its total volume remarkably smaller than the original layout. Figure 16 depicts the three selected designs. Information regarding dimensions of the optimized designs is listed in Table 3.

Table 3. Comparison of the Three Optimized Designs

	Solution 1	Solution 2	Solution 3
Total height	4037 mm	3837 mm	3537 mm
Total weight	48406.8 kg	45850 kg	40968 kg
Height of the bottom cylindrical chills	999 mm	999 mm	1149 mm
Thickness of the bottom cylindrical chills	160 mm	160 mm	160 mm

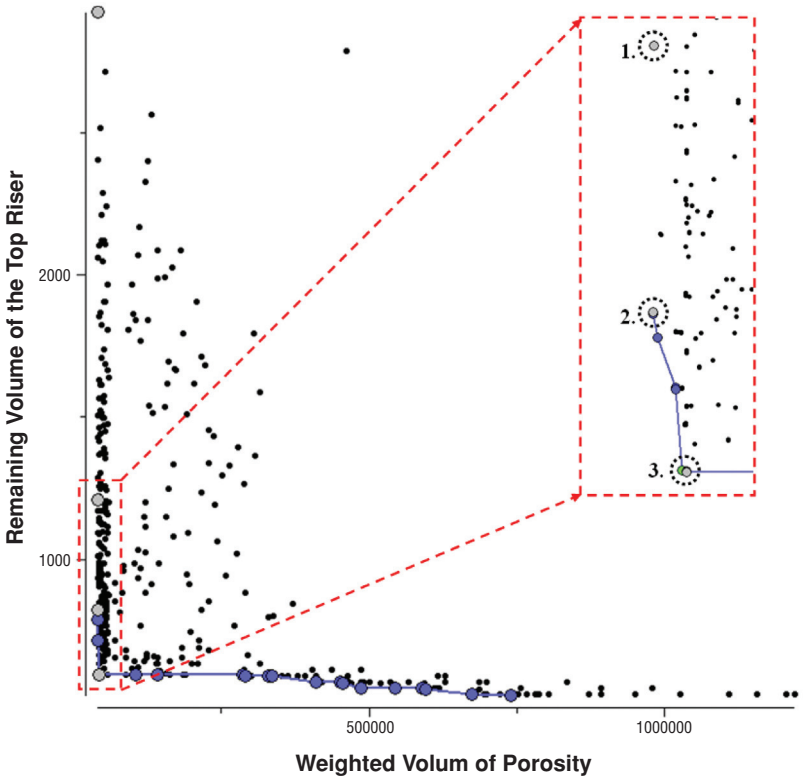

Figure 15. Design space with the highlighted Pareto set.

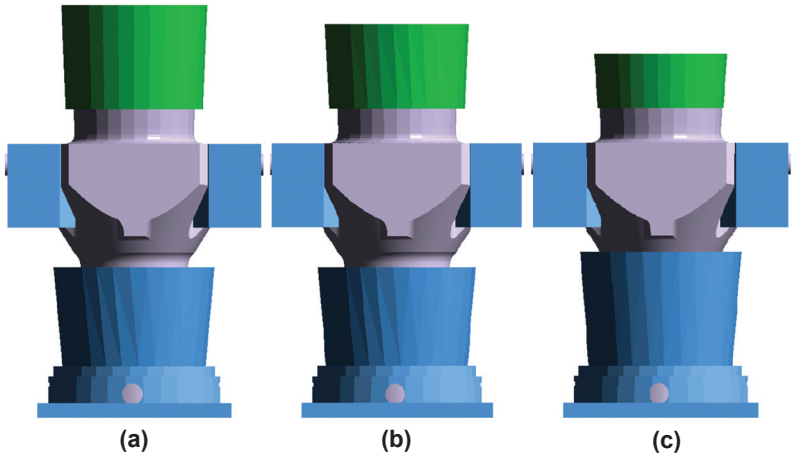

Figure 16. Three distinct designs proposed by the optimization tool.

Regarding the solidification patterns of the three optimized designs, no isolated liquid areas are forming in the bottom area as in the original layout, depicted in Figure 7. The bottom chill plate and the stair-type chill around the conical section induced directional solidification towards the thermal axis and the riser. Solidification patterns were checked over the entire solidification interval. It was found that none of these designs exhibit apparent isolated liquid areas although solution 3 is really on the edge later in solidification in an area right below the riser-neck, see Figure 17. The reason is that the riser is too small and the heaviest section of the casting slowly begins to be the last to solidify. If one should fully rely on the numerical results, solution 3 would be good enough for production. However, simulation does not take into account all crucial factors that occur in practice. For instance the quality of the melt can be compromised by a dirty ladle with residuals from the previous batch. Next could be the human factor, which often compromises the quality of a casting process. Having all this in mind it was decided together with the foundry not to go for solution 3 to avoid failure in production. But this solution is still shown and discussed here.

In Figure 18, the centerline porosity is expressed by the Niyama criterion. The light blue areas stand for values of 0,4 and lower which will contain macroscopic shrinkage. Everything above the 0,45 up to 1 will most likely be microporosity, not detectable by the radiography techniques. It is seen that despite solution 3 being on the edge, it still shows no occurrence of porosity in the casting body. Only the bottom pins contain small porous areas. The reasonable remedy for this was addressed earlier.

A similar situation applies for shrinkage porosity shown in Figure 19. The casting body appears to be porosity free in all three cases, except for the pins again.

The last assessment concerns the casting yield. The aim of the entire project has been primarily to eliminate the presence of various casting defects. Once this was achieved, the next step was to optimize the riser volume for the casting yield improvement. The results of this assessment are given in Table 4. Compared to the original design, the casting yield could be increased by approximately 25% if the optimized solution 3 was applied. Due to a high risk of shrinkage occurrence below the riser neck, solution 3 was not approved for production.

Table 4. Casting Yield Assessment

	Original Solution	Optimized Solution 1	Optimized Solution 2	Optimized Solution 3
Total Height	4337 mm	4037 mm	3837 mm	3537 mm
Total Weight	59640 kg	48406.8 kg	45850 kg	40968 kg
Casting Yield	55.36 %	61.76 %	72.01 %	80.59 %

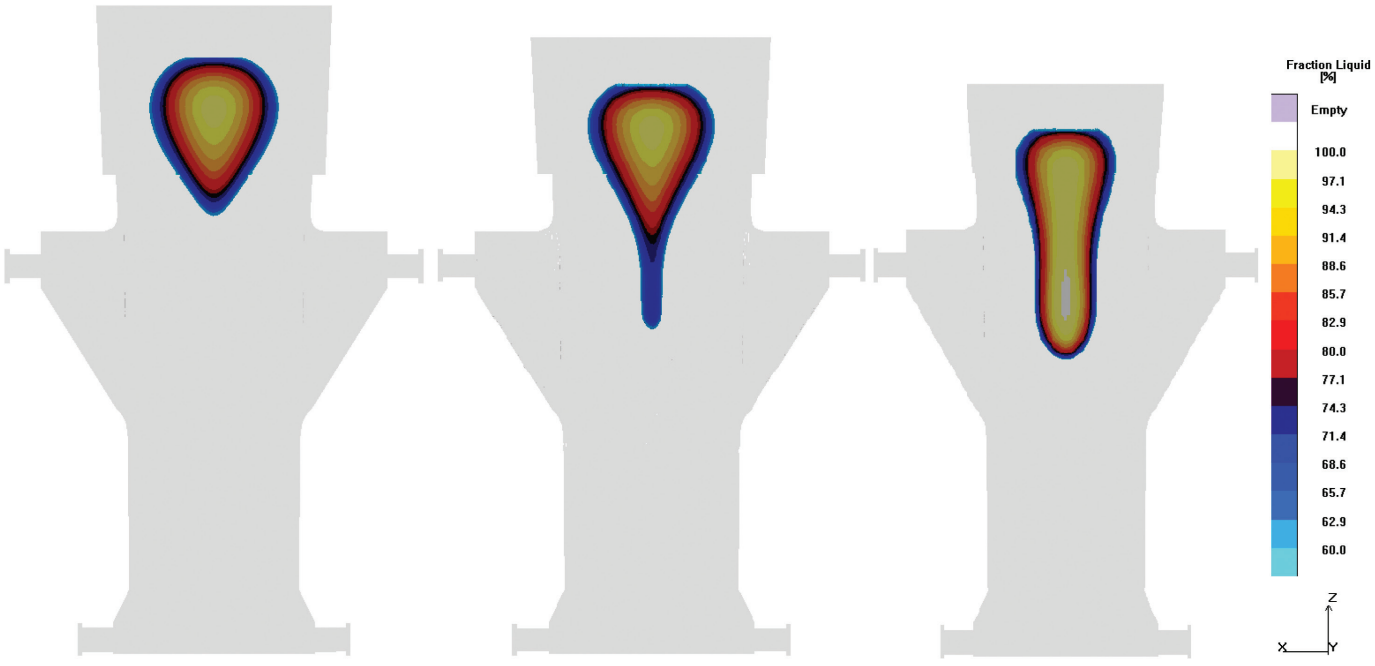

Figure 17. Solidification pattern of the three optimized designs at 90% solidified.

Conclusions

This work showed a study of a multi-objective optimization problem that has been carried out for a steel forging ram produced by the gravity sand casting technique. The main idea of this case study was to demonstrate how fully computerized optimization can be effectively utilized in daily foundry practice. The optimization objectives were to minimize the remaining volume of the top riser and avoid (minimize) shrinkage and centerline porosity in the casting body.

The first step was to thoroughly analyze the original casting layout provided by the foundry. Both filling and solidification analyses were performed and potential flaws and defects were revealed. The results of filling indicated

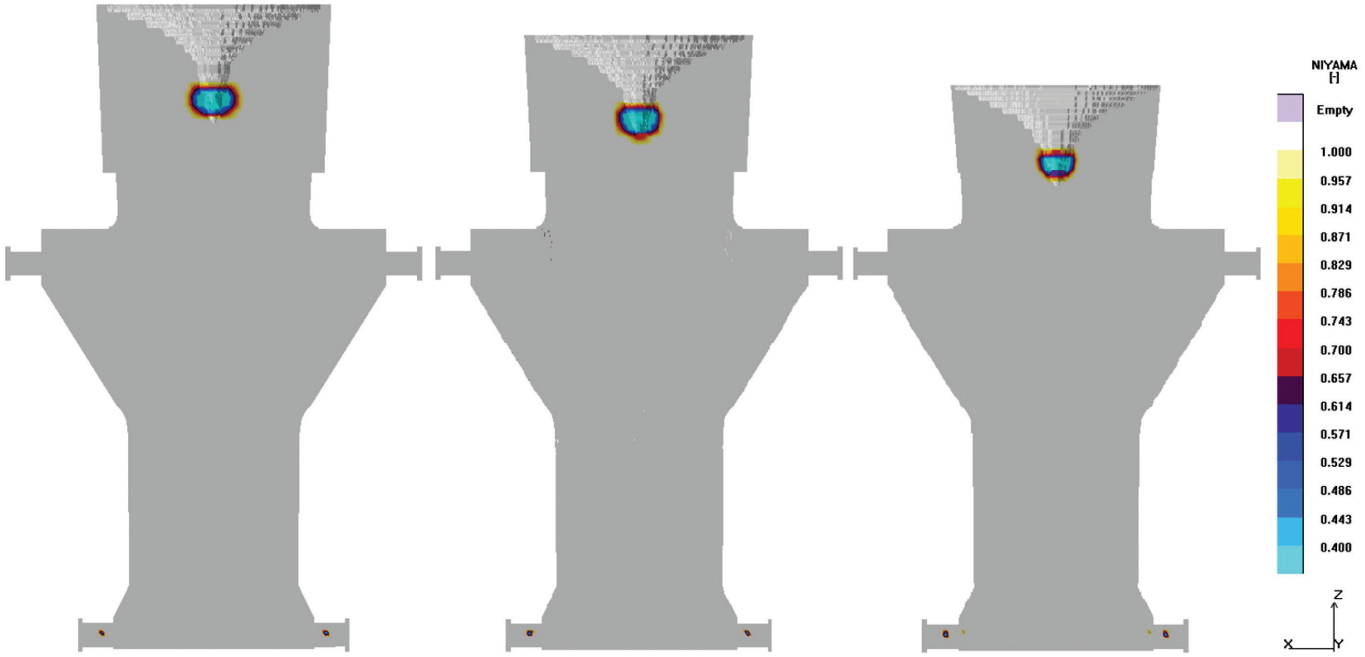

Figure 18. Occurrence of centerline porosity in the optimized designs.

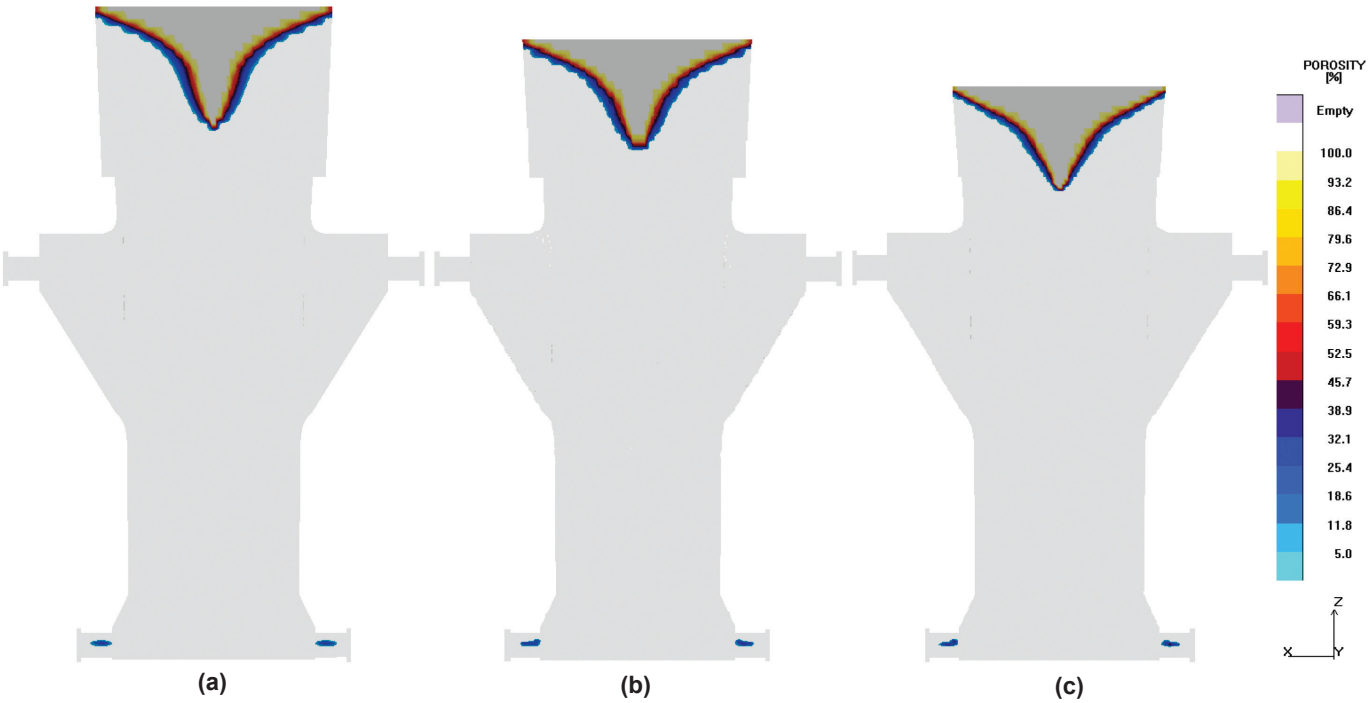

Figure 19. Occurrence of macroscopic shrinkage in the optimized designs.

a massive melt aspiration in the downsprue section due to the accelerating melt and the constant cross-section. Using this type of a gating system, it was impossible to control the melt velocity whatsoever, which then led to a formation of fountains and subsequent melt oxidation in the mould cavity. As to the solidification results, it was shown that due to improper cooling there was a tendency for cutting off liquid areas from the feeding path. A consequence was a formation of shrinkage and centerline porosity in the bottom cylindrical area of the part. These results were verified by casting trials performed by the foundry. Therefore it was decided to redesign the gating system from the bottom-fill to the side- fill type, rearrange the chills, and implement a new chill plate underneath the casting to promote cooling of that area. It showed that the filling pattern improved significantly, avoiding problems with fountains in the mould cavity. The surface turbulence is still present, but as long as the cross-section area of the filling channels remains constant and the velocity is uncontrolled, no further improvement is feasible. The new chill arrangement caused significant improvements in the solidification pattern. More pronounced cooling established steeper temperature gradients and induced directional solidification in the problematic bottom area, totally eliminating the shrinkage-related defects.

The manually-optimized solution served as a reference case for the geometry optimization of the riser and chills. In the multi-objective optimization case, the riser and chills dimensions have been applied as design variables together with the ranges of variation. In addition, optimization objectives together with potential constraints have been introduced into the optimizer together with the number of initial designs and generations in which the optimal solutions should be found. Three distinct solutions were selected from the design space. The first one represented a modest approach (relatively large riser), the middle one was still a safe solution but the riser was much smaller, and the third solution represented the very risky solution with the highest casting yield. It turned out that all three designs yielded different solidification patterns compared to the initial design. This was attributed to the change in the riser dimensions and the rearranged chills. No residual liquid pools were spotted; however there were some indications of potential problems in the third solution. Concerning the macro and micro-shrinkage in the optimized designs, the only problematic areas were in the riser head and bottom pins. The casting body seemed free of porosity. Eventually it was decided together with the foundry not to consider the last solution for production due to a high risk of failure in production. In other words, when taking the human factor into consideration, the risk of porosity extending from the riser to the casting body is too high. Last, findings regarding the casting yield showed that when correctly utilizing multi-objective optimization, it is feasible to substantially increase the casting yield and thus reduce production costs.

Acknowledgements

The authors would like to thank the Vitkovice Heavy Machinery a.s. for identifying the case study and providing us with the casting data necessary to perform the relevant simulations and the photographs of the metallographic analysis for this case study.

REFERENCES

1. MAGMAsoft simulation software, MAGMA GmbH, Aachen, Germany
2. Svensson, I.L., Seifeddine, S., Hattel, J.H., Thorborg, J., Kotas, P., "On Modelling of Microstructure Formation, Local Mechanical Properties and Stress-Strain Development in Aluminium Castings", *Proc. Int. Conf. On Modelling of Casting, Welding and Advanced Solidification Processes,* MCWASP XII, Vancouver BC, Canada, pp. 129-136 (2009).
3. Seifeddine, S., Wéssen, M., Svensson, I.L., "Use of Simulation to Predict Microstructure and Mechanical Properties in an As-Cast Aluminium Cylinder Head: Comparison with Experiments", *Metallurgical Science & Technology*, vol. 24, no. 2, pp. 27-33 (2007).
4. Herman, A., Marousek, L., "The Verification of Computer Simulation for High Pressure Casting Technology", Technológia 2003. Bratislava: Faculty of Mechanical Engineering of the Slovak Technical University, p. 56 (2003).
5. Sturm, J., Hepp, E., Enger-Walter, A., "*Integration of Casting Simulation into Crash Simulation"* 20th CAD-FEM Users` Meeting 2002, International Congress on FEM Technology, Lake Constance, Germany (2002).
6. Kotas, P., "Numerical Optimization of Die Filling and of High-Pressure Die Cast Deformation", Master Thesis, Technical University of Denmark, Lyngby, Denmark (2007).
7. Hattel, J.H., *Fundamentals of Numerical Modelling of Casting Processes*, 1st ed., Kgs. Lyngby: Polyteknisk Forlag (2005).
8. Egner-Walter, A., "Prediction of Distortion in Thin-Walled Die Castings", *Casting Plant and Technology International*, vol. 23, no. 1, pp. 24-33 (2007).
9. Monroe, C., Beckermann, C., "Deformation during Casting of Steel: Model and Material Properties", in *Proceedings of the 61st Technical and Operating Conference,* SFSA, Chicago, IL (2007).
10. Poloni, C., Pediroda, V., *GA Coupled with Computationally Expensive Simulations: Tools to Improve Efficiency, Chapter Genetic Algorithms and Evolution Strategies in Engineering and Computer Science*, pp. 267-288. John Wiley and Sons (1997).
11. Fonseca, C., Fleming, P., "Genetic Algorithms for Multiobjective Optimization: Formulation, Discussion and Generalization", In Genetic Algorithms, Proceedings of the 5th International Conference, USA, pp. 416-423 (1993).

12. MAGMAfrontier 4.4 Reference Manual (2005).
13. Hahn, I., Hartmann, G., "Automatic Computerized Optimization in the Die Casting Processes", *Casting Plant & Technology International,* vol. 24, no. 4 (2008).
14. Gramegna, N., Baumgartner, P., Kokot, V., "Capabilities of New Multi-Objective Casting Process Optimization Tool", IDEAL International Conference, Lecce, Italy (October 2005).
15. Kokot, V., Bernbeck, P., "Integration and Application of Optimization Algorithms with Casting Process Simulation", *Proc. Int. Conf. On Modelling of Casting, Welding and Advanced Solidification Processes,* MCWASP X, Destin, Florida, pp. 487- 494 (May 2003).
16. Goldberg, D.E., *Genetic Algorithms in Search, Optimization & Machine Learning*, Addison Wesley Longmann, Inc., (1989).
17. Tutum, C.C., Hattel, J.H., "Optimization of Process Parameters in Friction Stir Welding Based on Residual Stress Analysis – A Feasibility Study", *Science and Technology of Welding and Joining* (In Press).
18. Deb, K., *Multi-Objective Optimization Using Evolutionary Algorithms*, John Wiley & Sons, (2001).
19. Deb, K., "Unveiling Innovative Design Principles by Means of Multiple Conflicting Objectives", *Engineering Optimization*, vol. 35, no. 5, pp. 445-470 (2003).
20. Tutum, C.C., "Optimization of Thermo-Mechanical Conditions in Friction Stir Welding", PhD Thesis, Technical University of Denmark, ISBN 978-87-89502-89, (2009).
21. Sobol, I., "On the Systematic Search in a Hypercube", *SIAM Journal on Numerical Analysis*, vol. 16, issue 5, pp. 790-793 (1979).
22. Niyama, E., Uchida, T., Morikawa, M., Saito, S., "Method of Shrinkage Prediction and its Application to Steel Casting Practice", *AFS Int. Cast. Met. J.,* vol. 7, no. 3, pp. 52-63 (1982).
23. Carlson, K.D., Beckermann, C., "Prediction of Shrinkage Pore Volume Fraction Using a Dimensionless Niyama Criterion", *Metallurgical and Materials Transactions A,* vol. 40A, pp. 163-175 (2009).
24. Carlson, K.D., Ou, S., and Beckermann, C., "Feeding of High-Nickel Alloy Castings," *Metallurgical and Materials Transactions B*, vol. 36B, pp. 843-856 (2005).
25. Jain, N., Carlson, K.D., Beckermann, C., "Round Robin Study to Assess Variations in Casting Simulation Niyama Criterion Predictions," in *Proceedings of the 61st Technical and Operating Conference*, SFSA, Chicago. IL (2007).
26. Carlson, K.D., Ou, S., Hardin, R.A., Beckermann, C., "Development of a Methodology to Predict and Prevent Leaks Caused by Microporosity in Steel Castings," in *Proceedings of the 55th Technical and Operating Conference,* SFSA, Chicago IL (2001).
27. Hardin, R.A., Ou, S., Carlson, K.D., Beckermann, C., "Development of New Feeding Distance Rules Using Casting Simulation; Part I: Methodology", *Metallurgical and Materials Transactions B*, vol. 33B, pp. 731-740 (2002).
28. Campbell, J., *Castings*, Second Edition. Elsevier Butterworth-Heinemann (2003).
29. Wang, L., and Beckermann, C., "Prediction of Reoxidation Inclusion Composition in Casting of Steel", *Metallurgical and Materials Transactions B,* vol. 37B, pp. 571-588 (2006).
30. Hansen, S.S., "Reduced Energy Consumption for Melting in Foundries", PhD Thesis, Technical University of Denmark, ISBN 978-87-91035-63-5 (2007).
31. Beckermann, C., "Modelling of Macrosegregation: Applications and Future Needs", *Int. Mater. Rev.*, vol. 47, pp. 243-261 (2002).
32. Beeley, P., *Foundry Technology*, Second Edition, Butterworth – Heinemann, (2001).
33. Porter, D.A., Easterling, K.E., *Phase Transformations in Metals and Alloys*, Second Edition, Taylor & Francis Group (2004).

Technical Review and Discussion

A Casting Yield Optimization Case Study: Forging Ram

P. Kotas, C. Tutum, J. Hattel, Technical University of Denmark, Lyngby, Denmark
O. Šnajdrová, Vitkovice Heavy Machinery A.S., Ostrava, Czech Republic
J. Thorborg, Technical University of Denmark, Lyngby, Denmark, MAGMA GmbH, Aachen, Germany

Reviewer: Can any sensitivities be evaluated after all the simulations are run to determine if other factors should be studied, e.g. upper chills required or effect on riser size?

Authors: *A classical sensitivity analysis is possible to carry out in the optimization software. It was done to evaluate if both of our objective functions are sensitive to the pre-defined design variables. And they are. However, this analysis was not stated in the paper, due to its already large size. If the question is whether the optimization software proposes some more design variables or factors that might be influential , the answer is NO, this was not done and is not possible to do. Every time, a user has to define all the variables, constraints, objectives and other parameters and the software only works with those.*

Reviewer: Were any trials run for the optimized solution to ensure casting soundness and that no other defects were created due to the recommended changes?

Authors: *No casting trials based on the optimized solutions and proposals have been performed by the foundry yet. However, there is a promise from them to take our results into considerations, apply the findings and perform the riser volume reduction in the next casting batch.*

C PAPER – III

Kotas, P., Tutum, C.C., Andersen, S., Hattel, J.H., "*Autonomous Optimization of a Solidification Pattern and its Effect on Porosity and Segregation in Steel Castings*", Accepted for an Oral Presentation at the 115th Metalcasting Congress, Schaumburg, April 2011, USA. To be published in AFS Transactions 2011.

Autonomous Optimization of a Solidification Pattern and its Effect on Porosity and Segregation in Steel Castings

P. Kotas
Technical University of Denmark, Department of Mechanical Engineering, Kgs. Lyngby, Denmark

C.C. Tutum
Technical University of Denmark, Department of Mechanical Engineering, Kgs. Lyngby, Denmark

S. Andersen
MAGMA Foundry Technologies, Inc., 10N. Martingale Road, Schaumburg, IL 60173, USA

J.H. Hattel
Technical University of Denmark, Department of Mechanical Engineering, Kgs. Lyngby, Denmark

ABSTRACT

The present paper considers optimization of a solidification pattern of a gravity sand-cast steel part. That is, the choice of proper riser and chill designs has been investigated using genetic algorithms while simultaneously considering their impact on centerline porosity and macrosegregation distribution. This was accomplished by coupling a casting simulation software package with an optimization module. The casting process of the original casting design was simulated using a transient 3D thermal model incorporated in a commercial simulation software package to determine potential flaws and inadequacies. After this initial assessment, a new geometrical model was suggested with the redesigned gating system and rearranged chills to obtain better filling and solidification patterns. Based on the improved model, relevant optimization targets and constraints were defined. One multi-objective optimization case with two conflicting objectives was considered in which minimization of the riser volume together with minimization of centerline porosity and elimination of macrosegregation issues were performed.

Key Words: Casting process simulation, genetic algorithms, riser volume optimization, casting yield, steel casting, macrosegregation, centerline porosity, shrinkage porosity

INTRODUCTION

Nowadays, a general trend is to reduce production costs as much as possible in order to stay competitive and attractive for potential and current customers. In this context, virtual prototyping and testing by numerical simulation offer an efficient way of reducing product development time as well as costs of producing prototypes, shortening lead time and eliminating scrap.
Metal casting process simulation is used to provide detailed information about the mold filling, solidification and solid state cooling, and with that, also information about the local microstructure, non-uniform distribution of mechanical properties and subsequently residual stress and distortion build-up[1-6]. Casting simulation tries to use physically realistic models without overtaxing the computer. At the same time the simulations need to give applicable results in the shortest time possible. Unfortunately, numerical simulations can only test one "state", while conclusions from calculations or subsequent optimization still require an engineer's interpretation and decision after each of the simulation runs. Understanding the process enables a foundry engineer to make decisions that can affect both the part and the rigging to improve the final quality.
The objectives which drive the designers are generally well defined: improving the component quality, achieving homogeneous mechanical characteristics, maximizing the casting yield, increasing the production rates, etc. It is very complex and time consuming to achieve all these objectives at the same time due to the high number of variables involved. In many foundries the only applied optimization is still based on intuition and thus on the trial-and-error method. While, when using numerical simulation, in the case of an error, only a virtual casting is spoiled, no raw material is wasted, no mould is produced and above all no production loss is experienced.
Rapid development of high performance computing has substantially shortened the calculation time needed for one variant of the casting process to be analyzed. Over night it is feasible to calculate numerous versions and layouts in almost unlimited configurations. The advantage of having such short calculation times can only be utilized providing that a computer can automatically analyze calculated variants with respect to the predefined objectives (e.g. maximum feeding, low porosity, low air entrapment etc.) and subsequently create new variants and analyze them in the same manner to achieve the optimal solution. By integrating such software for casting process simulation with an optimization algorithm (in this case the Multi-Objective Genetic Algorithm, MOGA[7] which

should not be confused with the non-elitist MOGA developed by Fonseca and Fleming[8]), a computer based optimization tool is established which is able to determine optimal values of user-defined design variables thereby optimizing a given casting process with respect to defined objectives. Subsequently such system can readily provide optimal solutions for any kind of casting processes[9-11].

This paper details multi-objective optimization of a solidification pattern of a steel forging ram and its effect on shrinkage porosity and macrosegregation pattern. Numerical multi-objective optimization is carried out by coupling the general-purpose casting simulation software package MAGMASOFT® with the add-on optimization module MAGMA*frontier*.

The study includes three different layouts. The initial layout is provided by a foundry (Vitkovice Heavy Machinery) that manufactures the forging ram. The second layout with manually rearranged gating system and chills is also provided by the foundry although some changes in the layout are made by the authors, and the third layout is purely generated by the numerical optimization. All of the designs are simulated including the filling of the mold cavity to obtain an accurate temperature field inside the casting for the following solidification simulation. However, only results from the solidification simulation are presented and discussed. In case of the first layout no computerized optimization is involved. The second layout is taken as a reference or starting solution for the following autonomous optimization. The last design is a result of multi-objective optimization. Conclusions and proposals are made from the various investigations and findings in the study, and are presented in the last section of the paper.

MODELLING PROCEDURE

DESCRIPTION OF THE CASTING

The project involves a large (59.6 ton, maximum dimensions 5.3 x 2.4 x 2.3 m) steel forging ram, **Figure 1a** made of a low carbon steel alloy DIN 1.1120, poured into furan bonded silica sand with an insulated top riser, shown in **Figure 1b**. The main cylindrical padding is insulating, the melt surface is covered by an exothermic powder and on top of that additional insulating powder is applied. The original casting arrangement is bottom-filled assuming an initial pouring temperature of 1540°C (2084 deg. F). The filling time is 120s. One hour after filling, additional top filling of the riser takes place to compensate for the volumetric shrinkage and to induce favorable temperature gradients. The chill bricks are placed around the lower cylindrical section of the casting to facilitate directional and progressive solidification towards the riser and to prevent potential macrosegregation-related flaws.

FILLING AND SOLIDIFICATION ANALYSIS

Casting process simulation starts with a geometry defined as a 3D CAD model of the casting, mold, gating, chills, riser and the insulating padding. Material group definition is done in the software's preprocessor. Next, the geometry is properly meshed and all necessary information relating to the molten metal chemistry, pouring temperature; flow properties, interface heat transfer coefficients (HTC), thermodynamic properties, and mechanical properties must be introduced into the system. Regarding HTC at the casting/mould interface, it is assumed temperature independent and it was set to be 800 W/m^{2}K. This assumption holds only for gravity sand casting for which the solidification results are relatively insensitive to the HTC since the thermal properties of the sand typically dominate the cooling of the casting. The assumption is that in sand casting the contact between the melt and the mould is poor from the very beginning due to the rough surface of the mould. As a result, there is a high resistance to heat removal, giving low interface HTC. When the casting shrinks during solidification and solid state cooling, an air gap is formed in the casting/mould interface, additionally increasing resistance to the heat removal. Nevertheless, since the heat transfer has been poor from the very beginning the decrease in HTC due to volumetric changes is not that decisive for the results and the HTC can be assumed more or less constant (low) over the entire casting process.

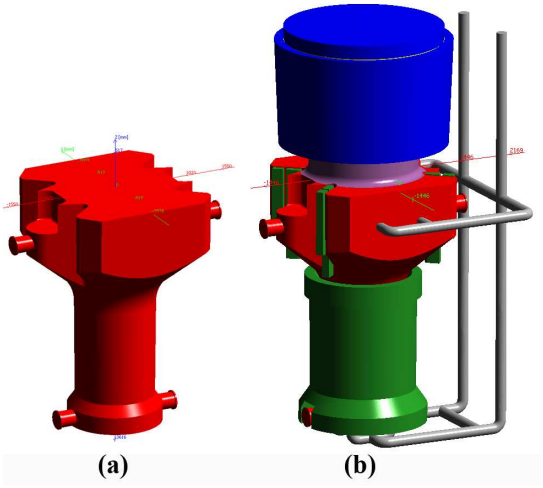

Fig. 1. The cast part used in the project and the initial casting layout. The casting is indicated red, chills indicated green; insulation is denoted dark blue, (Property of Vitkovice Heavy Machinery, a.s.).

After all process parameters are entered, filling of the casting can be simulated. A flow rate boundary condition is selected to control the filling process which accounts for a change in overpressure during filling using bottom-pour ladles. Once filling is modeled, resulting temperature fields in the casting are taken and used as an input for the subsequent heat transfer calculation during solidification and solid-state cooling of the casting. The heat transfer calculation gives temperature fields and distributions of various defects arising during solidification and further cooling. Results predicting defects occurrence, i.e. shrinkage porosity, centerline porosity, macrosegregation

etc., are used to evaluate the casting soundness and its overall quality.

The formation of centerline porosity is represented by the Niyama criterion[12]. It is a local thermal parameter defined as the relationship between the thermal gradient (G) in K/mm and the cooling rate (R) in K/s, both of which are assessed at a specified temperature near the end of solidification, see eq. (1). Shrinkage porosity predicted by the Niyama criterion usually forms in the mushy region at high solid fractions. At lower solid fractions, the pressure drop which governs this type of porosity is negligibly small. Therefore, in a casting simulation, the Niyama criterion is always evaluated at a temperature near the end of the solidification interval. In the present study, the Niyama criterion is evaluated at a temperature 10% of the solidification range above the solidus temperature.

$$Niyama = \frac{G}{\sqrt{R}} \qquad \text{Equation 1}$$

With the help of the Niyama criterion, it is feasible to predict the presence of centerline shrinkage porosity, i.e. micro- and macro-shrinkage in steels, caused by shallow temperature gradients[13-15]. It indicates that in regions that solidify quickly, there must be hot metal nearby to establish a high gradient to feed the shrinkage during solidification.

Based on literature search and findings provided by the manufacturer, it is determined that the critical Niyama value for macro-porosity for this particular steel alloy is Ny_{macro}= 0.45 $(K \cdot s)^{1/2}$/mm. Everything above this value is assumed to be a micro-shrinkage that will not be detected via common radiography The second threshold value for micro-porosity, above which the material is completely sound is set to be Ny_{micro}= 1 $(K \cdot s)^{1/2}$/mm. The Niyama criterion only predicts feeding-distance related shrinkage; it does not explicitly predict hot spots in a casting, and it does not predict gas porosity[12].

Macrosegregation refers to solute inhomogenities at the macroscopic scale in metal alloy castings and range in scale from several milimeters to even meters. These compositional variations have a negative impact on final properties, i.e. microstructure, mechanical properties, and in-service behavior of a cast part. Macrosegregation is caused by relative movement or flow of segregated liquid and solid within the mushy zone during solidification.

There are four major causes of macrosegregation, these are [16]:

(a) *Macrosegregation associated with solidification shrinkage*, i.e. flow that feeds the solidification shrinkage and the contractions of the liquid and solid during cooling,

(b) *Macrosegregation associated with natural or forced convection*. If the velocity of the liquid is perpendicular to the solute gradient, no macrosegregation occures. However, macrosegregation is induced when the flow enters or exits the mushy zone.

(c) *Macrosegregation associated with grain movement*. As long as the grains move with the same velocity as the liquid, there is no macrosegregation. However, equiaxed grains have a tendency to sediment or, in certain cases, to float, giving rise to macrosegregation.

(d) *Macrosegration associated with deformation of the solid network* in the mushy zone due to thermal and shrinkage stress, head pressure, or external forces on the solid shell. In other words, the mushy solid behaves like a sponge causing the liquid to be expelled (when in compression) or sucked in (when in tension).

Flow due to thermal and solutal gradients in the liquid leads to formation of so-called channel segregates, commonly referred to A- segregates or freckles. Freckles are typically initiated by convective instabilities above or inside the mushy zone, i.e. when the velocity of the liquid in the mushy zone exceeds that of the isotherm and the segregated interdenritic liquid becomes less dense than the overlying bulk liquid of original composition. This phenomenon eventually leads to open channels, i.e. local remelting due to solid fraction decrease, in the mush through which the solute-rich and low-density liquid flows upward into the bulk liquid region. These open channels are associated with local increase in permeability which allows for the liquid to flow more easily, thus enhancing remelting and macrosegregation. When the channels eventually freeze, they appear as pencil-like chains of equiaxed crystals that are highly enriched in solute[17]. It has been shown in the literature[16] that if temperature gradients and the casting speed, i.e. isotherm velocity, are high enough, freckles are less likely to form. One could thus argue that in this regard centerline shrinkage and channel segregations follow a similar trend although, they are not necessarily governed by the same physical phenomena. It means that in principle enhanced thermal gradients and progressive directional solidification with sufficiently tapered pool of liquid metal[18] should decrease a risk of both of these defects. Therefore in this present work, the major focus will be put on optimizing the chilling system to evoke steeper thermal gradients and to establish a pronounced progressive solidification pattern.

OPTIMIZATION PROCEDURE

In the present study, unknown shapes and sizes of the top riser and the chills are sought by means of autonomous optimization to obtain a better solidification pattern of the casting. This issue has been addressed by defining the problem as a multi-objective optimization problem (MOP) by combining multiple conflicting criteria, i.e. minimization of the riser volume and minimization of centerline shrinkage porosity and macrosegregation, respectively. The multi-objective genetic algorithm (MOGA)[9] has been applied to handle these multiple objectives. In the following sections, a brief description of MOP and genetic algorithms is given followed by an introduction to the considered optimization problem.

INTRODUCTION TO MOP AND MOGA

Most engineering design activities require a solution of multi-disciplinary and multi-objective optimization

(MOO) problems which usually deal with conflicting design objectives. In the case of single-objective optimization problems, it is easier to identify the optimal solution as compared to the case of MOO where there is more than one criterion to satisfy, i.e. hence more than one best (elite) solution to consider. As it was put forward by Goldberg[19] "if we refuse to compare apples to oranges, then we must come up with a different definition of optimality, one that respects the integrity of each of our seperate criteria" which points out the concept of Pareto Optimality, correlated to the fundamental concept of domination. Since the concept of domination allows a way to compare solutions with multiple objectives, most MOO algorithms use this domination concept to search for non-dominated solutions, i.e. the ones that constitute the Pareto-front as shown **in Figure.2(c)**. This concept can be explained with a simple example in a 2D objective space, in which the minimization of both objective functions (i.e. f_1 and f_2) is considered, as shown in **Figures.2(a-c)**. In **Figure.2(a)**, point-1 representing a solution or a design which splits the 2D objective space into two zones: the first zone (the shaded region); the set of the points dominated by point-1, and the second zone; the set of points not dominated by point-1 (the remaining three quadrants), i.e. the non-dominated or noninferior set of points. Thus, the two conditions stated below need to be satisfied if point-1 dominates point-i, where point-i is any other design point in the objective space[20]

- point-1 is no worse than point-i in all objectives.
- point-1 is strictly better than point-i in at least one objective.

These two statements give a general description for the comparison of the two solutions in terms of "betterness", hence emphasizing the applicability of this comparison for other types or combinations of conflicting objectives besides the minimization – minimization type as shown in **Figures.2(a-c**), i.e. maximization - maximization, maximization – minimization as well as minimization - maximization.

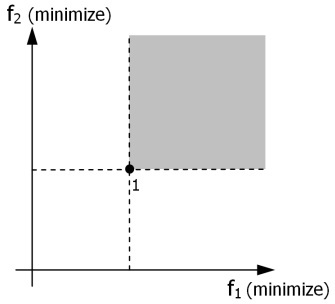

Figure 2. (a) The two separate sets of solutions defined with respect to point-1: i) the set of dominated solutions (the shaded region), ii) the set of non-dominated solutions (adapted from [22]) [23].

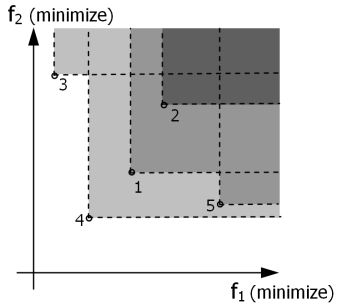

Figure 2. (b) Each solution in a population has its own sets of dominated and non-dominated solutions (inspired by [24]) [23].

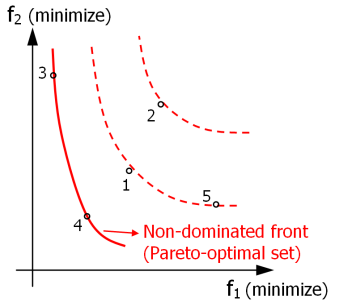

Figure 2. (c) The dominated and non-dominated (Pareto-optimal) fronts [23].

In case of having a population composed of e.g. five points as shown in **Figure.2(b)**, a need for an overall relation of dominance arises, i.e. the one-to-one comparison made for point-1 should be generalized for each point. **Figure.2(b)** shows the distribution of these five points together with their domination regions which are distinguished with different tones of colors and it is clearly seen that point-4 dominates points-1, 2 and 5 with respect to all objectives, while point-3 dominates all other points (i.e. strictly better) only with respect to the first objective for the given distribution. However, since points-3 and 4 are not dominated by any other points, they constitute the non-dominated front which is also called the Pareto-optimal front, see **Figure. 2(c)**, in an MOO context. A similar comparison will reveal that point-1 and point-5 constitute the next domination front which in itself is dominated by the Pareto front and shown as the closest dashed line to the Pareto front in **Figure.2(c)**[22].

Population-based evolutionary algorithms are typically able to provide a larger spectrum of Pareto-optimal solutions without any additional problem specification as in some algorithms designed specifically for the SOO problems. This ideal approach of evolutionary MOO algorithms replaces some of the potential weaknesses of gradient based algorithms in some cases, e.g. when having a non-continuous or non-convex search space. The availability of trade-off solutions, representing varying preference levels between chosen objectives, makes it easier for a user to choose a particular solution for subsequent implementation[25-27].

PROBLEM STATEMENT – OPTIMIZATION OF THE RISER AND CHILLS

The optimization problem here is defined as the goal of finding the most suitable shapes of the top riser and the chills surrounding the casting, which provide a set of trade-off solutions for the minimization of two conflicting objectives. These are, (i) to design the top riser so, that the casting is sound (i.e. with minimum centerline shrinkage porosity and evenly distributed concentration profiles of solute elements) and (ii) at the same time having a top riser's volume as small as possible to increase the casting yield. In this context, 'casting yield' is defined as the

gross weight including the riser and the gating system divided by the weight of the fettled casting.
Prior to optimization, it was decided by the manufacturer to redesign the chills. The primary aim is to facilitate directional and progressive solidification towards the top riser to eliminate potential porosity and channel segregation, i.e. A- and V-type segregates. To achieve this, a cooling plate is added underneath the casting and wedge shaped chill blocks are added adjacent the "head" area of the casting. In order to place the plate, the gating system has to be modified from bottom filling to side filling. Also, new vertical runners are added to support filling in higher sections of the casting. Furthermore, the chills around the cylindrical section are rearranged a bit. In order to ensure sufficient cooling of the very bottom, thicker chills are added around the conical bottom section of the casting, see **Figure 11** Solution 1. Besides the mentioned geometrical changes, all casting and simulation parameters remain the same as in the first casting arrangement.
The manually refined casting layout is taken as a reference solution to compare the optimization results with. It has been decided to try to reduce the size of the top riser as much as possible to increase the casting yield, providing that there will be no defects occurring in the casting due to the riser's reduced size. When the riser and the chills are transformed into parametric objects, the optimization process is initiated. The design variables (those which are subjected to optimization) are: dimensions of the chills- height and thickness of the bottom cylindrical chills, and of the top riser –its height, bottom and top diameters, and the top diameter of the riser neck. It would be very time consuming to calculate thermal convection and segregation for each design during the optimization cycle. Thus, only selected designs constituting the final Pareto line are analyzed with respect to macrosegregation.
The initial population for the MOGA algorithm containing 100 unique designs is provided by the Sobol DOE sequence generating technique which is a quasi-random sequence. The points in this type of sequence are maximally avoiding each other, so the initial population fills the design space in a uniform manner. The assumed optimization problem is constrained only by the predefined ranges of variation of the design variables. The directional cross-over, the selection and the mutation probabilities of 0.6, 0.3 and 0.1, respectively, are chosen for running 20 generations giving in a total number of 2000 possible solutions. In addition, elitism is applied to support convergence in the optimization problem. Elitism is a GA operator (in general, an evolutionary algorithm operator) to keep the best designs found so far in the evolution of the generations.

RESULTS AND DISCUSSION

In the two following sections, results obtained from the simulations and casting trials are presented and discussed. First, the numerical and experimental results from the original casting assembly are analyzed to establish a base case. Then, the results from the multi-objective optimization problem (riser volume and chill size optimization) are presented. At the end a comparison of the casting yield of the original and the optimized designs is carried out.

CASTING TRIAL AND SIMULATION RESULTS- ORIGINAL LAYOUT

The original casting arrangement depicted in **Figure 1b** was cast using the process parameters indicated in the beginning of this paper. The casting was then sectioned, etched and surface treated to provide information regarding its microstructure and mainly solidification related issues for further comparison with the numerical solution. **Figure 3** shows the lower part of the casting, i.e. vertical cut through the part.
In that figure, two types of solidification induced defects are found. The first one is a shrinkage porosity which formed in the centre of the casting section. At this point it is quite difficult to estimate the exact type of porosity, i.e. centerline porosity or shrinkage porosity. Most likely this defect occurred due to limited feeding ability of the riser. In other words, the problematic area is out of the effective feeding distance of the top riser. The second type of the defect is referred to as channel segregation, namely A- and V-type. This defect formed most likely due to an improper solidification pattern caused by inadequate cooling from the chills. Local remelting occurred in the mushy zone giving rise to open channels of highly segregated liquid.

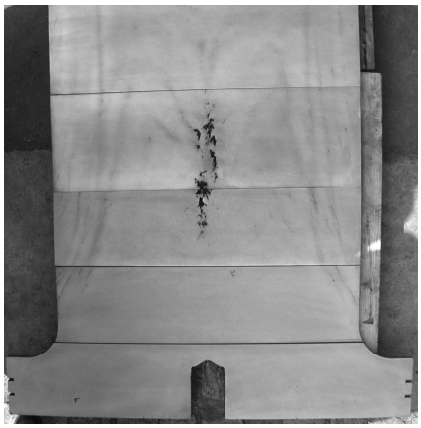

Fig. 3. Results from the casting trial- presence of porous areas and bands of macrosegregation, (Courtesy of Vitkovice Heavy Machinery, a.s.).

The same casting layout was simulated, both with respect to filling and solidification. The filling analysis provides proper temperature fields inside the casting for the subsequent solidification analysis. The thermal analysis during solidification evaluates the effectivity of the top riser and the cooling ability of the chills placed around the cylindrical section of the cast part.

In **Figure 4** it is seen that during the solidification process, particularly at 45 % solidified, there are indications of choking off liquid pools in the lower cylindrical section of the casting. When the liquid melt supply is cut off and drained, areas solidifying last will be short of melt so when they are going to solidify no compensation for the volumetric shrinkage will be available, forming a hot spot and leading to shrinkage porosity, **Figure 5**. The chills cool the cylindrical section faster, compared to the bottom area in which the cooling rate is lower due to the enlarged cross-section and no chills. No other issues with isolated liquid areas which would cause shrinkage porosity have been spotted during solidification. A remedy would be either to increase the thickness of the chills towards the bottom area or to redesign the gating system so that there is a chance to add a chill plate underneath the casting bottom. Cooling of the bottom of the casting would be significantly promoted and progressive directional solidification towards the riser would be established.

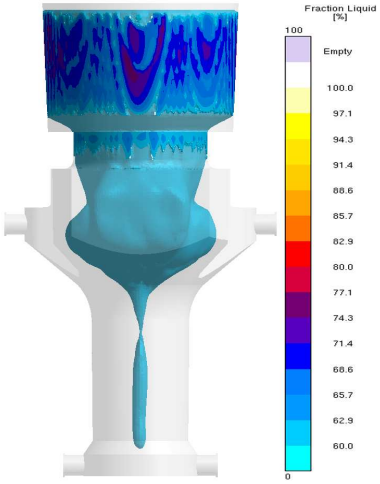

Fig. 4. Indication of an isolated liquid pool in the lower area of the cast part at 45% solidified.

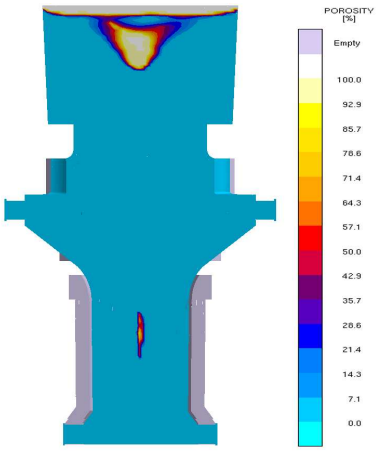

Fig. 5. Presence of shrinkage porosity caused by improper feeding during solidification.

Figure 6 shows the numerically predicted presence of centerline porosity, i.e. represented by the Niyama criterion, in the lower casting area together with results obtained from the casting trial. It is seen that indeed, the porous areas occured in the casting where the isolated liquid pool was once present and in the area which is out of reach of the riser`s effective feeding distance. Looking at the size of the defect area, a very good agreement with the numerical solution is seen. The close correlation also justifies the use of the Niyama threshold value of 0.45 for this particular steel alloy. However, it should be emphasised that the geometrical extension of the shrinkage obtained numerically, to some extend is approximate due to its dependecy on the mesh quality.

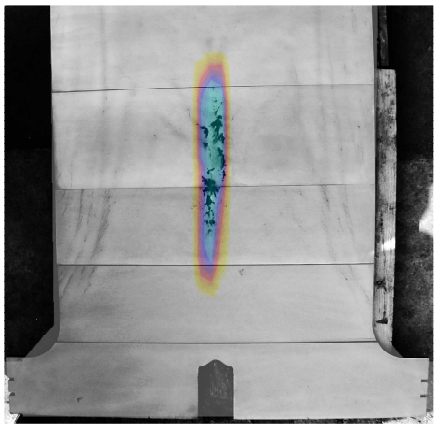

Fig. 6. Prediction of the centerline macro/micro shrinkage and its experimental validation obtained from the foundry.

Figure 7 is a plot of the predicted convection patterns in the bulk liquid and mushy zones during solidification, namely at 7, 11 and 20% respectively. The vectors indicate the direction and velocity of both, the liquid and the mush during solidification. Based on this information one can estimate whether channel segregates will form or not, and where. In essence, just due to density changes the solidifying elements in the mush have higher density than the liquid in the central areas and thus they will sediment down and push the lighter liquid upwards. However, if a strong upward flow within the solidifying mush occurs this could indicate that a narrow channel has been opened, local remelting has occured and highly segregated liquid can flow through, giving rise to a freckle. Indirectly it implies that the cooling ability of the surrounding chills is poor to retain steep thermal gradients and thus to prevent upward, localized flow. Obviously in practice it is nearly impossible to completely avoid channel segregation since the geometry of the casting together with the shape of the chills and of the riser would have to be designed extremely well and still it would not be 100% sure that no problems would occur. Although, by establishing a proper directional and progressive solidification pattern, potential freckles can be either ”pushed“ deep into the casting so that they do not show on the surface during machining

operations or are partially eliminated. Problematic areas with a high risk of freckles are implied by black arrows in the figure. As compared to the casting trial, quite good agreement with the numerical prediction of freckles has been found.

It can also be seen that the V-shaped segregates that formed in the real casting, seen in the photo in **Figure 3,** match very well with the predicted pattern which also resembles a V shape. This might however be a coincidence as the resolution of small scale

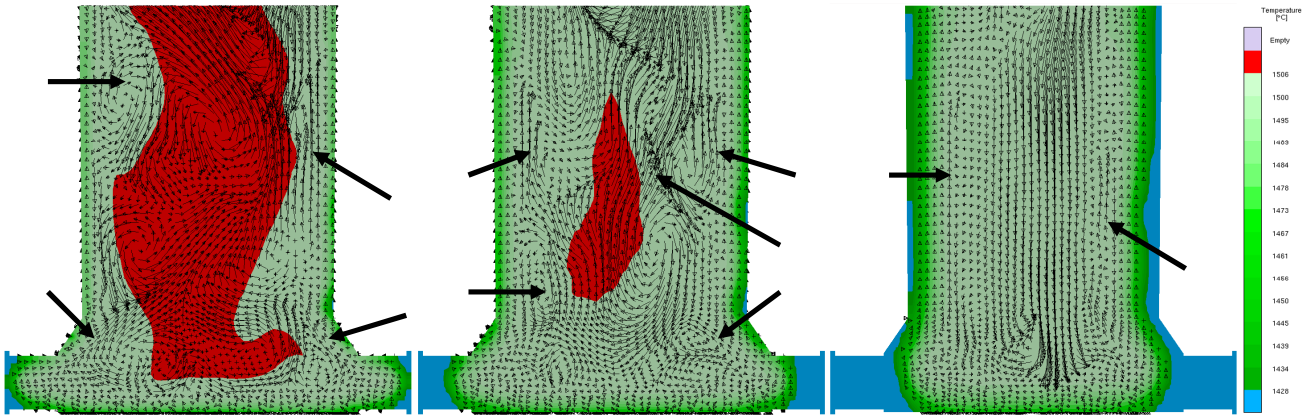

Fig. 7. Convection patterns and velocity vectors at 7, 11 and 20% solidified

Figure 8 shows the predicted carbon macrosegregation pattern in the completely solidified casting placed on top of the photo of the sectioned casting, while **Figure 9** shows the numerical predictions for the entire cast part. It can be seen that the strong flow has created a carbon rich region in the centre of the casting.

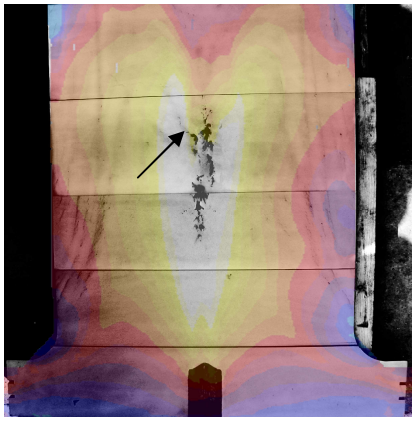

Fig. 8. Calculated and experimentally obtained final C macrosegregation pattern.

It affirms that areas solidifying last, i.e. the hot spots, will be rich in solute elements. These elements have been rejected and pushed away to the remaining liquid by the progressing solidifying front due to their lower solubility at decreasing temperatures, causing positive segregation in the last area to solidify. Due to the isolated liquid pool which has also been a hot spot, all solute elements ended in that region with nowhere to escape, causing positive segregation. These macrosegregation predictions have been compared with the experiment, i.e. samples from the central region have been analyzed with respect to solute composition, and a reasonable agreement has been found.

macrosegregation features such as A or V segregates in large castings is still beyond the current capabilities of the macrosegregation model in the applied software.

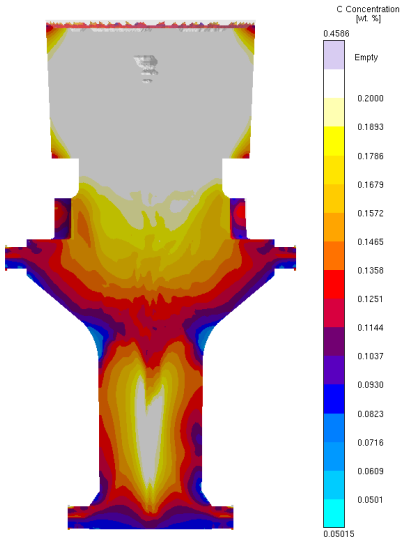

Fig. 9. C macrosegregation pattern for the entire casting

OPTIMIZED RISER AND THE CHILLING SYSTEM

The primary reason for autonomous optimization has been to find a more suitable design of the top riser and of the surrounding chills to increase the casting yield and at the same time to avoid formation of solidification related issues such as centerline porosity, shrinkage porosity and channel segregates seen in the original casting layout. The gating system has been changed from bottom to side filling to be able to place the chill plate underneath the casting. On top of that, cylindrical chills and the riser have been transformed into parametric objects and

subjected to optimization as design variables. The most important condition in assessing the size of the riser has been to avoid the shrinkage pipe penetrating into the riser neck area or even to the casting body. Such designs are then rejected as unsuitable.

The objective space for the optimization problem in **Figure 10** is constructed by two following objectives: Minimization of centerline porosity and minimization of the remaining volume of the top riser. The first objective is represented by the Weighted Volume Niyama criterion which expresses the total volume of areas having issues with centerline porosity. The remaining volume of the riser is then calculated as the geometrical volume of the riser minus the volume of the shrinkage pipe in the riser.

The blue line is the Pareto line which is comprised of the non-dominated trade-off solutions. However, it is still up to the user to determine which solution out of the Pareto set will be the most desirable. In other words, the user has to decide whether he/she wants to minimize the riser as much as possible, at the cost of increased porosity or to have a porosity-free casting with a slightly larger riser, but still smaller than the initial design.

Two distinct designs have been selected. The first one does not lie on the Pareto front and represents the reference solution with the largest riser volume. This solution, even though it appears in the optimization results has not undergone a proper multi-objective optimization. It is entirely based on the manual rearrangement of the chills and the top riser remained unchanged, i.e. it has the same dimensions and casting yield as the original solution. The second design highlighted by the red dashed circle represents the case with the lowest amount of centerline porosity and somewhat reduced remaining volume of the riser.

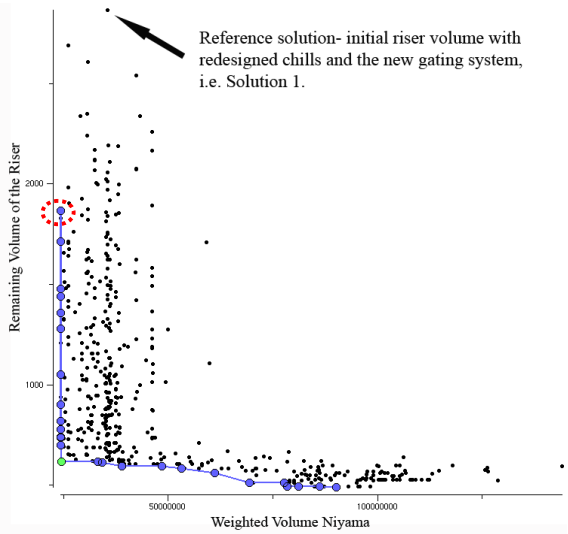

Fig. 10. Design space with the highlighted Pareto set.

The two selected designs have then been evaluated with respect to filling and solidification in the standard simulation environment. The results from filling are not presented. The geometries of the two designs are captured in **Figure 11.** There are a few reasons for choosing what at first glance could appear as modest or conservative designs. First, the primary goal has been to eliminate the presence of centerline porosity and to minimize channel segregation issues as compared to the original solution. To satisfy this objective the focus has been on solutions located very close to the Y-axis, representing minimum centerline shrinkage in **Figure 10**. Centerline shrinkage is directly affected by a pressure drop inside the casting, derived from Darcy`s law of flow in porous media, which represents resistance to feeding of a particular area.

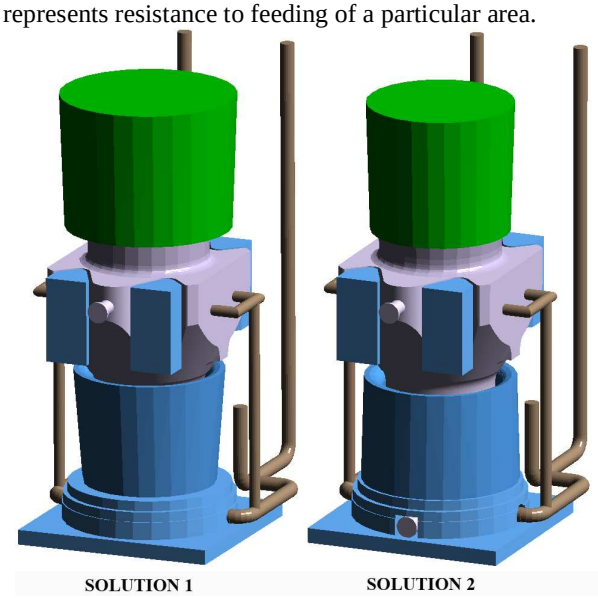

Fig. 11. Selected designs proposed by the optimizer.

To keep the pressure gradient sufficiently high to ensure efficient feeding flow, the height and the total volume of the riser should not be too small. Next, centerline shrinkage usually forms at areas with shallow thermal gradients. To establish steep thermal gradients, the riser should again be sufficiently large and the dimensions of the chills should be chosen so that progressive and directional solidification towards the riser is provided. Considering segregation, it is also known that having steep thermal gradients due to intense chilling results in a finer dendritic microstructure imposing higher resistance for channel segregates to form. Moreover if a progressive and directional solidification pattern exists, it helps to move the highly segregated remaining liquid towards the riser. For this reason one could deduce that centerline shrinkage and macrosegregation phenomena could in principle be treated by the same remedy. Obviously it does not mean that they are driven by the same physical phenomena.

After this brief reasoning we can make an assumption that if the design of the riser and chills yields a favorable solidification pattern, i.e. steeper thermal gradients, directional and progressive solidification, enhanced feeding, to prevent centerline porosity, issues with channel segregation should be reduced somewhat and the

macrosegreation profile should be positively changed as well.

If macrosegregation was not considered in the optimization case, designs with much smaller riser volumes could be chosen with no major risk of issues with porosity. This has been shown in the previous work by the authors[21] where macrosegregation has been disregarded; therefore the selected designs reached much higher casting yields. Information regarding dimensions of the optimized designs is listed in **Table 1**.

Table 1.Comparison of the two optimized designs

	Solution 1	Solution 2
Riser height	1350 mm	1300 mm
Riser bottom D	1660 mm	1380 mm
Riser top D	1760 mm	1463 mm
Height of the cylindrical chills	1150 mm	1050 mm
Bottom thickness of the cylindrical chills	100 mm	220 mm
Top thickness of the cylindrical chills	190 mm	190 mm
Total weight	59650 kg	51143 kg

Regarding the solidification patterns of the two selected designs, no isolated liquid areas have been forming in the bottom area as in the original layout, depicted in **Figure 12**. The bottom chill plate and the new chills around the cylindrical section evoked directional solidification towards the thermal axis and the riser. Solidification patterns were checked over the entire interval. It is also seen, that solution 2 has a more pronounced progressive solidification pattern compared to solution 1, and meaning that the solidifying front progresses towards upper areas in a V shape pattern which is desirable mainly with respect to segregation. The favorable solidification pattern in solution 2 has to do with the dimensions of the top riser and the chills which are different as compared to solution 1. Solution 1 has conical chills extending upwards while solution 2 has conical chills extending downwards, see **Table 1**. Due to more intense heat removal at the top of the cylindrical chills in solution 1, a tendency for choking the remaining liquid pipe is observed, similar to the initial case.

Figure 13 shows the new distribution of centerline porosity. It shows that due to the optimized design of the chills, steeper thermal gradients inside the casting have been achieved. These gradients have changed the morphology of the mushy zone, i.e. decreased its extent, decreased its permeability due to finer grains giving rise to very small and widely distributed pores not detectable via radiographs, etc. Besides that, a more favorable solidification pattern has been evoked, which has led to more enhanced feeding of the remote bottom area. The light blue areas stand for values of 0.45 and lower which will contain macroscopic shrinkage. Everything above 0.45 up to 1 will most likely be microporosity not detectable by radiography techniques. It shows that the casting body and even the riser neck will be free of any porosity issues. Only the bottom pins contain small porous areas. The reasonable remedy would be to enlarge the draft towards the main casting body.

The same pattern applies for shrinkage porosity. The main porous region has been found in the top riser, forming a shrinkage pipe which in both cases has not penetrated even to the riser neck. This can be seen in **Figure 13** as the missing area on the top of the riser.

Fig. 12. Fraction liquid at 45% solidified for the two optimized solutions.

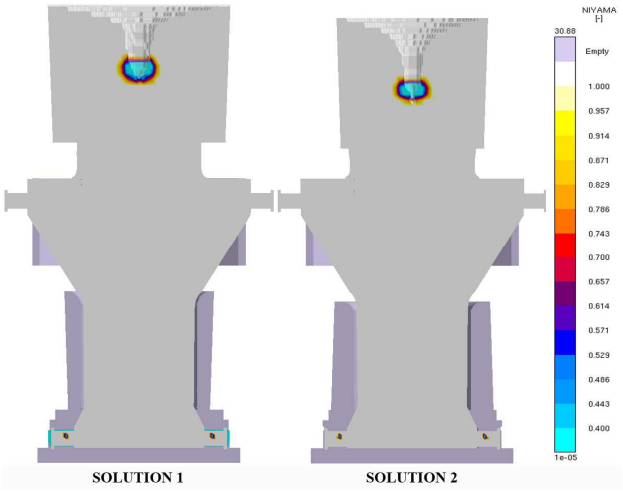

Fig. 13. Comparison of centerline porosity in the optimized designs.

Figure 14 illustrates how the solidification progresses inside the casting and its influence on the convection pattern for both of the optimized designs. Now it is obvious that the optimized chills have induced steeper thermal gradients that have decreased the size of the mushy zone denoted by green color. As compared to the initial situation depicted in **Figure 7,** the liquid area is present for a longer period of time and in a much larger

scale. Steeper gradients have caused an evolution and growth of much finer grains, thereby decreasing the permeability of the mush. Consequently, resistance towards liquid/solid movement and to opening liquid channels which give rise to channel segregates is therefore much higher. Convection is denoted by the vector arrows.

Figure 15 implies the situation at 31% solidified. The probability of forming some channel segregates is rather high for both solutions as quite large streams of upward moving liquid/solid have been observed. Although if any such channel segregates form, they will be found deep enough in the casting not to show on the casting surface after machining operations.

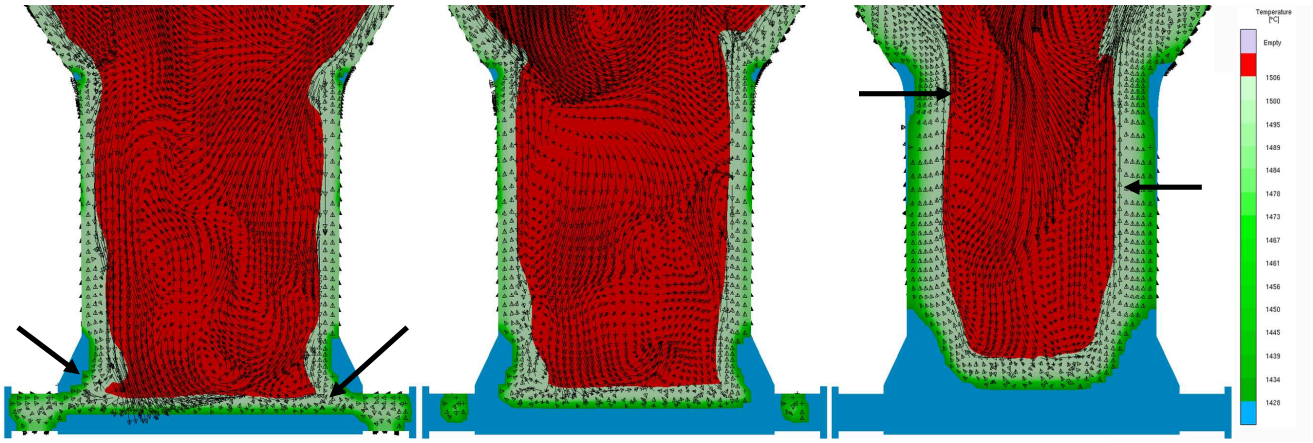

Fig. 14(a). Solidification processing and convection patterns at 7, 11 and 20% solidified respectively for SOLUTION 1.

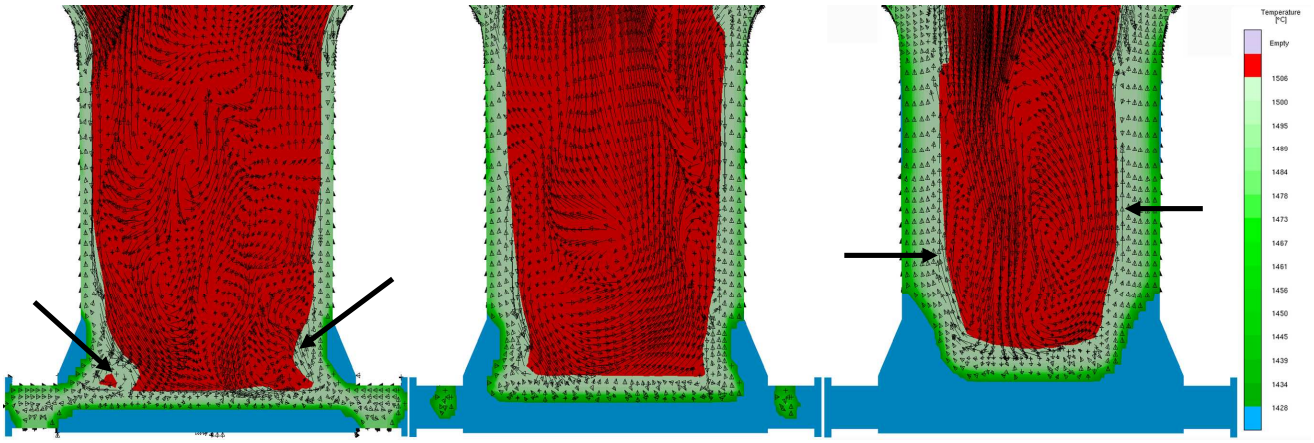

Fig. 14(b). Solidification processing and convection patterns at 7, 11 and 20% solidified respectively for SOLUTION 2

Potential issues with channel segregates are again highlighted by the black thick arrows. At 7% solidified areas adjacent to the bottom pins are very prone to channel segregation because of a sudden increase of velocity oriented upwards and a subsequent local remelting. Moreover due to choking the pins from the open feed path, porosity will form and a positively segregated region will occur which is subsequently proven in **Figure 16**. At 20% solidified the first indications of potential channel segregates at the cylindrical area are noticed. However, there is very little chance that these will form at all since they are in direct contact with the liquid melt which is highly permeable.

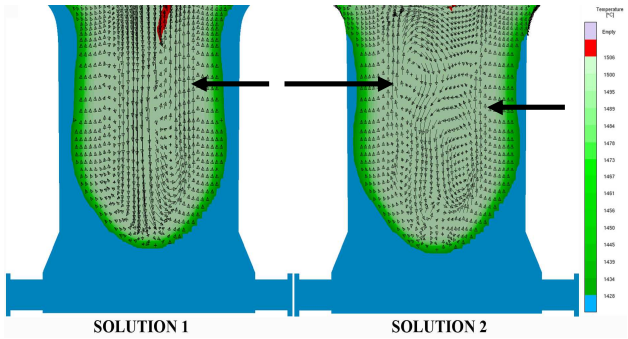

Fig. 15. Convection patterns at 31% solidified for the two optimized solutions.

As a consequence of the modified solidification and convection pattern new macrosegregation profiles have been expected for both optimized solutions. These are captured in **Figure 16**. One can recognize an apparent improvement in the sense that the carbon is distributed more uniformly over the entire lower section which exhibited high positive segregation in the initial layout, see **Figure 9**. When it comes to the under-riser section, solution 1 appears to have a slightly more favorable carbon distribution, while solution 2 seems to have that region highly segregated and thus worse as compared to the original solution. This is for sure attributed to the riser size and shape.

The forging application, for which this part is used, sets high requirements on the under-riser area which should exhibit very good mechanical properties. For this reason, solution 1 would be more beneficial. It should be noted that solution 1 has already been cast according to the optimization results. It has been evaluated, tested and no problems have occurred whatsoever.

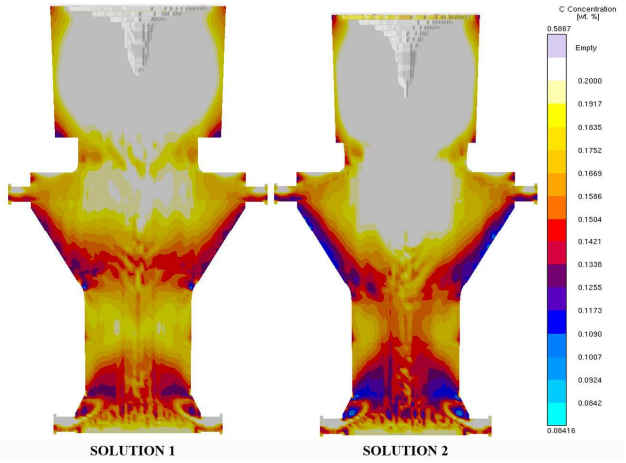

Fig. 16. Carbon macrosegregation patterns for the two optimized solutions.

The last assessment concerns the casting yield. The aim of the entire project has been to eliminate the presence of various casting defects via determination of the proper design of the riser and chills. Simultaneously, increased casting yield has been pursued by optimization. Results of this assessment are given in **Table 2**. Compared to the original design the casting yield could be increased by approximately 19% with no apparent risk of centerline shrinkage and segregation issues.

Table 2. Casting yield assessment

	Original solution	Solution 1	Solution 2
Total weight	59640 kg	59640 kg	51143 kg
Casting Yield	55.36 %	55.36 %	64.9 %

CONCLUSION

This work presented an attempt to perform multi-objective optimization of the solidification pattern of a large steel forging ram. The main idea of this study was to demonstrate how the fully computerized optimization can be effectively utilized for solving several conflicting objectives in daily foundry practice. The intention was to prove that macrosegregation can be addressed by optimization even without prescribing it as one of the objectives which would not be feasible time-wise. It was found that by optimizing the solidification pattern so that directional and progressive solidification with steep thermal gradients is established, one could relatively easily handle multiple issues like porosity and segregation.

The optimization objectives were minimization of the remaining volume of the top riser and the avoidance (minimization) of centerline porosity through which the elimination of macrosegregation issues, particularly channel segregates in the casting body was expected.

The first step was to analyze the original casting layout provided by the foundry. Both filling and solidification analyses were performed and potential flaws and defects were revealed. The result of the improper solidification pattern together with poor chilling was a formation of shrinkage and centerline porosity in the bottom cylindrical area of the part. Besides that, channel segregates were identified in the casting body. These findings were verified by casting trials performed at the foundry. It was thus decided to redesign the gating system from the bottom-fill to the side- fill type, rearrange the chills and implement a new chill plate underneath the casting to promote more intense cooling of that area.

The manually-optimized solution, i.e. solution 1, served as a reference or starting solution for the autonomous multi-objective optimization of the solidification pattern. In the optimization problem, the dimensions of the riser and the chills were applied as design variables together with the allowed ranges of variation. After optimization, one solution was selected from the design space.

The new chill arrangement caused significant improvements in the solidification patterns in both of the solutions. More pronounced cooling established steeper temperature gradients and induced progressive and directional solidification in the problematic bottom area, totally eliminating the shrinkage-related defects. The only porous areas were found in the riser head and in the bottom pins. The casting body seemed free of porosity.

New convection and macrosegregation patterns were obtained giving favorable and promising results. Due to steeper thermal gradients the mushy zone got reduced, its permeability was lowered imposing higher resistance for liquid-solid movement and for potential channel segregation. The resulting carbon distribution seemed more uniform over the casting body, mainly in case of solution 1. As to the under-riser area (in solution 1) which will be heavily cyclically loaded during service, it is

likely to have similar mechanical properties as compared to the initial solution.
Last, findings regarding the casting yield showed that when correctly utilizing multi-objective optimization, it is possible to increase the casting yield substantially and thus reduce production costs.

ACKNOWLEDGEMENTS

The authors would like to thank the Vitkovice Heavy Machinery for identifying the case study and providing us with the casting data necessary to perform the relevant simulations and the photographs of the metallographic analysis for this case study.

REFERENCES

1. MAGMAsoft simulation software, MAGMA GmbH, Aachen, Germany
2. Kotas, P., Hattel, J.H., Thorborg, J., Svensson, I.L., Seifeddine, S., *Proc. International Ph.D. Foundry Conference*, Brno, Czech Republic, (2009).
3. Seifeddine, S., Wéssen, M., Svensson, I.L., *Metallurgical Science & Technology*, Vol. 24, No. 2, pp. 7-, (2007).
4. Sturm J., Hepp, E., Enger-Walter, A., *20th CAD-FEM Users` meeting 2002, International Congress on FEM Technology*, Lake Constance, Germany, (2002)
5. Egner-Walter, A., *CP+T Casting Plant + Technology International*, Vol. 23, no. 1, pp. 24-29, (2007).
6. Monroe, C., Beckermann, C., *Proceedings of the 61st Technical and Operating Conference, SFSA*, Chicago, IL, (2007).
7. Poloni, C., Pediroda, V., *GA coupled with computationally expensive simulations: tools to improve efficiency, chapter Genetic Algorithms and Evolution Strategies in Engineering and Computer Science*, pp. 267-288. John Wiley and Sons, (1997).
8. Fonseca, C., Fleming, P., *5th International Conference on Genetic Algorithms*, USA, (1993).
9. MAGMAfrontier 4.4 Reference Manual, (2005).
10. Hahn, I., Hartmann, G., *Casting Plant & Technology*, Vol. 24, no. 4, (2008).
11. Gramegna, N., Baumgartner, P., Kokot, V., IDEAL International Conference, Lecce, Italy, (October 2005).
12. Niyama, E., Uchida, T., Morikawa, M., Saito, S., *AFS Int. Cast. Met. J.*, Vol. 7, No. 3, pp 52-63, (1982).
13. Carlson, K.D., Beckermann, Ch., *Metallurgical and Materials Transactions A*, Vol. 40A, pp. 163-175, (2009).
14. Carlson, K.D., Ou, S., and Beckermann, C., *Metallurgical and Materials Transactions B*, Vol. 36B, pp. 843-856, (2005).
15. Hardin, R.A., Ou, S., Carlson, K.D., Beckermann, C., *Metall. Mater. Trans. B*, Vol. 33B, pp. 731-740, (2002).
16. Dantzig, J.A., Rappaz, M., *Solidification*, EPFL Press, (2009).
17. Schneider, M.C., Gu, J.P. Beckermann, C., Boettinger, W.J., Kattner, U.R., *Metallurgical and Materials Transactions A*, Vol. 28A, pp. 1517- 1531, (1997).
18. Sigworth, G.K., Wang, C., *AFS Trans*, vol. 100, pp. 989–1004, (1992).
19. Goldberg, D.E., *Genetic Algorithms in Search, Optimization & Machine Learning*, Addison Wesley Longmann, Inc., (1989).
20. Deb, K., *Multi-Objective Optimization Using Evolutionary Algorithms*, John Wiley & Sons, (2001).
21. Tutum, C.C., Hattel, J.H., *Science and Technology of Welding and Joining*, Vol. 15, No. 5, pp. 369- 377, (2010).
22. Poles, S.: 'MOGA-II: An improved Multi-Objective Genetic Algorithm. Technical Report'; 2003, ESTECO s.r.l.
23. Tutum, C.C., *PhD thesis*, Technical University of Denmark, Kongens Lyngby, Denmark, 2009.
24. E. Zitzler, E., *PhD Thesis*, Swiss Federal Institute of Technology (ETH), Zurich, Switzerland, 1999.
25. Kotas, P., Tutum, C.C., Snajdrova, O., Thorborg, J., Hattel, J.H., *International Journal of MetalCasting*, Vol. 4, Issue 4, (2010).
26. Deb, K., *Engineering Optimization*, Vol. 35, No. 5, pp 445-470, (2003)
27. Deb, K., Proc. Genetic and Evolutionary Computation Conf. (GECCO 2006), Seattle, WA, USA, July 2006, ACM, Vol.2, 1629–1636.

D PAPER – IV

Kotas, P., Thorborg, J., Tutum, C.C., Hattel, J.H., "*Elimination of Hot Tears in Steel Castings by Means of Solidification Pattern Optimization*", Metallurgical and Materials Transactions B, 2011 (Submitted).

Elimination of Hot Tears in Steel Castings by Means of Solidification Pattern Optimization

P. Kotas
Technical University of Denmark, Department of Mechanical Engineering, Kgs. Lyngby, Denmark

J. Thorborg
MAGMA GmbH, Kackertstrasse 11, D-52072, Germany

C.C. Tutum
Technical University of Denmark, Department of Mechanical Engineering, Kgs. Lyngby, Denmark

J.H. Hattel
Technical University of Denmark, Department of Mechanical Engineering, Kgs. Lyngby, Denmark

ABSTRACT

A methodology of how to exploit the Niyama criterion for elimination of various defects such as centerline porosity, macrosegregation and hot tearing in steel castings is presented. The tendency of forming centerline porosity is governed by the temperature distribution close to the end of the solidification interval, specifically by thermal gradients and cooling rates. The physics behind macrosegregation and hot tears indicate that these two defects are also heavily dependent on thermal gradients and pressure drop in the mushy zone. The objective of this work is to show that by optimizing the solidification pattern, i.e. establishing directional and progressive solidification with the help of the Niyama criterion, macrosegregation and hot tears issues can be both minimized or entirely eliminated.
An original casting layout was simulated using a transient 3D thermal fluid model incorporated in a commercial simulation software package to determine potential flaws and inadequacies. Based on the initial casting process assessment, multi-objective optimization of the solidification pattern of the considered steel part followed. That is, the multi-objective optimization problem of choosing proper riser and chill designs has been investigated using genetic algorithms while simultaneously considering their impact on centerline porosity, the macrosegregation pattern and primarily on hot tear formation.

Key Words: Casting process simulation, genetic algorithms, solidification pattern optimization, macrosegregation, centerline porosity, hot tearing

INTRODUCTION

Twenty years after the introduction of simulation software for foundries into the industry, casting process simulation has become an accepted tool for process and design lay-out.
Metal casting process simulation is used to provide detailed information about the mold filling, solidification and solid state cooling, and with that, also information about the local microstructure, non-uniform distribution of mechanical properties and subsequently residual stress and distortion build-up[1-9]. Casting simulation tries to use physically realistic models without overtaxing the computer. At the same time the simulations need to give applicable results in the shortest time possible.
Due to the multitude of factors affecting the quality of castings and the complex interactions of physics, metallurgy and casting geometry, empirical knowledge is the main source on which “optimized manufacturing engineering” is based. Foundry simulation can quantify experience but unfortunately, it can only test one “state” or layout. It provides insights into the root causes of problems, while conclusions from calculations or subsequent optimization still require an engineer’s interpretation and decision after each of the simulation runs. This means that a continuous improvement involves “trial and error”- both in reality and in simulation.
In recent years the usage of simulations software has improved and now integrates parallel processing computers. It is feasible to calculate numerous versions and layouts in almost unlimited configurations. The advantage of having such short calculation times can only be utilized providing that a computer can automatically analyze calculated variants with respect to predefined objectives (e.g. maximum feeding, low

porosity, low air entrapment etc.) and subsequently create new variants and analyze them in the same manner to achieve the optimal solution. By integrating such software for casting process simulation with an optimization algorithm, a computer based optimization tool is established which is able to determine optimal values of user-defined design variables thereby optimizing a given casting process with respect to predefined objectives[10].
Autonomous optimization uses the simulation tool as a virtual test field. By modifying pouring conditions, gating designs or process parameters, the software tries to find the optimal route to fulfill the desired objective. Several parameters can be changed at the same time and be evaluated independently from each other. Autonomous optimization tools combine the classical approach of foundry engineers, to find the "best compromise" with validated physics. This not only further reduces the need for trial runs to find the optimal process window, but also allows an in-depth evaluation of many parameters and their individual impact on providing a robust process. Subsequently such system can readily provide optimal solutions for any kind of casting processes[11-16].
This paper details multi-objective optimization of the solidification pattern of a steel wedge shaped casting and its effect on defects distribution, i.e. hot tears.
The study includes two distinct layouts. The initial layout is provided by a manufacturing foundry. The second layout is generated by the numerical optimization tool. Both of the designs are simulated including the filling of the mold cavity to obtain an accurate temperature field inside the casting for the following solidification simulation. After the filling simulation, a thermal analysis together with stress-strain calculations are performed to get an insight into the thermal behavior of the cast part together with predictions of thermally induced stresses and strains. In case of the first layout no computerized optimization is involved. Conclusions and proposals are derived from the various investigations and findings in the study, and are presented in the last section of the paper.

METHODS

DESIGN OF THE CASTING LAYOUT

The project involves a large (84,6 ton, max height = 4280mm, max width = 2881mm) steel wedge-shaped casting made of a low carbon steel alloy DIN 1.1165, (GS30Mn5), poured into a furan bonded silica sand mould. Two insulated top risers are placed on top of the casting, directly above the critical regions with the highest mass accumulation, shown in **Figure 1**. The main cylindrical padding is insulating, the melt surface is covered by an exothermic powder and on top of that additional insulating powder is applied. The original casting arrangement is filled from the bottom, which is generally considered the best way of avoiding disintegration of the melt during mold filling[17], assuming an initial pouring temperature of 1550°C. The filling time is estimated to 120s. Two bottom-pour ladles accommodating a total volume of 86 tons are simultaneously used to fill the casting. One hour after filling, additional top filling of the risers takes place to compensate for the volumetric shrinkage and to induce favorable temperature gradients. Directional and progressive solidification shall also be promoted with the help of cooling chills that are properly placed, mainly at the bottom of the casting. These chills are placed approximately 30mm deep in the sand mould, i.e. non-contact chills, to avoid the risk of hot tears when using contact chills.

Fig. 1: The initial casting layout investigated in this work after shake out from the sand mould and after burning off the top risers.

NUMERICAL MODELLING

The casting process simulation starts with the geometry defined as a 3D CAD model of the casting, mold, gating, chills, riser and the insulating padding, see **Figure 2**.

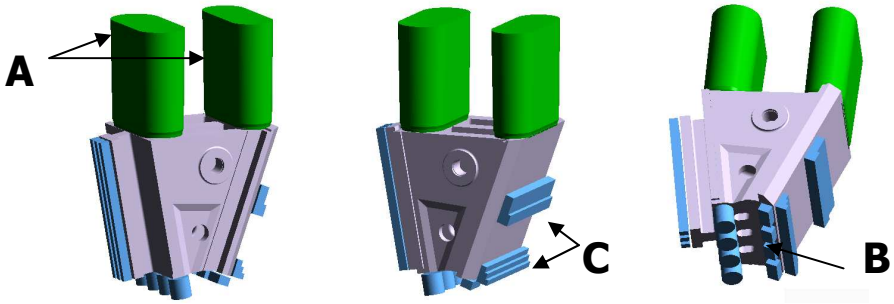

Fig. 2: 3-D visualization of the original casting layout with its characteristic feeder design and chill patterns applied in the initial numerical calculations. This layout was then subjected to optimization. Characters A, B, C indicate groups of design variables for the subsequent optimization.

Material group definition is made in the software's preprocessor. Next, the geometry is properly meshed and all necessary information relating to the molten metal chemistry, pouring temperature; flow properties, interface heat transfer coefficients (HTC), thermodynamic properties, and mechanical properties must be introduced into the system.

In the mesh generator of MAGMAsoft, Solver 5 for filling simulations has been applied to take advantage of improved features, (as compared to lower level CFD-solvers in the software), such as variable viscosity, improved wall friction model, improved pressure-velocity calculations and also a Cartesian cut-cell method which is applied to the equations, i.e. momentum equations, pressure equation, thermal energy equation, free surface equation and venting model, to minimize the effect of the stair-step profiles of the boundary in the calculation mesh, i.e. Cartesian grid[1].

The summary in **Figure 3** shows an overview of the sequence of casting simulation modules.

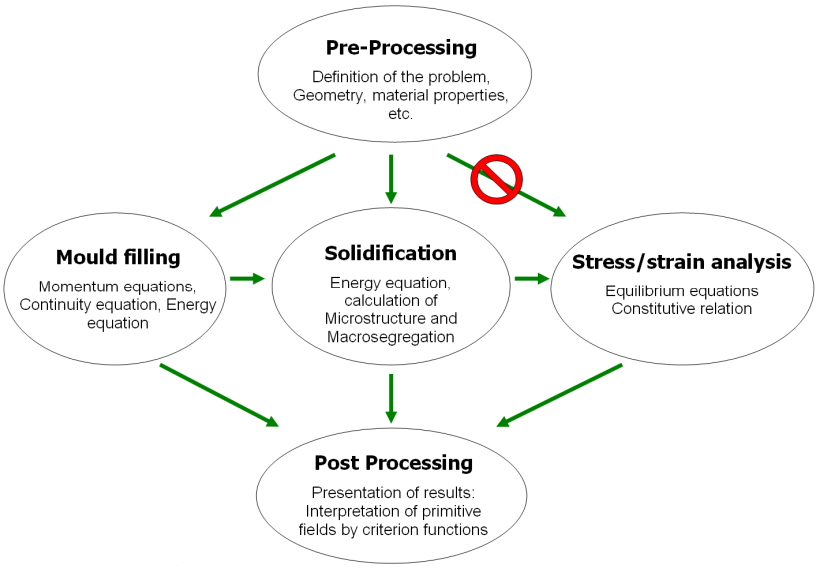

Fig. 3: Flow diagram of the interrelationship of casting simulation modules, figure inspired by Hattel[18].

When all process parameters are entered, filling of the casting can be simulated. A flow rate boundary condition is selected to control the filling process which accounts for a change in overpressure during filling using bottom-pour ladles. Once filling is modeled, the resulting temperature fields in the casting are taken and used as an input for the subsequent heat transfer calculation during solidification and solid-state cooling of the casting. The heat transfer calculation gives temperature fields and distributions of various defects arising during solidification and further cooling. Results predicting defects occurrence, i.e. shrinkage porosity, centerline porosity, macrosegregation etc., are used to evaluate the casting soundness and its overall quality. Only after computing the temperatures the deformation can be evaluated. When stress-strain prediction is needed, an additional simulation is run. Temperature and porosity both drive deformation by casting shrinkage. In reality,

deformation occurs at the same time as the temperatures are dropping and porosity is forming. It is usually accepted to calculate the deformation in a sequence and not as a codependent calculation. The validity of the distortion prediction is dependent on representative simulation results obtained for the temperature distribution. Not only representative final results are needed, but the entire calculated history must be validated to predict the final casting shape and residual stresses[19]. An outline of the simulation analyses performed at various stages of this project is given in **Table I**.

Table I. – Indication of the differences in complexity of the simulation analyses for the original and final layouts as compared to the optimization procedure.

	Filling	Solidification		Stress-strain analysis	Hot tear analysis
		Thermal analysis	Convection, macrosegregation		
Original layout	YES	YES	YES	YES	YES
Optimization procedure	NO	YES	NO	NO	NO
Optimized layout	YES	YES	YES	YES	YES

BACKGROUND ON DEFECTS FORMATION

CENTERLINE POROSITY- THE NIYAMA CRITERION

In modeling of casting processes, special criteria have been developed to indicate areas of the casting where particular problems, e.g. shrinkage, hot tears or mould erosion, can be expected. A very important part of the solidification analysis is the evaluation of the feeding efficiency. Several criterion functions have been suggested for that purpose. A criterion function based on only the temperature gradient for predicting centerline porosity was suggested by Pellini[20] as early as in 1953. Later on, in 1982, this criterion was improved by Niyama[21]. By comparing the results of solidification simulations and observations of centerline shrinkage problems in steel castings, Niyama and co-workers were able to relate the development of centerline shrinkage to the temperature gradient and cooling rate, both of which are assessed at a specified temperature near the end of solidification, see **Eq. 1**. Shrinkage porosity predicted by the Niyama criterion usually forms in the mushy region at high solid fractions. At lower solid fractions, the pressure drop which governs this type of porosity is negligibly small. Therefore, in a casting simulation, the Niyama criterion is always evaluated at a temperature near the end of the solidification interval.

$$Niyama = \frac{G}{\sqrt{\dot{T}}} \qquad \text{Equation 1}$$

With the help of the Niyama criterion, it is feasible to predict the presence of centerline shrinkage porosity, i.e. micro- and macro-shrinkage in alloys with short freezing range such as steels, caused by shallow temperature gradients[22-24]. It indicates that in regions that solidify quickly, there must be hot metal nearby to establish a high gradient to feed the shrinkage during solidification.

Although at first glance, the Niyama criterion may appear to be purely an empirical relationship, it also has a physical interpretation. The model begins with Darcy's law, which relates the interdendritic feeding-flow velocity to the pressure drop across the mushy zone, see **Eq. 2**.

$$\frac{dP}{dx} = \frac{\mu_L (1 - f_S)}{K} u_L \qquad \text{Equation 2}$$

where p is the pressure, μ is the viscosity of the liquid, f_S is the solid fraction, K is the permeability of the mushy zone and u_l is the liquid velocity in the mushy zone (i.e., shrinkage velocity). By making simplifying assumptions about the functional form of the solid fraction-temperature curve and the permeability, Niyama et al., were able to analytically integrate the one dimensional (1-D) form of Darcy's law to demonstrate that

$$\Delta P = M \cdot (\dot{T}/G)^{-2} = \frac{M}{Niyama^2} \qquad \text{Equation 3}$$

where ΔP is the pressure drop across the mushy zone and M is a material constant. This inverse relationship shows that the pressure drop increases as the *Niyama* value decreases. If an assumption is made that porosity forms at a critical pressure drop, then this critical value is more likely to be exceeded when the *Niyama* value is small[18]. By comparing experimentally observed shrinkage porosity patterns in cast-steel cylinders to

corresponding casting simulations, Niyama et al. discovered that, indeed there was a threshold value of *Niyama* below which shrinkage was typically present. When the *Niyama* value decreases below a critical value, small amounts of micro-shrinkage begin to form. As the *Niyama* value decreases further, the amount of micro-shrinkage increases until it becomes detectable on a standard radiograph. This transition occurs at a second critical value. Both of these threshold values are heavily dependent on the composition of the alloy and in some cases on the casting process conditions.

While the presence of the temperature gradient in **Eq. 1** is not surprising, and implies that shrinkage porosity will form in regions of low *G*, the presence of the cooling rate in the denominator may at first seem counterintuitive. The Niyama criterion predicts that shrinkage porosity increases with increasing cooling rate, because the feeding-flow velocities and the resulting pressure drop across the mushy zone are higher for higher solidification rates. One could also say that if the cooling rate is high, there is not enough time to supply the required melt into the needy area to compensate for the volumetric shrinkage and consequently a pore will form. It follows that the beneficial effect of a chill, for example, is due to the increase in the temperature gradient the chill provides; the concomitant increase in the cooling rate near a chill is actually counterproductive with regard to avoiding shrinkage porosity[22].

The Niyama criterion only predicts feeding-distance related shrinkage for short freezing range cast alloys; it does not explicitly predict hot spots in a casting, and it does not predict gas porosity[21].

In this paper it will be shown how the centerline porosity, represented by the Niyama criterion can be effectively used to eliminate both macrosegregation and hot tearing by optimizing temperature distribution and primarily thermal gradients in the casting.

MACROSEGREGATION

Solute composition inhomogenity on the macroscopic scale of a casting- a phenomenon commonly known as macrosegregation – is undesirable for several reasons. First, such inhomogenity cannot be removed by heat treatment, as the time required for solid state diffusion to occur at this scale is prohibitive. Second, macrosegregation results in spatial variations of the mechanical properties after heat treatment and thus in in-service behavior of a cast part due to the concomitant spatial variations in the amount, nature and size of the precipitates. Third, macrosegregation can lead to the formation of gross compositional defects such as freckles, also called segregated chimneys. Macrosegregation is caused by relative movement or flow of segregated liquid and solid within the mushy zone during solidification. There are four major causes of macrosegregation, these are [25]:

(a) *Macrosegregation associated with solidification shrinkage*, i.e. flow that feeds the solidification shrinkage and the contractions of the liquid and solid during cooling.

(b) *Macrosegregation associated with natural or forced convection*. If the velocity of the liquid is perpendicular to the solute gradient, no macrosegregation occurs. However, macrosegregation is induced when the flow enters or exits the mushy zone.

(c) *Macrosegregation associated with grain movement*. As long as the grains move with the same velocity as the liquid, there is no macrosegregation. However, equiaxed grains have a tendency to sediment or, in certain cases, to float, giving rise to macrosegregation.

(d) *Macrosegreation associated with deformation of the solid network* in the mushy zone due to thermal and shrinkage stress, head pressure, or external forces on the solid shell. In other words, the mushy solid behaves like a sponge causing the liquid to be expelled (when in compression) or sucked in (when in tension).

Flow due to thermal and solute gradients in the liquid leads to formation of so-called channel segregates, commonly referred to A- segregates or freckles. Freckles are typically initiated by convective instabilities above or inside the mushy zone, i.e. when the velocity of the liquid in the mushy zone exceeds that of the isotherm and the segregated interdendritic liquid becomes less dense than the overlying bulk liquid of original composition. This phenomenon eventually leads to open channels, i.e. local remelting due to solid fraction decrease, in the mush through which the solute-rich and low-density liquid flows upward into the bulk liquid region. These open channels are associated with local increase in permeability which allows for the liquid to flow more easily, thus enhancing remelting and macrosegregation. When the channels eventually freeze, they appear as pencil-like chains of equiaxed crystals that are highly enriched in solute[26]. It has been shown in the literature[25] that if temperature gradients and the casting speed, i.e. isotherm velocity, are high enough, freckles are less likely to form. One could thus argue that in this regard centerline porosity and channel segregations follow a similar trend although; they are not necessarily governed by the same physical phenomena. It means that in principle enhanced thermal gradients and progressive directional solidification with sufficiently tapered pool of liquid metal[27] should decrease the risk of both of these defects. Therefore in the present work, the major focus will be put on optimizing the chilling system to evoke favorable thermal gradients and to establish a pronounced progressive and directional solidification pattern.

HOT TEARS

Hot tearing is one of the most common and serious defects encountered in large steel castings. Hot tear defects require extensive rework, which significantly increases costs. In some instances, several iterations of part inspection repair and heat treatment can be required, which are both labor and energy intensive. Hot tear defects that are not properly repaired or are not discovered, can result in failure initiation sites during service. These troublesome defects can occur internally in a casting or on the surface of the casting. These cracks may be large and visible to the naked eye or small and found only by magnetic particle inspection. They are caused by a combination of thermal effects, such as hot spot size, and casting restraint, like cores in cylindrical castings. In addition, the composition can affect hot tearing tendency. Physically, two factors contribute to hot tearing in the mushy zone. Hot tears are formed when the mushy zone is cut off from liquid feeding and is under tensile loading[28].

First, liquid feeding is the flow of liquid metal into the mushy zone to account for volumetric shrinkage as the liquid becomes solid. The mushy zone accumulates volumetric changes both through shrinkage, which is the density change as liquid metal solidifies to solid metal, and by the externally imposed volumetric strain from e.g. thermal contraction. The mushy zone is analogous to a sponge as shown in **Figure 4**. Initially, liquid may flow through, like the sponge, but as solidification continues the permeability of the sponge decreases which restricts liquid metal flow. Eventually the flow is cut off and the remaining liquid pockets become isolated. As long as the liquid pressure is sufficient to drive liquid into the pockets, no porosity will form. But when the pockets become isolated the liquid will not feed the contraction during solidification and porosity forms. With this approach, hot tear should not occur as long as there is no lack of feeding of the solid phase with the liquid. This was the basis for Feurer[29] who used hindered feeding as a driving factor for porosity and hot tear occurrence. He focused on the pressure of the liquid present between the grains and argued that a hot tear will nucleate as a pore if the liquid is no longer able to fill these interdendritic openings caused by the solidification shrinkage. He considered that the feeding depends on the permeability of the mushy zone which is largely dependent on the thermal gradients and cooling rates. Later on, a two-phase model of the semi-solid dendritic network was developed by Farup[30] in which the pressure drop of the liquid phase in the mush together with tensile stress caused by thermal contraction of the solid are considered as a cause of hot tear formation. This supports the assumption that it must be possible to eliminate hot tears by means of the Niyama criterion which is a pure thermal criterion and is physically linked to the pressure drop over the mushy zone as seen in **Eq. 3**.

Second, tensile solid deformation is also necessary for hot tears. In the sponge analogy, tensile deformation stretches the sponge. Alternatively, compressive deformation squeezes the sponge and may eliminate porosity and hot tears. Tensile deformation can result when the thermal contraction of the solid areas of the casting are restrained. Restrained thermal contraction may occur, when metal surrounds a core or if an already solid casting feature pins the contraction at a hot spot. When the mushy zone in a hot spot is being deformed in tension, solid dendrites or grains are pulled apart. This circumstance is illustrated schematically in **Figure 4**.

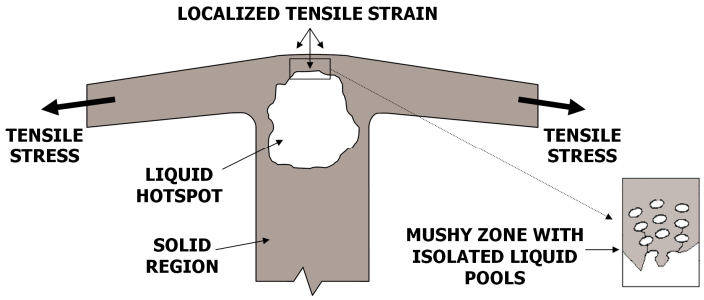

Fig. 4: Schematic of a deformed mushy zone. Tensile stress in one area can evoke tensile strains localized in a distinct area. If that area is still mushy and improperly fed, the tensile strains can easily facilitate hot tearing in that weak spot. Figure inspired by Monroe[31].

As the solid colder pieces at the edge of the mushy zone are pulled apart by contraction, additional liquid metal must flow into the mushy zone to fill this space. If liquid is not available under tensile loading, due to the feeding flow being cut off, additional porosity may form. This porosity forms late in the solidification, along grain boundaries and it is the initiation site for a hot tear.

Considering the composition of the melt, the addition of sulfur and phosphorus will not change the fundamentals mentioned above. Instead, sulfur and phosphorus will segregate to the grain boundaries and depress the solidus temperature. As mentioned before, this last liquid to solidify is on grain boundaries, which under tensile deformation will easily separate. The depressed solidus temperature increases the time that tensile

strain may accumulate when flow is cut off[32]. Hence one can see that unfavorable macrosegregation profiles in the casting also facilitate hot tearing to a large extent.
The right conditions for hot tearing can occur from (1) casting design; normal contraction of thinner sections causing deformation or restraint of thicker sections which cool more slowly, or (2) bulk resistance of the mold and core, which prevents contraction of a casting, or (3) the rigging design, especially if feeding is marginal, by providing additional restraints or due to the high thermal gradients that are often needed to achieve directional solidification. In a complex-shaped casting, hot tearing may occur as a result of the combined effect of the aforementioned causes[33]. A very thorough summary of many mechanisms of hot tearing and conditions that may lead to it is given in the work of Eskin and Katgerman[34].

OPTIMIZATION PROCEDURE

In the present study, unknown optimal shapes and sizes of the two top risers as well as the chills are sought by means of autonomous optimization to obtain a better solidification pattern of the casting which would eliminate the likelihood of hot tearing. This issue has been addressed by defining the problem as a multi-objective optimization problem (MOP) via combining multiple conflicting criteria, i.e. the minimization of the riser volume together with the minimization of the presence of centerline porosity. The decisive factors for the occurrence of centerline porosity, macrosegregation and hot tears are the same, i.e. low thermal gradients combined with an unprogressive solidification pattern. Therefore, the focus has been put on elimination of hot tears by the minimization of centerline porosity by establishing enhanced thermal gradients and a progressive solidification pattern inside the casting. The multi-objective genetic algorithm (MOGA) [35] has been applied to handle these multiple objectives. In the following sections, a brief description of MOP and genetic algorithms is given followed by an introduction to the optimization problem at hand.

INTRODUCTION TO MOP AND MOGA

When multi-objective optimization is utilized, the user defines not only the degrees of freedom for the process parameters but also a number of objective functions which may be conflicting and are to be either minimized, maximized, or a combination of these. This often results in having multiple *trade-off* solutions associated with different amount of *gains* and *sacrifices* among multiple criteria, providing that the objectives are conflicting.
In case of single-objective optimization problems, it is easier to identify the optimal solution as compared to the case of MOP where there is more than one criterion to investigate and satisfy, hence more than one best (elite) solution to consider.
As it was put forward by Goldberg[36] "if we refuse to compare apples to oranges, then we must come up with a different definition of optimality, one that respects the integrity of each of our seperate criteria" which points out the concept of Pareto Optimality, correlated to the fundamental concept of domination. Since the concept of domination allows a way to compare solutions with multiple objectives, most MOP algorithms use this domination concept to search for non-dominated solutions, i.e. the ones that constitute the Pareto-front as shown **in Figure 5(c)**. This concept can be explained with a simple example in a 2D objective space, in which the minimization of both objective functions (i.e. f_1 and f_2) is considered, as shown in **Figures 5(a-c)**. In **Figure 5(a)**, point-1 representing a solution or a design which splits the 2D objective space into two zones: the first zone (the shaded region); the set of the points dominated by point-1, and the second zone; the set of points not dominated by point-1 (the remaining three quadrants), i.e. the non-dominated or noninferior set of points. Thus, the two conditions stated below need to be satisfied if point-1 dominates point-i, where point-i is any other design point in the objective space[37]

- point-1 is no worse than point-i in all objectives.
- point-1 is strictly better than point-i in at least one objective.

These two statements give a general description for the comparison of the two solutions in terms of "betterness", hence emphasizing the applicability of this comparison for other types or combinations of conflicting objectives besides the minimization – minimization type as shown in **Figures 5(a-c**), i.e. maximization - maximization, maximization – minimization as well as minimization - maximization. . In case of the aforementioned minimization-minimization problem, it is formulated as follows[36, 38]

$$(\forall j : f_j(x_1) \leq f_j(x_i)) \bigcap (\exists k : f_k(x_1) < f_k(x_i)) \qquad \text{Equation 4}$$

where x_1 represents point-1 in **Figure 5(a)** and x_i represents any design point-i in the same 2D objective space. **Eq. 4** can be put in words as; at least ($\exists$) in one objective, design-1 is "strictly less" than design-i, while in others ($\forall$) they might be equal.
In case of having a population composed of e.g. five points as shown in **Figure 5(b)**, a need for an overall relation of dominance arises, i.e. the one-to-one comparison made for point-1 should be generalized for each

point. **Figure 5(b)** shows the distribution of these five points together with their domination regions which are distinguished with different tones of colors and it is clearly seen that point-4 dominates points-1, 2 and 5 with respect to all objectives, while point-3 dominates all other points (i.e. strictly better) only with respect to the first objective for the given distribution. However, since points-3 and 4 are not dominated by any other points, they constitute the non-dominated front which is also called the Pareto-optimal front, see **Figure 5(c)**, in an MOO context. A similar comparison will reveal that point-1 and point-5 constitute the next domination front which in itself is dominated by the Pareto front and shown as the closest dashed line to the Pareto front in **Figure 5(c)**[39].

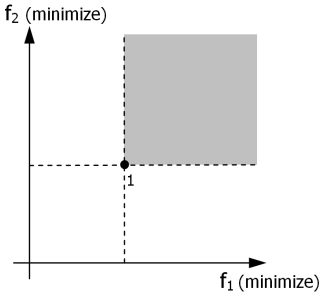

Figure 5(a) The two separate sets of solutions defined with respect to point-1: i) the set of dominated solutions (the shaded region), ii) the set of non-dominated solutions (adapted from [39]) [40].

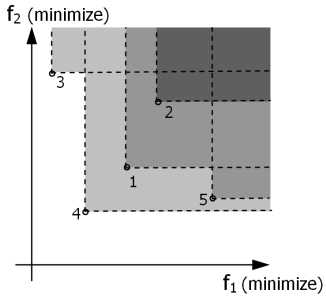

Figure 5(b) Each solution in a population has its own sets of dominated and non-dominated solutions (inspired by [38]) [40].

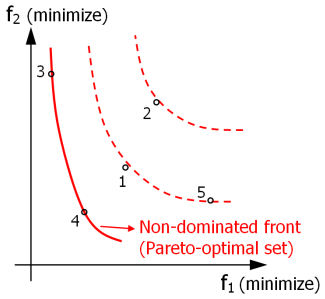

Figure 5(c) The dominated and non-dominated (Pareto-optimal) fronts [40].

The actual optimization cycle is initiated by establishing a first generation, i.e. set of solutions, containing a user-defined amount of individuals, referred to as initial population or Design Of computational Experiments (DOE). Each individual represents one configuration for the considered set of design variables, i.e. the dimensions of the top risers together with the dimensions and the position of the chills. For each of these designs an analysis of solidification and solid-state cooling is performed and the values for the requested output variables are calculated. The output data is used to evaluate and compare the different designs. After the first generation has been calculated, the optimization algorithm evaluates the designs with respect to the objective functions and constraint(s) and subsequently generates a new set of solutions using mathematical mechanisms that follow the concept of natural genetics, i.e. selection, reproduction, cross-over and mutation. This iterative evolution strategy is consequently referred to as a Genetic Algorithm[33]. The flow chart of the above described optimization procedure is depicted in **Figure 6.**

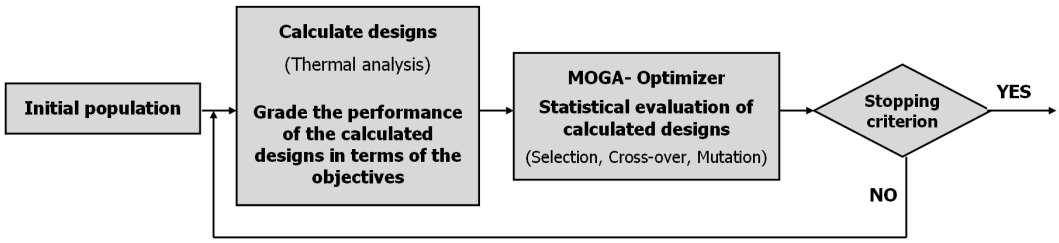

Fig. 6: Flow chart of the optimization process (adapted from [41]).

GAs do not need any gradient information in their search process. Thus, they are very suitable for black-box (e.g. commercial software) optimization applications. Moreover, as compared to classical optimization techniques based on a single solution approach, genetic algorithms can effectively utilize distributed computing facilities because of their population based approach, i.e. all individuals (designs) can be computed independently. GAs are typically able to provide a larger spectrum of Pareto-optimal solutions without any additional problem specification as in some algorithms designed specifically for the SOP problems. This ideal approach of evolutionary MOO algorithms replaces some of the potential weaknesses of gradient based algorithms in some cases, e.g. when having a non-continuous or non-convex search space. The availability of trade-off solutions, representing varying preference levels between chosen objectives, makes it easier for a user to choose a particular solution for further implementation[41-45].

OPTIMIZATION OF THE SOLIDIFICATION PATTERN

As briefly mentioned above, the optimization problem is defined as the goal of finding the most suitable shapes of the two top risers and the proper placement and shapes of chills surrounding the casting, which provide a set of trade-off solutions for the minimization of two conflicting objectives. These are, (i) to design the top risers and the surrounding chills so that the casting is sound (i.e. with minimum centerline shrinkage porosity, evenly distributed concentration profiles of solute elements and no hot tears) and (ii) at the same time having top risers' volume as small as possible to increase the casting yield. In this context, 'casting yield' is defined as the weight of the fettled casting divided by the gross weight including the riser and the gating system. This unconstrained multi-objective problem can then be expressed in mathematical terms as

$$\begin{aligned} &\text{Minimize:} \quad f_1(\mathbf{x}) = \mathbf{V_{riser}} \\ &\text{Minimize:} \quad f_2(\mathbf{x}) = \mathbf{Weighted\ Volume\ Niyama} \\ &\qquad x = \{a_{1-5}, b_{1-4}, c_{1-12}\} \end{aligned} \qquad \text{Equation 5}$$

$$\text{where } \mathbf{Weighted\ Volume\ Niyama} = \sum_{\substack{i=1 \\ Niyama_i < Niyama_{cr}}}^{N_{cell}} V_i \cdot 2^{\,\mathrm{int}\left(10 \cdot \frac{Niyama_{crit} - Niama_i}{Niyama_{crit}}\right)} \qquad \text{Equation 6}$$

where V_i is a volume of a cell, $Niyama_{crit}$ is a critical value of 0.7. Information received from the weighted volume Niyama values is regarding the volume of the mesh affected by a poor Niyama value, i.e. below the critical value of 0.7.

Prior to optimization, it is necessary to parameterize the model in order to vary considered design / process parameters. The primary aim of the optimization process is then to change the solidification pattern of the casting so that hot tears are eliminated. In other words, to establish directional and progressive solidification towards the top risers with favorable thermal gradients, to eliminate centerline and shrinkage porosity and segregation issues. As it was already discussed above all of these phenomena directly promote hot tearing.

In total there have been 21 independent design variables (those which are changed / updated during optimization) used in the optimization procedure, which are: placement and dimensions of the chills- height, width and thickness, and of the top risers –their height, bottom and top diameters. The design variables were split into three groups and are highlighted in **Figure 2,** where group A(a_{1-5}) contains all variables for the two top risers, group B(b_{1-4}) contains variables for the four bottom brick-like chills and group C(c_{1-12}) comprises variables for the two sets of chills on the right hand side of the casting. It would be very time consuming to calculate thermal convection, segregation and hot tears prediction for each design during the optimization cycle. Thus, only the selected designs constituting the final Pareto line are analyzed with respect to macrosegregation and hot tearing, see **Table I**.

The initial population for the MOGA containing 100 unique sets of designs is provided by the Sobol DOE sequence generating technique which is a quasi-random sampling technique[46]. The points in this type of sequence are maximally avoiding each other, so the initial population fills the design space in a uniform manner. The assumed optimization problem is constrained only by the predefined ranges of variation of the design variables. The directional cross-over, the selection and the mutation probabilities of 0.6, 0.3 and 0.1, respectively, are chosen for running 20 generations giving in a total number of 2000 solutions. In addition, elitism is applied to accelerate convergence in the optimization problem. Elitism is a GA operator (in general, an evolutionary algorithm operator) which saves the best designs found so far during the evolution of the generations.

RESULTS AND DISCUSSION

In the following sections, results obtained from the simulations and casting trials are presented and discussed. First, the numerical and experimental results from the original casting assembly are analyzed to establish a base case. Then, the results from the multi-objective optimization problem (riser volume and chill size optimization) are presented.

CASTING AND SIMULATION RESULTS – ORIGINAL LAYOUT

The original casting arrangement depicted in **Figure 2** was cast using the process parameters indicated in the beginning of this paper. After the shake out, a massive hot tear was found in the middle rib, going diagonally from the left top riser down to the right, across the top cylindrical core, see **Figure 7**. The rib was found to be torn completely from both sides. Obviously, this defect was impossible to repair weld, making the casting a scrap. The hot tear was found before burning off the two top risers.

Since hot tears can be assumed to be driven by the thermal behavior of the casting, the major emphasis was put on the solidification stage and its optimization by means of the Niyama criterion.

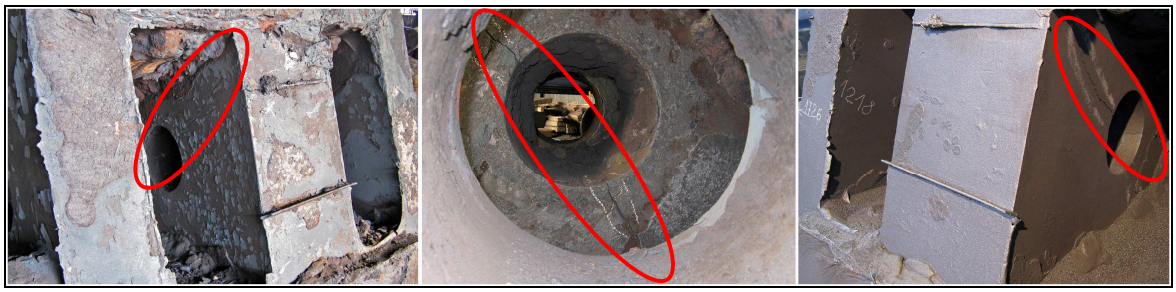

Fig. 7: View on the location of the hot tear in the middle rib of the steel casting. This hot tear occurred on both sides of the middle rib.

The first numerical analysis concerned filling of the sand mould cavity. **Figure 8** captures the situation in the early stages of the filling process. It shows that the gating system is not designed well enough to ensure smooth and calm filling without massive surface turbulence. Due to the non-tapered sprues and runners the flow velocity is not controlled whatsoever and the melt enters the mould cavity with high velocity. Consequently, it leads to jetting and splashing establishing a highly turbulent flow pattern[47]. Surface turbulence contributes to air entrapment but primarily to folding of oxide bi-films[48]. These oxide films are then drifted by the propagating metal and end up somewhere in the solidifying casting structure. Areas containing oxide films exhibit impaired mechanical properties[49], thus if these areas full of oxide films are subjected to some loads, either external or internal, they could readily serve as tear or crack initiation sites. The only option in this case would be to redesign the gating system so that the velocity of the melt is controlled and lowered to avoid the above mentioned deficiencies. For instance, one could apply choke elements at the bottom of each sprue to partially avoid air aspiration during the free fall in the sprue area. Runners should be reworked so that the melt enters the cavity from all the gates at the same time with the same or similar velocity. Runner extensions should be installed to absorb kinetic energy of the flowing metal and hence lower the entrance velocity. The last element from the gating system that should be avoided or at least redesigned is the two vertical runners. Their function is to supply the upper region of the casting with fresh and hot melt during later stages of the filling process. However, with the current design, the melt reaches the top of those runners much earlier than desired and initiates the so-called waterfall effect which is seen in **Figure 7** at 8% filled. This is a notoriously known effect that substantially adds to the surface turbulence. Nobody questions that it is very important to supply the upper section with hot melt to promote favorable thermal gradients but the position and shape of the two vertical runners must be changed so that they do not start filling too early.

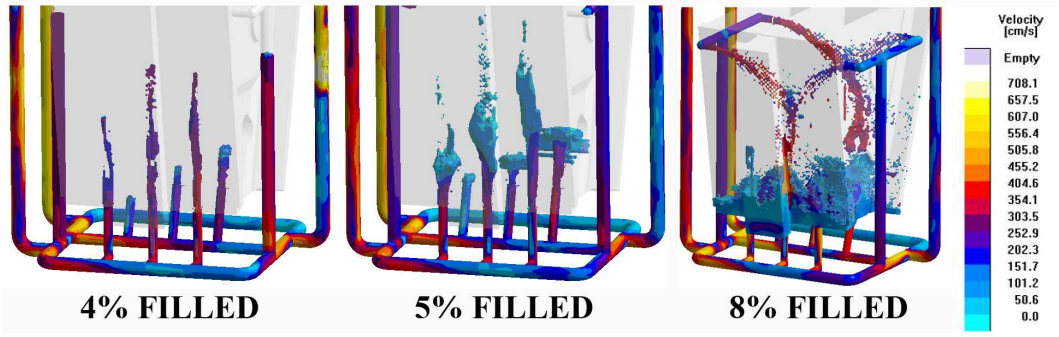

Fig. 8: Initial stages of the filling process in case of the original casting arrangement suggesting highly turbulent entry of the metal to the mould causing jetting and also a waterfall effect due to improperly designed gating system.

Figure 9 outlines the Niyama criterion which usually indicates regions prone to centerline porosity due to low thermal gradients. This time it has been used to show regions with very steep gradients and low cooling rates and, hence areas potentially susceptible to hot tearing. Having large temperature differences over a small or narrow region implies that large thermal strains will be evoked due to this sudden temperature change, which will be later verified in the thermo-mechanical analysis. Low cooling rates suggest that the cooling is hindered and, that the particular area remains weak for a longer time. This again favors hot tearing. One can see that the area above the top cylindrical core experiences large temperature differences in two very narrow channels,

exactly at the area where the hot tear was found in the real casting. Since the Niyama criterion is evaluated at the end of the solidification interval it was necessary to check how the casting behaves thermally speaking during the entire solidification interval.

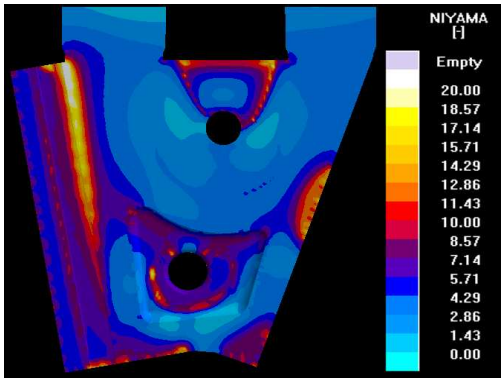

Fig. 9: The Niyama criterion used to highlight areas with high thermal gradients for the considered casting. Areas with high Niyama values exhibit steep thermal gradients and low cooling rates.

Figure 10 implies that already at 40% solidified a small region above the top core solidifies at a much higher rate than the surrounding areas. This trend persists throughout the entire solidification interval. Having an area which solidifies much quicker than the surroundings generally leads to large thermally induced tensile strains. Also, the cold area has gained strength and volumetrically contracts while the surroundings are still semi-solid and weak. The consequence of this thermal imbalance can easily be a hot tear located at the boundaries of the cold and hot regions.

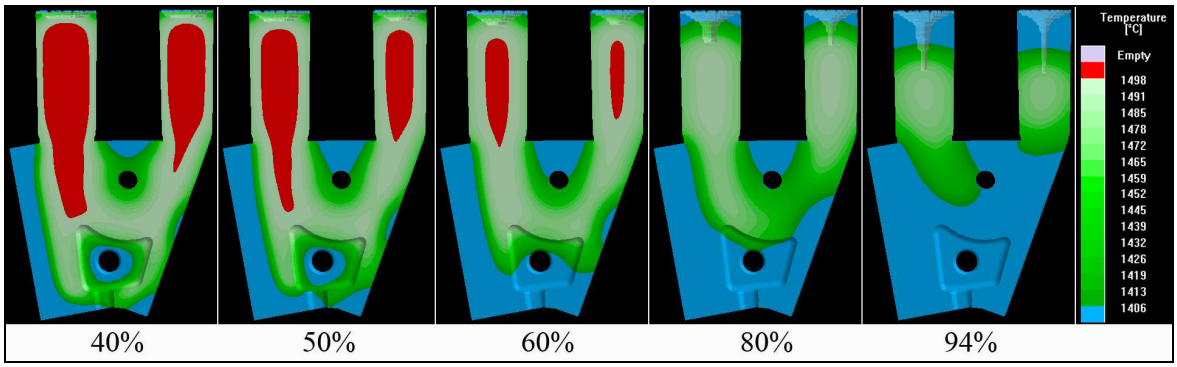

Fig. 10: Temperature distribution in the solidification interval of the original casting layout. It is expected that the sudden temperature change in the area between the risers might induce thermal straining at the boundaries of the cold and hot regions and consequently a hot tear. Blue color denotes a completely solid region, all of the shades of green stand for the mushy zone and the red color stands for the liquid.

As mentioned earlier, unbalanced or improper concentration profiles of the solute elements can also promote hot tearing. As seen in **Figure 11**, the profiles of three elements, i.e. carbon, phosphorus and sulfur, are definitely unfavorable with respect to hot tearing. One can see that in all three cases there are regions with positive segregation very close to the problematic area where the tear formed. Having positively segregated areas means that they will exhibit impaired mechanical properties, i.e. carbon causes local embrittlement, sulfur and phosphorus suppress solidification temperature and thus increase the risk of hot tearing. Mainly in case of carbon and sulfur, notice the white region denoting positive segregation indicated by black arrows, following exactly the same pattern as the hot tear in the real casting in **Figure 7**.

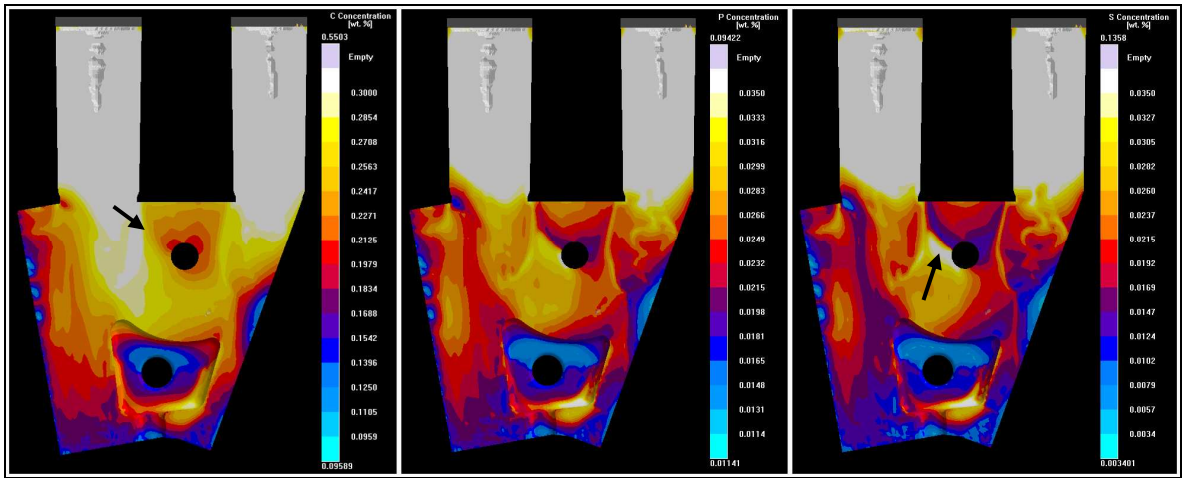

Fig. 11: Concentration profiles of three solute elements (left) carbon, (middle) phosphorus, (right) sulfur. Highly segregated regions exhibit impaired mechanical properties, increasing the risk of hot tearing. The black arrows highlight the most risky areas in terms of hot tear susceptibility.

Figure 12 captures the maximal principal strain rate inside the casting at two different stages of solidification. One might argue why we should be concerned about what goes on at that early stage of solidification when hot tears usually form much later. The reason is that at 40% solidified; the cold "triangular" area starts to form above the top core, as indicated in **Figure 10**. Therefore, that particular area is already in the late stage of its solidification, due to the uneven solidification pattern of the entire casting and thus hot tears can form there already at 40% solidified. Indeed, one can see in **Figure 12** that the significant temperature difference coupled with a volumetric contraction lead to rather severe thermally induced tensile straining in that area. Also, it is now obvious that the top core represents a mechanical restraint to the free contraction as the peak values of the strain rate are adjacent to the core. Hence one may assume that the hot tear initiated there and propagated diagonally to the top.

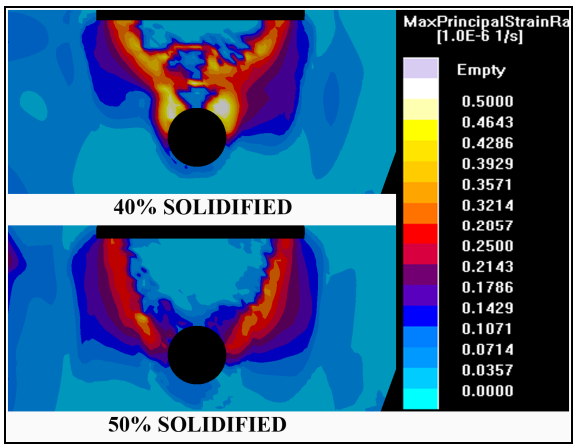

Fig. 12: Maximal principal strain rate contributing to hot tearing. The effect of the top cylindrical core as a mechanical restraint to free contraction is seen. The "fastest" deformation occurs right at the region where the hot tear was found in the real casting.

Figure 13 depicts the final prediction of the hot tear occurrence in the casting as a consequence of the coupled physical phenomena mentioned above. Notice a very good correlation with the results obtained from the casting trial. There is one more area in the hot tear results that might be of concern. It is located in the lower central section of the casting above the bottom cylindrical core. One of the possible reasons why the hot tear did not occur in the bottom area in reality is the stress redistribution in the casting after the top hot tear opened up. So, when the hot tear formed in the central rib, the residual stress stored in the casting may have got released in a form of deformation and the stress pattern of the entire casting changed and the bottom tear did not initiate. Although, there is no clear evidence which would verify this statement.

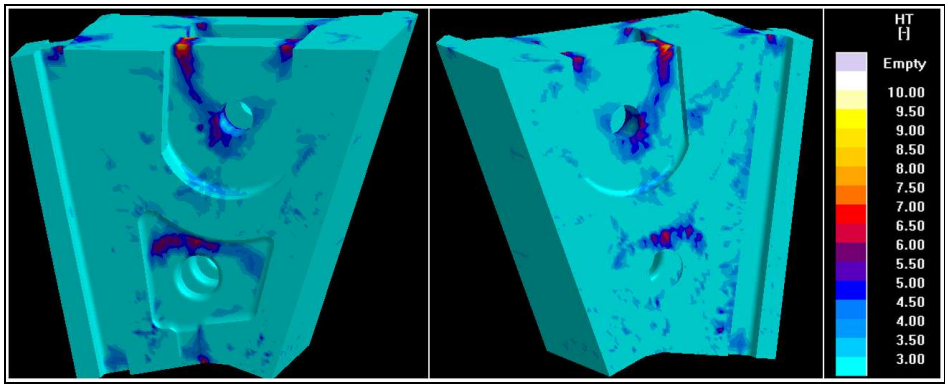

Fig. 13: Hot tear prediction obtained from the numerical stress-strain analysis. Colored areas indicate regions most susceptible to hot tearing. A good agreement with the experimental results is seen in terms of the predicted hot tear in the central rib.

A conclusion can be that the hot tear was in essence evoked by a combination of multiple factors, (i) an uneven temperature distribution inducing high thermal gradients concentrated over a very narrow area, (ii) by unfavorable concentration profiles of solute elements which are also heavily dependent on the temperature profiles and, (iii) by a mechanical restraint due to the presence of the top core which hindered free volumetric contraction of the solidifying cast part.

CASTING AND SIMULATION RESULTS – OPTIMIZED LAYOUT

As already mentioned, the primary goal of autonomous optimization based on process simulations has been to find a more suitable design of the two top risers and of the surrounding chills to establish a directional and progressive solidification pattern which would eliminate the formation of solidification related issues such as centerline porosity, shrinkage porosity, macrosegregation and hot tears which were present in the original casting layout.

The gating system has been changed somewhat to achieve a more uniform and smooth flow pattern to avoid excessive oxidation. On top of that, chills and risers have been transformed into parametric objects and subjected to optimization as design variables. The most important condition in assessing the size of the riser has been to avoid the shrinkage pipe penetrating into the riser neck area or even to the casting body. Such designs are then instantly rejected since they are unsuitable.

The objective space for the optimization problem is constructed by the two following conflicting objectives (i) minimization of the remaining riser volume and (ii) minimization of the weighed volume Niyama of the casting body, **Figure 14**. After the optimization run the user has to decide which design among multiple optimal solutions will be the most desirable for him/her. Whether he/she wants to minimize the riser as much as possible, at the cost of increased porosity or to have a porosity-free and sound casting with a slightly larger riser, but still smaller than the initial design. Obviously, the optimized design must contain less centerline porosity than the original casting layout. This is why only Pareto optimal solutions located in the blue region are considered. All other solutions are disregarded since they exhibit more centerline porosity than the initial layout, which is not desirable. These six solutions were subsequently analyzed in terms of shrinkage porosity, which is an additional criterion for evaluating the overall soundness of the casting. It was found that solution 4 had the best response in terms of shrinkage porosity and solution 1 was only slightly worse than 4. The other four designs showed much worse response and therefore they were disregarded. Since the primary aim of the optimization procedure was to search for the solution with the lowest amount of centerline porosity, solution 1 was selected, although it had the largest volume of the two top risers from all of the trade-off solutions. However, the objective of minimizing the riser volume was still met by solution 1, which actually exhibited a significant decrease in the riser volume as compared to the original solution. By picking solution 1, one could argue that single objective optimization could have been applied. True, however, the benefit of multi-objective optimization is that the user has a selection of many trade-off solutions lying on the Pareto line which may fulfill his/her preferences that he/she would never be able to explore, or be aware of other potential alternatives, while using the single objective approach.

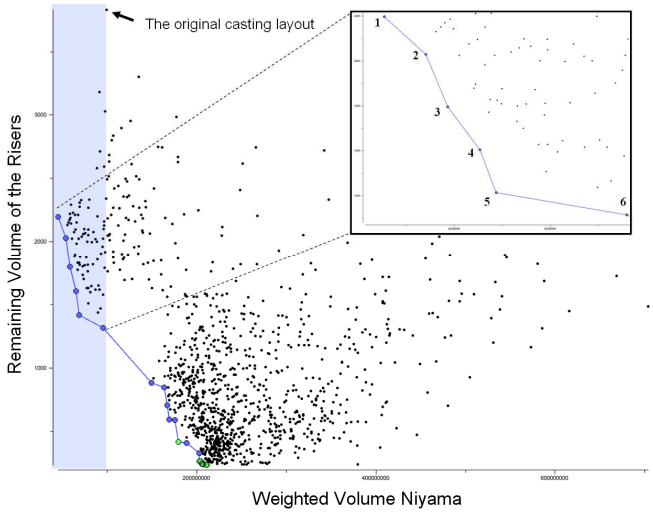

Fig. 14: The objective space where all the computed designs are stored. The blue line represents the Pareto optimal front which comprises the best trade-off solutions in terms of the predefined optimization objectives. The light blue color indicates the area from which the best solution is selected. The enlarged view on the six Pareto designs is located on the right upper corner.

One design was selected from the objective space for further analysis. The selected design has then been evaluated with respect to filling, solidification as well as stresses and strains in the standard simulation environment. The geometry of the preferred design is captured in **Figure 15.**

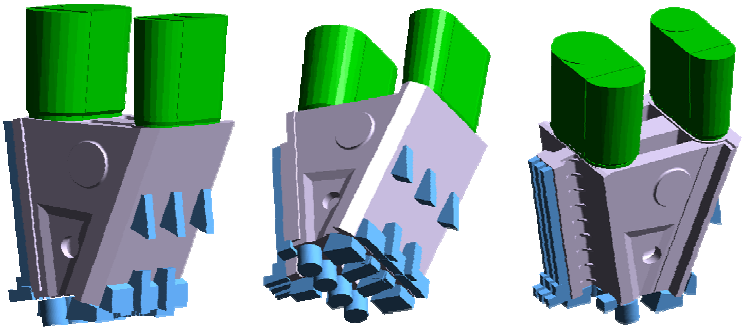

Fig. 15: New casting layout after optimization. Dimensions of the two top risers together with dimensions and location of the surrounding chills were varied during optimization.

There are a few reasons for choosing such a design. First, the primary goal has been to eliminate the presence of centerline porosity and through that to minimize segregation issues and occurrence of hot tear.
As discussed earlier, centerline shrinkage is directly affected by a pressure drop inside the casting, derived from Darcy`s law of flow in porous media, which represents resistance to feeding of a particular area. To keep the pressure gradient sufficiently high to ensure efficient feeding flow, the height and the total volume of the risers should not be too small. Next, centerline shrinkage usually forms at areas with shallow thermal gradients. To establish steep thermal gradients, the risers should again be sufficiently large and the dimensions and placement of the chills should be chosen so that progressive and directional solidification towards the risers is imposed. Considering segregation, it is also known that having steep thermal gradients due to intense chilling results in a finer dendritic microstructure imposing higher resistance for channel segregates to form. Moreover if a progressive and directional solidification pattern exists, it helps to move the highly segregated remaining liquid towards the riser. As to the hot tears, it has been shown earlier in the text that an adequate solidification pattern with good feeding, favorable thermal gradients and concentration profiles should eliminate hot tears in castings.
For this reason one could deduce that centerline shrinkage, macrosegregation phenomena and hot tears could in principle be treated by the same remedy. Obviously it does not mean that they are driven by the same physical phenomena.
After this brief reasoning one can make the assumption that if the design of the risers and chills yields a favorable solidification pattern, i.e. steeper and uniformly distributed thermal gradients, directional and

progressive solidification, enhanced feeding, to prevent centerline porosity, the macrosegreation profiles should be positively changed, as well as hot tear susceptibility minimized.
Figure 16 shows how the thermal gradients changed due to the performed optimization adjustments. It is seen that due to the new shape of the risers, combined with newly placed chills with optimized design and due to the removed top core, the high thermal gradients got eliminated from the area where the hot tear occurred. The large area on the left hand side of the casting indicates steep thermal gradients accumulated over a relatively narrow region, hence implying potential hot tearing. In reality, there are narrow ribs placed along that area to prevent hot tearing as seen in **Figures 15** and **21**. Since they are very narrow and it would require an extremely fine mesh to consider them during calculations, these were not modeled. Hence, this critical area predicted by the numerical solver can be disregarded.

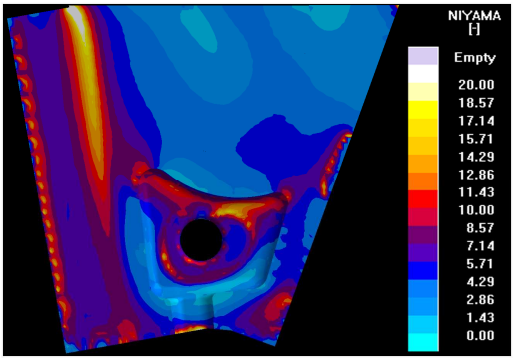

Fig. 16: Thermal gradients in the cast part after optimization. No obvious high thermal gradients located in a narrow band-like area as in the original casting arrangement are seen. The risk of hot tears has been minimized in the previously critical region.

The optimization adjustments have also led to a new distribution of temperature in the casting domain, **Figure 17**. There is no longer that "triangular" area solidifying much faster as compared to the surroundings, evoking thermal imbalance and subsequent thermal tensile strains. Now it appears that the casting solidifies directionally and progressively from the bottom and from the sides towards the two top risers. This should for sure lower the risk of hot tearing in that problematic area as well as in the entire casting domain.

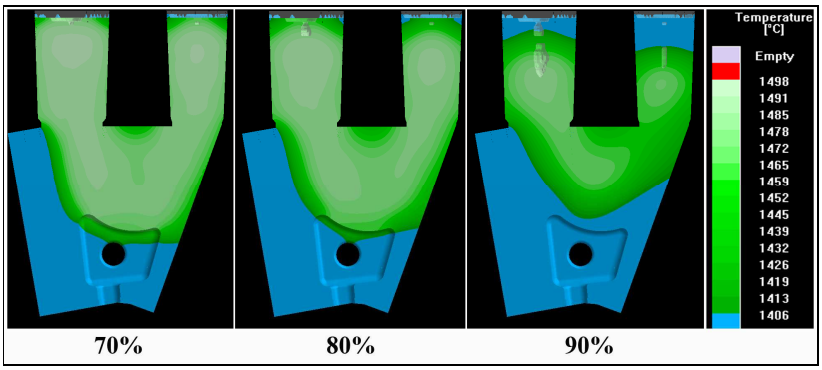

Fig. 17: Temperature profiles at different stages of solidification in the optimized layout. No indications of sudden temperature changes as were identified in the original layout. The likelihood of a hot tear is very low in the previously critical area. Blue color denotes a completely solid region, all of the shades of green stand for the mushy zone and the red color stands for the liquid phase.

The changes in the solidification pattern have naturally led to a redistribution of the characteristic solute elements in the casting, represented by their concentration profiles. It is shown in **Figure 18** that the concentration profiles of the selected three elements are now more balanced and favorable implying that the positively segregated region will be found mostly in the riser region. This state is much more beneficial with respect to hot tear susceptibility as compared to the original state. However, a question arises whether the mechanical properties would be sufficiently good in the area between the two risers due to positive segregation. The manufacturer noted that no special requirements for that specific area as to the mechanical properties were determined by the final customer. Therefore this solution would be suitable for subsequent production. Minor improvements in the segregation might be expected during the heat treatment that the part will undergo afterwards, especially during homogenization.

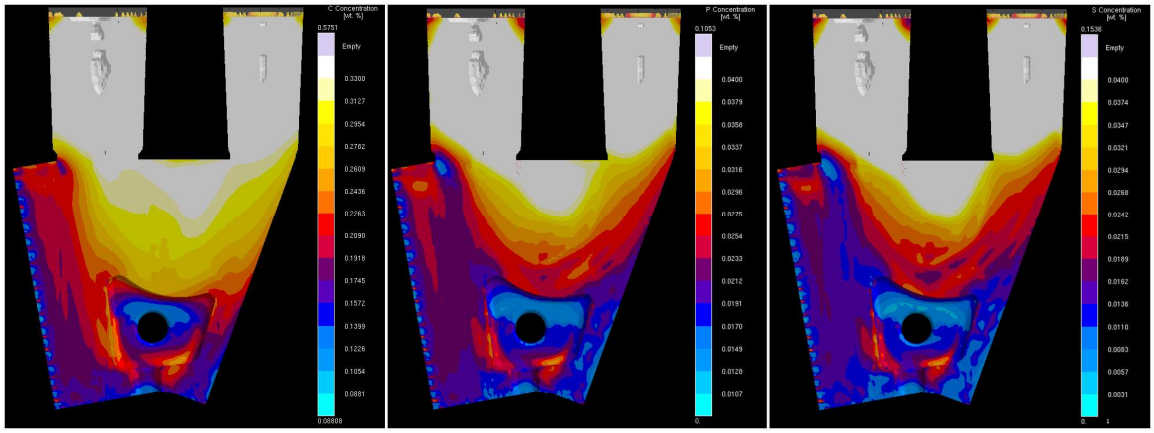

Fig. 18: More uniform concentration profiles in the optimized steel casting due to the more favorable solidification pattern, (left) carbon, (middle) phosphorus, (right) sulfur. The positively segregated area is now located mainly in the two top risers and partially in the under-riser region.

When we look at the maximal principal strain rates during the solidification interval of the optimized layout in **Figure 19** it shows that, in the previously critical area there are no more signs of high tensile straining hence eliminating the risk of hot tearing. The potentially critical area in the lower central region of the casting is not to be worried about. Each numerical solver always highlights some risky areas, but it is very important to assess also the magnitude of it. The peak values on the scale are so low as compared to the state in the original layout (see **Figure 12)**, that it becomes apparent that the thermally induced strains will not cause any major problems in relation to hot tearing.

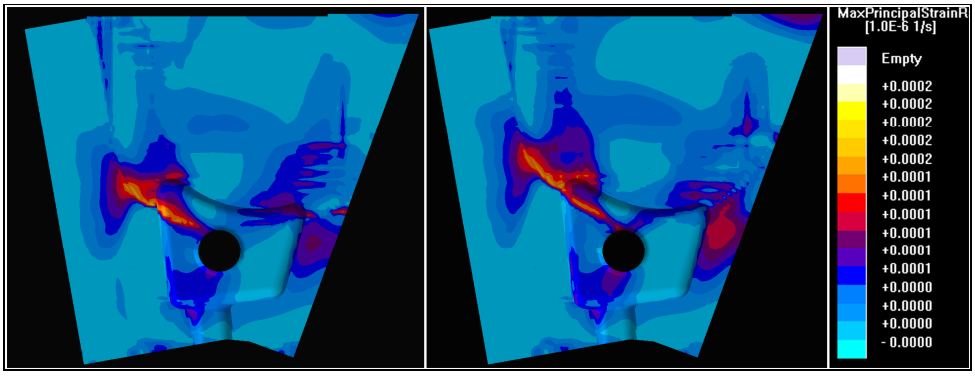

Fig. 19: Maximal principal strain rate in the optimized layout. Note the difference in the scale as compared to Figure 12.

Consequently, due to the optimized solidification pattern in which directional and progressive solidification toward the heaviest section has been established, the risk of hot tearing got entirely eliminated in the problematic area in the middle rib, **Figure 20**. There is only one small place in the casting which might be prone to hot tearing. It is found in the lower central area, right above the bottom core. However, when considering all the above investigated criteria such as temperature profiles during solidification, the Niyama criterion, segregation profiles and strain rates, it can be assumed that this area will not be of concern in production and hot tear will most likely not form. Also, the peak value on the scale is much lower as compared to the original solution where the tear was found.

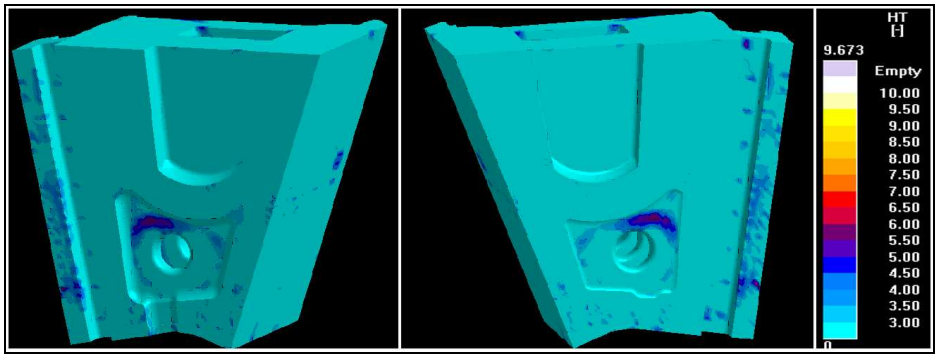

Fig. 20: Hot tear prediction in the optimized casting layout. The middle rib appears hot tear free. The other indication in the lower central area will most likely induce no hot tearing. This can be deduced from its value on the color scale.

Based on the findings obtained from the multi-objective optimization run, a new casting layout has been proposed and applied in production, see **Figure 21**. After it was cast, the part was inspected, both visually and by the prescribed NDT techniques, and no major defects or problems that would ultimately destroy the casting were found.

Fig. 21: The steel casting which was manufactured based on the optimization results, after its shakeout. It exhibited no hot tears whatsoever. Protective ribs have been applied for the real casting. They were not assumed during simulations since they would require extremely fine meshing.

CONCLUSION

This work presented an attempt to perform multi-objective optimization of the solidification pattern of a large steel wedge shaped casting. The main purpose of the study was to demonstrate how the autonomous optimization procedure based on simulations can be effectively utilized for solving several conflicting objectives in daily foundry practice. More specifically, to prove that hot tearing can be relatively easily addressed by optimization even without prescribing it as one of the objectives which would not be feasible computational time-wise. It was found that by optimizing the solidification pattern so that directional and progressive solidification with favorable thermal gradients is established, one could relatively easily handle multiple phenomena like centerline porosity, macrosegregation and hot tears.

The optimization objectives were prescribed as (i) minimization of the remaining volume of the top riser and (ii) minimization of centerline porosity through which the elimination of hot tear occurrence in the middle rib was expected.

The first step was to analyze the original casting arrangement provided by the foundry to figure out major reasons for the hot tear to form. Filling, solidification and stress/strain analyses were performed to capture all physical phenomena and potential flaws and defects which may contribute to hot tearing. The result of the improper solidification pattern, i.e. abrupt temperature drops over a narrow region, together with poor chilling and the presence of a top cylindrical sand core as a mechanical restraint were all contributing to the formation of a hot tear in the middle rib of the casting body. Besides that, unfavorable concentration profiles of multiple solute elements were identified in the casting body leading to highly segregated regions very close to the critical area which favored hot tearing. These findings were verified by casting trials performed at the foundry. A very good agreement with the casting results was found.

In the optimization problem, the dimensions and positions of the two top risers and the chills were prescribed as design variables together with the allowed ranges of variation. After optimization, one solution was selected from the design space.
The new shapes of the top risers and the new chill arrangement led to significant improvements in the solidification pattern of the selected optimized solution. More pronounced cooling established favorable temperature gradients and induced progressive and directional solidification not only in the problematic area but also in the entire casting. New convection and macrosegregation patterns were obtained giving favorable and promising results. Due to steeper thermal gradients the mushy zone got reduced, its permeability was lowered imposing higher resistance for liquid-solid movement and for potential channel segregation. The resulting carbon, phosphorus and sulfur distributions seemed more uniform over the casting body. After removing the top sand core there was no longer a mechanical restraint to free volumetric contraction of the casting in the area just below the top core. All of these features and improvements completely eliminated the susceptibility to hot tearing in the entire casting which was also proved during the subsequent production.

REFERENCES

1. MAGMAsoft simulation software, MAGMA GmbH, Aachen, Germany
2. Kotas, P., Hattel, J.H., Thorborg, J., Svensson, I.L., Seifeddine, S., *Proc. International Ph.D. Foundry Conference*, Brno, Czech Republic, (2009).
3. Seifeddine, S., Wéssen, M., Svensson, I.L., *Metallurgical Science & Technology*, Vol. 24, No. 2, pp. 7- , (2007).
4. Sturm J., Hepp, E., Enger-Walter, A., *20th CAD-FEM Users` meeting 2002, International Congress on FEM Technology*, Lake Constance, Germany, (2002).
5. Egner-Walter, A., *CP+T Casting Plant + Technology International*, Vol. 23, no. 1, pp. 24-29, (2007).
6. Gunasageram, D.R., Finnin, B.R., Polivka, F.B., Materials Science and Technology, Vol. 23, Nr. 7, pp. 847-856, (2007).
7. Domkin, K., Hattel, J.H., Thorborg, J., *Journal of Materials Processing Technology*, (2009).
8. Kotas, P., Master Thesis, Technical University of Denmark, Lyngby, Denmark, (2007).
9. Lin, Z., Monroe, C.A., Huff, R.K., Beckermann, C., *Proc. Int. Conf. On Modelling of Casting, Welding and Advanced Solidification Processes, MCWASP XII*, Vancouver, Canada, pp. 329 – 336, (June 2009).
10. Kokot, V., Bernbeck, P., *Proc. Int. Conf. On Modelling of Casting, Welding and Advanced Solidification Processes, MCWASP X*, Destin, Florida, pp. 487- 494, (May 2003).
11. MAGMAfrontier 4.4 Reference Manual, (2005).
12. Hahn, I., Hartmann, G., *Casting Plant & Technology*, Vol. 24, no. 4, (2008).
13. Hahn, I., Sturm, J.C., *Proc. World Foundry Congress*, Hangzhou, China, (2010).
14. Tsoukalas, V.D., *Proc. IMechE*, Vol. 222 Part B: J. Engineering Manufacture, (2008).
15. Tsoukalas, V.D., *Materials and Design*, Vol. 29, pp. 2027–2033, (2008).
16. Gramegna, N., Baumgartner, P., Kokot, V., *IDEAL International Conference*, Lecce, Italy, (October 2005).
17. Campbell, J., *Mat. Sci. Tech*., Vol. 4, pp. 194-204, (1988).
18. Hattel, J.H., *Fundamentals of Numerical Modelling of Casting Processes*, 1st ed., Kgs. Lyngby: Polyteknisk Forlag, (2005).
19. Monroe, C., Beckermann, C., *Proc. of the 61st Technical and Operating Conference*, SFSA, Chicago, IL, (2007).
20. Pellini, W.S., AFS Transactions, Vol. 61, pp 61-80, (1953).
21. Niyama, E., Uchida, T., Morikawa, M., Saito, S., *AFS Int. Cast. Met. J*., Vol. 7, No. 3, pp 52-63, (1982).
22. Carlson, K.D., Beckermann, C., *Metallurgical and Materials Transactions A*, Vol. 40A, pp. 163-175, (2009).
23. Carlson, K.D., Ou, S., and Beckermann, C., *Metallurgical and Materials Transactions B*, Vol. 36B, pp. 843-856, (2005).
24. Hardin, R.A., Ou, S., Carlson, K.D., Beckermann, C., *Metall. Mater. Trans. B*, Vol. 33B, pp. 731-740, (2002).
25. Dantzig, J.A., Rappaz, M., *Solidification*, EPFL Press, (2009).
26. Schneider, M.C., Gu, J.P. Beckermann, C., Boettinger, W.J., Kattner, U.R., *Metallurgical and Materials Transactions A*, Vol. 28A, pp. 1517- 1531, (1997).
27. Sigworth, G.K., Wang, C., *AFS Trans*, vol. 100, pp. 989–1004, (1992).
28. Monroe, C., and Beckermann, C., *Mater. Sci. Eng. A*, Vol. 413-414, pp. 30-36, (2005).

29. Feurer, U., Giessereiforschung, Vol.28, Issue.2, pp 75-80, (1976).
30. Farup, I., Mo, A., Metallurgical and Materials Transactions A, Vol.31, Issue.5, pp 1461-1472, (2000).
31. Monroe, C., Ph.D. Thesis, University of Iowa, (2008).
32. Wong, Y. M., Han, H. N., Yeo, T., OH, K.H., ISIJ International, vol. 40, no. 2, pp. 129-136, (2000).
33. Bhattacharya, U.K., Adams, C.M., Taylor, H. F., *AFS Trans*., Vol. 60, pp. 675, (1952).
34. Eskin, D.G., Katgerman, L., Metallurgical and Materials Transactions A, Vol.38A, Issue 7, pp 1511-1519, (2007).
35. MAGMAfrontier 4.4 Reference Manual, (2005).
36. Goldberg, D.E., *Genetic Algorithms in Search, Optimization & Machine Learning*, Addison Wesley Longmann, Inc., (1989).
37. Deb, K., *Multi-Objective Optimization Using Evolutionary Algorithms*, John Wiley & Sons, (2001).
38. Zitzler, E., Ph.D. Thesis, Swiss Federal Institute of Technology (ETH), Zurich, (1999).
39. Poles, S.: 'MOGA-II: An improved Multi-Objective Genetic Algorithm. Technical Report'; ESTECO s.r.l., (2003).
40. Tutum, C.C., *PhD thesis*, Technical University of Denmark, Kongens Lyngby, Denmark, (2009).
41. Tutum, C.C., Hattel, J.H., *Science and Technology of Welding and Joining*, Vol. 15, No. 5, pp. 369-377, (2010).
42. Kotas, P., Tutum, C.C., Snajdrova, O., Thorborg, J., Hattel, J.H., *International Journal of MetalCasting*, Vol. 4, Issue 4, (2010).
43. Kotas, P., Tutum, C.C., Andersen, S., Hattel, J.H., *115th Metalcasting Congress*, Schaumburg, USA, (2011), (accepted for oral presentation).
44. Deb, K., *Engineering Optimization*, Vol. 35, No. 5, pp 445-470, (2003).
45. Kor, J., Chen, X., Hu, H., *IEEE International Symposium on Intelligent Control*, Saint Petersburg, Russia, (2009).
46. Sobol, I., *SIAM Journal on Numerical Analysis* 16, (1979).
47. Campbell, J., "Castings Practice, the 10 Rules of Castings", Elsevier Butterworth-Heinemann, (2004).
48. Campbell, J., "Castings", Elsevier Butterworth-Heinemann, (2003).
49. Dai, X., Yang, X., Campbell, J., Wood, J., Materials Science and Technology, Vol. 20, Nr. 4, pp. 505 – 513, (2004).

E INDUSTRIAL REPORT

Kotas, P., Hattel, J.H., "*Casting Process Optimization of a Large Steel Ring With Respect to Centerline Porosity and Channel Segregates*", 2011.

Danmarks Tekniske Universitet

Industrial Report

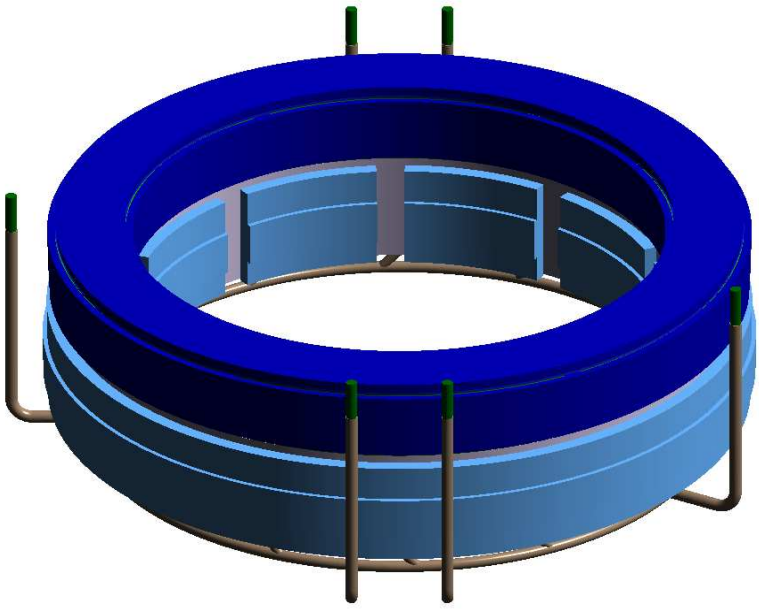

Casting Process Optimization of a Large Steel Ring With Respect to Centerline Porosity and Channel Segregates

Petr Kotas
Jesper Hattel

Process Modelling Group
Department of Mechanical Engineering
Technical University of Denmark
Produktionstorvet, Kgs. Lyngby
2800, Denmark

Table of Contents:

Casting Process Optimization of a Large Steel Ring With Respect to Shrinkage Porosity and Channel Segregates

P. Kotas
Technical University of Denmark, Department of Mechanical Engineering, Kgs. Lyngby, Denmark

J. Hattel
Technical University of Denmark, Department of Mechanical Engineering, Kgs. Lyngby, Denmark

INTRODUCTION

This project was assigned and successfully completed in a framework of research collaboration between the process modeling group of DTU and Vitkovice Heavy Machinery a.s – one of the largest steel foundries in Europe.
The aim of this project was to optimize an entire casting process of a large (246 ton) steel ring with the objective of eliminating problems with macrosegregation, particularly with channel segregates also referred to as freckles. Moreover, it was requested by the managing director of the foundry to increase the casting yield by optimizing the shape of the top riser. However, even after the yield optimization, the overall quality of the casting had to remain superior, i.e. concentration profiles, freckles, shrinkage porosity and hot tears had to be avoided.
The project was divided into two sections. The first section comprised two very thorough numerical analyses of mould filling and solidification; both accomplished using the commercial simulation software package MAGMAsoft®. Outcomes of the filling analysis were the following: detailed information regarding the filling pattern, i.e. whether surface turbulence or a risk of oxide inclusions would be of concern, subsequent defects prediction, and above all the temperature distribution in the casting caused by the filling pattern. The solidification analysis provided valuable insights into the temperature distribution during solidification and the subsequent solid state cooling. Moreover, it was possible to identify critical areas such as hot spots, areas with inadequate and/or restricted feeding, or areas with thermal imbalance that may evoke thermal stresses and strains. Based on this information, defects that may form due to the aforementioned shortcomings were investigated. Last, convection and macrosegregation profiles were assessed in order to predict possible issues with macrosegregation or with channel segregates and to compare these predictions with experimental results obtained from the foundry. The stress strain analysis was not required by the foundry since the original casting has already been cast and no hot tears were found in the casting. The cause of rejection was the presence of hundreds of channel segregates extending to the surface. The outline of the simulation analyses performed in this project is given in **Table I**.

Table I – Indication of the differences in complexity of the simulation analyses for the original and final layouts as compared to the optimization procedure

		Solidification			
	Filling	Thermal analysis	Convection, macrosegregation	Stress-strain analysis	Hot tear analysis
Original layout	YES	YES	YES	YES	YES
Optimization procedure	NO	YES	NO	NO	NO
Optimized layout	YES	YES	YES	YES	YES

The second section was entirely devoted to autonomous optimization with a goal of finding the “most optimal” solution to the predefined objectives. The objectives were: (i) the minimization of the riser volume and (ii) the minimization of the presence of centerline porosity. For this purpose, a built-in optimizer MAGMA*frontier*, which is based on multi-objective genetic algorithms, was applied. One may ask, why did we not prescribe minimization of the macrosegregation as one of the optimization objectives because this is what we want to achieve? Macrosegregation optimization would not be feasible since the calculation time for convection and

macrosegregation analysis is approximately one day on a standard multi-processor work station and approximately 1000 -2000 of design variants needs to be calculated during optimization in a search for the optimal solution. It was found in literature that both centerline porosity and macrosegregation are influenced and governed by the same physical phenomenon- the thermal gradient. In essence, if centerline porosity is eliminated by increasing thermal gradients and by establishing a progressive solidification pattern, concentration profiles denoting macrosegregation should be positively affected as well, thereby suppressing the tendency to channel segregation in the cast part. After selecting the most favorable design layout in terms of the predefined objectives, this design was again analyzed with respect to filling, solidification and stress-strain to evaluate the impact of the optimized features on the overall behavior. The findings and proposals from this study were presented to the management of the foundry and were evaluated as suitable for subsequent implementation. This report is not considered as a scientific manuscript. It was written as a final report to the foundry personnel in which all results and proposals are summarized and presented.

DESCRIPTION OF THE ORIGINAL CASTING ARRANGEMENT

The project involves a large steel ring weighing approximately 246 tons, (max height = 2175mm, measured from the bottom of the ring to the top of the riser, max diameter = 7909mm, measured on the top surface of the riser) made of a low carbon steel alloy DIN 1.1165, (GS30Mn5), poured into a furan bonded silica sand mould. A riser is placed on top of the ring to establish favorable thermal gradients and to facilitate feeding, see **Figure 1**.

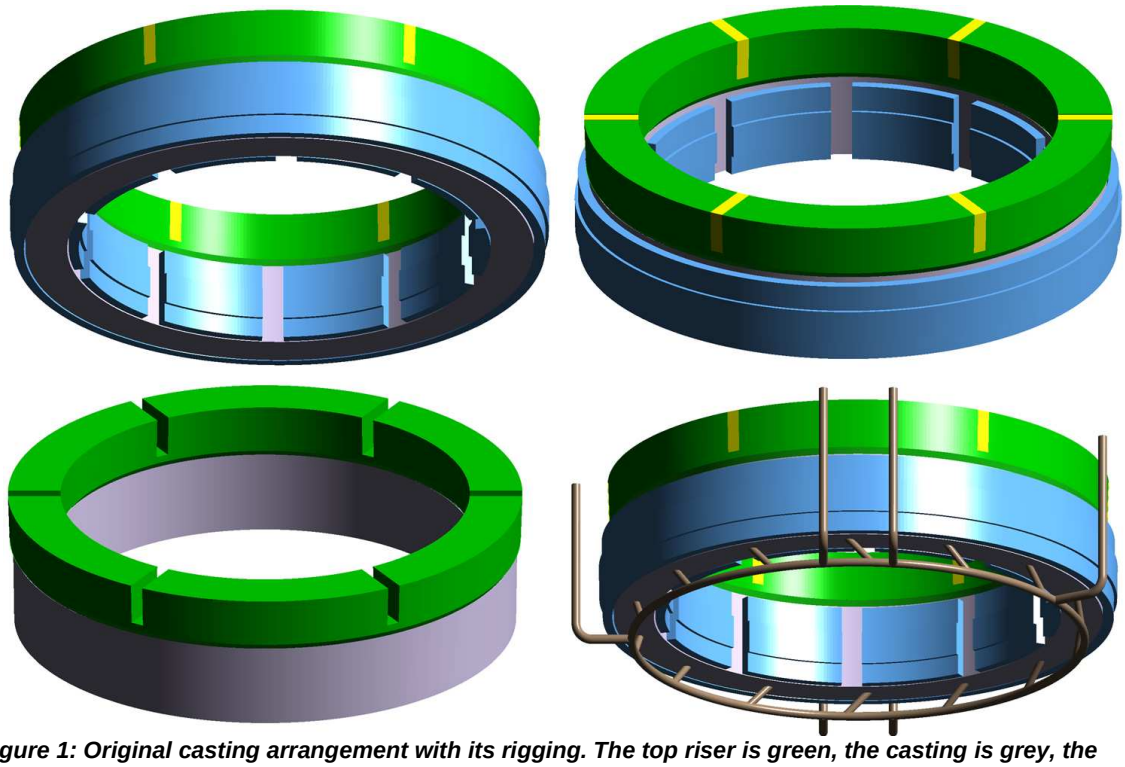

Figure 1: Original casting arrangement with its rigging. The top riser is green, the casting is grey, the gating system is brown, cores are yellow and chills are light blue.

The riser is equipped with 6 brick-shaped sand cores to ease the subsequent machining, i.e. the riser is burned off with an automatic torch. The main cylindrical padding is insulating, the melt surface is covered by an exothermic powder and on top of that additional insulating powder is applied. The original casting arrangement is filled from the bottom, which is generally considered the best way to avoid disintegration of the melt during mold filling, assuming an initial pouring temperature of 1540°C. The filling time is estimated to 180s. Four bottom-pour ladles accommodating a total volume of 216 tons are simultaneously used to fill the casting. Two hours after filling additional filling of approximately 40 tons is applied to refill the top riser. A separate gating system is used for that. In order to intensify cooling of the casting and to establish directional solidification, a set of chills were placed on both the outer and the inner side of the ring. These chills are placed approximately 30mm deep in the sand mould, i.e. non-contact chills, to lower the risk of hot tears when using contact chills. No chills are placed underneath the casting.

FLUID FLOW ANALYSIS FOR THE INTIAL CASTING LAYOUT

As to the filling stage, it occurs that the gating system was designed relatively well. To claim this, it was necessary to look at the behavior of the moving melt especially while entering the casting cavity. From the filling sequence in **Figure 2**, one can argue that the melt entry itself was quite calm. This means that no severe surface turbulence, e.g. jetting or splashing was observed and already from 4% filled the melt propagates very smoothly upwards. This can be attributed to the inclined position of the thin gates, the so-called tangential gates.

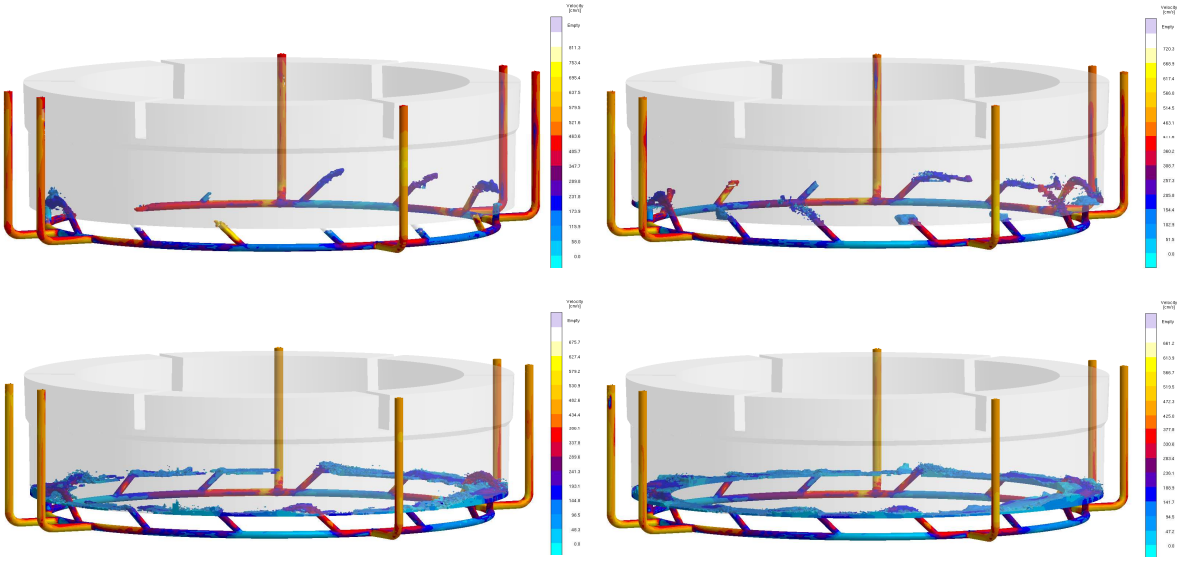

Figure 2: Velocity fields at initial stages of the filling process, 1, 2, 3 and 4% filled respectively. The behavior of the melt in terms of the surface turbulence can be assessed from these images.

The problem with turbulent behavior of the propagating melt is that it causes air entrapment and folding of oxide bi-films, generally referred to as oxide inclusions. The biggest threat of having entrapped oxides in the melt is that nobody can precisely predict where they end up after filling at the solidified structure.
Oxide inclusions cause severe problems already during machining operations where they can show up on the machined surface as black stains or lines. Besides that, areas with accumulated oxides exhibit impaired mechanical properties and thus may compromise the in-service performance of the given cast part. Very often these bi-films are connected with shrinkage porosity and may also be linked to the casting's surface. Then, while service loading, this may lead to an ultimate failure of the casting. Some theories also suggest that oxide bi-films also promote hot tearing since they can easily open up or "unfold" during deformation of the mushy zone. The results of the metallographic and microstructure analysis of the steel ring showed that indeed, oxide inclusions both, dispersed and film-like, and other non-metallic impurities were found in the casting structure, see **Figure 3**. It was found that these impurities were mainly located near the porous areas, in segregated regions and also right at the channel segregates. These findings support the theory of Prof. Campbell from Cambridge University who attributes the occurrence of channel segregates to the presence of oxide bi-films. He suggests that during solidification when castings undergo volumetric shrinkage, these folded oxide bi-films can easily unfold and make it easier for the interdendritic liquid, rich on solute elements to flow upwards through this newly opened channel.

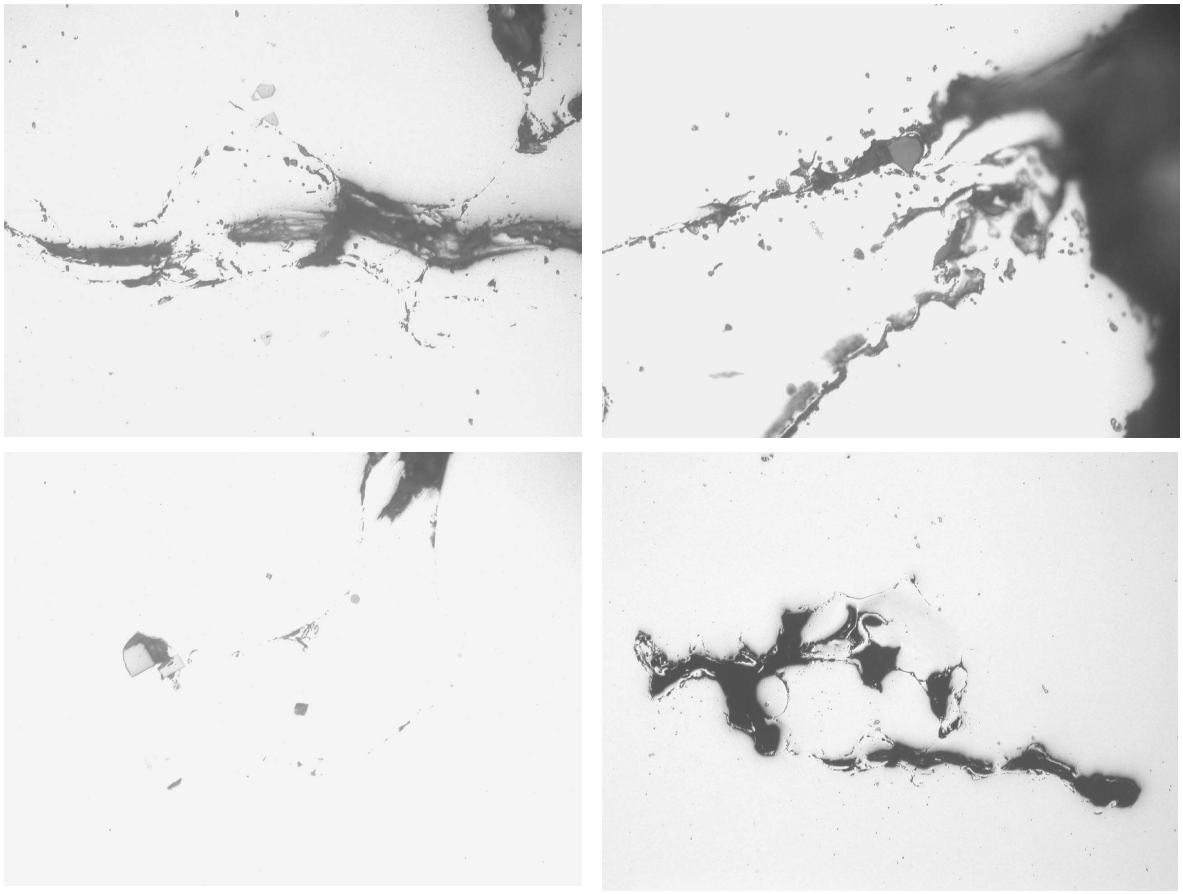

Figure 3: Presence of oxide films in the casting structure- obtained from the metallographic analysis. Property of Vitkovice Heavy Machinery a.s.

Although the gating system is reasonably good, there is still one proposal that should be considered by the manufacturing foundry. It should always be ensured that the melt will enter the casting cavity from all the thin gates at the same time which is not fulfilled in this case. It would be enough to split the runner ring into few sections so that the melt coming from various ladles does not impinge with other streams from different ladles. Moreover the runner cross section area should be sequentially reduced based on the number of thin gates being filled from the same runner.

If the entry velocity was to be further reduced, runner extensions should be placed to absorb some of the kinetic energy of the melt or the cross section area of the thin gates should be enlarged a bit.

SOLIDIFICATION ANALYSIS OF THE ORIGINAL CASTING LAYOUT

The objective of the solidification analysis was to identify potential problems that might arise due to the improper solidification pattern of the casting because of its geometry. The initial temperature field was acquired from the fluid flow analysis. **Figure 4** depicts the temperature field right after the filling was completed. It is evident that the casting has already started solidifying from its surfaces towards the centre due to the presence of the chills. The shape and placement of the chills played an important role during solidification of the casting. It occurs that the casting solidifies directionally toward its centre but not directionally towards the top riser, the isotherms are nearly vertical, primarily because of an insufficient cooling from the bottom. The bottom of the casting was continuously filled with the fresh and hot melt coming from the gating system and hence continuously heated up. Already based on this figure, one may anticipate some issues with shrinkage porosity or macrosegregation in the bottom part of the casting due to an inadequate, i.e. non-progressive, solidification pattern.

It also appears that the outer surface of the casting cools down more rapidly as compared to the inner surface. The inner surface is not capable of rapid cooling since the inner core gets heated up by the converging heat coming from the casting. Therefore, if any channel segregates formed, they would most likely be more pronounced in areas adjacent to the inner surface. Usually, foundries just try to "push" the A-segregates deep into the casting so that they do not occur on the surface. Although, one should always consider that these highly segregated bands exhibit completely different mechanical properties, usually much impaired. Therefore, the primary aim should be not just to "hide" this defect from the customer but take all the possible precautions to eliminate them. This problem can only be tackled by intensifying the cooling on the inner surface of the ring.

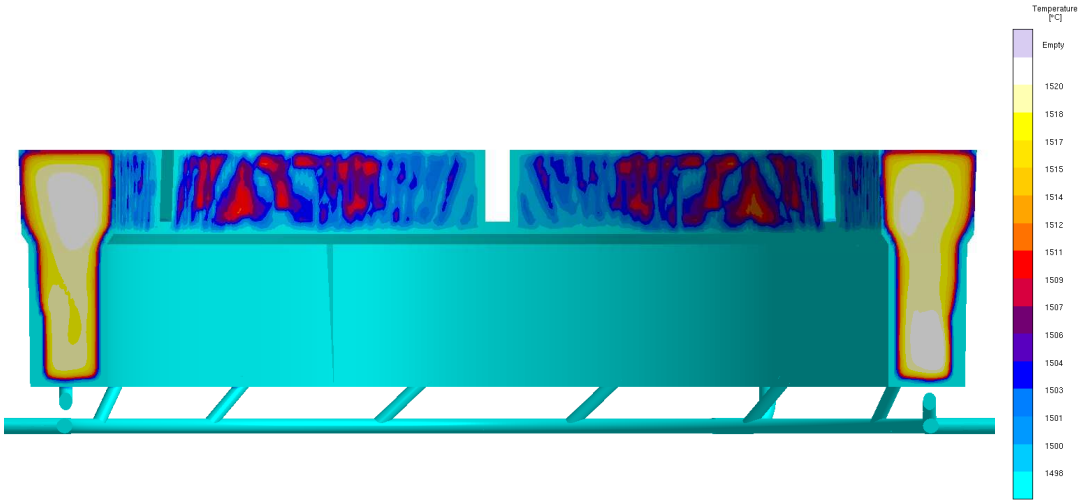

Figure 4: Temperature field right after the filling process is ended. The cyan color stands for solid phase; everything else is either the mush or liquid.

Figure 5 captures the situation at 30% solidified. It is evident that the casting removes its heat much faster from its outer surface than on its inner surface. In addition, there is no doubt about the unprogressive solidification pattern meaning, that the casting does not solidify progressively from the bottom towards the heaviest section.

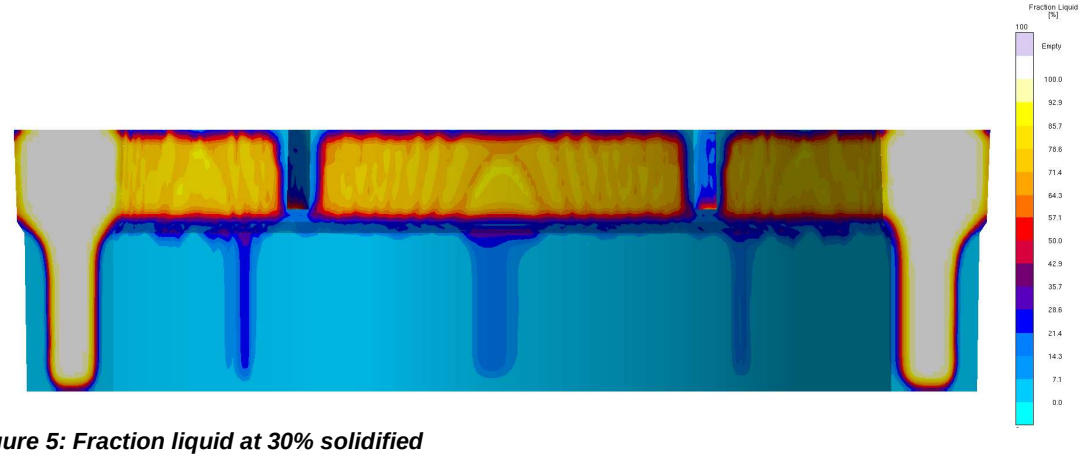

Figure 5: Fraction liquid at 30% solidified

Due to the unfavorable solidification pattern as well as improper placement and shapes of the steel chills, small pools of residual liquid got isolated from the feeding path during solidification, see **Figure 6**. These areas which lack the necessary melt to compensate for the volumetric reduction are then very likely to contain shrinkage porosity. The critical spots are encircled and the consequent shrinkage porosities are predicted in **Figure 7**.

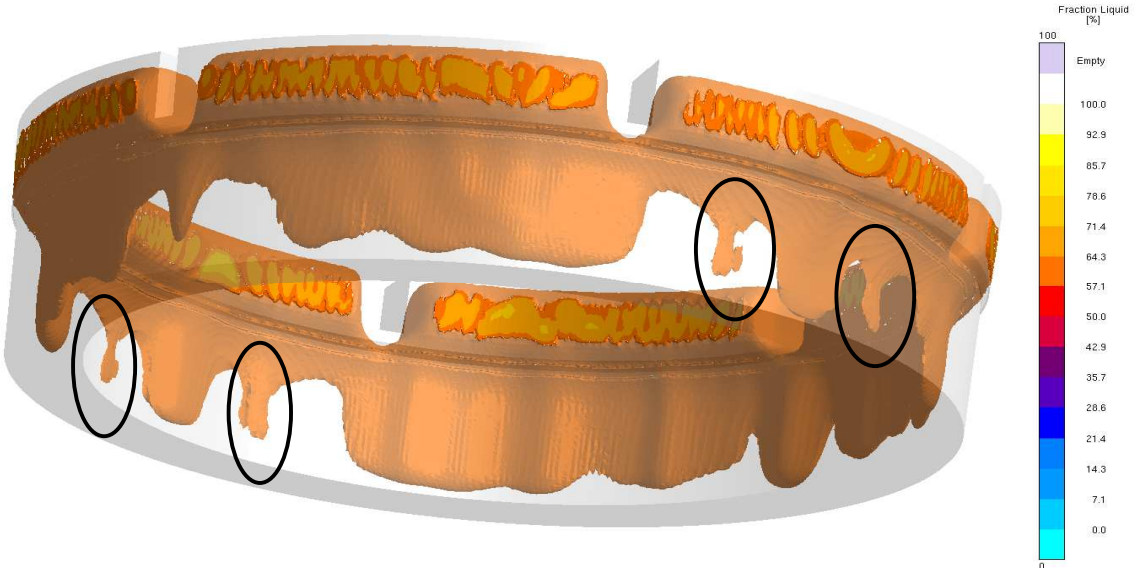

Figure 6: Amount of fraction liquid at the moment when the choking of the liquid pools took place in the casting.

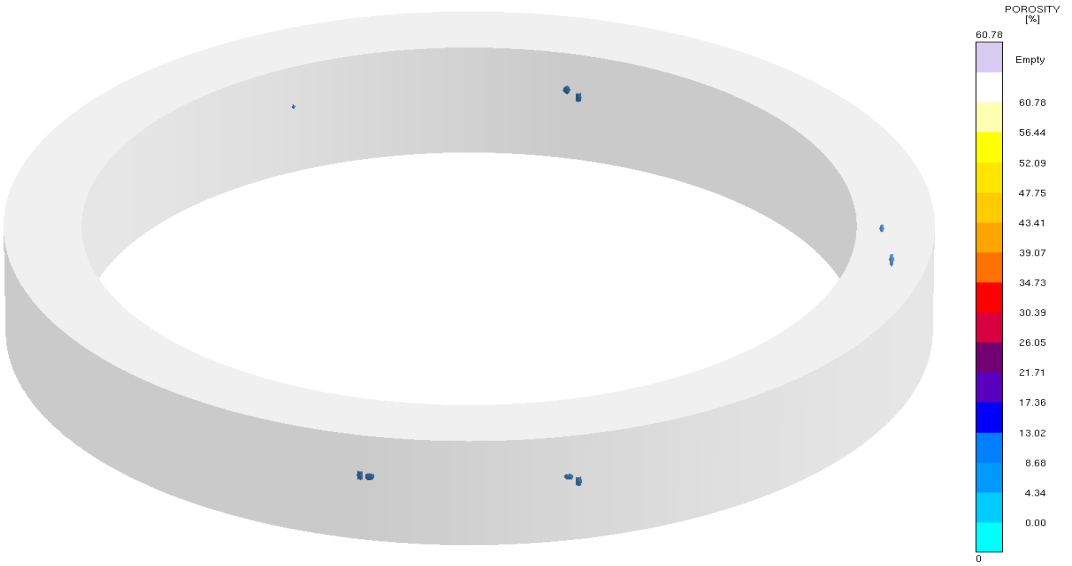

Figure 7: Predicted amount and distribution of porosity in the original casting layout. X-Ray feature was applied to hide all areas containing less than 10% porosity.

When it comes to centerline porosity and microporosity which are both represented by the Niyama criterion, see **Figure 8**, the most decisive factors for their occurrence are low thermal gradients in a combination with high cooling rates. If there is an area of a casting in which the thermal gradient is rather flat- which in essence is always in a thermal axis of a casting, a riser cannot effectively supply the required amount of fresh melt to that needy area. One could rephrase it, that the riser does not have the “power” to push the melt through the solidifying structure, the so-called mush. Or that this troublesome place is too far from the effective feeding zone of the given riser. The impact of the cooling rate can be formulated as follows: if the cooling rate is too high, the solid dendrites grow too rapidly and there is not enough time to deliver the necessary melt into those areas to compensate for the volumetric shrinkage caused by the dendrite growth. Pores then form at these areas as a consequence. This type of defect can be relatively easily eliminated by intense cooling which in general enhances thermal gradients, but also cooling rates. Based on this reasoning, it occurs that it is crucial to support

cooling from the bottom of the casting by a adding chill plate underneath the casting. This should promote an establishment of directional and progressive solidification, hence partially eliminating the channel segregates or pushing them deep enough to the casting so that they would not appear on its surface. This new chill system will however require certain changes in the gating system. To be specific, the bottom gating has to be changed to side gating to accommodate the bottom chill plate. The modifications will be presented and discussed in the section devoted to optimization.

Figure 8: Numerically predicted presence of centerline porosity inside the original casting arrangement.

The occurrence of macrosegregation together with the channel segregates can be predicted by simulating thermal convection inside the solidifying casting, i.e. in the solidification interval where liquid and solid phase coexist. Note that thermal convection must be checked over the whole solidification interval in order not overlook potential freckling anywhere in the mushy zone.

Macrosegregation refers to a solute inhomogenity at the macroscopic scale in metal alloy castings and range in scale from several millimeters to even meters. These compositional variations have a negative impact on final properties, i.e. microstructure, mechanical properties, and in-service behavior of the cast part. Macrosegregation is caused by relative movement or flow of segregated liquid and solid within the mushy zone during solidification.

Flow due to thermal and solute gradients in the liquid is responsible for the formation of channel segregates, commonly referred to as A- segregates or freckles. Freckles are typically initiated by convective instabilities above or inside the mushy zone, i.e. when the velocity of the liquid in the mushy zone exceeds that of the isotherm and the segregated interdendritic liquid becomes less dense than the overlying bulk liquid of original composition. This phenomenon eventually leads to open channels, i.e. local remelting due to solid fraction decrease, in the mush through which the solute-rich and low-density liquid flows upward into the bulk liquid region. These open channels are associated with local increase in permeability which allows for the liquid to flow more easily, thus enhancing remelting and macrosegregation. When the channels eventually freeze, they appear as pencil-like chains of equiaxed crystals that are highly enriched in solute.

There is quite a lot of evidence in the literature that if temperature gradients and casting speed, i.e. isotherm velocity, are high enough, freckles are less likely to form. One could thus argue that in this regard centerline shrinkage and channel segregations follow a similar trend although; they are not necessarily governed by the same physical phenomena. It means that in principle enhanced thermal gradients and progressive directional solidification with a sufficiently tapered pool of liquid metal should decrease the risk of both of these defects. Since both of these defects are found in the current casting, the major focus will be put on optimizing the chilling system to evoke steeper thermal gradients and to establish a pronounced progressive solidification pattern to get rid of both of them.

Another type of channel segregates is the V-segregates. Unlike freckles, they are found at or around the thermal axis of the casting and very often, they are found very close to porous areas. As to my knowledge, no apparent V-segregates were found in the casting which was sectioned and thoroughly inspected with respect to macro- and microstructure. A few snapshots of the sectioned original casting are seen in **Figure 9**.

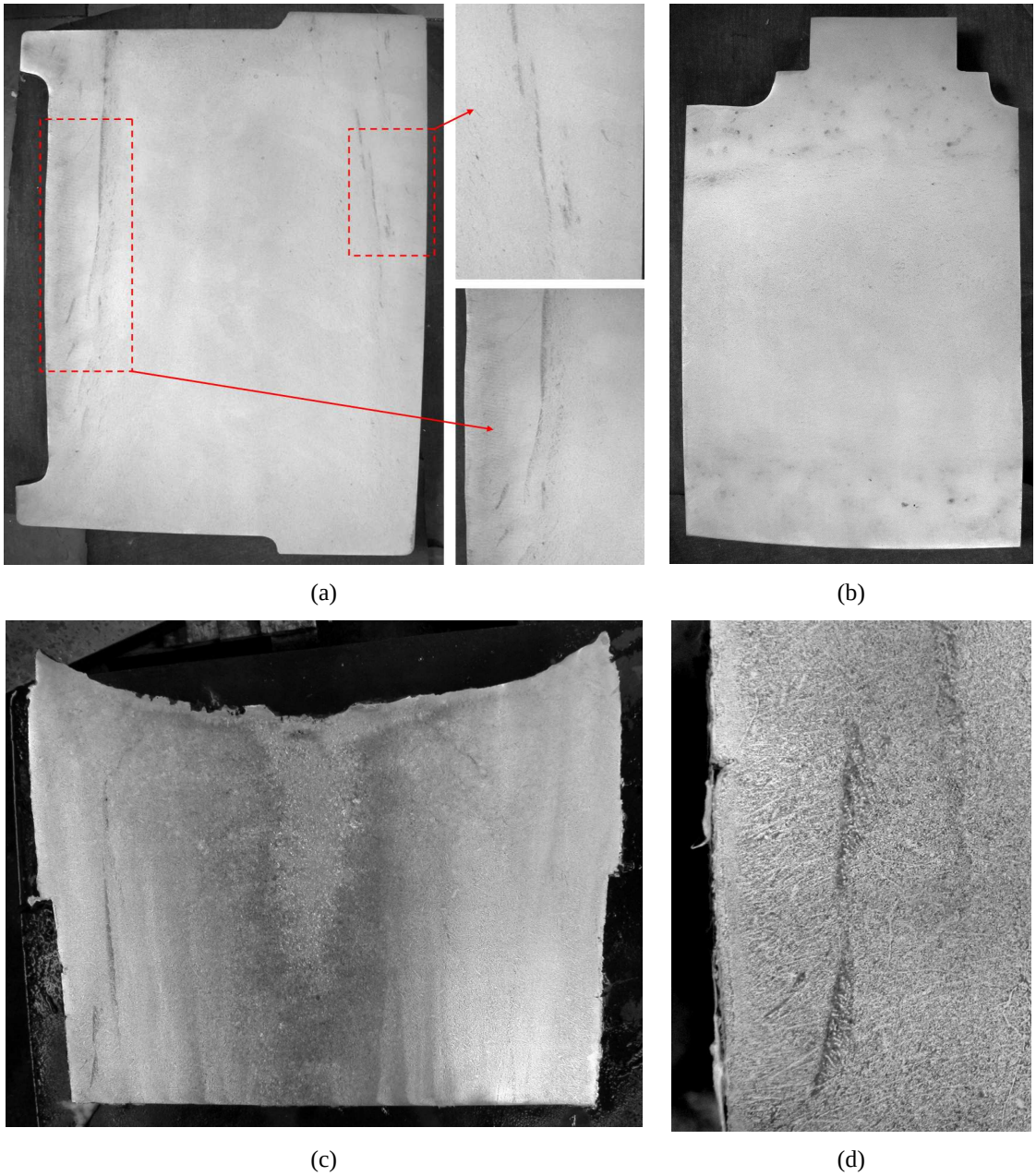

(a) (b)

(c) (d)

Figure 9: (a) longitudinal cut through the steel ring with highlighted A-segregates, (b) transverse cut through the under-riser area denoting the appearance of channel segregates as black dots, (c) cut through the riser showing the pronounced macrosegregation and also porosity and (d) a detailed view on the A-segregated in the riser area. Property of Vitkovice Heavy Machinery a.s.

Figure 10 captures the temperature distribution during the solidification interval, velocity vectors for thermal convection and hence potential initiation sites for A-segregates, i.e. freckles are indicated by the black arrows. A sudden upward-oriented flow in the mush suggests that the permeability of the mushy zone got decreased and that the interdendritic liquid which is rich on various solute elements is able to float up. This means that the buoyancy force causing this flow overruled the retarding frictional force and made the interdendritic liquid flow up as explained earlier in the text. Moreover it is observed both, with the numerical results and with experimental findings in **Figure 9(a)** that the inner surface of the ring is more prone to freckling due to suppressed heat removal as compared to the outer surface. It means that the inner core will heat up fast and will not be able to remove the heat fast enough due to the "converging" heat transfer. As one could see, a relatively good agreement with reality was achieved using the convection profiles during solidification.

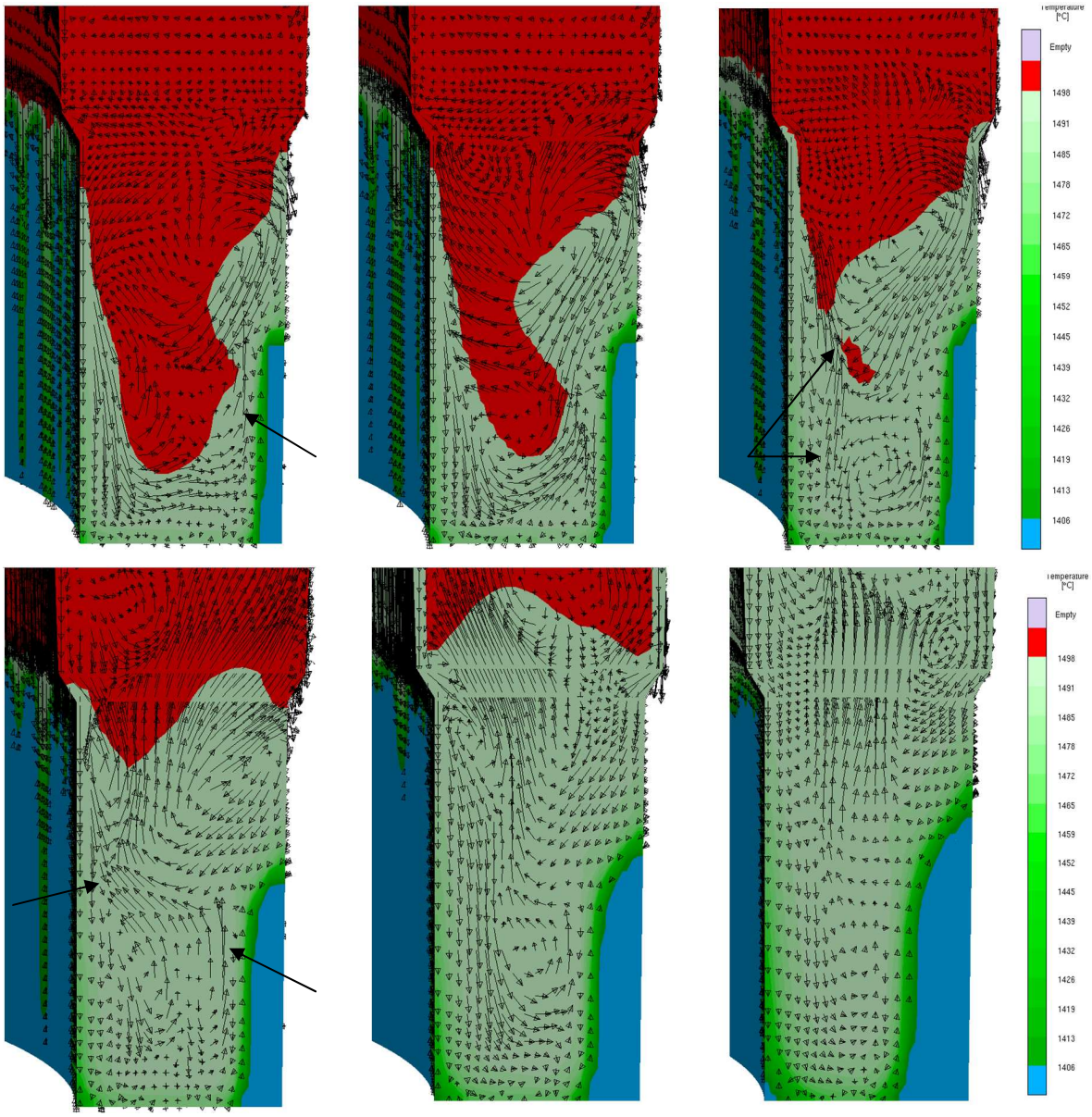
Temperature [°C]
Empty
1498
1491
1485
1478
1472
1465
1459
1452
1445
1439
1432
1426
1419
1413
1406

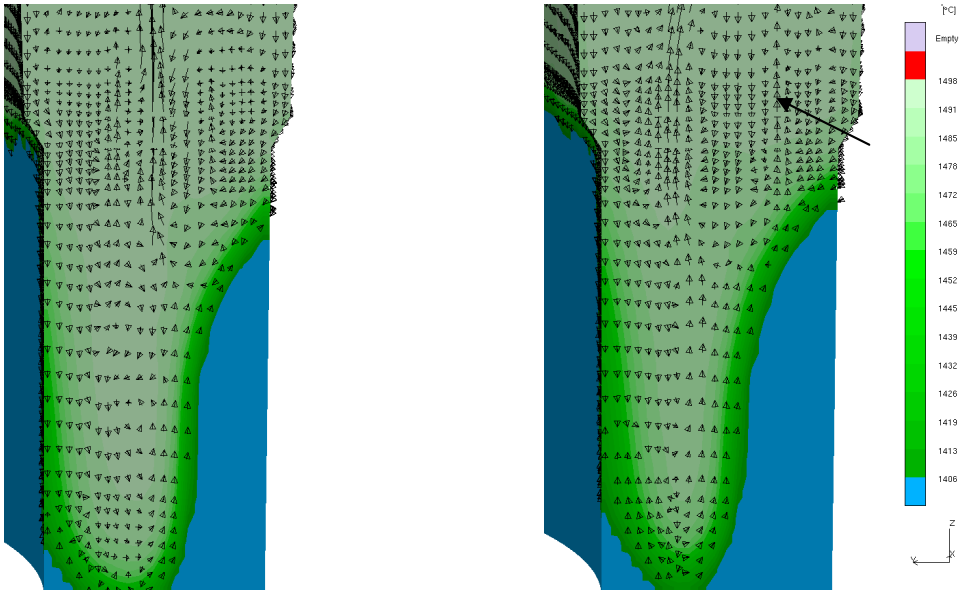

Figure 10: Temperature profiles and convection patterns in a solidifying steel ring casting at8, 10, 12, 14, 20, 30% 40 and 50% solidified. Black arrows indicate potential initiation sites for freckles.

A direct consequence of thermal convection in a solidifying structure is macroscopic segregation of solute elements. It is well known that areas solidifying last contain the largest amount of these solute elements which are rejected from the solid phase into the liquid due to lowered solubility during the temperature drop. Therefore, the residual liquid will have the highest concentration of these elements from the entire casting. Generally it is desired to have uniform concentration profiles of the alloying elements in the casting for the sake of good mechanical properties and to restrict the presence of the positively segregated region to the risers which will eventually be cut off. If the risers are under dimensioned, improperly placed or if the chills are insufficient, the casting could easily wind up having the highly segregated region in the actual casting body. For this reason one could claim that the solidification pattern directly influences macrosegregation.
The series of **Figures 11-14** show concentration profiles of three different solute elements present in the casting microstructure. These figures support the assumption that the solidification pattern has a substantial impact on the macrosegregation in castings. Due to the unprogressive solidification towards the top riser and also due to inadequate chilling from the inner side and from the bottom of the steel ring, the area exhibiting positive segregation is found to be very close to the inner surface and penetrates deep into the casting almost to its bottom.

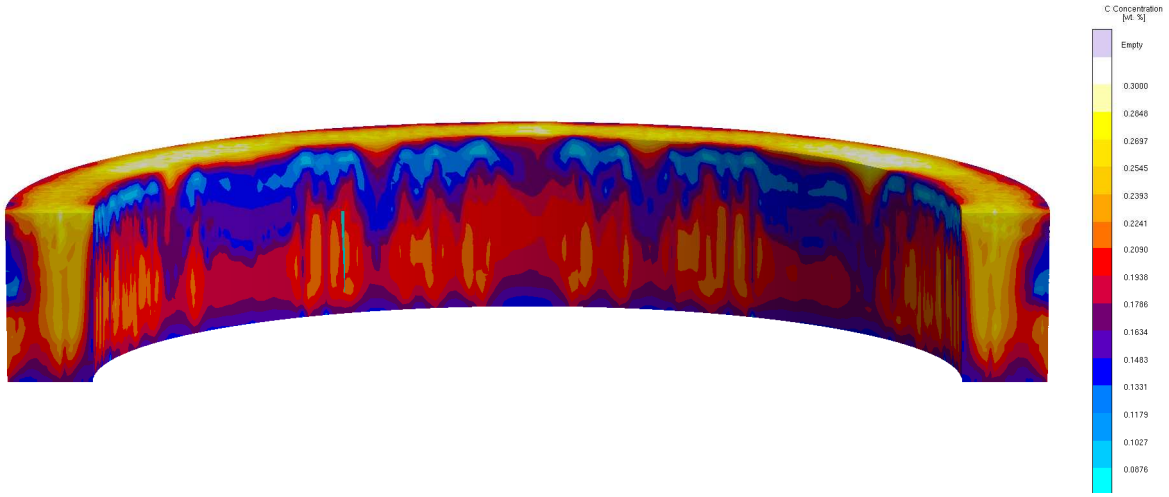

Figure 11: Concentration profile of C for the original casting design. Everything what is white contains more solute elements than is the nominal composition in the liquid state.

An area highlighted red in **Figure 12** implies a tendency towards the so-called inverse segregation. We must only talk about a tendency since that area is not really positively segregated, but is close to it. The inverse

segregation occurs are areas adjacent to chills which solidify the first and rapidly. Nevertheless, this area is not of concern and no related issues are expected.

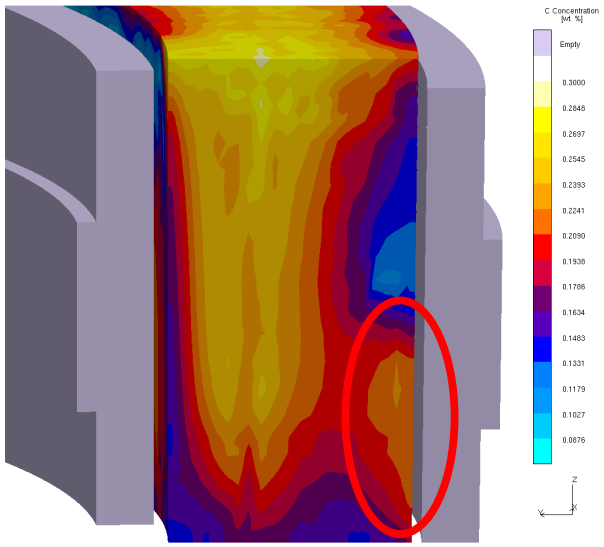

Figure 12: A detailed view of a concentration profile of carbon in the original casting layout.

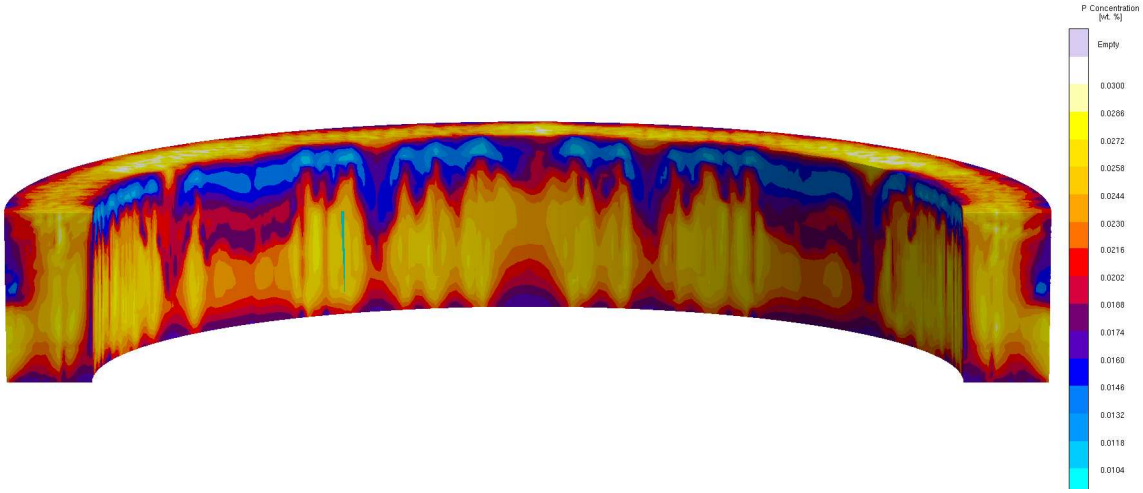

Figure 13: Concentration profile of P for the original casting design. Everything what is white contains more solute elements than is the nominal composition in the liquid state.

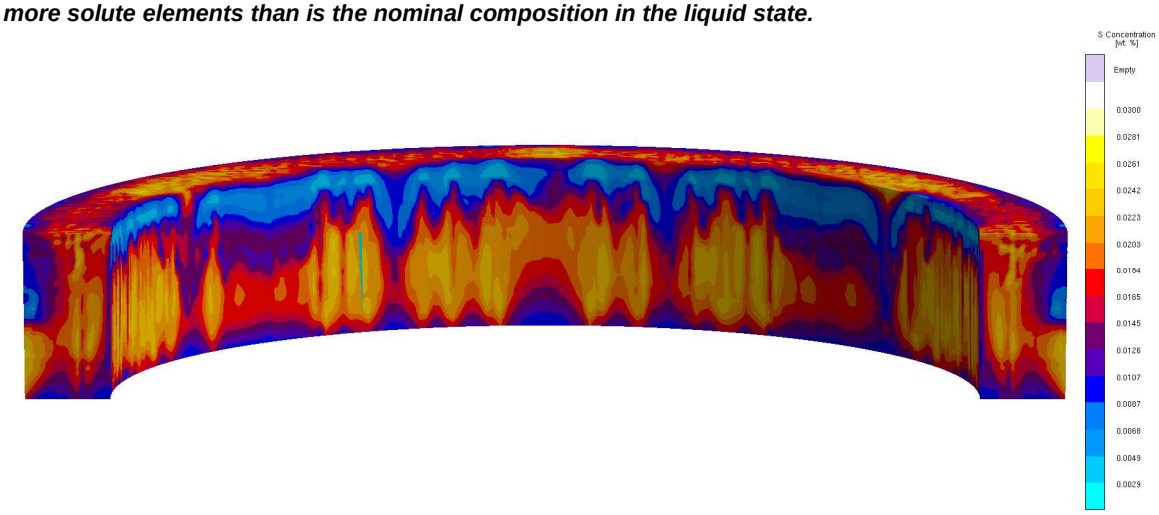

Figure 14: Concentration profile of S for the original casting design. Everything what is white contains more solute elements than is the nominal composition in the liquid state.

The stress-strain analysis was not performed because it was not required by the collaborating foundry. However, it is still possible to get an impression whether the casting may have stress-strain related problems already from the solidification analysis. A way how to kind of indicate potential problems related to high thermal straining and thereby with hot tears is again to use the Niyama criterion. This time we want to highlight areas with the largest thermal gradients and low cooling rates which can be found in the casting very late in the solidification interval, see **Figure 15**. If these thermal conditions are localized in a narrow or small area, this would imply that high thermally induces strains are to be expected there. Moreover, if these areas are mechanically restrained from free contraction, it can easily induce a hot tear. The thermal behavior of the casting implies that feeding of these "problematic" areas should be fine. Besides, there is not any apparent mechanical constraint which may hinder the free contraction. Therefore, I would not expect any hot tear to be found in the real casting.
The real casting which was cast based on this initial layout exhibited only minor tears/cracks on the outer surface at areas which were heavily affected by the flame torch while burning off the top riser. Before the riser removal, no tears or cracks had been observed by the personnel. These minor tears/cracks can be attributed to large temperature differences concentrated over a very narrow region while removing the riser.

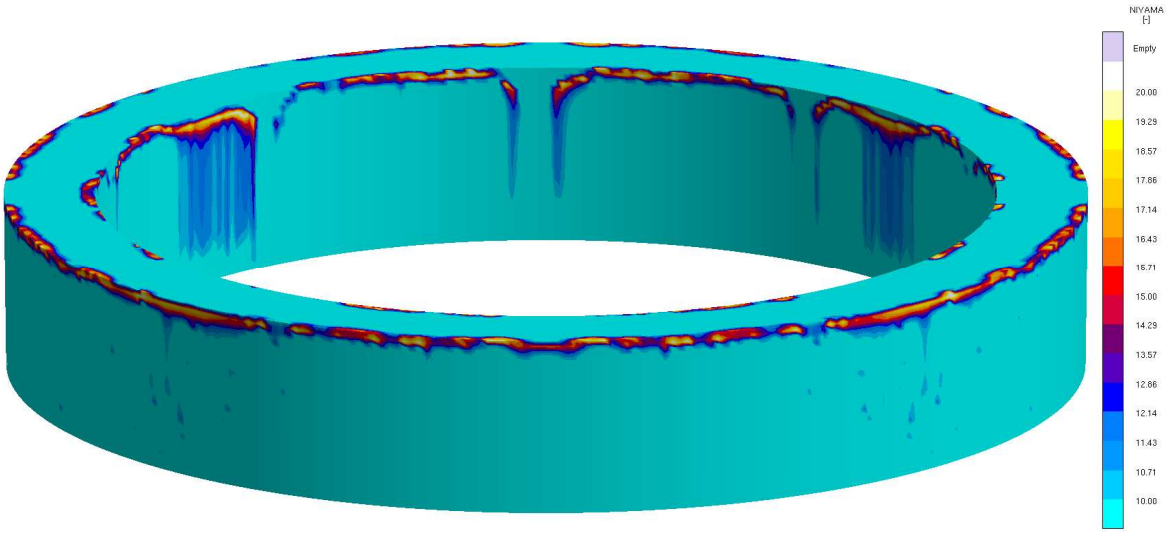

Figure 15: The Niyama criterion is used to highlight areas with high thermal gradients, i.e. yellow color shades. Areas with high Niyama values exhibit steep thermal gradients and low cooling rates. If they are concentrated over a narrow range the risk of hot tears is increased.

CONCLUSION:
This section can be concluded with a few proposals for improvement. Due to the improper layout of the chills the casting did not solidify progressively and directionally towards the open top riser. It eventually led to formation of unfavorable concentration profiles of solute elements which also promoted channel segregates mainly near the inner surface. These channel segregates were later discovered during the subsequent machining operations and were a major cause of rejection. Besides that, areas suffering with centerline and shrinkage porosity were identified both by the numerical simulation software package and by NDT techniques, i.e. non-destructive testing techniques. Considering that this particular steel ring will be used in the cement industry as a load-bearing platform for a large cement mill, this current state of the casting, i.e. porosity and channel segregates present in the structure, is for sure unacceptable for service.
My recommendation is to add chills underneath the casting to evoke more intense cooling from the bottom. I would make these chills in direct contact with the casting for increased efficiency. Additionally, I would recommend optimizing the shape of the chills on both inner and outer side of the casting for inducing favorable thermal conditions, i.e. directional and progressive solidification towards the riser. If the system of the chills is designed properly to promote intense cooling, the total volume of the top riser could be reduced somewhat, thus increasing the casting yield and still eliminating shrinkage and centerline porosity. Based on the relation between the centerline porosity and macrosegregation, a more uniform distribution of the solute elements can be expected.

OPTIMIZATION PROCEDURE

During the riser optimization I followed the guidelines and boundaries that we have set and agreed upon together with the foundry representatives at the project's kick-off meeting. I also took economic aspects into consideration, mainly how expensive it would be for the foundry to apply my optimization proposals. For this reason I decided to keep the shape of the top riser the same and let the numerical optimizer only seek for the most suitable number and location of the small sand breaker cores present in the riser area. I believe that this solution will be much cheaper compared to designing a brand new shape of the riser. Besides, having more of these breaker cores will make the cutting/ burning process of the riser easier. The optimizer was „allowed" to vary the thickness, and the number of these breaker cores (the number of breaker cores ranges 4 – 20). Optimization results suggested that the most optimal solution to casting yield would be to use 12 breaker cores with a slightly larger thickness than in the original arrangement. Thanks to that, the total weight of the casting will be decreased by 7.7 tons and at the same time, the risk of porosity formation and other related issues will not experience an increase with respect to the original solution. The material and dimensions of the insulating padding surrounding the top riser remained unchanged. **Table II** gives information regarding the impact of the optimized riser on the total weight of the casting. The casting and its optimized rigging can be seen in **Figure 16 (left)**.

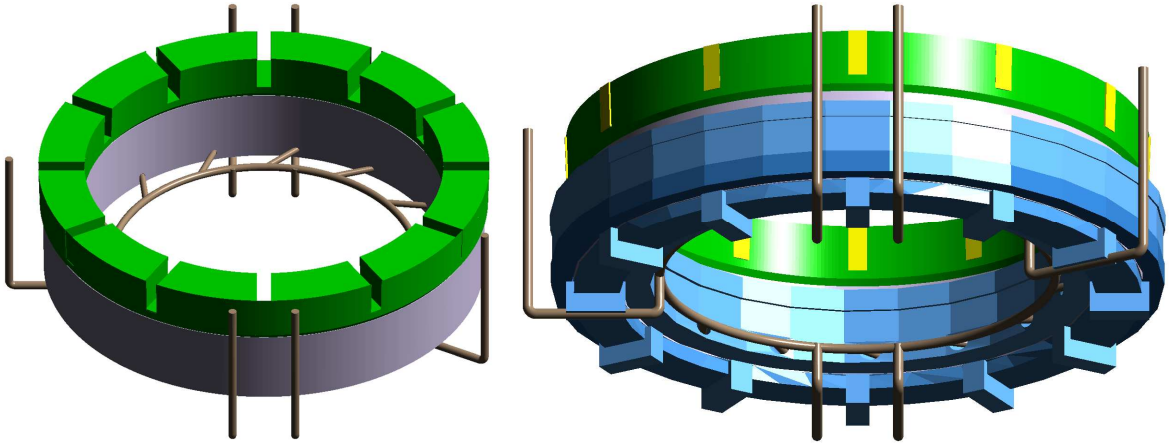

Figure 16: Optimized casting design with new layouts of the top riser, chills and the gating system. The top riser is green, the casting is grey, the gating system is brown, cores are yellow and chills are light blue.

I am convinced that this is a very effective solution to the riser optimization task with minimum production costs related to applying these modifications. Nonetheless, if Vitkovice Heavy Machinery would be interested in performing more radical changes, the parametric model is fully prepared.

Another objective of the optimization study was to completely redesign the system of the chills, i.e. inner and outer, to eliminate issues with centerline and shrinkage porosity and consequently with channel segregates. As mentioned before, a driving force for segregation in general is an inadequate solidification pattern combined with low thermal gradients.

As shown before, due to the gating system being placed below the casting, combined with no chilling from the bottom and unsatisfactory cooling from the sides, problems associated with unprogressive solidification towards the riser were identified in the original technological layout.

Table II – Effect of the optimized riser shape on material consumption.

	Weight of the riser	**Total weight of the casting system**
Original solution	109,5 t	253,7 t
Optimized solution	101,8 t	246 t
Material saved	7,7 t	7,7 t

A decision was made to place a chill plate underneath the casting. In practice it will not be a one-piece ring chill, it will be comprised of steel blocks being in good contact with each other. For their higher efficiency they were made in a direct contact with the casting. It showed that if these bottom chills were in no contact, the

thermal effect on the casting would be nearly zero. Therefore, in order to promote cooling from the bottom, these chills must be in direct contact with the casting. The side chills are non-contact and are placed approximately 20 to 25mm from the casting, in the sand mould. Since the technologists from the foundry insisted on keeping them non-contact under all circumstances it has to be accepted that these non-contact chills will be by far less effective than if they were in contact with the casting. The chills were transformed into parametric objects in the simulation software so that they would be editable by the optimized. Allowed ranges of variation were determined for all elements or units that would undergo optimization. The chills were split into three sections (top, middle and bottom) in order to vary their thicknesses and heights independently. The independent design variable were: The thickness and height of each section The dimension of the chills which were selected by the optimizer as the most optimal are listed in **Table III.**

Table III. - Dimensions of the optimized chills

Outer chill	**Inner chill**	**T1**	270 mm
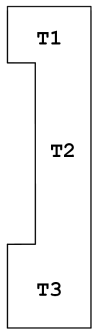	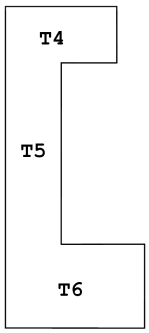	**T2**	245 mm
		T3	270 mm
		T4	300 mm
		T5	250 mm
		T6	400 mm

The thickness of the bottom chills was again determined by the optimizer, 200 mm.
One could notice in **Figure 15(right)** that 12 thicker chill elements were used at areas above which the sand breaker cores were located in the riser. An idea behind this was to intensify cooling and to split the feeding zones of the top riser to make it more effective. These thicker chill segments are also in direct contact with the casting. Their height was suggested to be 300 mm.
Since the bottom chills were added into the system, it was necessary to rearrange the gating system so that the thin gates are attached to the casting from a side. To avoid the melt impinging on the mould wall which may cause mould erosion, tangential thin gates were employed. The main circular runner was placed into the central core. A reason for putting the circular runner to the central core was that, if any hot tears occurred around the thin gates on the casting's surface due to sudden cross-section change, it would be easier to remove them since there are much larger machining allowances on the inner side of the ring.
As to the actual positioning of the thin gates, they go directly „through" the side chills and are placed as close to the bottom of the casting as possible to avoid any „waterfall" effect during filling. All of these modifications in the gating system design were made manually together without numerical optimization.

FILLING ANALYSIS FOR THE OPTIMIZED CASTING LAYOUT OF THE STEEL RING

After simulating the filling stage with the new gating system, several conclusions have been drawn. It was found that the new gating system was again designed reasonably well. As in the first filling analysis, the major focus was put on turbulent behavior of the flowing melt at the initial stages of the filling process, when the melt was entering the mould cavity.
Since the melt now enters the cavity from the side, it was required to pay attention to potential mould erosion caused by the impinging metal on the mould wall. If one thoroughly checks the filling sequence outlined in **Figure 17** where the filling velocities are captured, it can be seen that no significant problems should arise. Nevertheless several shortcomings of the new gating system design must be pointed out. The most obvious one is that the melt does not enter the mould cavity from all thin gates at the same time and with the same velocity. Maybe the first shortcoming could be partially neglected. One could argue that since the casting is so large, the fact that the melt is not entering the mould cavity at the same time from all the gates will not harm the final quality, unlike in the high pressure die casting process. But the second shortcoming really matters. Those areas where the melt flows with higher velocity will be more prone to potential mould erosion. Besides, surface turbulence will be more significant there. A remedy could be to incorporate choke elements into the runner and/or to add runner extensions to absorb some of the kinetic energy of the melt. By dividing the circular runner

into a few independent sections, the streams of the metal coming from different downsprues would not collide in the runner but would flow smoothly into the mould cavity.

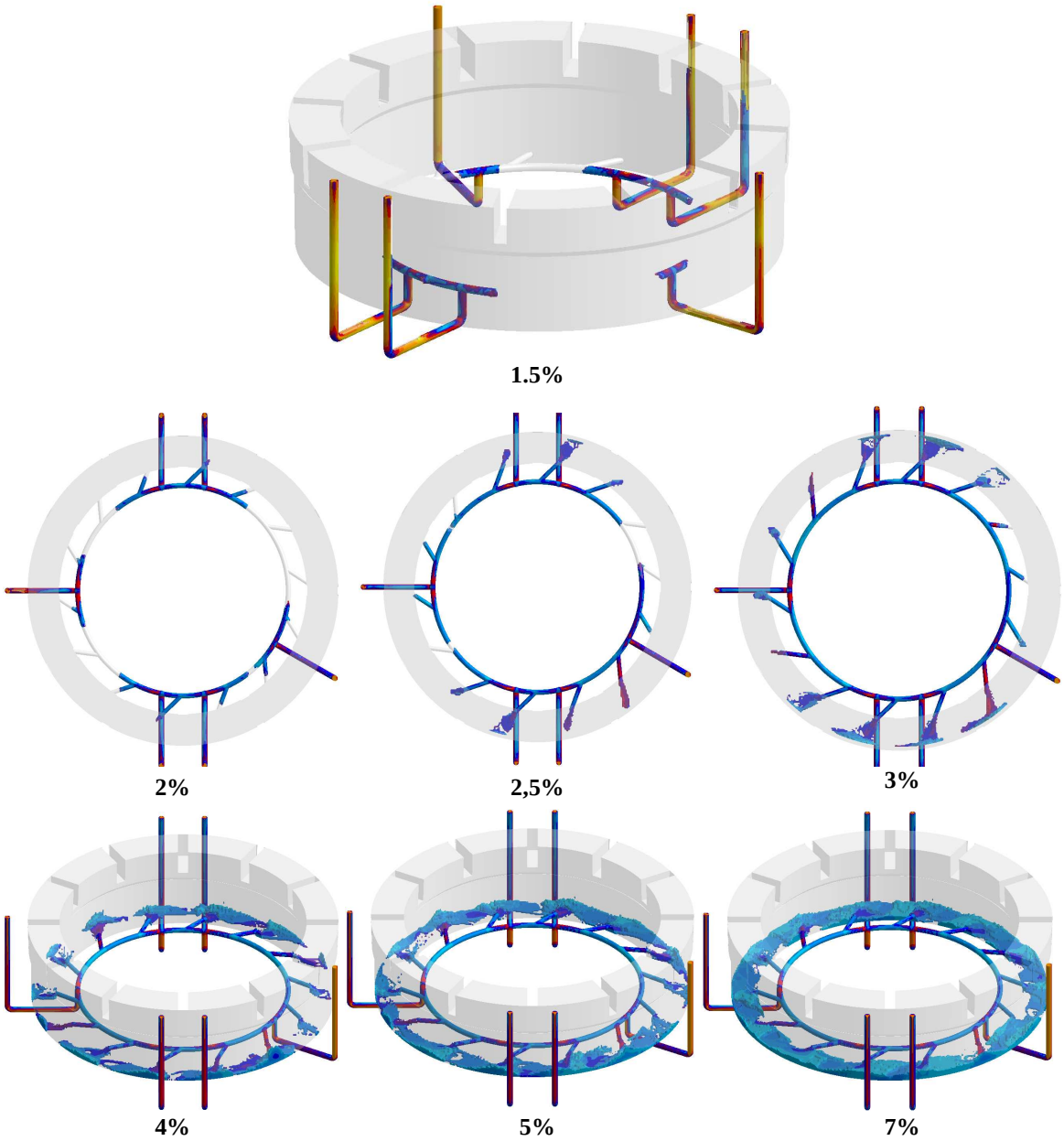

Figure 17: Velocity fields at the initial stages of filling of the optimized casting using the new design of the gating system.

SOLIDIFICATION ANALYSIS FOR THE OPTIMIZED CASTING LAYOUT

The objective of the numerical optimization carried out entirely in MAGMA*frontier* was (i) to increase the casting yield by changing the shape and the volume of the top riser and (ii) to eliminate the presence of centerline porosity by increasing thermal gradients in the casting and through that to eliminate or push the channel segregates deep enough so that they do not show up on the machined surface.
In this section the impact of all of the performed modifications on the solidification pattern and on the defects occurrence is investigated and discussed.
The initial temperature distribution in the optimized casting layout was obtained from the fluid flow calculations. As seen in **Figure 18** the casting has already started to solidify from its surfaces and also a little bit from the bottom due to the presence of the new bottom chills. Although, if we check the color scale we can notice that the temperature is more or less the same all over the casting. It suggests that when modeling

solidification of large castings, one may assume uniform initial temperature distribution. It then (in some cases) allows skipping the filling simulations. However, for accurate results all stages of the casting should always be considered. New shapes and the arrangement of chills started to play a significant role during solidification and not during filling.

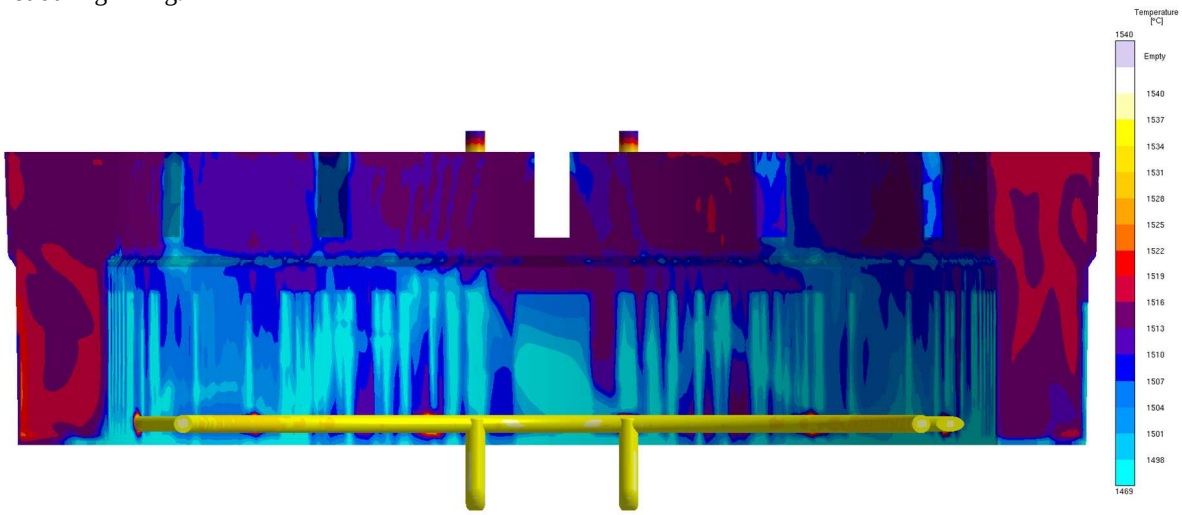

Figure 18: Temperature distribution just after the completion of the filling stage. A more or less uniform distribution of temperature is seen. It points out that the filling is "so quick" as compared to the total mass and the subsequent solidification time that is does not affect the temperature difference nearly at all-for very large castings.

Figure 19(a) outlines what is happening at 30% solidified in terms of the fraction liquid, i.e. how much liquid is present and where. The casting still removes its heat slightly faster from its outer surface than from the inner surface. But the situation at the bottom of the casting has improved a lot after adding the bottom chills. Now we can finally start talking about a tendency to directional and progressive solidification towards the heaviest section of the casting. For sure, this should improve the situation with centerline porosity and hopefully with channel segregates.

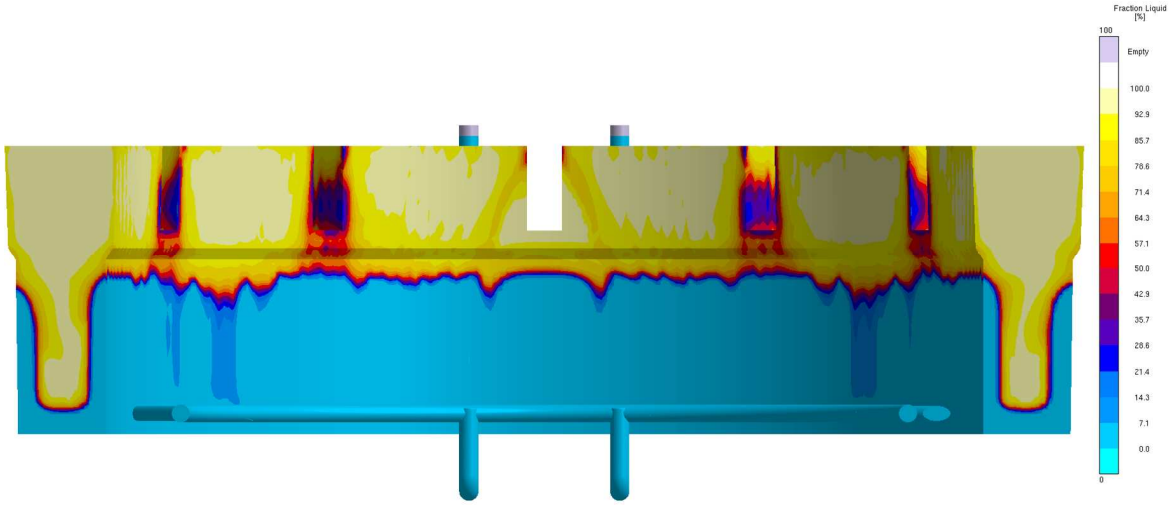

Figure 19(a): Fraction liquid at 30% solidified in the optimized casting layout showing its solidification pattern.

While evaluating the solidification results, it followed that it will not be necessary to use the thicker chill elements below the casting at areas, above which the breaker cores are placed. This statement is based on **Figure 19(b)**, where it is evident that the thicker chill elements have basically no influence on the distribution of the liquid fraction and hence on feeding efficiency of each riser element.

Figure 19(b): Fraction liquid at 30% solidified in the optimized casting layout. Solid areas are filtered out and appear transparent. No choking of residual liquid pools was spotted during solidification.

Obviously the new solidification pattern had a positive impact on the distribution of shrinkage porosity in the casting, see **Figure 20.** Except for two very small isolated porous regions the casting body seems completely sound. The X-Ray function in MAGMAsoft was set to show only areas where the porosity level exceeded 10%. Even when the threshold value was lowered to 5% these two small spots increased only a bit and no new ones emerged. I personally think that nothing will be detected by the NDT techniques and that these areas can be neglected.

Regarding the centerline porosity and microporosity which are expressed by the Niyama criterion, they depend on thermal gradients and cooling rate. As already mentioned, if thermal gradients are low, the mushy zone will be very large and it will be difficult for the riser to supply all the necessary melt through the semi solid region. The cooling rate then expresses the time dependency of feeding.

Thanks to the pronounced cooling which evoked sufficient thermal gradients in the critical areas, the problem with centerline porosity is believed to be resolved, see **Figure 21**.

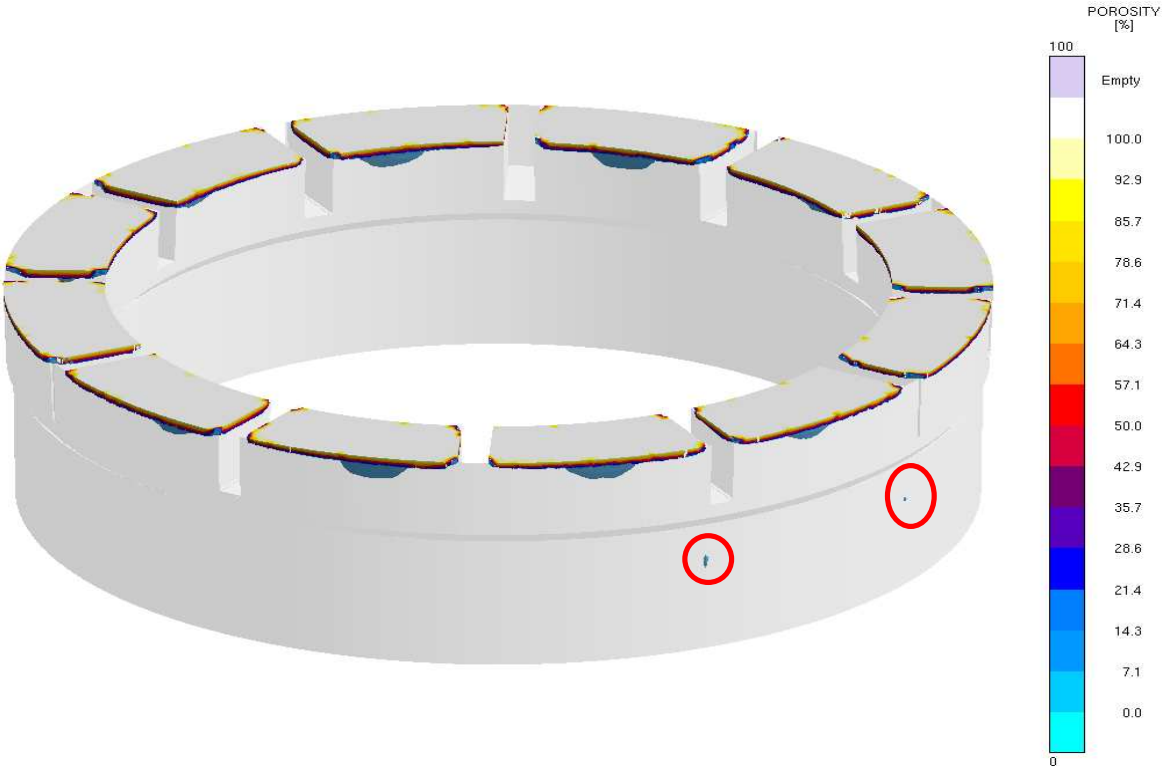

Figure 20: Prediction of shrinkage porosity in the optimized casting layout. Only areas containing more than 10% of porosity are seen. These are encircled red.

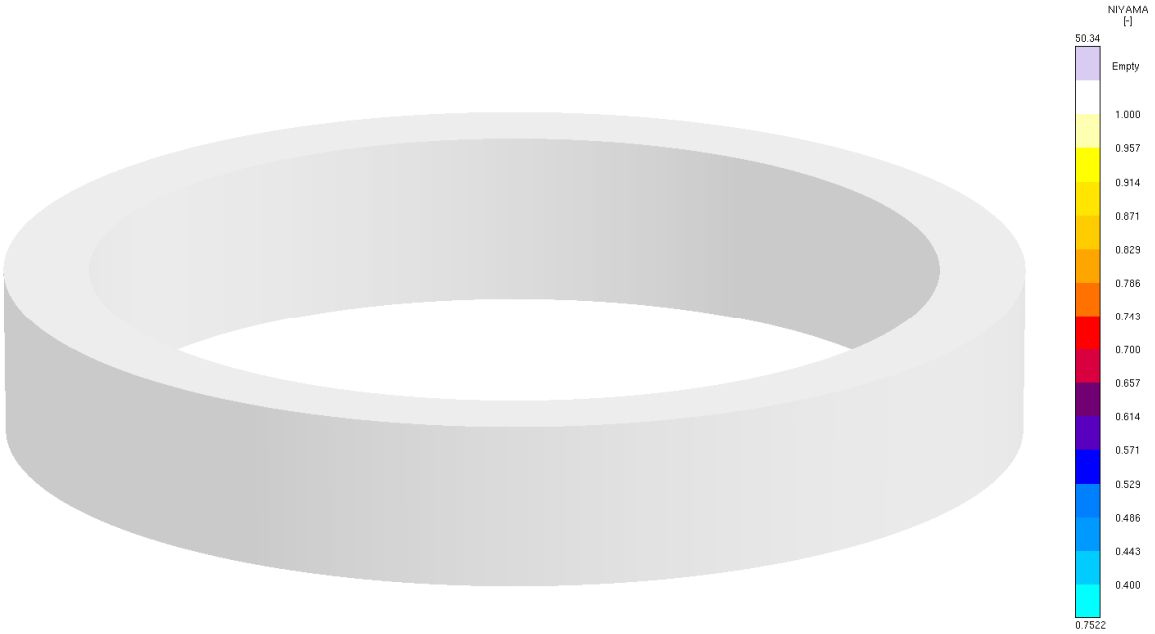

Figure 21: Prediction of centerline porosity inside the optimized casting. No indications of centerline porosity were observed.

In the assessment of the thermal convection and the movement of the mushy zone I focused on the potentially most critical area of the casting when it comes to the channel segregates. This area is found underneath each breaker core, see **Figure 22**. Why exactly this area? Because it does not have a riser on top and thus the thermal gradients will be much flatter and the likelihood of channel segregation is higher there.

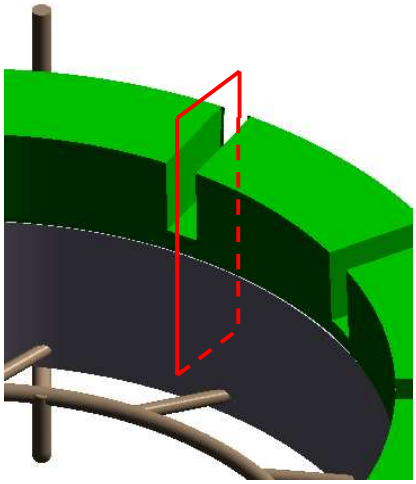

Figure 22: Outline of the cross-section most prone to segregation issues. This area was investigated in terms of convection and macrosegregation.

High thermal gradients will narrow down the mushy zone and will not „allow“the highly segregated liquid to start flowing up. Their effect on the character of the mushy zone is depicted in **Figure 23**. It again supports our conviction that it is feasible to optimize the entire solidification pattern and also reduce macrosegregation related issues just by prescribing the minimization of the centerline porosity as one of the optimization objectives. This is quite an interesting finding which makes it possible to optimize the macrosegregation issues without setting it as the optimization objective. During this particular optimization run, two thousand of thermal calculations are being performed in a search for the most optimal solution. One standard convection and segregation analysis which is necessary for this purpose takes roughly 24 hours on a standard up-to-date multi-core work station, using a reasonably fine computational grid. Thus it is not feasible to calculate thousands of such analyses. When we prescribe minimization of the centerline porosity as an objective, we sort of by-pass this issue. In order to satisfy this objective, thermal gradients must be increased, directional and progressive solidification established. All this reduces the extent of the mushy zone and the highly segregated residual liquid is pushed into to the riser, see **Figure 23**. Moreover, the resistance to channel segregates is higher due to the reduced permeability of the mush. Now we can see more „organized“or controlled movement of the mush with very few indications of potential freckles.

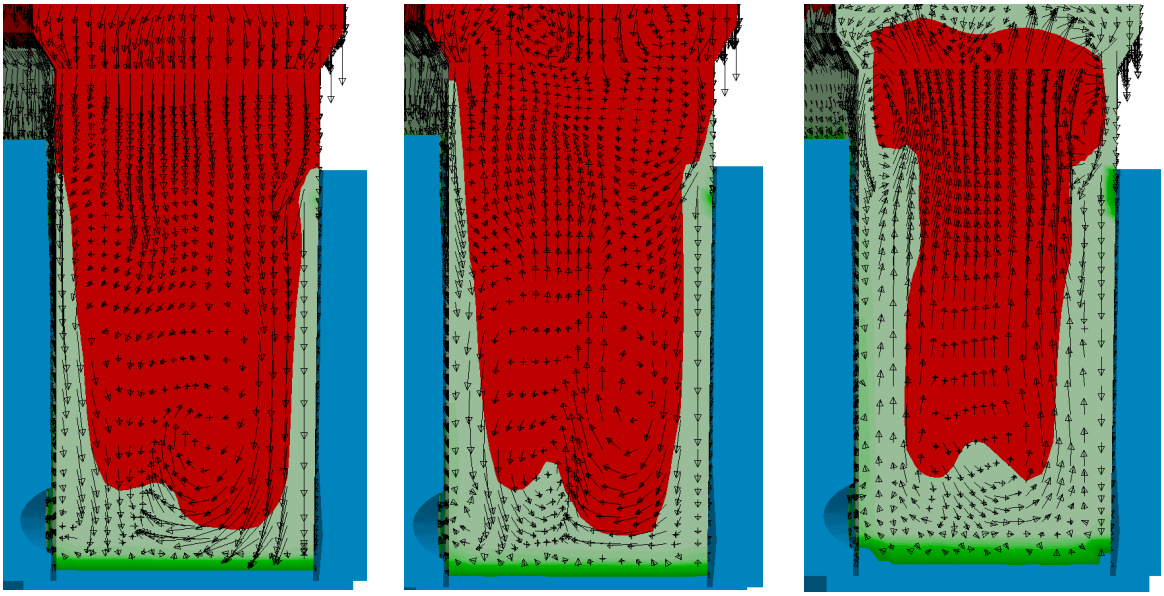

6% 7% 10%

Figure 22(a): Temperature distribution and velocity fields in the early stages of solidification in the optimized casting. The vectors show the direction of the flow of the melt and the interdendritic liquid. Blue color denotes a completely solid region, all of the shades of green stand for the mushy zone and the red color stands for the liquid phase.

Just for clarity, while assessing macrosegregation, more than one area of the casting was investigated but no apparent indications of freckling were found. I believe that if any issues with channel segregates were encountered, it would happen in the area under the breaker core which is presented in **Figure 23.** Although I think that even there no problems should be expected.
The only place where a freckle could possibly form is highlighted in **Figure 23(b)** and is denoted by a black arrow. Nevertheless, it would be deep enough not to show up on the machined surface.

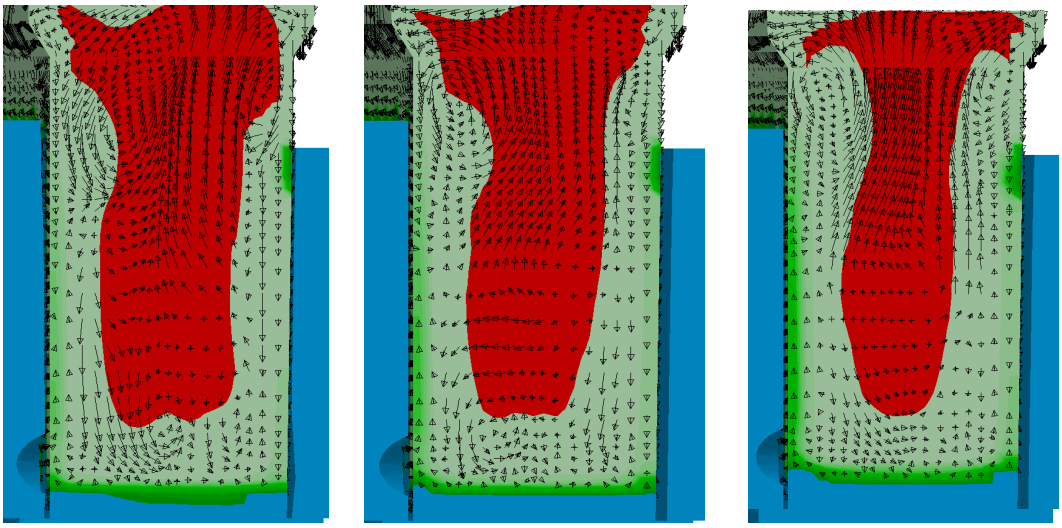

12% 14% 17%

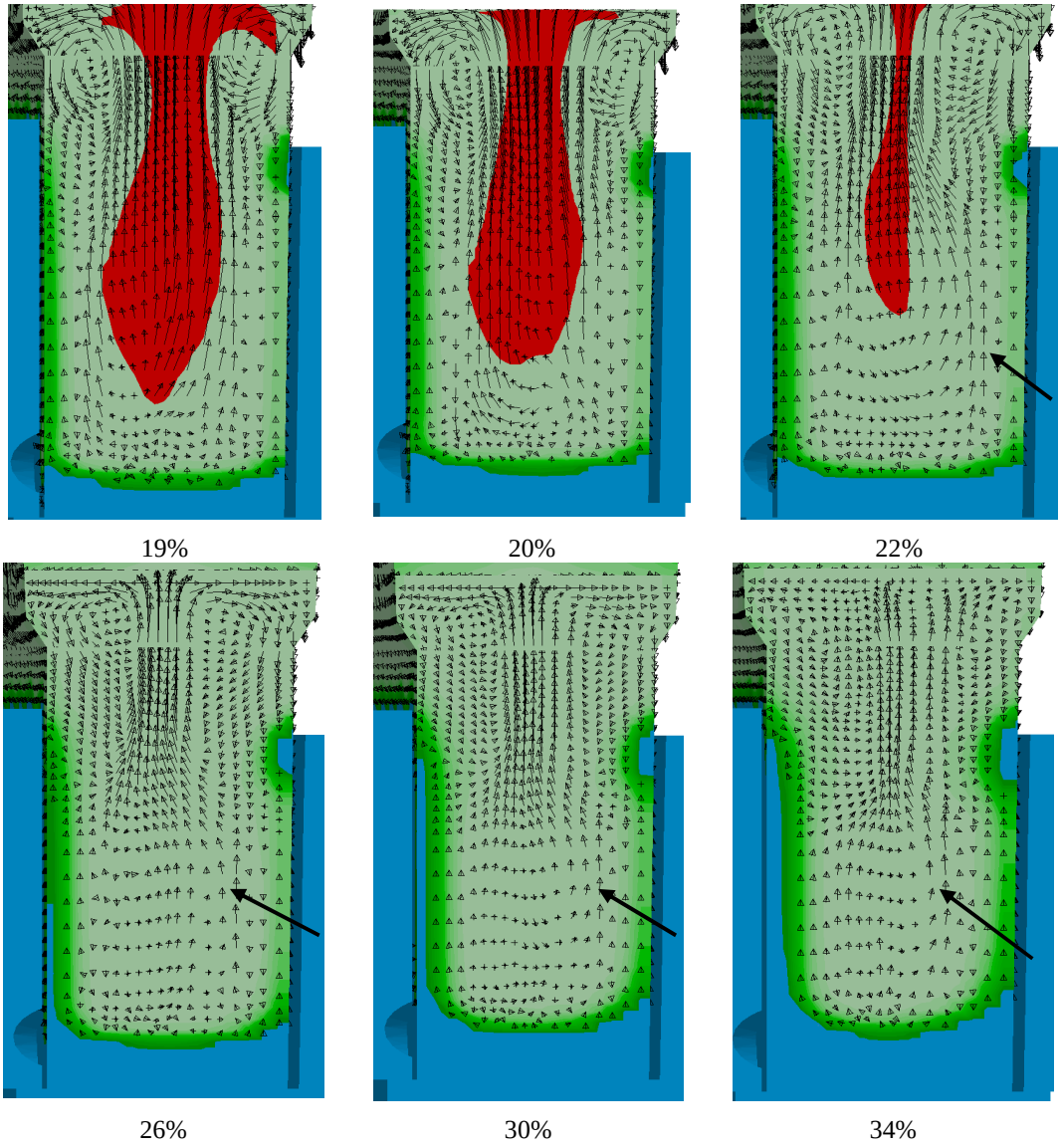

Figure 23(b): Temperature distribution and velocity fields at 12-34% solidified in the optimized casting layout. The four black arrows emphasize the area at which a potential freckle might form. Blue color denotes a completely solid region, all of the shades of green stand for the mushy zone and the red color stands for the liquid phase.

Figures 24-26 show concentration profiles of three major solute elements. The optimized solidification pattern obviously changed the distribution of these elements in the casting. A very beneficial feature of the new distribution is that the positively segregated region is only located in the riser area and does not penetrate into the body. To be really certain that the positive segregation will not affect the under-riser area, a few more modifications in the taper of the riser or the shape of the chills would have to be made. As to the casting body itself, a rather uniform distribution of the elements is observed. The bottom area now exhibits negative segregation that is caused by sedimentation of the primary dendrites which are heavier than the solute elements which in return are rejected to the bulk liquid and pushed up. This was not the case in the original layout due to the insufficient cooling from the bottom. The two negatively segregated bands right under the riser are most likely caused by the vortices seen in **Figure 23** which „washed away“ the solute elements into the bulk liquid leaving those areas poor on solutes**.** Generally it applies that an area in the mushy zone, from which the interdendritic liquid enters the liquid, will be poor on the solutes and vice versa. One more explanation for having these bands is deformation of the mushy zone which will be shown in the stress-strain analysis. Else, the concentration profiles are quite favorable which again support our assumption that it is possible to optimize the segregation issues by establishing a proper solidification pattern. And this solidification pattern is established based on the optimization objective - the minimization of centerline porosity.

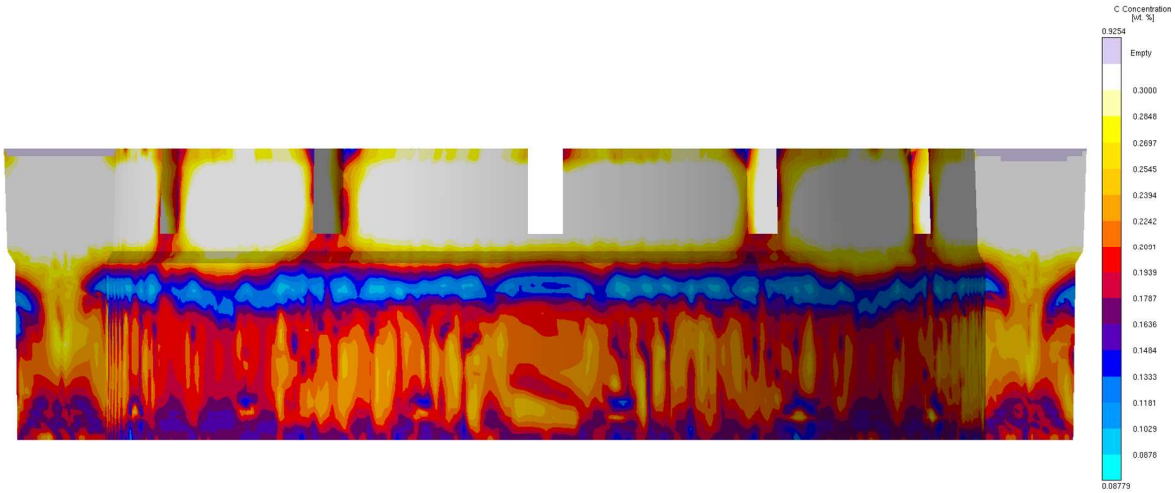

Figure 24: Concentration profile of C for the optimized casting design. Everything what is white contains more solute elements than is the nominal composition in the liquid state.

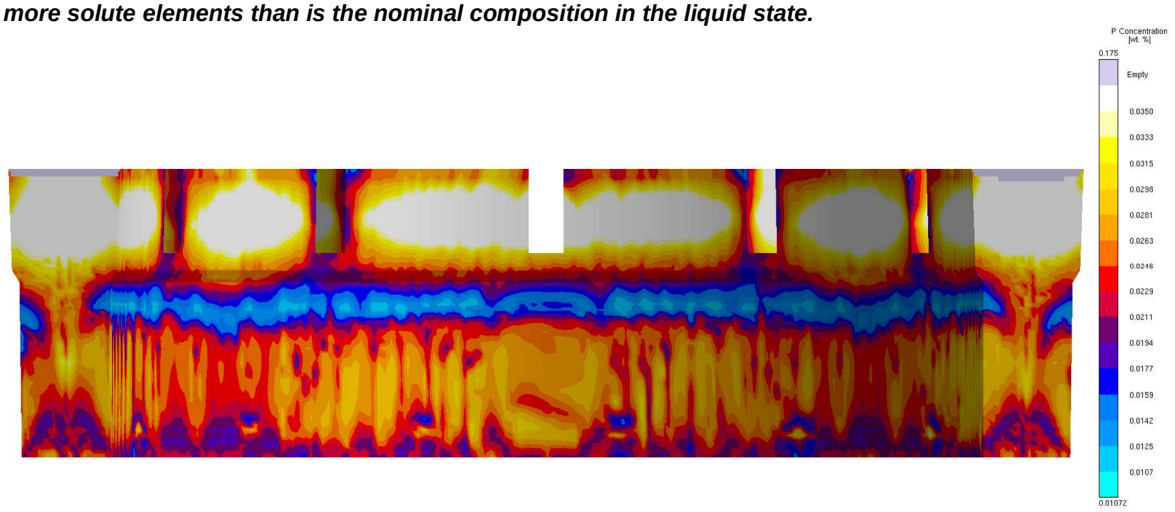

Figure 25: Concentration profile of P for the optimized casting design. Everything what is white contains more solute elements than is the nominal composition in the liquid state.

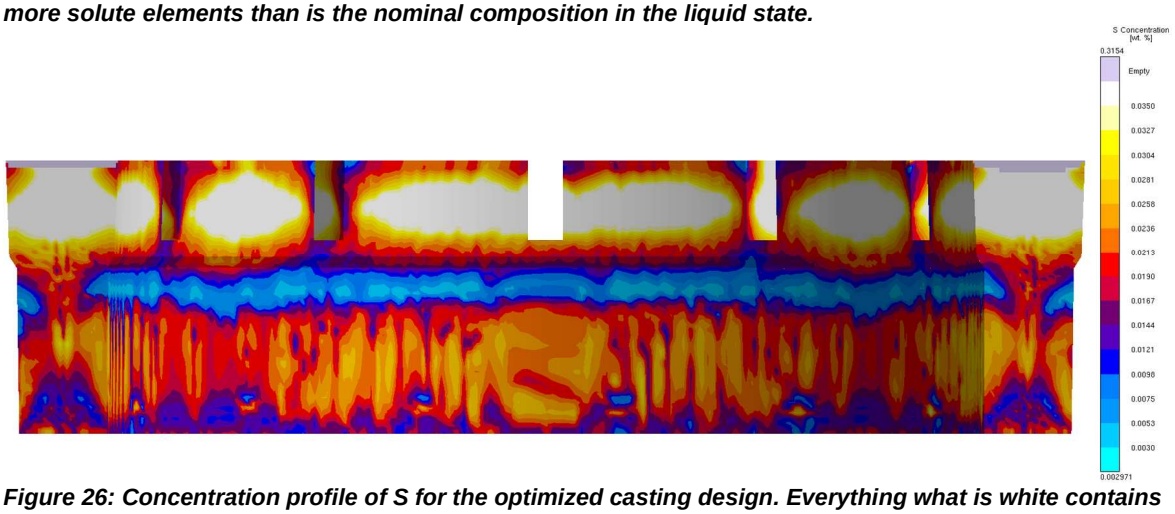

Figure 26: Concentration profile of S for the optimized casting design. Everything what is white contains more solute elements than is the nominal composition in the liquid state.

CONCLUSION

A numerical optimization was performed for the case of a large steel ring. In this study, the optimization was aimed at minimizing the total riser volume to obtain a better casting yield and at minimizing centerline porosity which should also “take care of” the issue with macrosegregation.

This new methodology where macrosegregation is addressed by means of the reduction of the centerline porosity makes it possible to perform a full optimization with thousands of analyzed variants without having to calculate segregation and convection in each of them, which would take for ever. Since both the centerline porosity and macrosegregation are heavily dependent on thermal gradients and cooling rates, it was expected that if proper thermal gradients with directional and progressive solidification pattern are established, the centerline porosity and macrosegregation will be both eliminated. This was proved and showed on the optimization results.
In order to achieve progressive and directional solidification with thermal gradients high enough, the dimensions of the riser and the chills were turned to parametric objects and optimized. Moreover, chills were added underneath the casting to support cooling from the bottom. Therefore the gating system was redesigned from bottom-fill to side-fill.
The total volume of the top riser got reduced by 7.7 tons while the solidification pattern got improved substantially. It resulted in a complete elimination of the centerline porosity and in a more uniform distribution of the solute elements in the microstructure. The risk of channel segregates was also lowered significantly due to much steeper thermal gradients which decreased the size of the mushy zone.

STRESS STRAIN ANALYSIS

In the stress strain analysis the focus was on predicting potential hot tears in the optimized casting layout. The issue of hot tearing was not considered during optimization, see **Table I**. The selected design was checked to make sure that, before approving it for production no hot tears would occur.
Since no "real" hot tears were found after casting the original casting, no issues with hot tearing were expected even now. In the worst case, I would expect minor tears at the contact area between the casting and the gating system. This is the only place with significant thickness difference which might be susceptible to hot tearing.
However, after assessing the stresses and strains induced during the solidification interval, it occurred that there might be a problem with hot tearing on the inner surface right under the riser, as depicted in **Figure 27**. The hot tear was found along the entire inner diameter. Just by looking at the casting geometry, the presence of the hot tear does not make much sense. The geometry is very simple with no apparent section changes, sharp corners or stress concentrators.

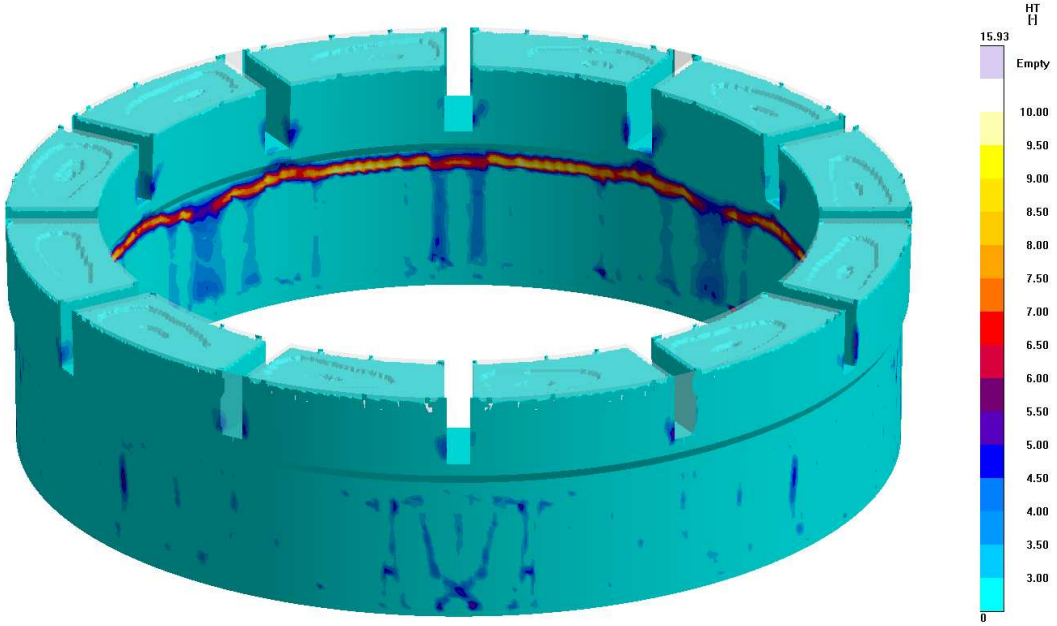

Figure 27: Hot tear prediction in the optimized casting layout. The most susceptible areas are indicated by the yellow color on the color scale. The higher the number on the scale the higher risk of hot tearing.

To explain the occurrence of hot tears and to estimate whether they would occur or not one has to look at the influencing factors for hot tears. The most decisive factors are hot spots being insufficiently fed combined with thermal tensile straining. First we will investigate the thermal fields inside the casting. **Figure 28** indicates that during solidification, the solidification front propagates both from the sides and from the bottom. However, there is an area (indicated by black arrows) which retains its temperature more or less constant for a relatively long time interval. The surrounding areas solidifying faster might then evoke tensile straining in the z axis due

to volumetric contraction. So the slowly solidifying area cannot exert much resistance to this deformation since it is still very weak. Hence it might actually end up being pulled apart and open up the tear. The tensile straining is seen in **Figure 29** where high tensile strains (white areas), are observed in the problematic area.

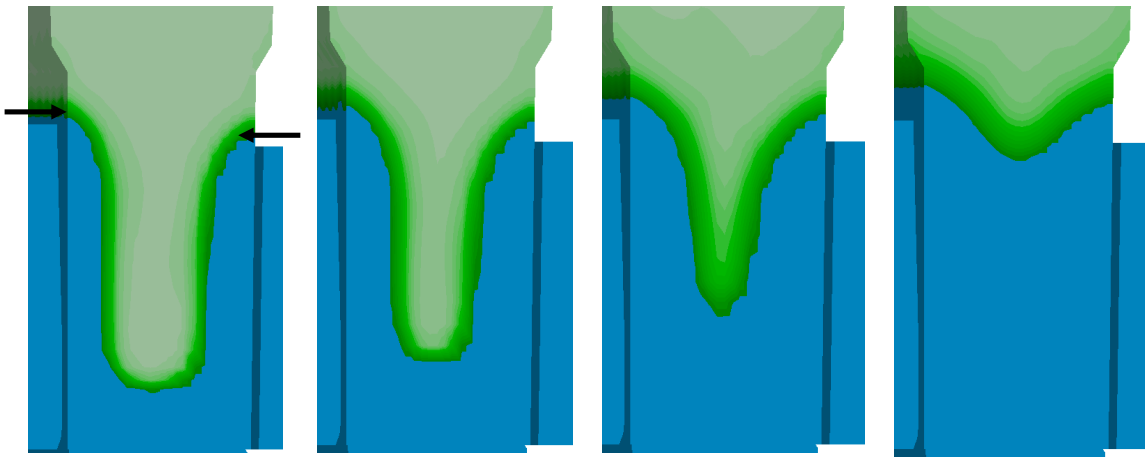

Figure 28: Thermal fields during solidification affecting the likelihood for hot tearing. Blue color denotes a completely solid region, all of the shades of green stand for the mushy zone.

The thermally induced straining would actually explain whey there are the two band-shaped areas with a pronounced negative segregation, see **Figures 24-26**. One cause of segregation is deformation of the mushy zone where the mushy zone can be pictured as a sponge. If the sponge is compressed, the liquid is rejected out of it, if it is in tension; the liquid is being sucked into the sponge. If one imagines that the problematic area is being pulled apart, it tries to suck in new liquid. Since it is located adjacent to the casting surface, there is no place to get that required melt. Therefore the solute rich melt is being sucked inwards from the outer region which makes it poor on these solutes.

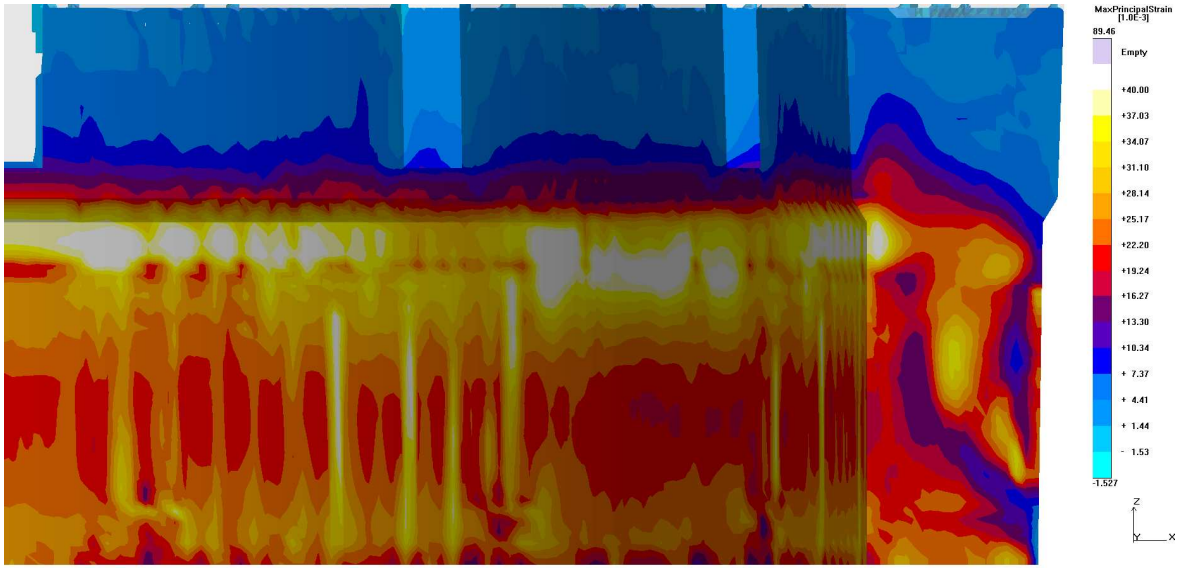

Figure 29: Maximum principal strain during the solidification interval of the optimized casting. It emphasizes areas which will undergo very rapid deformation- white areas in the figure.

The Niyama criterion was applied again to highlight areas with high thermal gradients and low cooling rates in the search for potential hot tears. It is seen that compared to the original solution, the size and magnitude of the risky areas decreased significantly.

I personally believe that no major problems with hot tears should be seen in reality. The geometry just does not look as if it facilitates hot tearing. Moreover, there is no hot spot that would not be fed properly. The solidification pattern is much more favorable than the original one where no real hot tears were found after casting-if we do not consider the crack after removing the riser. All numerical software packages will always

find the most critical area. One must always check the severity and magnitude of that potential defect. For this reason I think that, MAGMA identified the most dangerous areas extremely well; however in reality, this defect may not occur due to its magnitude- at least in my opinion.

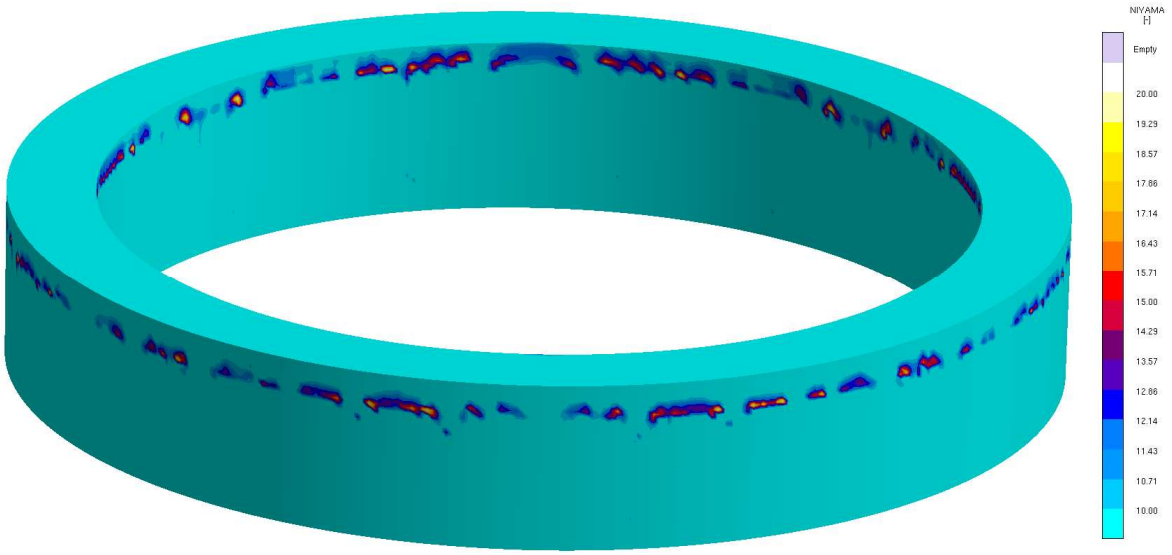

Figure 29: The Niyama criterion was again applied to highlight areas with high thermal gradients and low cooling rates which may induce thermal strains.

In **Figure 29** all of the least dangerous areas were filtered from the hot tear susceptible area to highlight only the most significant. It shows that if any hot tear formed it would not be continuous and deep but isolated and most likely only on the surface.

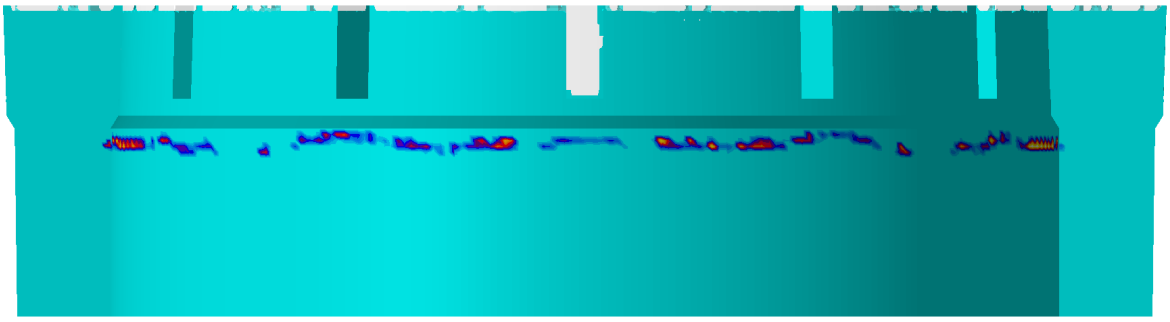

Figure 30: The "hottest" candidates for hot tearing. The less severe areas were filtered out and appear light blue.

Monday, January 10, 2011 I personally called a senior technologist from Vitkovice Heavy Machinery to inform about the current status of the optimized steel ring. At this moment, the optimized steel ring is at the machining shop. The roughing and the final cleaning have already been carried out and only 5 black dots which may imply A-segregates have been found on the surface. In the original design, there were literally hundreds of them on the surface. No hot tear has been found. Since the machining operations are still not completely finished, we do not dare to make the final conclusion, although till now everything seems very good.